Mirko Meboldt · Christoph Klahn *Editors*

Industrializing Additive Manufacturing — Proceedings of Additive Manufacturing in Products and Applications — AMPA2017

Springer

Industrializing Additive Manufacturing — Proceedings of Additive Manufacturing in Products and Applications — AMPA2017

Mirko Meboldt · Christoph Klahn
Editors

Industrializing Additive Manufacturing — Proceedings of Additive Manufacturing in Products and Applications — AMPA2017

Springer

Editors
Mirko Meboldt
pd|z Product development Group Zurich
ETH Zürich
Zürich
Switzerland

Christoph Klahn
Inspire AG
Zürich
Switzerland

ISBN 978-3-319-66865-9 ISBN 978-3-319-66866-6 (eBook)
DOI 10.1007/978-3-319-66866-6

Library of Congress Control Number: 2017952386

© Springer International Publishing AG 2018
This work is subject to copyright. All rights are reserved by the Publisher, whether the whole or part of the material is concerned, specifically the rights of translation, reprinting, reuse of illustrations, recitation, broadcasting, reproduction on microfilms or in any other physical way, and transmission or information storage and retrieval, electronic adaptation, computer software, or by similar or dissimilar methodology now known or hereafter developed.
The use of general descriptive names, registered names, trademarks, service marks, etc. in this publication does not imply, even in the absence of a specific statement, that such names are exempt from the relevant protective laws and regulations and therefore free for general use.
The publisher, the authors and the editors are safe to assume that the advice and information in this book are believed to be true and accurate at the date of publication. Neither the publisher nor the authors or the editors give a warranty, express or implied, with respect to the material contained herein or for any errors or omissions that may have been made. The publisher remains neutral with regard to jurisdictional claims in published maps and institutional affiliations.

Printed on acid-free paper

This Springer imprint is published by Springer Nature
The registered company is Springer International Publishing AG
The registered company address is: Gewerbestrasse 11, 6330 Cham, Switzerland

Preface

"Industrializing Additive Manufacturing" is the proceedings of the first scientific conference on *Additive Manufacturing in Products and Applications AMPA 2017.* The conference provides a platform for the exchange of ideas and knowledge among engineers, designers, and managers. Its objective is to support real-world value chains by developing additively manufactured serial products.

Additive Manufacturing (AM) often has been referred to as a future production technology enabling the next industrial revolution. Additive processes offer very different characteristics when compared to conventional manufacturing processes, such as almost unlimited freedom in design and an efficient digital process chain allowing for lot size one manufacturing. Many AM processes were invented between the mid-1980s and the early 2000s. Researchers all over the world dedicated their work to understanding and improving AM materials and processes. Thanks to them, we now have access to a large variety of industrial AM machines and commercially available materials.

Yet still we are just at the beginning of an industrialization of AM. There are several challenges to face in regard to quality, productivity and robustness of processes, and a demand for new materials. Nevertheless, it can be clearly stated that Additive Manufacturing by now is a mature process ready for industrial production. Engineers in industry do not question the operational readiness of the processes anymore. Their concern now is how to benefit from Additive Manufacturing and how to integrate AM into their existing product development and production processes. Having a reproducible process delivering parts of sufficient quality and acceptable costs is only the starting point for the industrialization of AM. Additive Manufacturing is taking the next step on its journey toward a broad range of series production, and we are facing many new scientific challenges.

Transforming the potential benefits of Additive Manufacturing into a successful industrial or end-user product is a challenge to all disciplines along the product development process. Designers and engineers need strategies to help them identify the right applications, tools, and methods for an efficient design process using the freedom of design to create benefits for users as well as the manufacturer. Production engineers have to assess Manufacturing Readiness Levels, implement

AM machines into the existing production chain, ensure an efficient operation, and establish quality assurance and control mechanisms. Examples for AM-specific topics on the economic side are make-or-buy decisions, supply chain organization, new business models, and converting Unique Selling Propositions in additional revenue.

The topics of *Additive Manufacturing in Products and Applications* cover all topics necessary to develop and produce successful products.

- Design Tools & Methods: Identifying and designing AM parts
- Process Chain Integration: Setting up a safe and efficient production infrastructure
- Business Cases of AM Applications: Quantifying the benefits of AM
- Unique Customer Benefits: Learning from good and unusual examples
- Teaching and Training: Bringing knowledge and experience to new users

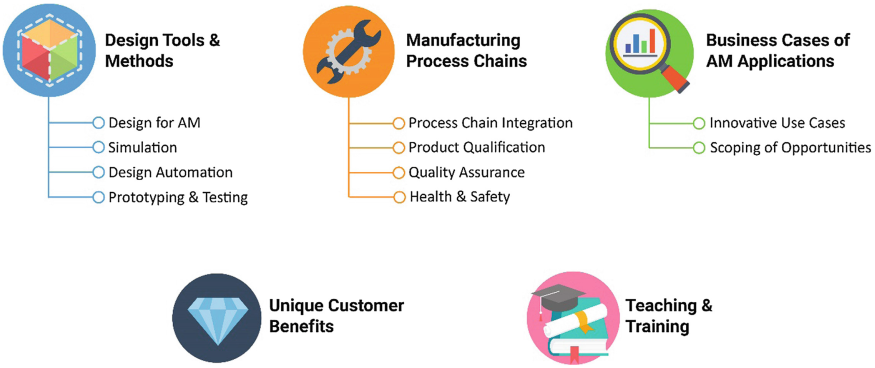
Design Tools & Methods
Design for AM
Simulation
Design Automation
Prototyping & Testing
Manufacturing Process Chains
Process Chain Integration
Product Qualification
Quality Assurance
Health & Safety
Business Cases of AM Applications
Innovative Use Cases
Scoping of Opportunities
Unique Customer Benefits
Teaching & Training

We would like to thank everyone who contributed to the success of the *Additive Manufacturing in Products and Applications* conference: Thanks to the authors for their valuable papers and talks, to the members of the industrial and scientific committees for their hard but fair reviews and for chairing sessions, to the participants of the sessions for the fruitful discussions, and last but not least to all those who supported the conference in the background.

Mirko Meboldt
Christoph Klahn

Organization

Organizing Committee

Mirko Meboldt	ETH Zürich, pd|z
Christoph Klahn	inspire AG, ipdz
Filippo Fontana	ETH Zürich, pd|z
Martin Stöckli	inspire AG
Petra Kahl	inspire AG
Daniel Türk	ETH Zürich, pd|z
Kornelia Kunstmann	inspire AG, ipdz

Members of the Industrial Committee

Matthias Baldinger	Additively AG
Ralf Becker	Schunk GmbH & Co. KG
Steffen Beyer	Airbus Safran Launchers
Paul Fickel	Daimler AG
Klaus Müller-Lohmeier	Festo AG & Co. KG
Gonzalo Rey	Moog Inc.
Thomas Scheiwiller	Bühler AG
Kai Schimanski	Premium Aerotec GmbH

Members of the Scientific Committee

Guido Adam	Universität Paderborn, Direct Manufacturing Research Center (DMRC)
Stefano Brusoni	ETH Zürich, Technology and Innovation Management

Olaf Diegel	Lund University, Product Development
Jens Ekengren	Örebro University, Mechanical Engineering
Claus Emmelmann	TU Hamburg, iLAS; Laser Zentrum Nord
Paolo Fino	IIT Torino
Richard Hague	University of Nottingham, EPSRC Centre for Additive Manufacturing
Russel Harris	University of Leeds
Erik Hofmann	University St. Gallen, LOG - Research Institute for Logistics Management
Andreas Kirchheim	ZHAW, Zentrum für Produkt- und Prozessentwicklung (ZPP)
Dieter Krause	TU Hamburg, Produktentwicklung und Konstruktionstechnik
Gideon Levy	TTA Technology Turn Around
Mirko Meboldt	ETH Zürich, pd|z
Wilhelm Meiners	Fraunhofer ILT
Torbjorn Netland	ETH Zürich, Production and Operations Management
Alberto Ortona	SUPSI, Hybrid Materials Laboratory
Maren Petersen	Universität Bremen, Institute Technology and Education
Manfred Schmid	inspire AG, icams
Adriaan Spierings	inspire AG, icams
Klaus-Dieter Thoben	University Bremen, IKAP
Anna Valente	SUPSI, IRoS
Konrad Wegener	ETH Zürich, IWF
Gerd Witt	Universität Duisburg-Essen

Contents

Design Tools and Methods

Evolution of Design Guidelines for Additive Manufacturing - Highlighting Achievements and Open Issues by Revisiting an Early SLM Aircraft Bracket 3
Christoph Klahn, Daniel Omidvarkarjan, and Mirko Meboldt

A Design Method for SLM-Parts Using Internal Structures in an Extended Design Space 14
Rene Bastian Lippert and Roland Lachmayer

Exploring the Impact of Shape Complexity on Build Time for Material Extrusion and Material Jetting 24
Patrick Pradel, Richard Bibb, Zicheng Zhu, and James Moultrie

Novel Optimised Structural Aluminium Cross-Sections Towards 3D Printing 34
Konstantinos Daniel Tsavdaridis, Jack Antony Hughes, Lukas Grekavicius, and Evangelos Efthymiou

Manufacturing Process Chain

Finite Element Modeling of Ceramic Deposition by LBM(SLM) Additive Manufacturing 49
Qiang Chen, Gildas Guillemot, Charles-André Gandin, and Michel Bellet

Analysis of the Influence of Shielding and Carrier Gases on the DED Powder Deposition Efficiency for a New Deposition Nozzle Design Solution 59
Federico Mazzucato, Andrea Marchetti, and Anna Valente

On-Demand Spare Parts for the Marine Industry with Directed Energy Deposition: Propeller Use Case 70
Wei Ya and Kelvin Hamilton

Macroscopic Finite Element Thermal Modelling of Selective Laser Melting for IN718 Real Part Geometries 82
Yancheng Zhang, Gildas Guillemot, Charles-André Gandin, and Michel Bellet

Additive Manufacturing of Piezoelectric 3-3 Composite Structures 93
Miriam Bach, Tutu Sebastian, Mark Melnykowycz, Tony Lusiola, D. Scharf, and Frank Clemens

Additive Manufacturing of Semiconductor Silicon on Silicon Using Direct Laser Melting 104
Marie Le Dantec, Mustafa Abdulstaar, Matthias Leistner, Marc Leparoux, and Patrik Hoffmann

Additive Manufacturing of Complex Ceramic Architectures 117
Oscar Santoliquido, Giovanni Bianchi, and Alberto Ortona

Process Chain Integration

An Advanced STEP-NC Platform for Additive Manufacturing 127
Renan Bonnard

Additive Manufacturing on 3D Surfaces 137
Olivier Chandran, Sebastien Lani, Danick Briand, Barthelemy Dunan, and Guy Voirin

Integrated Platform for Multi-resolution Additive Manufacturing 145
Paul Delrot, Damien Loterie, Demetri Psaltis, and Christophe Moser

Enhanced Toolpath Generation for Direct Metal Deposition by Using Distinctive CAD Data 152
Daniel Eisenbarth, Florian Wirth, Kevin Spieldiener, and Konrad Wegener

Performance Simulation and Verification of Vat Photopolymerization Based, Additively Manufactured Injection Molding Inserts with Micro-Features 162
Michael Mischkot, Thomas Hofstätter, Ifigeneia Michailidou, Carlos Herrán Chavarri, Andreas Lunzer, Guido Tosello, David Bue Pedersen, and Hans Nørgaard Hansen

Additive Repair Design Approach: Case Study of Transverse Loading of Aluminum Beams 169
Zghair Yousif and Lachmayer Roland

Quality Assurance

Controlled Porosity Structures in Aluminum and Titanium Alloys by Selective Laser Melting 181
Flaviana Calignano, Giulio Cattano, Luca Iuliano, and Diego Manfredi

Development and Optimization of an Innovative Double Chamber Nozzle for Highly Efficient DMD 191
Andrea Marchetti, Federico Mazzucato, and Anna Valente

***In Situ* and Real-Time Monitoring of Powder-Bed AM by Combining Acoustic Emission and Artificial Intelligence** 200
K. Wasmer, C. Kenel, C. Leinenbach, and S.A. Shevchik

Quality Related Effects of the Preheating Temperature on Laser Melted High Carbon Content Steels 210
Livia Zumofen, Christian Beck, Andreas Kirchheim, and Hans-Jörg Dennig

Business Cases

Additive Manufacturing in Automotive Spare Parts Supply Chains – A Conceptual Scenario Analysis of Possible Effects 223
Timo Eggenberger, Katrin Oettmeier, and Erik Hofmann

Selection of High-Variety Components for Selective Laser Sintering: An Industrial Case Study 238
Filippo Fontana, Enrico Marinelli, and Mirko Meboldt

Process Setup for Manufacturing of a Pump Impeller by Selective Laser Melting 252
Marc Huber, Jonas Ess, Martin Hartmann, Andreas Würms, Robin Rettberg, Thomas Kränzler, and Kaspar Löffel

Hybrid Integration; Case Study with Sun Sensor for Cube Satellites 264
Nenad Marjanović, Jérémy Disser, Frédéric Zanella, Jürg Schleuniger, Alessandro Mustaccio, Rolando Ferrini, Marc Schnieper, and Eyad Assaf

Temperature Monitoring of an SLM Part with Embedded Sensor 273
Philipp Stoll, Bastian Leutenecker-Twelsiek, Adriaan Spierings, Christoph Klahn, and Konrad Wegener

Unique Customer Benefits

Integration of Fiber-Reinforced Polymers in a Life Cycle Assessment of Injection Molding Process Chains with Additive Manufacturing 287
Thomas Hofstätter, Niki Bey, Michael Mischkot, Philippe M. Stotz, David B. Pedersen, Guido Tosello, and Hans N. Hansen

Advantages in Additive Manufacturing for a Medium Format Metrology Camera 296
Ralph Rosenbauer, Filippo Fontana, Heidi Hastedt, Thomas Luhmann, David Ochsner, Dirk Rieke-Zapp, and Robin Rofallski

Patient Specific Implants from a 3D Printer – An Innovative Manufacturing Process for Custom PEEK Implants in Cranio-Maxillofacial Surgery 308
Florian M. Thieringer, Neha Sharma, Azagen Mootien, Ralf Schumacher, and Philipp Honigmann

Teaching and Training

Work-Process Orientated and Competence Based Professional Training for Skilled Workers in Laser Additive Manufacturing 319
Christian Daniel, Bianca Schmitt, and Maren Petersen

Why Education and Training in the Field of Additive Manufacturing is a Necessity 329
Andreas Kirchheim, Hans-Jörg Dennig, and Livia Zumofen

The Experience Transfer Model for New Technologies - Application on Design for Additive Manufacturing 337
Bastian Leutenecker-Twelsiek, Julian Ferchow, Christoph Klahn, and Mirko Meboldt

Decision-Making in Additive Manufacturing – Survey on AM Experience and Expertise of Designers 347
Johanna Spallek and Dieter Krause

Author Index 361

Design Tools and Methods

Evolution of Design Guidelines for Additive Manufacturing - Highlighting Achievements and Open Issues by Revisiting an Early SLM Aircraft Bracket

Christoph Klahn[1(✉)], Daniel Omidvarkarjan[2], and Mirko Meboldt[2]

[1] Inspire AG, Zürich, Switzerland
`klahn@inspire.ethz.ch`
[2] ETH Zurich, Product Development Group Zurich pd|z, Zürich, Switzerland
`http://www.pdz.ethz.ch/`

Abstract. Design knowledge is important for the success of new technologies. This is especially true for Additive Manufacturing technologies like Selective Laser Melting (SLM), which offer a higher degree of freedom, but also very different restriction in design compared to conventional manufacturing technologies. An analysis of current and previous designs from aerospace and motorsports identifies important drivers in Design for Additive Manufacturing. To visualize the advances in design knowledge an SLM aircraft bracket is re-designed based on today's state of the art almost 10 years after its initial design for additive manufacturing. The analysis reveals important factors for a "good" design. In early designs the focus of engineers was on the manufacturability of the part itself, while the capabilities of CAD tools limited the designer. Nowadays designs show a more holistic view on the manufacturing process chain and the part's application, e.g. by integrating provisions for conventional post-processing and fatigue optimized shapes and surfaces. Some issues are still open and need to be addressed in the next generation of guidelines, tools and equipment.

Keywords: Additive Manufacturing · Selective Laser Melting · Design guideline · Aircraft bracket

1 Introduction

The Additive Manufacturing (AM) process of Selective Laser Melting (SLM) is suited to produce metal parts for industrial and end-user applications in a layer-by-layer process based on a 3D-CAD-model by melting sections of a powder-bed with a laser. The process was developed by Meiners in 1999 [1]. In the following years the industrial maturity of process and machinery increased. Today different sizes of machines are commercially available for industrial direct part production. The range of powder materials took a similar development. Nowadays different

© Springer International Publishing AG 2018
M. Meboldt and C. Klahn (eds.), *Industrializing Additive Manufacturing - Proceedings of Additive Manufacturing in Products and Applications - AMPA2017*,
DOI 10.1007/978-3-319-66866-6_1

steels, aluminum-, titanium- and nickel-based alloys are commercially available and new metal groups and alloys are in the development e.g. Inconel IN738LC [2] and the scandium modified aluminum Scalmalloy [3].

The main driver in these developments are the applications and demands of industrial sectors. The adoption of Additive Manufacturing to a new sector generates research questions that need to be answered before AM-parts can enter the market. One sector with an early interest in Selective Laser Melting was the aerospace industry.

The aerospace industry is interested in Additive Manufacturing, and in particular in Selective Laser Melting, because of AM's main differences compared to conventional manufacturing: Manufacturing costs are primarily determined by part volume. The lot size and the geometrical complexity of a part have little to no influence on manufacturing time and costs. This helps aircraft manufacturers and operators in addressing two challenges:

- Aircrafts are not build in large quantities. The best-selling civilian models of the two largest large aircraft manufacturers count in total 9486 delivered Boeing 737 since 1967 [4] followed by 7564 delivered Airbus single aisle aircrafts since 1987 [5]. Production numbers for individual parts can be even lower due to customer specific variants in cabin layout, engines etc.
- Operating costs and payload put a constant pressure on aircraft manufacturers and operators to save weight. Greene stated that a 1% reduction of the gross weight of an aircraft reduces the fuel consumption by 0.25–0.75% [6,7]. This is a significant saving, because the fuel costs dominate operating costs [8].

The use of Additive Manufacturing allows designing and producing highly optimized aircraft parts at low lot sizes.

In 2008 a master thesis at Airbus evaluated different brackets of cabin monuments and re-designed one of them. The objectives were to show the weight saving potential of Selective Laser Melting and to serve as a technology demonstrator highlighting the design potentials of this young production technology [9]. The milled bracket of the Airbus A380 Upper Deck Cabin Crew Rest Compartment (UD-CCRC) depicted in Fig. 1(a) was selected. Figures 1(b) and (c) show the result of the re-design.

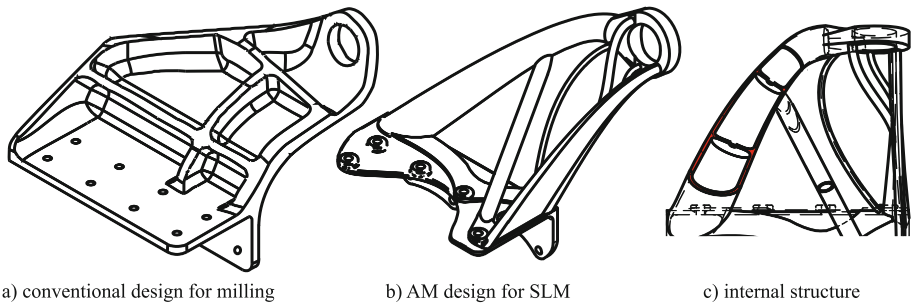
a) conventional design for milling b) AM design for SLM c) internal structure

Fig. 1. Bracket designs (a) for Aluminum milling and (b) initial design for Selective Laser Melting of TiAl6V4 with (c) internal bamboo structure [9]

The bracket in Fig. 1(b) and (c) reflects the design knowledge on Selective Laser Melting in 2008. We revisited this bracket to analyze the advances in design knowledge during the past decade and show the impact by applying the current state of art on the same design task.

2 Review of Existing Design Guidelines

Knowledge on designing for Selective Laser Melting was scarce in the year 2008. Selective Laser Melting was described as a near-net-shape process capable of producing almost any part. Available literature on design for AM focused on quantifying design limitations e.g. feasible hole diameters, wall thicknesses etc. [10–13]. Only few works provided guidance in the conceptual design phase [14, 15]. The design knowledge can be summarized by the following points [10–15]:

- Surface quality is best on vertical walls and decreases on sloped surfaces due to the staircase effect. Upskin surfaces, pointing in build directions are better than downskin surfaces facing the build platform.
- Support for overhanging structures is needed on downskin surfaces exceeding a certain angle. Support structure removal is tedious; therefore supports should be avoided by design and part orientation.
- Vertical holes and bores do not require support, if the top curvature is below a certain diameter.
- Internal cavities require an opening for powder removal.
- Thin-walled structures require a minimum thickness and should not be oriented parallel to the coater direction to avoid deformation and bending.
- Mechanical properties show an anisotropy in strength with lower values in build direction.

In the years following the design of the aircraft bracket design rules increased steadily in number and level of detail. Most publications focused on providing values for the limitations of manufacturing for design elements in specific materials and applications [16–20]. This type of design rules supports engineers primarily in the detailed design phase and ensure that the part is feasible to be manufactured. These works reflect the increasing understanding of the consolidation process and the effects of material, powder and process parameters on mechanical properties, thermal stress, and other quality characteristics.

In contrast to these specific design rules, methods and principles addressing the challenges of concept development are still rare [21]. They often focus on presenting design solutions within an application, e.g. conformal cooling for injection molding tools [22,23]. In the development of lightweight designs for aerospace applications, the advantages of Selective Laser Melting are the ability to design parts very close to the results of a topology optimization and incorporate bionic principles to reduce stress peaks [24,25].

3 Design Task and Requirements

In 2008's design task the aircraft bracket depicted in Fig. 1(a) was selected for a re-design to demonstrate the design potentials of Additive Manufacturing. The bracket is a component of the Upper-Deck Cabin Crew Rest Compartment of an Airbus A380. It is screwed onto the upper edge of this large cabin monument and a tie-rod is bolted to the swivel-eye, connecting the monument to the aircraft's fuselage. The dimensioning load case is a static force of approx. 11 kN pulling on the swivel-eye under emergency landing conditions. The type and position of the interfaces should remain the same although interfaces no longer necessary can be omitted. The wall and ceiling panels of the cabin limit the available space. It was decided to change the material from Aluminum to Titanium TiAl6V4, because of its higher strength. This allowed a further reduction in part volume, which was already known to be a major cost driver [26].

A topology optimization was performed in ANSYS 11 based on the dominant load case, constraints and the available space. The program used the SIMP-algorithm to calculate the density distribution depicted in Fig. 2.

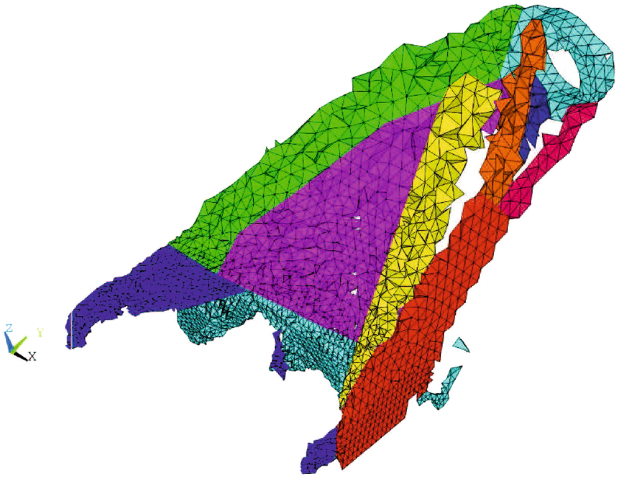

Fig. 2. Result of the topology optimization [9]

The result of the topology optimization was the basis of the initial SLM-design in 2008 and will be used in the revisited design. To perform a new topology optimization with a modern program would make it difficult to separate the effects of optimization capabilities and design knowledge. At the same time it is not expected to receive fundamentally different optimization results, because today's topology optimizers still use the SIMP-algorithm [27,28].

4 Initial SLM-Design of the Year 2008

The initial SLM-Design of the bracket and its internal structure is depicted in Fig. 1(b) and (c). The most prominent design feature is a hollow arm holding the swivel-eye. Two design elements increase the bending stiffness of the arm: an internal bamboo-like structure and a shear area connecting the arm to the corner of the attachment surfaces.

The two perpendicular plates forming the attachment to the monument were reduced in volume to save weight by cutting away low-stressed sections and reducing the thickness of both plates. In the assembly only the bracket was up to change, the other components in the bill of materials of the Crew Rest Compartment were required to be kept the same. Therefore the thickness of the plates at the positions of the screws was maintained at the original value. In topology optimizations the material is concentrated to form the optimum load path. A side effect of this concentration can be seen at the screws' positions. The load on the swivel-eye was directed to a few screws, which were highly stressed while others were almost load free. To remain within the design allowable of each threaded insert of the monument the plates had to be stiffened to transfer some of the load from overstressed screws to adjacent screws. Attachment points with a low load were omitted to save weight and assembly time.

In FEM-Simulations the bracket showed a smaller displacement and lower maximum stress compared to the conventional UD-CCRC-bracket. The weight of the bracket was reduced by 50%, despite the change to a material with a higher density. Table 1 summarizes the key properties of the designs.

The design process of the SLM-bracket consisted of identifying a suitable component for an AM re-design, developing a principal solution to fulfill the functional requirements (in this case by topology optimization) and creating a detailed design, which meets all requirements and can be manufactured. This approach proved to be successful in designing Additive Manufactured functional parts and is still in use today [28].

Table 1. Comparison of conventional bracket design, initial SLM bracket design and SLM re-design

	Conventional design [9]	Initial SLM design (2008) [9]	SLM re-design (2017)
Material	Aluminum alloy	TiAl6V4	TiAl6V4
Volume	421.6 cm^3	146.8 cm^3	140.2 cm^3
Mass	1.32 kg	0.65 kg	0.62 kg
Displacement of swivel eye	1.2 mm	1.0 mm	2.0 mm
Max. v. Mieses Stress	295 MPa	582 MPa	428 MPa
Safety factor (v. Mieses)	1.28	1.50	1.64

It is therefore worth mentioning a few lessons learned from 2008's initial design of the SLM-bracket. Most issues during the design process originated from software programs and interfaces. The result of the SIMP topology optimization is a density distribution in a mesh of finite elements resembling the design space. Exporting the cloud of high-density elements from the FEM-software into a file than can be used in the CAD-program was impossible. The CAD design process started from scratch based on a video of the rotating element cloud and an analysis of the load type of different sections. This interpretation proved to be helpful and led to the patented idea of the bamboo structure [29]. One has to be aware of the limitations of optimization algorithms. Human engineering judgment is needed to adapt the numeric optimum to the context of the application. During detailed design the CAD-software was often brought to its limits by intersecting freeform surfaces. The use of complex shapes caused difficulties and a keen eye will find a few areas on the SLM bracket, which are not well designed in terms of local stress peaks. Figure 3 shows examples of big notches which could not be avoided due to the inability of the CAD to create fillets at the intersection of curved surfaces.

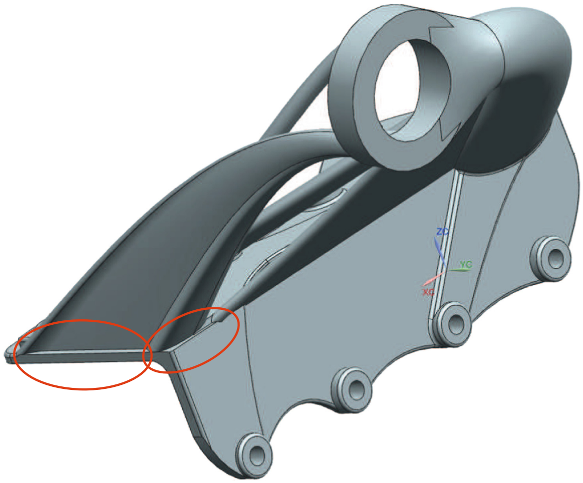

Fig. 3. Notch in the CAD model of the initial SLM-design due to limited capabilities of CAD program

Today's CAD-programs offer tools for a modeling 3D freeform surfaces and improved interfaces and workflows between different modeling environments. This largely improves the design capabilities although it is still possible to run into numeric problems when using freeform curves, surfaces and solids to model a complex part. Voxel-based solutions don't have these restrictions because they describe a geometry by placing material in a three-dimensional grid. This comes at the price of large amounts of data and a loss of parametric design. The CAD-software Siemens NX 10 was used for the re-design.

5 Re-designed Bracket of the Year 2017

The initial SLM-bracket was developed at a time where little design knowledge was published. To illustrate the impact of today's design and process expertise on a design for SLM the design task in Sect. 3 was repeated using the current state-of-the-art. The resulting design is depicted in Fig. 4.

Advancements in design process, tools, and the awareness of the whole production process chain led to significant differences between the bracket shown in Fig. 4 and the initial design in Fig. 3.

The design process followed the approaches of an early part orientation based on an ideal design [30] and subsequent detailed design for additive manufacturing [17,19,20] in a function driven design strategy [31].

The intermediate result of the first design stage was similar, because of the same starting point and similar manufacturing process capabilities. The outcome of the topology optimization was used to determine the orientation at the beginning of the design process instead of designing a part and later on testing different orientation. In this phase the effect of today's design knowledge was a higher efficiency of the process with less iterations in late design stages. For the detailed design a framework of curved beams was chosen over other concepts like hollow structures, straight beams, or shear areas. These concepts were derived from an analysis of various SLM-Designs found in literature [21,32]. This decision was based on two factors: curved beams are expected to show less distortion due to thermally induced stress and surfaces need to be accessible for post-processing. This post-processing is necessary because rough surfaces reduce the fatigue performance [33–36]. A bamboo structure like the one of the initial SLM-design is favorable in terms of static stress and stiffness, but is not recommended for dynamic loads today. Therefore the part depicted in Fig. 4 was designed without internal structures or sharp, concave corners. This allows an

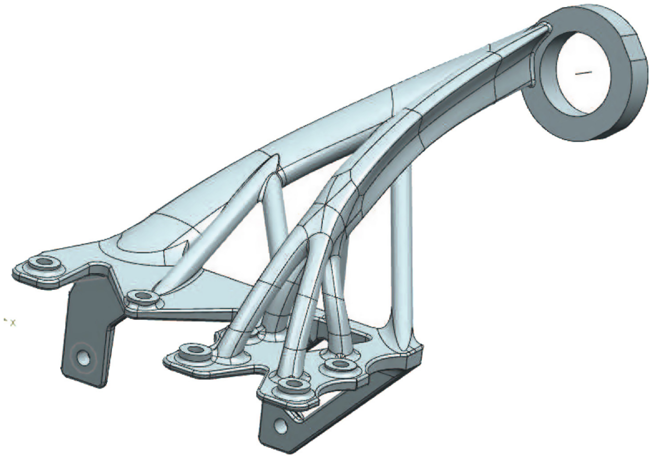

Fig. 4. New bracket design for Selective Laser Melting

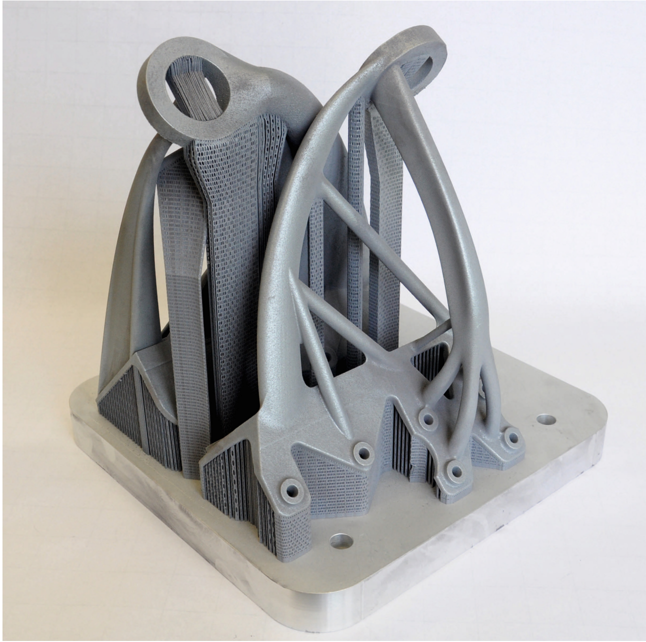

Fig. 5. Initial SLM bracket and re-designed bracket build on a Concept Laser M2 Dual Laser Machine

efficient surface treatment by sandblasting and vibration grinding. Further provisions for machining were made by adding parallel surfaces for clamping and planes for referencing. The design process was more efficient than in the first SLM- design, although the used CAD-program didn't offer a dedicated "Design for Additive Manufacturing"-module. The software provided modules to create freeform elements and interfaces to FEM-simulations. A CAD-tool to check the draft angles of casting parts was re-purposed to analyze the need for support on overhanging surfaces. Table 1 summarizes the key properties of each design iteration.

To validate the assumptions of a reduced SLM manufacturing time and less manual labor for post-processing both CAD-models were prepared in Materialize Magics to be manufactured from TiAl6V4. The total manufacturing time for one bracket was estimated to be 89 h for the initial SLM design and 66 h for the re-design. The reduction of total build time by 25% is due to the large reduction of support needed on overhanging surfaces. The main cost drivers of part volume and build-job height are similar for both brackets and don't have much influence on the difference in build time.

The ratio between initial design and re-design was confirmed by the build-job depicted in Fig. 5. For financial reasons AlSi10Mg and a layer thickness of 50 μm were chosen to produce both parts on a Concept Laser M2 Dual Laser Machine. One Laser was assigned to each part to document the exposure time separately.

One Laser exposed the sections of the initial design in total for 24 h 52 min, while the sections of the re-design were exposed by the other Laser for 16 h 45 min. The time to add a new layer of powder was shared by both brackets. The re-design based on today's design guidelines reduced the build time of a single bracket by 21%, compared to the build time of the initial design. The re-designed bracket needed less support structures, which reduced the required manual labor to separate the parts from the build plate and remove the supports from the brackets.

6 Conclusion

Revisiting a design from the early days of Selective Laser Melting in the aircraft industry increased the awareness of the different influences in designing for this technology. The general restrictions of the SLM process were already discussed at time of the initial design. Since then the process related design knowledge progressed in understanding the reasons behind the restrictions and quantifying design reference values for different materials. What really made a difference are the methods to organize the workflow and to overcome restrictions, e.g. the early determination of part orientation based on an ideal design, together with design principles for easier post-processing.

Engineers find a growing number of inspiring designs to support the creative aspect of a design process. Collecting these design solutions and transferring the hidden expertise into another application takes a lot of time and expertise and is not feasible parallel to the everyday work of an engineer in industry. Compiling, structuring and condensing real-life design solutions is therefore an ongoing task for design research.

References

1. Meiners, W.: Direktes Selektives Laser Sintern einkomponentiger metallischer Werkstoffe. Berichte aus der Lasertechnik. Shaker, Aachen (1999)
2. Cloots, M., Uggowitzer, P.J., Wegener, K.: Investigations on the microstructure and crack formation of IN738LC samples processed by selective laser melting using Gaussian and doughnut profiles. Mater. Des. **89**, 770–784 (2016)
3. Spierings, A.B., Dawson, K., Voegtlin, M., Palm, F., Uggowitzer, P.J.: Microstructure and mechanical properties of as-processed scandium-modified aluminium using selective laser melting. CIRP Ann. - Manufact. Technol. **65**(1), 213–216 (2016)
4. Boeing Company: Orders & deliveries (2017). http://www.boeing.com/commercial/#/orders-deliveries
5. Airbus SAS: The market/orders and deliveries (2017). http://www.airbus.com/company/market/orders-deliveries/
6. Lee, J.J., Lukachko, S.P., Waitz, I.A., Schafer, A.: Historical and future trends in aircraft performance, cost and emissions. Annu. Rev. Energy Env. **26**, 167–200 (2001)
7. Greene, D.L.: Commercial air transport energy use and emissions: is technology enough? In: Conference on Sustainable Transportation-Energy Strategies (1995)

8. Johnson, V.S.: Minimizing life cycle cost for subsonic commercial aircraft. J. Aircr. **27**(2), 139–145 (1990)
9. Klahn, C.: Topologische Optimierung der Gestaltung von lasergenerierten Funktionsbauteilen der Luftfahrttechnik. Diplomarbeit. Institute of Laser and System Technologies (iLAS), TU Hamburg-Harburg, Hamburg (2008)
10. Onuh, S.O., Yusuf, Y.Y.: Rapid prototyping technology: applications and benefits for rapid product development. J. Intell. Manuf. **10**, 301–311 (1999)
11. Trenke, D.: Konstruktionsregeln für eine Rapid Tooling gerechte Gestaltung von Werkzeugen und Prototypen. IMW - Institutsmitteilung **25**, 85–90 (2000)
12. Rehme, O., Emmelmann, C.: Reproducability for properties of selective laser melting products. In: Beyer, E., Dausinger, F., Ostendorf A., Otto, A. (eds.) Proceedings of the Third International WLT-Conference on Lasers in Manufacturing 2005. AT-Fachverlag, München (2005)
13. Aumund-Kopp, C., Petzoldt, F.: Laser sintering of parts with complex internal structures. In: Lawcock, R., Lawley, A., McGeehan, P.J. (eds.) Advances in Powder Metallurgy & Particulate Materials - 2008, pp. 85–97. Metal Powder Industries Federation, Princeton (2008)
14. Burton, M.J.: Design for rapid manufacture: developing an appropriate knowledge transfer tool for industrial designers. Ph.D. thesis, Loughborough University, Loughborough (2005)
15. Hopkinson, N., Hague, R.J., Dickens, P.M. (eds.): Rapid Manufacturing: An Industrial Revolution for the Digital Age. Wiley, Chichester (2006)
16. Thomas, D.: The development of design rules for selective laser melting. Ph.D. thesis, University of Wales Institute, Cardiff (2009)
17. Adam, G.A.O., Zimmer, D.: Design for additive manufacturing - element transitions and aggregated structures. CIRP J. Manufact. Sci. Technol. **7**, 20–28 (2014)
18. Adam, G.A.O.: Systematische Erarbeitung von Konstruktionsregeln für die additiven Fertigungsverfahren Lasersintern, Laserschmelzen und Fused Deposition Modeling, Forschungsberichte des Direct Manufacturing Research Centers, vol. 1. Shaker, Aachen (2015)
19. Kranz, J., Herzog, D., Emmelmann, C.: Design guidelines for laser additive manufacturing of lightweight structures in TiAl6V4. J. Laser Appl. **27**, S14001 (2015)
20. Verein Deutscher Ingenieure - VDI: Additive Fertigungsverfahren - Konstruktionsempfehlungen für die Bauteilfertigung mit Laser-Sintern und Laser-Strahlschmelzen (2015)
21. Wohlers, T.T., Caffrey, T.: Wohlers Report 2015: 3D Printing and Additive Manufacturing State of the Industry Annual Worldwide Progress Report. Wohlers Associates, Fort Collins (2015)
22. Vogel, H., Tangwiriyasakul, C., Emmelmann, C.: Analysis of cooling channel design for injection molds manufactured by laser freeform fabrication. In: Vollertsen, F. (ed.) Proceedings of the Fourth International WLT-Conference on Lasers in Manufacturing 2007. AT-Fachverlag, München (2007)
23. Meckley, J., Edwards, R.: A study on the design and effectiveness of conformal cooling channels in rapid tooling inserts. Technol. Interface J. **10**(1), 1–28 (2009)
24. Emmelmann, C., Petersen, M., Kranz, J., Wycisk, E.: Bionic lightweight design by laser additive manufacturing for aircraft industry. In: Ambs, P., Curticapean, D., Emmelmann, C., Knapp, W., Kuznicki, Z.T., Meyrueis, P.P. (eds.) SPIE Eco-Photonics 2011 Sustainable Design, Manufacturing, and Engineering Workforce Education for a Green Future, vol. 8065. Society of Photo-Optical Instrumentation Engineers (SPIE), Strassburg (2011)

25. Emmelmann, C., Sander, P., Kranz, J., Wycisk, E.: Laser additive manufacturing and bionics: redefining lightweight design. Phys. Procedia **12**, 364–368 (2011)
26. Kruth, J.P., Vandenbroucke, B., Vaerenbergh, J.V., Mercelis, P.: Benchmarking of different SLS/SLM processes as rapid manufacturing techniques. In: International Conference on Polymers and Moulds Innovations (PMI). University of Texas, Gent (2005)
27. Bendsøe, M.P.: Optimal shape design as a material distribution problem: structural optimization, computer-aided optimal design of stressed systems and components. Struct. Optim. **1**(4), 193–202 (1989)
28. Kantareddy, S.N.R., Ferguson, I., Frecker, M., Simpson, T.W., Dickman, C.J.: Topology optimization software for additive manufacturing: a review of current capabilities and a real-world example. In: ASME 2016 International Design Engineering Technical Conferences and Computers and Information in Engineering Conference, p. V02AT03A029. Charlotte, NC (2016)
29. Klahn, C., Gysemberg, R., Rehme, O.: Stütze für ein im Selective Laser Melting-Verfahren herstellbares Flugzeugstrukturbauteil. German Patent DE 10 2008 044 759 B4 (2010)
30. Leutenecker-Twelsiek, B., Klahn, C., Meboldt, M.: Considering part orientation in design for additive manufacturing. Procedia CIRP **50**, 408–413 (2016)
31. Klahn, C., Leutenecker, B., Meboldt, M.: Design strategies for the process of additive manufacturing. Procedia CIRP **36**, 230–235 (2015)
32. Carter, W.T., Erno, D.J., Abbott, D.H., Bruck, C.E., Wilson, G.H., Wolfe, J.B., Finkhousen, D.M., Tepper, A., Stevens, R.G.: The GE aircraft engine bracket challenge: an experiment in crowdsourcing for mechanical design concepts. In: 25th Solid Freeform Fabrication Symposium (SFF 2014), pp. 1402–1411. University of Texas, Austin, TX (2014)
33. Leuders, S., Thöne, M., Riemer, A., Niendorf, T., Tröster, T., Richard, H.A., Maier, H.J.: On the mechanical behaviour of titanium alloy TiAl6V4 manufactured by selective laser melting: fatigue resistance and crack growth performance. Int. J. Fatigue **48**, 300–307 (2013)
34. Edwards, P., Ramulu, M.: Fatigue performance evaluation of selective laser melted Ti-6Al-4V. Mater. Sci. Eng., A **598**, 327–337 (2014)
35. Spierings, A.B., Starr, T.L., Wegener, K.: Fatigue performance of additive manufactured metallic parts. Rapid Prototyp. J. **19**(2), 88–94 (2013)
36. Brandl, E., Heckenberger, U., Holzinger, V., Buchbinder, D.: Additive manufactured AlSi10Mg samples using selective laser melting (SLM): microstructure, high cycle fatigue, and fracture behavior. Mater. Des. **34**, 159–169 (2012)

A Design Method for SLM-Parts Using Internal Structures in an Extended Design Space

Rene Bastian Lippert(✉) and Roland Lachmayer

Institute of Product Development,
Leibniz Universität Hannover, Hannover, Germany
`lippert@ipeg.uni-hannover.de`

Abstract. Selective laser melting enables the production of cavities as well as internal structures and thus opens up new lightweight potentials for mechanically loaded components. This paper describes a design method for weight-optimization by applying internal structures in an extended design space compared to conventional models. Based on a pedal crank as a demonstrator, the objective is a maximum weight reduction with predefined stresses and a homogeneous stress distribution. The basic dimensioning of the design space is limited by assembly and application restrictions. By using computer aided design tools and topology optimization in an iterative procedure, a step wise confinement of the design space takes place. Concerning the same interfaces and functions as the conventional pedal crank, new model generations with the advantage of force flow adapted structures are built up. Using Finite Element Method, a continuous evaluation of the impact from a change of design towards the weight/stress ratio is performed. The created models are evaluated regarding their weight reduction in order to select the most efficient one. The final model has a large-volume geometry with the simultaneous integration of internal structures and cavities. A validation compared to the initial model as well as to a model with conventional design space and selective areas with internal structures quantifies the optimization result. Based on the acquired knowledge from this comparison, an estimation of the weight reduction potential concerning the design method is given.

1 Introduction

Additive Manufacturing is used for the production of prototypes and tools. Also direct manufacturing, and thus the additive fabrication of end products to use or assemble directly, becomes increasingly more important [1, 2]. Due to the mechanical properties of the final components, especially selective laser melting serves as a continuous substitute as well as a supplement to conventional manufacturing processes [3, 4].

A major benefit in designing structural components using selective laser melting is the potential of light weight constructions [5, 6]. Here, the layer-wise and selective solidification permits new lightweight designs, such as manufacturing freeform geometries, undercuts or cavities [7–9]. To enlarge the weight-saving potential, internal structures can be implemented. These are defined as "repeatable elements for the substitution of solid volumes with the objective to vary the material arrangement on a

© Springer International Publishing AG 2018
M. Meboldt and C. Klahn (eds.), *Industrializing Additive Manufacturing - Proceedings of Additive Manufacturing in Products and Applications - AMPA2017*,
DOI 10.1007/978-3-319-66866-6_2

macroscopic level without affecting the material properties" [10]. The challenge is the integration of load optimized internal structures in order to reduce the component weight without a significant increase of stresses, so that the life expectancy is not influenced [11, 12]. Here, computer-aided tools can be used to predict the component failure and to provide a force flow adapted orientation of internal structures [13, 14]. Previous studies have shown that the weight of a component can be reduced by around 30% using internal structures in conventional shapes [15, 16]. Based on these investigations, the present paper describes an analysis to increase weight saving by moving away from the conventional shapes and utilizing an extended design space.

2 Design Method

A computer-aided design method to implement internal structures in mechanically loaded components is described. It is distinguished into five sequentially arranged sections, which are characterized by an iterative procedure, shown in Fig. 1.

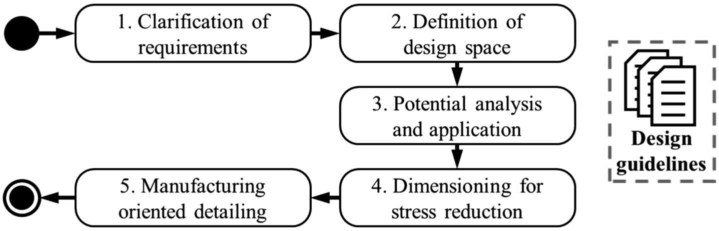
1. Clarification of requirements
2. Definition of design space
3. Potential analysis and application
4. Dimensioning for stress reduction
5. Manufacturing oriented detailing
Design guidelines

Fig. 1. Integrated design method using computer-aided modeling and simulation tools

To clarify the requirements (1), information about force application points, amount of load vectors as well as the stress state of the component has to be figured out. This information can be calculated or recirculated from life cycle data. Furthermore, a design space (2) has to be defined, which is limited by effective areas as well as assembly and application restrictions. Based on information about the mechanical behavior of internal structures and requirements of the component, suitable structures have to be selected and transferred into the design space (3) selectively. The structures and transition areas are optimized regarding stress reduction and a homogeneous stress distribution (4). The new model generation is finally validated regarding manufacturability (5) by considering design guidelines for detailing.

2.1 Design Guidelines for Internal Structures

To fulfill requirements of the manufacturing process in the early development stages, design guidelines have to be considered [17, 18]. In form of knowledge storages, such as checklists or design catalogues, these guideline provides standard values to ensure manufacturability [19]. For example, boundary conditions for minimal wall thickness or diameter, depending on the building direction of a component, are defined [20, 21].

Design guidelines are partially available for different parameter sets, which describe a specific machine and material. Furthermore, general statements are available, which define optimal orientation, arrangement or positioning of components in the process chamber or the necessity for cleaning openings [18]. As shown in Fig. 2, using the example of a honeycomb, minimum wall thicknesses, realizable overhangs and 45° angles to avoid support structures have to be considered. Furthermore, the element size b is limited by a minimal diameter.

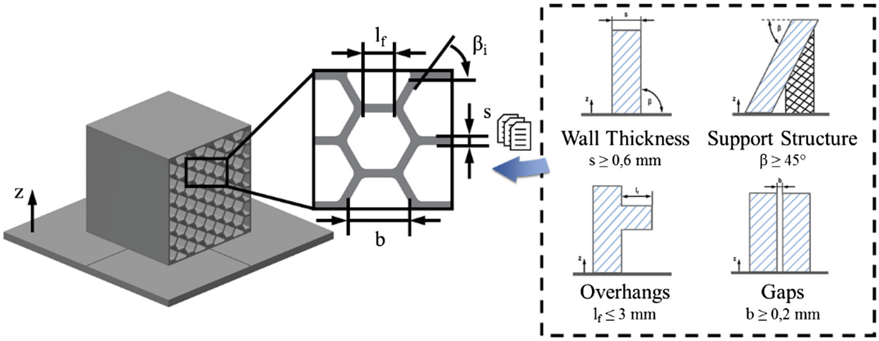

Fig. 2. Relevant design guidelines concerning the example of honeycomb structures

2.2 Simulation Environment

A material database to specify the anisotropic behavior of a selective laser melting component is defined. Using this database during computer-aided modeling and simulation, the consideration of building directions is possible. Analogous to conventionally processed materials, powder alloys for selective laser melting differ in mechanical properties depending on the post-process. Thus, the properties after the building process and a post-heat treatment are different. In practice, selective laser melting components are predominantly used after heat treatment, because internal stresses are reduced and the material properties are homogenized. Based on the example of AlSi10Mg alloy - which is used in this paper for validation - material characteristics after heat treatment (300 °C for 2 h) are shown in Fig. 3 [22, 23]. Besides the static properties, the stress-cycle (S-N) curve for calculating the fatigue properties is set [15].

	x-/y- direction	z-direction
E-Modul [kN/mm²]	70	60
Density [g/cm³]	2,67	2,67
Poisson's ratio	0,3	0,3
Tensile strength [kN/mm²]	345	350
Yield strength [kN/mm²]	245	245
Elongation at fracture [%]	12	11
Shear modulus [kN/mm²]	2,436 (yz/ xz)	2,6315 (xy)

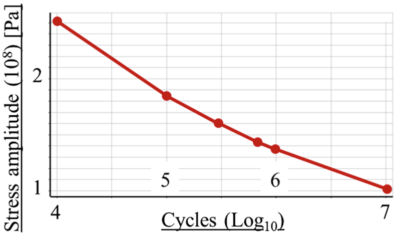

Fig. 3. Properties and S-N curve for AlSi10Mg after heat treatment [24–28]

3 Adaption of a Demonstrator

To validate the design method, a pedal crank is used as a demonstrator. The objective is a maximal weight reduction with constant internal (von Mises) stresses compared to conventional models (respectively material characteristics). Except considering relevant interfaces, the component dimensions are freely selectable.

3.1 Clarification of Requirements

The initial model is conventionally manufactured with AlSi10Mg alloy and has a weight of m = 217.45 g. Two interfaces for fixing the bottom bracket and the pedals define the length l = 170 mm, as depicted in Fig. 4-a. According to Sullivan und Chris, different load cases occur during the lifecycle. In assumption of an idealized model, in which torsional forces are neglected (due to the external force introduction), the critical load case is pure bending [16, 29]. In combination with the load vector F_{max} = 2.250 N, which represents the maximum occurring forces with an additional safety factor, the bending load is used for further optimization [29].

3.2 Definition of Design Space

As shown in Fig. 4-b, the design space is limited by assembly and application restrictions as well as the size of the process chamber (machine Eosint M280). This rough estimation is used as an input for topology optimization (using material characteristics shown in Fig. 3) in order to narrow down the design space. Figure 4-c shows the optimization results as an iterative elimination of the volume elements with the lowest stresses (Ansys Workbench 17.0). It can be seen that an asymmetric topology occurs. For the following potential analysis and selection of an internal structure, the optimization result is rebuilt as shown in Fig. 4-d.

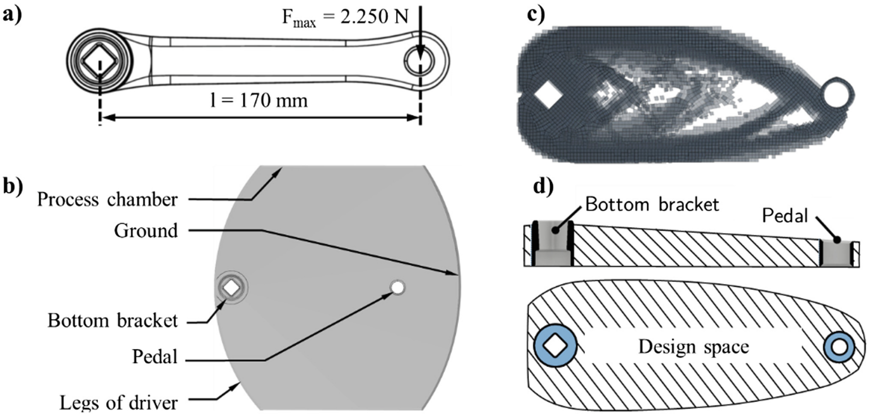

Fig. 4. Definition of design space (a) Relevant load case of the initial model (b) Assembly and application restrictions (c) Result of topology optimization (d) Extended design space

In order to identify a suitable internal structure to be integrated in the design space, the asymmetrical shape is neglected in the first iteration. The results are considered again while dimensioning for stress reduction. Hence, the topology is iteratively adapted to the asymmetric shape.

3.3 Potential Analysis and Application

Preliminary investigations at the institute describe the modeling and simulation of digital specimens with internal structures [9]. In addition to the application of computer-aided tools, the results are validated by analyzing physical specimens with a static test bench. The acquired knowledge is summarized in a design catalog, which allows the selection of a load optimized structure, when the load case is predefined. The essential criterion to select a suitable structure is low weight with high stiffness. Based on the findings summarized in the design catalog, suitable structures for bending loads are selected. Using CAD, these structures are modeled within the design space (e.g. see Fig. 5 - right) as separate concept models and are simulated by applying a structural mechanical analysis. The results are shown in Fig. 5 as a relation between (von Mises) stress and weight. Local stress peaks occurring on non-optimized transition regions (structure is unfavorably cut) are neglected. Furthermore, the stress/weight ratio of the initial model, the allowable stress σ_{all} of AlSi10Mg as well as an objective area are depicted.

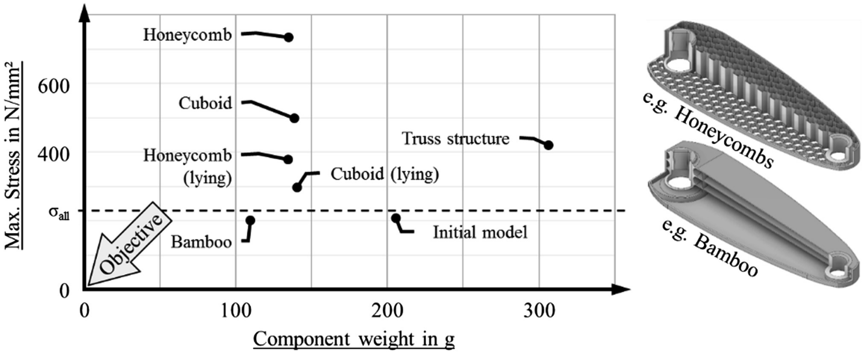

Fig. 5. Stress/weight ratio for concept models with different internal structures in the extended design space

Due to the high material effort, the concept model ‘truss structure’ (1) shows a higher component weight compared to the initial model. ‘Honeycombs’ and ‘cuboids’ show improved weight savings. However, the stresses partly increase significantly ($\sigma_{max} >> \sigma_{allowable}$).

The concept model ‘bamboo’ already shows a synthesis between maximum stresses and component weight and thus is selected for the further optimization.

3.4 Dimensioning for Stress Reduction

To define a preliminary design, the topology of the concept model ‘bamboo’ undergoes a rough adaption to the asymmetrical shape originating from the topology optimization (see Fig. 6-a). It can be seen that high stresses occur in the area of the bearing ($\sigma \approx 280$ N/mm^2), which exceed the allowable value $\sigma_{\text{allowable}} \approx 245$ N/mm^2. Furthermore, low stresses occur along the neutral axis.

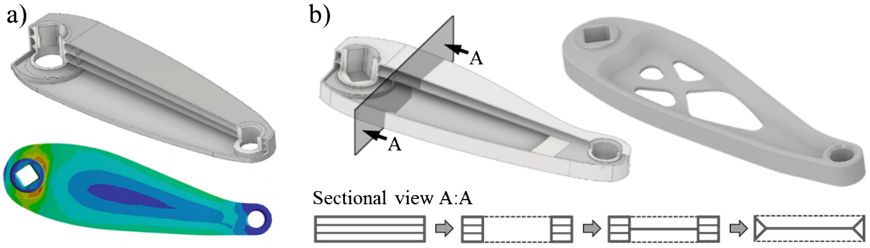

Fig. 6. Optimizing the topology for stress reduction (a) Adapting the outer shape (b) Adapting the cross-sectional area

In a first step, the areas with low stresses are optimized by removing material according to the optimization results (see Fig. 6-b). Starting from the concept model with a constant cross-sectional area (A:A), various preliminary designs are examined. As a result, a hollow profile with 45°-surfaces is provided in the outer areas. The less stressed area is substituted by a thin layer without cavities. Due to this modification, material can be saved and manufacturability can be improved by reducing overhangs.

After adapting both, the outer shape and the cross-section area, the stress distribution of the preliminary design can be improved, as depicted in Fig. 7-a. However, the maximum stress is still critical. Against this background, the areas near the bearing has to be optimized. After evaluating different strategies for the material distribution, an adapted “core” is built up, shown in Fig. 7-b. Holes are used for maximum weight reduction. The optimization of the preliminary design results in a homogeneous stress distribution with maximum stresses ($\sigma \approx 240$ N/mm^2) below the allowable values.

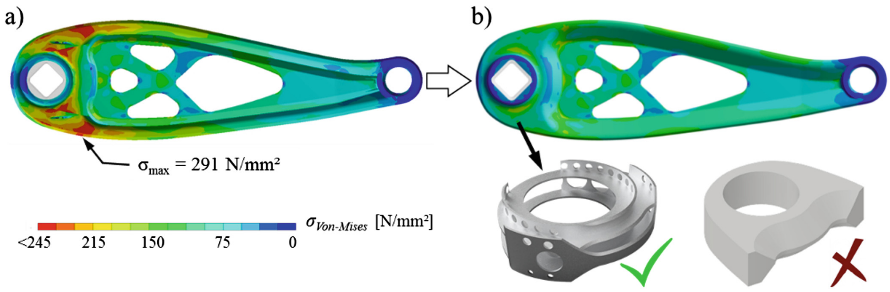
a)
b)
σ_{max} = 291 N/mm²
$\sigma_{Von\text{-}Mises}$ [N/mm²]
<245
215
150
75
0
✓
✗

Fig. 7. Stress distribution while dimensioning (a) Adapted cross-sectional area (b) Stress-optimized model

3.5 Manufacturing Oriented Detailing

The preliminary design is finally evaluated in comparison to the design guidelines. Therefore, the orientation and position of the model in the process chamber has to be defined. After weighing the criteria for production time, accuracy, loading capacity due to anisotropy, post-process effort and avoiding damage by the coater, the orientation and position is set as depicted in Fig. 8.

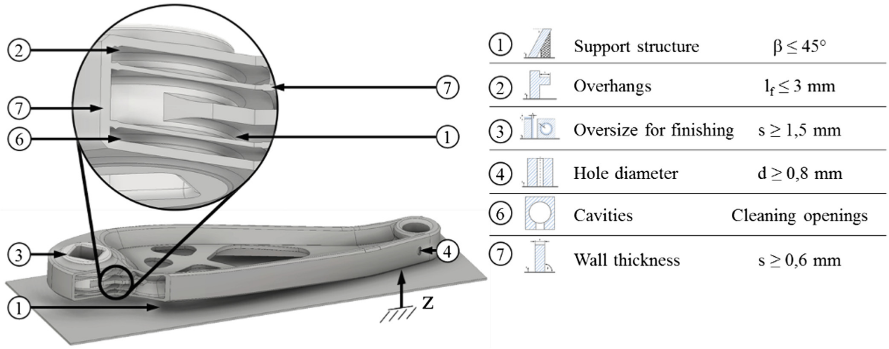
②
⑦
⑥
③
①
⑦
①
④
z
① Support structure β ≤ 45°
② Overhangs $l_f \leq 3$ mm
③ Oversize for finishing s ≥ 1,5 mm
④ Hole diameter d ≥ 0,8 mm
⑥ Cavities Cleaning openings
⑦ Wall thickness s ≥ 0,6 mm

Fig. 8. Relevant design guidelines for the optimized model of the pedal crank

Due to the horizontal positioning various areas result, which are limited by design guidelines. For example, down skin surfaces - normal vector is negative in respect to z direction - have to be investigated with regards to necessity of support structures. Supports are unavoidable between the component and building platform, but can be easily removed in post-process. In the components' interior, supports are forbidden, because removing them is impossible. Consequently, cavities as well as internal structures are limited by maximum overhangs and angles. Considering this restriction, all down-skin surfaces can be manufactured without lowering in negative z direction during manufacturing.

Besides specific values, general guidelines for removing excess material have to be considered. As depicted in Fig. 8, cleaning openings are provided on a slightly loaded area of the surface. The sizing of the openings is limited by the minimum diameter in z direction. Furthermore, the consideration of minimizing stress peaks and avoiding supporting structures is necessary during designing.

4 Conclusion

The optimized model is manufactured with AlSi10Mg using an Eosint M280 machine. As depicted in Fig. 9-a, the process parameters for core and skin exposure are set. Figure 9-b shows the result from manufacturing process after thermal (300 °C for 2 h) and mechanical post-processing (removing support structures and shot peening). The outer shape shows a high accuracy corresponding to the CAD model. To evaluate the accuracy of the internal structure, a mechanically sliced model is shown in addition. The estimation shows, that an accurate realization of the inner structures without deformation took place.

	Power in W	Speed in mm/s
Core	370	1.300
Up-/ Downskin	370	775
Postcontours	370	230

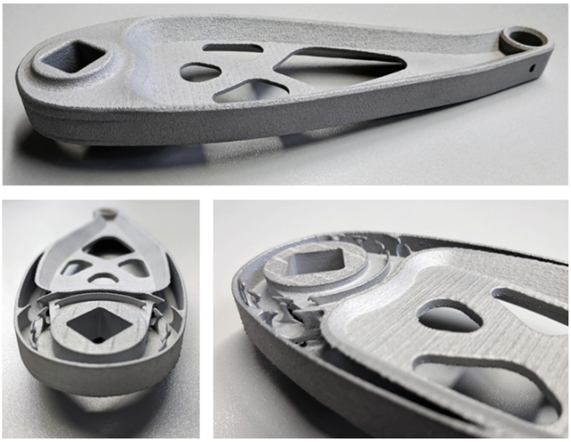

Fig. 9. Process parameters (Eos EoSint M280) and results from manufacturing process

Internal surfaces with a down-skin angle $\beta > 45°$ have a good surface quality. As expected, overhangs show an increased surface roughness. Compared to the weight of the initial model ($m \approx 217$ g), a weight saving of about 55% is achieved. Due to its complexity, the new optimized model ($m \approx 88$ g) cannot be manufactured using conventional technologies. In comparison to previous investigations, in which the shape of the initial model is maintained, further weight savings are achieved. The maximum (von Mises) stresses increased marginally, but are located below the allowable value $\sigma_{\text{allowable}}$.

A high optimization effort is necessary to achieve the obtained results. A rough transfer of a structure as a concept model can be performed in a first iteration without great effort. However, the stress- and manufacturing-oriented detailing of the preliminary design increase this effort significantly.

In addition to influences during modeling and simulation, internal structures have an effect on the in- and post-process. On one hand, the manufacturing time is affected. On the other hand, the post-process is challenging. This concerns the quality control of internal surfaces for comparison with the CAD geometry. Furthermore, internal structures hinder conventional mechanical finishing, which is necessary to improve mechanical behavior.

In the next step, the fatigue performance has to be simulated in order to calculate life expectancy. In addition, physical models have to be analyzed by performing static and fatigue tests. The acquired results are compared with the digital models. The objective is to describe design guidelines for covering surface roughness and mechanical properties in form of safety values during the design phase.

The challenge to implement the integrated design method is reproducibility and automation. Stress- and manufacturing-oriented detailing is strongly component specific and can only be generalized with difficulty. First approaches describe the parameterized density variation based on the amount of internal stresses.

References

1. Gibson, I., Rosen, D., Stucker, B.: Additive Manufacturing Technologies: 3D Printing, Rapid Prototyping, and Direct Digital Manufacturing. Springer (2015). ISBN 978-1-4939-2112-6
2. Gartner Marktforschungsunternehmen: Hype cycle for emerging technologies maps the journey to digital business (2014). www.gartner.com. Accessed 17 June 2016
3. Gebhardt, A.: Generative Fertigungsverfahren: Additive Manufacturing und 3D Drucken für Prototyping – Tooling – Produktion, 4th edn. Hanser (2013)
4. Poprawe, R., et al.: Production systems: recent developments in process development, machine concepts and component design. In: Advances in production Technology. Springer (2015)
5. Emmelmann, C., Sander, P., Kranz, J., Wycisk, E.: Laser additive manufacturing and bionics: redefining lightweight design. Phys. Proc. **12**, 364–368 (2011)
6. Teufelhart, S.: Geometrie- und belastungsgerechte Optimierung von Leichtbaustrukturen für die additive Fertigung. Additive Fertigung, Seminarbericht (2012)
7. Lippert, R.B., Lachmayer, R.: Topology examination for additive manufactured aluminum components. In: Proceedings of the 3rd DDMC, Berlin, Germany (2016)
8. Hague, R., Mansour, S., Saleg, N.: Design opportunities with rapid manufacturing. Assem. Autom. **23**(4), 346–356 (2002)
9. Chen, T., Fritz, S., Shea, K.: Design for mass customization using additive manufacturing: case-study of a balloon-powered car. In: Proceedings of the 20th ICED15, Milan, Italy (2015)
10. Lippert, R.B., Lachmayer, R.: Bionic inspired infill structures for a light-weight design by using SLM. In: Proceedings of the 14th DESIGN Conference, Dubrovnik, Croatia (2016)
11. Smith, M., et al.: Finite element modelling of the compressive response of lattice structures manufactured using the selective laser melting technique. Int. J. Mech. Sci. **67**, 28–41 (2013)
12. Lachmayer, R., Lippert, R.B., Fahlbusch, T.: 3D-Druck beleuchtet – Additive Manufacturing auf dem Weg in die Anwendung. Springer, Germany (2016). ISBN 978-3-662-49055-6
13. Ullah, I., et al.: Performance of bio-inspired kagome truss core structures under compression and shear loading. J. Compos. Struct. **118**, 294–302 (2014)
14. Reinhart, G., Teufelhart, S.: Load-adapted design of generative manufactured lattice structures. Phys. Proc. **12**, 385–392 (2011)
15. Lippert, R.B., Lachmayer, R.: Einflussfaktoren innerer strukturen im gestaltungsprozess von strukturbauteilen für das selektive laserstrahlschmelzen. In: Proceedings of the 14th Rapid. Tech, Erfurt, Germany (2017)
16. Lachmayer, R., Lippert, R.B.: Additive Manufacturing Quantifiziert. Springer, Heidelberg, May 2017. ISBN 978-3-662-54112-8
17. Vayre, B., et al.: Designing for additive manufacturing. In: 45th CIRP Conference on Manufacturing Systems (2012)
18. VDI 3405 Part 3: Additive manufacturing processes, rapid manufacturing - design rules for part production using laser sintering and laser beam melting. Beuth, Berlin, Germany (2015)

19. Roth, K.: Konstruieren mit Konstruktionskatalogen - Band 1: Konstruktionslehre, 3. Auflage. Springer, Germany (2000). ISBN 978-3-642-17466-7
20. Zimmer, D., Adam, G.: Direct manufacturing design rules. In: Innovative Developments in Virtual and Physical Prototyping (2012)
21. Kranz, J., Herzog, D., Emmelmann, C.: Design guidelines for laser additive manufacturing of lightweight structures in TiAl6V4. J. Laser Appl. **27**, S14001 (2015)
22. EOS GmbH: Material data sheet EOS Aluminium AlSi10Mg. EOS GmbH (2014)
23. DIN EN 515:2016-01: Aluminium und Aluminiumlegierungen - Halbzeug - Bezeichnungen der Werkstoffzustände. Beuth Verlag (2015)
24. Tang, M., Pistorius, P.C.: Oxides, porosity and fatigue performance of AlSi10Mg parts produced by selective laser melting. Int. J. Fatigue **94**, 192–201 (2016)
25. Brandl, E., Heckenberger, U., Holzinger, V., Buchbinder, D.: Additive manufactured AlSi10Mg samples using Selective Laser Melting (SLM): microstructure, high cycle fatigue, and fracture behavior. Mater. Des. **34**, 159–169 (2012)
26. Kempen, K., Thijs, L., Van Humbeeck, J., Kruth, J.P.: Mechanical properties of AlSi10Mg produced by selective laser melting. Phys. Proc. **39**, 439–446 (2012). doi:10.1016/j.phpro.2012.10.059
27. Anyalebechi, P.: Effect of process route on the structure, tensile, fatigue properties of aluminum alloy steering knuckles. Int. Foundry Res. **63**(3), 32–43 (2011)
28. Humbeeck, J.V., Thijs, L.: PFC: AlSi10Mg parts produced by Selective Laser Melting (SLM). Miguel Godino Martínez. Industrial Engineering. Specialty: Materials (2013)
29. Sullivan, S., Chris, H.: Weight Reduction Case Study of a Premium Road Bicycle Crank Arm Set by Implementing Beralcast® 310, Vancouver (2013)

Exploring the Impact of Shape Complexity on Build Time for Material Extrusion and Material Jetting

Patrick Pradel[1](✉), Richard Bibb[1], Zicheng Zhu[2],
and James Moultrie[2]

[1] Loughborough Design School, Loughborough University, Loughborough, UK
p.pradel@lboro.ac.uk
[2] Department of Engineering, University of Cambridge, Cambridge, UK

Abstract. "Complexity for free" has often been claimed as one of the main opportunities of additive manufacturing (AM). Many examples have proven how, for highly complex and intricate geometries, additive manufacturing is the only available route. However, the implications that shape complexity has on part cost have not been thoroughly explored. This is especially relevant for series production where optimisation of building time can lead to significant cost savings. This study explores how shape complexity impacts build time in Material Extrusion (ME) and Material Jetting (MJ). A screening experiment is presented where the impact of 'area', 'size' and 'increase in perimeter' on build time is analysed. The results show that these three factors influence building time in ME, while only 'size' has a significant effect in MJ. Our results challenge the mainstream assumption that all AM processes provide "Complexity for free" while presenting preliminary indications on how to design efficient components for ME and MJ.

Keywords: Design for additive manufacturing · Shape complexity · Design for cost · Costing · Additive manufacturing

1 Introduction

It has been widely promoted that in Additive Manufacturing (AM) there is no correlation between shape complexity and part cost. Among the first who attempted to define the opportunities of AM, Hague et al. stated that AM could produce "any complexity of geometry without any increase in cost" [1]. Similarly, Gibson et al. suggested that when using AM, designers can exploit "complex geometries without causing any additional increase in time and cost" [2]. While, Lipson argued that AM "drastically reduces the cost of making complexity" [3]. Likewise, industry has advocated that complex parts could be created rapidly, inexpensively and practically with AM processes [4]. Although these contributions were significant as they marked the first efforts to define AM opportunities in design, they did not explore the implications of shape complexity with empirical studies. The claims in the papers may be

© Springer International Publishing AG 2018
M. Meboldt and C. Klahn (eds.), *Industrializing Additive Manufacturing - Proceedings of Additive Manufacturing in Products and Applications - AMPA2017*,
DOI 10.1007/978-3-319-66866-6_3

based on comparing AM to other more established methods of manufacture. What they did not consider was the comparison of different shapes or how design might be optimized for a specific AM process.

In addition, the development of cost models for AM shows that shape complexity has not been considered in detail. For instance, Xu et al. were among the first to propose a cost model for AM. In their equation for calculating the fabrication time, the authors considered the volume of the solid part as the only geometrical variable [5]. More recently, Baumers et al. [6] focused their cost model on machine productivity without addressing the implications of shape complexity. In their generic cost model for AM, Gibson et al. considered shape complexity as a correction factor for calculating the average cross-sectional area of a part [2]. This correction factor, derived from Pham and Wang [7], considered the printing time in laser sintering differences between geometries with identical cross-sectional area but dissimilar area distribution. The authors proposed to define shape complexity as a ratio between the actual part volume and the bounding box. However, since this correction factor was devised from laser-based systems (e.g. Laser Sintering and Stereolithography) [7] where the build time is influenced by the speed of the laser scanner; it may not apply to other AM technologies such as nozzle-based systems (e.g. Fused Deposition Modelling and Laser Engineering Net Shape), line-wise system (e.g. Material Jetting and Binder Jetting) or layer-wise systems (e.g. Digital Light Processing and Continuous Digital Light Processing) where the build time is affected by other factors such as the deposition speed of the material [8, 9].

In specific cost models for FDM, shape complexity has been widely neglected and accounted for only through software simulation of building time and material consumption [10, 11]. Only recently, Urbanic and Hedrick [8] hinted at the problem of shape complexity, discussing how intricate surfaces increase the building time. According to the authors, the building time in FDM is directly related to the perimeter travel distances and the volume of the component. Because the travel speed of the outer delimiting contour is slower than the speed of the raster infill, components with intricate external surfaces would result in higher building times and therefore prove more expensive. Although this was a first attempt to consider the implications of shape complexity in FDM, the paper did not offer an adequate investigation on the issue.

In a previous work, we investigated the relation between shape complexity and build time in ME using as a case study a simple load cell holder [12]. The results indicated that in ME, shape complexity seems to have a remarkable impact on both build time and material consumption; challenging the assumption that in ME “Complexity is Free”. However, that experiment presented some limitations.

- First, it considered only one AM process therefore limiting the generalization of the results.
- Additionally, the case used for the experiment was interesting in addressing a real case scenario, but it failed to isolate the shape complexity from the area.
- Finally, it did not provide any indication of the perimeter length and the magnitude of its impact.

To address these issues and improve our understanding of the topic, we carried an experiment aimed at:

- Further validating the result of the previous experiment.
- Isolating shape complexity from other factors such as area and size.
- Comparing the results with other AM technologies.
- And providing guidance for design practice.

2 Method

To make the problem of shape complexity in AM more manageable, we decided to consider only the complexity provided by the geometry of the layers; therefore, transforming a 3D problem into a 2D problem. This decision was chosen since the principal variable in build time is layer deposition on the x-y axis; whereas build time in the z axis is chiefly dictated by the movement of the build platform which is typically fixed. In fact, given the nature of AM, 3D geometries can be considered as a stack of 2D layers.

As factors for characterizing the 2D geometrical complexity of a layer, three factors were considered:

- **Area:** i.e. the area of the layer in which the material has been deposited.
- **Size:** i.e. the overall dimensions of the minimum bounding box of the layer.
- **Increase in perimeter:** i.e. the total length of the perimeter. Since perimeter is not an independent variable, we did not consider it as an absolute value, but rather as an increase in length compared to the perimeter of the shape with identical size and area.

The three factors where variate at two levels (high and low) following the structure of a 2^3 factorial design [13]. Table 1 presents the 2^3 factorial design with factors and levels. For the 'Area', 500 mm^2 were chosen as indicative of 'low' level while 900 mm^2 as representative of a high level. For 'Size', we defined 'low' as a shape with a minimum bounding box of 35 mm × 35 mm and 'high' a shape with a minimum bounding box of 70 mm × 70 mm. An increase in perimeter of 0% was considered 'low' while a percentage increase of 15% was considered a sufficient indication for a 'high' level. An internal hole was added to the components to be able to variate independently the area and the size.

Table 1. Experimental plan.

Factors	Low level (−)	High level (+)
A: Area (mm^2)	500	900
B: Size (mm)	35	75
C: Increase in perimeter (%)	0	15

The CAD package SolidWorks 2016 was used to design the shapes according to the factorial experimental design. The shapes were designed to fit into a square bounding box of 35 mm or 70 mm side. These dimensions were considered appropriate since it allowed the shapes to be produced quickly whilst remaining large enough to provide indications for the study. The bounding box and the internal hole were used to contain the shapes and at the same time ensure that the different geometries had identical size and area (i.e. therefore controlling the area and size factors). Figure 1 shows how the different shapes were conceived.

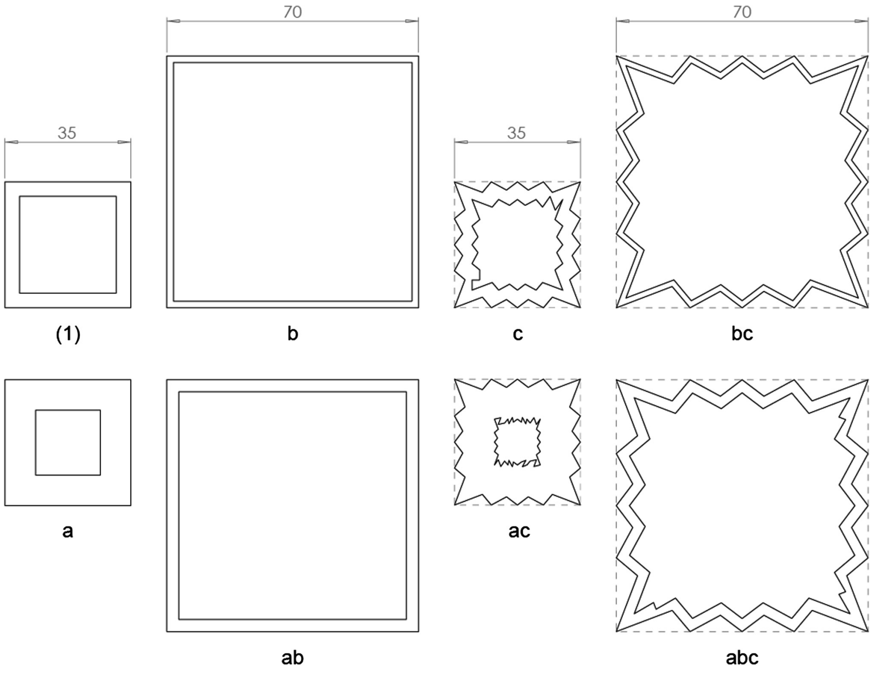

Fig. 1. Construction of the sample shapes.

The geometries where then extruded to a height of 5 mm. The height was kept constant. The shapes generated are presented in Table 2 along with their area, size and perimeter variation.

Table 2. Samples generated for the experiment.

Run	Area (mm^2)	Size (mm)	Perimeter (mm)	Increase in perimeter (%)
(1)	500	35	248	0
a	900	35	212	0
b	500	70	545	0
ab	900	70	533	0
c	500	35	293	15
ac	900	35	249	15
bc	500	70	641	15
abc	900	70	627	15

2.1 Experiment

To explore the validity of the findings of our previous experiment, we decided to test two diametrically opposed AM process categories: Material Extrusion (ME) and Material Jetting (MJ). ME was chosen because it provides further validation for the results of the previous experiment and it is an example of vector technology, while MJ was chosen because it was considered a good example of a raster AM technology. In fact, in the previous experiment, we hypothesized that our findings could be theoretically generalized to all vector based technologies (e.g. fused deposition modelling, laser sintering and stereolithography), while we assumed they were not applicable to raster based approaches such as MJ. Therefore, we assumed that MJ could provide a stark contrast to our results and indications regarding generalizability.

The machines used for producing the samples were an Object Connex 500, which was used to test the samples for MJ; and a Stratasys Dimension sst1200es, which was used to test the samples for ME. Table 3 shows the settings of the machines used during the experiment.

Table 3. Settings of the machines

	Material jetting	Material extrusion
Machine	Objet connex 500	Stratasys dimension sst 1200es
Software	Objet studio version 9.2.8.3	CatalystEX version 4.4
Printing mode	Digital material	
Material	VeroClear™	ABS-P43™ model (Ivory)
Orientation	Auto orient	Auto orient
Layer resolution	0.03 mm	0.2540 mm
Finish	Glossy	
Model interior	Solid	Sparse - low density
Support infill		Sparse
Number of layers	202	30

The samples were produced randomly and replicated three times with each machine for a total number of 24 replicas for each technology.

Build time was selected as the dependent variable since it can be considered one of the main drivers for cost of production in AM. Build time accounts for the machine's amortization, energy consumption and productivity [6, 9].

For ME, the build time was measured with the app 'Clock' of an IPhone 5S from the instant the print head started to deposit the material of the first layer to the instant in which the print head stopped depositing material. For the MJ, the build time was taken with the same device starting from the instant the machine was completely heated to when the machine completed the component and the building plate moved to the home (lowest) position.

The data was then compiled and analyzed using Excel 2016 and SPSS v23. A three-way ANOVA test was used to analyze the data and provide the statistical significance for the different factors [13].

3 Results

Figure 2 shows the samples produced during the experiment while Table 4 reports the overall results.

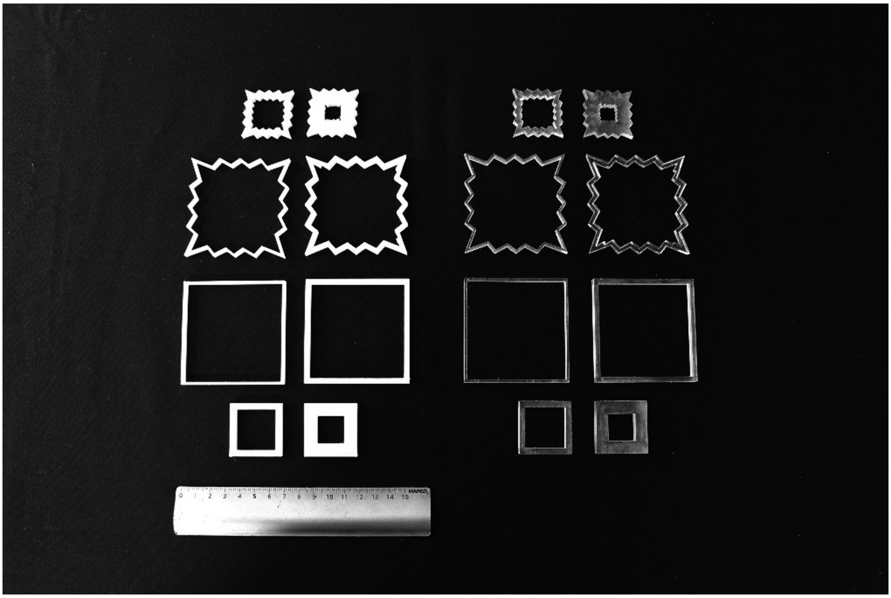

Fig. 2. A sample of the printed shapes.

Table 4. Build time of the samples in seconds.

Run	ME replicate 1	ME replicate 2	ME replicate 3	MJ replicate 1	MJ replicate 2	MJ replicate 3
(1)	892	892	892	1304	1305	1303
a	947	941	940	1303	1304	1304
b	1160	1160	1161	2915	2918	2913
ab	1635	1634	1635	2914	2916	2913
c	1010	1013	1015	1306	1302	1303
ac	1122	1124	1124	1302	1304	1303
bc	1226	1224	1226	2922	2916	2919
abc	1758	1776	1772	2920	2919	2919

3.1 Shape and Build Time in Material Extrusion

Table 5 presents the results of the ANOVA for build time in ME. The results of the experiment show a direct strong correlation between the three factors and the build time.

Table 5. ANOVA for build time in material extrusion.

Source	Type III sum of squares	df	Mean square	F	Sig.	Percentage contribution
AREA	521265.375	1	521265.375	36795.203	.000	24.4%
SIZE	1239876.042	1	1239876.042	87520.662	.000	57.9%
INCREASE IN PERIMETER	93875.042	1	93875.042	6626.474	.000	4.4%
AREA * SIZE	274990.042	1	274990.042	19411.062	.000	12.8%
AREA * INCREASE IN PERIMETER	6240.375	1	6240.375	440.497	.000	0.3%
SIZE * INCREASE IN PERIMETER	3927.042	1	3927.042	277.203	.000	0.2%
AREA * SIZE * INCREASE IN PERIMETER	30.375	1	30.375	2.144	.162	0.0%
Error	226.667	16	14.167			
Total	37859591.000	24				
Corrected total	2140430.958	23				

A. R Squared = 1.000 (Adjusted R Squared = 1.000)

The results suggest that size (F (2;24) = 87520.662, p < .05) accounts for more than 50% of the variation, area (F (2;24) = 36795.203, p < .05) for roughly a quarter and their combined effect (F (2;24) = 19411.062, p < .05) for the 12.8%. Increase in perimeter (F (2;24) = 6626.474, p < .05), which was our indicator of complexity, has also a significant impact and it accounts for 4.4% of the variation. The other effects appear to provide instead either a very low contribution (e.g. AREA * INCREASE IN PERIMETER and SIZE * INCREASE IN PERIMETER) or they were not significant (e.g. AREA * SIZE * INCREASE IN PERIMETER).

3.2 Shape and Build Time in Material Jetting

Table 5 presents the results of the ANOVA for MJ. In MJ, the results indicate that size (F (2;24) = 5065517.851, p < .05) is the only indicator of build time. Although, 'increase in perimeter' and the combined effect of 'size' and 'increase in perimeter' seem to be significant (p < .05), their percentage contribution (<0.0%) is neglectable. This is consistent with our initial hypothesis that shape complexity does not affect line-wise systems. Additionally, it also shows that the area of the layer does not alter printing time as shown in the ANOVA results reported in Table 6.

Table 6. ANOVA for build time in material jetting.

Source	Type III sum of squares	df	Mean square	F	Sig.	Percentage contribution
AREA	1.042	1	1.042	.338	.569	0.0%
SIZE	15618680.042	1	15618680.042	5065517.851	.000	100.0%
INCREASE IN PERIMETER	22.042	1	22.042	7.149	.017	0.0%
AREA * SIZE	.042	1	.042	.014	.909	0.0%
AREA * INCREASE IN PERIMETER	.375	1	.375	.122	.732	0.0%
SIZE * INCREASE IN PERIMETER	35.042	1	35.042	11.365	.004	0.0%
AREA * SIZE * INCREASE IN PERIMETER	1.042	1	1.042	.338	.569	0.0%
Error	49.333	16	3.083			
Total	122498731.000	24				
Corrected total	15618788.958	23				
A. R Squared = 1.000 (Adjusted R Squared = 1.000)						

4 Discussion and Conclusion

For ME, the results of this experiment seem to confirm the conclusions of our previous paper while adding more insights on the individual effects provided by ‘area’, ‘size’ and ‘increase in perimeter’ on build time. Although all three factors affect build time, ‘size’ has the strongest impact and therefore should be carefully considered when designing components for ME. ‘Area’ has also an important impact on build time. Moreover, it must be considered that we used a ‘low density’ infill in this experiment and with a ‘solid’ infill a more prominent effect could be expected. Regarding the ‘increase in perimeter’, our experiment shows that it has also an impact on build time; however, this impact is significantly smaller than those of ‘size’ and ‘area’. This might be due to the amount of ‘increase in perimeter’ which was rather minor (15%). We do not exclude that increasing the perimeter of higher values might have a more noticeable influence. Additionally, we observed a much larger impact of ‘increase in perimeter’ at small scales i.e. approaching the resolution of the ME machine (Please see ‘ac’ build time).

This might suggest that designers should first consider the first two factors (i.e. ‘area’ and ‘size’) and then address the later (‘increase in perimeter’). Components with low size, area, and perimeter should result more ‘efficient’ for ME. If the design target is to minimize cost, build time can be reduced by minimising area, size and perimeter of the component. However, in practice this is seldom possible, we therefore suggest adopting a ‘priority’ approach. From this we can draw the following design principles for ME:

- Minimise component size.
- Minimise layer area.
- Minimise perimeter length.

Similarly, for MJ, the results show that 'size' is the main effect, but differently they also indicate that there is no correlation between 'area' or 'increase in perimeter' and build time. This confirms our initial hypothesis that build time in raster systems is driven only by size. The implications for this are manifold. First, in MJ shape complexity is really for "free" and the build time of complex geometries is the same of simple ones given the size remains the same. However, it does not necessary imply that designers should not carefully consider components' geometry when designing for MJ. In fact, if size is the only driver, shapes that minimise it or that make full advantage of it should be preferred. Building big hollow shapes, such as shape 'b', might not be the most efficient way of using this technology. Therefore, the design principles for MJ that we can draw from this experiment are the following:

- Minimise component size.
- Avoid 'empty' big spaces.
- Use design space effectively.

These considerations can also have implications for part consolidation. If part consolidation increases the size of the component, designers should have to address the trade-off between increasing build time and reducing assembly cost. We imagine there could be cases in which a straight part consolidation is not the most convenient design approach.

This experiment presented different limitations. For instance, we considered only two dimensional geometries without investigating the impact on the z axis. Although there is an assumption that shape complexity does not impact build time on the z axis, future studies will have to prove this assumption. Moreover, in this experiment we have tested only relative small components (35 mm to 70 mm side). It cannot be excluded that at large scales (i.e. closer to the size of building plate), with a substantially higher number of layers or by filling the building plate, the same results will be obtained. Future studies will have to investigate these scenarios.

References

1. Hague, R.J., Campbell, I., Dickens, P.: Implications on design of rapid manufacturing. Proc. Inst. Mech. Eng. Part C J. Mech. Eng. Sci. **217**, 25–30 (2003). doi:10.1243/095440603762554587
2. Gibson, I., Rosen, D.W., Stucker, B.: Additive manufacturing technologies: 3D printing, rapid prototyping, and direct digital manufacturing, First edi (2010). doi:10.1007/978-1-4419-1120-9
3. Lipson, H.: The shape of things to come: frontiers in additive manufacturing. In: Frontiers of Engineering, pp. 33–43 (2011). http://www.chinatranslation.net/upload/956445282.pdf
4. Comb, J.: Designing parts for direct digital manufacturing. Adv. Mater. Process. **168**, 22–24 (2010)

5. Xu, F., Wong, Y.S., Loh, H.T.: Toward generic models for comparative evaluation and process selection in rapid prototyping and manufacturing. J. Manuf. Syst. **19**, 283–296 (2001). doi:10.1016/S0278-6125(01)89001-4
6. Baumers, M., Dickens, P., Tuck, C., Hague, R.J.M.: The cost of additive manufacturing: machine productivity, economies of scale and technology-push. Technol. Forecast. Soc. Change. **102**, 193–201 (2016). doi:10.1016/j.techfore.2015.02.015
7. Pham, D.T., Wang, X.: Prediction and reduction of build times for the selective laser sintering process. Proc. Inst. Mech. Eng. – Part B – Eng. Manuf. **214**, 425–430 (2000). doi:10.1243/0954405001517739
8. Urbanic, R.J., Hedrick, R.: Fused deposition modeling design rules for building large, complex components. Comput. Aided. Des. Appl. **4360**, 1–21 (2015). doi:10.1080/16864360.2015.1114393
9. Gibson, I., Rosen, D.W., Stucker, B.: Additive manufacturing technologies: rapid prototyping to direct digital manufacturing, Addit. Manuf. Technol. Rapid Prototyp. Direct Digit. Manuf. 1–459 (2010). doi:10.1007/978-1-4419-1120-9
10. Mello, C.H.P., Martins, R.C., Parra, B.R., Pamplona, E.D.O., Salgado, E.G., Seguso, R.T.: Systematic proposal to calculate price of prototypes manufactured through rapid prototyping an FDM 3D printer in a university lab. Rapid Prototyp. J. **16**, 411–416 (2010). doi:10.1108/13552541011083326
11. Grujovic, N., Pavlovic, A., Sljivic, M., Zivic, F.: Cost optimization of additive manufacturing in wood industry. FME Trans. **44**, 386–392 (2016). doi:10.5937/fmet1604386G
12. Pradel, P., Bibb, R., Zhu, Z., Moultrie, J.: Complexity is not for free: the impact of component complexity on additive manufacturing build time. In: RPDM 2017, n.d.: pp. 1–7
13. Montgomery, D.C.: Design and Analysis of Experiments, 6th edn. Wiley, Hoboken (2004)

Novel Optimised Structural Aluminium Cross-Sections Towards 3D Printing

Konstantinos Daniel Tsavdaridis[1(✉)], Jack Antony Hughes[2],
Lukas Grekavicius[3], and Evangelos Efthymiou[4]

[1] School of Civil Engineering, Institute for Resilient Infrastructure,
University of Leeds, Woodhouse Lane, Leeds LS2 9JT, UK
k.tsavdaridis@leeds.ac.uk
[2] Robert Bird Group, Level 2 Harling House,
47-51 Great Suffolk St, London SE1 0BS, UK
jack.hughes@robertbird.com
[3] Cundall, 4th Floor, Partnership House, Regent Farm Road, Gosforth,
Newcastle upon Tyne NE3 3AF, UK
l.grekavicius@cundall.com
[4] Department of Civil Engineering, Institute of Metal Structures,
Aristotle University of Thessaloniki, 54124 Thessaloniki, Greece
vefth@civil.auth.gr

Abstract. In the last decades, the deployment of aluminium and its alloys in engineering fields has been increased significantly, due to the material's special features accompanied by supportive technological and industrial development such as the extrusion manufacturing method. However, the extent of aluminium structural applications in building activities is still rather limited, and barriers related to strength and stability issues prevent its wider use. In the context of topology optimisation, appropriate design in aluminium cross-sections can overcome inherent deficiencies, such as the material's low elastic modulus.

The current study investigates the application of structural topology optimisation to the design of aluminium beam and column cross-sections, through a combination of 2D and 3D approaches, with focus on post-processing and manufacturability. Ten unique cross-sectional profiles are proposed based on structural testing through Finite Element Analysis (FEA). Conclusions attempt to highlight the general characteristics of the optimised aluminium cross-sections as well as the benefits of the using extrusion and 3D printed manufacturing methods in order to realise these results.

Keywords: Manufacturing processes · Aluminium structural members · Novel cross-section design · Structural topology optimisation · SIMP technique · Extrusion · 3D printing

1 Introduction

Aluminium is a unique material that has the potential of competing within the construction industry. Successful application of aluminium alloys in structural engineering is connected to its inherent physical and mechanical properties: low density, which

© Springer International Publishing AG 2018
M. Meboldt and C. Klahn (eds.), *Industrializing Additive Manufacturing - Proceedings of Additive Manufacturing in Products and Applications - AMPA2017*,
DOI 10.1007/978-3-319-66866-6_4

allows reduced loads on foundations and easier construction process; excellent corrosion resistance, which reduces its maintenance requirements; and the extrusion process, which allows the production of members with efficient and optimised cross-sections [1]. In particular, although available for some other non-ferrous metals, such as brass and bronze, it is with aluminium that the extrusion process has become a major manufacturing method [2]. The extrusion process allows aluminium sections to be formed in an almost unlimited range of shapes, while a significant advantage is the ability to produce sections that are very thin relative to their overall size [3]. Additive manufacturing and in particular 3D printing process delivers similar advantages in the design and fabrication of monolithic structural elements of complex shapes, and in particular those are irregular along the length of the member.

Aluminium cross-sections are separated into four classes based on b/t ratio limits of reinforced and un-reinforced parts. When compared to standardise steel sections, aluminium cross-sections are often asymmetric, more complex, contain thin walls and are reinforced with ribs, bulbs and lips [4]. Local instability is, therefore, the governing factor when designing such sections. Another factor that is linearly related to buckling resistance of beams and columns is the stiffness of cross-sections (*EI*). To compensate for the low elastic modulus and achieve higher stiffness, the moment of inertia has to be increased. When considering standard shapes this would result in deeper and slenderer sections, which are more susceptible to buckling. However, sections obtained through advanced topology optimisation techniques can achieve a high I-value with an optimal amount of material.

Structural topology optimisation is based on the principle of optimising the number and size of openings within a design space, in order to satisfy the applied loading and constraints. There are numerous topology optimisation techniques available in the literature. The currently most popular one is the Solid Isotropic Material Penalisation (SIMP) technique, which is based on discretising the design domain into finite elements and utilising FE analysis to vary the densities in each element. Depending on the intensity of stresses, the elements are characterised as being low, high or intermediate density [5]. The process is iterative until convergence is reached.

Topologies may resemble complex natural forms; therefore, it is often up to the designer to interpret them. Interpretation is a crucial part of the overall optimisation process and needs to be performed carefully with consideration of manufacturing and practicality factors. This has been unaddressed in the existing literature [6–8], which is limited to a selection of a few load conditions and there have not been any attempts made yet at optimising aluminium cross-sections. Therefore, this study aims to utilise the complimentary of the co-authors in optimisation and aluminium and propose new efficient structural shapes by conducting cross-sectional topology optimisation analysis of 6063-T6 aluminium alloy beams and columns. It is intended to achieve a minimum possible weight with maximum stiffness, as weight savings can render significant reductions in manufacturing and construction costs, as well as environmental impact.

2 Manufacturing Processes

Aluminium is presently extracted exclusively from bauxite, however, it also exists in other minerals within the earth’s crust to make it the third most abundant element. Combined with the high recyclability rate of the end product, this ensures that there is adequate material for continued sustainable construction for an almost indefinite period.

Once combined with its alloying elements, the new material is classed as being a casting or wrought alloy, dependent on whether it is to be melted before casting. As a result, most hot rolled and extruded applications utilise wrought alloys. The heat treatment process is then followed by quenching and ageing, during which the majority of hardening occurs.

The current state-of-the-art manufacturing process for aluminium member is the extrusion process Fig. 1(a)-left. The extrusion process creates cross-sectional shapes by forcing hot metal, in the form of a billet, through an opening called a die (e.g., porthole and bridge dies). The corresponding cross-section then matches the profile of the die, regardless of it complexity. This enables designers to create specific sections to meet requirements, simply by producing the appropriate die; such as the complex shapes shown in Fig. 1(a)-right. This method provides a relatively high quality result with national specifications allowing a deviation of approximately 5% from the nominal thickness.

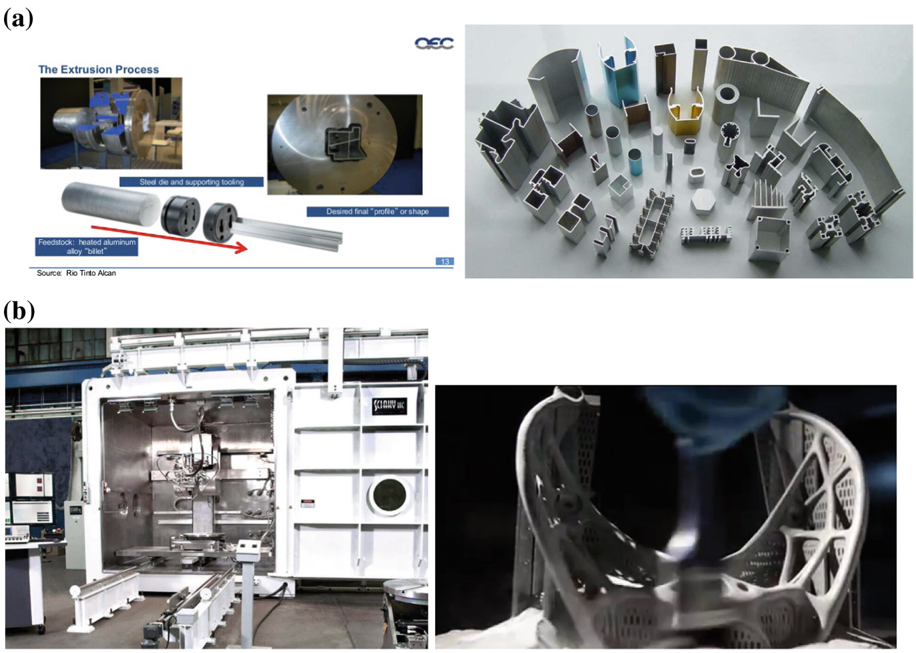
(a)
The Extrusion Process
Steel die and supporting tooling
Desired final "profile" or shape
Feedstock: heated aluminum alloy "billet"
Source: Rio Tinto Alcan
13
(b)

Fig. 1. (a) Extrusion process (left) and products (right) (b) Biggest 3D printer (left) and manageable complexity of product design (right)

The cost influencing criterial as being very similar to those for rolled sections, however, specific costs may vary dramatically for bespoke die designs. In general, costs for hollow sections have been reported as being up to five times more expensive than solid or open profiles. Cheaper manufacture methods are available, such as shell casting rather than die casting, however, larger tolerances for imperfection may be expected.

On the other hand, recently, designers are pushing technologies to realise the full potential of 3D printing and overcome material quality, monitoring, and size limitations (Fig. 1(b) – the biggest 3D printing for metallic members). This method of fabrication is a new process of making a 3D solid object directly from a digital model. It is an additive process where successive layers of material are laid down in a controlled way to achieve the desired (optimised) shape, replacing traditional machining techniques, dealing with material removal through cutting and splitting, sawing/drilling/rounding off, and CNC turning/milling. There are three 3D printing techniques such as: (i) Extrusion type – Fuse Deposition Modelling (FDM) used for thermoplastics: PLA, ABS, nylon, alumide (a mix of nylon and aluminium); (ii) Granular type – Selective Laser Sintering (SLS) used for thermoplastics, metal powders, and ceramic powders; (iii) Liquid type – Multi Jet Modelling (MJM) used for acrylic plastic.

The cost of the 3D printing is comparable to the one of the extrusion process, but cannot be precisely evaluated since massive production is required while the industry is still experimenting. For this reason, this paper contributes to the effort demonstrating the need for larger scale 3D printers as well as focus on high production of structural elements through comprehensive comparisons between typical structural aluminium cross-section members that can be produced by extrusion process, and fully optimised structural aluminium members that can only be manufactured by 3D printers. Table 1 below, is the first attempt to compare the pros and cons of the two aforementioned manufacturing processes and draw the overall picture of the current state-of-the-art.

Table 1. Overview of manufacturing processes

	Extrusion	3D Printing
Advantages	• Length (long span, <30 m) • Quick production (20–70 m/min) • Similar cost to cold forming • No trimming or milling is required • Very few imperfections and residual stresses	• No supply chain is required • Achieve any optimised complex shape (decrease weight to stiffness ratio)
Disadvantages	• Constant cross-section along the length of the member • Need pre-production of the die • Can be five times more expensive than solid or open profile	• Size limitations (so far) • Brittle performance in certain occasions • Cracking control is required • Roughness control is required (direction dependent) • Time expensive process • Certain models only suitable for limited temperature range

3 Topology Optimisation Approach

This research undertook a combination of approaches, in order to consider all necessary degrees of freedom identified in Fig. 2. A 2D approach was used to identify a wide variety of cross-sectional profiles, however this approach did not consider variations in bending and shear along the length of the member. A 3D approach was then used to provide a series of comparative cross-sectional slices, to capture the effect of this variation. All optimisation was performed using Altair Engineering's software package HyperWorks v13.0. Through this, more than 40 different combinations of loading and support conditions were analysed. Loading conditions were chosen with reference to the standard cross-section classification procedure for outstand and internal compression elements given by codified provisions [9].

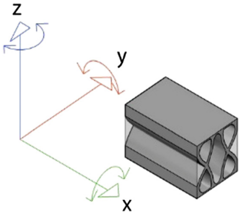

Fig. 2. Considered directions of rotation and translation

Linear static analysis was performed on an elastic material model with the following properties: Young's modulus of 70 GPa, Poisson's ratio of 0.3, shear modulus of 27 GPa and density of 2700 kg/m^3. Shell elements with a nominal size of 1 mm and solid elements with a nominal size of 5 mm were used to model the 2D and 3D members, respectively. All models have been optimised for minimum compliance (therefore maximum stiffness) subject to a constraint on the final volume fraction of 0.275. Manufacturability is addressed through constraints on symmetry and a minimum member size of 7 mm. This optimisation problem has been validated in both the 2D and 3D cases. When compared to the results obtained in existing literature [6, 8] a close agreement of the patterns has been identified.

Identical analysis has been performed to compare topologies obtained with aluminium and steel. Aluminium alloy 6063-T6 (with a tensile strength of 245 N/mm^2) was compared to grade S355 steel with Young's modulus of 210 GPa and Poisson's ratio of 0.3. Identical topologies reveal that the optimisation constraints and geometry are dominant, therefore the results are applicable to both materials.

A 100 × 100 mm square section has been chosen as the initial design domain in order to provide maximum flexibility in the resulting topologies. So as to provide a comparison however, sections with aspect ratios of 100 × 200 mm and 200 × 100 mm have also been optimised. Figure 3 demonstrates that very similar density plots are achieved regardless of the aspect ratio, therefore the sections may be adapted into similar forms as required.

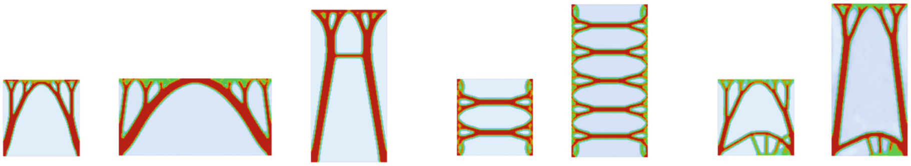

Fig. 3. Topologies of cross-sections with various aspect ratios

Topology optimisation results must be carefully interpreted into a suitable structure. The results are highly sensitive to geometry, so a method of post-processing multiple results to allow for these sensitivities is proposed. The contour plots shown previously have been smoothed with a density threshold of 0.3 using Altair Engineering's OSSmooth and extracted into AutoCAD. Afterwards, the results from multiple loading and support conditions have been overlaid and presented in a form appearing similar to x-rays. These show the most frequently stressed material to be darker in colour and allow for the interaction of various load cases to be considered.

Optimisation processes for lightweight structures typically result in thin-walled cross-sections. When combined with aluminium's lower modulus of elasticity, local instability modes including distortional and local buckling are typically dominant. In order to minimise the likelihood of these failures, optimal placement of compression members and stiffeners is of vital importance. Using the described post-processing method, this stability criterion should be satisfied by comparing the typical stresses in cross-sections subjected to torsion, compression, yielding and one or two plane buckling.

4 Topology Optimisation of Cross-Sections

Beams. Pinned supports to 2 and 4 nodes are compared, in order to propose sections suitable for simply supported and fixed beams respectively. Major axis bending and torsion have then been applied. Figure 4 shows 5 beam cross-sections developed after processing. Section properties are then presented in Table 2. For beams that are primarily subjected to bending about one axis only, the proposed sections are symmetric about one plane. Asymmetric cross-sections are also included for additional stiffness when subjected to torsion. Regardless of the applied symmetry, it is noticed that the topology results have a similar moment of inertia about both axes.

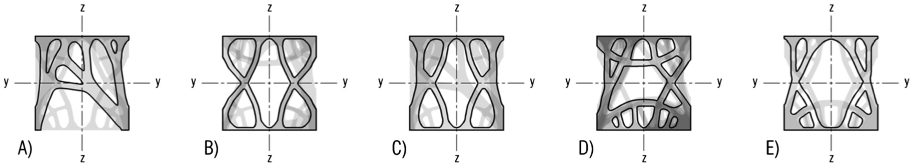

Fig. 4. Post-processing of beam cross-sections

Table 2. Beam section properties

Section	A	B	C	D	E
Area [cm^2]	44.39	30.32	39.43	48.84	37.82
Moment of inertia, y [cm^4]	340.26	337.32	399.50	528.69	436.66
Moment of inertia, z [cm^4]	448.14	312.46	423.15	479.10	426.65

3D optimisation was performed on a 2 m extruded 100 mm square beam, with total of six different loading and support combinations; including the case of fixed supports and a uniformly distributed load to the top flange as shown in Fig. 5(a). These reveal constant cross-sections such as elliptical hollow profile across 45–50% of the length of the beam. The remaining portion shows three distinct regions of low stress at approximately ¼, ½, and ¾ of the span, as seen in Fig. 5(b). These regions are observed to correspond with the intersections of the lines of principal tensile and compressive stresses in a homogeneous beam.

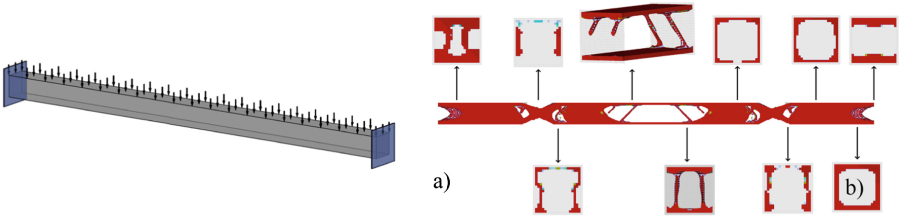

Fig. 5. Beam 3D optimisation input (a) and resulting topology with cross-sectional slices (b)

Columns. Optimisation of 2D column cross-sections with various support and loading conditions was initially attempted. Sections with two and four corner pin supports were analysed, subjected to axial compression, which include failure by yielding and one or two plane buckling. Column cross-sections found in practice are most commonly symmetric and have high buckling resistance about one or more axes depending on specific applications, hence this logic is followed in developing the final cross-sections shown in Fig. 6. The first attempt considers a column under pure compression, such cross-sectional profile would reach its yield stress limit and experience material failure. The shape resembles a standard double webbed compound column cross-section used in the industry. The second attempt considers column failure due to buckling. Figure 6B and C represent a cross-sectional profile of a column having high stiffness in the y-y axis. The cross-sections are a combination of resulting stress plots with loading replicating compression and bending of a member as it buckles. Therefore, they are applicable in cases when an eccentric axial load or a moment are applied triggering one plane buckling. Sections presented in Fig. 6D and E are resistant to compression and buckling in two axes. These profiles have equal stiffness in both axes and appear more resistant to local buckling. The section properties are presented in Table 3.

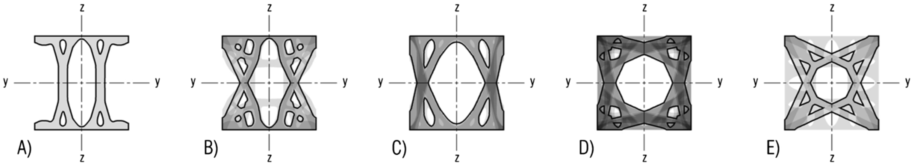

Fig. 6. Post-processing of column cross-sections

Table 3. Column section properties

Section	A	B	C	D	E
Area [cm^2]	35.36	49.95	52.00	59.13	49.10
Moment of inertia, y [cm^4]	461.63	565.23	582.67	608.38	442.67
Moment of inertia, z [cm^4]	224.58	449.33	578.80	608.38	442.67

3D optimisation was performed on a 2 m extruded 100 × 100 mm square column with fixed-pinned supports as shown in Fig. 7(a). An axial compressive load was applied at the top and loads triggering buckling in two planes – in the middle of the member. Symmetry manufacturing constraint was applied to the model about y-y and z-z axes. When subjected to two plane buckling the column developed concentrations of material at the four corners (Fig. 7), resembling a box section at multiple locations along the length of the member. Formation of a web connecting the flanges is also observed in the middle of the member at the location of the lateral load. The box shape of the cross-section could be related to the fully symmetric profiles obtained through 2D optimisation (Fig. 6D and E).

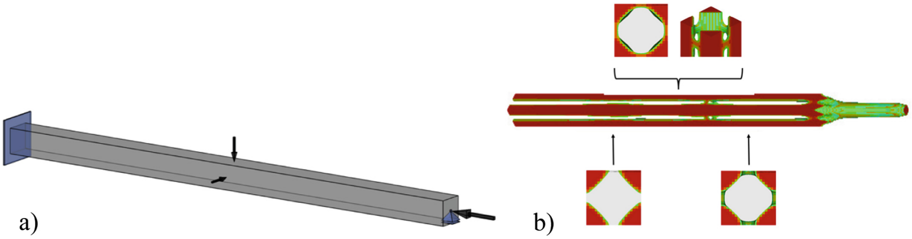

Fig. 7. Column 3D optimisation input (a) and resulting topology with cross-sectional slices (b)

5 Finite Element Analysis

Analysis Parameters. Finite element analysis (FEA) software ANSYS v14.0 is adopted in this study to assess the performance of the unique cross-sectional shapes. Geometrical and material non-linear analysis was employed, which takes into account the plastic behaviour of aluminium.

Results - Beams. Two of the optimised beam cross-sections developed have been tested through the FE analysis. In order to provide a reliable benchmark for how suitable the optimisation method is for developing new cross-sections, the two chosen have been compared against a selection of three conventional and two additional novel cross-sections, each of which are shown in Fig. 8. SHS and UB profiles have been included within the compared cross-sections as they are also available as steel profiles. A conventional Y-profile has then also been included, as an additional section that is only used in aluminium. Two novel cross-sections are then additionally included within the comparison, one of which is the result of previous optimisation studies by Kim and Kim [10]. As in the optimisation analysis, the models adopt a 100 mm square cross-section, and have been tested with lengths of both 2 m and 1 m in order to consider both extremities of span to depth ratios with 20 and 10.

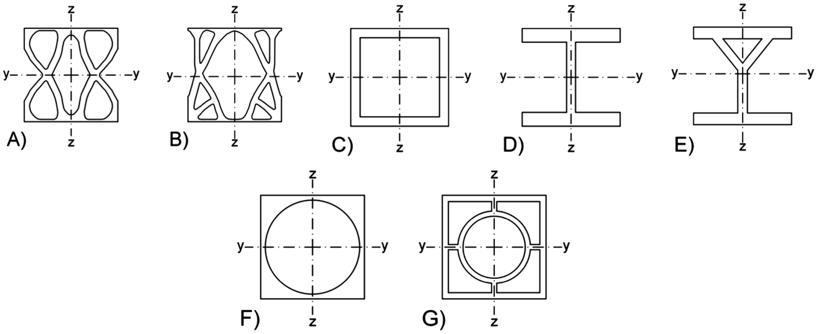

Fig. 8. Beam cross-sections employed in finite element analysis

All beams analysed have been subject to a uniformly distributed pressure to the top flange, along with a variety of two different support conditions. The first set of models have been analysed with fully fixed ends to prevent both translation and rotation, whilst the second set was modelled using a pinned bottom flange.

The members with 2 m length experienced significant plastic deformation and clearly demonstrate that serviceability criteria are the critical design aspect. Each of the members was able to resist the maximum applied load of 2 MPa, however they show significant mid-span deflections that are unacceptable in practice. At this ultimate load, the optimised cross-section A shows the least deflection, and the conventional SHS showing the most. Due to the large deflections however, the failure load of the members has been taken as that at a serviceability limit of the deflections of span/250. At the 8 mm deflection limit imposed by this criterion the performance of the various cross-sections dramatically differs, with the conventional sections marginally out-performing the optimised profiles. Due to the large mid-span deflections seen in the beams analysed with span-depth ratios of 20, it was considered necessary to analyse a series of stockier beams at span-depth ratios of 10. Pinned supports have been used in this set of results, to enable failure of the cross-sections at the high stress concentrations observed near the supports. These members were subjected to identical loading, and due to their alternate dimensions experienced much more acceptable levels of deflection at the ultimate load. The failure loads and corresponding deflections are presented in Table 4, along with the load-deflection curves in Fig. 9. The results show a much larger variation in the experienced deflections and failure loads, and therefore enable a clearer comparison when looking at the load-deflection curve.

Table 4. Analysis results for 1 m pinned beams

Section	A	B	C	D	E	F	G
Ultimate pressure [N/mm^2]	1.75	1.69	1.82	1.63	1.89	1.95	1.61
Von-Mises stress [MPa]	179.91	169.81	169.91	179.67	177.16	169.80	185.52
Mid-span deflection [mm]	12.98	13.69	16.82	18.49	23.93	11.45	20.83

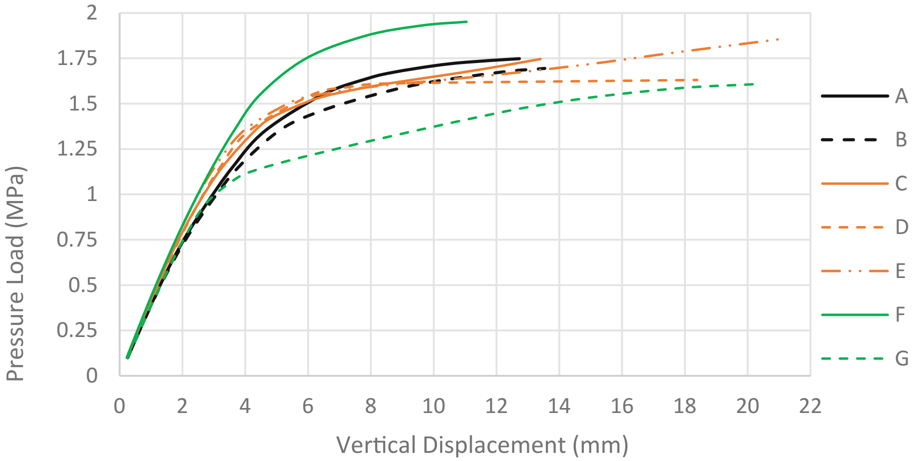

Fig. 9. Load-deflection curves for 1 m pinned beams

Both optimised cross-sections A and B have performed well in this comparison, and show relatively low levels of deflections. Novel cross-section F is quite significantly the most efficient however, showing both the highest failure load and the lowest deflection simultaneously.

Results - Columns. Two of the optimised shapes were chosen to be analysed; one with large stiffness in one axis and one with equal stiffness about both axes. In addition, two conventional and two novel shape sections with similar mass were chosen for a comparative analysis similarly to the beams. The tested cross-sectional profiles are shown in Fig. 10.

The models were constrained with pined support conditions. All translational degrees of freedom were restrained at both ends, apart from the one in the axial direction at one end. A compressive axial load was applied to the column extrusions by specifying pressure on the top face. The critical buckling loads and their corresponding deflections were extracted for all cross-section models (shown in Table 5). The performance of all sections is also presented in the load-deflection curve Fig. 11.

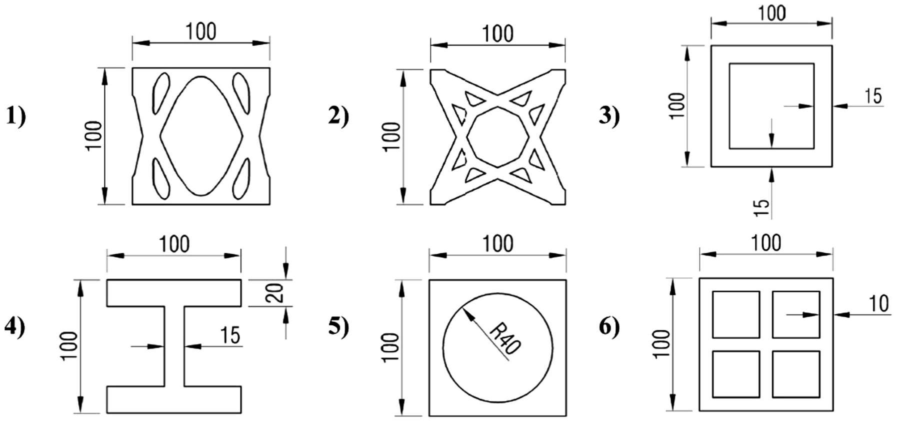

Fig. 10. Column cross-sections employed in finite element analysis

Table 5. Analysis results for 2 m pinned columns

Section	1	2	3	4	5	6
Ultimate load [N/mm^2]	154.09	144.94	151.01	144.94	155.44	151.01
Deflection at mid-span [mm]	0.67	1.66	0.53	1.43	0.59	0.72
Max lateral deflection [mm]	0.72	1.80	0.58	1.58	0.64	0.78
Vertical deflection [mm]	4.43	4.29	4.38	4.27	4.47	4.40

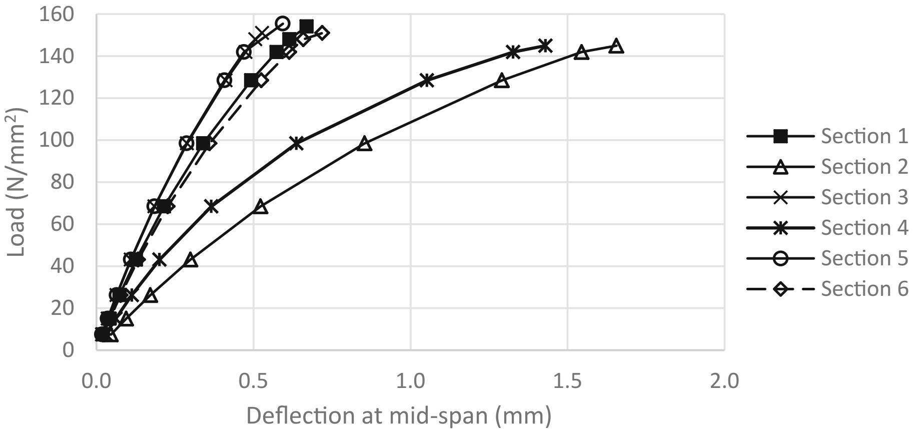

Fig. 11. Load-deflection curves for 2 m pinned columns

A clear separation between Sections 2 and 4, and the rest of the specimens is observed with Sections 2 and 4 indicating the worst performance. Despite the same load limit, Section 2 shows a worse response due to the largest magnitude of the lateral deflection at mid-span. Even though Section 4 (H-section) column stiffness in the minor axis (z-z) is lower than any other sections, it does not experience the largest deflection. Instead, Section 2 was the one that performed poorly in terms of lateral deflection. Thus, it can be concluded that Section 2 has the smallest stiffness and load-capacity out of all the specimens, despite being one of the two optimised cross-sectional profiles. Analysis results for Section 5 indicate the best performance. This box section with a circular hollow, despite possessing a smaller cross-sectional area, performed better than a standard box section (Section 3). Section 1 – one of the two optimised cross-sections – indicated a better performance than most within the comparison. Therefore, Section 1 is only slightly weaker than the stiffest (Section 5). Sections 3 and 6 also performed relatively well. Surprisingly, a square box section without internal stiffeners (Section 3) performed better than a square box section with stiffeners (Section 6).

6 Concluding Remarks

Extrusion processes and 3D printing provides engineers the freedom to design structural products that cannot be manufactured with traditional ways such as the typical steel members made through a cold or a hot formed process. Especially, the most recently developed 3D printed manufacturing process, is a process of adding material, as opposed to subtracting material in the classic methods, and allows for more intricate optimised shapes that inherently provide strength and stiffness. This has given engineers an unprecedented chance to design lighter, more organic looking products which are aesthetically pleasing and practical and fully exploit the advanced optimisation tools to design new structural elements. Moreover, 3D printing offers another benefit to design engineers; no supply chain is required. The final product does not need welding and bolting anymore and this guarantees its long lasting performance.

In this paper, new cross-sectional topologies for aluminium structural members have been investigated through structural topology optimisation. A series of unique cross-sections have been generated using the SIMP technique, subject to different loading and support conditions. A tailored method for post-processing the 2D planar results is presented which aimed to address stability and manufacturability criteria. In this way, different density plots have been overlaid to identify the most frequently stressed areas of the cross-section, which resulted in five novel section profiles for beams and columns. A 3D optimisation approach was also presented to identify correlation between 2D and 3D results.

Both approaches for beams and columns predominantly result in complex hollow-like sections, with a large central opening and other smaller peripheral openings. Due to the square (but also the rectangular) design domain, most sections have a similar moment of inertia about both axes. Beam sections have an approximately central neutral axis despite only one plane of symmetry has been applied. As it was expected, all column sections are symmetric about both axes and have high or equal stiffness about one or two axes, respectively. Four of the optimised cross-sections are compared with a range of more conventional aluminium profiles under static loads using a FEA package. Results for beams and columns are presented, and indicate that the optimised cross-sections are able to provide a large stiffness and out-perform some conventional profiles, with one typology demonstrating the best efficiency for both beams and columns. The next step of this research project is to experimentally test the optimised scaled beam and column members manufactured through extrusion and 3D printing processes, with scope to investigate their structural performance under bending, compression (and combined actions) as well as fatigue. Due to the 3D printing process, surface roughness and crack control should be also checked at that stage in order to achieve similar stiffness in static and cyclic loads. Thus, safety factors will be employed in an attempt to allow Eurocode 9 for the design of such 3D printed and optimised aluminium structural elements.

References

1. Mazzolani, F.M.: Aluminium Alloy Structures. CRC Press, London (1994)
2. Muller, U.: Introduction to Structural Aluminium Design. Whittles Publishing, Scotland (2011)
3. Dwight, J.: Aluminium Design and Construction. E & FN SPON, London (1999)
4. Mazzolani, F.M. (ed.): Aluminium structural design. In: CISM- International Center for Mechanical Sciences- Courses and Lectures, vol. 443. Springer, New York, Udine, Italy (2003)
5. Bendsoe, M.P., Sigmund, O.: Topology Optimization: Theory, Methods, and Applications. Springer Science & Business Media, Berlin (2013)
6. Anand, K., Misra, A.: Topology optimization and structural analysis of simple column and short pressurized beams using optimality criterion approach in ANSYS. IRJET **02**(3), 1408–1415 (2015)
7. Bochenek, B., Tajs-Zielińska, K.: Minimal compliance topologies for maximal buckling load of columns. Struct. Multidisc. Optim. **51**(5), 1149–1157 (2015)
8. Zuberi, R.H., Zhengxing, Z., Kai, L.: Topological optimization of beam cross section by employing extrusion constraint. In: Proceedings of ISCM II and EPMESC XII, vol. 1233(1), pp. 964–969 (2010)
9. CEN/TC250/SC9, EN 1999-Eurocode 9: Design of aluminium structures- Part 1-1: General structural rules, CEN-European Committee for Standardisation, Brussels, Belgium (2007)
10. Kim, Y., Kim, T.: Topology optimization of beam cross sections. Int. J. Solids Struct. **37**(3), 477–493 (2000)

Manufacturing Process Chain

Finite Element Modeling of Ceramic Deposition by LBM(SLM) Additive Manufacturing

Qiang Chen, Gildas Guillemot, Charles-André Gandin, and Michel Bellet(✉)

Cemef, Mines ParisTech, PSL Research University,
UMR CNRS, 7635 Sophia Antipolis, France
`michel.bellet@mines-paristech.fr`

Abstract. The Marangoni effect caused by surface tension gradient is modeled. The resulting convection flow in the melt pool is demonstrated with different values of the Marangoni coefficient. Its influence on the temperature distribution, the shape of melt pool and thus the shape of solidified track is presented. The role of Marangoni convection on the stability of melt pool and the surface quality of the final track are also discussed.

Keywords: Additive Manufacturing · Selective Laser Melting · Melt pool shape · Surface tension · Marangoni effect

1 Introduction

Additive Manufacturing (AM) is largely developed during the last decade and many processes become available for different materials. Among them, Laser Beam Melting (LBM), or Selective Laser Melting (SLM) process gets peoples' attention, especially in the aeronautic industry, for the fabrication of complex parts like turbines. On the other hand, ceramic materials like the $Al_2O_3 - ZrO_2$ eutectic are of interest for this kind of parts, due to their good performance at high temperature. However, traditional forming processes of ceramics are limited by the geometrical complexity of parts. Thus, the application of LBM(SLM) may be a solution as it is reported that fully dense parts with near net shape can be achieved [1].

In LBM(SLM) process, the surface tension and Marangoni effect play an important role in the creation of convection flow in the melt pool. These convection flows can eventually modify the temperature distribution and the melt pool shape, thus leading to a different solidified track shape. The surface tension results also into surface oscillations and even interrupted fragments of the melt pool (balling effect) when the length/circumference ratio of melt pool attains a limit [2]. The balling effect was observed and analyzed by Gu and Shen [3], and reproduced by numerical simulation by Khairallah *et al.* [4]. Moreover, the Marangoni effect also appears in the process, induced by the surface tension evolution with respect to temperature. It is considered to be very important both

© Springer International Publishing AG 2018
M. Meboldt and C. Klahn (eds.), *Industrializing Additive Manufacturing - Proceedings of Additive Manufacturing in Products and Applications - AMPA2017*,
DOI 10.1007/978-3-319-66866-6_5

for the melt pool shape and the temperature distribution inside it [5]. Under this effect, the convection flow is driven from low toward high surface tension domain. Yuan and Gu [6] developed a 3D finite volume method taking into account the Marangoni effect for SLM of TiC/AlSi10Mg nanocomposites. A wider and shallower melt pool was obtained with a negative Marangoni coefficient. Qiu *et al.* [7] modeled the surface tension and Marangoni flow together with recoil pressure with regularly packed Ti-6Al-4V powder particles. They recognized the significant influence of Marangoni force and recoil pressure on the melt splashing and thus the instability of melt pool. Khairallah *et al.* [4] used a fine-scale model with randomly packed 316 L stainless steel powder particles. They concluded that the Marangoni flow induces the circulation of melt flow and hence cools the location of the laser spot. It can also result into liquid spattering away from the surface due to the low viscosity of liquid.

In this work, a Finite Element (FE) model with level set formulation is proposed for the simulation of LBM(SLM) [8]. It is implemented in the numerical simulation library *Cimlib*, developed in *Cemef*. The Marangoni effect is considered, in addition to the surface tension. The resulting convection flow is presented and its influence on the temperature distribution is demonstrated. The melt pool shape under different Marangoni coefficients is also discussed, together with its consequence on the solidified track shape.

2 Modeling

The system consists of the gas and material domain, as shown in Fig. 1. Although we intend to process the ceramic of $Al_2O_3-ZrO_2$ eutectic in the project, we do begin with pure alumina due to its simple properties compared to $Al_2O_3-ZrO_2$ eutectic and tests have been carried out by our collaborators. This choice simplify the modeling, but the model developed here is certainly more general and can be used for other materials. Thus, alumina is chosen in our modeling, both for the substrate and the powder. The porous powder layer is deposited on the fully dense substrate. The densification by the melting of powder is modeled through the variation of apparent density. A level set at the gas and material boundary is employed in order to follow the evolution of the surface of melt pool (driven by the surface tension, the Marangoni effect, etc.) and solidified track. The precision of level set is guaranteed by the mesh adaptation. All conservation equations are averaged over the whole system with different material properties for gas and material domains. Principal assumptions are as follows:

- the powder is assimilated to a continuum;
- no powder projection is considered (*i.e.* no powder loss);
- the possible residual porosity is not modeled (*i.e.* no release of dissolved gas to form pores; no gas entrapment accounted for).

2.1 Level Set Method

As schematized in Fig. 1, the gas/material boundary is immersed in the system and a level set (LS) function ψ is defined to track this boundary ($\psi = 0$). This

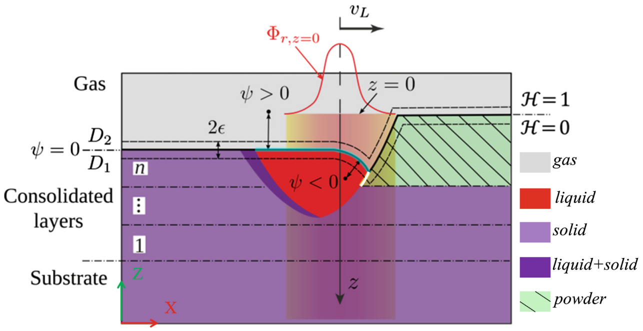

Fig. 1. Modeling schema of AM by LBM(SLM) with the level set method to track gas/material boundary $\psi = 0$.

is a signed distance function with respect to the boundary which is taken as positive in the gas and negative in the material domain. A continuous transition zone is then introduced around the boundary with a half-thickness ϵ, where a Heaviside function ψ is defined continuously:

$$\mathcal{H}(\psi) = \begin{cases} 0 & \text{if } \psi < -\epsilon \, (\text{material}) \\ \frac{1}{2}\left[1 + \frac{\psi}{\epsilon} + \frac{1}{\pi}\sin\left(\frac{\pi\psi}{\epsilon}\right)\right] & \text{if } \mid \psi \mid \leqslant \epsilon \\ 1 & \text{if } \psi > \epsilon \, (\text{gas}) \end{cases} \tag{1}$$

The local value of any global property $\{\chi\}$ is averaged between two domains by the Heaviside [9] function:

$$\{\chi\} = \mathcal{H}\chi^{D_2} + (1 - \mathcal{H})\chi^{D_1} \tag{2}$$

where $\langle\chi\rangle^{D_i}$ ($i = 1$ for material and $i = 2$ for gas) denotes the volume average property homogenized between phases. This treatment is used for density, enthalpy, thermal conductivity, absorption and viscosity. It avoids the sudden change of properties and reduces the difficulty of numerical resolution.

2.2 Governing Equations

At first, the unsteady heat transfer equation taking into account the convection and diffusion is solved:

$$\frac{\partial\{\rho h\}}{\partial t} + \nabla \cdot \{\rho h \boldsymbol{u}\} - \nabla \cdot (\{\kappa\}\nabla T) = \{\dot{q_L}\} - \{\dot{q_r}\} \tag{3}$$

where T is the temperature, ρ is the density, h is the enthalpy per unit mass and λ is the thermal conductivity. The convection velocity, $\boldsymbol{u}$, is deduced by the solving the Navier-Stokes equation. $\dot{q}_r$ is the heat loss by radiation at the material surface. The volume heat source based on the Beer-Lambert law, $\dot{q}_L$, writes:

$$\dot{q}_L\left(r, z\right) = (1 - R)\,\frac{P_L}{2\pi\sigma_L^2}\exp\left(-\frac{r^2}{2\sigma_L^2}\right)\alpha\exp\left(-\int_0^z \alpha \mathrm{d}\,l\right) \tag{4}$$

where R is the reflection coefficient at the material surface, P_L is the nominal laser power, α is the local absorption coefficient, r is the radial distance to the laser axe and z is the flux propagation direction. σ_L is the standard deviation of the Gaussian distribution. It is equal to $R_L/2$ if no laser dispersion in powder is considered.

The velocity is calculated in the whole system by the resolution of the momentum conservation equation:

$$\{\rho\}\left(\frac{\partial\{\boldsymbol{u}\}}{\partial\, t} + \left(\{\boldsymbol{u}\}\cdot\nabla\right)\{\boldsymbol{u}\}\right) - \nabla\cdot\{\underline{\underline{\boldsymbol{\sigma}}}\} = \boldsymbol{f}_s + \boldsymbol{f}_m + \{\rho\}\boldsymbol{g} \tag{5}$$

where $\boldsymbol{u}$ is the velocity, $\boldsymbol{f}_s$ is the surface tension force, $\boldsymbol{f}_m$ is the Marangoni force, $\boldsymbol{g}$ is the gravity, and $\underline{\underline{\boldsymbol{\sigma}}}$ is the stress tensor respecting a compressible Newtonian constitutive law [8]. The surface tension $\boldsymbol{f}_s$ and the Marangoni force $\boldsymbol{f}_m$ can be respectively expressed by:

$$\boldsymbol{f}_s = \gamma\kappa\boldsymbol{n}, \quad \boldsymbol{f}_m = \frac{\partial\gamma}{\partial\, T}\nabla_s T \tag{6}$$

where γ is the surface tension coefficient, $\kappa = -\nabla\cdot\boldsymbol{n}$ is the average curvature, $\boldsymbol{n}$ is the unit vector normal to the interface and $\nabla_s T = \nabla T - (\nabla T\cdot\boldsymbol{n})\,\boldsymbol{n}$ is the surface temperature gradient. Note that both the surface tension and Marangoni force are imposed at the gas/liquid interface (light blue curve in Fig. 1) and at the powder/liquid boundary (white curve in Fig. 1). As these interfaces are immersed in the system, $\boldsymbol{f}_s$ and $\boldsymbol{f}_m$ are multiplied by the Dirac function $\delta(= \partial\mathcal{H}/\partial\psi)$ using the CSF method [10] to transform them into volumetric forces. The momentum conservation is coupled with the mass conservation:

$$\nabla\cdot\{\boldsymbol{u}\} = \dot{\theta} \tag{7}$$

where $\dot{\theta}$ is the shrinkage rate deduced from the variation of apparent density [8].

The velocity obtained by solving Eqs. (5) and (7) is used to update the gas/material boundary by the transport of the level set function ψ:

$$\frac{d\psi}{dt} = \frac{\partial\psi}{\partial\, t} + \boldsymbol{u}^{LS}\cdot\nabla\psi = 0 \tag{8}$$

where $\boldsymbol{u}^{LS}$ denotes the velocity at the boundary represented by $\psi = 0$. However, the distance obtained by this resolution is only geometrically valid at the boundary $\psi = 0$. Therefore, ψ is recomputed after the resolution of Eq. (8) by a geometrical method [11] with respect to the new position $\psi = 0$.

2.3 Simulation Configuration

The dimension of the whole system is $3 \times 0.5 \times 1.1\,\mathrm{mm}^3$. The substrate with a height of 1 mm is at the bottom and a layer of powder with thickness 30 µm is deposited on it. The rest corresponds to the air domain. A laser beam with an effective power $P_L(1-R) = 80\,\mathrm{W}$ and a radius $R_L = 35\,\mu\mathrm{m}$ is applied. It moves from position $(X_S, Y_S) = (0.2, 0.25)$ mm to position $(X_E, Y_E) = (2.8, 0.25)$ mm with a scanning velocity of $0.3\,\mathrm{m\ s^{-1}}$. At the end, the heat source is abruptly switched off but the simulation continues until all the liquid is solidified. Boundary conditions and material properties are given in Tables 1 and 2, more details can be found in [8]. The Marangoni coefficient $\partial\gamma/\partial T$ is compared in literature with values varying between -4.8×10^{-4} to $-6 \times 10^{-5}\,\mathrm{N\,m^{-1}\,K^{-1}}$ [12].

Table 1. Boundary conditions for thermal and mechanical resolutions

	Thermal	Fluid mechanic
Bottom	Imposed convection with heat transfer coefficient	$\boldsymbol{u} = 0$
4 lateral faces	$h_T = 40\,\mathrm{W\,m^{-2}\,K^{-1}}$	$\boldsymbol{u} \cdot \boldsymbol{n} = 0$
Top	Adiabatic	Free

Table 2. Alumina properties used in simulation

Properties	Value	Unit	Ref.
Alumina density	3800	$\mathrm{kg\,m^{-1}}$	[13]
Gas density	1.3	$\mathrm{kg\,m^{-3}}$	
Specific enthalpy of alumina	Fig. 5(a) in [8]	$\mathrm{J\,kg^{-1}}$	[14]
Heat capacity of gas	1000	$\mathrm{J\,kg^{-1}\,K^{-1}}$	
Alumina conductivity	$5.5 + 34.5\exp(-0.0033T)$ $T \in [25, 1300]$ °C	$\mathrm{W\,m^{-1}\,K^{-1}}$	[15]
Gas conductivity	0.024	$\mathrm{W\,m^{-1}\,K^{-1}}$	
Viscosity of liquid alumina	0.069	Pa s	[16]
Viscosity of gas	2.4×10^{-5}	Pa s	
Surface tension liquid/gas	0.67	$\mathrm{N\,m^{-1}}$	[17]

The Marangoni effect is investigated by case 1 to 3 with $\partial\gamma/\partial T = -2 \times 10^{-4}$, 0 and $2 \times 10^{-4}\,\mathrm{N\,m^{-1}\,K^{-1}}$, respectively. However, $\partial\gamma/\partial T$ is only used for taking into account the Marangoni effect, while a constant $\gamma = 0.67\,\mathrm{N\,m^{-1}}$ is always taken for the surface tension, considering its small variation under $\partial\gamma/\partial T$.

3 Results and Discussion

Figure 2(a) shows the temperature field and the iso-contours for case 1. One can note that the tail shape of the iso-contour changes during cooling, from a convex

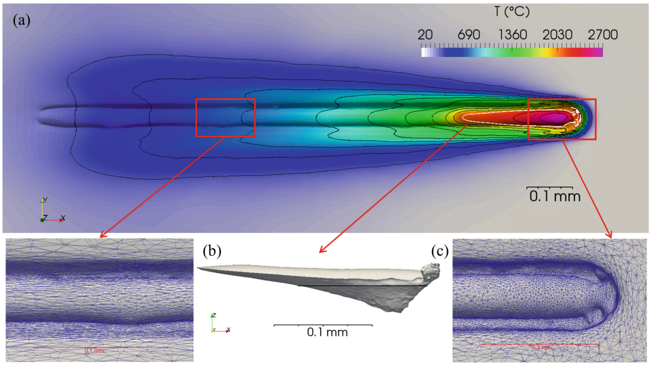

Fig. 2. (a) Temperature field (top view) with iso-contours (black line, 300 to 2700 °C with the step $\Delta T = 200$ °C, white line for $T = T^l = 2104$ °C); (b) the shape of melt pool (black lines for the surface position of substrate) and (c) the mesh at $t = 4$ ms of case 1.

contour shape at high temperature to a non-convex shape at low temperature. For instance, the iso-contour $T = 1100$ °C reveals a tail hotter than the powder on the sides while it is inversed for $T = 300$ °C. This is due to the low thermal conductivity of the powder, leading to a slower heat extraction. The melt pool shape is presented in Fig. 2(b). It has a long tail and its penetration depth into the substrate is about 50 µm. The mesh adaptation is shown in Fig. 2(c). Generally, the mesh size is fine in the melt pool and coarse in the scanning direction in the solidified track. The surface with high curvature (*e.g.* droplets at the front of melt pool) is furtherly refined and well represented.

The temperature field with iso-contours is shown in Fig. 3 for case 1 to 3. Compared with case 2, case 1 with negative $\partial\gamma/\partial T$ shows a slightly wider (more visible for the iso-contours $T = 2300$ and 2500 °C) and longer melt pool, while

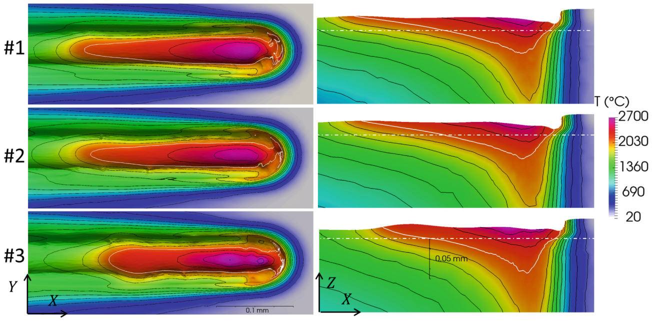

Fig. 3. Comparison of temperature distribution with iso-contours (same as Fig. 2) and the shape of melt pool (top and longitudinal cut view) in case 1 to 3 at $t = 4$ ms. Dashed white line represents the surface of substrate.

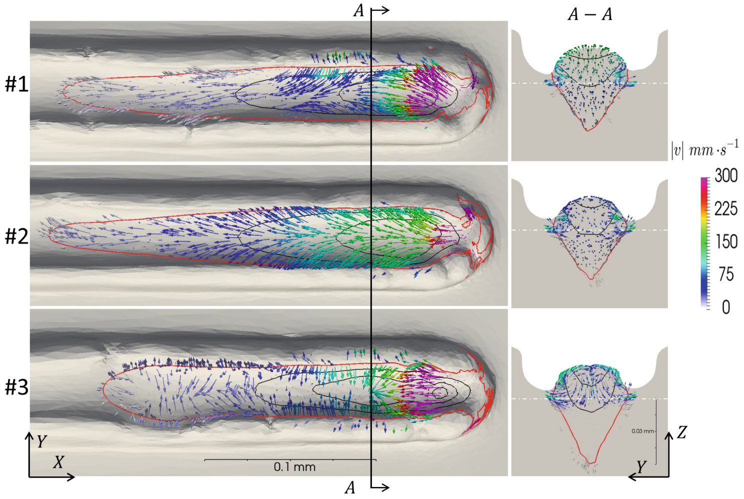

Fig. 4. Comparison of velocity field (top and transversal cut view) in case 1 to 3 at $t = 4$ ms, together with the temperature iso-contours $T = T^l = 2104$ °C (red), $T = 2300$, 2500, 2700 °C (black).

the influence on the depth is not obvious. This is due to the centrifugal convection flow from the high to the low temperature region (*i.e.* from low to high γ value). This convection flow can homogenize the temperature in the melt pool. For case 3 with positive $\partial\gamma/\partial T$, the Marangoni effect creates a centripetal convection from low to high temperature region (*i.e* from low to high γ value), thus leading to a shorter and narrower melt pool. Even though it is not very evident, one can note that from the case 1 to 3, the melt pool becomes deeper and deeper. To understand this effect, the convection flow induced by Marangoni force is shown in Fig. 4 in both top and transversal cross sections. Firstly, for all cases, at the front of the melt pool, there is an unstable zone with high velocity. It is caused by condensation of melted powder in liquid droplets that falls into the pool to feed it. This phenomenon results into a wave towards the tail of the melt pool, together with heat flux. For case 1 with negative $\partial\gamma/\partial T$, one can see that the fluid has a tendency to flow toward the two sides of the melt pool. It is more evident in the cut view $A - A$. At the center of the melt pool, the liquid rises up. Two convection cells are seen with opposite and outward directions. The melt pool is thus expanded by the liquid movement driven at the surface, from the center to the two sides of melt pool. This means that the heat at the center is also taken away to the two sides. However, as the Marangoni force applies only at the gas/liquid interface, the convection cells are limited at certain depth ($\sim 15\,\mu$m) bellow the substrate surface. By contrast, the convection cells are inversed in case 3 with $\partial\gamma/\partial T$. Liquid moves inward from the sides to the center at the melt pool surface. At the symmetric plan, the liquid flows downward, trying to dig into the melt pool, consequently forming a deeper pool. The heat is indeed taken away from the surface center to the depth of the melt pool. It should be mentioned that the Marangoni effect is not very pronounced on the melt pool shape due to the high viscosity of alumina.

Figure 5 aims at comparing the surface oscillations of the solidified track. Color code represents the track height with respect to the substrate surface. Height iso-contours are also presented, showing clearly surface oscillations through hills and valleys. The quasi-periodical stable regime begin after a scanning distance of about 0.2 mm. Comparing the color contrast between hills and valleys for each case, one can easily find that the oscillations increase from case 1 to case 3. In fact, in case 3, the track has tendency to be fragmented at the valleys. This does not occur as melt pool solidification takes place before fragmentation, thus ensuring a continuous track. With a longer melt pool, the balling effect may appear. There are less surface oscillations in case 1. This may be due to the liquid movement from hills to valleys with a negative $\partial\gamma/\partial T$. It means that a negative $\partial\gamma/\partial T$ may help to obtain a smoother surface and avoid balling effect. This observation may be useful for the process as we may change $\partial\gamma/\partial T$ by slightly modifying the material composition or by consciously choose the protection gas.

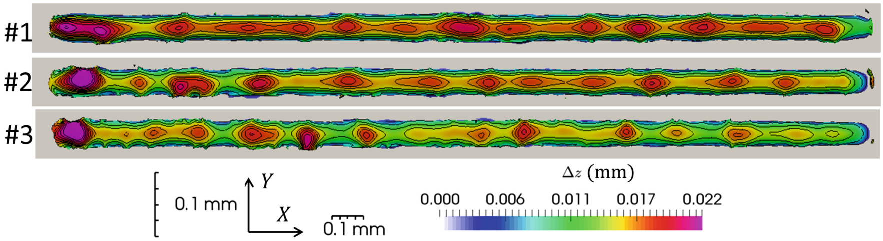

Fig. 5. Height of solidified tracks with respect to the substrate surface and iso-contours in case 1 to 3. Note that it is scaled by factor 2 in the Y direction.

4 Conclusions

In this work, the Marangoni effect in LBM(SLM) is modeled and presented by FE simulation with a LS approach at the scale of track formation. The convection flow induced by Marangoni force is shown, as well as its important influence on the temperature field and the melt pool shape. A negative Marangoni coefficient leads to a wider and longer melt pool while a positive coefficient results into a shorter, narrower and deeper one. The influence of Marangoni effect on the surface quality is also investigated. A negative Marangoni coefficient may help to decrease the surface oscillations of final tracks. This leads to a better thickness homogeneity of the next powder layer and improves the quality of developed tracks.

Acknowledgements. This work has been conducted within the framework of the CEFALE project, part of the ACLAME program funded by the Institut CARNOT MINES (Paris, FR). The authors would like to thank Christophe Colin, Jean-Dominique Bartout, Marie-Hélène Berger and Liliana Moniz Da Silva Sancho from MINES ParisTech Centre des Matériaux (Evry, FR) for invaluable information regarding AM by LBM(SLM) and ceramic materials.

References

1. Hagedorn, Y.-C., Wilkes, J., Meiners, W., Wissenbach, K., Poprawe, R.: Net shaped high performance oxide ceramic parts by selective laser melting. Phys. Proc. **5**, 587–594 (2010). doi:10.1016/j.phpro.2010.08.086
2. Gusarov, A.V., Yadroitsev, I., Bertrand, Ph., Smurov, I.: Heat transfer modelling and stability analysis of selective laser melting. App. Surf. Sci. **254**, 975–979 (2007). doi:10.1016/j.apsusc.2007.08.074
3. Gu, D., Shen, Y.: Balling phenomena in direct laser sintering of stainless steel powder: metallurgical mechanisms and controls methods. Mater. Des. **30**, 2903–2910 (2009). doi:10.1016/j.matdes.2009.01.013
4. Khairallah, S.A., Anderson, A.T., Rubenchik, A., King, W.E.: Laser powder-bed fusion additive manufacturing: physics of complex melt flow and formation mechanisms of pores, spatter, and denudation zones. Acta Mater. **108**, 36–45 (2016). doi:10.1016/j.actamat.2016.02.014
5. Chan, C., Mazumder, J., Chen, M.M.: A two-dimensional transient model for convection in laser melted pool. Meta. Trans. A **15**, 2175–2184 (1984). doi:10.1007/BF02647100
6. Yuan, P., Gu, D.: Molten pool behavior and its physical mechanism during selective laser melting of TiC/AlSi10Mg nanocomposites: simulation and experiments. J. Phy. D: App. Phy. **48**, 035303 (2015). doi:10.1088/0022-3727/48/3/035303
7. Qiu, C., Panwisawas, C., Ward, M., Basoalto, H.C., Brooks, J.W., Attallah, M.M.: On the role of melt flow into the surface structure and porosity development during selective laser melting. Acta Mater. **96**, 72–79 (2015). doi:10.1016/j.actamat.2015.06.004
8. Chen, Q., Guillemot, G., Gandin, C.-A., Bellet, M.: Three-dimensional finite element thermomechanical modeling of additive manufacturing by selective laser melting for ceramics materials. Add. Manu. **16**, 124–137 (2017). doi:10.1016/j.addma.2017.02.005
9. Desmaison, O., Bellet, M., Guillemot, G.: A level set approach for the simulation of the multipass hybrid laser/GMA welding process. Comput. Mater. Sci. **91**, 240–250 (2014). doi:10.1016/j.commatsci.2014.04.036
10. Brackbill, J.U., Kothe, D.B., Zemach, C.: A continuum method for modeling surface tension. J. Comput. Phys. **100**, 335–354 (1992). doi:10.1016/0021-9991(92)90240-Y
11. Shakoor, M., Scholtes, B., Bouchard, P.-O., Bernacki, M.: An efficient and parallel level set reinitialization method - application to micromechanics and microstructural evolutions. Appl. Math. Model. **39**, 7291–7302 (2015). doi:10.1016/j.apm.2015.03.014
12. Paradis, P.-F., Ishikawa, T.: Surface tension and viscosity measurements of liquid and undercooled alumina by containerless techniques. Jap. Soc. App. Phy. **44**, 5082–5085 (2005). doi:10.1143/JJAP.44.5082

13. Morrell, R.: Handbook of Properties of Technical & Engeering Ceramics. H.M.S.O, London (1985)
14. Chase, M.W.: Thermochemical tables. NIST-JANAF (1998)
15. Touloukian, Y.S., Kirby, R.K., Taylor, R.E., Lee, T.T.R.: Thermal expansion - nonmetallic solids. Thermophys. Prop. Matter. **13**, 176–177 (1984)
16. Kawai, Y., Shiraishi, Y.: Handbook of Physico-chemical Properties at High Temperatures, ISIJ (1988)
17. Lihrmann, J.M., Haggerty, J.S.: Surface tensions of alumina-containing liquids. J. Am. Ceram. Soc. **68**, 81–85 (1985). doi:10.1111/j.1151-2916.1985.tb15269.x

Analysis of the Influence of Shielding and Carrier Gases on the DED Powder Deposition Efficiency for a New Deposition Nozzle Design Solution

Federico Mazzucato(✉), Andrea Marchetti, and Anna Valente

SUPSI, University of Applied Science and Arts of Southern Switzerland,
6928 Manno, Switzerland
`{federico.mazzucato,andrea.marchetti,`
`anna.valente}@supsi.ch`

Abstract. In Direct Energy Deposition of metal parts the powder deposition efficiency is defined as the ratio of the nominal metal powder feed rate to the amount of powder directly involved in the component manufacture. Generally, the powder particles falling into the molten pool represent only a small portion of the total amount of metal particles nominally provided by the feeding system (less than 50% for most of the commercial systems), deteriorating the process performances in terms of powder waste, production time and increasing the production costs. For constant laser power, laser scan speed, and laser spot diameter, the deposition efficiency is primarily associated to the nozzle geometry, feeding system, and powder characteristics (e.g. particle size distribution, particle shape and size).

The current work focuses on the analysis and characterization of the performances of a new generation of high efficiency nozzles with an enhanced design which adopts the inert Argon gas for a double purpose of Shielding and Carrier. The proposed analysis consists in designing and executing an experimental campaign structured as a full factorial Design of Experiments to map the impact of Shielding gas, Carrier, and Ti-6Al-4V powder mass flow on the deposition efficiency by monitoring the resulting geometry of the powder flow. A numerical CFD simulation is also carried out to verify the possibility in deducing a control logic to modulate the aforementioned process parameters on a custom feeding system demonstrator. The metal powder and the benefit of the approach are assessed with regards to an industrial use case.

Keywords: Direct laser deposition · Deposition nozzle solution · Deposition powder efficiency

1 Introduction

Direct Energy Deposition (DED) [1] systems employing powder feeding are getting a large employment in industrial sectors such as aerospace, automotive, and biomedical thanks to its capability to realize Functionally Graded Structures (FGS) with innovative shapes and enhanced functionalities, limiting the metal powder consumption compared

© Springer International Publishing AG 2018
M. Meboldt and C. Klahn (eds.), *Industrializing Additive Manufacturing - Proceedings of Additive Manufacturing in Products and Applications - AMPA2017*,
DOI 10.1007/978-3-319-66866-6_6

to the Selective Laser Melting (SLM) technology. Nevertheless, these systems are highly sensitive to working conditions [2–4] and a still critical process challenge is related to the high energy consumption and production costs related to the process [5]. In particular, the deposition efficiency (also called catchment efficiency) provided by the actual feeding systems remains still low when fine laser spots are employed, deteriorating the overall success and performance of DED technology and increasing both the material waste and the production time [6]. The actual feeding systems employ deposition head with different deposition nozzle solutions that ensure different performances. The common deposition configurations are:

- off-axis configuration, where the deposition head is provided by only one later nozzle not aligned with the laser beam;
- coaxial nozzle configuration, where a conical powder flow ensure an homogeneous powder deposition that surrounds the melt pool;
- multiple-nozzles configuration, where several deposition nozzles not aligned with the laser beam (up to 8 [7]) are arranged around the melt pool providing an omnidirectional powder feeding.

The off-axis deposition nozzle configuration finds large application in welding and cladding laser based technologies, thanks to its capability to get thicker coating layers compared to the traditional technologies, getting an excellent bonding between coating and substrate with reduced pore and crack formation. In DED systems, this solution can ensure very high deposition efficiency (close to 90% [8]) when a perfect alignment between powder and laser beam happens. Nevertheless, its performances strongly depend on the traverse speed if other process parameters are held constant, showing significant limitations in the case of high complex geometric patterns with bidirectional motions and limiting the capabilities of a DED system [9]. On the contrary, coaxial and multiple nozzle configurations ensure a constant and homogeneous powder deposition surrounding the melt pool, independently from the geometry of the pattern and allowing the manufacture of parts with a very complex shape. These nozzle solutions find a widespread employment in DED technology even if their deposition efficiency remains quite low (less than 50%).

The advantages related to the coaxial- and multi-nozzle configurations have encouraged several authors to dedicate attention and efforts in the improvement of the performances of several deposition nozzle solutions, characterizing their fluid-dynamics and powder particle distributions. Lin in [10] underlined how the deposition efficiency in DED strongly depends on the relative dimension between molten pool and cross-sectional area of the powder flow reaching the deposition plane. Particularly, he demonstrated that the Carrier mass flow affects the particle trajectories and an enhanced catchment efficiency is possible by limiting the enlargement of the powder flow in correspondence to the deposition plane. Zhu et al. observed that the local geometry of the substrate affected the powder particle concentration in correspondence to the molten pool, indicating the need to vary the feeder's parameters dynamically to ensure the higher deposition efficiency during the process. Zekovic et al. [12] demonstrated that the stand-off distance plays an important role for an accurate part manufacture and for preventing nozzle damages. Zhang et al. [13] improved the DED deposition efficiency building a deposition vacuum chamber and replacing Argon with Helium as Carrier gas, but increasing the overall cost of the system. Other authors as Yang [14] proposed numerical model to optimize the nozzle geometry with focus in reducing the spread of the powder flux during deposition. Despite the big efforts and researches, for multiple-nozzle deposition head the spread of the powder flow in correspondence to the deposition plane remains still large with an extension ranging between 6 and 8 mm [11, 15, 16], with a consequent very low deposition efficiency for DED systems adopting laser spots of 1 mm or smaller [1].

In this paper, the performances of an innovative double chamber nozzle solution for a multiple-nozzles deposition head are investigated, thus evaluating the shape of the powder flow at the exit of the nozzle outlet and characterizing the spread of the powder particles in correspondence to the deposition plane. Two prototype nozzles are installed in a testing deposition chamber and a high-speed camera is employed to detect the width variation of the powder flow during the experimental analysis. The results are employed to validate a numerical CFD model. The employment of an annular Shielding flux external to the Carrier-powder mixture results to be an effective solution in limiting the spread of the powder flow, reducing the dispersion of the powder particles. This work is part of a bigger research work that has the ambition to design a tailored deposition closed loop control to improve the catchment efficiency of DED systems employing laser spots of 1 mm or finer. The rest of the paper is structured as it follows: Sect. 2 outlines the metal powder and the equipment employed during the experimental tests; Sect. 3 describes the experimental plan and the employed method for image analysis; Sect. 4 briefly introduces the adopted CFD model; Sect. 5 introduces and discusses the obtained experimental results; and Sect. 6 deals with the final conclusions.

2 Material and Equipment

The metal powder employed during this experimental investigation is a gas atomized Ti-6Al-4V powder with a powder grain size ranging between 45 and 105 μm (supplier: EOS GmbH - Electro Optical Systems). Only one batch of metal powder is tested since only the effectiveness of this nozzle solution is investigated. Table 1 outlines the chemical composition of Ti-6Al-4V metal powder.

Table 1. Chemical composition of Ti-6Al-4V powder employed during the experimental tests.

Al (%)	V (%)	C (%)	Fe (%)	O (%)	N (%)	Ti (%)
6	4	0.1	0.3	0.02	0.05	balance

The deposition nozzle solution [17] designed at the Department of Innovative Technologies (DTI) of SUPSI (Manno-CH) is represented in Fig. 1(a) and (b). It consists in a double chamber coaxial nozzle where the central powder-gas flow is shielded by an external annular flux of inert gas with the task to:

- protect the molten pool from oxidation even for no-hermetic deposition chamber;
- limit the spread of the powder flow coming out from the nozzle outlet and reduce the material waste during the deposition process.

In opposition to other nozzle solutions for cladding and welding process, which employ an external shielding gas [8], this modular deposition nozzle allows a more compact design of the deposition head and a lower stand-off distance between the nozzle outlet and the deposition plane. The reduction in the stand-off distance has the double benefit of both increasing the effectiveness of the Shielding gas in limiting the rebounding of the powder particles on the metal substrate, and reducing the laser energy attenuation caused by metal powder scattering and reflection. No more details or additional drawing can be provided since there is a patent pending concerning the deposition nozzle solution introduced in this paper. The chosen Carrier and Shielding inert gas is Argon. Two deposition nozzles are placed with an inclination of 30° inside a custom deposition chamber demonstrator represented in Fig. 1(c). The deposition nozzles are connected with a flexible feeding system that allows the independent and precise control of Shielding, Carrier, and powder mass flow required for the experimental tests.

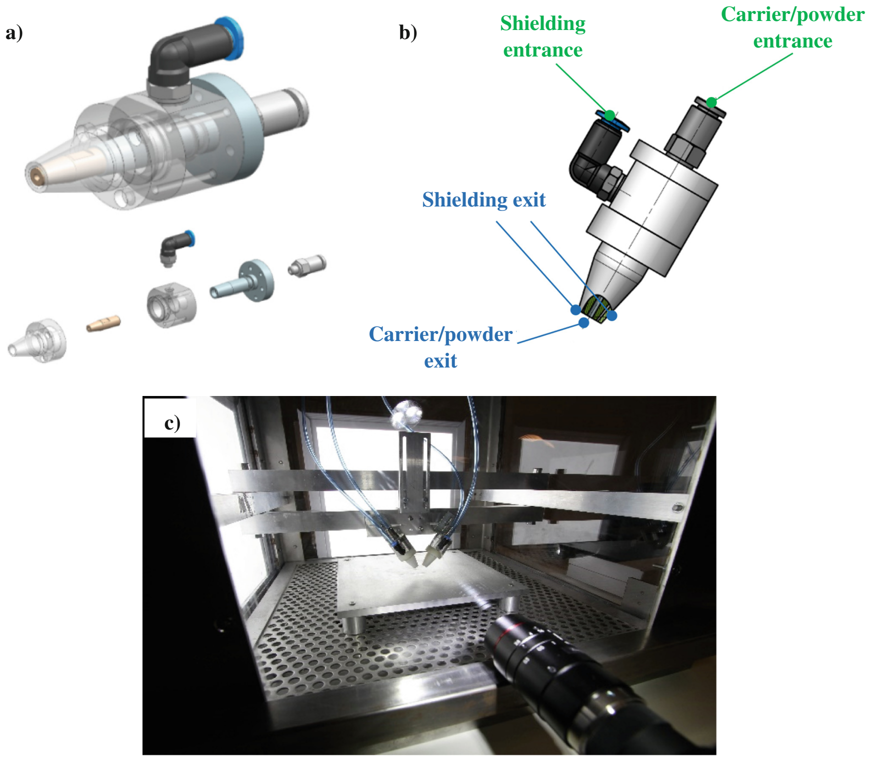

Fig. 1. (a) New deposition nozzle solution; (b) Scheme of the entrance and exit of the Shielding and Carrier gases; (c) Custom feeding system demonstrator at SUPSI.

3 Experimental Procedure

The objective of this experimental campaign is to investigate the performances of a new nozzle solution analysing the powder spread at 15 mm from the nozzle outlet (i.e. the location of the deposition plane). Such objectives have been investigated with a 2 × 3 × 2 full factorial design, according to Design of Experiments (DoE) approach, taking into account the Carrier, Shielding, and powder mass flow rate as experimental factors (see Table 2) and recognising three process conditions (see Fig. 2):

- only one active nozzle without the presence of the substrate;
- two active nozzles without the presence of the substrate;
- two active nozzles with the presence of a flat substrate placed at 15 mm from the centre of the nozzle outlet to evaluate the efficiency of the nozzle solution.

The experimental levels for the experimental factors are chosen following the common ranges adopted in DED [18] whereas a flat substrate is chosen to reproduce the process condition at the first layer deposition. The spread of the powder particles is analysed detecting the 95% of the total powder flow width at the deposition plane. The experimental results are investigated taking into account a confidence interval of 95% and running 3 repetitions for each parameter settings. A high-speed acquisition camera is employed to record the variation of the powder flow for every combination of process parameters.

Table 2. Evaluated experimental factors.

Process parameters for 1 nozzle	Low level	Medium level	High level
Carrier mass flow rate (kg/s)	$4.51e^{-05}$		$5.41e^{-05}$
Shielding flow rate (kg/s)	0	$1.95e^{-04}$	$2.92e^{-04}$
Powder feed rate (g/s)	0.1		0.14

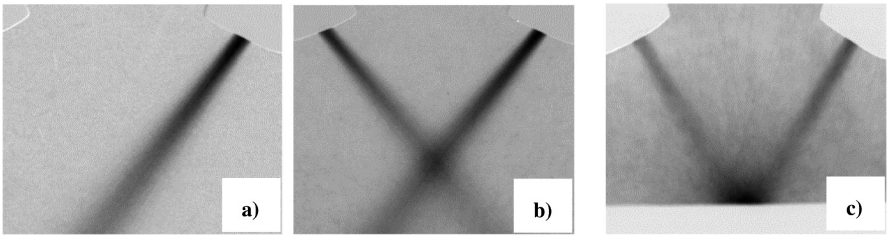

Fig. 2. (a) One active nozzle; (b) 2 active nozzles; (c) 2 active nozzles with substrate at 15 mm.

3.1 Image Analysis Method

The method employed to characterize and measure the shape and width variation of the powder flow is an image based analysis method performed with the open software ImageJ [19]. For each combination of process parameters, the powder flow coming out from the nozzle outlet is recorded after 30 precautionary seconds of flow stabilization. Ten images are extracted from each experimental video and averaged each other to improve the image quality, reducing the presence of undesired floating powder particles which can deteriorate the edges of the powder flow (see Fig. 3a). From the resulting averaged image, the corresponding image background is subtracted and a “binary-mask” filter is applied to show up the profile contours of the powder-gas mixture (see Fig. 3b). The shape of the powder flow is characterized tracing 10 evaluation planes equally spaced as shown in Fig. 3b.

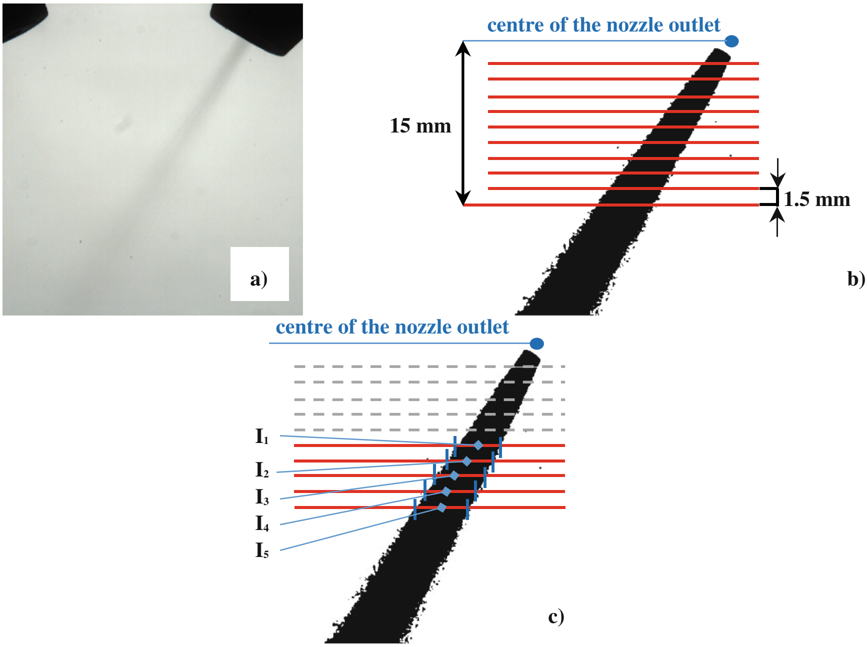

Fig. 3. (a) Acquired image; (b) Evaluation planes on the image filtered by binary-mask (mm); (c) The five planes employed for the intensity threshold detection.

The intensity threshold required for applying the “binary-mask” filter is determined applying an iterative method that forces an equal total intensity of the powder flow on the last five evaluation planes, following the equation below (see Fig. 3c):

$$\frac{\sum_{k=1}^{5} I_k}{5} - \left(\frac{\sum_{k=1}^{5} I_k}{5}\right) 5\% < I_k < \frac{\sum_{k=1}^{5} I_k}{5} + \left(\frac{\sum_{k=1}^{5} I_k}{5}\right) 5\% \quad \forall \mathrm{k} = 1, \ldots, 5 \quad (3.1)$$

where I_k is the total intensity enclosed by the powder flow contours in correspondence of the five evaluation planes located between 15 and 9 mm from the nozzle outlet.

This iterative methodology is performed for every averaged image extracted from the 108 experimental videos.

4 CFD Modeling

The employed numerical model is based on the actual State of the Art on CFD simulations applied at DED process, where the particle powders are modelled as a discrete phase dispersed into a continuous phase represented by the Argon inert gas. This approach is widely employed in the scientific literature to simulate fluid-dynamics problems when a low volume fraction of powder particles is dispersed and dragged by the gas [20, 21]. The numerical simulations are executed through ANSYS ® FLUENT software taking into account a control volume big enough to allow the complete development of the powder flow at the exit of the deposition nozzle. In the case of 2 active nozzles, a symmetry condition is assumed. The powder grain size distribution is considered uniform with an average diameter of 70 µm, neglecting collision between particles.

5 Results and Short Discussion

Table 3 summarizes the experimental results when no substrate is employed. In the case of only one active nozzle, the effects of Shielding gas (p-value = 0.000) and of powder feed rate (p-value = 0.001) are significant. By increasing the powder feed rate from 0.1 to 0.14 g/s, the 95% of the total spread of the powder flow at 15 mm decreases from 4.58 to 4.43 mm in average, thus obtaining an average absolute variation of −9.8% when no Shielding is applied. This proves the effectiveness of the suggested nozzle design. Indeed, it ensures a high particle powder concentration focused at the centre of the flow, thus limiting the powder dispersion. The influence of the Shielding gas on the powder flow profile is consistent for every evaluated combination of process parameters. The external flow of inert gas compacts the powder particles at the exit of the nozzle. Indeed, it contrasts the effect of the gravity force that tends to deflect the powder particles from the nominal trajectory imposed by the nozzle geometry (see Fig. 4a). Increasing the Shielding mass flow rate from 0 to $2.92e^{-04}$ kg/s, the spread of the powder flow at 15 mm from the nozzle outlet reduces up to −14.6% in average. To have a quantitative estimation of the advantage in terms of catchment efficiency, further deposition tests are required where the weight of the realized samples is compared with the nominal quantity of powder provided during the process. Nevertheless, a preliminary estimation of the influence of this nozzle solution on the deposition efficiency can be made considering the geometrical ratio between the nominal area of the melt pool and the projected area of the powder flow on the deposition plane. In this context, taking into account a nominal circular melt pool with a diameter of 1 mm, the deposition efficiency increases from 5% to 7%, indicating an increase close to the 50% of the catchment efficiency when no Shielding is applied. In terms of material and cost saving, an increase in the catchment efficiency from 5% to 7% determines a material saving of 0.9 kg and a significant cost saving of 207 EUR for the manufacture of a small-medium size full-dense part in Ti-6Al-4V with a volume of 33000 mm^3.

Table 3. Summary of the experimental results without the presence of the substrate.

1 active nozzle	Powder feed rate = 0.1 g/s				Powder feed rate = 0.14 g/s			
	Carrier = $4.51e^{-05}$ kg/s		Carrier = $5.41e^{-05}$ kg/s		Carrier = $4.51e^{-05}$ kg/s		Carrier = $5.41e^{-05}$ kg/s	
	95% width (mm)	Variation (%)	95% width (mm)	Variation (%)	95% width (mm)	Variation (%)	95% width (mm)	Variation (%)
Shielding = 0 kg/s	4.93	–	4.98	–	4.77	–	4.97	–
Shielding = $1.95e^{-04}$ kg/s	4.33	−12	4.57	−8.3	4.41	−7.6	4.33	−12.8
Shielding = $2.92e^{-04}$ kg/s	4.29	−13	4.35	−12.7	4.22	−11.5	3.91	−21.3
2 active nozzles	Powder feed rate = 0.2 g/s				Powder feed rate = 0.28 g/s			
	Carrier = $9.02e^{-05}$ kg/s		Carrier = $1.08e^{-04}$ kg/s		Carrier = $9.02e^{-05}$ kg/s		Carrier = $1.08e^{-04}$ kg/s	
	95% width (mm)	Variation (%)	95% width (mm)	Variation (%)	95% width (mm)	Variation (%)	95% width (mm)	Variation (%)
Shielding = 0 kg/s	5.73	–	6.34	–	5.27	–	5.56	–
Shielding = $3.9e^{-04}$ kg/s	5.11	−10.9	5.22	−17.8	4.40	−16.5	5.68	−2.3
Shielding = $5.84e^{-04}$ kg/s	5.29	−7.8	5.58	−12.1	5.32	−1.1	5.64	−1.5

In the case of 2 active nozzles without the presence of substrate, the powder feed rate has a negligible effect (p-value = 0.064) compared to the Shielding (p-value = 0.001) and Carrier gas (p-value = 0.000). By increasing the Carrier gas from $9.02e^{-05}$ to $1.08e^{-04}$ kg/s, the spread of the powder flow increases (see Table 3). This is mainly due to the increase in the Carrier inertia that reduces the effect of the Shielding gas. Moreover, the influence of the Shielding gas is not linear as happened in the process condition with only one active nozzle. In this case, the experimental analysis shows a significant reduction in the powder particles diffusions for medium values of the Shielding gas, followed by a critical enlargement at the highest values. For medium values of the Shielding gas, the 95% of the powder flow width at 15 mm decreases up to −11.8% in average, whereas for higher mass flow rates the width only decreases up to −5.6%. The reason of this behaviour could be related to the location where the two powder flows meet each other. Indeed, increasing the Shielding mass

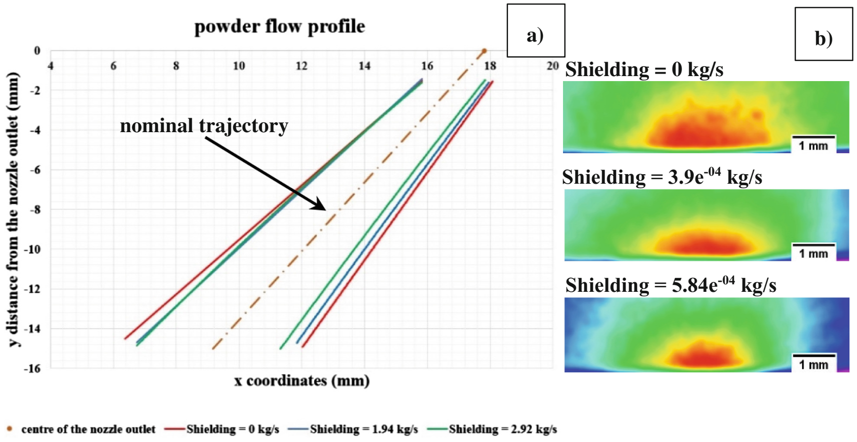

Fig. 4. (a) Influence of the Shielding gas on the powder flow profile (1 active nozzle); (b) Influence of the Shielding gas with the presence of the substrate (2 active nozzles, Carrier = $1.08e^{-04}$ kg/s, powder feed rate = 0.2 g/s)

flow rate from $3.9e^{-04}$ to $5.84e^{-04}$ kg/s the zone where the two powder flows meet each other results to be lowered in comparison with the previous case. This phenomenon affects the measurements since the deposition plane is no more located at 15 mm from the nozzle outlet.

Concerning the case of 2 active nozzles with the presence of the substrate at 15 mm from the nozzle outlet, the acquired images are strongly affected by an high concentration of bouncing powder particles that degrade the image analysis and prevent the application of the image based method discussed in the Sect. 3.1.

For this reason, only a qualitative analysis is possible: it implies evaluating the spectrum of the powder particles distribution in correspondence to the surface of the substrate. Figure 4b shows the effect of the Shielding gas for constant values of Carrier mass flow rate and powder feed rate. The zone with the higher particle concentration results to be qualitatively smaller for higher values of the Shielding mass flow rate. Nevertheless, to have a feedback and a quantitative analysis of the influence of Shielding, Carrier, and powder mass flow on the deposition efficiency of the process under this process conditions, further experimental tests are required.

6 Conclusions

In this paper, a new solution of double chamber deposition nozzle for DED application is introduced and its performances evaluate. The influence of the Shielding mass flow rate, Carrier flow rate, and powder feed rate on the spread of the powder flow coming out from the deposition nozzle is analysed characterising the 95% of the width of the powder flow at 15 mm from the nozzle outlet. The main outputs coming out from this experimental analysis are:

- the three evaluated process conditions show a significant effect of the Shielding mass flow rate;
- for 1 active nozzle, increasing the Shielding mass flow rate up to $2.92e^{-04}$ kg/s the 95% of the deposition area reduces up to −14.6% with a consequent increase in the deposition efficiency;
- a rough estimation of the catchment efficiency show an improvement close to 50% when the Shielding mass flow increases from 0 to $2.92e^{-04}$ kg/s;
- the Shielding gas compacts the powder flow reducing the effect of both the gravity force and Carrier gas inertia that are the main responsible of the spreading of the powder flow;
- during the experimental campaign, the suggested deposition nozzle shows to be an effective solution to reduce the powder spread and improve the performance of DED technology;
- to have a quantitative evaluation of the performance of the deposition nozzles in terms of catchment efficiency, further experimental tests are required, where the weight of the deposited part is compared with the nominal powder feed rate provided during the process;
- the employed CFD model does not fit the experimental results correctly, but an enhanced CFD model is necessary to simulate the process properly.

Acknowledgements. The research has been partially funded by European H2020 Borealis Project (Grant agreement no: 636992).

References

1. Thompson, S.M., Bian, L., Shamsaei, N., Yadollahi, A.: An overview of direct laser deposition for additive manufacturing; part I: transport phenomena, modeling and diagnostics. Addit. Manuf. **8**, 36–62 (2015). doi:10.1016/j.addma.2015.07.001
2. Pinkerton, A.J., Li, L., Lau, W.S.: Effect of powder geometry and composition in coaxial laser deposition of 316L steel for rapid prototyping. CIRP Ann. – Manuf. Technol. **52**, 181–184 (2003). https://doi.org/10.1016/S0007-8506(07)60560-5
3. Kakinuma, Y., Mori, M., Oda, Y., Mori, T., Kashihara, M., Hansel, A., Fujishima, M.: Influence of metal powder characteristics on product quality with directed energy deposition of Inconel 625. CIRP Ann. – Manuf. Technol. **65**, 209–212 (2016). https://doi.org/10.1016/j.cirp.2016.04.058
4. Boisselier, D., Sankaré, S.: Influence of powder characteristics in laser direct metal deposition of SS316L for metallic parts manufacturing. Phy. Proc. **39**, 455–463 (2012). https://doi.org/10.1016/j.phpro.2012.10.061
5. Pinkerton, A.J.: Advances in the modeling of laser direct metal deposition. J. Laser Appl. **27**, S15001 (2015). doi:10.2351/1.4815992
6. Huang, Y., Khamesee, M.B., Toyserkani, E.: A comprehensive analytical model for laser powder-fed additive manufacturing. Addit. Manuf. **12**, 90–99 (2016). doi:10.1016/j.addma.2016.07.001
7. Ding, Y., Dwivedi, R., Kovacevic, R.: Process planning for 8-axis robotized laser-based direct metal deposition system: a case on building revolved part. Robot Cim-Int. Manuf. **44**, 67–76 (2017). doi:10.1016/j.rcim.2016.08.008
8. Arnold, J., Volz, R.: Laser powder technology for cladding and welding. J. Therm. Spray Technol. **8**, 243–248 (1999). doi:10.1007/s11666-999-0001-3
9. Laeng, J., Stewart, J.G., Liou, F.W.: Laser metal forming processes for rapid prototyping – A review. Int. J. Prod. Res. **38**, 3973–3996 (2010). doi:10.1080/002075400501761111
10. Lin, J.: A simple model of powder catchment in coaxial laser cladding. Opt. Laser Technol. **31**, 233–238 (1999). doi:10.1016/S0030-3992(99)00046-8
11. Zhu, G., Li, D., Zhang, A., Tang, Y.: Numerical simulation of metallic powder flow in a coaxial nozzle in laser direct metal deposition. Opt. Laser Technol. **43**, 106–113 (2011). doi:10.1016/j.optlastec.2010.05.012
12. Zekovic, S., Dwivedi, R., Kovacevic, R.: Numerical simulation and experimental investigation of gas-powder flow from radially symmetrical nozzles in laser-based direct metal deposition. Int. J. Mach. Tool Manuf. **47**, 112–123 (2007). doi:10.1016/j.ijmachtools.2006.02.004
13. Zhang, B., Coddet, C.: Numerical study on the effect of pressure and nozzle dimension on particle distribution and velocity in laser cladding under vacuum base on CFD. J. Manuf. Processes **23**, 54–60 (2016). doi:10.1016/j.jmapro.2016.05.019
14. Yang, N.: Concentration model based on movement model of powder flow in coaxial laser cladding. Opt. Laser Technol. **41**, 94–98 (2009). doi:10.1016/j.optlastec.2008.03.008
15. Smurov, J., Doubenskaia, M., Zaitsev, A.: Comprehensive analysis of laser cladding by means of optical diagnostics and numerical simulation. Surf. Coat. Technol. **220**, 112–121 (2013). doi:10.1016/j.surfcoat.2012.10.053

16. Kovaleva, I., Kovalev, O., Zaitsev, A., Smurov, I.: Numerical simulation and comparison of powder jet profiles for different types of coaxial nozzles in direct material deposition. Phys. Proc. **41**, 810–872 (2013). doi:10.1016/j.phpro.2013.03.160
17. Brugnetti, I., Colla, M., Marchetti, A., Valente, A.: Nozzle apparatus for direct energy deposition. Patent pending, App Number: EP16201499 (2016)
18. Task 3.1 Borealis project. http://www.borealisproject.eu/project/
19. ImageJ v1.51 k. https://imagej.nih.gov/ij/
20. Tabernero, I., Lamikiz, A., Ukar, E., de Lacalle, L.L.N., Angulo, C., Urbikain, G.: Numerical simulation and experimental validation of powder flux distribution in coaxial laser cladding. J. Mater. Process. Technol. **210**, 2125–2134 (2010). doi:10.1016/j.jmatprotec.2010.07.036
21. Wen, S.Y., Shin, Y.C., Murthy, J.Y., Sojka, P.E.: Modeling of coaxial powder flow for the laser direct deposition process. Int. J. Heat Mass Trans. **52**, 5867–5877 (2009). doi:10.1016/j.ijheatmasstransfer.2009.07.018

On-Demand Spare Parts for the Marine Industry with Directed Energy Deposition: Propeller Use Case

Wei Ya[1,2,3] and Kelvin Hamilton[4](✉)

[1] Faculty of Engineering Technology,
Department of Mechanics of Solids, Surfaces & Systems (MS3),
University of Twente, P.O. Box 217, 7500 AE Enschede, The Netherlands
[2] Materials innovation institute (M2i),
P.O. Box 5008, 2600 GA Delft, The Netherlands
[3] Rotterdam Additive Manufacture Fieldlab (RAMLAB),
Scheepsbouwweg 8 - K03, 3089 JW Rotterdam, The Netherlands
[4] Autodesk BV, Taurusavenue 3, 2132 LS Hoofddorp, The Netherlands
`kelvin.hamilton@autodesk.com`

Abstract. As additive manufacturing (AM) gains greater industrial exposure, there is a drive towards defining practical, high-value processes and products. Defining viable business cases is critical to ensure successful technology adoption. Given the marine industry's slow uptake of AM, the potential of Wire Arc Additive Manufacturing (WAAM) to produce spare parts on demand is promising. It has the potential to reduce storage and transportation costs of spare parts by bringing production closer to end use locations.

Using a propeller as a familiar marine industry object for a case study, the authors focused and explored four different design iterations to highlight the opportunity and design freedom offered through AM for development time and cost reductions by producing components on a needs basis in close proximity to where they are required. Designing, preparing for manufacture, manufacturing and post processing these components exposes a considerable portion of the process chain from a hardware and software perspectives.

Current trend towards producing locally along with the intersection of Wire and Arc AM, the flexibility offered by software and hardware coupled with high cost pressures of the marine industry make this spare part on-demand concept particularly attractive.

Keywords: Additive Manufacturing (AM) · Wire Arc Additive Manufacturing (WAAM) · Propeller · Design · Welding strategy · Maritime

1 Introduction

Sustainable development and economic pressure drive industries to develop new technologies to reduce cost by repairing or regenerating damaged components [1]. In the past decades, additive manufacturing (AM) has moved from a novel manufacturing process in mainstream research and heading towards industrial applications across multiple sectors [2, 3].

© Springer International Publishing AG 2018
M. Meboldt and C. Klahn (eds.), *Industrializing Additive Manufacturing - Proceedings of Additive Manufacturing in Products and Applications - AMPA2017*,
DOI 10.1007/978-3-319-66866-6_7

Metal AM implementations via different deposition techniques have been reviewed by Frazier [4]. Although current AM research focuses on high energy beam with powder based processes [5–9], Wire Arc AM (WAAM) is one of the promising technologies to sustainably produce large components in a short time due to its low setup cost and relatively high deposition rates. Research focus has centred around aerospace [10] however, in the maritime industry, adoption of AM has been slow therefore, defining and demonstrating viable business cases becomes critical in ensuring successful adoption.

Consider the propeller, a familiar maritime object made from corrosion resistant materials by either casting, forging, or by welding blades to a central hub. Casting typically consists of the following manufacturing steps: designing, molding, and casting, heat treatments, grinding and polishing. Casting porosities need to be inspected if a new design is produced [11]. These times consuming steps were reviewed by Degu and Sridhar [12].

For WAAM to be a viable manufacturing process for propellers, it must meet the business drivers important to the industry. Primarily it would need to offer one or more of the following: (i) cost effective production; (ii) cost reduction in supplier the chain; (iii) comparable or enhanced product quality. This paper focuses on the design and manufacturing process chain (workflow) to achieve the first two requirements. Four different design iterations and fabrication are investigated and aimed at reductions in time and cost. This paper also explores the concept of spare parts on demand as a route to reducing spare parts stockpiles by producing components on a needs basis near to where they are needed. In this case, production was done at the Port of Rotterdam's RAMLAB facility, where a minimalist footprint aims to reduce cost by reducing time and the supply chain itself.

Material used and their properties are mentioned, however this is not the focus of this present paper. Detailed material metallurgical and mechanical properties measurements will be presented in future publications for the proper and intended maritime material. The obtained final manufacturing design and WAAM workflow will be used to implement future production.

2 Setup, Materials and Experiments

Setup and Welding Wire Used. WAAM experiments were performed using Active Wire Production (AWP, MAG welding with 80 Ar/20 CO_2 shielding gas) with a Panasonic TM-1400WG3-AWP 6-axis welding robot and an additional 2-axis workpiece manipulator (type YA-1RJC62) with a maximum handling capacity of 300 kg. Lincoln Electric SG II welding wire (diameter 1.0 mm and Table 1 shows its composition) was used in experiments primarily due to its low cost as this study focuses on design exploration. Experimental conditions are shown in Fig. 1. Optimal conditions were obtained and the corresponding weld bead geometry and processing conditions were used as inputs into the AM module of Autodesk's PowerMILL software to create weld paths for deposition and for controlling and creating effective robot configurations.

Table 1. Chemical compositions of SG II welding wire.

Element	C	Mn	Si	P	S	Cu	Mo
Wt.%	0.07–0.10	1.4–1.6	0.7–1.0	max 0.025	max 0.025	max 0.30	-

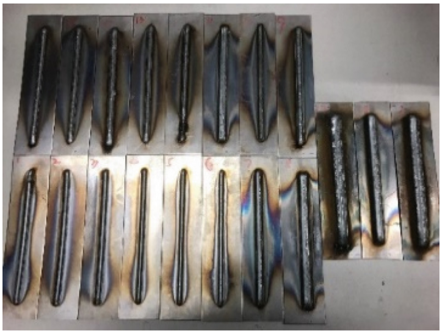

- Welding wire (SG II)
- Thin ST37 steel plate (250 x 60 x 3 mm)
- With active cooling and clamping
- Deposition rate (1.05 – 3.14 kg/hour)
- Welding current (85 – 200 A)
- Welding voltage (16.4 – 23 V)
- Welding speed (0.2-0.4 m/min)
- Shielding gas (80 Ar/20 CO2, 16-20 l/min)

Fig. 1. Samples and tested conditions.

Deposition Efficiency. To minimize geometrical errors (< ± 0.1 mm), deposition rate and efficiency were evaluated based on equations and methods presented by Ya [1]. Figure 2 shows that dense, porosity-free and crack-free layers can be produced with the optimal weld conditions. This figure also shows the layer welding direction perpendicular to the building direction.

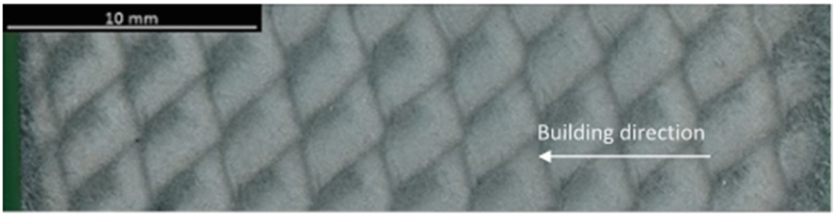

Fig. 2. Dense deposited weld layers.

Figure 3 shows the change of efficiency and microhardness with the energy input. Microhardness was measured with the LECO microhardness tester (LM100AT). As high energy input reduces the cooling rate, larger grains/phases are expected to appear in the weld microstructure which do reduce the hardness. Desirable welding conditions can be derived from Fig. 3 where the material retains enough hardness (energy input of 500 J/mm and 1.2 kg/h of deposition rate).

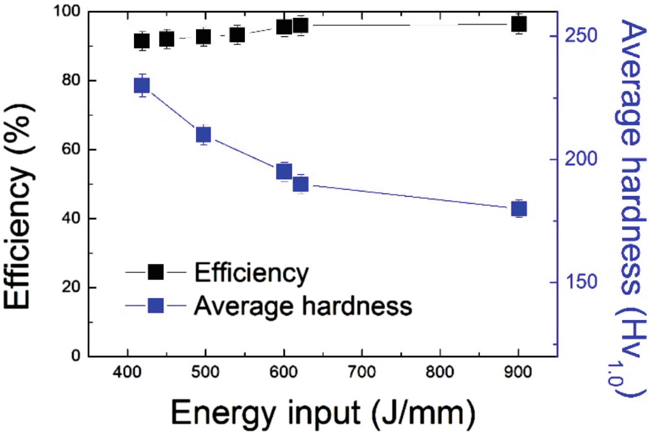

Fig. 3. Efficiency and microhardness.

Deposition Strategies. Two deposition strategies were investigated by depositing two walls (dimensions: 380 × 28 × 500 mm) as shown in Fig. 4. The lateral displacement (step over) between adjacent weld was 3.8 mm and the single weld track width and height are 5.2 mm and 2 mm respectively. After each deposited layer, the torch was moved up 2.75 mm and its travel direction was reversed to control the build-up of material at deposition start and end positions. Samples were then prepared from the deposited walls for standard mechanical tests. The measured results are comparable to the referenced values from the wire manufacturer. The effects of depositing conditions and strategies on material properties will not be discussed as this paper focuses on design aspects.

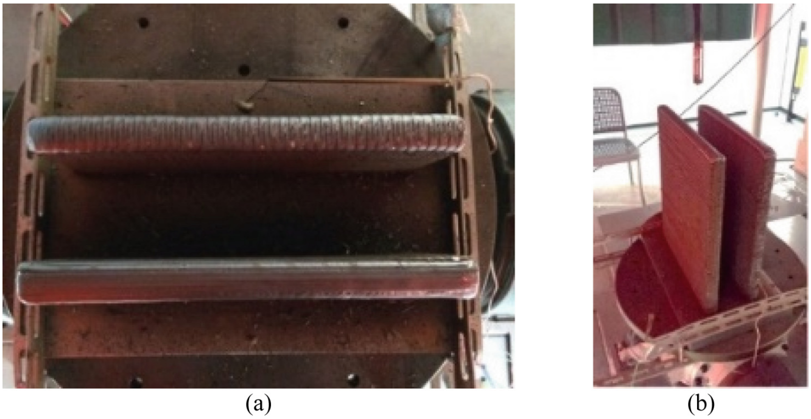
(a) (b)

Fig. 4. Two wall deposited with different patterns, (a) top view; (b) side view.

3 Process Chain: Design Exploration and Manufacture

With appropriate material properties and AM process conditions known, the designed propeller can be manufactured. The propeller shapes were used to investigated not only the new-found design freedom enabled by AM but the suitability of both rapid prototyping and rapid manufacturing. The thermal and negative geometric effects on the part as it is built were considered during the preform creation stage. To avoid excessive heat and distortion during deposition, an active cooling system was used for thermal management. The four designs are described in Figs. 5, 7, 9, and 11.

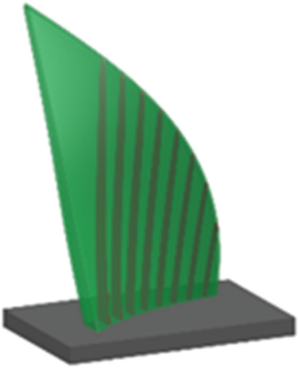

Fig. 5. Single blade with hollow shell (500 mm high).

Design #1 (Fig. 5): Single blade (~ 0.5 m in height) deposited using a single weld bead contour strategy to create a hollow shell blade with 5 mm nominal wall thickness. Additional 5 mm thick stiffening braces across the length of the blade were constructed to provide stiffness. This design explores the potential of manufacturing a hollow

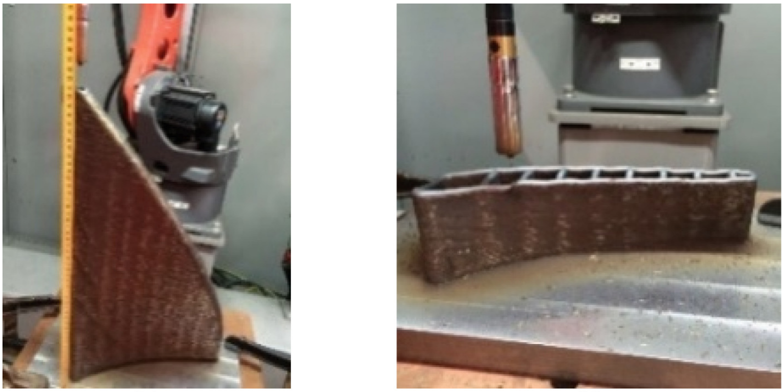

(a) (b)

Fig. 6. As-deposited shape of Design #1, (a) during deposition; (b) after deposition.

propeller which cannot be manufactured with traditional techniques. By changing how material is distributed, this concept can be rapidly prototyped as less material needs to be deposited. The design was manufactured as shown in Fig. 6. Alternately, during service, a single blade of a propeller may be damaged. Regenerating the damaged blade with AM will help to reduce the cost of down time.

Design #2 (Fig. 7): Full propeller (∼0.5 m in diameter) with four hollow blades deposited using an oscillation strategy to create blades with 10 mm nominal thick walls. Although the blades are hollow, excess material (>15 mm thick) was left on the leading and trailing edges to improve the overall strength of the blades. Additional material was deposited to allow the realisation of the final blade fillet with the shaft.

This design, like Design #1, follows the rapid prototyping concept to manufacture a full hollow propeller. It shows the limitation of substrate shapes on design is minimum. The manufactured propeller is shown in Fig. 8.

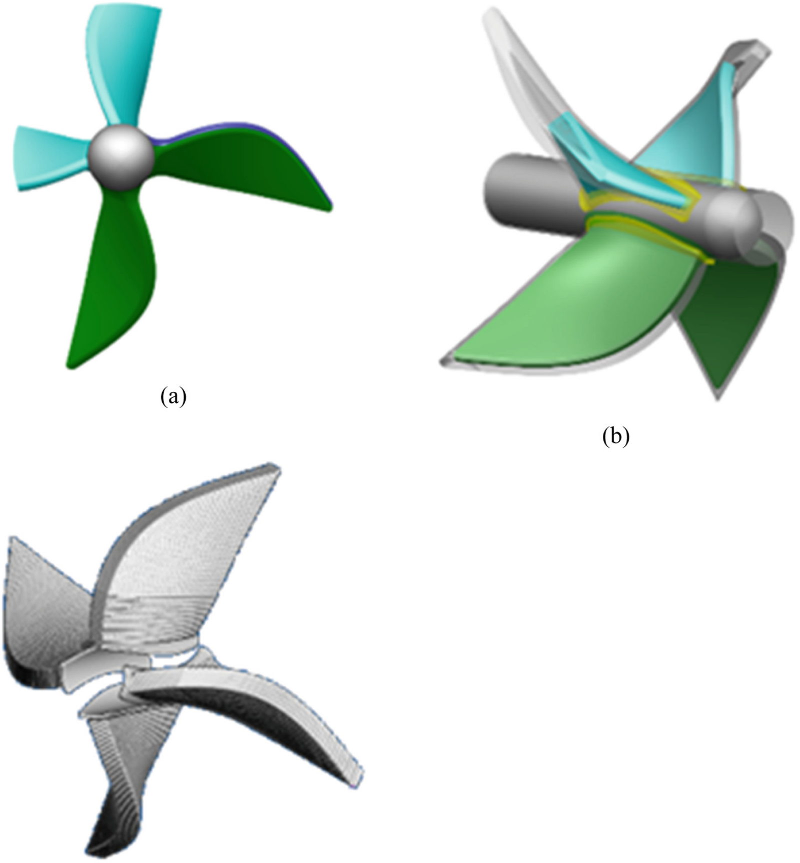
(a)

(b)

(c)

Fig. 7. Full propeller with four hollow blades, (a) Final propeller shape; (b) overlay of the deposition preform; (c) material deposition model (weld paths) – Ø500 mm tip to tip

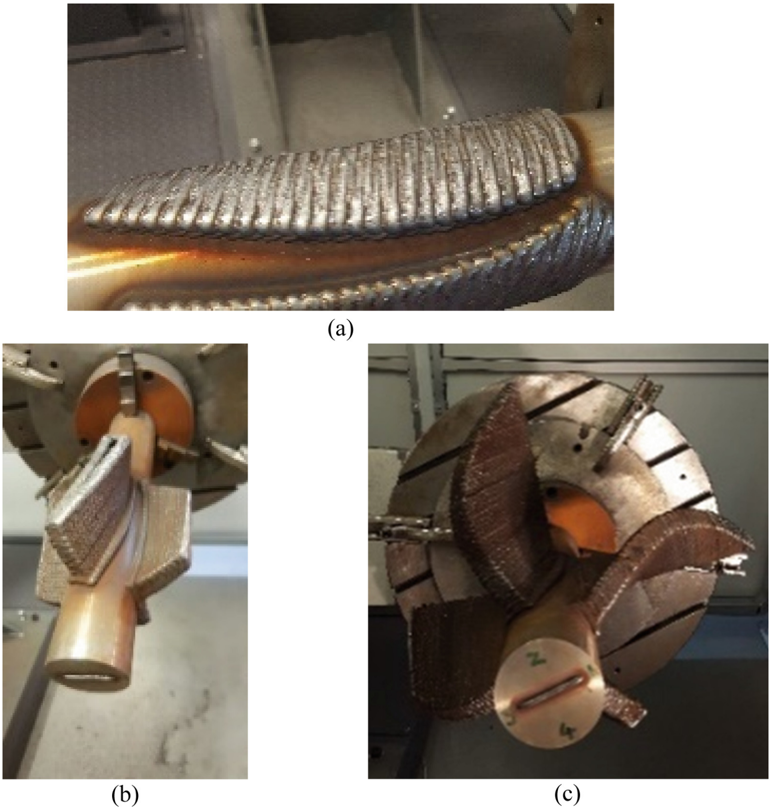

Fig. 8. As-deposited shape of Design #2, (a) initial; (b) during; (c) after deposition

Design #3 (Fig. 9): Propeller (~1.0 m in diameter) with three solid blades deposited using multiple conformal parallel weld tracks to create blades with 15 mm nominal wall thickness. Excess material was deposited to be able to realise the final blade fillet with the shaft. The design was manufactured and shown in Fig. 10.

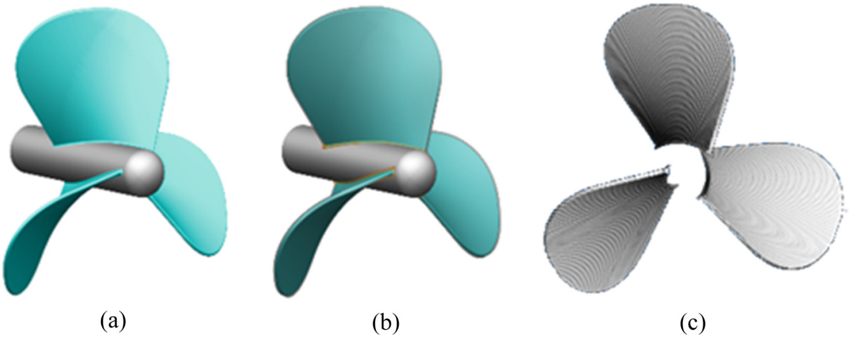

Fig. 9. Three solid blade propeller, (a) net shape; (b) near net shape; (c) deposition model

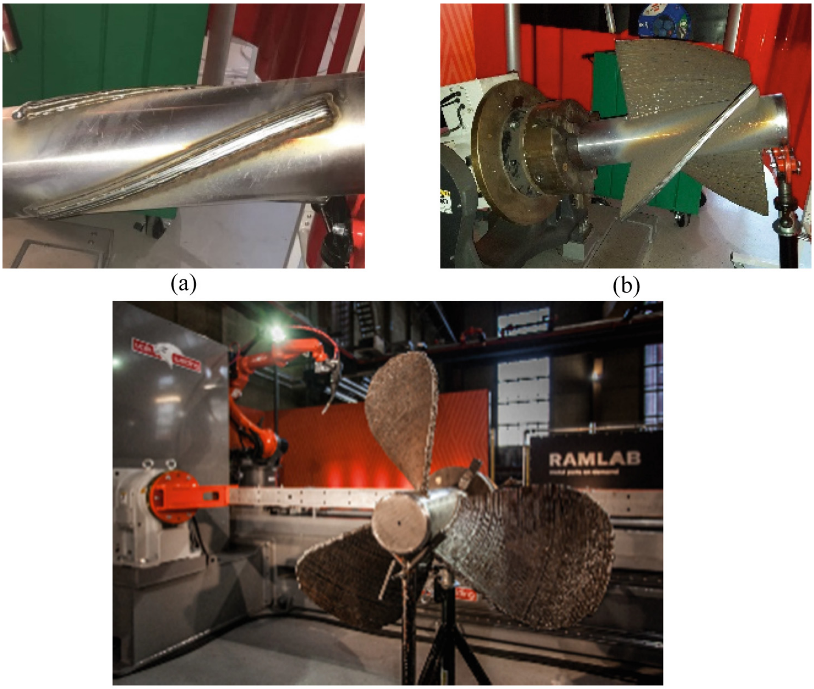

(a) (b) (c)

Fig. 10. As-deposited shape of Design #3, (a) initial; (b) during; (c) after deposition – Ø1000 mm tip to tip.

Design #4 (Fig. 11): Propeller (0.36 m in diameter) deposited using multiple conformal parallel weld tracks to create blade with variable wall thickness. Additional material was deposited to allow the realisation of the final blade fillet with the shaft.

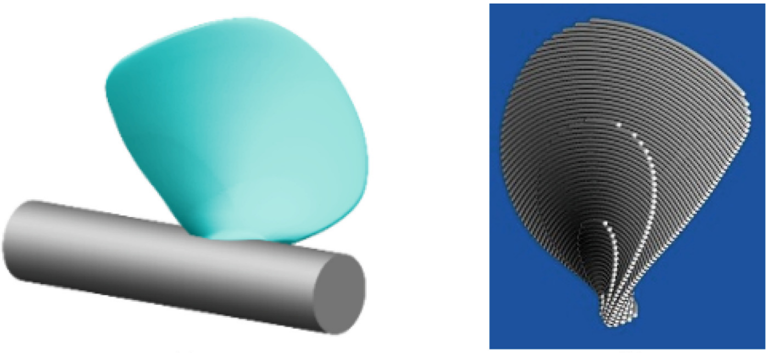

(a) (b)

Fig. 11. Single solid blade Ø360 mm tip to tip.

This design is an improved version of Design #3 with additional material added to allow a variable thickness fillet to be created. Less processing and post machining time is required with this design as the additional material is near to the required net shape of the final part. This near-net shape deposition is realized and manufactured propeller is shown in Fig. 12.

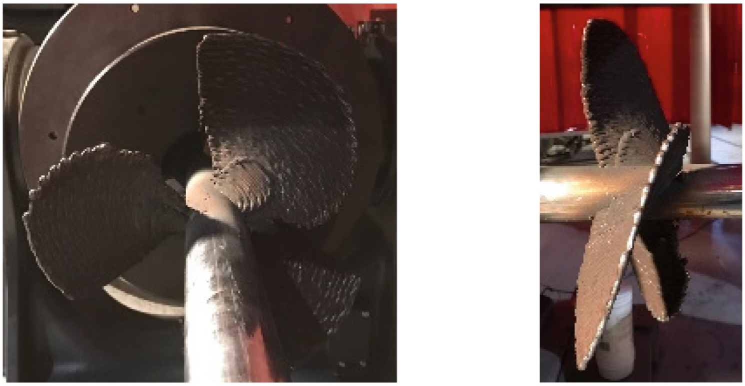
(a) (b)

Fig. 12. As-deposited shape of Design #4, (a) initial deposition; (b) after deposition.

Both Design #1 and #2 explore new design concepts that are otherwise impossible/difficult to manufacture, however, through AM, new design concepts can be conceived and prototypes rapidly produced to shorten the design cycle. Designs #3 and #4 both take conventionally designed CAD models to AM manufacture without any redesign.

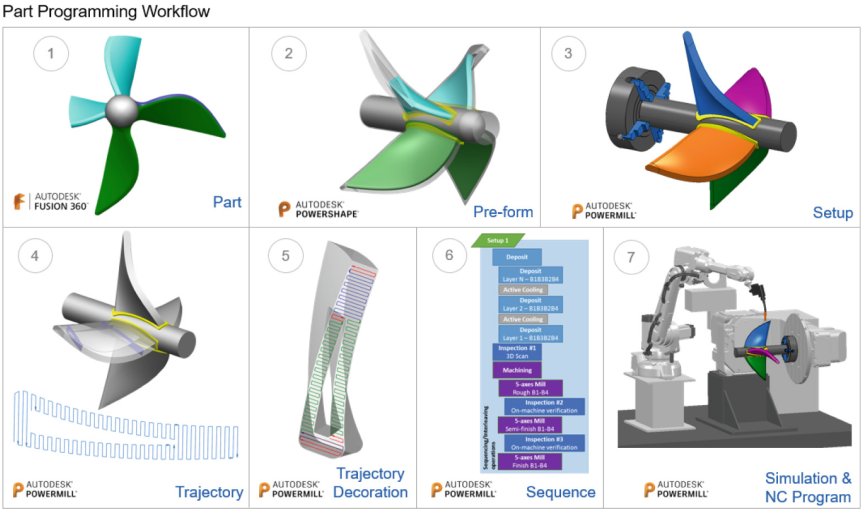
Part Programming Workflow
1
AUTODESK FUSION 360
Part
2
AUTODESK POWERSHAPE
Pre-form
3
AUTODESK POWERMILL
Setup
4
AUTODESK POWERMILL
Trajectory
5
AUTODESK POWERMILL
Trajectory Decoration
6
Setup 1
Deposit
Deposit Layer N – B1B3B2B4
Active Cooling
Deposit Layer 2 – B1B3B2B4
Active Cooling
Deposit Layer 1 – B1B3B2B4
Inspection #1 3D Scan
Machining
5-axes Mill Rough B1-B4
Inspection #2 On-machine verification
5-axes Mill Semi-finish B1-B4
Inspection #3 On-machine verification
5-axes Mill Finish B1-B4
Sequencing/Interleaving operations
AUTODESK POWERMILL
Sequence
7
AUTODESK POWERMILL
Simulation & NC Program

Fig. 13. Software programming workflow for Design #2.

From a rapid manufacture/production perspective, this highlights that there are subsets of components that are suited for rapid AM reproduction with reduced production time. This avoids spare-parts piles up in the warehouse. For either route, the part programming software workflow used for design exploration and manufacturing can be identical as illustrated in Fig. 13. Software used for each step are given to show extent of the process chain.

4 Post-processing

Each of the four designs produced a near net shape propeller which therefore require post processing to bring these components to their final as-desired forms. Two post processing techniques were successfully explored to give the desired surface finish. Using conventional manual grinding tools, the surfaces of Design #1 and Design #3 were brought to acceptable surface finish (Fig. 14). To ensure that the blades are within tolerance, a non-contact optical scanner was used to validate and control the surfaces. For Design #2, 5-axis CNC milling was utilized to remove excel material from the as-built geometry (Fig. 15). On-machine verification with a touch probe and optical scanning methods were utilized to control the final as-machined surfaces.

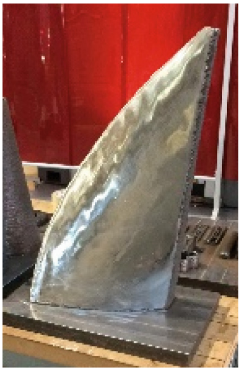

Fig. 14. Ground face of Design #1 and #3.

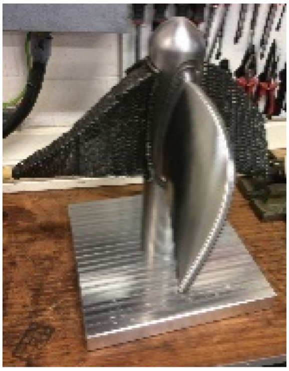

Fig. 15. CNC machined blade of Design #2

5 Discussion and Conclusion

Through design exploration and manufacturing of marine propellers with WAAM, the authors show the potential for added value for industrial applications. The traditional manufacturing method for propellers in general has a lead time of over 30 days. The cost and time can be reduced through the removal of time consuming steps such as molding and casting. This creates an opportunity for quicker production turnaround. It is known in the shipbuilding industrial that winglets on blade tips increase efficiency of propellers in the order of 1–4% [13]. Up to now propellers with tip modified blades are hardly used due to the high manufacturing cost, as blade tips tend to brake off during casting processes. WAAM has a great potential of enabling these kinds of propeller design. With fuel bills of large ships running in the order of millions per year, a few percent efficiency gain has a positive effect on the business case of WAAM.

With this newfound design freedom, not only can rapid prototyping be realized but rapid production can be implemented as well. This would enable locally produce spare parts on demand from CAD to offer a marked opportunity to reduce storage and transportation costs while reducing production time by shortening the design iteration from a rapid prototyping perspective. Existing maritime components could already be manufactured by WAAM as an alternative to conventional methods. Components such as complex double curved parts of the bow section of special purpose vessels. These components are now often machined from solid metal blocks or built up from plate material requiring many man hours for shaping, leading to cost of 30–50 euro/kg of structure. These kind of prices are in theory also achievable with WAAM which could make it a competitive alternative method.

WAAM of maritime components has a positive effect on the supply chain of component manufacture. Ships consist of many mission critical systems where failure could result in the ship no longer able to fulfil its tasks. The propeller is a very mission critical component where damaged from say a grounding event could leave the ship unable to sail. Given that many ships operate on contracts posing heavy penalties on unavailability of the ship, conventional manufacture on mission critical components carry long lead times which create financial risks. WAAM can significantly reduce the lead time of some components where even at higher cost price, WAAM produced components could alleviate the risk, ultimately reducing overall cost.

WAAM has the potential to be a viable manufacturing process for maritime components like propellers primarily because it offers the possibility to realize time and cost effective production of component as well as reducing the overall size of the supply chain by producing them locally.

Acknowledgment. This research is carried out under project number T16022 within the framework of the Research Program of the Materials innovation institute M2i (www.m2i.nl). The authors thank Valk Welding, Autodesk and other partners of RAMLAB for their support. The authors also thank MSc. C. Goulas for his assistance with the experiments and MSc. Kees Custers from DAMEN Shipyards for his insights on the business drivers.

References

1. Ya, W.: Laser materials interactions during cladding: analyses on clad formation, thermal cycles, residual stress and defects. Enschede (2015)
2. Kannan, G.B., Rajendran, D.K.: A review on status of research in metal additive manufacturing. In: Advances in 3D Printing & Additive Manufacturing Technologies, pp. 95–100 (2017)

3. Huang, S.H., Liu, P., Mokasdar, A., Hou, L.: Additive manufacturing and its societal impact: a literature review. Int. J. Adv. Manuf. Technol. **67**(5–8), 1191–1203 (2013)
4. Frazier, W.E.: Metal additive manufacturing: a review. J. Mater. Eng. Perform. **23**(6), 1917–1928 (2014)
5. Li, J., Wu, B.I.L.L.Y., Myant, C.O.N.N.O.R.: The Current Landscape for Additive Manufacturing Research. Imperial College, Londaon (2016)
6. Gupta, N., Weber, C., Newsome, S.: Additive Manufacturing: Status and Opportunities (2012)
7. Costabile, G., Fera, M., Fruggiero, F., Lambiase, A., Pham, D.: Cost models of additive manufacturing: a literature review. Int. J. Ind. Eng. Comput. **8**(2), 263–283 (2017)
8. Bikas, H., Stavropoulos, P., Chryssolouris, G.: Additive manufacturing methods and modelling approaches: a critical review. Int. J. Adv. Manuf. Technol. **83**(1–4), 389–405 (2016)
9. Wong, K.V., Hernandez, A.: A review of additive manufacturing. ISRN Mechanical Engineering (2012)
10. Qiu, X.: Effect of Rolling on Fatigue Crack Growth Rate of Wire and Arc Additive Manufacture (WAAM) Processed TITANIUM. Cranfield University, Cranfield (2013)
11. Carlton, J.: Marine Propellers and Propulsion. Butterworth-Heinemann, Oxford (2013)
12. Degu, Y.M., Sridhar, K.: Marine propeller manufacturing – a new approach. Am. J. Eng. Res. (AJER) **03**, 207–211 (2014)
13. Bertram, V.: Practical Ship Hydrodynamics. Elsevier, Amsterdam (2012)

Macroscopic Finite Element Thermal Modelling of Selective Laser Melting for IN718 Real Part Geometries

Yancheng Zhang(✉), Gildas Guillemot, Charles-André Gandin,
and Michel Bellet

Mines ParisTech, PSL Research University, Centre de Mise en Forme des Matériaux,
UMR CNRS 7635, Sophia Antipolis, France
{yancheng.zhang,gildas.guillemot,charles-andre.gandin,
michel.bellet}@mines-paristech.fr

Abstract. A 3D finite element model is developed to study heat exchange during the selective laser melting (SLM) process. The level set functions are used to track the interface between the constructed workpiece and non-melted powder, and interface between the gas domain and the successive powder bed layers In order to reach the simulation in macroscopic scale of real part geometries in a reasonable simulation time, the energy input and the formation of the additive deposit are simplified by considering them at the scale of an entire layer or fraction of each layer. The layer fractions are identified directly from a description (e.g. using G-code) of the global laser scan plan of the part construction. Each fraction is heated during a time interval corresponding to the exposure time to the laser beam, and then cooled down during a time interval equal to the scan time of the laser beam over the considered layer fraction. The global heat transfer through the part under additive construction and the powder material non-exposed to the laser beam is simulated. To reduce the computational cost, mesh-adaptation is adopted during the construction process. The proposed model is able to predict the temperature distribution and evolution in the constructed workpiece and non-melted powder during the SLM process at the macroscale, for parts made of complex geometry. Application is shown for a nickel based material (IN718), but the numerical model can be easily extended to other materials by using their data sets.

Keywords: Selective laser melting · Macroscopic finite element thermal modelling · Level set · Adaptive mesh · G-code

1 Introduction

Selective laser melting (SLM) is an advanced form of the selective laser sintering (SLS) process with full melting of the powder bed particles takes place by using one or more lasers. It was developed by Fockele and Schwarze in cooperation

© Springer International Publishing AG 2018
M. Meboldt and C. Klahn (eds.), *Industrializing Additive Manufacturing - Proceedings of Additive Manufacturing in Products and Applications - AMPA2017*,
DOI 10.1007/978-3-319-66866-6_8

with the Fraunhofer institute of laser technology in 1999 and then commercialized with MCP Realizer250 machine by MCP HEK Gmbh (now SLM Solutions Gmbh) in 2004 [1]. It received great interest for both research and industry aspects. Different metal alloys have been widely tested by SLM process [2–5]. Besides, the ceramic materials are also studied [6]. To avoid the costly trial and error approach by repeated experiments, numerical modelling is introduced for the simulation of different concurrent physical phenomena involved in the process [7].

The finite element (FE) method is usually selected for the numerical model in meso and macro scales. In the meso-scale, it's possible to predict the phase transformation, the formation of melt pool profiles and bead shapes [6]. In the macro scale, the predictions of temperature and residual stress are preferred [8–10].

By the thermal analysis, it's possible to improve the process parameters and optimize the designed the geometry size and the support structure [10]. To reach the thermal analysis in macro model, Zaeh et al. created a three dimensional FE-model to investigate of transient physical effects in SLM called SIMUSINT [11]. For present macro scale models, the regular shape workpiece is usually selected and powder bed is rarely considered [7]. The objective of the present approach is to develop a finite element thermal model of SLM by depositing the energy at the scale of a layer fraction for the workpiece of a complex geometrical form and taking into account the non-melted powder bed.

2 Modelling Strategy

Figure 1 presents a schematic of the FEM strategy. Firstly, the geometry of the workpiece, Ω_{WP}, is given by information extracted from a computer-aided design (CAD) model. It includes the useful component of the part plus the supports, which constitute the full consolidated geometry produced by SLM. The CAD model is immersed in a larger analysis domain Ω also embedding a bottom substrate, Ω_S, and enough gas, Ω_G, to full surround the CAD model. A level set function ψ is defined (red line in Fig. 1) that divides Ω into two regions, the material, Ω_M ($\psi < 0$) and the above gas Ω_G ($\psi > 0$), thus defining the $\Gamma_{M/G}$ boundary ($\psi = 0$). The level set function ψ is updated by

$$\psi^{t+\triangle t} = \psi^t - \triangle Z_T \tag{1}$$

where t is the time step and $\triangle Z_T$ is the layer thickness. The workpiece is split into the bottom constructed part, Ω^M_{WP}, and the top virtual part to be built, Ω^V_{WP}. At a given time during the construction of the part, the complement to $\Omega_G \cup \Omega_M$ in Ω_M is the powder bed, Ω_{PD}, that was not exposed to SLM. The level set function φ is also defined to track the $\Gamma_{WP/PD}$ boundary in the material domain. Finally, the whole domain Ω can be expressed as $\Omega = \Omega_G \cup \Omega_M$, where $\Omega_M = \Omega_{PD} \cup \Omega^M_{WP} \cup \Omega_S$.

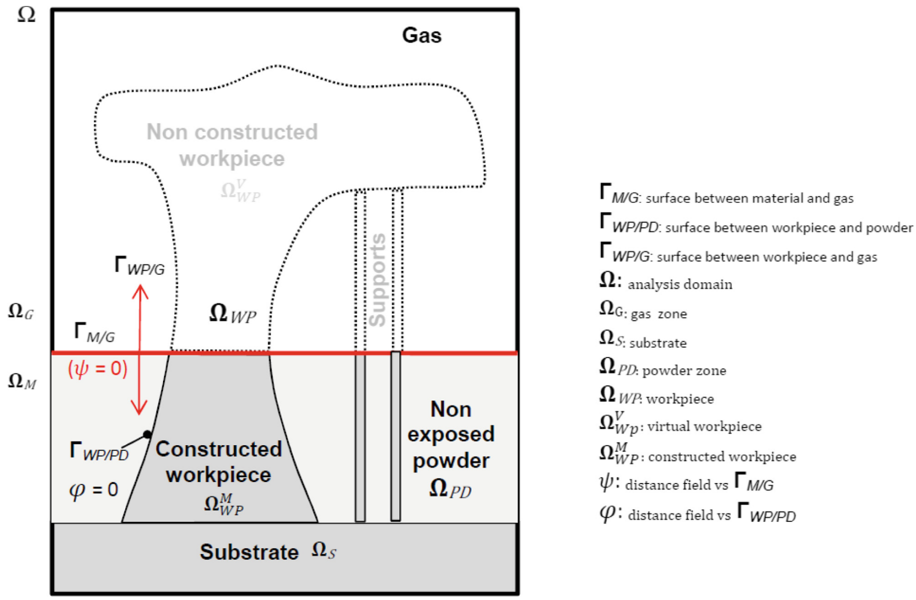
Ω
Gas
Non constructed workpiece
Ω^V_{WP}
Supports
$\Gamma_{WP/G}$
Ω_G
$\Gamma_{M/G}$
Ω_{WP}
$(\psi = 0)$
Ω_M
$\Gamma_{WP/PD}$
$\varphi = 0$
Constructed workpiece
Ω^M_{WP}
Non exposed powder
Ω_{PD}
Substrate Ω_S
$\Gamma_{M/G}$: surface between material and gas
$\Gamma_{WP/PD}$: surface between workpiece and powder
$\Gamma_{WP/G}$: surface between workpiece and gas
Ω: analysis domain
Ω_G: gas zone
Ω_S: substrate
Ω_{PD}: powder zone
Ω_{WP}: workpiece
Ω^V_{Wp}: virtual workpiece
Ω^M_{WP}: constructed workpiece
ψ: distance field vs $\Gamma_{M/G}$
φ: distance field vs $\Gamma_{WP/PD}$

Fig. 1. Scheme of the macro model

2.1 G-code Interpreter Module

Based on CAD information, the laser scan path is generated in the form of a G-code file, by a software tool known as a "slicer". The slicer intersects the CAD model with a series of planes in order to define a set of cross sections. For each plane, both perimeter and infill trajectories are computed to produce a layer [12]. In the present work, the discretized laser trajectories are extracted from the G-code. Then each trajectory is interpreted and transferred to the finite element thermal solver. Each layer can in turn be decomposed into several layer fractions, according to the effective scan path and a critical length, as illustrated in Fig. 2. A size of 52 mm is selected as the critical length in this work, and more "time-averaged" effect will be obtained for the temperature with higher value.

2.2 Scheme for Energy Input

Instead of applying the successive thermal input along the laser path, a different strategy is proposed in this work. Each layer fraction is heated during a time interval corresponding to the effective time during which the powder bed is exposed to the laser beam. By the discretization of laser trajectory in macro model, the time interval t^{lf}_{heat} is approximated by the time of the laser point passing one laser diameter.

$$t^{lf}_{heat} = \frac{\phi_L}{v_L} \tag{2}$$

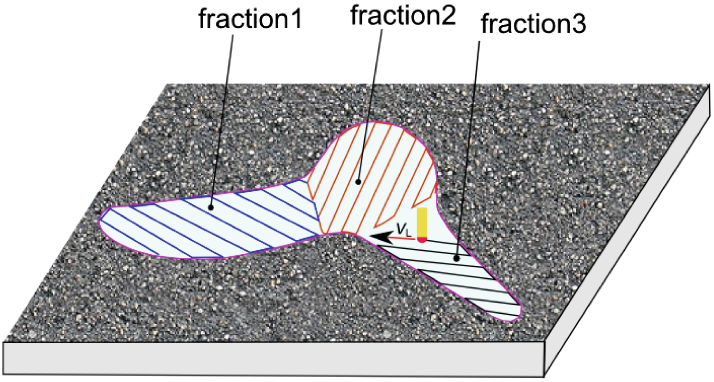

Fig. 2. Decomposition of a layer into fractions

where ϕ_L is the laser beam diameter and v_L is the laser velocity. The scanning time of each layer fraction t^{lf}_{scan} can be directly deduced from the exploitation and analysis of the laser scan file. It is then assumed that after being heated during the time interval t^{lf}_{heat}, the layer fraction cools (as well as the rest of domain Ω_M) during the time difference: $t^{lf}_{cool} = t^{lf}_{scan} - t^{lf}_{heat}$.

The heat flux ($\dot{q}_L$) that should be applied to the layer fraction during the heating time t^{lf}_{heat} can be easily calculated by the following energy balance,

$$(1-R)\ P_L\ t^{lf}_{scan} = S^{lf}\ \dot{q}_L\ t^{lf}_{heat} \tag{3}$$

where P_L is the nominal laser power, R is the reflexion coefficient of the laser radiation at the surface of the powder bed, and S^{lf} is the surface of the layer fraction. Actually, for the numerical implementation, this heat input is uniformly applied to the whole thickness Δz_t of the powder bed, using a volumetric heat source ($\dot{Q}_L$). This uniform volume source is then given by:

$$\dot{Q}_L = \frac{(1-R)\,P_L}{S^{lf}\,\Delta z_t}\frac{t^{lf}_{scan}}{t^{lf}_{heat}} \tag{4}$$

2.3 Refining and Unrefining the Mesh

To consider both the computationally elegant and physically realistic performance, the local mesh size and the total mesh number must be controlled. To refine the mesh in the deposited layer, an objective metric M is defined by applying the error estimation method [13] to the Heaviside function $H(\psi)$ according to the boundary $\Gamma_{M/G}$ and to the Heaviside function $H(\varphi)$ related to the boundary $\Gamma_{WP/PD}$.

$$\mathbf{M}_{\{\vec{n},\vec{\tau_1},\vec{\tau_2}\}} = \begin{bmatrix} 1/h_n^2 & 0 & 0 \\ 0 & 1/h_{\tau_1}^2 & 0 \\ 0 & 0 & 1/h_{\tau_2}^2 \end{bmatrix} \tag{5}$$

where h_n is the mesh size in the normal direction of the interface corresponding to the progress direction of the workpiece upper interface. Similarly h_{τ_1} and h_{τ_2} are mesh sizes in the two tangent directions of the interface. In addition, to avoid numerical perturbations in time and space associated with thermal shock, the local mesh size h should follow the mesh limitation condition [14]:

$$h \leq \sqrt{\frac{\kappa \Delta t}{\rho c_p}} \tag{6}$$

where Δt is the time step, κ the thermal conductivity, ρ is the density and c_p is the specific heat of the material at the local position.

For the constructed workpiece and gas far from the heated zone, an unrefining strategy is also applied by the adaptive remeshing technique.

3 Application

Using the strategy presented above, SLM of a part made of the nickel-based alloy IN718 in argon gas is simulated.

3.1 Geometrical Parameters

As shown in Fig. 3(a), the simulated domain is $30 \times 30 \times 16\,\text{mm}^3$, including the 1 mm-thick substrate. The workpiece under construction is initially immersed in the non-consolidated powder bed. Argon gas is considered over the powder bed, the height of this gas domain decreasing continuously during construction to reach a minimum value of 4 mm at the end of the process.

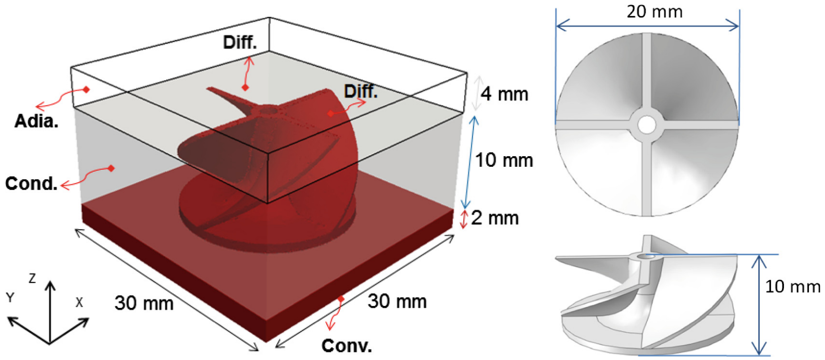

(a) simulated system (b) 3d view

Fig. 3. Geometrical description of the studied case showing: (a) the part to be constructed in red color, while the surrounding powder bed is in grey color, and the gas domain is in white color. (b) the top and perspective views of the part

The workpiece is an impeller with 4 spiral blades, the thickness of which is 1 mm. The radius of the lower plate and the height of the workpiece are 10 mm. Moreover, a vertical central hole goes through the workpiece (Fig. 3(b)). The deposition of energy is considered by layer fractions, which are based on the laser trajectories from the G-code description as detailed previously. Besides, the additional cooling time between the layers (Δt_{dwell}) of 15 s is considered.

3.2 Thermal Modelling

The temperature history is calculated by a 3D Lagrangian transient thermal analysis considering solid and powder properties of the metallic materials as well as argon gas properties. The local properties are estimated by a mixing rue based on the defined two level set functions ψ and φ.

Concerning the boundary conditions (as shown in Fig. 3(a)), the conductive heat exchange with machine environment is considered for the lateral surface of the material part, while the convective heat exchange is considered for bottom surface. The adiabatic condition is applied for the external surface of the gas zone ($\partial \Omega_G \cap \partial \Omega$). For the interfaces of $\Gamma_{M/G}$ and $\Gamma_{WP/PD}$, only the diffusive heat exchange is considered.

The thermal properties of the different simulated materials together with the parameters of thermal exchange and the laser inputs are given in Table 1. In the initial stage to develop this strategy, the thermal properties are considered as constant values, the temperature dependant properties will be implemented in the future model.

Table 1. Material properties and process conditions [7,15]

	Properties	Workpiece	Powder bed	Argon gas
Materials	Density, ρ [$\mathrm{kg\,m^{-3}}$]	8185	3191.5	1.3
	Thermal conductivity, κ [$\mathrm{W\,m^{-1}\,K^{-1}}$]	10.8	0.19	0.024
	Specific heat, C_p [$\mathrm{J\,kg^{-1}\,K^{-1}}$]	427	427	1000
Heat exchange	Ambient temperature, T [°C]	20		
	Convection coefficient, h [$\mathrm{W\,m^{-2}\,K^{-1}}$]	15		
	Emissivity	0.25		
Laser	Nominal power, P [W]	96		
	Scan speed, v_L [$\mathrm{mm\,s^{-1}}$]	55.03		
	Reflexion coefficient, R	0.45		
	Diameter of laser beam, ϕ_L [mm]	0.2		
	Thickness of deposited layer, Δz [mm]	0.2		
	Inter-layer dwell time, Δt_{dwell} [s]	15		

3.3 Mesh Adaptation

As shown in Fig. 4(a), the mesh in the gas region far from the construction front is coarse, while the zone close to the construction front is kept fine enough to avoid thermal shock. For the constructed workpiece, fine elements are located at its surface to preserve the geometrical shape, while coarser ones can be found inside Fig. 4(b). By the adaptive strategy, the number of elements in the system can be stabilized around 2 million, and the computation time reaches 17 h on a 50 processor cluster.

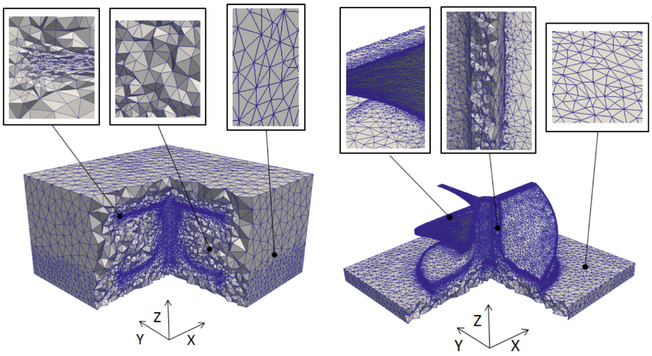

(a) Entire model (b) Constructed workpiece

Fig. 4. Illustration of the mesh adaptation, close to the end of the simulation process: the mesh is shown (a) in the entire model, evidencing refining at the $\Gamma_{M/G}$ boundary and unrefining in the powder bed far from the workpiece and (b) details of the mesh close to the substrate and within the manufactured component, illustrating variations in the vivinity of the $\Gamma_{WP/PD}$

3.4 Model Validation

By the above strategy, the adiabatic boundary condition is assumed to validate the energy conservation for the prescribed model. The energy evolution is given in Fig. 5 for the calculated value and the input one, respectively. In the final stage

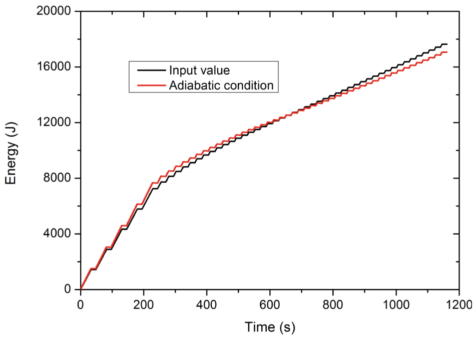

Fig. 5. Energy comparison with adiabatic boundary condition

of the simulation, 3% difference is obtained for the calculated energy compared with the theoretical input one, which means the developed model is acceptable form the energy point of view.

3.5 Simulation Results

After cooling down with a final dwelling time of 15s, the simulated result for the temperature field of the entire model is given in Fig. 6(a) at the end of the 50 layers. By removing the upper gas zone, the material zone is presented in Fig. 6(b). This presentation allows observing the temperature distribution in the powder bed and in the consolidated workpiece along the top and lateral surfaces. The highest temperature located in the last heated zones is around 610 °C, while the lowest temperature, around 52 °C, appears along the lateral surfaces. By removing the non-exposed powder, a vertical temperature gradient can be seen in the part, the temperature in the bottom plate and the 400 °C (Fig. 6(c)). To better evaluate the 3D temperature distribution, vertical and horizontal profiles are displayed in Fig. 7(a). The chosen lines (H2 and V2) in the cold zone go through one blade, while the ones in the hot zone (H1 and V1) intersect the longitudinal axis of the geometry. Even if the temperature tends to be homogeneous in the cold zone (green color in Figs. 7(b)), transitions can be found for the blue lines H2 and V2 (Figs. 7(c) and 7(d)). Line H2 traverses the powder and one blade, while V2 goes through substrate, workpiece, powder, blade, powder and gas, as indicated by the red circles read from left to right. The capture lines in the hot zone go through the red colour in Fig. 7(b). The vertical line V1 successively crosses the substrate from 0 to 2 mm, the powder bed from 2 to 12 mm and argon gas from 12 to 16 mm. The temperature in the substrate varies slightly, while the temperature increases in the powder and decreases in the gas zone with high temperature gradient. The horizontal line H1 crosses several times the powder and the workpiece when the central hole is encountered. The corresponding variations in the temperature profile can clearly

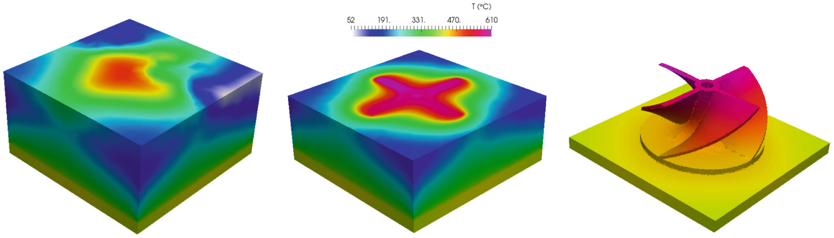

(a) Whole model

(b) Workpiece with non-exposed powder

(c) Workpiece with substrate (powder bed removed)

Fig. 6. Temperature distribution in the simulated system, at the end of the construction process

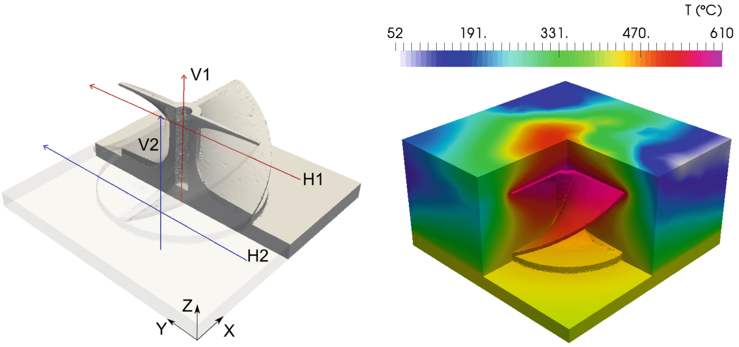

(a) Capture lines (b) section view

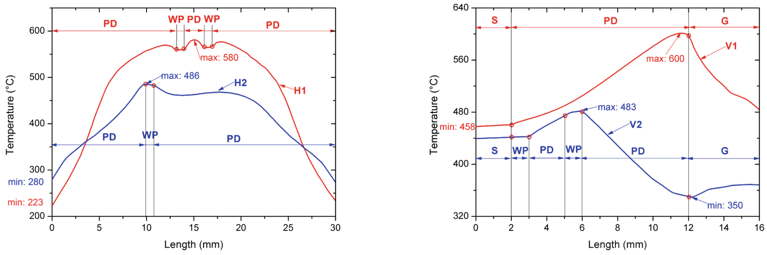

(c) horizontal direction (d) vertical direction

Fig. 7. Temperature profiles through the entire model with H1 (X = 15 mm, Y = [0, 30] mm, Z = 8 mm), V1 (X = 15 mm, Y = 15 mm, Z = [0, 16] mm), H2 (X = 7 mm, Y = [0, 30] mm, Z = 5 mm), V2 (X =7 mm, Y = 11 mm Z = [0, 16] mm)

be seen. Due to the low thermal conductivity, the temperatures in the powder are still high after 15 s dwelling time for each layer construction.

For profiles (H1, V1) in the construction center, the maximum temperature always locates at the powder zone, and the temperature gradient of the powder is higher than that of the workpiece. For the profiles out of the center (H2, V2), the maximum temperature locates the interface between workpiece and powder.

4 Conclusions

A 3D finite element thermal model at the macroscopic scale of the constructed workpiece has been developed. The simulation encompasses the non-consolidated powder bed and the surrounding gas. A layer fraction strategy based on the G-code description of the global laser scan plan for a complex geometrical workpiece has been implemented. The level set functions are used to track the interfaces of material-gas and workpiece-powder. Using an adaptive mesh technique, local refinement and de-refinement of the mesh is continuously controlled in the whole model during the construction process in a reasonable computation time.

By the transient thermal analysis, the temperature gradient in the material zone can be easily observed: the temperature in the substrate tends to be homogeneous, while the temperature gradient near the interface is high. The boundary conditions are applied in a reasonable way by considering the non-exposed powder. The influence of the latter on the temperature profile of the entire model can be easily observed. The developed 3D macroscopic model can be applied to the thermal analysis of SLM additive manufacturing of metal parts, without limitation regarding the geometrical complexity.

Due to the simplification of fraction layer, the local high temperature fluctuations encountered by the deposited material (due to the successive laser impacts) might not be well reproduced by such a macro calculation. However, regarding the global build up of stress(at the scale of the part), it's essentially of a more "time-averaged" temperature history that can be effectively captured by such model. It will be interesting in the future to see whether such hypotheses are correct by comparing calculated stress and distortions with the measured ones.

5 Outlook

The next developments will consider temperature dependent material properties and the implementation of a thermo-mechanical module in order to predict the stress build-up in the part during its construction. In addition, the comparison with the experimental measurements, it's in progress. Based on the validated model by experiments, the parametric optimisation of SLM process will also be expected.

References

1. Bhavar, V., Kattire, P., Patil, V., Singh, R.: A review on powder bed fusion technology of metal additive manufacturing. In: The 4th International Conference and Exhibition on Additive Manufacturing Technologies, AM 2014, Banglore, India, 1–2 September 2014 (2014)
2. Thijs, L., Verhaeghe, F., Craeghs, T., Van Humbeeck, J., Kruth, J.-P.: A study of the microstructural evolution during selective laser melting of Ti-6Al-4V. Acta Mater. **58**, 3303–3312 (2010). doi:10.1016/j.actamat.2010.02.004
3. Qiu, C., Adkins, N.J.E., Attallah, M.M.: Microstructure and tensile properties of selectively laser-melted and of HIPed laser-melted Ti-6Al-4V. Mater. Sci. Eng. A. **578**, 230–239 (2013). doi:10.1016/j.msea.2013.04.099
4. Yadroitsev, I., Krakhmalev, P., Yadroitsava, I.: Hierarchical design principles of selective laser melting for high quality metallic objects. Addit. Manufact. **7**, 45–56 (2015). doi:10.1016/j.addma.2014.12.007
5. Aboulkhair, N.T., Everitt, N.M., Ashcroft, I., Tuck, C.: Reducing porosity in AlSi10Mg parts processed by selective laser melting. Addit. Manufact. **1–4**, 77–86 (2014). doi:10.1016/j.addma.2014.08.001
6. Chen, Q., Guillemot, G., Gandin, C.-A., Bellet, M.: Three-dimensional finite element thermomechanical modeling of additive manufacturing by selective laser melting for ceramic materials. Addit. Manufact. (2017, accepted, in press)

7. Denlinger, E.R., Jagdale, V., Srinivasan, G.V., El-Wardany, T., Michaleris, P.: Thermal modelling of Inconel 718 processed with powder bed fusion and experimental validation using in situ measurements. Addit. Manufact. **11**, 7–15 (2016). doi:10.1016/j.addma.2016.03.003
8. Fu, C.H., Guo, Y.B.: Three-dimensional temperature gradient mechanism in selective laser melting of Ti-6Al-4V. J. Manufact. Sci. Eng. **136**(6), 061004 (2014). doi:10.1115/1.4028539
9. Heigel, J.C., Michaleris, P., Reutzel, E.W.: Thermo-mechanical model development and validation of directed energy deposition additive manufacturing of Ti-6Al-4V. Addit. Manufact. **5**, 9–19 (2015). doi:10.1016/j.addma.2014.10.003
10. Belle, L.V., Boyer, J.C., Vansteenkiste, G.: Investigation of residual stresses induced during the selective laser melting process. Key Eng. Mater. **554–557**, 1828–2834 (2013). doi:10.4028/www.scientific.net/KEM.554-557.1828
11. Zaeh, M.F., Branner, G., Krol, T.A.: A three dimensional FE-model for the investigation of transient physical effects in selective laser melting. In: 4th International Conference on Advanced Research in Virtual and Physical Prototyping, VRAP 2009, 6 –10 October 2009. Taylor and Francis/Balkema, Leiria (2010)
12. Steuben, J.C., Iliopoulos, A.P., Michopoulos, J.G.: Discrete element modeling of particle-based additive manufacturing processes. Comput. Methods Appl. Mech. Eng. **305**, 537–561 (2016). doi:10.1016/j.cma.2016.02.023
13. Coupez, T.: Metric construction by length distribution tensor and edge based error for anisotropic adaptive meshing. J. Comput. Phys. **230**, 2391–2405 (2011). doi:10.1016/j.jcp.2010.11.041
14. Fachinotti, V.D., Bellet, M.: Linear tetrahedral finite elements for thermal shock problems. Int. J. Numer. Methods Heat Fluid Flow **16**(5), 590–601 (2006). doi:10.1108/09615530610669120
15. Sih, S.S., Barlow, J.W.: The prediction of the emissivity and thermalconductivity of powder beds. Part. Sci. Technol. **22**(4), 427–440 (2004). doi:10.1080/02726350490501682a

Additive Manufacturing of Piezoelectric 3-3 Composite Structures

Miriam Bach[1], Tutu Sebastian[2], Mark Melnykowycz[2], Tony Lusiola[2], D. Scharf[2], and Frank Clemens[2](✉)

[1] Institute of Ceramic, Glass and Construction Materials,
TU Bergakademie Freiberg, Agricolastraße 17, 09596 Freiberg, Germany
[2] Laboratory for High Performance Ceramics,
Empa – Swiss Federal Laboratories for Materials Science and Technology,
Überlandstrasse 129, 8600 Dübendorf, Switzerland
`frank.clemens@empa.ch`

Abstract. Fused deposition of ceramics (FDC) is an additive manufacturing technique, were thermoplastic filaments are used for the fabrication of intricate structures that are difficult or impossible to produce with traditional techniques. This processing technique is utilized in the domestic and industrial appliance market. However, this simple and cheap manufacturing method is not widely used for the fabrication of traditional, high performance or functional ceramics. The objective of this contribution is to manufacture grid structures by means of FDC and subsequently investigate their electromechanical properties. Highly loaded ceramic - EVA (ethyl vinyl acetate) based filament is produced, as a feedstock for FDC. After successful printing and sintering of the grid structures, ferroelectric investigations were performed. Moreover, the grid structures are impregnated with a polymer resin resulting in a piezoelectric 3-3 composite that can be used as a hydrophone in under water noise detection.

Keywords: Fused deposition of ceramics · Additive manufacturing · Thermoplastic processing · PZT · $BaTiO_3$

1 Introduction

Piezoelectric materials have the ability to convert electrical energy to mechanical vibrations or vice versa depending on their applications. Although monolithic ceramics are relatively inexpensive and show good piezoelectric properties, the direct applications are limited due to the mismatch in acoustic impedance between the media and ceramic through which signals are transmitted or received [1]. Piezoelectric composites, which consist of a piezoelectric ceramic embedded in an inactive polymer phase provides an alternative solution. Researches have proved that piezoelectric composites show better properties compared to monolithic ceramics for ultrasonic applications due to better acoustic impedance matching and lower dielectric permittivity [2]. The properties of a composite can be tailored to suit the applications by changing the ceramic/polymer volume fractions and the constituent materials. The connectivity of the ceramic phase within the polymer matrix also governs the final electromechanical

© Springer International Publishing AG 2018
M. Meboldt and C. Klahn (eds.), *Industrializing Additive Manufacturing - Proceedings of Additive Manufacturing in Products and Applications - AMPA2017*,
DOI 10.1007/978-3-319-66866-6_9

properties and Newnham *et al.* proposed ten connectivity patterns for a 2-phase system, where each phase could be continuous in zero, one, two or three dimensions [3]. The internationally accepted nomenclature are (0-0), (0-1), (0-2), (0-3), (1-1), (1-2), (1-3), (2-2), (2-3) and (3-3), where the first number in the parenthesis represents the connectivity of piezoelectric active phase and the second number refers to the polymer inactive phase [3]. A series of different types of connectivity of the 2-phase composite system is shown in Fig. 1.

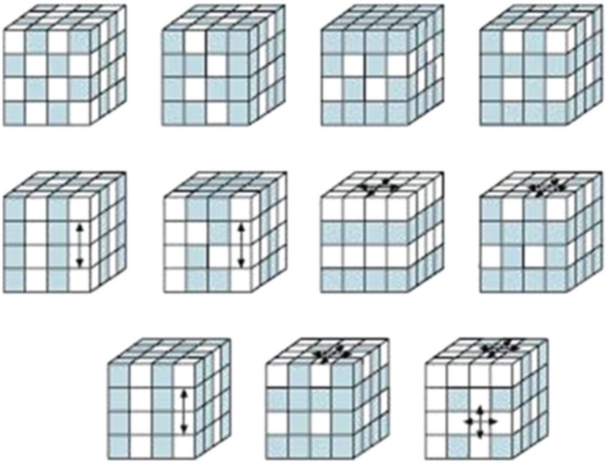

Fig. 1. Different types of connectivity of the 2-phase composite system [4]

Various processing techniques have been used to fabricate piezoelectric composites [5–9]. Empa has prior experience in fabricating 1-3 fibre composites using extrusion and 0-3 composite fibers [10, 11]. Techniques such as injection moulding and dice & fill method are also used widely to produce 1-3 and 2-2 composites [12, 13]. 3-3 composites are fabricated mainly using lost mould method [14]. Since the mould needs to be burned out and the inability to rapidly prototype samples restricts the wide scale usage of this technique. In this contribution, additive manufacturing via fused deposition modelling of ceramics was used to fabricate 3-3 composites that overcome these drawbacks and provides flexibility in the fabrication process. Fused deposition modelling of ceramics is a 3D printing process that extrudes a continuous thermoplastic filament to form it into a continuous profile and is particularly useful at producing complicated models layer by layer [7]. With this technique, complicated structures can be made and modified by changing the computer aided design (CAD) file. Furthermore, complicated shapes such as curved surface, used for focussing ultrasound beams can be fabricated easily. While fused deposition technique is not as cost effective as mass production, the new 3D printing technologies have permitted the ability to build intricate structures and prototypes by reducing high costs in time and capital [15].

The 3-3 connectivity composites discussed in this contribution is particularly used in hydrophone applications for under water low frequency noise exploration [16]. Hydrophone sensitivity is characterized by hydrostatic voltage constant (g_h), which is the electric field generated during the applied hydrostatic stress. It is calculated using the formula $g_h = d_h/(\varepsilon_0 * \mathrm{K})$, where d_h is the hydrostatic strain constant, ε_0 is the permittivity of free space and K is the dielectric constant [16]. However in this article, the focus is given on the fabrication of 3-3 composites and suitability of the same for hydrophone applications will be discussed in a future contribution.

The flexibility offered by the fused filament fabrication process enables the volume fraction of the piezoelectric ceramic phase in a 3D printed 3-3 structure to be varied, by varying the width and spacing within the ceramic grid structure. Among the many ferroelectric ceramic materials, two of the most widely researched ones, lead zirconate titanate (PZT) and barium titanate (BT) owing to their superior piezoelectric, ferroelectric and dielectric properties [17] and was thus used in this work to produce scaffolds with a grid structure. By showing the feasibility of this process, would enable the processing of several useful types of complex shaped monolithic and composite ferroelectric devices.

2 Experimental

The production of fused deposition ceramic structures is divided into several steps which include production of the thermoplastic feedstock, extruding the filament, 3D printing, debinding, sintering and the measurement of the ferroelectric properties. For the feedstock formulation, density, BET and grain size of the ceramic powders are essential. The density of the commercially obtained PZT and BT powder was measured with the Helium pycnometer (Accu-Pyc II 1340, Micromeritics, USA), specific surface area was determined by BET (Beckman-Coulter SA3100, Beckman-Coulter, USA) and particle size was measured using laser diffraction (LS 230, Beckman Coulter, USA). Phase analyses of the ferroelectric powders were performed using X-ray diffraction (XRD, X'Pert Pro MPD, PANalytical, Netherlands). To identify the phase composition, perovskite peaks were examined from the 2θ angles 20–60°.

2.1 Preparation of Feedstock

Feedstocks of PZT EC65 (Harris corporation, USA) and BT (Ferro, GmbH) were prepared using a high-shear mixer (Haake PolyLab Mixer Rheomix 600, Thermo Fisher Scientific), mixing with the thermoplastic polymer i.e. Ethyl vinyl acetate copolymer (EVA, DuPont, USA) and stearic acid (Sigma Aldrich, GmbH). The preparation parameters of the feedstocks are shown in Table 1. The extrusion was performed with the Rosand RH7 Flowmaster (Bohlin Instruments - Malvern Instruments, UK). The filaments were extruded into a beaker and were tailored to be flexible enough to wind on a roll for use with the 3D printer.

Table 1. Preparation parameters for thermoplastic feedstock

Ceramic	vol.% ceramic	vol.% SA	vol.% EVA	Applied monolayer's SA
PZT	49.0	10.4	40.5	7.5
BT	52.0	5.6	42.4	3.0

2.2 3D Printing of Feedstock

The 3D printer was built from a 3D printer construction kit (Velleman K8200/3Drag with a Bulldog XL drive mechanism and E3D hot end). A glass plate was used as the printing bed covered with a tape (width: 50 mm, length: 50 m, thickness: 0.14 mm) from 3D-printerstore.ch. The K8200 was built from open source hardware and software, allowing physical component and software modification. At the other side of the frame, the unpowered roll pushes the filament against the powered roll. When the pressure is too high, the filament may buckle and when the filament is too soft, then it is not forced through the channel, extruder and the nozzle resulting in clogging. A 0.8 mm nozzle was used with a printing temperature between 150 °C to 180 °C and the printing bed was heated to 60 °C. Structures with a printing gap range of 0.15 mm to 0.4 mm were fabricated. 3D scaffolds with the infill percentages between 10 vol.% and 100 vol.% were printed for PZT. A schematic of 3D printing process and the printed grid structure is shown in Fig. 2. BT filament was only used for printing scaffolds with 50 vol.% filling.

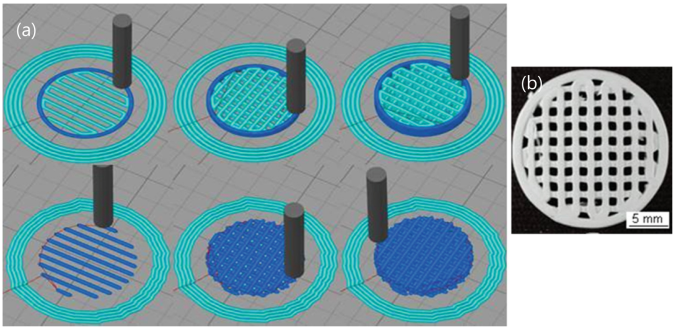

Fig. 2. (a) Simulation of 3D printing and (b) 50 vol.% BT ceramic scaffold structure

The discs were printed with a diameter of 20 mm, a thickness of 2 mm. 8 layers were printed by cross-ply design. The model was programmed with OpenSCAD and saved in a STL file format (STereoLithographie). The 3D printer is programmed by Simplyfy3D software.

2.3 Debinding and Sintering of 3D Printed Ceramic Structures

For the thermal treatment (debinding and sintering processing step), PZT scaffolds were debinded for 2 h at 500 °C followed by sintering at 1200 °C whereas $BaTiO_3$ scaffolds were debinded at 500 °C for 2 h followed by sintering at 1350 °C for 5 h. The debining and sintering profile used for the PZT and BT scaffolds are shown in Fig. 3. Because of the different sintering behaviour, PZT samples were sintered using the furnace (Pyrotec PY12H, GmbH) and BT samples were sintered using the furnace (Nabertherm LHT 04/17, Switzerland). The samples were heated at 3 °C/min until 200 °C followed by 0.25 °C/min until 500 °C. The samples were further heated up to their respective sintering temperatures. For the PZT scaffolds, alumina crucible was coated with 0.08 g zirconium dioxide powder (NANOVATION, GmbH) and 0.92 g lead zirconate powder (Sigma-Aldrich Chemie GmbH) per disc to achieve vapour pressure during sintering, to restrict lead oxide volatilization. 1 g of PZT powder was also added to the sintering base as a bed to avoid the disc sticking to the crucible [18]. Al_2O_3 powder is used to seal the crucible completely.

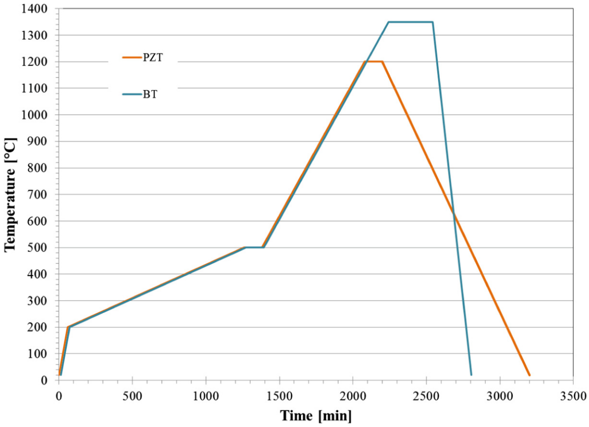

Fig. 3. Debinding and sintering profile for PZT and BT scaffolds

2.4 Piezoelectric Composite Fabrication

Sintered PZT ceramic scaffolds were impregnated with epoxy EpoThin™ 2 (Buehler, GmbH), consisting of resin and hardener that are mixed in a volume ratio of 2:1 to fabricate piezoelectric 3-3 composites. Curing was executed at room temperature for at least 9 h. The samples were polished on both sides parallel to each other until first layer of ceramics is exposed, using the polishing machine (Struers Tegramin 30, Switzerland) with a 40 µm diamond pad and ground with water.

2.5 Characterization of 3D Printed Ceramic Structures

On the scaffolds, electrodes with a diameter of 8 mm were prepared from silver paste (Electrodag 5195, Henkel, GmbH), placed in the centre on both sides of each disc and fired at 150 °C for 15 min. Ferroelectric and piezoelectric behaviour of each sintered disc was measured with a piezoelectric evaluation system, aixPES (aixACCT, GmbH), the details of this setup has been described previously [19–21]. A sketch of the instrument is shown in Fig. 4. To prevent arcing and extract excessive heat while applying high electric field, sample was immersed in silicone oil (Therm 180, Lauda Dr. R. Wobser GmbH & Co. KG).

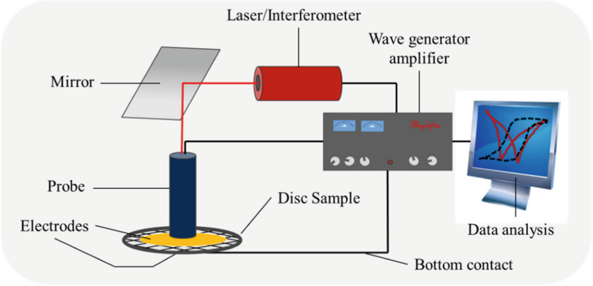

Fig. 4. Sketch of the FerroFib equipment with scaffold sample structure between two electrodes

The large signal polarization and strain hysteresis as a function of applied electric field was recorded at 0.1 Hz and 2 $kVmm^{-1}$. After these measurements the samples were electrically poled with a direct current at an electric field of 2 $kVmm^{-1}$ for 300 s at room temperature. Small signal stimulus (100 V at 0.2 Hz) was applied, and the displacement was measured with a laser interferometer.

3 Results and Discussion

Powder properties of the used ceramic materials are given in Table 2. Both materials have similar d_{50}. However the PZT powder has a slightly higher mean value and a smaller d_{10}. This will result in a larger grain size distribution.

Table 2. Powder properties of the ceramic

Powder	Properties					
	SSA in m^2/g	ρ in g/cm^3	d_{10} in µm	d_{50} in µm	d_{90} in µm	Mean in µm
PZT	1.325	8.01	0.89	1.67	5.91	2.77
BT	2.21	6.10	1.03	1.74	3.43	2.00

X-ray diffraction of as-received and sintered powders is shown in Fig. 5. It is clear that all the analysed powders are of single phase and no impurities can be detected. PZT show rhombohedral and tetragonal phases (43–46°) which correspond to morphotropic phase boundary (MPB) composition. Peaks at 2θ values 43.7°, 44.9° correspond to tetragonal phase and 2θ value at 44.3° correspond to the rhombohedral phase. The as-received BT powder is of tetragonal phase, as characterized by the peak splitting in 200_p peak. During heat treatment/sintering of the PZT powder at 1200 °C, due to lead loss, the morphotropic phase became predominantly tetragonal rich [22, 23]. This is characterized by the double peak splitting of the 200_p pseudocubic peak. As expected, heat treatment of BT powder did not result in any change of the chemical composition.

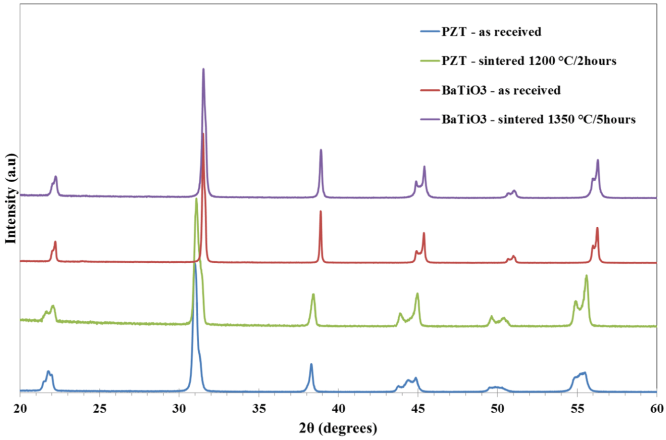

Fig. 5. X-ray diffraction of as-received and sintered BT and PZT ceramic powders

3.1 3D-Printing

The extruded filament was wound on a spool and fed into a feeder of the commercial 3D printer for FDC process. Hence, the filament must exhibit certain flexibility so as not to break while this process. In Fig. 6, the flexibility of PZT and BT filament is shown. It is evident that PZT filament displays higher flexibility than BT and is therefore much easier to feed into the printer. Nevertheless, filament made of BT was still able to be fed in the printer as smaller fragments and continuous printing can still be achieved. The white lines displayed in Fig. 6 represent angular distances of 30° each.

In Fig. 7, PZT ceramic scaffolds of ceramic filling content from 10–100% are shown. All the samples were printed at a temperature of 150 °C and a nozzle-bed gap of 0.2 mm was used.

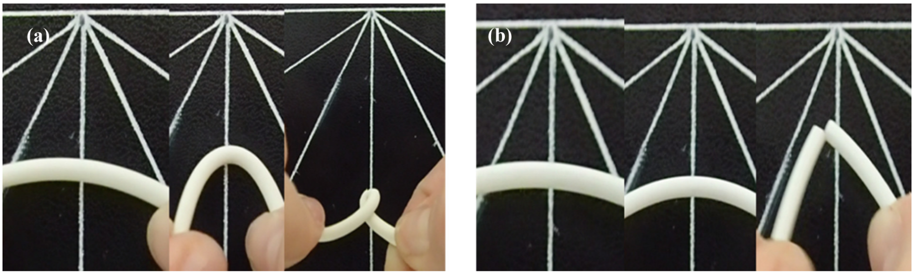

Fig. 6. Proof of flexibility with PZT (a) and BT (b)

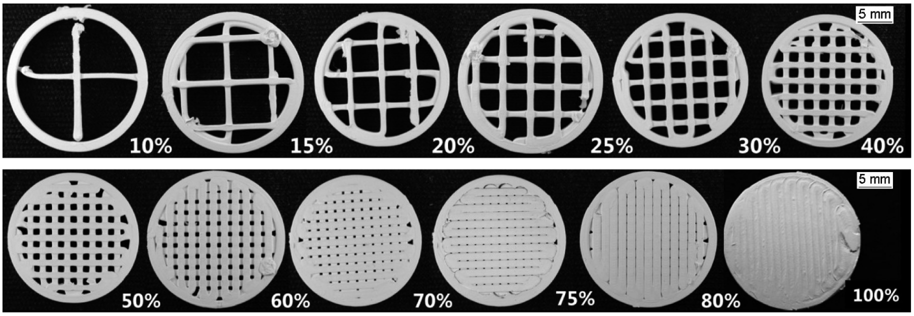

Fig. 7. Printed grid structure of PZT with different filling content (vol.%)

3.2 Piezoelectric Composites

Piezoelectric composites with 3-3 connectivity were fabricated by impregnating sintered PZT ceramic scaffolds with an epoxy resin. Since the piezoelectric properties of PZT are much higher than BT, only 3D printed PZT scaffolds are considered here for making piezoelectric 3-3 composites. A series of samples were investigated with ceramic volume contents starting from 10 to 70 vol.%. The electromechanical properties of these samples were measured at 2 kVmm^{-1} at room temperature. The results are shown in Figs. 8 and 9. As expected, increase of ceramic content in the 3-3 composite results in an increase of remnant polarization (Fig. 10(a)), piezoelectric constant and strain (Fig. 10(b)). However discrepancies can be observed for low filling level, like <25 vol.%, since the sample was too lossy. The sample with ceramic content of 80% formed blisters while sintering as evident from the multiple cracks visible in the micrograph, see, Fig. 11. Hence the investigation is limited to 70% maximum ceramic loading. The coercive field of all the samples seems to fall within a narrow range. Any noticeable change in d_{33} and the maximum strain could be observed with increasing ceramic content. It could be expected that embedding the ceramic in a polymer resin would restrict its displacement (clamping effect) on application of an electric field. However, it seems that the used resin has negligible effect on the strain behavior.

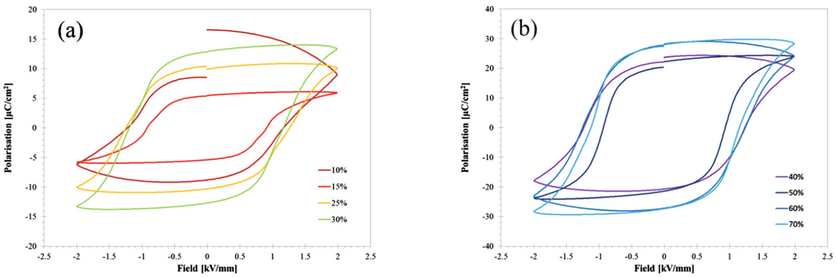

Fig. 8. PE loops for 3-3 piezoelectric composites

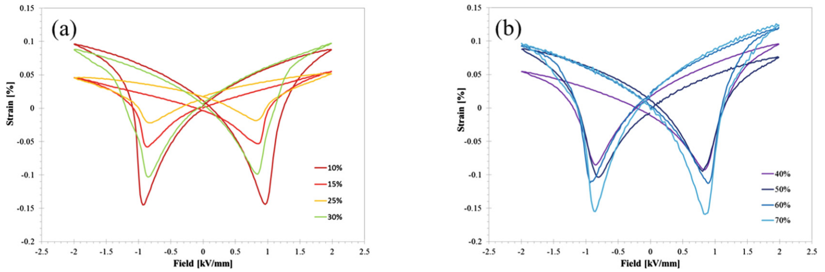

Fig. 9. SE loops for 3-3 piezoelectric composites

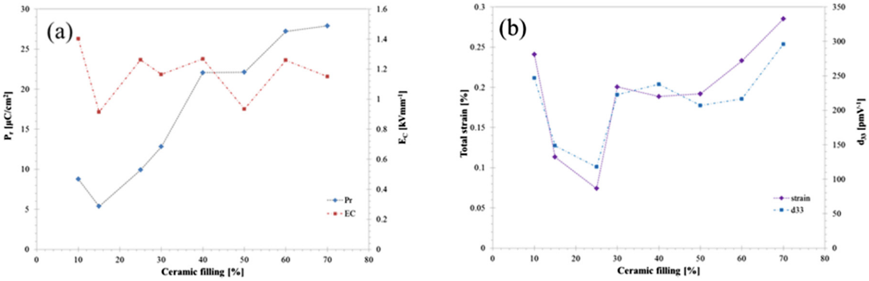

Fig. 10. Electromechanical properties for 3-3 piezoelectric composites

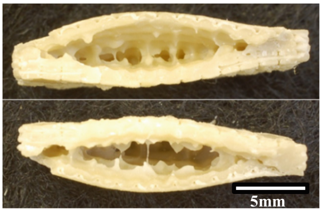

Fig. 11. Cross section of sintered PZT void grid structured ceramic samples (80% ceramic filling level). Blisters are formed on the surface of sample representing too much ceramic loading.

4 Conclusions

Additive manufacturing, especially Fused Deposition of Ceramics was successfully used for manufacturing ferroelectric PZT and BT grid/scaffold structures. The ceramic powder was compounded with a thermoplastic (EVA) binder and a surfactant (SA) to prepare a highly load filament as the feedstock for 3D printing process. Both lead and lead-free ferroelectric grid structures were fabricated successfully. PZT grid structures were further processed into piezoelectric composites and their electromechanical properties were studied in detail. It was found that a maximum of electromechanical properties can be attained at a ceramic filling level of 70 vol.% of ceramic.

This contribution acts as a proof of concept showing intricate structures with electroceramic materials can be fabricated for various applications using fused deposition technique. Further enhancement in printing performance, especially optimizing the layer height, along with improved binder burn out and sintering process shall lead to dense ceramic end products and over and above to outstanding ferroelectric properties. Interestingly, already at low powder content a d_{33} $\sim$245 pm/V could be achieved. Only P_r depends significantly on the ceramic content in the 3-3 composite structure. Total strain, piezoelectric constant and coercive field values show larger deviation and does not show a significant difference in relation to the ceramic content in the piezoelectric composite.

Acknowledgements. The authors would like to acknowledge the COST Action MP 1202; SBFI No.C14.0991 and C14.0099 and the SNF No. 206021 133833 for financing the project and the new equipment.

References

1. Gururaja, T.R.: Piezoelectrics for medical ultrasonic imaging. Am. Ceram. Soc. Bull. **73**(5), 50–55 (1994)
2. Skinner, D.P., Newnham, R.E., Cross, L.E.: Flexible composite transducers. Mater. Res. Bull. **13**(6), 599–607 (1978)
3. Newnham, R.E., Skinner, D.P., Cross, L.E.: Connectivity and piezoelectric-pyroelectric composites. Mater. Res. Bull. **13**(5), 525–536 (1978)
4. Newnham, R.E., et al.: Composite piezoelectric transducers. Mater. Des. **2**(2), 93–106 (1980)
5. Bandyopadhyay, A., et al.: Processing of piezocomposites by fused deposition technique. J. Am. Ceram. Soc. **80**(6), 1366–1372 (1997)
6. Calignano, F., et al.: Overview on additive manufacturing technologies. Proc. IEEE **105**(4), 593–612 (2017)
7. Safari, A., Allahverdi, M., Akdogan, E.K.: Solid freeform fabrication of piezoelectric sensors and actuators. J. Mater. Sci. **41**(1), 177–198 (2006)
8. Savakus, H.P., Klicker, K.A., Newnham, R.E.: PZT-epoxy piezoelectric transducers: a simplified fabrication procedure. Mater. Res. Bull. **16**(6), 677–680 (1981)
9. Waller, D.J., et al.: Lead zirconate titanate fiber/polymer composites prepared by a replication process. J. Am. Ceram. Soc. **73**(11), 3503–3506 (1990)

10. Clemens, F.J., et al.: Microstructural and electromechanical comparison of different piezoelectric PZT based single fibers and their 1-3 composites. In: 2010 IEEE International Symposium on the Applications of Ferroelectrics (ISAF) (2010)
11. Sebastian, T., Lusiola, T., Clemens, F.: Ferroelectric hybrid fibers to develop flexible sensors for shape sensing of smart textiles and soft condensed matter bodies. Smart Mater. Struct. **26** (4), 045003 (2017)
12. Klicker, K., Schulze, W., Biggers, J.: Piezoelectric composites with 3-1 connectivity and a foamed polyurethane matrix. J. Am. Ceram. Soc. **65**(12), C208–C210 (1982)
13. Bowen, L.J., French, K.W.: Fabrication of piezoelectric ceramic/polymer composites by injection molding. In: 1992 Proceedings of the 8th IEEE International Symposium on Applications of Ferroelectrics, ISAF 1992. IEEE (1992)
14. Rittenmyer, K., et al.: Piezoelectric 3-3 composites. Ferroelectrics **41**(1), 189–195 (1982)
15. O'Donnell, J., et al.: All-printed smart structures: a viable option? In: SPIE Smart Structures and Materials + Nondestructive Evaluation and Health Monitoring. International Society for Optics and Photonics (2014)
16. Safari, A., Akdogan, E.K.: Rapid prototyping of novel piezoelectric composites. Ferroelectrics **331**(1), 153–179 (2006)
17. Jaffe, B., Cook Jr., W.R., Jaffe, H.: The Piezoelectric Effect in Ceramics, in Piezoelectric Ceramics, Chap. 2, pp. 7–21. Academic Press (1971)
18. Heiber, J., et al.: Properties of $Pb(Zr, Ti)O_3$ fibres with a radial gradient structure. Acta Mater. **55**(19), 6499–6506 (2007)
19. Bortolani, F., et al.: High strain in (K,Na)NbO3-based lead-free piezoelectric fibers. Chem. Mater. **26**(12), 3838–3848 (2014)
20. Lusiola, T., et al.: Low shear compounding process for thermoplastic fabrication of ferroelectric lead-free fibres. J. Eur. Ceram. Soc. **34**(10), 2265–2274 (2014)
21. Lusiola, T., et al.: Ferroelectric KNNT fibers by thermoplastic extrusion process: microstructure and electromechanical characterization. Actuators **4**(2), 99 (2015)
22. Kozielski, L., et al.: PZT Microfibre defect structure studied by Raman spectroscopy. J. Phys. D: Appl. Phys. **43**(41), 415401 (2010)
23. Heiber, J., et al.: Ferroelectric characterization of single PZT fibers. J. Intell. Mater. Syst. Struct. **20**(4), 379–385 (2009)

Additive Manufacturing of Semiconductor Silicon on Silicon Using Direct Laser Melting

Marie Le Dantec(✉), Mustafa Abdulstaar, Matthias Leistner,
Marc Leparoux, and Patrik Hoffmann

Laboratory for Advanced Materials Processing, Empa – Swiss Federal
Laboratories for Materials Science and Technology, Thun, Switzerland
Marie.ledantec@empa.ch

Abstract. Currently, Additive Manufacturing (AM) is limited to three classes of materials: ceramics, polymers and metals. Even within these classes, only a small number of materials can be processed by AM, either in a powder bed approach or in a direct energy deposition approach.

We propose to extend AM to a new class of materials: semiconductors. We process silicon powders by direct laser melting (DLM), and we present the experimental setup in details.

AM in general and more precisely DLM of brittle materials is challenging due to thermal stresses and cracks that build up during the process. In this contribution, we demonstrate the possibility of attaching Si pillars built by DLM to a monocrystalline wafer by increasing the pre-heating temperature of the substrate thanks to a hot plate.

Keywords: Silicon · Direct laser melting · Thermal stress

1 Introduction

Additive manufacturing (AM) is an innovative production technology which has been increasingly attracting attention during the past few years. It holds promise in a wide variety of fields including aerospace and defense, medical applications and automotive industries. It provides numerous advantages over conventional manufacturing, such as a high degree of customization, material savings, design of complex parts and creation of lightweight pieces.

Currently, three categories of materials have mostly been studied for AM: ceramics, polymers and metals. There is a need to extend AM to new materials as “improvements to feedstock materials or development of new materials could have a direct impact on facilitating more widespread use of AM” [1].

This contribution investigates silicon as a potential material for AM, to open new horizons for both semiconductor and AM technologies. Semiconductor nanoparticles (such as TiO_2) have already been used in AM materials as additives to improve their mechanical properties [2]. Free form patterning of Si has been achieved by means of layers of chemical vapor deposition of silicon followed by Ga ion implantation by FIB and etching [3]. The features obtained had dimensions ranging from dozens of nanometers to micrometers. However, only one paper was found to have tried AM of a

© Springer International Publishing AG 2018
M. Meboldt and C. Klahn (eds.), *Industrializing Additive Manufacturing - Proceedings of Additive Manufacturing in Products and Applications - AMPA2017*,
DOI 10.1007/978-3-319-66866-6_10

semiconductor material in a powder-bed approach: El-Desouky et al. [4] managed to melt Bi_2Te_3 powders by SLM, opening novel routes to a new class of materials.

Currently, the semiconductor industry is able to make 2.5D structures out of Si, mostly through materials removal approach usually involving photolithography and etching. 3D structures are obtained by more complicated SOI technologies. However, the third dimension is missing to reach total freedom in design, which could be provided by AM. Additionally, it would be interesting to have an alternative process for producing a small number of high-aspect ratio structures on a wafer. In this case, one could avoid material waste caused by extensive etching and decrease the need for harmful chemicals such as HF. Potential applications in MEMS or watch parts are imaginable. Moreover, as standard and most well-known semiconductor, silicon is a good starting point to study the feasibility of AM of semiconductors. Silicon has not yet been published as a possible material in AM using a powder-bed or a direct energy deposition approach.

Silicon is very brittle at room temperature, which makes it difficult to process without cracking due to thermal stresses caused by high thermal gradients across the wafer during the process. In AM of metals, this problem has already been encountered with various other materials. For the alloy Fe-30Al-10Ti, Weisheit and Rolink [5] showed that DLM was only possible if the piece was pre-heated above 700 °C. Rolink et al. showed that Fe–28Al should be pre-heated to 200 °C to obtain defect free samples by DLM [6]. The brittle-to-ductile transition temperature of this alloy was 150 °C. Rittinghaus et al. [7] showed that the titanium alloy Ti-48Al-2Nb-2Cr could not be processed without defects unless an inert atmosphere and pre-heating above 700 °C were used. This temperature also corresponds to the brittle-to-ductile transition of the material. Furthermore, silicon is very sensitive to oxidation.

In this paper, we demonstrate the feasibility of processing silicon powders by DLM by building perpendicular pillar-like shapes onto a monocrystalline silicon wafer. This simple geometry is best for preliminary experimental investigations.

2 Experimental

2.1 Direct Laser Melting (DLM) Setup

The set-up is a flexible research installation allowing for rapid modification or exchange of individual components. A large volume (550 mm height and 580 mm diameter) ultra-high vacuum (UHV) multiflange reactor of more than 200 kg weight acts as chamber and mechanical base for the installation. A photo of the setup is presented in Fig. 1. Flanges are used as feed-through for gases, powders, electric cables or as windows for the laser beam or optical observation purposes. The massive chamber allows for high acceleration and high speed movements of the integrated moving stages.

Moving Stages. Presently, three high precision linear motor driven stages are mounted to a x-y-z system (2 LINAX® Lxs 160F60 and 1 LINAX® Lxc 44F08 from Jenny Science, Switzerland), each with a resolution of 1 µm and an accuracy of ±2 µm. Therefore, this installation can reach a 3D precision of better than 5 µm. The stroke in x

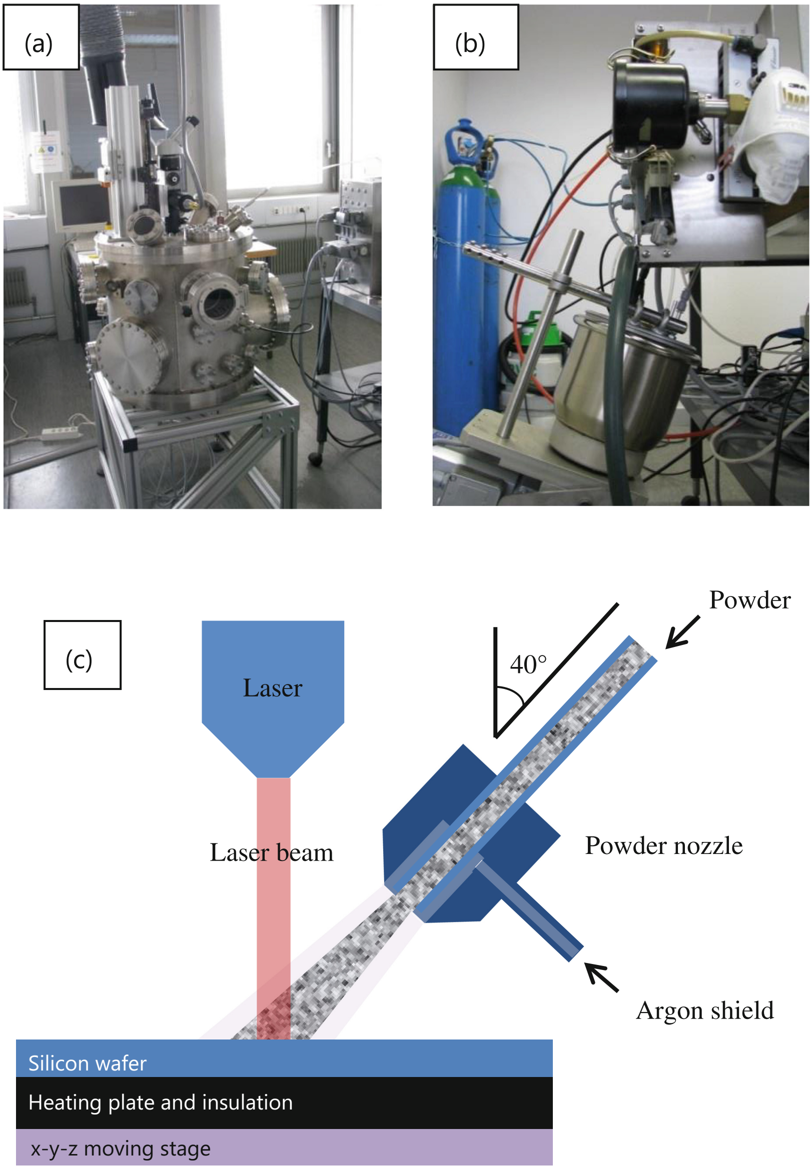
(a)
(b)
(c)
Laser
40°
Powder
Laser beam
Powder nozzle
Argon shield
Silicon wafer
Heating plate and insulation
x-y-z moving stage

Fig. 1. (a) Photo of the laser processing chamber, (b) photo of the powder feeding system and (c) schematic of the configuration inside the chamber

and y directions is 160 mm and 44 mm in the z-direction. Very high maximum speeds of 3 m/s in the x and y direction, and 2 m/s in the z direction, can respectively be reached. The 3 stages (and further stages, if added) are piloted by a Beckhoff TwinCAT3 PLC system with feed-back control and data I/O exchange up to 20 kHz (Beckhoff Automation AG, Switzerland). Furthermore, other parameters such as powder feeding rates, laser parameters such as pulse energy, pulse duration, pulse modulation and a laser trigger will be controlled also by this state-of-the-art control unit.

Laser. The illumination system used is a pulsed 1064 nm Nd:YAG solid state laser (SLS 200 C60 from LASAG AG, Switzerland). The Nd:YAG is excited with a pulsed flash lamp under free running pulse conditions. Pulse durations can be in the range of 0.1−20 ms and the energy limit per pulse is about 50 J. The laser beam is coupled into a 400 µm core diameter step index fiber (LL422 from Rofin-LASAG, Switzerland) to deliver the beam to the laser beam head (LLBK45, from Rofin-LASAG, Switzerland) fixed on a z-moving stage to adjust the image plane on the substrate surface. The fiber exit is magnified by 1.5, resulting in a focal spot of 600 µm diameter on the substrate plate. Average peak intensity of up to 177 MW/cm^2 can be delivered to the work-piece through the focal spot. The laser intensity is controlled through the flash lamp current, with a modulation frequency of 20 kHz. Due to the applied coupling into the multi-mode fiber a flat cone topped hat intensity profile is obtained (see Fig. 2, top line in the focal plane (0 mm) with about 20% intensity maximum in the center as compared to the edge). The laser intensity had to be strongly reduced for measuring the beam profile by a beam splitter and neutral density filters. The very large depth of field deforms this intensity profile slightly by increasing the distance between the lens and the observation plane by 0.5 mm and 1 mm, at 2 mm out of focus, the intensity profile approaches a Gaussian-like intensity distribution that widens with further increase of the distance.

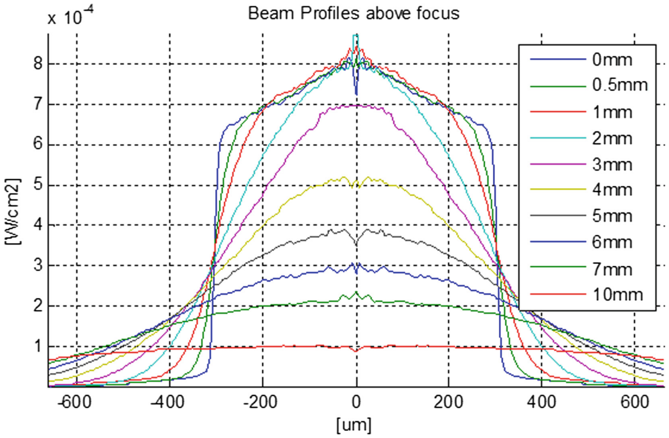

Fig. 2. Strongly reduced intensity beam profile in and out of focus for the pulsed 1064 nm Nd:YAG solid state laser (SLS 200 from LASAG AG, Switzerland)

Powder Feeder. The powder injection takes place through a lateral injection nozzle linked to a powder feeder. The powder jet center is aligned with the laser beam focus on the surface of the substrate (Fig. 1c). The powder feeder, Impakt$^{\mathrm{TM}}$, was purchased from P&S Powder and Surface GmbH in Germany. The feeder consists of a powder container, a feeder chamber with two cells and a control unit. It is connected to an Argon pressure bottle delivering the inert transport gas. The powder transport is based on the pressure difference between the feeder cells and the process chamber. The functional principle in brief: first, the feeder cell is evacuated using a vacuum pump, then powder is sucked into the cell due to the pressure difference between the powder container and the evacuated feeder cell. A filter membrane is retaining the powder in the cell. Argon is pressed into the powder containing feeder cell to increase the pressure and then the valve to the process chamber is opened leading to transport of the powder into the chamber. Continuous repetition of this process results in a pulsed powder transport. In our case, one cell was working at 5 Hz. Several chambers can run consecutively resulting in a pulsed quasi-continuous gas transported powder feed. The feeding rate can be changed by adjusting the vacuum (pressure) inside the intermediate chamber or by adapting the opening-closing time of the different valves governing the transport process.

The powder is sucked into the feeder cell from a rotating container, inclined with an angle of 25° with respect to horizontal, to keep powders moving. The container has a diameter of 20 cm and a height of 20 cm, and can contain up to 2 kg of powder. The sucking tube and the lid of the container are held in a fixed position. The container atmosphere is kept under a slight overpressure of Argon. A special stirring plate was mounted in the powder feeder container to keep the powder flowing during the feeding process. Two tubes are linking the cell and the nozzle: the first one made out of plastic, of inner diameter 4 mm and outer diameter 6 mm, followed by a stainless steel tube of inner diameter 3 mm and outer diameter 6 mm. The first tube is 105 cm long and the second one is 36.2 cm long.

Nozzle. The powder nozzle consists of two coaxial tubes. The inner one, for powder transportation, has an inner diameter of 3 mm and an outer diameter of 6 mm. The outer tube, for the argon shield, has an inner diameter of 7 mm. The argon supply is delivered through a tube placed perpendicularly to the powder tube (see Fig. 1c). The shielding gas flow of 14.6 L/min of argon protects the powder from remaining traces of water or oxygen in the process chamber. The argon flow is controlled through a flowmeter, and forms a laminar flow at the exit of the tube, according to the calculated Reynold’s number equal to 1500. The angle of the injection nozzle with respect to the laser beam is 40°, and the nozzle-to-substrate distance is 8 mm.

Hot Plate. A resistively heated silicon nitride hot plate (Bach Resistor Ceramics GmbH) was mounted on the moving stage to pre-heat the wafer substrates. Its temperature is controlled by a PID unit (LabHeat®, SAF Wärmetechnik GmbH) by reading out the signal of a K-type thermocouple recording the temperature of the plate. The hot plate is thermally isolated from the motion stage platform with a 15 mm thick ceramic plate.

2.2 Process

As schematically presented in Fig. 1c, the process was made under an Argon shielding gas at 14.6 L/min. The substrate was heated up in steps of 100 °C every 5 min to avoid overshooting. The final temperature of the hot plate was set to 980 °C. The heating cycle was realized under 14.6 L/min of argon to avoid further oxidation of the Si wafer. The laser started shooting to create a melt pool before the powders were injected. If not otherwise specified, the laser parameters were: output power set at 600 W, pulse duration 1 ms, frequency 50 Hz, resulting in 395 mJ per pulse. The pillars were built with a stage in z-motion, at a speed of 0.1 mm/s. The building time was about 50 s. However, the pillars are built at a slightly faster rate of about 0.12 to 0.16 mm/s. After growth, the laser, and the heating stage were switched off and the substrate cooled down to room temperature.

2.3 Materials

The silicon powder used in this study was obtained from the company Keyvest, Belgium. It was metallurgical grade, with 98% purity. The particle size distribution as given by the manufacturer was $d_{50} = 16.33$ μm, $d_{10} = 3.37$ μm and $d_{90} = 41.74$ μm. The powders are kept under vacuum at a temperature of 100 °C when not used, to avoid water adsorption and further oxidation.

The wafers used are p-doped (boron) monocrystalline test wafers having a resistivity ranging between 0.1 and 100 Ω cm, and thickness of 525 μm. Their orientation was <100> and they were polished on one side. The polished side was used in all the experiments presented.

2.4 Powder Characterization

The particle morphology was observed by Scanning Electron Microscopy Hitachi S-4800. The particle size distribution was analyzed by HELOS&RODOS Laser Diffraction Sensor of Sympatec GmbH. The powder oxygen content was determined by combustion and infrared analysis with a LECO TC-500. The powder was placed in a tin capsule with nickel chips. The sample was then melted in a graphite crucible in an electrode furnace at about 3000 °C. The oxygen was detected as CO_2 after reaction with the graphite crucible by quantitative infrared analysis.

2.5 Temperature Measurements

The temperature at the surface of the wafer was difficult to estimate. Optical methods are under investigation for wafer surface temperature measurements. So far, the hot plate was set to 980 °C, resulting in an estimated temperature of more than 700 °C at the surface of the wafer.

2.6 Pillar Characterization

All the samples produced by DLM were embedded in a resin and mechanically grinded to observe their cross-section. The morphology of the cross-sections as well as its microstructure were then observed by optical microscopy and scanning electron microscopy (Hitachi S-4800). The chemical analyses were performed by EDX analysis.

3 Results

3.1 Powder Characterization

Figure 3 illustrates the silicon powder size distribution with 3.37, 16.33 and 41.74 µm for D_{10}, D_{50} and D_{90}, respectively. The measured oxygen content was 0.7 wt%.

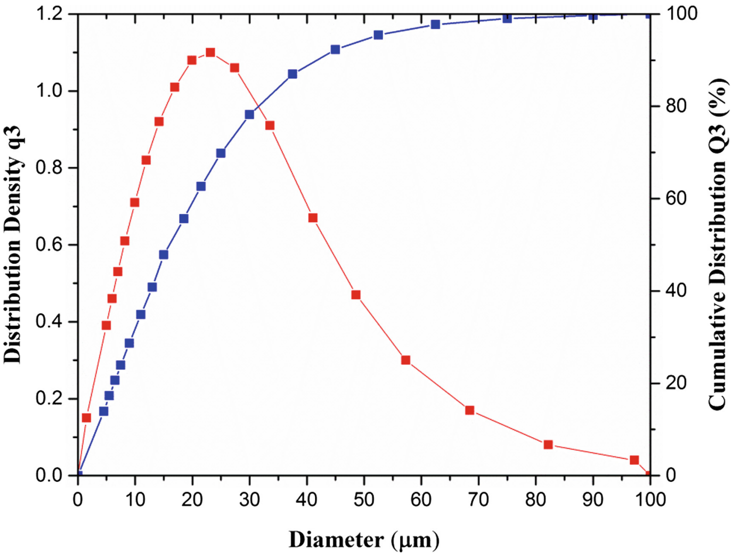

Fig. 3. Silicon powder particle size distribution

The morphology of the silicon powder investigated by Scanning Electron Microscopy is shown in Fig. 4. The particles show sharp edges and they are not spherical. They also show a broad particle size distribution. Thus, the flowability of the powder is poor even when it is dried in a furnace for several hours. Standardized flowability

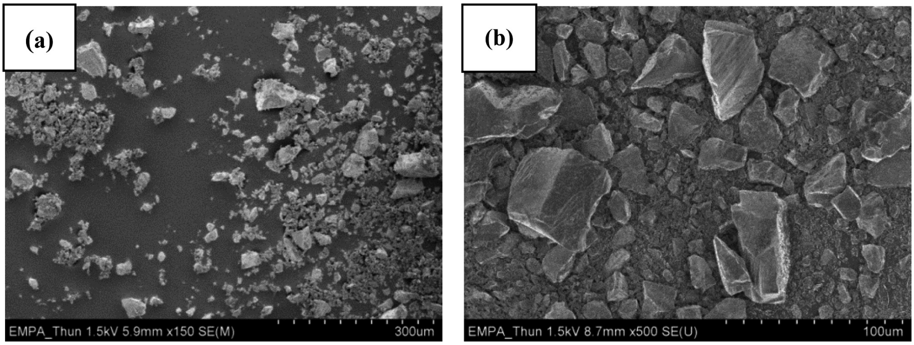
(a)
EMPA_Thun 1.5kV 5.9mm x150 SE(M)
300um
(b)
EMPA_Thun 1.5kV 8.7mm x500 SE(U)
100um

Fig. 4. SEM pictures of silicon powder: (a) low magnification and (b) higher magnification

measurements failed, as no powder was flowing through the 18 mm cone hole diameter resulting in no flowability value. Nevertheless the powder transport with the used pulsed powder feeder was realized.

X-ray fluorescence (XRF) of silicon powder is shown in Fig. 5. The results show that the powder is containing metallic impurities such as iron, nickel, manganese and tungsten. The Si signal size underestimates the amount of silicon, due to the lower atomic number of Si.

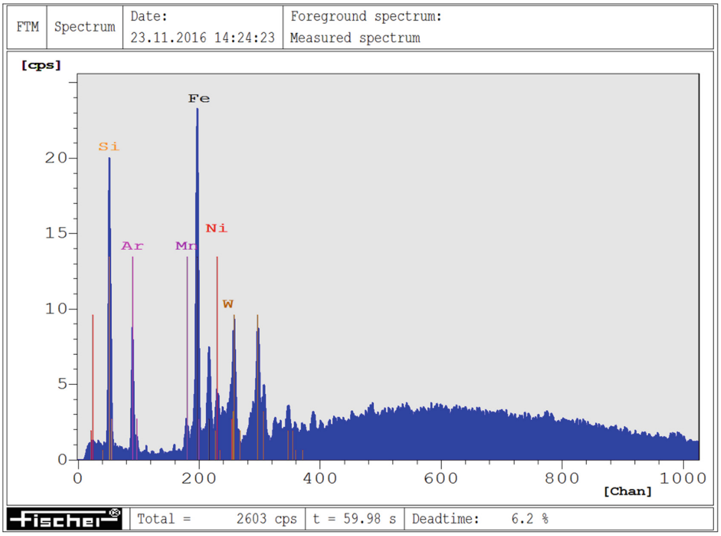

Fig. 5. X-ray fluorescence of silicon powder. The main contaminant was found to be Fe.

3.2 Deposition Experiments

The deposition process is carried out by switching the pulsed laser on for 1 to 2 s in order to preheat or melt the substrate before adding the powder supply. The latter modifies the temperature profile strongly due to adding "cold" powder and gas to the laser irradiated system. To which extend this shock cooling results in cracking of the substrate is presently under investigation.

Pillars Built at Room Temperature. Pictures of pillars built at room temperature on a wafer substrate are shown in Fig. 6. An optical microscope picture of the cross-section of a Si pillar built on a Si monocrystalline wafer at room temperature is shown on Fig. 7. The stage was moving at 0.1 mm/s. After processing, a large crack appears at the base of the pillar in contact with the wafer. However, the pillars could also be built into tall needles without breaking in the middle of the process, as shown in Fig. 6, thanks to the presence of unmolten sintered silicon powders that consolidated the base of the latter. However, the pillars were often broken at this very location.

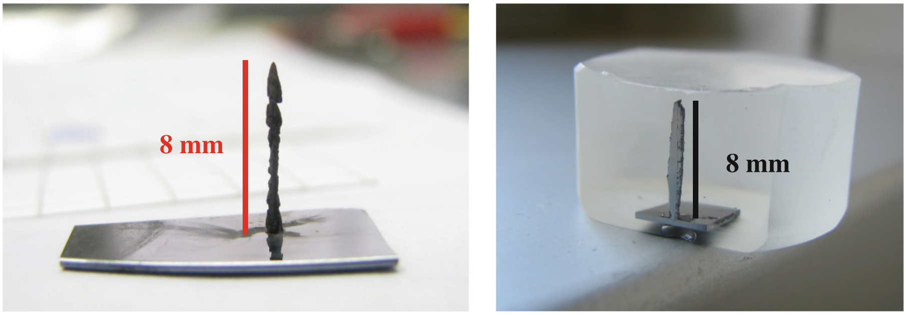

Fig. 6. (a) Photo of a Si pillar built on a monocrystalline wafer. The stage was moving in the z-direction at 0.1 mm/s. It was 8 mm tall. (b) Photo of a Si pillar embedded in resin and mechanically grinded to reveal its cross-section. Its height was 8 mm and width 600 µm.

Even if the base of the pillar is broken, it is still possible to embed it in resin because a large amount of consolidated powder is stuck around the pillar, making it stable enough for the embedding (see Fig. 7). It is unlikely that the pillar breaks during embedding because all of them clearly present different features from the ones for which the substrate heater was set to 980 °C. Moreover, its microstructure is discontinuous on both sides of the cracks: the wafer side shows a monocrystalline microstructure whereas the pillar side shows a multicrystalline microstructure (Fig. 8). This suggests that the crack appeared during laser processing.

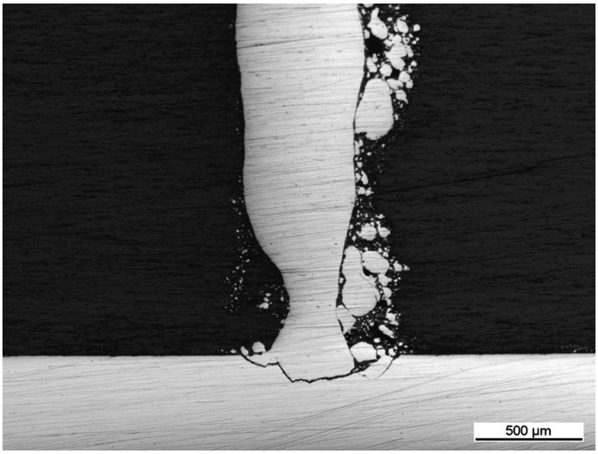

Fig. 7. Optical microscope observation of the cross-section of a Si pillar built on a monocrystalline Si wafer at room temperature. The stage was moving in the z-direction at 0.1 mm/s. The base of the pillar is not attached to the wafer, and presents a crack.

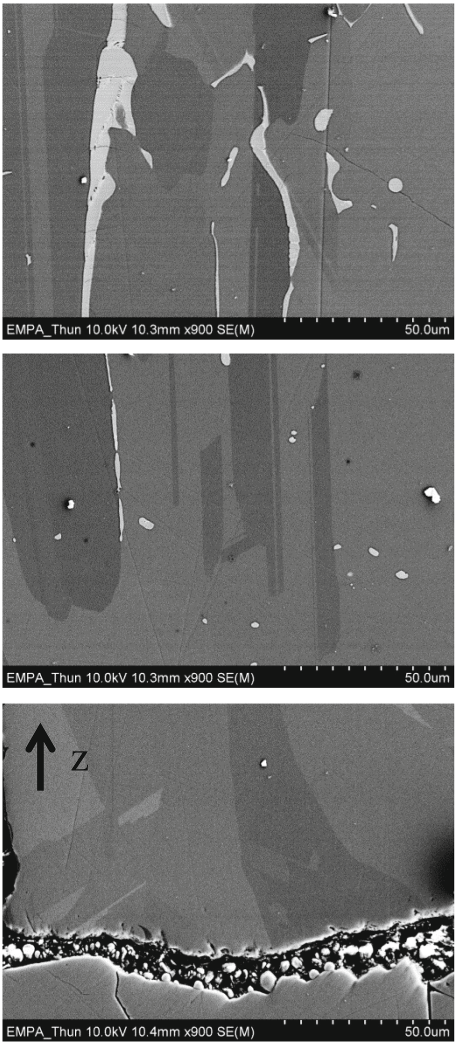
EMPA_Thun 10.0kV 10.3mm x900 SE(M) 50.0um
EMPA_Thun 10.0kV 10.3mm x900 SE(M) 50.0um
Z
EMPA_Thun 10.0kV 10.4mm x900 SE(M) 50.0um

z = 7 mm
Top of the pillar

z = 3 mm
Middle of the pillar

z = 0 mm
Base of the pillar

Fig. 8. SEM pictures of the microstructure of a Si pillar built at room temperature, with a power of 500 W (332 mJ per pulse). The stage was moving in the z-direction at a speed of 0.1 mm/s. The arrow represents the pillar building direction (z-direction). The microstructure shows directional growth. Inclusions of metallic impurities were found to be more numerous at the top of the pillar. The inclusions were mostly Fe and Al, as measured by EDX.

The microstructure of a pillar on the longitudinal cross-section was observed by SEM. The pictures are displayed in Fig. 8. From bottom to top, the grains are several dozens of micrometers long. The growth is directional, as we see elongated grains in the direction of pillar building. The pillars contained impurities. These impurities were more and more visible as we reach the top of the pillar. The SEM image also shows that they segregated at the grain boundaries. EDX analysis of the inclusions was performed.

It showed that they were mostly containing Fe, and some Al. XRF of the powders, displayed in Fig. 5 demonstrates that Fe is the main impurity in the Si powder used in the process. Moreover, stainless steel powder was also used previously in the same chamber. Therefore, we concluded that impurities were coming from these two sources. The use of metallurgical grade silicon instead of highly pure silicon on a highly pure silicon substrate can influence the microstructure.

Pillars Built with Pre-heating Under Ar with a Hot Plate Set at 980 °C. After setting the hot plate at 980 °C, and performing the heating ramp of the wafer under an inert gas shield of argon, we processed the powders under the same conditions as in Fig. 7. The cross-section of the obtained sample is presented in Fig. 9. This time, there is a clear connection between the wafer and the pillar. Some cracks can however be seen on the sides of the pillar.

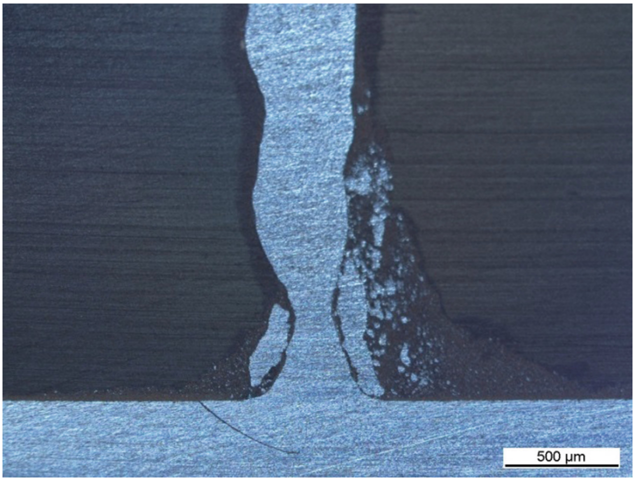

Fig. 9. Optical microscope observation of the cross-section of a Si pillar built on a monocrystalline Si wafer. The wafer was heated under a flow of Ar of 14.6 L/min. The hot plate was set at 980 °C. The pillar is now attached to the substrate, even if cracks are visible on the sides of the pillar.

4 Discussion

As seen in Fig. 8, when a crack appears between the wafer and the pillar, the latter's microstructure is polycrystalline, with directional growth. The directional growth of the pillar, as well as the impurity segregation location, are well-known phenomena described in the literature for crystal growth. Segregation coefficients of iron and aluminum impurities are $6.4.10^{-6}$ and 0.002 respectively [8]. Therefore, their concentration will be higher in the melt, hence their preferential location at the top of the pillar. They are also well-known for segregating at the grain boundaries. The directional growth is similar to the one we find in the crystal growth industry when the crystal is pulled out of the heating zone.

By pre-heating the silicon wafer prior to silicon deposition, successful attachment of the pillar to the wafer was obtained as presented in Fig. 9. We explain it by a reduction of the temperature difference between the substrate and the melt and therefore a reduction of thermal stresses during processing. Two different cases could be assumed: either the brittle-to-ductile transition temperature of our substrate was overcome by heating the latter with the hot plate, or simply reducing thermal gradients was sufficient to avoid cracking at the base of the structure.

As mentioned in the introduction, the AM process of many brittle alloys was successful when the substrate was heated at a temperature higher than the brittle-to-ductile transition. The brittle-to-ductile transition of silicon can range from 500 to 1000 °C. It is widely accepted that the brittle-to-ductile transition of silicon occurs over a very narrow range of temperatures, of the order of 10 K. However the transition temperature depends on the resistivity of the wafer. It also depends on the strain rate used in the experiments. The transition temperature can vary by 100 °C when the strain rate is changed by 10 times [9]. If the loading rate decreases, the transition temperature decreases as well [10]. Our wafers are p-doped test wafers having a resistivity ranging between 0.1 and 100 Ω cm (intrinsic to slightly doped, 10^{14} to 10^{16} atoms/cm^{3}). Hirsch et al. [9] found that for an intrinsic Si single crystal at the lowest strain rate the transition temperature was 550 °C. Therefore, it is possible that the brittle-to-ductile transition in our case is relatively low, below the temperature at which the silicon wafer has been pre-heated during our experiments. Therefore, the success in connecting the pillar to the wafer substrate could be owed to pre-heating of the substrate to a temperature higher than the brittle-to-ductile transition.

On the other hand, reducing thermal gradients throughout the structure by pre-heating the wafer substrate may also have been sufficient to reduce thermal stresses enough so that no cracking occurs at the interface between the wafer and the pillar.

Despite the attachment between the pillar and the wafer, horizontal cracks are often present in the Si pillar structure. During deposition, the pillar is much warmer than the wafer substrate, due to the pulsed laser exposure. On the contrary, when the laser is turned off, the pillar is convectively cooled by the continuous flow of argon shielding gas to a lower temperature than the pre-heated substrate. Therefore, a strong thermal gradient is present across the whole structure. Due to thermal expansion, stress is induced between the lower and the upper part of the structure, which could explain the cracking.

Cracks at the border between the melt pool and the unmolten material appear in all the samples, one shown as example in Fig. 9. Again too high thermal gradients between the wafer and the melt pool during processing could be the cause of these cracks. They could also be the results of high heating rate during the first laser pulses.

5 Conclusions

A home-built DLM system allowing transport of non-flowable powder in the form of an inert gas transported jet into a laser melt pool is described. This system enabled us to grow material perpendicular to the surface of a monocrystalline silicon wafer substrate. First results show that without wafer preheating the silicon pillars did not attach to the wafer probably due to thermal stresses caused by too high temperature gradients. However, the build pillars possess a multi-crystalline microstructure with directional growth along the direction of pillar building. Preheating the wafer probably above the brittle ductile transition temperature of the silicon wafer by setting the temperature of the hot plate to 980 °C pillars grew on the silicon wafer attached on the wafer, still showing a crack in the wafer close to the pillar.

In the future, improvements can be made by using the moving stage to grow pillars of better shape. Additionally, very slow cooling rate could be applied to avoid as much as possible the residual thermal stresses. Higher grade silicon will be used in further studies.

Acknowledgments. The authors would like to thank Bernhard von Gunten, Christoph Amsler and Mehari Asfaha for the technical support on building and improving the process chamber. We would also like to thank Renato Figi and Melanie Bürki for the combustion and infrared analysis measurements.

References

1. Jurrens, K., Energetics incorporated for NIST (National Institute for Standards and Technology): measurement science roadmap for metal-based additive manufacturing. Workshop Summary Report (2013)
2. Ivanova, O., Williams, C., Campbell, T.: Additive manufacturing (AM) and nanotechnology: promises and challenges. Rapid Prototyp. J. **19**(5), 353–364 (2013). doi:10.1108/RPJ-12-2011-0127
3. Fischer, A.C., Belova, L.M., Rikers, Y.G.M., Malm, B.G., Radamson, H.H., Kolahdouz, M., Gylfason, K.B., Stemme, G., Niklaus, F.: 3D free-form patterning of silicon by ion implantation, silicon deposition, and selective silicon etching. Adv. Func. Mater. **22**, 4004–4008 (2012). doi:10.1002/adfm.201200845
4. El-Desouky, A., Read, A., Bardet, P., Andre, M., LeBlanc, S.: Selective laser melting of a bismuth telluride thermoelectric material. In: Proceedings of Solid Freeform Fabrication Symposium, pp. 1043–1050 (2015)
5. Weisheit, A., Rolink, G.: Influence of process conditions in laser additive manufacturing on the microstructure evolution of Fe-Al alloys: a comparison of laser metal deposition and selective laser melting. In: AAM Workshop. MPIE, Düsseldorf (2016)
6. Rolink, G., Vogt, S., Senčekova, L., Weisheit, A., Poprawe, R., Palm, M.: Laser metal deposition and selective laser melting of Fe-28 at.% Al. J. Mater. Res. **29**(17), 2036–2043 (2014). doi:10.1557/jmr.2014.131
7. Rittinghaus, S.-K., Weisheit, A., Mathes, M., Vargas, W.G.: Laser metal deposition of titanium aluminides – a future repair technology for jet engine blades? In: 13th Proceedings of World Conference on Titanium, pp. 1205–1210. Wiley (2016)
8. Sakiotis, N.: Role of impurities in silicon solar cell performance. Sol. Cells **7**, 87–96 (1982)
9. Hirsch, P.B., Roberts, S.G., Samuels, J., Warren, P.D.: The brittle-to-ductile transition in silicon. In: Mechanics of Creep Brittle Materials 1, pp. 1–12. Elsevier Science Publishers Ltd. (1989)
10. Brede, M.: The brittle-to-ductile transition in silicon. Acta Metall. Mater. **41**(1), 211–228 (1993)

Additive Manufacturing of Complex Ceramic Architectures

Oscar Santoliquido, Giovanni Bianchi, and Alberto Ortona(✉)

HM Laboratory at MEMTI, SUPSI,
Strada Cantonale 2C, 6928 Manno, Switzerland
alberto.ortona@supsi.ch

Abstract. Additive manufacturing (AM) has the potential to revolutionise engineering because of its advantages in the product development phase. The revolution consists in the fact that components can be designed for their function and no longer for their manufacturability. This is already a reality for plastic and metallic components where new disruptive designs have been already produced at competitive costs.

Following the AM hype, the ceramic industry is now thinking to adopt this technique for industrial components. Stereolithography (SLA) is nowadays used to fabricate complex structures in all the material classes.

Two components designed for their function and produced by SLA are here presented along with their unique features. These components were developed for industrial applications in the automotive industry as well as for heat management (production, transfer and storage).

1 Introduction

Cellular structures are hybrid materials comprised of a solid and a gaseous phase. In random cellular materials their effective properties can be modified mostly by controlling the amount of the solid phase (i.e. their density). Periodic cellular structures though, are obtained by placing the solid phase according to a unit cell which is then reproduced into the space. The use of these structures allows a real material's engineering by working on their topology.

In a recent paper we reviewed different methods to design and produce cellular ceramic by 3D printing [1] while leaving the interested reader to a more general view on additive manufacturing of ceramics [2, 3] here focus on one of them: stereolithography. Several components were designed following end users' requirements and produced by SLA. These components were developed for industrial applications in the automotive industry as well as for heat management (production, transfer and storage). Before their final employment it is necessary to endorse some of their effective properties by experimental testing. In this work we show some of them, namely: pressure drop and heat exchange ability (for heat exchangers) and mechanical strength (for handling).

SLA is an additive manufacturing (AM) process in which ultraviolet (UV) light is used to cure a polymer. SLA was first used to manufacture polymeric structures, however further modifications allowed SLA to be used for processing ceramic

© Springer International Publishing AG 2018
M. Meboldt and C. Klahn (eds.), *Industrializing Additive Manufacturing - Proceedings of Additive Manufacturing in Products and Applications - AMPA2017*,
DOI 10.1007/978-3-319-66866-6_11

materials [4, 5]. Ceramic particles are dispersed in a resin containing a photo initiator. This reactive system allows the fabrication of three dimensional ceramic/plastic parts thanks to UV light that induces their polymerization and further thermal treatments. The object is built layer by layer, obtained by slicing a 3D numerical model (.stl file).

Printing flexibility of different geometrical features, high accuracy of ceramic structures are the main advantages of SLA. However, supporting structures during manufacturing are needed while printing (Fig. 1 bottom-left) [4].

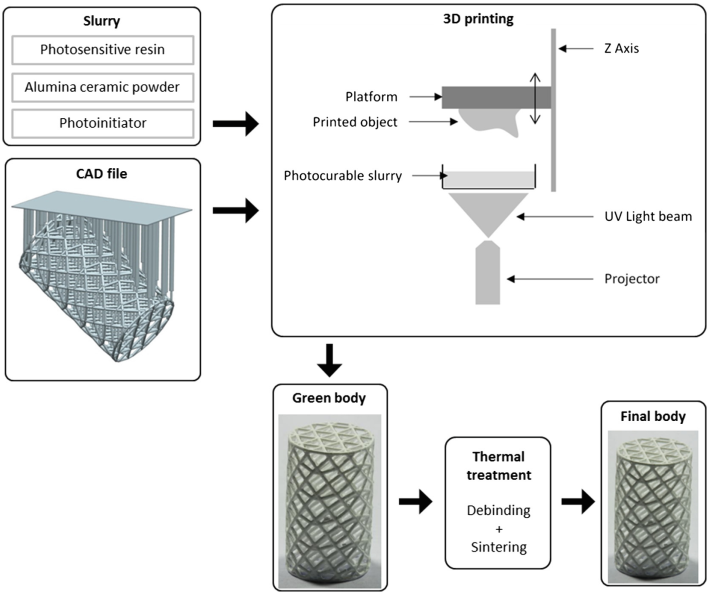
Slurry
Photosensitive resin
Alumina ceramic powder
Photoinitiator
CAD file
3D printing
Z Axis
Platform
Printed object
Photocurable slurry
UV Light beam
Projector
Green body
Thermal treatment
Debinding
+
Sintering
Final body

Fig. 1. Flowchart of the process developed

2 Experimental Procedure

A literature review helped us to formulate a suitable slurry (i.e. a dispersion of ceramic powders into the reactive monomer) for stereolithography. The composition of the slurry plays a fundamental role. According to [6–8], a stable suspension can be achieved by mixing a reactive resin with a diluent (constituting the UV curable system), and then adding a photo initiator and a dispersant. The ceramic powder represents the filler. Often, the particles are previously de-agglomerated and dried before dispersing them into the resin. Once cured, the polymer creates a rigid matrix around ceramic particles which confers cohesion to the body.

The final slurry receipt developed for this study comprises an acrylic resin TPGDA 56.8 vol% (Allnex, Luxenburg, Luxenburg) mixed with ceramic powders (D90: 2 µm) 42 vol% (Nabaltec, Schwandorf, Germany) and UV photo initiator: Irgacure 819 1.2 wt% (BASF, Ludwigshafen, Germany). Slurry was thoroughly mixed by ball mixing for 24 h with zirconia balls $\Phi = 8.5$ mm.

The main steps to generate a ceramic body from a three dimensional numerical model are shown in Fig. 1. In case of periodic structures, component design consists in building a large numerical domain made by staking cells and then intersecting it with a desired shape [1]. The edges and nodes of the resulting architecture are then substituted with cylinders and spheres respectively. Models were designed using commercial CAD software (UGS NX 10.0, Siemens, Munich, D) and a Matlab script (The Mathworks Inc., Natick, MA).

Printing was performed with a 3DLPrinter – HD 2.0 (RobotFactory, Mirano, Italy). Printing parameters were set as following: slice thickness: 0.05 mm, slice exposure time: 1.1 s.

The polymerized resin in the 3D printed body was subsequently removed by an appropriate thermal treatment at low temperatures. Then the sintering of the green part at high temperature ensured the final properties of the ceramic.

Thermal treatment (Nabertherm, Lilienthal, Germany) on the green bodies were performed as following: de-binding with 1 °C/min heating rate until 300 °C with a dwell of 0.5 h, followed by 0.8 °C/min up to 400 °C. Sintering of the part with a ramp of 2.5 °C/min up to 1600 °C with a dwell of 2 h.

3 Applications

This paragraph presents a couple of applications of periodic cellular architectures for high temperature, harsh working conditions. Their peculiarity stands in the opportunity to design these structures for their function without considering the limits brought by conventional ceramic manufacturing. Usually ceramic manufacturing utilizes molds or similar tools in order to shape the green body. With such an approach it is impossible to produce such architectures. As for metal or plastic additive manufacturing, ceramic 3D printing allows to realize components with unmatched properties: we show here some of them.

4 Automotive Catalytic Supports

In some industrial applications, like catalytic supports, foams structures are used. This solution presents several advantages over the standard honeycomb solution. On the other hand foams cannot be engineered in terms of their end user requirements since they employ random foams [9].

With our methodology [1] it was possible to produce catalyst for engine exhaust with the desired shape, optimized in terms of his final requirements [10–12].

Thanks to this method, smaller catalyst based on specifically designed engineered structures has been developed, with a very low amount of precious metal and without sacrificing pollutant conversion.

Another advantage of this technique is that the 3D printed strut has a surface area which is 26% wider than the nominal one (Fig. 2), thanks to the "staircase" morphology typical of this additive manufacturing process.

This larger surface means more reaction and better catalytic effect.

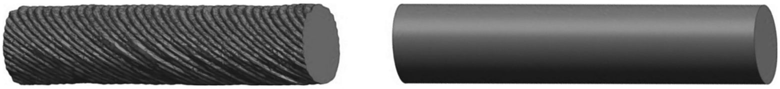

Fig. 2. 3D printed strut compared with a theoretical strut: on the left a strut surface reconstructed from CT micro tomography (source EMPA), on the right the surface of the corresponding strut realized by CAD.

On the other hand this "stair case" effect has some influence on the overall mechanical properties of the component. Ceramic architectures were printed five times with four different orientations in respect of the building direction with the goal to induce a different layering angle. Samples were tested under compression at 0.5 mm/min (Zwick/Roell Z050 Germany), cross head displacements and loads were recorded with a 5 kN load cell (Zwick/Roell, D).

Table 1 shows how this orientation affects mechanical properties of the component. An ideal orientation must be selected in order to trade off surface enhancement and mechanical properties.

Table 1. Mean failure load [N] and the standard deviation [N] for different printing angles of the same component. The orientation in respect to the building direction is depicted in the second row of the table.

Horizontal (A)	Horizontal (B)	Tilted (A)	Tilted (B)	Vertical
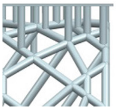	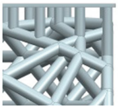	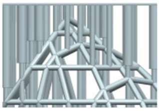	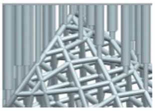	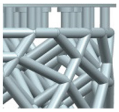
35.8 ± 16.2	27.0 ± 6.5	16.0 ± 6.6	21.4 ± 6.2	19.4 ± 6.7

5 Heat Exchangers

Currently, the demand for ceramic heat transfer systems is increasing to answer the needs of energy-intensive industry, such as in cement, metals and petro-chemical plants as well as in concentrated solar energy field. Tubular heat exchanger are widely used in several applications because they are easy to assemble and maintain. The drawback of this solution is its low efficiency [12] which is related with the capacity of the system to drain the heat from the outside to the air flowing inside it. Engineered cellular architectures, possibly inserted inside a dense tubular skin, enhance the heat exchange efficiency due to the favourable convection and radiation phenomena induced by the inner architecture [5, 12, 13].

Thanks to an high temperature pressure drop test rig developed in-house (Fig. 3), it was possible to measure these properties of the 3D printed ceramic architectures. A controlled air flow was forced into an alumina tube with and without alumina periodic architectures. The tube was then placed through a furnace which was heated in its central part (Fig. 3).

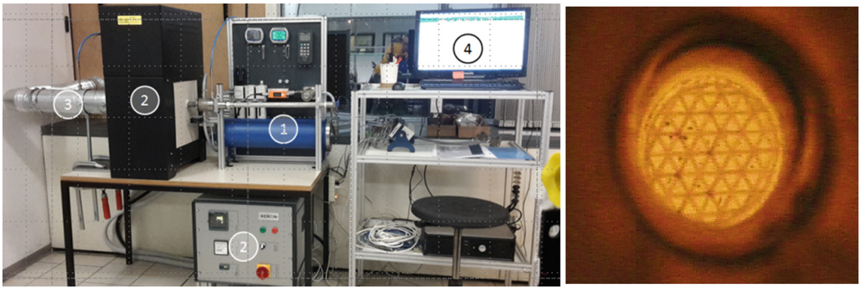

Fig. 3. On the left the test apparatus: (1) flow metering, (2) furnace, (3) exhaust, (4) control unit. On the right a ceramic architecture during high temperature test (700 °C)

Figure 4 compares the temperature of the air at the outlet with and without the presence of an alumina 3D printed lattice inside the tube. The outlet temperature increase significantly with the presence of the lattice. On the other hand the pressure drop increases as shown in Fig. 5.

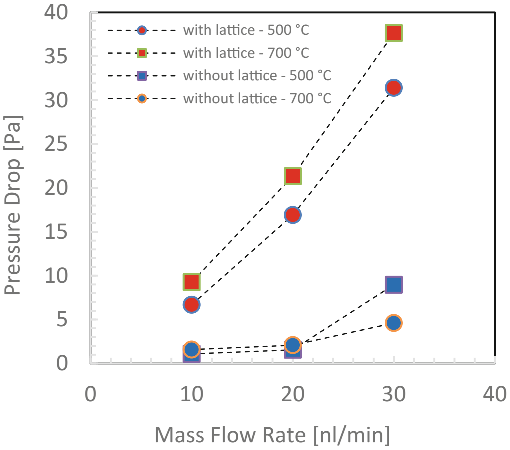

Fig. 4. Pressure drop vs mass flow rate

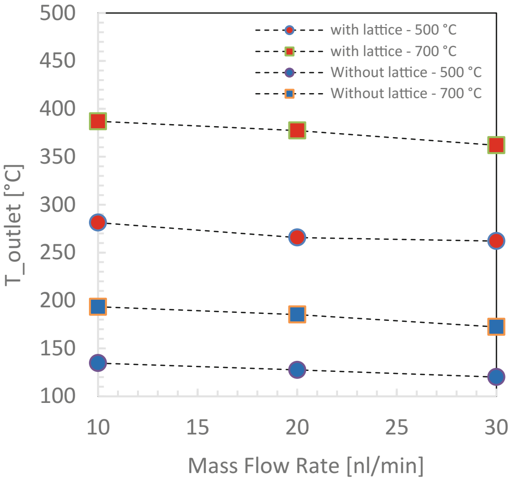

Fig. 5. Outlet temperature vs mass flow rate

Even though the lattice was made by alumina, known to have a low thermal conductivity (25 [W/m K] at room temperature for a 96% dense Al_2O_3), a significant increase of the heat exchange capability of the system was experienced. This because of the favourable combination of radiative and convective heat exchange regime introduced by the lattice. The overall efficiency can be increased depending on the cellular architecture employed without scarifying too much the pressure drop [12].

6 Conclusions

Stereolithography, modified for ceramic suspensions, allows the production of complex ceramic architectures with engineered features. Thanks to this technique complex structures can be designed and realized. Former simulation work allows to realize an optimal geometry in respect of the properties which needs to be maximised. Two examples of periodic ceramic architectures which were realized via this method were presented: a structure for automotive catalysts and a tubular heat exchanger.

References

1. Bianchi, G., Gianella, S., Ortona, A.: Design and additive manufacturing of periodic ceramic architectures. J. Ceram. Sci. Technol. **8**(1), 59–66 (2017)
2. Zocca, A., Colombo, P., Gomes, C.M., Günster, J.: Additive manufacturing of ceramics: issues, potentialities, and opportunities. J. Am. Ceram. Soc. **98**(7), 1983–2001 (2015)
3. Travitzky, N., Bonet, A., Dermeik, B., Fey, T., Filbert-Demut, I., Schlier, L., Schlordt, T., Greil, P.: Additive manufacturing of ceramic-based materials. Adv. Eng. Mater. **16**(6), 729–754 (2014)
4. Bandyopadhyay, A., Bose, S. (eds.): Additive Manufacturing. CRC Press (2015)

5. Griffith, M.L., Halloran, J.W.: Freeform fabrication of ceramics via stereolithography. J. Am. Ceram. Soc. **79**(10), 2601–2608 (1996)
6. Mitteramskogler, G., Gmeiner, R., Felzmann, R., Gruber, S., Hofstetter, C., Stampfl, J., Ebert, J., Wachter, W., Laubersheimer, J.: Light curing strategies for lithography-based additive manufacturing of customized ceramics. Addit. Manuf. **1**, 110–118 (2014)
7. Licciulli, A., Corcione, C.E., Greco, A., Amicarelli, V., Maffezzoli, A.: Laser stereolithography of ZrO_2 toughened Al_2O_3. J. Eur. Ceram. Soc. **24**(15–16), 3769–3777 (2004)
8. Hinczewski, C., Corbel, S., Chartier, T.: Ceramic suspensions suitable for stereolithography. J. Eur. Ceram. Soc. **18**(6), 583–590 (1998)
9. D'Angelo, C., Ortona, A.: Cellular ceramics produced by replication: a digital approach. Adv. Eng. Mater. **14**(12), 1104–1109 (2012)
10. Della Torre, A., Lucci, F., Montenegro, G., Onorati, A., Eggenschwiler, P.D., Tronconi, E., Groppi, G.: CFD modeling of catalytic reactions in open-cell foam substrates. Comput. Chem. Eng. **92**, 55–63 (2016)
11. Lucci, F., Della Torre, A., Montenegro, G., Eggenschwiler, P.D.: On the catalytic performance of open cell structures versus honeycombs. Chem. Eng. J. **264**, 514–521 (2015)
12. Lucci, F., Della Torre, A., von Rickenbach, J., Montenegro, G., Poulikakos, D., Eggenschwiler, P.D.: Performance of randomized Kelvin cell structures as catalytic substrates: mass-transfer based analysis. Chem. Eng. Sci. **112**, 143–151 (2014)
13. Vignoles, G.L., Ortona, A.: Numerical study of effective heat conductivities of foams by coupled conduction and radiation. Int. J. Therm. Sci. **109**, 270–278 (2016)

Process Chain Integration

An Advanced STEP-NC Platform for Additive Manufacturing

Renan Bonnard[1,2](✉)

[1] SENAI/SC Innovation Institute for Laser Manufacturing,
Manufacturing Systems and Embedded Systems, Florianópolis, Brazil
renan.bonnard@gmail.com
[2] Department of Mechanical and Mechatronics Engineering,
University of Brasilia, Brasília, Brazil

Abstract. Additive manufacturing processes, initially only reserved for the manufacturing of prototypes, now allow the manufacturing of high-value functional products with a wide range of materials. These processes can considerably change the process chain organization and therefore are growing interest in both academics and industrials. Despite these developments in this field, many problems remain on current digital chain that uses old format such as STL and G-code. A solution to challenge this issue is the development of a new digital chain based on the STEP-NC standard (Standard for the Exchange of Product Model Data compliant Numerical Control). This paper intends to propose a methodology for the integration of additive manufacturing to a new STEP-NC model. In order to illustrate this model's possibilities a STEP-NC Platform for Advanced Additive Manufacturing is presented. Finally the integration of this platform in a multi-process context and satisfying Industry 4.0 requirements is highlighted as perspective.

Keywords: Additive Manufacturing · STEP-NC · Digital thread · Digital chain · Industry 4.0

1 Introduction

Additive Manufacturing (AM) processes are defining by the ISO TC 261 standard as "the process of joining materials to make objects from 3D model data, usually layer upon layer, as opposed to subtractive manufacturing methodologies" [1]. They have known major changes for the past 30 years and have evolved from processes allowing prototypes manufacturing to the manufacture of functional products [2].

At the same time, the digital chain (also known as digital thread) of AM processes still uses old digital tools like STL (Surface Tessellation Language, 1987) and ISO 6983 also known as G-code (1982) [3]. Even though industrial companies are responding to competitive pressures by "digitizing" their process chain and have to manage huge amount of data [4]. In addition to this observation, new challenges for a manufacturing integrated in an advanced, intelligent and connected factory using cyber-physical systems, Internet of things and cloud manufacturing [5] include that the current digital chain is no more adapted and is one of the major issue of AM industrials and academics [6, 7].

© Springer International Publishing AG 2018
M. Meboldt and C. Klahn (eds.), *Industrializing Additive Manufacturing - Proceedings of Additive Manufacturing in Products and Applications - AMPA2017*,
DOI 10.1007/978-3-319-66866-6_12

Same issues have been identified for machining processes in the beginning of the 2000's and a solution to challenge the problem has been the development of the STEP-NC standard (Standard for the Exchange of Product model data compliant Numerical Control). This is a language of computerized numerical control (CNC) and a data model for the CAD-CAPP-CAM-CNC (Computer Aided Design, Computer Aided Process Planning, Computer Aided Manufacturing, Computer Numerical Control) chain, formalized as ISO 14649 [8] and ISO 10303 Application Protocol (AP) 238 [9], and has been developed by ISO TC184 SC1 and SC4 committees. Studies have been conducted for the evaluation of the relevance of STEP-NC for AM processes and all results agreed that STEP-NC is an appropriate format for AM [10–14].

In this context, this paper intends to evaluate the current situation of AM digital chain in order to identify fundamental requirements for new developments. Also, a new STEP-NC data model for AM and a platform compliant STEP-NC for AM are presented. And finally, a multi-process platform proposition satisfying Industry 4.0 requirements is highlighted as perspective.

2 Current Situation of Additive Manufacturing Digital Chain and Recent Alternatives

AM digital chain is composed of different steps involving different systems from the 3D CAD model of the product to the fabrication of the physical product. The adopted vision in this paper decomposes the AM digital chain in five main steps (see Fig. 1). Transitions between each step of the CAx chain are models conversions and/or parameters settings.

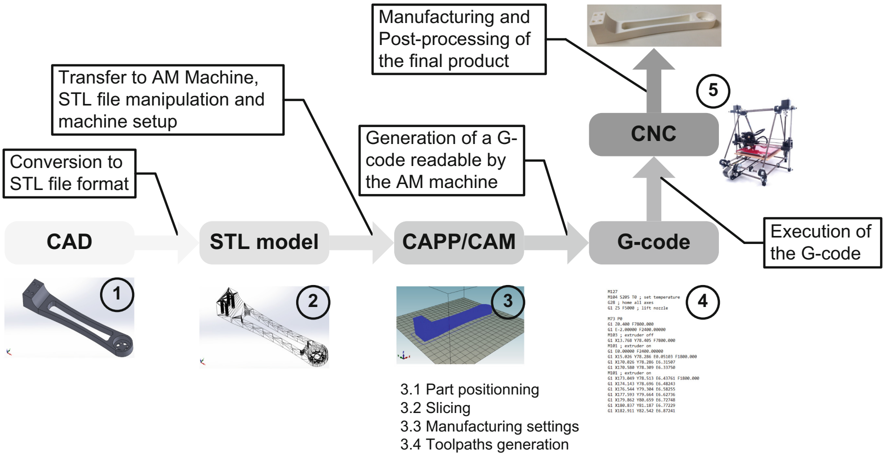
Manufacturing and Post-processing of the final product
Transfer to AM Machine, STL file manipulation and machine setup
Generation of a G-code readable by the AM machine
Conversion to STL file format
CNC
5
CAD
STL model
CAPP/CAM
G-code
Execution of the G-code
1
2
3
4
3.1 Part positionning
3.2 Slicing
3.3 Manufacturing settings
3.4 Toolpaths generation

Fig. 1. Current digital chain with STL format and G-code

The first step of the AM digital chain consists of the design of a 3D model of the product thanks to a CAD system, it can also be provided by a 3D scanner. This 3D model is converted in STL format which is the most commonly used standard for the AM CAM and/or hardware of the AM machine [15]. During this process of conversion many data concerning geometry, tolerancing, material and texture are lost [16, 17]. The next step is usually the set of manufacturing parameters and the definition of process planning, even if some AM systems accept directly the STL file. Most of the AM machines need a G-code file that contains basic axis movements and actions on the process. Finally the product is built on the AM system and some post-processing operations are operated.

At this stage, issues of the AM digital chain are identified as: (i) there is an important amount of files which can be responsible of redundancy and transparency problems, (ii) multiplication of format and digital supports does not enable to integrate simultaneous optimization., (iii) closed-loop manufacturing is hard to operate, (iv) digital chain is not modular and scalable, (v) bidirectional data flow and interoperability are not possible and (vi) digital chain is AM specific and does not allow multi-process manufacturing.

In parallel of STEP-NC developments other propositions have been made by the international community in order to solve the shortcomings of AM digital chain. This led to the proposition of two newer formats as a substitution of the STL standard: (i) AMF (Additive Manufacturing Format) and (ii) 3MF (3D Manufacturing Format). Both formats are XML [18] based file format defined by an XSD schema. AMF is developed by ASTM F42 committee on AM Technologies [19] and co-branded with the ISO TC 261 standards committee [20]. Its development is done with the idea of reducing the shortcomings of the STL format in relation to the new possibilities offered by AM processes. Principal qualities of this format are listed by Hiller and Lipson [19] as: simplicity, flexibility, evolutionary, easy understanding and open-source. The 3MF consortium, which is composed of CAD and AM software vendors, proposed in 2015 the 3MF [21]. It is developed to guarantee interoperability between CAD software and CAM solution and/or AM machines hardware. 3MF structure is organized in two parts: the 3MF core and, materials and properties.

These two solutions are real improvements of the de-facto STL standard for geometry representation. Despite of this, they are an answer of AM digital chain shortcomings only for the transition between CAD and CAM or AM hardware system. It does not propose a global approach in order to challenge to all digital chain challenges.

3 New Vision of the Digital Chain with STEP-NC Standard

As highlighted previously, AM digital chain is currently using old standards of the 1980s and 1990s, and do not challenge the 21st century manufacturing problematics. From this consideration, international works have been carried out in order to propose a new standard for CNC programming. The new STEP compliant NC standard is based on the Standard for Exchange of Product data model (STEP) [22]. Like every Application Protocol of STEP standard, there is an Application Reference Model (ISO 14649 [8]) and an Application Interpreted Model (ISO 10303 AP 238 [9]). ISO 10303-238 results of a mapping obtained from ISO 14649. Consequently AP 238 has the best integration in STEP ISO 10303 but it is more complex and increases data storage [23]. The presented study intends to use ISO 14649 standard for this reason.

AM digital chain compliant STEP-NC does not have to be seen as a STL replacement like AMF or 3MF but as a complete new rebuilding of manufacturing numerical chain. As illustrated in Fig. 2, STEP-NC enables new possibilities for the exchange of high-level data in the whole digital chain. With this standard the digital thread adopts a new overall logic with a unique data file which covers all design and manufacturing information that guarantees transparency, avoids loss of information and, allows bidirectional data flow and interoperability. In addition, its structure is feature-based that provides a generic file non machine depending and scalability. With this standard simulations and optimizations are possible in all stages of the digital chain and STEP-NC file is automatically updated. Finally with AP 219 [24] and Inspection in part 16 of ISO 14649 [25], the new digital chain provides closed-loop manufacturing [26] and possibly a knowledge database also allows cloud manufacturing [5].

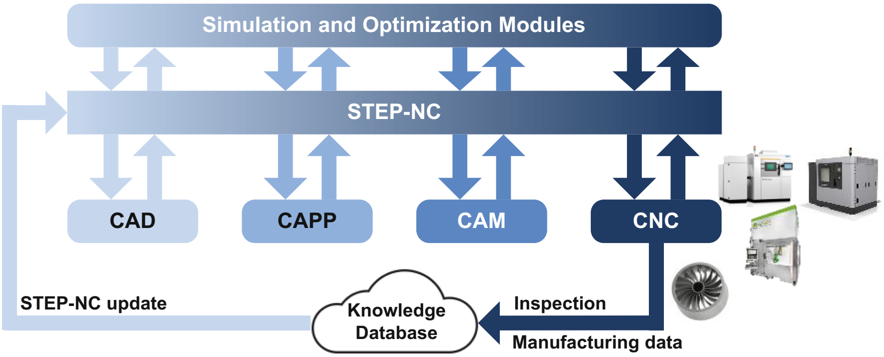

Fig. 2. STEP-NC digital chain.

4 Additive Manufacturing STEP-NC Model Proposition

ISO 14649 standard is developed for machining since the beginning of the 2000's. It is with the expansion of AM processes and their ability to manufacture functional product that the international committee has begun works for the integration of AM. A new ISO 14649 model obtained from data of a complete Hierarchical Object-Oriented Model of AM [27] has been proposed by ISO TC184/SC1 Committee in part 17 of ISO 14649 [28] and is still under review. This model is written in EXPRESS and EXPRESS-G, languages of the STEP-NC standard. The information contents of ISO 14649 are composed of: (i) task description, (ii) geometry description, (iii) structure and product model description, and (iv) tools and technology description. The task description contains the logical sequence of executable tasks and data types. Each workingstep's details are covered in the product model description in relation with the technology and tools description, and the geometry description.

As a result, a STEP-NC file of an AM part, based on features, can be defined (see Fig. 3). This test part is fabricated in ABS with a Fused Deposition Modeling (FDM) machine. STEP-NC file contains all information on workpiece, features, technology, strategy, part structure, geometry and tools.

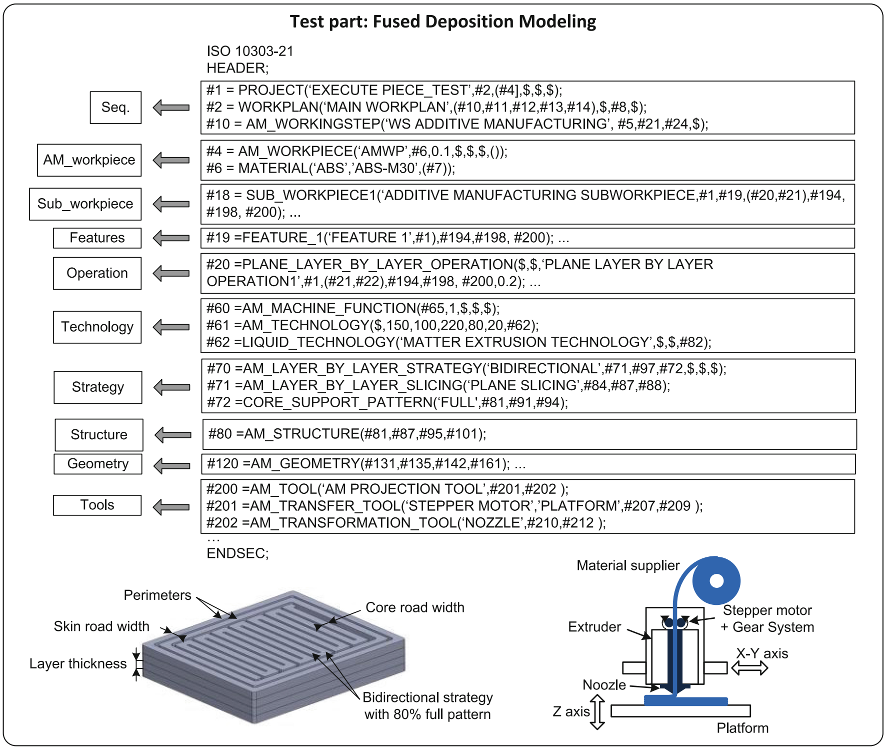
Test part: Fused Deposition Modeling
Seq.
AM_workpiece
Sub_workpiece
Features
Operation
Technology
Strategy
Structure
Geometry
Tools
Perimeters
Skin road width
Layer thickness
Core road width
Bidirectional strategy
with 80% full pattern
Material supplier
Extruder
Stepper motor
+ Gear System
X-Y axis
Noozle
Z axis
Platform

```
ISO 10303-21
HEADER;
#1 = PROJECT(‘EXECUTE PIECE_TEST’,#2,(#4],$,$,$);
#2 = WORKPLAN(‘MAIN WORKPLAN’,(#10,#11,#12,#13,#14),$,#8,$);
#10 = AM_WORKINGSTEP(‘WS ADDITIVE MANUFACTURING’, #5,#21,#24,$);
#4 = AM_WORKPIECE(‘AMWP’,#6,0.1,$,$,$,());
#6 = MATERIAL(‘ABS’,’ABS-M30’,(#7));
#18 = SUB_WORKPIECE1(‘ADDITIVE MANUFACTURING SUBWORKPIECE,#1,#19,(#20,#21),#194,
#198, #200); ...
#19 =FEATURE_1(‘FEATURE 1’,#1),#194,#198, #200); ...
#20 =PLANE_LAYER_BY_LAYER_OPERATION($,$,‘PLANE LAYER BY LAYER
OPERATION1’,#1,(#21,#22),#194,#198, #200,0.2); ...
#60 =AM_MACHINE_FUNCTION(#65,1,$,$,$);
#61 =AM_TECHNOLOGY($,150,100,220,80,20,#62);
#62 =LIQUID_TECHNOLOGY(‘MATTER EXTRUSION TECHNOLOGY’,$,$,#82);
#70 =AM_LAYER_BY_LAYER_STRATEGY(‘BIDIRECTIONAL’,#71,#97,#72,$,$,$);
#71 =AM_LAYER_BY_LAYER_SLICING(‘PLANE SLICING’,#84,#87,#88);
#72 =CORE_SUPPORT_PATTERN(‘FULL',#81,#91,#94);
#80 =AM_STRUCTURE(#81,#87,#95,#101);
#120 =AM_GEOMETRY(#131,#135,#142,#161); ...
#200 =AM_TOOL(‘AM PROJECTION TOOL’,#201,#202 );
#201 =AM_TRANSFER_TOOL(‘STEPPER MOTOR’,’PLATFORM’,#207,#209 );
#202 =AM_TRANSFORMATION_TOOL(‘NOZZLE’,#210,#212 );
...
ENDSEC;
```

Fig. 3. Example of an AM STEP-NC program of a FDM test part.

5 Advanced STEP-NC Platform for Additive Manufacturing Architecture

A STEP-NC file is almost impossible to read and write, therefore the elaboration of a STEP-NC Platform is the necessary step to interpret and execute STEP-NC data for oriented-object manufacturing. Many studies have illustrated STEP-NC platform for machining processes [29–31]. Works of Professor Hascoët in France leads to a multi-process platform including AM [31, 32] but the implementation have been done on a laser cladding machine equipped with an industrial CNC similar to subtractive machines. That is not the case of the majority of AM systems.

The architecture of the Open Intelligent STEP-NC Platform for Advanced Additive Manufacturing proposed, intends to be generic and possibly integrated in every AM systems (see Fig. 4). Eight principal modules of the platform have been identified. The first module is a CAD model whose format is ISO 10303-203 [33]. The second module, developed with Python and PythonOCC [34], is the identification of the AM features from the previous STEP model. The third module, also developed in Python provides the AM process-planning and a STEP-NC data file is generated (module 4). Modules five to seven are part of the open advanced CNC controller based on LinuxCNC solution [35]. Module 5 is composed of two sub-modules: a visualization and simulation module (using LinuxCNC tools) and a module that enables shop-floor modifications. Module 6 is an optimization module of the manufacturing. Module seven enables inspection and caption of machine monitoring data. Information of modules six and seven are then archived in a cloud knowledge data base. Optimizations and shop-floor modifications operate automatic update of the STEP-NC file. STEP-NC file also beneficiates the knowledge of past manufacturing thanks to the cloud database and it guarantees closed-loop manufacturing. Modules six to eight are still under development.

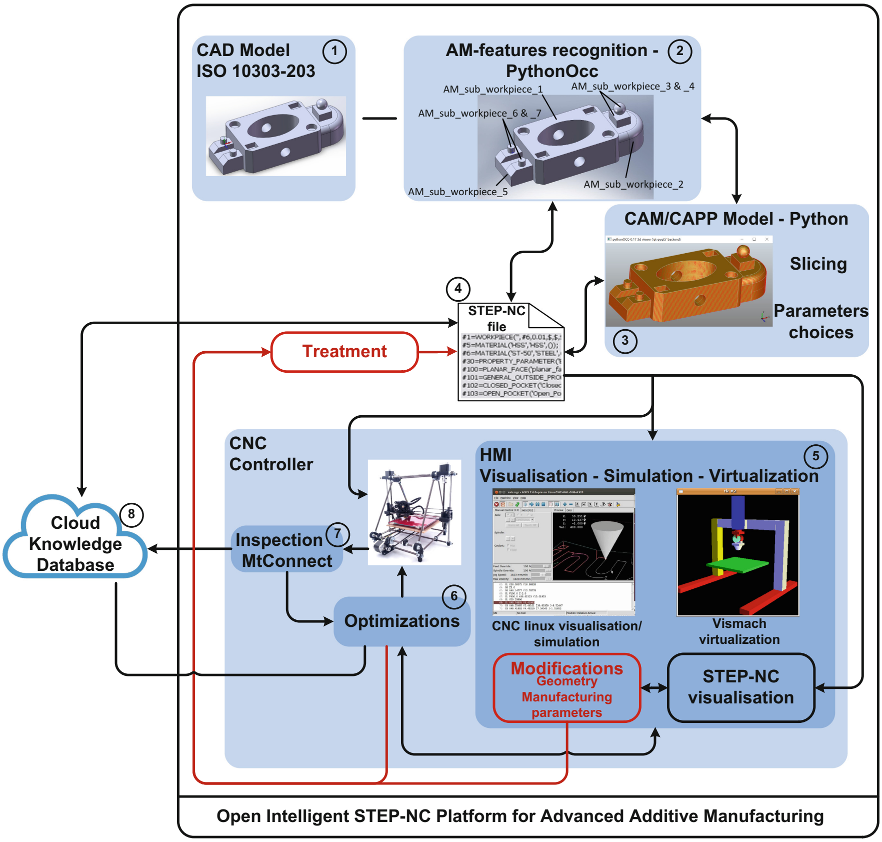
CAD Model
ISO 10303-203
①
AM-features recognition - PythonOcc
②
AM_sub_workpiece_1
AM_sub_workpiece_3 & _4
AM_sub_workpiece_6 & _7
AM_sub_workpiece_5
AM_sub_workpiece_2
CAM/CAPP Model - Python
Slicing
Parameters choices
③
④
STEP-NC file
Treatment
CNC Controller
HMI
Visualisation - Simulation - Virtualization
⑤
CNC linux visualisation/ simulation
Vismach virtualization
Modifications
Geometry
Manufacturing parameters
STEP-NC visualisation
Inspection MtConnect
⑦
Optimizations
⑥
Cloud Knowledge Database
⑧
Open Intelligent STEP-NC Platform for Advanced Additive Manufacturing

```
#1=WORKPIECE('',#6,0.01,$,$,$
#5=MATERIAL('HSS','HSS',());
#6=MATERIAL('ST-50','STEEL',
#30=PROPERTY_PARAMETER('
#100=PLANAR_FACE('planar_fa
#101=GENERAL_OUTSIDE_PRO
#102=CLOSED_POCKET('Closed
#103=OPEN_POCKET('Open_Po
```

Fig. 4. Open Intelligent STEP-NC Platform for Advanced Additive Manufacturing.

Experimental tests have been conducted to validate the AM STEP-NC data model and the open STEP-NC platform. These tests consisted of fabricating a test part (see Fig. 5). The test part comprised manufacturing a principal workpiece, the manufacturing of two AM features and a hole with material support, with a FDM machine. Each workpiece has different manufacturing parameters, which is normally not possible with classical process-planning for FDM, in order to validate new STEP-NC capabilities.

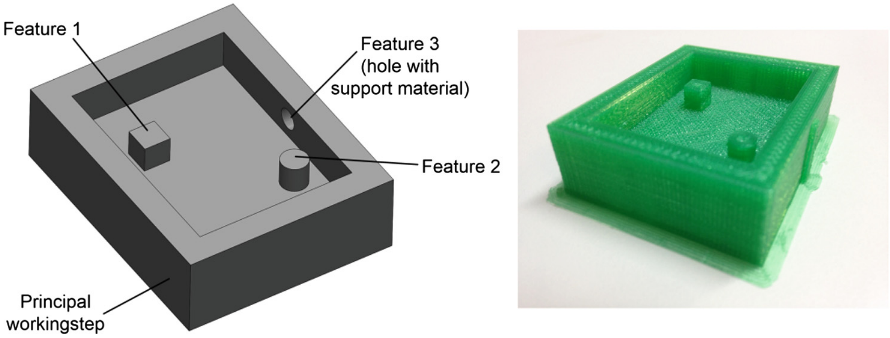

Fig. 5. Resulting test part manufactured on open STEP-NC platform.

Open Intelligent STEP-NC Platform for Advanced AM demonstrates advanced programming. The next section will illustrate how this platform enables also multi-process manufacturing.

6 Toward the Integration of Additive Manufacturing in a Multi-process STEP-NC Platform

An important concern in manufacturing industries is the possibility to combine additive and subtractive manufacturing. Indeed, with huge progresses in design for AM, it is now possible to manufacture lighter products than with machining, but with the same mechanical characteristics. In order to challenge this, many studies have been conducted in order to optimize both the design [36] and process-planning [37] of hybrid-manufacturing products. Such a manufacture is not easy to take in place because of different digital thread of additive and subtractive processes. STEP-NC is a perfect standard to address this problematic because of its unique feature-based structure integrating these two processes. The demonstration of a STEP-NC multi-process platform have been done by Professor Hascoët [31, 32].

The Fig. 6 illustrates the architecture toward a multi-process STEP-NC platform enabling cloud manufacturing in an industrial collaborative network. Each CNC of the machines' network is compliant STEP-NC. Then from the information of both design and production engineering a STEP-NC file is generated. The first algorithm analyses all manufacturing features of the file and determines for each feature which processes are the best thanks to a feature-based cloud manufacturing knowledge data base shared in the network. This database is alimented by inspection results and MTConnect's [38] manufacturing data. The second algorithm determines which machines can manufacture the product in terms of functional specification and which are available in order to complete manufacturing before deadline and with competitive price. Then a STEP-NC file is generated and the manufacturing is operated. These new developments for multi-process feature-based cloud manufacturing are still under development.

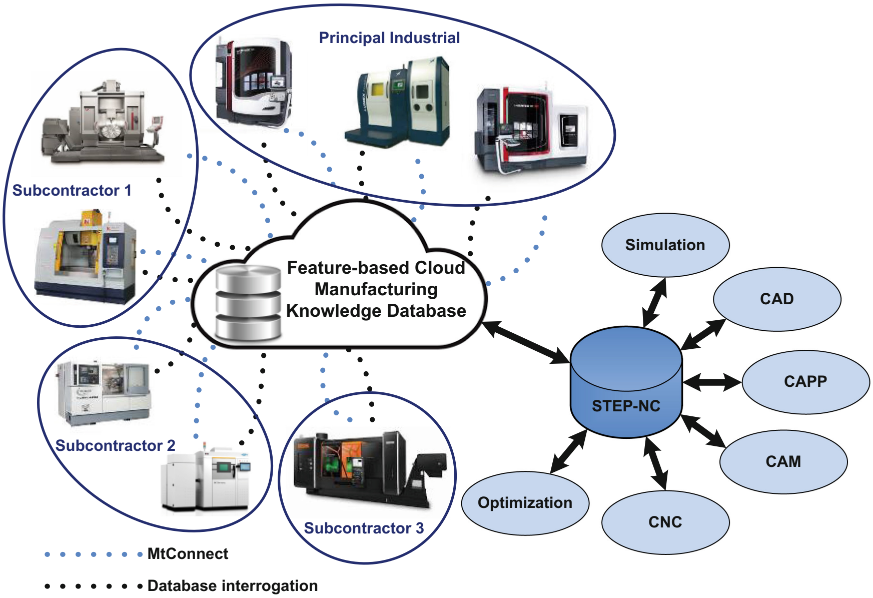
Principal Industrial
Subcontractor 1
Subcontractor 2
Subcontractor 3
Feature-based Cloud Manufacturing Knowledge Database
STEP-NC
Simulation
CAD
CAPP
CAM
CNC
Optimization
MtConnect
Database interrogation

Fig. 6. Intelligent multi-process STEP-NC platform for cloud manufacturing.

7 Conclusion

This paper proposes a new open and intelligent platform for advanced AM that can be implemented on every AM systems. The architecture of the platform enables the introduction of new modules for optimizing, simulating or monitoring. Some works are under development in this way for closed-loop manufacturing and integration of cloud manufacturing. Integrations of this platform in an intelligent multi-process platform enabling cloud manufacturing is also introduced and it is part of further developments toward advanced and intelligent manufacturing.

References

1. ISO 17296-1: Additive manufacturing - General principles - Part 1: Terminology (2015)
2. Wohlers, T.T., Caffrey, T., Campbell, R.I.: Wohlers report 2016: 3D printing and additive manufacturing state of the industry: annual worldwide progress report (2016)

3. ISO 6983-1: Numerical control of machines—Program format and definition of address words—Part1: Data format for positioning, line motion and contouring control systems (1982)
4. Mies, D., Marsden, W., Warde, S.: Overview of additive manufacturing informatics: “a digital thread”. Integr. Mater. Manuf. Innov. **5** (2016). doi:10.1186/s40192-016-0050-7
5. Lu, Y., Xu, X.: A semantic web-based framework for service composition in a cloud manufacturing environment. J. Manuf. Syst. **42**, 69–81 (2017). doi:10.1016/j.jmsy.2016.11.004
6. Pei, E., Ressin, M.: Investigating the Impact of CAD Data Transfer Standards for 3DP-RDM. Brunel University London, UK (2016)
7. Esmaeilian, B., Behdad, S., Wang, B.: The evolution and future of manufacturing: a review. J. Manuf. Syst. **39**, 79–100 (2016). doi:10.1016/j.jmsy.2016.03.001
8. ISO 14649-1: Industrial automation systems and integration - Physical device control - Data model for computerized numerical controllers - Part 1: Overview and fundamental principles (2003)
9. ISO 10303-238: Industrial automation systems and integration - Product data representation and exchange - Part 238: Application protocol: Application interpreted model for computerized numerical controllers (2007)
10. Bonnard, R., Mognol, P., Hascoët, J.-Y.: A new digital chain for additive manufacturing processes. Virtual Phys. Prototyp. **5**, 75–88 (2010). doi:10.1080/17452751003696916
11. Lipman, R., McFarlane, J.: Exploring model-based engineering concepts for additive manufacturing. In: Proceedings of the 26th Solid Freeform Fabrication Symposium, pp. 385–400, Austin (Texas) (2015)
12. Cha, J.-M., Suh, S.-H., Hascoet, J.-Y., Stroud, I.: A roadmap for implementing new manufacturing technology based on STEP-NC. J. Intell. Manuf. **27**, 959–973 (2016). doi:10.1007/s10845-014-0927-2
13. Bonnard, R., Hascoet, J.-Y.: Additive Manufacturing Digital Thread: State of the Art and Perspectives (2017)
14. Xiao, J., Anwer, N., Durupt, A., Le Duigou, J., Eynard, B.: Information exchange standards for design, tolerancing and additive manufacturing: a research review. Int. J. Interact. Des. Manuf. IJIDeM (2017). doi:10.1007/s12008-017-0401-4
15. Bohn, J.H.: File format requirements for the rapid prototyping technologies of tomorrow, pp. 878–883. University of Hong Kong, Hong Kong (1997)
16. Stroud, I., Xirouchakis, P.C.: STL and extensions. Adv. Eng. Softw. **31**, 83–95 (2000)
17. Bonnard, R., Mognol, P., Hascoët, J.Y.: Rapid prototyping project description in STEP-NC model. In: Proceedings of the 6th CIRP International Seminar on Intelligent Computation in Manufacturing Engineering, pp. 357–362, Naples, Italy (2008)
18. XML Technology (2015). https://www.w3.org/standards/xml/. Accessed 23 Nov 2016
19. Hiller, J.D., Lipson, H.: STL 2.0: a proposal for a universal multi-material additive manufacturing file format. In: Solid Freeform Fabrication Symposium, pp. 5–9. Citeseer, Austin, TX, August 2009
20. ISO/ASTM 52915: Specification for Additive Manufacturing File Format (AMF) Version 1.2 (2016). https://www.iso.org/obp/ui/#iso:std:iso-astm:52915:ed-2:v1:en. Accessed 23 Nov 2016
21. 3MF Consortium: 3MF (2016). http://www.3mf.io/. Accessed 23 Nov 2016
22. Pratt, M.J.: Introduction to ISO 10303—the STEP standard for product data exchange. J. Comput. Inf. Sci. Eng. **1**, 102 (2001). doi:10.1115/1.1354995
23. Xu, X.W., Wang, H., Mao, J., Newman, S.T., Kramer, T.R., Proctor, F.M., Michaloski, J.L.: STEP-compliant NC research: the search for intelligent CAD/CAPP/CAM/CNC integration. Int. J. Prod. Res. **43**, 3703–3743 (2005). doi:10.1080/00207540500137530

24. ISO 10303-219: Industrial automation systems and integration - Product data representation and exchange - Part 219: Application protocol: Dimensional inspection information exchange (2007)
25. ISO 14649-16: Industrial automation systems and integration - Physical device control - Data model for computerized numerical controllers - Part 16: data for touch probing based inspection (2004)
26. Danjou, C., Le Duigou, J., Eynard, B.: Manufacturing knowledge management based on STEP-NC standard: a closed-loop manufacturing approach. Int. J. Comput. Integr. Manuf. 1–15 (2016). doi:10.1080/0951192X.2016.1268718
27. Bonnard, R., Hascoët, J.-Y., Mognol, P., Zancul, E., Alvares, A.: Hierarchical Object-Oriented Model (HOOM) for Additive Manufacturing Digital Thread (2017)
28. ISO 14649-17: Industrial automation systems and integration - Physical device control - Data model for Computerized Numerical Controllers - Part 17: Process data for additive manufacturing processes (2016)
29. Suh, S.H., Lee, B.E., Chung, D.H., Cheon, S.U.: Architecture and implementation of a shop-floor programming system for STEP-compliant CNC. Comput.-Aided Des. **35**, 1069–1083 (2003). doi:10.1016/S0010-4485(02)00179-3
30. Xu, X.W.: Realization of STEP-NC enabled machining. Robot. Comput.-Integr. Manuf. **22**, 144–153 (2006). doi:10.1016/j.rcim.2005.02.009
31. Rauch, M., Laguionie, R., Hascoet, J.-Y., Suh, S.-H.: An advanced STEP-NC controller for intelligent machining processes. Robot. Comput.-Integr. Manuf. **28**, 375–384 (2012). doi:10.1016/j.rcim.2011.11.001
32. Laguionie, R., Rauch, M., Hascoet, J.Y.: A multi-process manufacturing approach based on STEP-NC data model. In: Bernard, A. (ed.) Global Product Development, pp. 253–263. Springer, Heidelberg (2011)
33. ISO 10303-203: Industrial automation systems and integration - Product data representation and exchange - Part 203: Application protocol: configuration controlled 3D designs of mechanical parts and assemblies (2011)
34. Paviot, T.: PythonOCC, 3D CAD/CAE/PLM development framework for the Python programming language, PythonOCC – 3D CAD Python (2016). http://www.pythonocc.org/. Accessed 19 Jan 2017
35. Torvalds, L.: LinuxCNC (2017). http://linuxcnc.org/. Accessed 16 Feb 2017
36. Kerbrat, O., Mognol, P., Hascoët, J.-Y.: A new DFM approach to combine machining and additive manufacturing. Comput. Ind. **62**, 684–692 (2011)
37. Newman, S.T., Zhu, Z., Dhokia, V., Shokrani, A.: Process planning for additive and subtractive manufacturing technologies. CIRP Ann. - Manuf. Technol. **64**, 467–470 (2015). doi:10.1016/j.cirp.2015.04.109
38. MTConnect (2015). http://www.mtconnect.org/. Accessed 15 Mar 2017

Additive Manufacturing on 3D Surfaces

Olivier Chandran[1,2], Sebastien Lani[1(✉)], Danick Briand[2],
Barthelemy Dunan[1], and Guy Voirin[1]

[1] CSEM SA, Jaquet droz 1, 2002 Neuchatel, Switzerland
sli@csem.ch
[2] EPFL, Microcity, 2002 Neuchatel, Switzerland

Abstract. Additive manufacturing (AM) is currently at the heart of the digital manufacturing trends. It englobes more than 15 different technologies. They are relying on the fabrication of a part made from mainly 1 or sometimes 2 materials with only 1 fabrication technology. In this study, we are developing technologies and materials to create 3D components on substrates or on 3D objects to form new components with an increase of functionality and complexity. We are particularly focusing on the realization of hybrids millimeter scale components for application in watch and medical field.

One example that we are presenting is the key technologies for the realization of a 3D printed prosthesis fitting the patient's morphology (for example a knee or an ankle) integrating printed force sensors for monitoring the pressure distribution over the prosthesis surface. It shall give the opportunity to analyze the motion of the prosthesis to detect potential need of kinesiotherapy, minor surgery for prosthesis adjustment or entire replacement in case of failure. It shall lead to a pain reduction and a better recovery of the motor function after surgery. The mechanical part of the prosthesis has been fabricated by Fused Deposition Modelling (FDM), electrical connections and sensors by Aerosol Jet Printing. Two different sensing technologies are under evaluation: LC resonant circuits, to avoid the need of communication circuit inside the prosthesis and resistive sensors.

Several others examples are presented over previously cited application fields.

1 Introduction

Additive manufacturing is not a recent technology as some of the principal technologies (FDM, SLA) are more than 25 years old. This number was the key in the development of the technology to a new level and a broader utilization. It corresponds to the end of the patent right, opening the field to new companies like Ultimaker©, Makerbot©, Formlabs©, supported by the crowdfunded generation to make affordable systems and open the marker to new users like academia, non-specialized industries, fablabs, and consumers. This dynamism is pushing the number of new functionalities and performances increase. One example is the release of a new SLA system, called CLIP "Continuous Liquid Interface Production" [1], enabling a continuous printing and then the disappearing of apparent layering of the process and the need of separation from a PDMS (or assimilate) film, and so increase the printing speed. Already SLS/SLM, is seeing the number of system manufacturers increasing as well as the

© Springer International Publishing AG 2018
M. Meboldt and C. Klahn (eds.), *Industrializing Additive Manufacturing - Proceedings of Additive Manufacturing in Products and Applications - AMPA2017*,
DOI 10.1007/978-3-319-66866-6_13

number of industrial applications, like in aerospace or medical market. One interesting recent fact is the 1.5 billion dollars investment from General Electric© on Arcam AB and SLM Solutions Group, demonstrating that the technology is ready for being used as an industrial manufacturing technology and no more only for rapid prototyping. And this is just the beginning as more patents will fall soon in the public domain.

What could be the next steps? Functionality and performance improvements will continue for at least 10 years and with the possibility to make and process new materials. This is a common trend to all technology developments. One additional trend, which is for us of high interest, is the apparition of some multi process and multi material printing systems, like the Aether1 for which CSEM is taking part to the beta test phase. It includes 2 FDM heads, up to 12 droplet heads, 8 syringes with the possibility to be heated at 200 °C, a UV LED, a laser for engraving and a CNC milling head. This system will allow many possibilities in bioprinting, printed electronics, functional objects and everything in between.

Additionally, one can imagine to combine different materials or technologies in different systems to obtain more complex or intelligent or "smart" systems. For example it can be silicon based microsystems with micrometer resolutions with 3D printing functions like sensors, actuators, mechanical (shock absorber…), or interfacing (fluidic channel, electrical connection, optical waveguide).

In this article, a study on "how to couple different AM technologies together?" will be presented with the application case of smart prosthesis. An introduction of the next steps and others applications will be concluded the study.

2 The Example of Smart Prosthesis

Mankind's history of physical trauma and injuries dates back to the birth of life itself, so does the ingenuity deployed and the apparatus envisioned to tackle and overcome any arising inconveniences. Since the artificial toe crafted under the Egyptian era, to the development of comprehensive limbs made necessary by wars, the technological development consistently matured the functionality, aesthetics and performance of prosthetic limbs. Nowadays, a higher life expectancy and an aging population causing a rise in prosthetic based surgery (estimated to grow by 174% between 2005 and 2030 for hip and knee arthroplasty surgeries [2]) is the main driver for prosthesis development. Foreseen by many as a strong driver too, the 3D printing role in the continuous improvement of prosthesis mimicking patient's morphology became more tangible with the fall into the public domain of key patents in 2009. Since then, many individuals strove toward the development of cost effective, "one fits them all", ready to print prosthetics, which eventually lead to the release of the Raptor Hand by e-NABLE (Fig. 1): a free prosthetic hand designed for kids suffering from atrophy or agenesis. Meanwhile, corporations focused on the development of high-end printed prosthesis based on CT-scan [3] to provide patients with the best health care.

Such developments paved the way for the further functionalization of printed parts namely with printed electronics. Thus enabling prosthesis to communicate and exchange data regarding the medical conditions of the prosthesis bearer (gait analysis, temperature, infection…).

Fig. 1. Evolution of prostheses with time. From left to right, Egyptian era, Victorian era, Modern era [4]

In 1966, Rydell [5] proposed the integration of a strain gauge in a prosthesis during a knee arthroplasty. Strain gauges were placed in the femoral head and the data collection was made possible through the use of wires, severed as soon as the study was finished. The overall purpose of this study was the determination of the forces acting on the femoral head prosthesis. The main challenges faced during this study dealt with the space available to fit the prosthesis with the strain gauges and the abnormal gait caused by the prosthesis. Similar development were carried out by Bergmann [6] in 1997 and Graichen et al. in 1999, with improved performances. Furthermore, more and more activities are ongoing through the acquisition of post-operative data to improve the fabrication of prosthesis, post-operative recovery procedure and evolution of the prosthesis with time up to its replacement. So far, mainly the post-operative procedure was evaluated.

The present study aims to develop the key technologies to fabricate smart prosthesis using only printing technologies giving the capability to produce patient custom based systems at a low cost with integrated force and/or temperature sensors. It will give the opportunity to massive application of the technology for prosthesis fabrication and data acquisition.

2.1 Sensors and Communication Solutions

One important part of the design of the force sensors and the communication system rely on the integration of batteries inside the prosthesis. 2 different solutions were evaluated.

The first proposed solution is relying on a RLC circuit, with the capacitor that can vary depending of the force applied and the inductance acting as the communication. A change in the capacitor will induce a frequency shift of the resonant LC circuit. An increase of the resistance will reduce the quality factor and so the sensitivity. This circuit do not need battery and is powered by the readout system, making it easy to be integrated.

The second proposed solution is relying on a metal resistive sensor also called strain gauge. The pressure will induce a deformation of the metal conductor changing its conductivity which is read by an electronics. This solution will require a battery, an integrated electronics with wireless communication.

2.2 Development of Key Fabrication Steps

The fabrication of the implant/prosthesis is achieved using a Fused Deposition Modeling printer (FDM), with material like PET-g and PLA, or a UV stereolithography printer (SLA), with material like poly-acrylate or poly-urethane. The sensors and conductive lines are realized with an Aerosol Jet printer (AJP) from Optomec© with capability to deposit conductive or dielectric inks from several hundred nanometers to several tens micrometers. It also presents the advantage to work to a distance up to 5 mm and to be programmed to have an in-plane our out-of-plane motion which is compatible with printing on a 3D surface made by additive manufacturing. The sintering of the ink was achieved with a photonic curing system from Novacentrix© giving the advantage to cure an ink at a high temperature without heating the substrate or damaging it.

Figure 2 presents the typical test structures for evaluating key fabrication technologies and a typical surface made by FDM with an average RMS roughness of 3.5 µm. Figure 3 demonstrates a typical challenge by forming a conductive line of several centimeters length on a FDM printed surface with some abrupt slope and also by dealing with photonic curing which is also creating defects and inhomogeneity during curing. It was also difficult to achieve low resistivity compared to oven curing or bulk material, particularly with gold ink for which typical annealing temperature is between 200 and 250 °C. Table 1 is resuming the best achieved results for the different tested material. It appears to be difficult to fully sintered Au ink without defects either on the metal lines or substrate (over-curing) or a low resistivity (insufficient curing). Because similar results were expected for silver, curing was only achieved on an oven and deposition on glass or SLA based substrate compatible with a curing temperature of 150 °C. Silver resistivity was 1.8 times the bulk value. For substrate with abrupt surface defects an epoxy resin was dispensed on the surface to achieve a smooth surface.

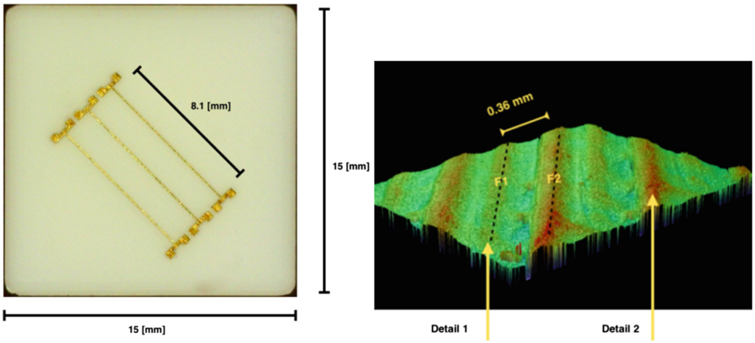

Fig. 2. (Left) typical test sample with an example of Au printed lines; (right) typical surface of a FDM printed samples.

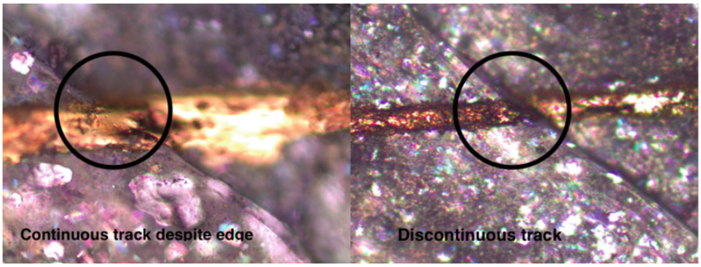

Fig. 3. Slopes as main reason of defects when printing on a FDM surface.

Table 1. Typical achieved resistivity for Au ink on different substrate and for different curing technics.

Substrate material	PET-g (FDM) Ra ~ 3.5 µm	PLA (FDM) Ra ~ 3.5 µm	Glass (microscope blade) Ra < 20 nm
Resistivity compared to Au bulk value	x12.9	x27.6	x2
Curing	Photonic	Photonic	Oven

2.3 Fabrication and Testing of Sensors

RLC Sensor

The fabrication of capacitive sensors was split in 2 parts, the coil and the capacitance. The coil design was consisting of an Ag layer of 1 to 1.5 µm thick. Table 2 is resuming the geometry of the coil fabricated. The resistance value is higher due to a higher bulk value of 2.5 times corresponding to a resistivity of 4.5×10^{-8} Ω m, taking into account the extra line width of 82 µm. An example of achieved coil is presented in Fig. 4(left). The capacitance is fabricated in 2 parts, both by UV stereolithography to obtain a sufficient accuracy (<25 µm) from a polymer-ceramic composite material from Tethon3D©. Silver ink was deposited on the surface without post processing, electrical contact was ensured all along the structure. So far achieved testing of RLC circuit have not shown any detectable change of capacity through the shift of the resonant frequency. The reason can be attributed to a low quality factor due to the higher resistance or a low capacity change (Fig. 5).

Table 2. Design and measured parameters of the coil.

	Avg. track width (µm)	Track spacing (µm)	Nb turns	Inductance (µH)	Resistance (Ω)
Design	60	340	7	0.75	130
Measured	82	318	7	2.9	232

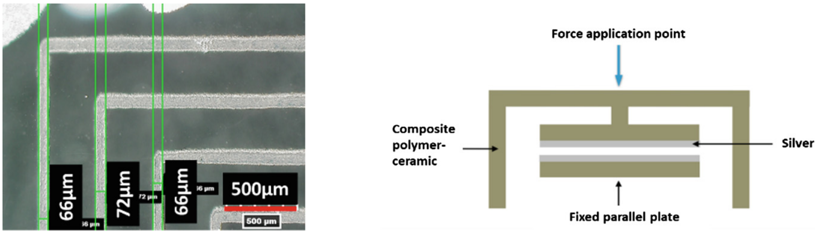
66µm
72µm
66µm
500µm
500 µm
Force application point
Composite polymer-ceramic
Silver
Fixed parallel plate

Fig. 4. (Left) typical printed coil; (right) concept of capacitive sensor with parallel plates.

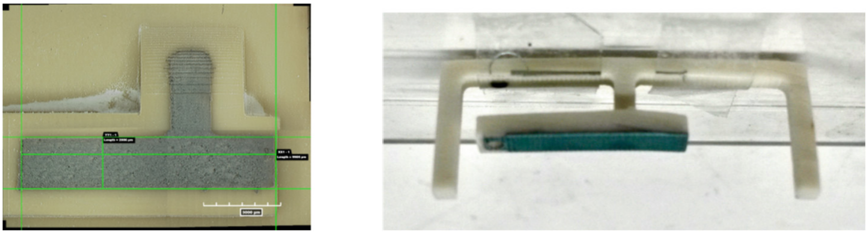

Fig. 5. (Left) fixed electrode of the capacitive sensor; (right) moveable electrode of the capacitive sensor.

Resistive Sensor

To evaluate the performance of the resistive sensors, a simple testing structure fabricated by UV stereolithography, with CLIP™ process with a representative roughness of FDM (several micrometers roughness) but resistant to a temperature up to 250 °C. An epoxy glue was dispensed at the surface to smooth the surface. Finally, the Ag resistance was deposited by AJP printing, followed by an annealing at 150 °C for duration of 30, 60 or 90 min. 2 different resistor designs (CLIP1 and CLIP2) were evaluated with different sensor lengths respectively 40.5 and 139.9 mm. The fabricated device with CLIP2 design is presented in Fig. 6(right).

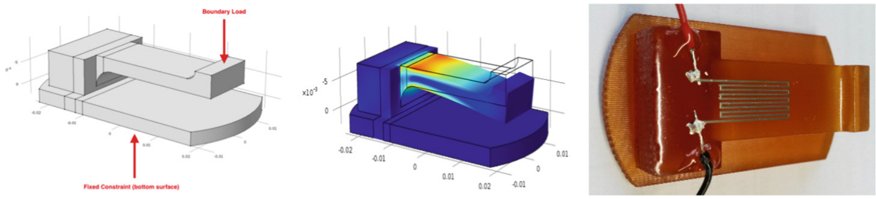
Boundary Load
Fixed Constraint (bottom surface)
x10⁻³
-5
0
-0.02
-0.01
0
0.01
0.02
-0.01
0
0.01

Fig. 6. (Left) testing structure design for resistive sensor; (center) FEA simulation of the structure; (right) fabricated testing structure with design sensor No. 2.

The resistance measured for each design and for each curing time is presented in Table 3. As expected, the resistance is decreasing with the curing temperature but the resistivity is far from the bulk value, particularly for the design CLIP2 with longer resistor. This is attributed to variation of the conductor section that vary along the resistance due to defects and surface roughness.

Table 3. Resistance value with respect to curing time.

Sample	30 min at 150 °C	60 min at 150 °C	90 min at 150 °C
CLIP1	569.7 Ω (223 × Bulk)	111.5 Ω (48 × Bulk)	82.2 Ω (33 × Bulk)
CLIP2	4578.7 Ω (652 × Bulk)	2129.7 Ω (303 × Bulk)	1259.6 Ω (179 × Bulk)

Drift and hysteresis were measured for the different designs and for different curing times. Drift measured for each device is composed of a transient state and a steady state, with values respectively of <0.1% and 0.01%. Transient state, with a time constant measured between 10 to 600 s respectively dependant to curing time (long curing time give shorter time constant), is attributed to a heating effect and to the curing level of the ink. Hysteresis, represented in Fig. 7 for sample CLIP2, was measured for an applied force of 10.5 N and repeated 3 times per curing time. Curing time of 30 min have a higher hysteresis than for 60 min and 90 min which lead to a lower stability. The design of CLIP2 was given a more stable gauge factor (GF) of 0.56 up to 0.68 (increasing with curing time).

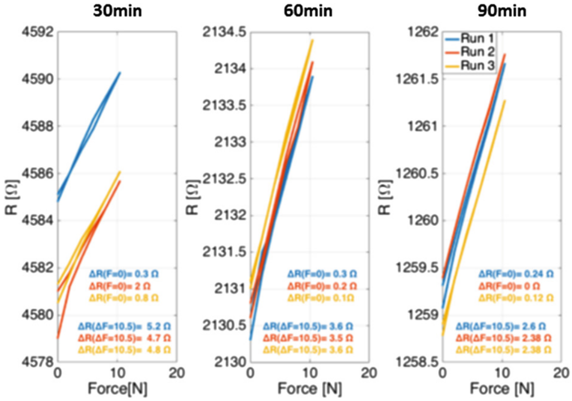

Fig. 7. Sensor response for different annealing time, from left to right: 30 min, 60 min and 90 min.

3 Discussion and Future Developments

Both sensing technologies were applied to a 3D printed components to evaluate their performances. So far, only metal resistive sensors have demonstrated sufficient sensitivity to be applied as force sensors on 3D printed prosthesis. Most of components fabricated by FDM and UV SLA are requiring a post processing prior AJP printing of a conductive ink. RLC sensors have to be redesigned with a higher capacity (gap reduction) value to compensate the low quality factor due to the high resistance of the conductive lines. Future developments will be directed to increase the conductive material thickness to reduce the total resistance. In parallel, the curing process will be optimized to reduce the resistivity to a lower value.

So far, sensors were tested on simple geometries and main steps will be to evaluate then of a closer geometry of prosthesis as for example presented in Fig. 8 for a knee prosthesis. Ideally, the sensors would further be integrated on the plastic spacer and being placed inside the parts thanks to layer by layer process of additive manufacturing. This concept will be evaluate using an Aether1™ printing system with the capacity to deposit materials with FDM, syringe or droplet dispensing. As, so far the integration of electronics and batteries are complex, particularly biocompatibility of these components, the RLC sensors are still the most promising technologies.

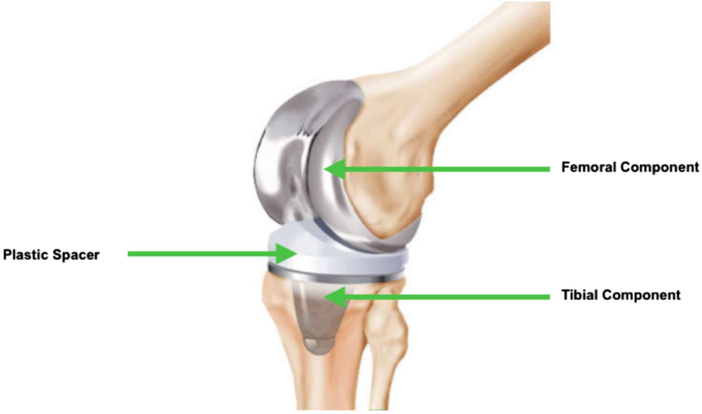

Fig. 8. Knee prosthesis with it components [7].

Such development could also easily be re-utilized for many applications and some are already of interest like 3D printing on microsystem or fully printed microfluidic chip with embedded electrical functionalities.

References

1. CLIP™ technology. http://www.carbon3d.com/
2. Kurtz, S., Ong, K., Lau, E., Mowat, F., Halpern, M.: Projections of primary and revision hip and knee arthroplasty in the United States from 2005 to 2030. J. Bone Joint Surg. (Am.) **89**(4), 780 (2007)
3. Johnson & Johnson's DePuy Synthes offering 3D printed "TruMatch" titanium facial and skull implants | 3D Printer News & 3D Printing News. http://3ders.org/
4. Prostheses Evolution History. http://www.amputee-coalition.org/
5. Rydell, N.W.: Forces acting on the femoral head-prosthesis: a study on strain gauge supplied prostheses in living persons. Acta Orthop. Scand. **37**(sup88), 1–132 (1966)
6. Graichen, F., Bergmann, G., Rohlmann, A.: Hip endoprosthesis for in vivo measurement of joint force and temperature. J. Biomech. **32**, 1113–1117 (1999)
7. Knee Replacement - Implants Subject to Recalls, Lawsuits

Integrated Platform for Multi-resolution Additive Manufacturing

Paul Delrot[1](✉), Damien Loterie[1], Demetri Psaltis[2], and Christophe Moser[1]

[1] Laboratory of Applied Photonics Devices, School of Engineering,
École Polytechnique Fédérale de Lausanne, 1015 Lausanne, Switzerland
`paul.delrot@epfl.ch`
[2] Laboratory of Optics, School of Engineering,
École Polytechnique Fédérale de Lausanne, 1015 Lausanne, Switzerland

Abstract. The integration of several printing techniques into a single platform requires to miniaturize each additive manufacturing tool.

With this aim in mind, we have developed a compact toolkit for high-resolution additive manufacturing of polymers. This toolkit is made of two ultra-thin nozzles, a multimode optical fiber (MMF) for the curing unit, and a glass capillary for the drop-on-demand device (DOD). Polymerization of micrometric patterns is achieved by delivering laser light in a structured manner through a 5-cm long, 200 µm-wide MMF. Along with this curing unit, the combined DOD device is made of a 10-cm long and 300-µm wide glass capillary through which viscous materials are delivered via laser-actuation.

We envision that our compact additive manufacturing toolkit could be integrated within other manufacturing platforms as an add-on tool, thus enabling multi-resolution processing.

Keywords: Laser · Direct-writing · Compact · Drop-on-demand · Laser-actuation

1 Introduction

The increasing interest in additive manufacturing (AM) over the recent years has led to the development of numerous printing techniques [1–3]. The resolution of these AM technologies ranges from the macro- [1] to the micro- [4] or even nano-scale [5]. Integrating various AM techniques into a single printing platform would allow multi-resolution processing of parts. A multi-resolution system would not only enable the embedment of fine details into bulk parts but would also dramatically improve the printing speed as well as the part functionality.

However current AM systems are large and require robotic arms to transfer parts from one AM platform to another [6]. Thus, the integration of several printing techniques into a single platform requires to miniaturize each additive manufacturing tool.

Here, we report on a compact toolkit we have developed for both dispensing and laser-processing polymer materials. This toolkit is made of two ultra-thin

© Springer International Publishing AG 2018
M. Meboldt and C. Klahn (eds.), *Industrializing Additive Manufacturing - Proceedings of Additive Manufacturing in Products and Applications - AMPA2017*,
DOI 10.1007/978-3-319-66866-6_14

nozzles, a glass capillary for the drop-on-demand device (DOD) and a multimode optical fiber (MMF) for the curing unit. The DOD device is made of a 10-cm long and 300-µm wide glass capillary through which materials are delivered via laser-actuation [7,8]. Micro-droplets of polymers, composite hydrogels (up to 20 Pa s viscosity) and proteins of size 50 µm to 300 µm have been successfully printed without degrading their functionality using this laser-actuated DOD system. Laser direct-writing through the 5-cm long, 200 µm-wide MMF is achieved by delivering and modulating continuous-wave laser light in a structured manner with a phase control system.

2 Materials and Methods

2.1 Laser Direct-Writing Through Multimode Optical Fibers

Micrometric patterns are produced through a MMF by adapting the endoscopic imaging setup (see Fig. 1(a)) of Loterie et al. [9].

Owing to their large number of modes, multimode fibers can transmit images with multiple pixels and a diffraction-limited resolution. Thus they represent a very compact means for image transfer. However, due to the different propagation constants of the different modes in the fiber, laser light coupled into a multimode fiber will be scrambled at the output resulting in an unstructured speckle pattern (see Fig. 1(b)). This limitation can be overcome by measuring

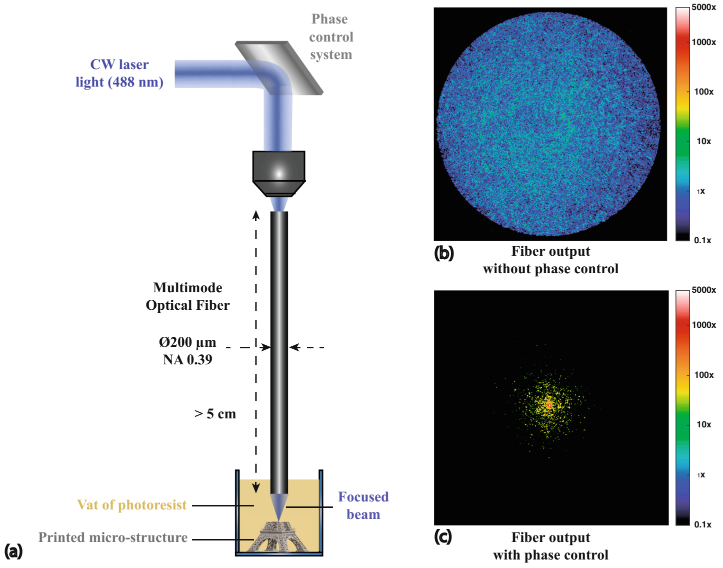
Phase control system
CW laser light (488 nm)
Multimode Optical Fiber
Ø200 µm NA 0.39
> 5 cm
Vat of photoresist
Printed micro-structure
Focused beam
(a)
5000x
1000x
100x
10x
1x
0.1x
(b) Fiber output without phase control
5000x
1000x
100x
10x
1x
0.1x
(c) Fiber output with phase control

Fig. 1. (a) Experimental setup for micro-additive manufacturing through a MMF (b) speckle observed at the distal tip of a MMF without phase control (c) focal spot generated through a MMF using a phase control system the transmission and propagation of the different modes inside the fiber, after which an image can eventually be reconstructed from the speckle pattern. Further details on the methods to characterize the fiber propagation constants and image reconstruction can be found in previous works [10,11].

In this work, CW laser light (Coherent, Sapphire 488 SF) is focused (see Fig. 1(c)) and scanned 200 µm ahead of the distal tip of a thin MMF (Thorlabs, FT200EMT, ϕ200 µm NA 0.39). As shown in Fig. 1(a), prior to being coupled in the fiber, light is modulated with a phase control system (Holoeye, Pluto) to account for the fiber modal scrambling. This modal scrambling is measured before each experiment using the methods described in [9]. In order to write micrometric polymer patterns, the fiber is dipped into a photoresist made of the organic polymer precursor trimethylolpropane triacrylate (TMPTA; >70%, Aldrich, USA) and 1wt% of the Norrish type II photoinitiator camphorquinone (CQ; 97%, Aldrich, USA) and 0.5wt% of the synergist Ethyl 4-(dimethylamino)benzoate (EDAB; =97%, Aldrich, USA). Confinement of the polymerization to the focal spot is enabled by oxygen scavenging of the free-radicals generated along the propagation of the beam into the photoresist, as demonstrated by Maruo and Ikuta [12].

2.2 Compact Drop-on-Demand System

Microdrops are produced at room temperature by focusing a 5-ns laser pulse (Continuum, ML-II, 532 nm) with a 10× microscope objective on a liquid-filled glass micro-capillary (see Fig. 2(a)). The experimental dynamics of a flow-focused droplet generation of a viscous Newtonian liquid (a mixture of water and glycerol at 80% (v/v), corresponding to a 67 mPa s viscosity at 25 °C) are described in Fig. 2(b–c). In Fig. 2(b) the liquid-air interface is highlighted with respectively a solid and dashed white line for clarity on the first two images corresponding to pre-firing and post-firing of the laser. Moreover, the lateral borders of the images correspond to the inner capillary walls. Distortion, due to the glass thickness of the capillary, is responsible for the black surroundings below the meniscus. Finally, in Fig. 2(c), the blue circles correspond to the pictures of Fig. 2(b). The dashed line is a spline interpolation of the jet dynamics and the dotted lines delimitates the phases of jetting. The inks were Newtonian water-glycerol mixtures and non-Newtonian polymer precursors such as TMPTA.

Absorption of the laser pulse by the stained ink leads to the generation of a cavitation bubble and a shockwave. The consequent impact of the pressure pulse on the liquid-air interface first accounts for the acceleration of the liquid. The liquid is further accelerated thanks to a flow-focusing phenomenon due to the concavity of the liquid's meniscus [8,13]. The subsequent thin jet is then slowed down by surface tension and the bubble collapse until it finally breaks up to form one or more droplets. Tagawa et al. [8] showed that, among other parameters, the contact angle θ is crucial for the generation of high-speed flow-focused jets, with narrow contact angles resulting in thinner and faster jets.

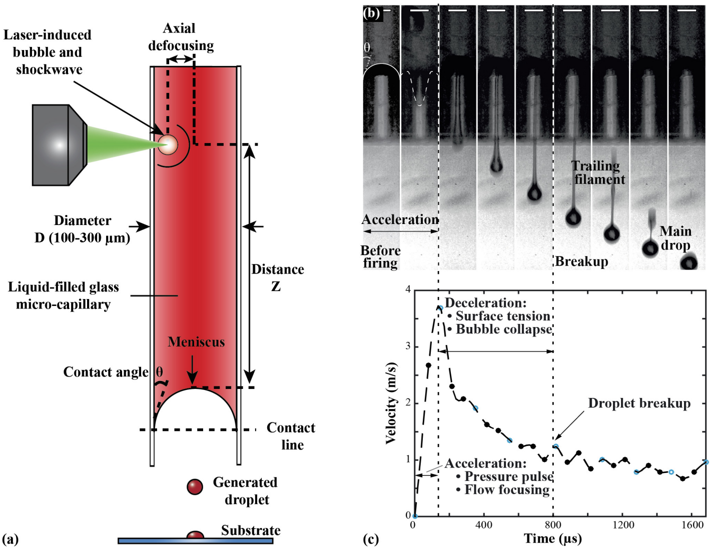
Laser-induced bubble and shockwave
Axial defocusing
Diameter D (100-300 µm)
Liquid-filled glass micro-capillary
Distance Z
Meniscus
Contact angle θ
Contact line
Generated droplet
Substrate
(a)
(b)
θ
Acceleration
Before firing
Trailing filament
Main drop
Breakup
Deceleration:
• Surface tension
• Bubble collapse
Droplet breakup
Acceleration:
• Pressure pulse
• Flow focusing
Velocity (m/s)
0
1
2
3
4
0
400
800
1200
1600
Time (µs)
(c)

Fig. 2. (a) Experimental setup and description of the experimental parameters impacting the droplet size and velocity (b) time-resolved imaging of the flow-focusing phenomenon. Scale bar: 200 µm (c) Interpolated jet dynamics corresponding to the droplet formation depicted in Fig. 2(b), adapted from [7].

3 Results and Discussion

3.1 Laser Direct-Writing Through Multimode Optical Fibers

Our first results show that two-dimensional micrometric patterns can be printed through an ultrathin multimode fiber onto a glass substrate with CW laser light, as shown in Fig. 3(a). The use of a CW laser to print micro-patterns deep into a photoresist represents a significant cost reduction compared to state-of-the-art systems relying on two-photon polymerization induced by the absorption of femtosecond laser pulses [5]. Moreover, our results show that the technique of CW laser direct-writing deep into a photopolymer originally demonstrated by Maruo and Ikuta [12] with a large numerical aperture (NA) microscope objective (NA = 1.0) can be extended to low-NA multimode optical fibers. However, as polymerization is a cumulative process, the overlap of several spots during the printing process of three-dimensional structures is likely to generate proximity effects and a divergence of the printed structure from the model [16]. Therefore, further developments accounting for proximity effects correction will be needed to print complex three-dimensional micro-structures with our compact fiber-based system.

3.2 Compact Drop-on-Demand System

Figure 3(b) also shows that the range of printable liquids with our laser-assisted drop-on-demand device is significantly broadened compared to conventional

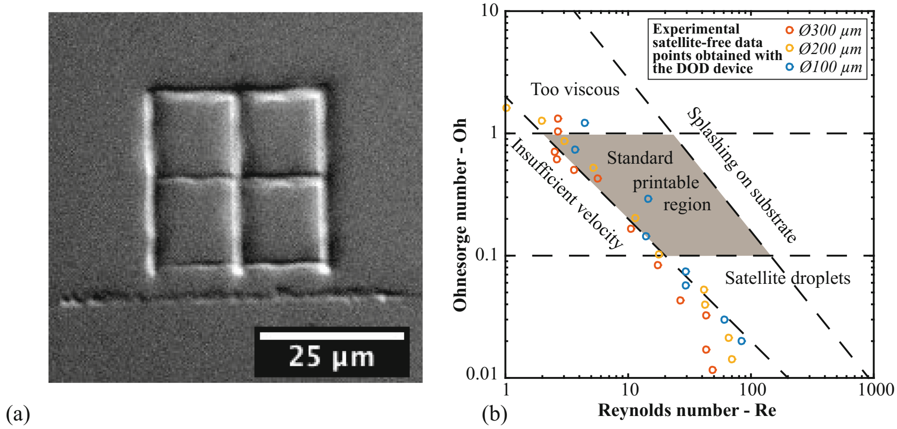

Fig. 3. (a) Two-dimensional pattern printed through a MMF in TMPTA (b) conventional inkjet printability region as defined in [14,15] superimposed with the experimental data points obtained with our laser-assisted flow-focusing device in the satellite- free jetting regime and with the water-glycerol Newtonian mixtures. Red, yellow and blue dots were respectively obtained for 300, 200 and 100-µm capillary diameters. Error bars are omitted for clarity, each data point is the results of at least 10 experiments, adapted from [7]

inkjet printing [7]. A standard printable region has been defined in the literature using two dimensionless numbers. The Reynolds number $Re = \frac{\rho R V}{\eta}$ represents the ratio of inertial and viscous forces, with ρ, R, V and η being respectively the liquid density, the drop diameter, the liquid velocity and the liquid dynamic viscosity. The Ohnesorge number $Oh = \frac{\eta}{\sqrt{\sigma \rho R}}$ corresponds to the ratio of the viscous forces over the geometric mean of the inertial and surface tension forces, with σ being the liquid surface tension. Using these dimensionless numbers, several criteria were derived from experimental measurements and numerical models [3,7,14] to map the regime for stable satellite-free drop generation from a nozzle in the frame of conventional thermal and piezoelectric inkjet printers (see gray region gray in Fig. 3(b)). By superimposing our experimental data points for viscous Newtonian water-glycerol mixtures to this diagram, we observe that the range of Ohnesorge numbers for which satellite-free droplets were generated is extended to $\sim 0.01 < Oh < \sim 1.5$ with our laser-assisted flow-focusing DOD system. The most plausible explanation for this extension of the satellite-free ejection regime with respect to conventional inkjet printers is that our device is less sensitive to viscosity owing to the flow-focusing phenomenon. Indeed, the measured initial velocities of the droplets correspond to $Re \sim 200$ for the least viscous inks and to $Re \sim 5$ for the most viscous ones. Hence, the initial acceleration phase was dominated by inertia for the range of viscous liquid studied, which is also consistent with previous works [13,17] on both inviscid and low-viscosity liquids.

3.3 Possible Industrial Applications of the System

Combining the curing unit (see Fig. 4(a)) and the DOD device would yield a compact multi-resolution additive manufacturing platform as illustrated in Fig. 4(b). Such a compact system could be used in the industry for rectifying AM parts that are not matching the specifications of the CAD model, thus reducing the number of iterations needed to print a compliant part.

However as seen in Fig. 4(a), the current experimental setups are large and future endeavours should be devoted to the miniaturization of the devices.

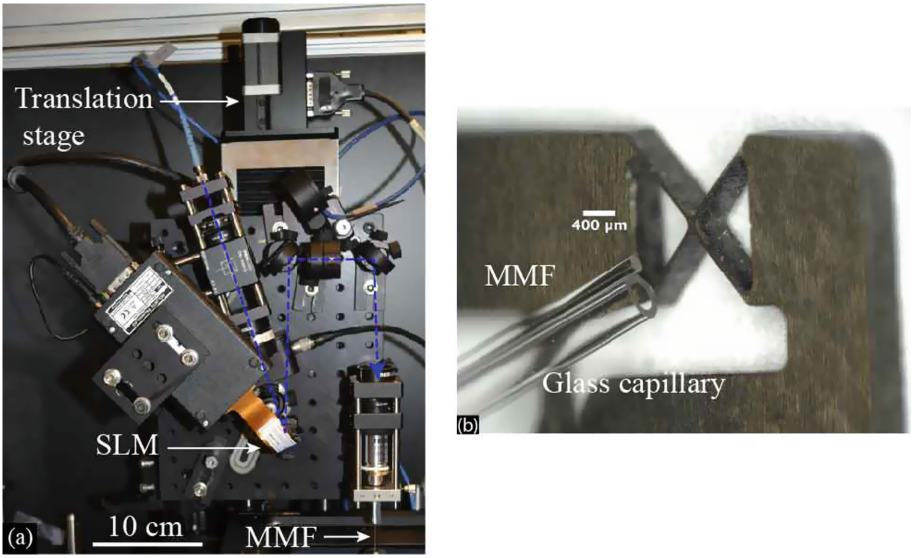

Fig. 4. (a) Experimental setup for single-photon printing through a MMF, SLM: Spatial Light Modulator. The dashed blue line indicates the path of the laser beam, which is first enlarged, modulated by the SLM and finally coupled in the thin MMF. The setup is mounted on a translation stage in an upright configuration in order to dip the MMF in the photopolymer. (b) Illustration of the proposed multi-resolution additive manufacturing system: a combination of the curing unit and the drop-on-demand system.

4 Conclusion

In this paper, we experimentally demonstrate satellite-free droplet generation via laser-actuation of viscous Newtonian and non-Newtonian inks as well as laser direct-writing through a 200-µm thin MMF of micro-patterns deep into a photopolymer.

Further miniaturization of the drop-on-demand device could be achieved by delivering the nanosecond laser pulses through a MMF inserted into the capillary instead of focusing light with a microscope objective. Moreover, combining the two tools we have developed into a compact device could enable their use as add-ons to other additive manufacturing platforms for multi-resolution processing.

References

1. Gibson, I., Rosen, D., Stucker, B.: Additive Manufacturing Technologies: 3D Printing, Rapid Prototyping, and Direct Digital Manufacturing, 2nd edn. Springer New York, New York (2015)
2. Murphy, S.V., Atala, A.: 3D bioprinting of tissues and organs. Nature Biotechnol. **32**(8), 773–785 (2014)
3. Hutchings, I.M., Martin, G.D.: Inkjet Technology for Digital Fabrication. Wiley, Hoboken (2012)
4. In'T Veld, B.H., Overmeyer, L., Schmidt, M., Wegener, K., Malshe, A., Bartolo, P.: Micro additive manufacturing using ultra short laser pulses. CIRP Ann. - Manuf. Technol. **64**(2), 701–724 (2015)
5. Fischer, J., Wegener, M.: Three-dimensional optical laser lithography beyond the diffraction limit. Laser Photonics Rev. **7**(1), 22–44 (2013)
6. MacDonald, E., Wicker, R.: Multiprocess 3D printing for increasing component functionality. Science **353**(6307), 1512–1515 (2016)
7. Delrot, P., Modestino, M.A., Gallaire, F., Psaltis, D., Moser, C.: Inkjet printing of viscous monodisperse microdroplets by laser-induced flow focusing. Phys. Rev. Appl. **6**(2), 024003 (2016)
8. Tagawa, Y., Oudalov, N., Visser, C.W., Peters, I.R., van der Meer, D., Sun, C., Prosperetti, A., Lohse, D.: Highly focused supersonic microjets. Phys. Rev. X **2**(3), 031002 (2012)
9. Loterie, D., Farahi, S., Papadopoulos, I., Goy, A., Psaltis, D., Moser, C.: Digital confocal microscopy through a multimode fiber. Opt. Express **23**(18), 23845–23858 (2015)
10. Papadopoulos, I.N., Farahi, S., Moser, C., Psaltis, D.: Focusing and scanning light through a multimode optical fiber using digital phase conjugation. Opt. Express **20**(10), 10583–10590 (2012)
11. Cižmár, T., Dholakia, K.: Exploiting multimode waveguides for pure fibre-based imaging. Nature Commun. **3**, 1027 (2011)
12. Maruo, S., Ikuta, K.: Submicron stereolithography for the production of freely movable mechanisms by using single-photon polymerization. Sens. Actuators A: Phys. **100**(1), 70–76 (2002)
13. Peters, I.R., Tagawa, Y., Oudalov, N., Sun, C., Prosperetti, A., Lohse, D., van der Meer, D.: Highly focused supersonic microjets: numerical simulations. J. Fluid Mech. **719**, 587–605 (2013)
14. Derby, B.: Inkjet printing of functional and structural materials: fluid property requirements, feature stability, and resolution. Annu. Rev. Mater. Res. **40**(1), 395–414 (2010)
15. Castrejón-Pita, A.A., Castrejón-Pita, J.R., Martin, G.D.: A novel method to produce small droplets from large nozzles. Rev. Sci. Instrum. **83**(11), 115105 (2012)
16. Wan, X., Menon, R.: Proximity-effect correction for 3D single-photon optical lithography. Appl. Opt. **55**(3), A1–A7 (2016)
17. Antkowiak, A., Bremond, N., Le Dizès, S., Villermaux, E.: Short-term dynamics of a density interface following an impact. J. Fluid Mech. **577**, 241–250 (2007)

Enhanced Toolpath Generation for Direct Metal Deposition by Using Distinctive CAD Data

Daniel Eisenbarth[1](✉), Florian Wirth[1], Kevin Spieldiener[2],
and Konrad Wegener[2]

[1] Inspire AG, ETH Zürich, Zürich, Switzerland
`eisenbarth@inspire.ethz.ch`
[2] Institute of Machine Tools and Manufacturing, ETH Zürich, Zürich, Switzerland
`http://www.inspire.ethz.ch`

Abstract. The additive process of Direct Metal Deposition shows great potential for the production and repair of large-scale metallic components due to its high deposition rate and easy integration into CNC machining and robot systems. Conventional CAM software applies only geometric information to calculate the toolpath, requiring still high manual input for the production of complex parts. An enhanced approach is proposed that gathers relevant information from product development and hands it over as "distinctive" CAD data, which describes a set of features that is used by the CAM system for the generation of the toolpath. Zigzag patterns, contour patterns as well as the combination called "hybrid toolpath" are discussed and distinctive data is applied to build thin-walled elements. The experimental validation reveals a high surface quality and shape accuracy of demonstrator parts built with optimized process parameters and toolpath strategies.

Keywords: Direct Metal Deposition · Laser cladding · Additive Manufacturing · Toolpath strategies · CAM

1 Introduction

Direct Metal Deposition (DMD) is a laser-based Additive Manufacturing (AM) process where metallic powder is directly blown into the melt pool. The moving processing head deposits a track, overlapping tracks form a layer, and multiple layers create a three-dimensional part. Since the DMD processing head is usually attached to a multi-axis machine, the design space is only limited by the available axis range. Further advantages are the high deposition rate, the control over the microstructure, and the ability to use multiple materials to produce graded components as stated by Gibson et al. [1]. Thus, DMD is suitable for the additive production of large-scale components, adding features to or repairing existing parts as described by Nowotny et al. [2]. However, the achievable part complexity using DMD is currently behind other AM processes. Shamsaei et al. [3] argue that one main reason for this deficit is the complexity of the toolpath generation

© Springer International Publishing AG 2018
M. Meboldt and C. Klahn (eds.), *Industrializing Additive Manufacturing - Proceedings of Additive Manufacturing in Products and Applications - AMPA2017*,
DOI 10.1007/978-3-319-66866-6_15

and its impact on the part properties. Therefore, the industrial use of DMD requires still a lot of manual input and adaptation for each individual application. This publication aims to contribute to the challenge of process automation by proposing an enhanced toolpath generation method, using distinctive CAD data. Applying this generation method in combination with further toolpath strategies shall result in a more reliable and predictable process for different geometric elements.

2 Concept of Distinctive CAD Data

Regarding the process chain from CAD data to the finished part, Gibson et al. [1] define eight steps that are generally applicable to all AM processes. These are:

1. CAD
2. Conversion to STL
3. Transfer to AM machine and STL file manipulation
4. Machine setup
5. Build
6. Removal
7. Post-processing
8. Application

The weak link in this process chain is the data transfer from CAD via STL to the machine: The STL file format is the most common interface in AM, describing any solid as a surface consisting of multiple triangles, each of them with a normal vector pointing to the outside. The advantage of the STL format is the standardized representation of any geometry. Conventionally, only the STL file and information about the desired material is handed over from the design to the manufacturing software system, which means from CAD to CAM. In comparison to technical drawings, which may contain dimensional, shape and position tolerances, the transfer via STL discards a lot of valuable engineering information at this stage. Due to the complexity of the DMD technology, manual input and expertise from manufacturing engineers is mostly required for CAM systems to generate the NC code from STL data. A newly developed standard is the AMF file format, but Gibson et al. [1] point out that it considers mainly the requirements of powder-bed and fused deposition modeling AM, such as data for color, material, and print orientation.

Hereafter, an approach is presented that takes advantage of the know-how and intention of the engineers who design and dimension the part as well as of the possibilities of current CAD systems. Besides the geometric shape, most parts possess functional and non-functional surfaces, leading to different shape and position tolerances as well as maximum surface roughness. Various applications lead to lowly and highly loaded sections and different load directions in the part. Support or clamping structures may be required for subsequent manufacturing steps (e.g. assembly), which are finally removed or fulfill no further function. This information is generated during product development and can be stored by distinctive CAD data. This term covers additional points, vectors, triangles, surfaces, solids or any other form of data output. If the CAM software is able to read these additional data, the manual effort by the manufacturing engineer can be reduced significantly. Furthermore, design engineers can consider the strengths and weaknesses of the DMD process in terms of "design for AM" during development, leading to higher process efficiency and lower manufacturing costs. Figure 1 illustrates the common process chain and the enhanced approach. Although this approach addresses primarily the needs of the DMD process, it can be beneficial for any industrial AM process with multiple input parameters.

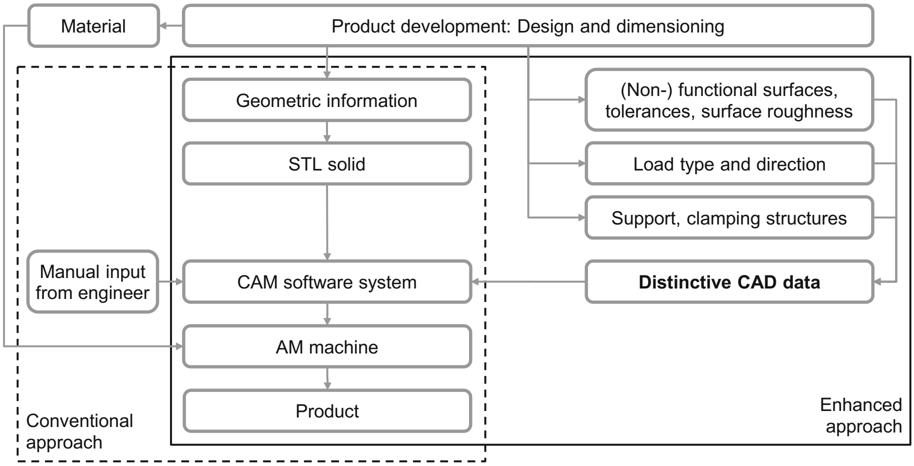
Material
Product development: Design and dimensioning
Geometric information
STL solid
Manual input from engineer
CAM software system
AM machine
Product
Conventional approach
(Non-) functional surfaces, tolerances, surface roughness
Load type and direction
Support, clamping structures
Distinctive CAD data
Enhanced approach

Fig. 1. Conventional and enhanced approach for an AM process chain

3 Toolpath Strategies

The toolpath of the processing head is one key factor for additive manufacturing. Together with the process parameters, it determines the achievable part complexity, quality and process efficiency in terms of time and resource consumption. Different geometries and part requirements demand different toolpath strategies. Additive technologies are characterized by a layer-wise buildup, where each layer is filled subsequently. Generally the layers have a constant thickness. Separating a solid geometry into various layers by CAM software is called "slicing".

A raster pattern is the easiest way to fill a surface. It is widely applicable and does not require special cases for calculation as described by Farouki et al. [4]. Due to the straight path, there are no inhomogeneities or defects which arise from turns of the processing head inside the part. However, Jin et al. [5] state that the surface quality of the wall is mostly insufficient. Changing the direction of the raster in each layer (e.g. by 90°) reduces the anisotropy in the material. Although for some applications, certain anisotropy of the mechanical properties can be beneficial. The high number of switch-on and switch-off events of the laser passing the boundary of the part creates discontinuities within the traveling melt pool. To overcome this problem, Rajan et al. [6] developed an algorithm that optimizes the raster direction regarding the number of laser beam interruptions. The zigzag pattern is the combination of all raster lines to a connected path. It reduces the number of on and off events, but creates the problem of under- and overfilling at turning points as described by Jin et al. [7]. Both raster and zigzag pattern cannot fill a surface exactly if the dimension of the part is no multiple of the track pitch. Otherwise, under- and overfilled areas are inevitable. Both patterns are not suitable for thin-walled parts, as they generate very short tracks and therefore plenty discontinuities.

An alternative approach is the contour pattern. Here, the contour of the surface equals the outermost toolpath. The adjacent paths are generated by a shrinking operation of the outer contour. The computation of contour toolpaths is challenging: The geometric algorithm named "straight skeleton" is able to process arbitrary two-dimensional surfaces, but has to consider multiple special cases as further described by Felkel and Obdrzalek [8]. Ding et al. [9] point out that under- and overfilling is a problem in the middle of the part where the inner paths meet. Farouki et al. [4] show that the contour pattern creates an almost seamless wall surface with the best achievable quality. Therefore, it is perfectly suited for thin-walled parts with constant wall thickness. A modification of the contour pattern is the spiral pattern which does not interrupt the laser beam, but is only applicable to simple geometries. The toolpath patterns of raster, zigzag, contour, and spiral are illustrated in Fig. 2.

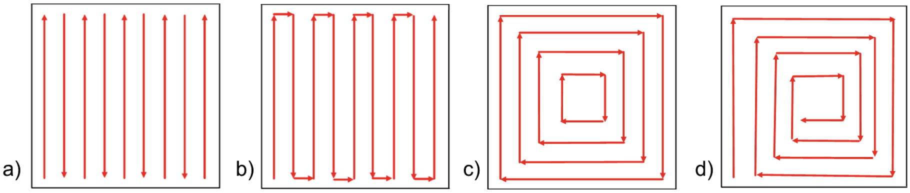

Fig. 2. Common toolpath patterns: (a) raster, (b) zigzag, (c) contour, (d) spiral

A hybrid strategy is a combination of different approaches. Combining zigzag and contour patterns provides several advantages: The surface of the wall is determined by the contour toolpath, whereas the inner quality is determined by the zigzag path, leading to both high surface quality and uniform filling of the inner structure. Different process parameters can be applied to each pattern in order to optimize the quality or process performance. The computational complexity is rather low, since the contour path follows the part boundary. Jin et al. [5] state that the biggest challenge of hybrid strategies is the interface between contour and zigzag path. There, under- and overfilling areas can occur, leading to bonding defects. The track distance and the resulting overlap of tracks are crucial parameters for an accurate interface. Figure 3 shows a possible hybrid toolpath for the demonstrator part “milling head”: A CAD file (a) is transferred to an STL model (b) and is sliced into various layers (c). The toolpath in one layer is depicted in (d). The blue line shows the outer contour path; the red lines depict the zigzag pattern. It can be seen that the zigzag pattern needs to be interrupted due to the intrusions.

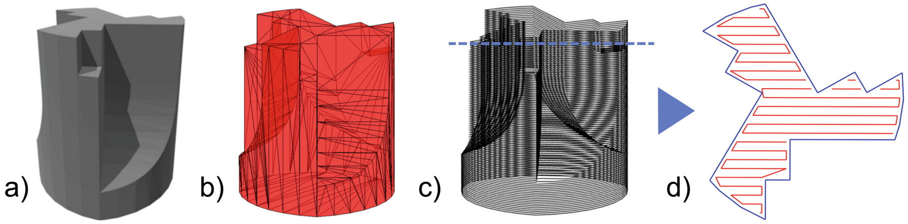

Fig. 3. Demonstrator “milling head”: (a) CAD part, (b) STL geometry, (c) sliced layers, (d) hybrid toolpath

4 Implementation of the CAM Algorithm

The objective of the presented research is to increase the achievable part complexity and quality by a reliable toolpath generation method, which is initiated by the designer in the CAD system. The goal is to make use of the engineer’s know-how to account for specific features, whereas the algorithm adds generally applicable strategies and calculates the toolpath according to a clear set of rules. The CAD system itself is not modified but used to provide multiple STL files that define the additive buildup with additional information, distinguishing functional and non-functional surfaces. A CAM software based on MATLAB has been developed at the institute. It reads STL files and multiple parameter sets, calculates the toolpath based on different strategies, and outputs the NC code to the DMD machine. It is currently limited to 3-axis buildup. A module for 5-axis DMD is being developed.

Figure 4 shows the demonstrator part “impeller”, which consists of both massive and thin-walled elements, namely the core cone and the blades. The blades and the outer wall are functional surfaces, requiring a low roughness for minimum friction. A suitable toolpath is then crucial. Within the conventional approach, the part would be represented by one volume as shown in image (a) of Fig. 4. An automated algorithm that distinguishes massive and thin-walled elements for arbitrary geometries would be complex and hard to control. This problem is eliminated by splitting the geometry into a zigzag subset and a contour subset in the CAD software, as shown by images (b) and (c). Thus, the massive interior of the impeller will be built by the zigzag subset, whereas the outer surface and the blades will be built by the contour subset. The minimum blade thickness here is two tracks as a back and forth movement of the processing head. For thicker blades, additional contour paths can be added by an enlarged contour subset, as shown in image (d). The advantage of distinctive CAD data is the full control of the toolpath already in the design phase of a part. Thus, either the geometry can be adapted to meet the manufacturing requirements of the DMD process, or the toolpath can be adjusted to prevent bonding defects. Image (e) depicts the hybrid toolpath in one layer.

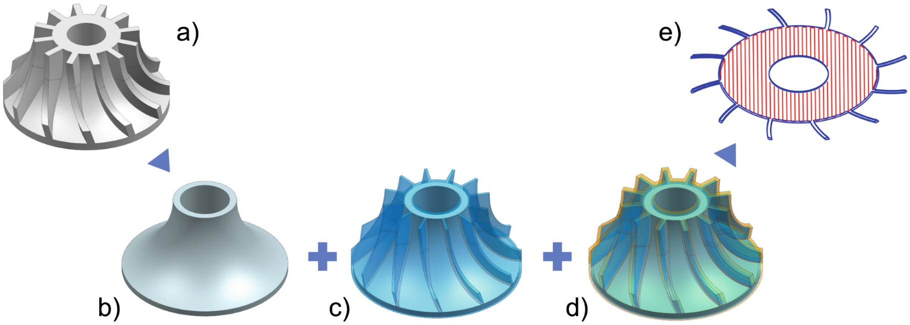

Fig. 4. Additional CAD data to model massive and thin-walled elements for the hybrid toolpath of the “impeller” demonstrator

Only if the blades exceed a certain thickness, it is suitable to fill the interior with a zigzag pattern. Tapered geometries are critical elements that need to be analyzed thoroughly, since the interface between zigzag and contour path is prone to bonding defects. A sharp edge can be realized by a single-track wall. Figure 5 shows the toolpath for a tapered geometry. Underfilling between the zigzag and the contour path in the edge can be prevented by optimized distance parameters. In order to create a sharp edge by a contour path, the laser is switched off at the tip and switched on again as soon as the paths diverge to a specific gap, as shown in the magnified area of Fig. 5. This strategy requires a local adaptation of the process parameters as described in the next section.

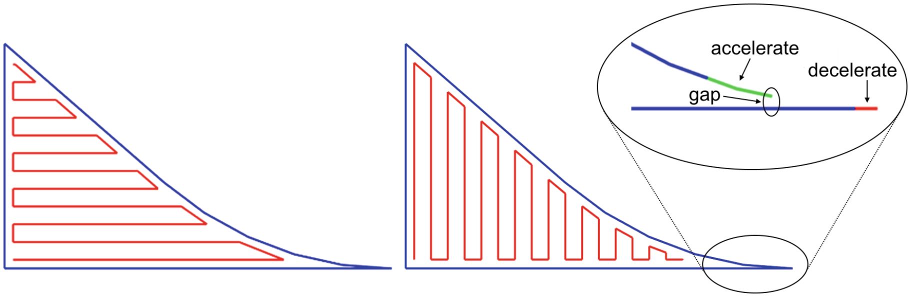

Fig. 5. Hybrid toolpath for a tapered geometry, showing 0° (left) and 90° (right) zigzag pattern and local parameter adaptation of the contour path in the sharp edge

5 Experimental Validation

The CAM algorithm has been validated by the fabrication and cross-sectional analysis of various demonstrator parts. A 5-axis CNC-machine “TRUMPF TruLaser Cell 7020” was used together with a 3 kW disk laser, emitting a laser beam with 1030 nm wave length. The processing head enables a variable laser spot size. The powder from the three-jet nozzle focuses in an area of 4 mm in diameter. All experiments were conducted with stainless steel type 1.4404 powder, having a grain size distribution from 45 to 106 µm. As substrate, bright steel grade S235JRC with a thickness of 8 mm was used.

The advantages of hybrid strategies are revealed by Fig. 6. The CAD geometry of the milling head is taken from Fig. 3. The process and toolpath parameters are listed in Table 1. Part (a) in Fig. 6 was made with a hybrid toolpath with constant process parameters as listed in column “zigzag”. It shows a poor surface roughness and bad shape tolerances. The resolution is too low to shape the pockets for the cutting inserts. For part (b), the contour path was optimized: A decreased laser spot size led to an increased surface quality. The laser spot size was adjusted in order that the height of two contour layers is equal to the height of one zigzag layer. The smaller laser spot size decreased the overall powder efficiency from 60% to 50%. Besides the improved surface roughness and shape tolerances, the pockets of part (b) are shaped accurately. The critical interface between the zigzag and the contour path does not show large bonding defects.

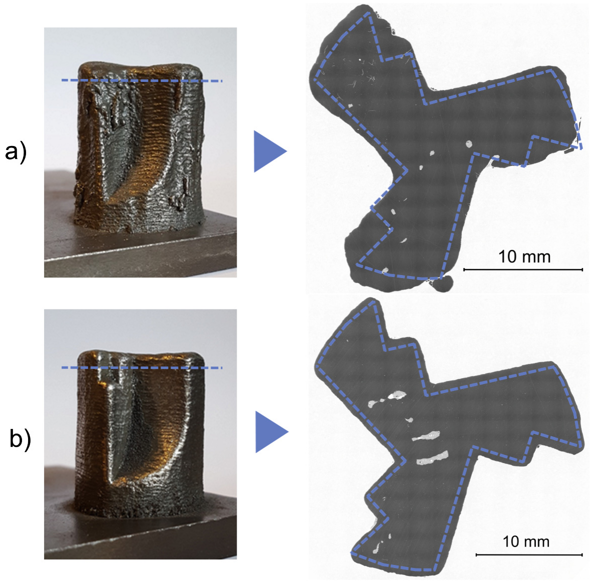

Fig. 6. Image and cross-section of the produced milling head, using standard zigzag (a) and optimized (b) process parameters for the contour toolpath, indicated by the dashed lines

Table 1. Process parameters for "milling head", "tapered geometry", and "impeller"

Parameter	Zigzag (a, b)	Contour (b)
Laser power	600 W	490 W
Laser spot size	2.7 mm	2.2 mm
Feed speed	830 mm/min	830 mm/min
Powder feed rate	6.5 g/min	6.5 g/min
Track pitch	1.1 mm	1.1 mm
Layer height	0.6 mm	0.3 mm

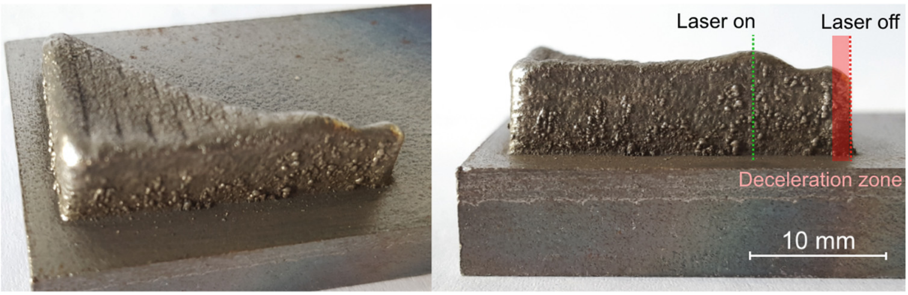

Fig. 7. Produced tapered geometry in isometric and side view, showing the laser on and off positions as well as the deceleration zone

However, the cross sections reveal lack of fusion in the interior of both parts, thus further optimization of the zigzag path is needed.

A tapered geometry with optimized parameters is shown in Fig. 7. The laser was switched on where the gap in the edge reaches 0.55 mm, visible by an accumulation of material. The sharp edge was built by a specific reduction of the feed speed (with constant laser power) before switching off the laser as depicted in Fig. 8. In this graph, the x-axis denotes the distance to the edge; the y-axis denotes the factor k that is multiplied with the feed speed. This profile was necessary to create an edge with constant buildup height. Using this strategy, an edge radius of less than 1 mm and a smooth transition within the tapered area could be achieved.

The impeller as shown in Fig. 9 was made with the same optimized parameters, leading to good shape accuracy of the blades. The cross section of a similar impeller proofs that the microstructure at the blade root is fully dense. The tip of the two-track blade is thickened due to the turn of the processing head. For larger, highly inclined blades, a 5-axis buildup would be required. Lack of fusion in the zigzag area is due to the small track length and the high number of laser-on and -off events, leading to an unstable melt pool.

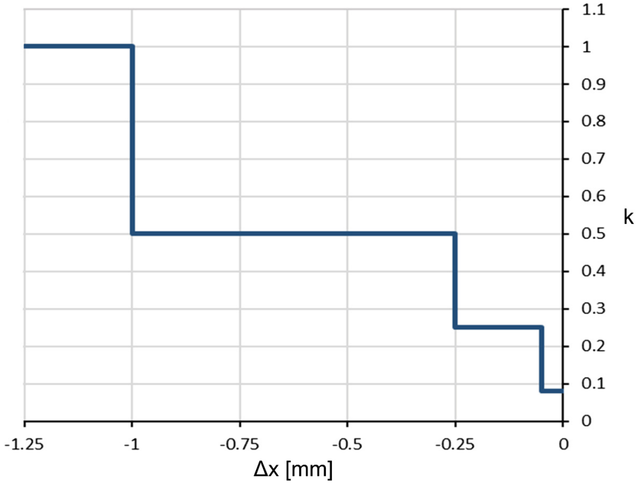

Fig. 8. Deceleration zone of the tapered geometry: Feed speed factor k as a function of the horizontal distance to the edge, where the laser is switched off

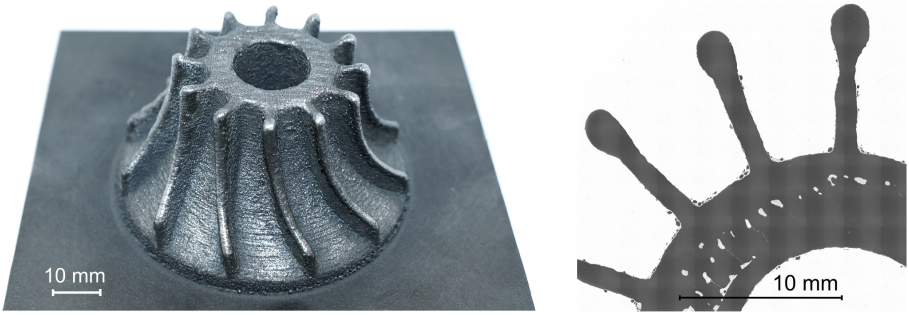

Fig. 9. Image and cross-section of the produced impeller

6 Conclusion

Toolpaths are a critical issue for the DMD process and constrain the achievable part complexity. It was stated that the enhanced approach of distinctive CAD data could reduce the required manual input for toolpath generation. By transferring additional information such as load directions or functional surfaces from the part development process to a CAM software, a suitable NC code can be calculated in a reliable and predictable manner. The hybrid toolpath is a combination of a zigzag filling and an outer contour path, showing various advantages regarding the process characteristics and the computational effort. By splitting a part into a zigzag subset and a contour subset in the CAD software, a CAM algorithm can calculate a suitable toolpath to build parts with both massive and thin-walled elements. Further optimization of the contour path and the process parameters lead to a significant increase in surface quality and shape accuracy, even for tapered geometries. Bonding defects at the interface of zigzag and contour path could be diminished. However, the zigzag pattern requires improvements to gain a fully dense microstructure. 5-axis toolpath strategies need to be developed for a further increase of the part complexity.

References

1. Gibson, I., Rosen, D., Stucker, B.: Additive Manufacturing Technologies. Springer, New York (2015)
2. Nowotny, S., Scharek, S., Beyer, E., Richter, K.H.: Laser beam build-up welding: precision in repair, surface cladding, and direct 3D metal deposition. J. Therm. Spray Technol. **16**(3), 344–348 (2007)
3. Shamsaei, N., Yadollahi, A., Bian, L., Thompson, S.M.: An overview of direct laser deposition for additive manufacturing; part ii: mechanical behavior, process parameter optimization and control. Addit. Manufact. **8**, 12–35 (2015)
4. Farouki, R.T., Koenig, T., Tarabanis, K.A., Korein, J.U., Batchelder, J.S.: Path planning with offset curves for layered fabrication processes. J. Manufact. Syst. **14**(5), 355–368 (1995)
5. Jin, G.Q., Li, W.D., Gao, L.: An adaptive process planning approach of rapid prototyping and manufacturing. Robot. Comput.-Integr. Manufact. **29**(1), 23–38 (2013)
6. Rajan, V., Srinivasan, V., Tarabanis, K.A.: The optimal zigzag direction for filling a two-dimensional region. Rapid Prototyping J. **7**(5), 231–241 (2001)
7. Jin, Y., He, Y., Xue, G., Fu, J.: A parallel-based path generation method for fused deposition modeling. Int. J. Adv. Manufact. Technol. **77**(5), 927–937 (2015)
8. Felkel, P., Obdrzalek, S.: Straight skeleton implementation. In: Proceedings of Spring Conference on Computer Graphics, pp. 210–218. http://citeseerx.ist.psu.edu/viewdoc/summary?doi=10.1.1.131.7175
9. Ding, D., Pan, Z., Cuiuri, D., Li, H.: A practical path planning methodology for wire and arc additive manufacturing of thin-walled structures. Robot. Comput.-Integr. Manufact. **34**, 8–19 (2015)

Performance Simulation and Verification of Vat Photopolymerization Based, Additively Manufactured Injection Molding Inserts with Micro-Features

Michael Mischkot(✉), Thomas Hofstätter, Ifigeneia Michailidou,
Carlos Herrán Chavarri, Andreas Lunzer, Guido Tosello,
David Bue Pedersen, and Hans Nørgaard Hansen

DTU Mechanical Engineering, Produktionstorvet 427A/314,
2800 Kongens Lyngby, Denmark
`micmi@mek.dtu.dk`

Abstract. Injection molding soft tooling inserts manufactured additively with vat photopolymerization represent a valid technology for prototyping and pilot production of polymer parts. However, a significant drawback is the low heat conductivity of photopolymers influencing cycle time and part quality. In this research, the thermal performance of a $20 \times 20 \times 2.7\,\text{mm}^3$ injection molding insert was simulated. A thermal camera was used to assess the quality and accuracy of the simulation. Both, simulation and measurements showed that the temperature cycle during injection molding becomes stationary within 3 to 5 cycles. After 2800 injection molding cycles, the experiment was stopped and the insert was still intact.

Keywords: Additive manufacturing · Micro injection molding · Soft tooling · Simulation

1 Introduction

Soft tooling injection molding inserts manufactured with vat photopolymerization enable fast and cost effective prototyping and pilot production. Available materials generally enable either high accuracy or have high resitance to heat [1]. The lifetime of vat photopolymerization soft tooling inserts has been reported mainly in the two- to three-digits cycle range [3,5]. However, [2] reported a lifetime of more than 2500 cycles when injection molding polyethylene low-density with carbon fiber-reinforced soft tooling inserts. The suitability of additive manufacturing for the production of inserts for micro injection molding has been demonstrated, e.g. in [3,4]. This research benchmarks the thermal performance of vat photopolymerization soft tooling injection molding inserts against conventional injection molding with a brass insert.

© Springer International Publishing AG 2018
M. Meboldt and C. Klahn (eds.), *Industrializing Additive Manufacturing - Proceedings of Additive Manufacturing in Products and Applications - AMPA2017*,
DOI 10.1007/978-3-319-66866-6_16

2 Materials and Methods

2.1 Design of Test Part

The test part consisted of a cuboid structure comprising two heart shaped structures (Fig. 1). The cuboid's outer dimensions were $20 \times 20 \times 2.7\,\text{mm}^3$. In addition, two cuboid structures with micro cylinders (800 µm diameter, (300 µm high) were present.

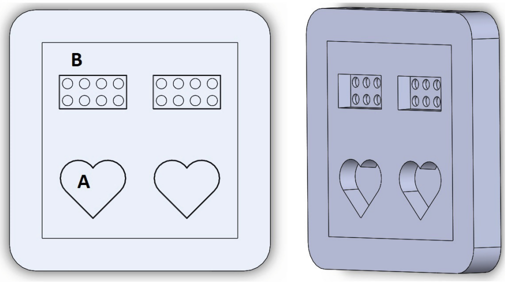

Fig. 1. CAD model of test part. Areas A and B are marked with letters.

2.2 Tooling

The inserts were manufactured in SOMOS®perform using a stereolithography vat photopolymerization printer.

2.3 Simulation

Five injection molding cycles were simulated in COMSOL Multiphysics®. One injection molding cycle consisted of the following periods resulting in a total cycle time of 20 s.

- Injection and packing: 8.5 s
- Mold opening, cooling down, and mold closing: 11.5 s

The material properties of the photopolymer were set to 0.167 W/mK for the thermal conductivity, 1100 kg/m^3 for the density, and 1400 J/kgK for the heat capacity.

2.4 Injection Molding and Thermal Imaging

An Engel®injection molding machine was used to injection mold acrylonitrile butadiene styrene (ABS) with an injection pressure of 300 bar.

A thermal camera (FLIR®A655sc) was installed and driven down from above the machine to take thermal images when the mold was open. About five seconds

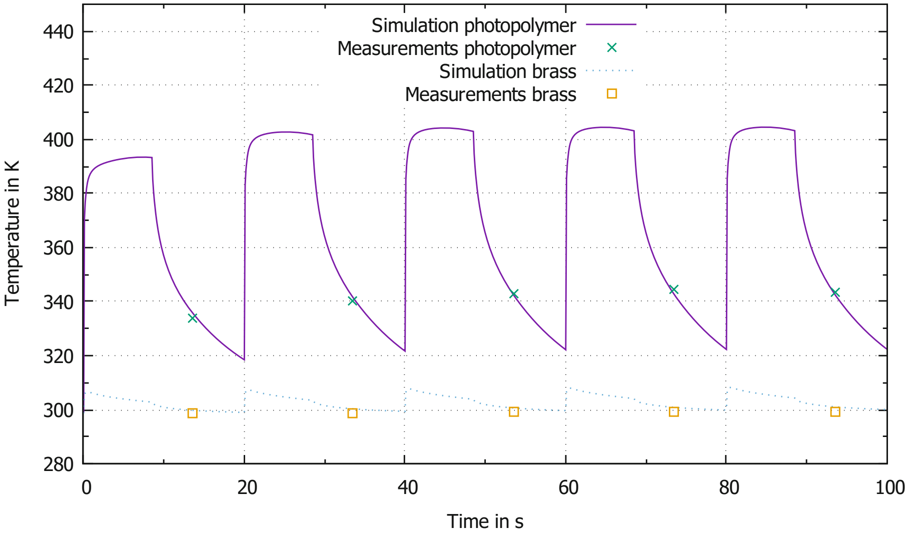

Fig. 2. Simulated and measured temperature development over the first five injection molding cycles.

passed from when the mold started opening to when the camera could start taking images. The images were analyzed with the camera manufacturer's software requiring the emissivity of the photopolymer. As a consequence, the emissivity was calibrated and set to 0.95.

Two different temperature measurements were conducted:

- An image series over 100 injection molding cycles (one image taken after each cycle). The first five cycles are presented in Fig. 2.
- A video capture of the natural cooling process after one injection molding cycle (2 frames per second, Fig. 3)

2.5 Metrological Assessment

The injection molded parts as well as the inserts were analyzed with a scanning electron microscope (SEM) as well as a laser scanning microscope (OLYMPUS Lext®). SEM pictures were taken before injection molding, after about 100 shots and after 2800 shots.

3 Results

3.1 Comparison of Thermal Simulations and Temperature Measurements

Figure 3 shows that the measured values (starting 5 s after mold opening) are matching the simulated values closely. Consequently, it can be assumed that

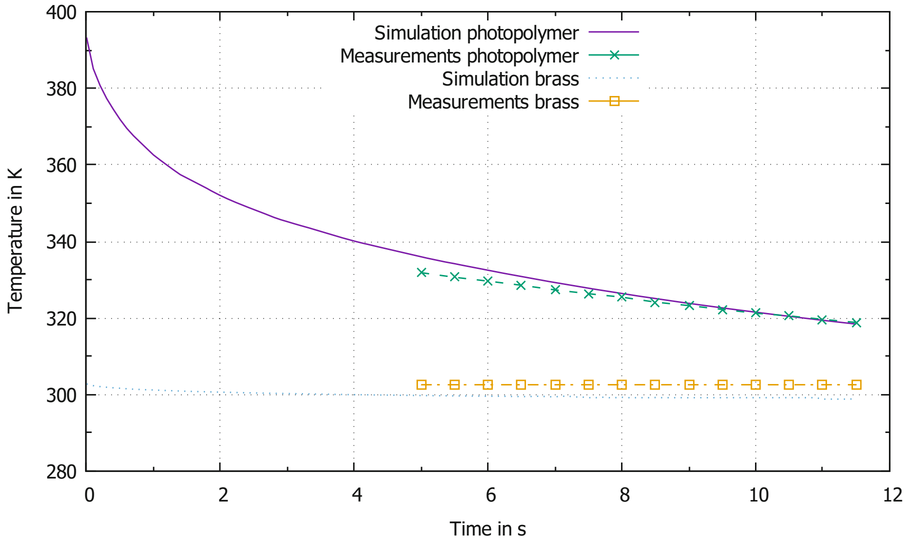

Fig. 3. Simulated and measured temperature development during the first injection molding cycle after mold opening.

the simulation presents a plausible calculation of the temperature development over the whole injection molding cycle, providing valuable information for future research and investigations on thermal ageing of soft tooling inserts.

3.2 Temperature Development

The temperature cycles became stationary within three to five cycles in both simulations and measurements.

The maximum temperature present on the insert was found to be below 410 K.

The high thermal inertia of the photopolymer became visible in Fig. 2 since the photopolymer insert was still heating up when the brass insert already started cooling down.

Figure 4 shows the temperature development in the insert symmetry plane as well as in a local symmetry plane in the heart/cuboid/cylinder region of the insert.

3.3 Insert Life Time

A soft tooling micro injection molding insert was used successfully for 2800 shots of ABS. The insert was still intact after the experiment which demonstrates a significant improvement when compared to, e.g., [2].

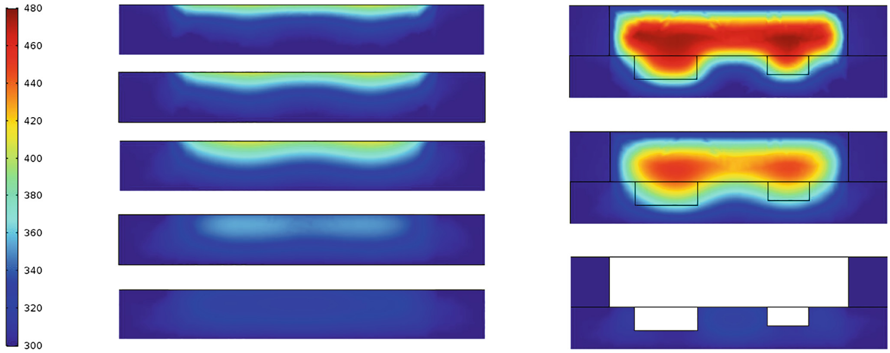

Fig. 4. Temperature development in the insert symmetry plane (left column: after 3, 5, 8.5, 12, and 17 s from top to bottom) and in a local symmetry plane in the heart/cuboid/cylinder region of the insert (right column: after 3, 8.5, and 17 s from top to bottom). In the right column, the ABS injection molded part is present during the injection and packing phase (8.5 s).

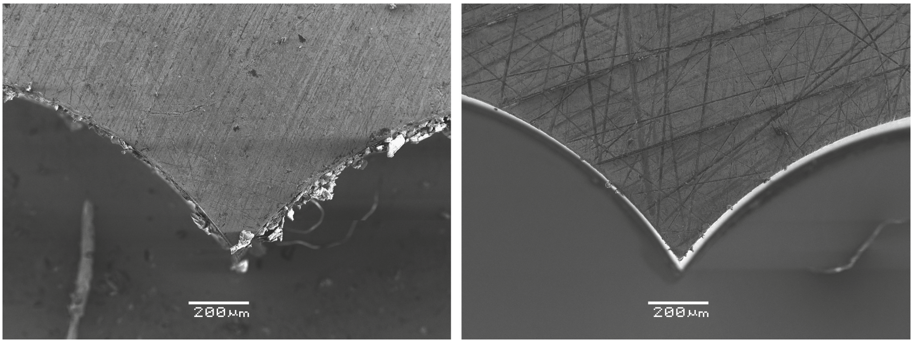

Fig. 5. Area A of a brass insert before injection molding (left) and after about 100 shots ABS (right).

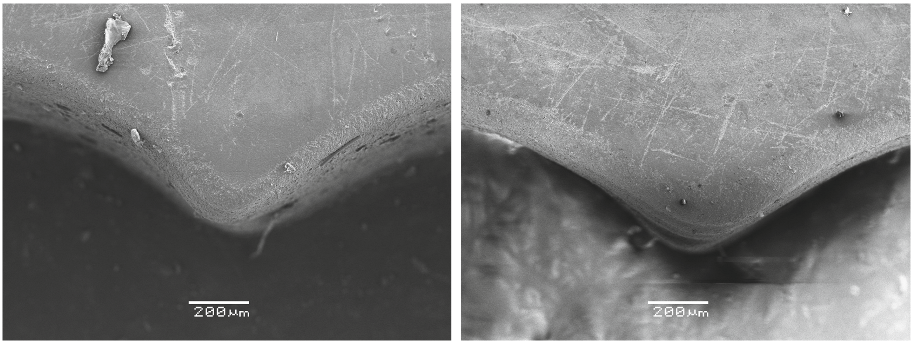

Fig. 6. Area A of a photopolymer insert before injection molding (left) and after about 100 shots (right).

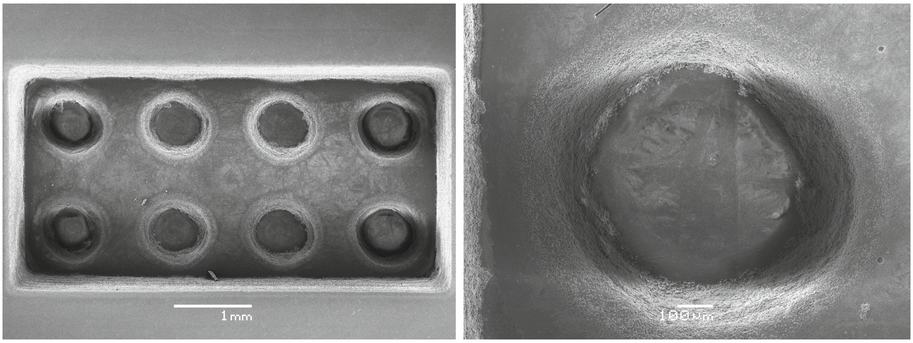

Fig. 7. Area B of a photopolymer insert after 2800 shots ABS.

3.4 Inserts Before and After Injection Molding

Figures 5, 6, and 7 show SEM images of the inserts before and after injection molding. On the photopolymer insert, no insert degradation or wear was detected during metrological analysis with a laser scanning microscope after 2800 injection molding cycles.

4 Conclusions

- The thermal simulation was found to be an accurate tool for the investigation of the temperature development in the injection molding inserts.
- The very low thermal conductivity of the photopolymer compared to brass (ca. 650× smaller) leads to a significantly longer injection molding cycle time (the cooling time was set to 11.5 s for an insert geometry of $20 \times 20 \times 2.7\,\mathrm{mm}^3$).
- After 2800 injection molding cycles with ABS, the photopolymer insert was still intact which represents a significant increase in lifetime when compared to numbers reported in, e.g., [1] or [2]. No insert wearing was detected in a metrological analysis with an SEM and laser scanning microscopy.

Suggestions for Future Research: It is suggested to investigate

- thermal simulations with a larger insert geometry,
- model fiber-reinforced and/or coated injection molding inserts to quantify the influence of these modifications on cycle time and insert lifetime,
- the thermal ageing process to increase the predictability and reliability of vat photopolymerization soft tooling inserts.

Acknowledgements. The research presented in this paper was carried out and financed in the framework of a project between the Technical University of Denmark (DTU) and the Manufacturing Academy of Denmark (MADE), (http://en.made.dk). Funding from Innovation Fund Denmark (http://innovationsfonden.dk/en) is greatly acknowledged.

References

1. Stucker, B., Gibson, I., Rosen, D.W.: Additive Manufacturing Technologies (2015)
2. Hofstätter, T., Mischkot, M., Pedersen, D.B., Tosello, G., Hansen, H.N.: Evolution of surface texture and cracks during injection molding of fiber-reinforced, additively-manufactured, injection molding inserts. In: Proceedings of ASPE Summer Topical Meeting 2016: Dimensional Accuracy and Surface Finish in Additive Manufacturing (2016)
3. Lantada, A.D., Piotter, V., Plewa, K., Barié, N., Guttmann, M., Wissmann, M.: Toward mass production of microtextured microdevices: linking rapid prototyping with microinjection molding. Int. J. Adv. Manufact. Technol. **76**(5–8), 1011–1020 (2015)
4. Mischkot, M., Zhang, Y., Gøtje, A.S., Pedersen, D.B., Tosello, G., Hansen, H.N: Influence of injection-molding process parameters on part replication of microstructures with additively-manufactured soft tooling inserts. In: WCMNM World Congress on Micro and Nano Manufacturing (2017)
5. Rajaguru, J., Duke, M., Au, C.: Development of rapid tooling by rapid prototyping technology and electroless nickel plating for low-volume production of plastic parts. Int. J. Adv. Manufact. Technol. **78**(1–4), 31–40 (2015)

Additive Repair Design Approach: Case Study of Transverse Loading of Aluminum Beams

Zghair Yousif(✉) and Lachmayer Roland

Gottfried Wilhelm Leibniz Universität Hannover, Hannover, Germany
`zghair@ipeg.uni-hannover.de`

Abstract. The repair process for complex components is complicated and time consuming, and the traditional repair methods cannot handle these challenges. Therefore, introducing new solutions to repair parts is a necessity in the industrial world. Additive manufacturing is considered one of the modest manufacturing techniques. Using this technique in components repair is the state of the art in the industry of maintenance. This paper is based on previous work to develop an additive repair design approach, with focus on the Selective Laser Melting technique. A bending load case on beams made of two metals (cast part and sintered part) is discussed, and the induced stresses and deflections are investigated for various building directions and interface planes geometries. The used metals of the cast parts are Al-6082 and Al-7075 alloys, and the used powder to build-over with the Selective Laser Melting machine is AlSi10Mg. The analysis carried out by means of a finite element numerical model to estimate bending loading and the induced flexural stresses. Experimental work is implemented, and all analytical and experimental results are discussed and compared. This work aims to develop scientific basics for parts repair using additive manufacturing technologies.

1 Introduction

Components usually suffer from wear, distortion, defects and cracks during their life cycle, and sometimes repairing is considered more cost effective and time saving than replacing these components. For complex geometry, especially for aerospace components, the repair process becomes more complicated, and the traditional repair methods cannot handle these challenges. Therefore, introducing new solutions by using additive manufacturing techniques to repair parts is necessary [1]. Since the additive technologies are used in repair, the term "Additive Repair" can be defined as "additive manufacturing process for reconstruct and modify prebuilt components" [1]. Companies like RPM Innovations, have already provided services using laser deposition technologies, such as laser engineered net shaping, advanced additive manufacturing and repair and laser repair technology (LRT) [2]. Siemens has already used additive repair technology to repair gas turbines [3]. EOS Company also stated the possibility to use additive manufacturing to repair damaged tool inserts [4]. "The experimental results show also that the parts built-up additively (part of an aluminum extrusion die) withstand the high mechanical and thermal loads which occur during hot aluminum extrusion" Hölker said [5]. Huan Qi., used Laser powder deposition based method

© Springer International Publishing AG 2018
M. Meboldt and C. Klahn (eds.), *Industrializing Additive Manufacturing - Proceedings of Additive Manufacturing in Products and Applications - AMPA2017*,
DOI 10.1007/978-3-319-66866-6_17

called Laser Net Shape Manufacturing (LNSM) to repair turbine compressor airfoil in his research due to the advantage of fine microstructure, small heat affected zone and to cast superior material properties [6]. Among diverse established additive layer manufacturing technologies, Selective Laser Melting (SLM) has become a promising manufacturing route for engineering parts, and that's due to its higher accuracy, god surface quality and less post machining compared to laser deposition method. From the other side, contributing SLM technology within machine elements repair is a big challenge, because of all variants surrounding the element in its working space, and the process limitations. Such as, loads and the way they act. The size of parts has to be considered, because of limited building rooms sizes. Also the available metals powders used in SLM machine are not covering a wide range. The additive repair process using SLM is based on preparing the damaged part to get a plane smooth surface so that it would be possible to build over it, and then to design and prepare a CAD model of the volume that has to be substituted, and finally to start the building process to get final repaired part. In this work, a method for conceptual design of Additive Repair is defined, and investigated to facilitate the steps required to make the conceptual designs for component repair for the designer. Since SLM can only build on flat planes, two possible building procedures of the added volume are introduced to satisfy the load type and magnitude. Later a transvers load case is defined, and the possible solutions to design the added volume are discussed. Six possible solutions are implemented numerically and experimentally for two selected metals. Finally, the results are compared and discussed.

2 Developed Method for Conceptual Design of Additive Repair

All design approaches must verify the relationship between the applied stresses on a part and the strength of its metal [7]. By taking all the advantages of additive manufacturing process, and specifying all the process capabilities and constraints, the designing process can be modified by AM technologies [8]. The objective of this approach is to define a methodology to help the designers in the early conceptual phase of a design process to design the damaged volume of parts by taking the advantage of additive manufacturing abilities. This methodology consists of two main steps (see Fig. 1). The first one is to define a new metals library, in which each metal alloy powder is assigned to be weld-able with several metal alloys. So that, it would be possible to know which powder fits to the metal of the part intended to repair, and that the bonding between the two metals are strong enough to carry the same loads. After analysis and the specifications of the part to be repaired are proposed, the second step is to make the design concept of the added repaired volume. The designer has to take the stress concentration planes in consideration, the position of cut plane (where the added volume will start from), the building direction and number of building stages. The designer has also the possibility to modify the added repaired volume in accordance with service conditions, and optimizing in relation to the specifications and the manufacturing constraints.

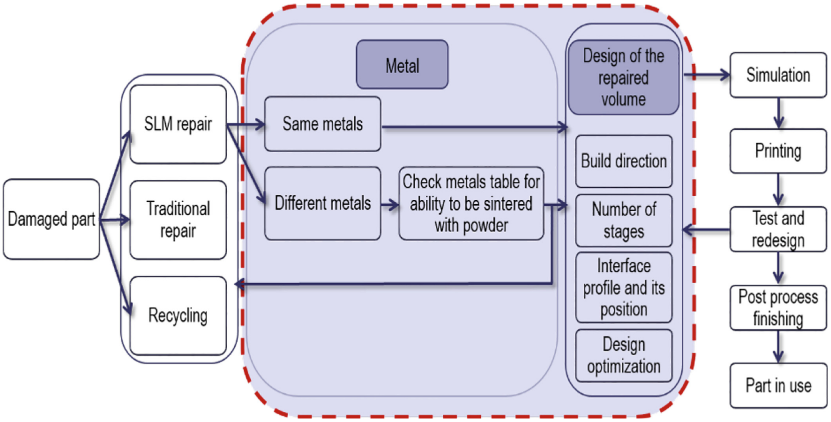
Damaged part
SLM repair
Traditional repair
Recycling
Metal
Same metals
Different metals
Check metals table for ability to be sintered with powder
Design of the repaired volume
Build direction
Number of stages
Interface profile and its position
Design optimization
Simulation
Printing
Test and redesign
Post process finishing
Part in use

Fig. 1. Developed design method for additive repair.

This paper is based on previous work [9, 10]. The metals selection and the interface planes design and building strategies will be adopted from it. One of the load cases will be investigated to verify and assign some design principals to the interface plane between the damaged part and its added repaired volume.

3 Beam Under Transverse Load

All mechanical parts, during operation, are subjected to variants of static or dynamic loads. The building direction in SLM is considerable, and the metal produced is orthotropic. Building in vertical direction will produce less durable structure than the other directions [11, 12]. So, care must be taken during the design of the repaired volume of the part, and designer have to find the best building position according to the load type that will be applied on part, even if it divides the building process into more than one building stage. The loads, in which parts in engines or structures could be subjected to, are mainly either a tension, compression, torsion or bending loads, and in many cases it could be a combination of more than one of them. In this work, a bending load case of simply supported beam is investigated. According to the beam theories of maximum transverse and shear stresses, and to the limitations of the SLM machines to build over plane surfaces, six profiles of the interface between the original and sintered volume are designed. The design is mainly made to avoid the maximum stresses in the interface plane, and to take in consideration the ability to be built with SLM machine. Figure 2 shows the six suggested profiles, and the corresponding loads positions. The participated metals that will be used as the damaged cast models are Al-6082 and Al-7075 aluminum alloys respectively, and the metal powder that will be used for repair is AlSi10Mg aluminum alloy.

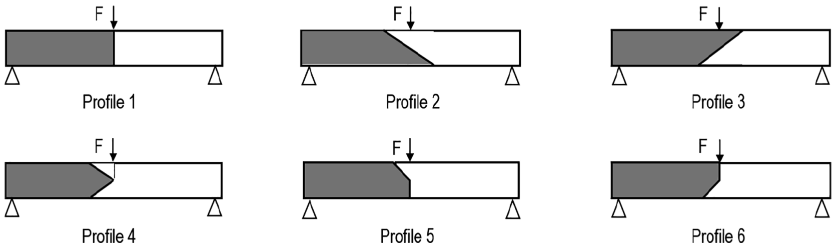
F
Profile 1
Profile 2
Profile 3
Profile 4
Profile 5
Profile 6

Fig. 2. Different interface planes profiles for simply supported beams under transverse load.

4 Case Study: Simply Supported Beam Under Static Transverse Load

4.1 Numerical Analysis

In this part of the work, a numerical analysis with finite element method will be implemented to determine stresses, deflections in specimens and the location of the expected fracture zone. The analysis will study the transverse load case on the six profiles, and the deflection of 19 selected points on the upper surface of the specimens. Consider the simply supported beam shown in Fig. 3 with length L, subjected to a load F over half its length. From the beam theories, the maximum flexural stress within the elastic limit is given by $\sigma_{max} = \frac{3FL}{2bh^2}$, where b, h are the dimensions of the cross sectional area of the beam. Since the models are made out of two metals and each metal has a different modulus of elasticity, the expected deformations and stresses of each half are not the same. For the given metal combination, the simulated applied force will be determined according to the weakest metal by using maximum transverse stress formula. For the case study beam, where the length is taken as 80 mm, and the square cross section dimension as 10 mm, the loads within the elastic limit must not exceed the values shown in Table 1. When the bilinear metals behaviors are defined, and all the geometry entities, meshing specs, boundary conditions, loads and analysis settings are set up, then the solve is executed.

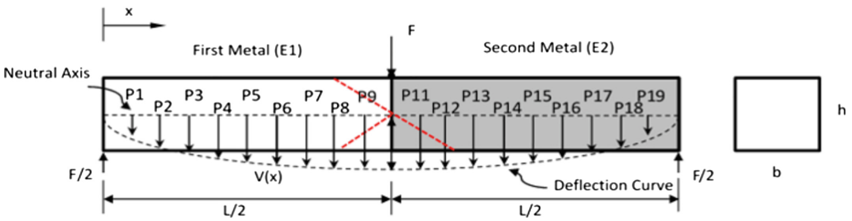
x
F
First Metal (E1)
Second Metal (E2)
Neutral Axis
P1
P2
P3
P4
P5
P6
P7
P8
P9
P11
P12
P13
P14
P15
P16
P17
P18
P19
F/2
V(x)
Deflection Curve
F/2
L/2
L/2
h
b

Fig. 3. Deflection curve of a two metals beam.

Table 1. Metals yield stresses and corresponding transverse yield forces.

Material	Yield stress (MPa)	Applied force for yield stress (N)
Al-6082	200	1666.67
Al-7075	400	3333.34
AlSi10 Mg	216	1800
6082 + AlSi10 Mg	200	1666.67
7075 + AlSi10 Mg	216	1800

On the upper surface of each model, the deflection readings of the 19 points are recorded. By drawing these readings against the beam length, the deflection curves of the beams are obtained for each profile (see Fig. 4).

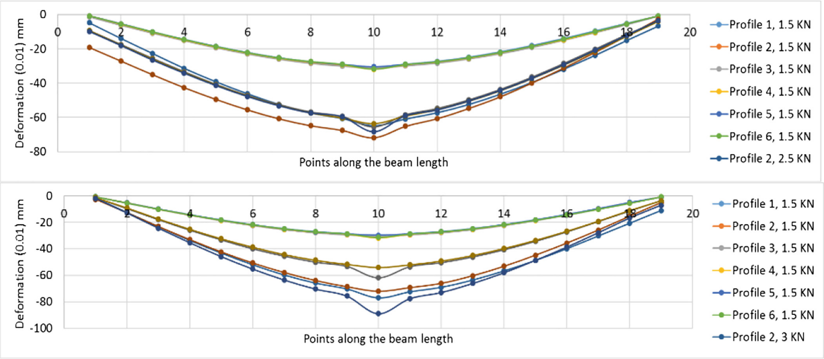

Fig. 4. Simulated deflection curves of the beams at 1.5 KN and 2.5 KN for (a) Al-6082/AlSi10Mg, (b) Al-7075/AlSi10Mg.

4.2 Experimental Analysis

The design of the interface plane layer, between the cast and sintered part, depends on the layer thickness and the laser power required to melt the cast part in sufficient depth to perform good bonding between the two metals. The laser power required varies from one metal to another, depending on different variables. In this work, the building strategy, including the interface plane design, part orientation and building direction, will be adopted from previous work that verified successfully in tension loads [9, 10]. First, the cast part of the specimens is machined, and fixed in the supposed position inside the building room in the machine. The machine used in this experiment is EOS 280M. Later, all the machine parameters are set up, and the CAD model of the second half of the specimens is uploaded. Six models are built in one building stage, while the rest are built in two building stages. At the end, all specimens are cleaned and machined to the final dimensions, and 19 points are marked on the surface to enable later the measurement of the deflection along the beam length. Figure 5 shows the specimens after each building step.

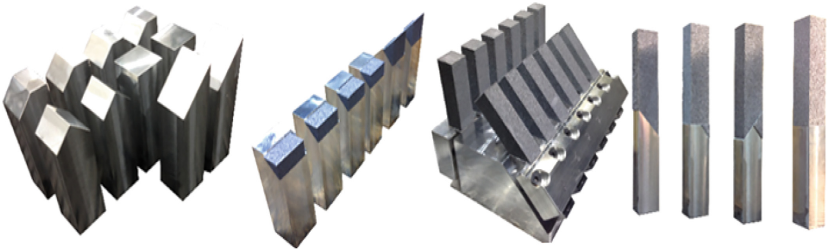

Fig. 5. Specimens building steps. (a) cast part, (b) First stage, (c) Second stage, d. final model.

5 Results and Discussion

The test of the models is performed by using a bending test bench at room temperature. The load is applied with 500 N increment, and the force deformation curve is obtained for all profiles. The deflection of the marked points is recorded at different loads, and hence the deflection curves are obtained. It could be observed from Fig. 6 that all fractures are located in the interface planes, but with different total deflections and fracture loads. To recognize which of the six profiles represent the best solution to stand against the transvers loads, all the theoretical, numerical and experimental curves should be examined and compared. The adopted criteria to evaluate the best profiles is depending on the stress produced on the middle of the lower surface of the beam, the total deflection of the midpoint, and finally on the percentage deflection difference (the difference in deflection of two symmetric points in each half of the specimen around the midpoint). The lower value is the better profile. Figure 7 shows the values of the above parameters for different loads, simulated and tested, and the percentage deflection difference is taken for the points 7 and 13 on the cast and sintered parts respectively. For the Al-6082/AlSi10 Mg specimens, the simulation values show that Profiles 1, 2 and 6 have lower stress values within the interface plane area, but the other profiles are only around 6% higher. Deflection at 1.5 KN load is almost the same for all profiles, while at 2.5 KN load the variation is about 12% from profile 5 to profile 3. Profiles 2 and 6 show the best percentage deflection difference between point 7 and 13 of the specimens within the elastic limit, while profile 6 is the best at higher load

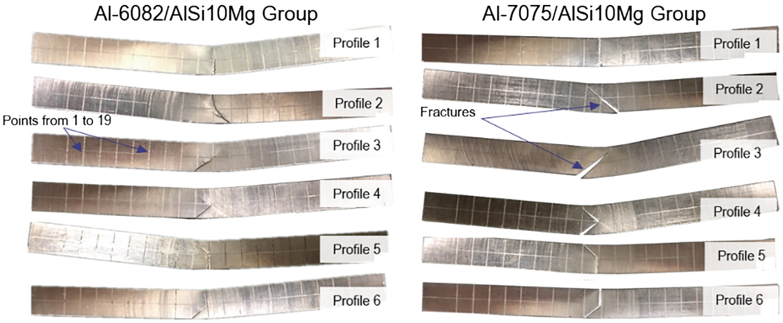

Fig. 6. Fractures location of the specimens, (a) Al-6082/AlSi10 Mg, (b) Al-7075/AlSi10 Mg.

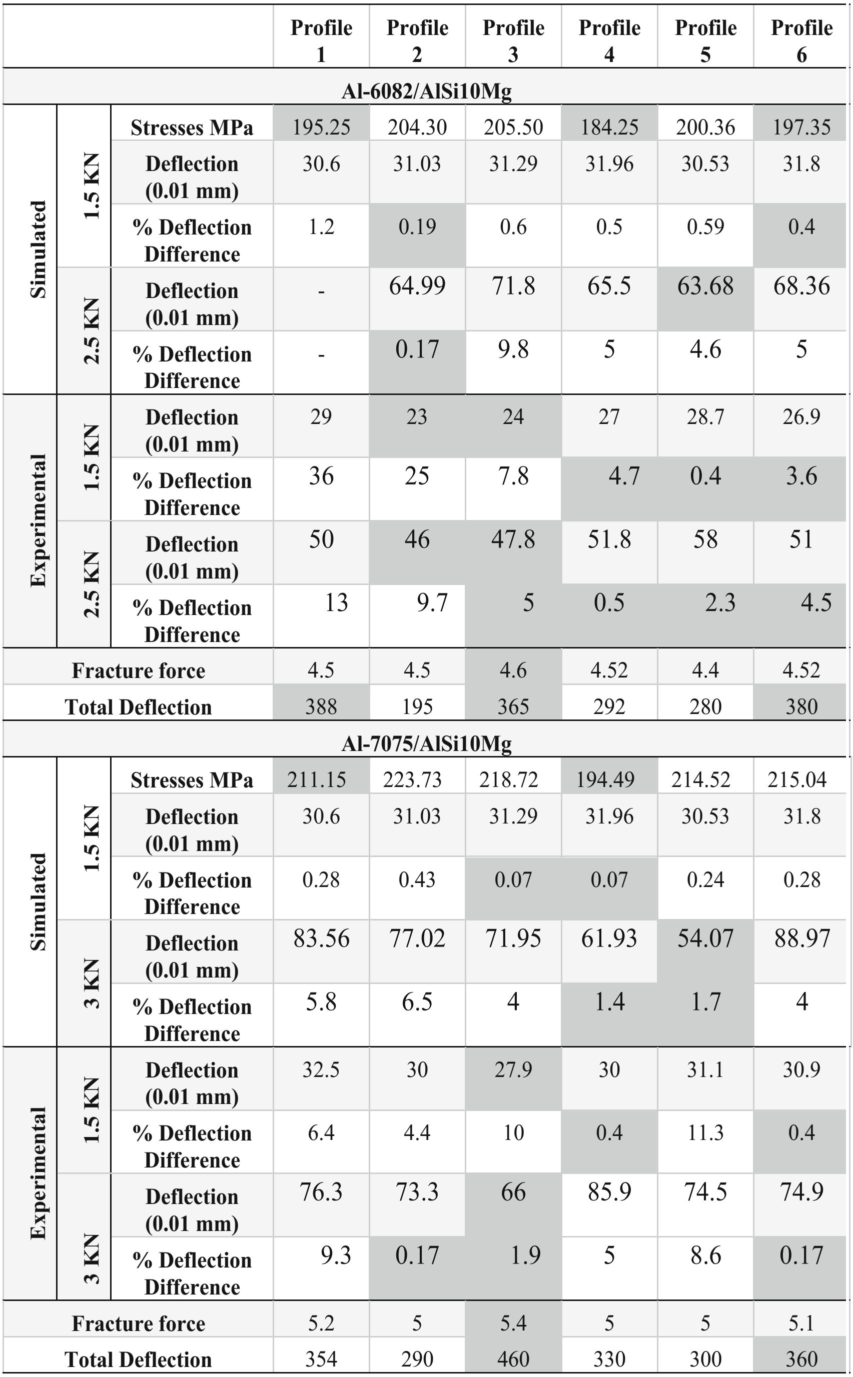

			Profile 1	Profile 2	Profile 3	Profile 4	Profile 5	Profile 6
Al-6082/AlSi10Mg								
Simulated	**1.5 KN**	**Stresses MPa**	195.25	204.30	205.50	184.25	200.36	197.35
		Deflection (0.01 mm)	30.6	31.03	31.29	31.96	30.53	31.8
		% Deflection Difference	1.2	0.19	0.6	0.5	0.59	0.4
	2.5 KN	**Deflection (0.01 mm)**	-	64.99	71.8	65.5	63.68	68.36
		% Deflection Difference	-	0.17	9.8	5	4.6	5
Experimental	**1.5 KN**	**Deflection (0.01 mm)**	29	23	24	27	28.7	26.9
		% Deflection Difference	36	25	7.8	4.7	0.4	3.6
	2.5 KN	**Deflection (0.01 mm)**	50	46	47.8	51.8	58	51
		% Deflection Difference	13	9.7	5	0.5	2.3	4.5
Fracture force			4.5	4.5	4.6	4.52	4.4	4.52
Total Deflection			388	195	365	292	280	380
Al-7075/AlSi10Mg								
Simulated	**1.5 KN**	**Stresses MPa**	211.15	223.73	218.72	194.49	214.52	215.04
		Deflection (0.01 mm)	30.6	31.03	31.29	31.96	30.53	31.8
		% Deflection Difference	0.28	0.43	0.07	0.07	0.24	0.28
	3 KN	**Deflection (0.01 mm)**	83.56	77.02	71.95	61.93	54.07	88.97
		% Deflection Difference	5.8	6.5	4	1.4	1.7	4
Experimental	**1.5 KN**	**Deflection (0.01 mm)**	32.5	30	27.9	30	31.1	30.9
		% Deflection Difference	6.4	4.4	10	0.4	11.3	0.4
	3 KN	**Deflection (0.01 mm)**	76.3	73.3	66	85.9	74.5	74.9
		% Deflection Difference	9.3	0.17	1.9	5	8.6	0.17
Fracture force			5.2	5	5.4	5	5	5.1
Total Deflection			354	290	460	330	300	360

Fig. 7. Readings and results used in the profiles evaluating criteria.

beyond the yield. The Experimental results show that within the elastic limit, profiles 2 and 3 have lower deflection values. The percentage deflection difference of profiles 4, 5 and 6 are less than the other profiles with a considerable value. Beyond the elastic limit, profiles 2 and 3 keep the lower deflection, and the percentage deflection difference of profile 3 decreases. The average fracture force for all specimens is 4.5, but the total deflection is differing with a percentage of 99%.

The simulation of Al-7075/AlSi10 Mg specimens within the elastic limit shows that profile 1 and 4 have the lowest stress values, followed by profiles 5 and 6. There is no considerable difference in the deflection values, or the percentage deflection difference of all profiles. When the load increased beyond the elastic limit, the deflection of profiles 1 and 6 are increased rapidly. The percentage deflection difference of profiles 4 and 5 is lower than the other profiles. The experimental results within the elastic limit indicate that profile 3 has a slight difference in deflection compared to the other profiles, while the percentage deflection difference of profiles 4 and 6 is positively noticeable. The recorded values of deflection of profile 3 beyond the yield is relatively lower than the others. The best recorded values of the percentage deflection difference are for profiles 2, 3 and 6. The average fracture force is 5.1 KN, and the total deflection of all profiles differ with 36%. According to the above discussion, the highlighted blocks of the experimental work in Fig. 7 are considered as a positive grade. By summing these grades for each profile of both groups, then profile 3 gets 5 points and profile 6 gets 3 points. Both profiles have good percentage deflection differences and high total deflection. The simulation results predict the deflection of the first specimens group within the elastic limit with an approximate error of 17% from the experimental results, while within the plastic region, the deflection error is around 8%. But the results of percentage deflection difference, within the elastic and plastic regions, deviate strongly from the experimental results, and it differ from profile to another. For the second group of specimens, the deflection error between simulation and experimental results within the elastic limit is around 2%, and varies from 5% to 18% beyond the elastic limit. The same big error for percentage deflection difference is noticed within both elastic and plastic regions.

6 Conclusions

It can be concluded that the best interface profiles to carry a static transvers load without very big difference in deflection between the cast part and the sintered part are profiles 3 and 6, for both specimen's groups. The bonding between the cast and sintered halve of the specimen for these profiles are strong enough to carry 4.6 KN for the Al-6082/AlSi10 Mg and 5.4 KN for the Al-7075/AlSi10 Mg specimens although the transverse fracture load for pure AlSi10 Mg powder is 5 KN. Which means, especially for the second group, this profile enhanced the specimen strength. The ANSYS error is acceptable for the deflection calculation in both regions, elastic and plastic. But the error of the percentage deflection difference is not acceptable, and therefore it is not adopted. In the next work steps, a post heat treatment of the repaired part will be studied, and another case study will investigate a dynamic bending load for another demonstrator, to evaluate the efficiency of the selected profiles in a life cycle test.

References

1. Lachmayer, R., Lippert, R.B., Fahlbusch, T.: (Hrsg.) 3D-Druck beleuchtet – additive manufacturing auf dem Weg in die Anwendung. Springer Vieweg Verlag, Berlin Heidelberg, Mai 2016 (2016). ISBN: 978-3-662-49055-6
2. Laser engineered net shaping advances additive manufacturing and repair. http://www.rpm-innova-tions.com/laser_deposition_technology_advances_additive_manufacturing_and_repair
3. Navrotsky, V., Graichen, A., Brodin, H.: Industrialisation of 3D printing (additive manufacturing) for gas turbine components repair and manufacturing. VGB Power Tech – Autorenexemplar
4. Tool Repair with Additive Manufacturing by EOS. http://www.eos.info/industries_markets/tooling/tool_repair
5. Hölker, R., Tekkaya, A.E.: Advancements in the manufacturing of dies for hot aluminium extrusion with conformal cooling channels. Int. J. Adv. Manuf. Technol. **83**, 1209–1220 (2015). doi:10.1007/s00170-015-7647-4
6. Qi, H., Azer, M., Singh, P.: Adaptive toolpath deposition method for laser net shape manufacturing and repair of turbine compressor airfoils. Int. J. Adv. Manuf. Technol. **2010**(48), 121–131 (2009)
7. Ponche, R., Hascoet, J.Y., Kerbrat, O., Mognol, P.: A new global approach to design for additive manufacturing. J. Virtual Phys. Proto-typing **7**(2), 93–105 (2012)
8. Vayre, B., Vignat, F., Villeneuve, F.: Designing for additive manufacturing. In: 45th CIRP Conference on Manufacturing Systems, Procedia CIRP, vol. 3, pp. 632–637 (2012)
9. Zghair, Y., Lachmayer, A.: Additive repair design approach: case study to repair aluminium base components. In: Accepted in International Design Conference – Design. Vancouver, Canada (2017)
10. Zghair, Y.: Rapid repair hochwertiger Investitionsgüter. In: Lachmayer, R., Lippert, R., Fahlbusch, T. (eds.) Additive Manufacturing Quantifiziert, pp. 196–229. Springer, Heidelberg (2017). ISBN: 978-3-662-54112-8
11. Zghair, Y.A., Lachmayer, R., Klose, C., Nürnberger, R.: Introducing selective laser melting to manufacture machine elements. In: International Design Conference – Design 2016, Dubrovnik – Croatia (2016)
12. Strößner, J., Terock, M., Glatzel, U.: Mechanical and microstructural investigation of nickel-based superalloy IN718 manufactured by Selective Laser Melting (SLM). Adv. Eng. Mater. **17**(8) (2015)

Quality Assurance

Controlled Porosity Structures in Aluminum and Titanium Alloys by Selective Laser Melting

Flaviana Calignano[1](✉), Giulio Cattano[1,2], Luca Iuliano[3], and Diego Manfredi[1]

[1] Istituto Italiano di Tecnologia, Center for Sustainable Future Technologies IIT@Polito, Corso Trento, 21, 10129 Turin, Italy
{flaviana.calignano,giulio.cattano, diego.manfredi}@iit.it
[2] Department of Applied Science and Technology, Politecnico di Torino, Corso Duca degli Abruzzi, 24, 10129 Turin, Italy
[3] Department of Management and Production Engineering, Politecnico di Torino, Corso Duca degli Abruzzi, 24, 10129 Turin, Italy
luca.iuliano@polito.it

Abstract. Stochastic and non-stochastic porous structures, are used in a variety of applications such as biomedical implants, heat exchangers mass and gas separation, water purification, energy conversion and storage due to their interesting combinations of physical and mechanical properties, such as high stiffness in conjunction with very low specific weight or high gas permeability combined with high thermal conductivity. Among the technologies for the production of these porous structures, the additive manufacturing (AM) processes, such as the powder bed based selective laser melting (SLM), are of particular interest. In order to obtain this kind of structures with SLM, it is important to know the relationship between process parameters and material employed. A series of experiments were carried out to analyze the influence of the main SLM process parameters on the width and continuity of manufacture of non-stochastic porous structures and to manufacture stochastic porous structures through the scanning strategy.

Keywords: Non-stochastic porous structure · Stochastic porous structure · Selective laser melting · Aluminum alloy · Titanium alloy

1 Introduction

Selective laser melting (SLM) or laser powder bed fusion (LPBF) process as defined by ISO/ASTM 52900, is an additive manufacturing (AM) technology which allows to build metal components with complex shapes, thanks to manufacture by melting subsequent layers of powders, starting from a three-dimensional (3D) computer aided-design (CAD) model. This has made the SLM technology, in recent years, very attractive for engineering designers who have the opportunity to fabricate new shapes, including porous structures, without the use of fixtures, tooling and mold. This

© Springer International Publishing AG 2018
M. Meboldt and C. Klahn (eds.), *Industrializing Additive Manufacturing - Proceedings of Additive Manufacturing in Products and Applications - AMPA2017*,
DOI 10.1007/978-3-319-66866-6_18

characteristic of SLM reduces and/or eliminates the design constraints of conventional manufacturing processes, expanding the design freedom, but also inserting a new set of process-specific design rules. Some of these new constraints are visible in one of the most promising applications of AM technologies: the realization of stochastic (random) and non-stochastic (periodic) porous structures, that are difficult or impossible to be produced by conventional manufacturing. Stochastic porous structures have been used as filters for years because they exhibit important filter properties such as fine filtration capacity, good particle retention, mechanical properties, corrosion resistance [1–4]. Instead, non-stochastic porous structures have been main utilized in applications such as heat exchangers and biomedical prostheses. Only recently, thanks to the metal AM technologies, non-stochastic porous structures have been used to create a filter design with holes in-line to the direction of fluid flow [1]. Burns [5] and Vijayakumar et al. [6] have suggested that AM technology such as SLM could be used in improving the filters efficiency and in reducing manufacturing costs. There are numerous designs for these structures, including octahedron, hexagon and rhombic dodecahedron that exhibit different mechanical properties [7]. In the recent years, some studies have focused on a kind of non-stochastic structures that are the thin wall porous structures. These structures offer higher surface area per unit volume, which increases their efficiency and may be applied, for example, in catalytic converter systems [4]. Some researchers have studied the relations between process parameters, CAD model, composition and microstructure of the obtained thin wall structures and/or the realization of these structures directly using process parameters. Yadroitsev et al. [4] analyzes the accurate reproduction of the parts geometry, strategy of manufacturing thin-walled 3D filters and filters with customized pattern of the micron-sized channels from stainless steel, nickel alloys and metal–polymer powders. Abele et al. [8] studied the generation of thin wall elements in stainless steel through the analysis of the influences of the SLM process parameters (laser power, scan speed, and hatch distance) on porosity. Porosity, permeability, pore size distribution, and tensile strength were also correlated. For example, Song et al. [9] investigated the W-Cu alloy thin wall components manufactured using directly the SLM process parameters. The effects of size and overlapping of melt pool on the thickness of single track wall were analyzed. Mumtaz and Hopkinson [10] analyzed the influence of laser pulse modes on width and surface quality of thin walls from Inconel 625 in the range of 400–500 μm. Stamp et al. [11] developed a scanning strategy for manufacturing porous structures in commercially pure titanium using the SLM. Zhang et al. [12] investigated the influence of scan line spacing on the SLM-made porous implants in Ti6Al4V alloy for biomedical applications.

The purpose of this study was to analyze the influence of the manufacturing strategy in the creation of stochastic and non-stochastic porous metals in AlSi10Mg and Ti6Al4V alloys by SLM. The aluminum alloy exhibits several properties such as low density, high strength-to-weight ratio and high thermal conductivity, resistance to corrosion that makes AlSi10Mg lightweight structures ideal for architectural, marine, and automotive applications. The titanium alloy due to its high corrosion resistance, very high specific strength and biocompatibility has a range of applications including customized medical implants, like lattice structures with mechanical properties optimized for compatibility with bones, and aerospace components.

2 SLM Process

The non-stochastic structures designed for automotive, aerospace and biomedical applications often contain features with dimensions of 1 mm or smaller, such as thin walls, which are often near the limit of the SLM process. The SLM process starts from the creation of a three-dimensional CAD (computer-aided design) model subsequently converted into STL format readable by AM software. In this software, the part is oriented on the building platform and support structures for overhanging surfaces are inserted to avoid cracks, warping and collapse from the part. Once the final STL file has been created, the 3D model is sliced in layers and the file is saved again in the format required by the SLM machine. The process consists on a recoating system that spreads uniformly a thin layer of metal powder over the building platform, and then the laser melts the powder following the cross section of the layer. Once the layer is solidified, the building platform is lowered and the chain is repeated until the part is finished. During the melting process the metal undergoes several cycles of rapid melting followed by fast cooling and solidification [13–18]. The change in phase of the metal from powder to liquid to solid is accompanied by shrinkage in the metal volume [19, 20]. The melt pool shape as well as the heat transfer and thermal flow are also significantly affected by local arrangement of powder particles in the powder bed which can vary from location to location due to randomness of the particles distribution. The volume shrinkage and thermal gradients together can lead to warpage and distortion which results in dimensional inaccuracies and loss of quality in the final part. As a result, thin and small features generated by SLM process often include defects such as un-melted powder inclusions, internal voids, cracks and shape irregularities [21–23]. Therefore, the factors that influence mainly the geometrical characteristics of the parts produced by SLM are: the building orientation of the part, the support structures, the properties of the powders, and the principal process parameters. To manufacture a SLM part, it is necessary to identify the correct orientation of the part on the building platform and, consequently, the correct positioning of the support structures required by process in order to fix the part to the platform, to conduct excess heat away from the part and to prevent the warping and/or collapse of the part [24]. Powder particles size, shape and distribution, and main process parameters, such as scanning strategy, laser power and speed, are also key factors for understanding quality control in SLM processes [25, 26]. Recent studies [27–29] have shown that the particle size distribution of a metallic powder has a high influence on the density, the surface quality and the mechanical properties of the samples by SLM.

2.1 SLM Scanning Strategy

Initially, all contour of the layer structure is exposed with a selected laser power and contour speed. As the diameter of the melted zone is usually larger than the laser diameter, it is necessary to compensate the dimensional error and the laser beam must be shifted by half the width from the contour to the inside, to make sure that the contour of the later part will correspond exactly to the original CAD data. This correction of the position is called Beam Offset (BO) [25]. The BO value is again defined with respect to the edge of the boundary, and if this value is higher or less than the correct value, the particles of the irradiated region may be not melted or over-melted.

Then, during hatching, the laser beam moves line after line several times to assure that the melting process can unroll completely. The distance between the lines is called hatching distance (h_d). If the h_d of the adjacent melt pools is appropriate, the manufactured parts are dense and with high precision. Instead, if the distance is too small, the melt line would be too large because too much overlap. If there is not enough h_d between the melt pools, the melt line would appear as dots. Depending on the h_d values, it is possible to obtain a controlled porosity inside the parts.

Many scanning options are provided in commercial SLM machines which include hatch pattern (or scanning strategy) in order to reduce residual stress and deformations through influencing the heat intensity input distributions [4]. Four choices for hatch pattern selection are generally available, i.e., along *x*, along *y*, both in *xy* or alternating in *xy* as shown in Fig. 1. Scanning can be done either along x or along y (Fig. 1a and b). If both in *x* and *y* options are selected than there will be double exposure on the layer, once along *x* and then along *y* (Fig. 1c). In alternating in *xy* choice, direction of scanning is changed for alternating layers (Fig. 1d). Figure 1e shows the direction of scanning rotated of 67° between consecutive layers.

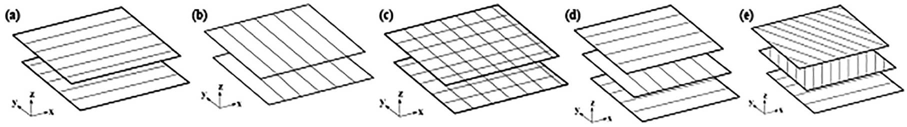

Fig. 1. Different hatch patterns or scanning strategies [30]

3 Materials and Methods

3.1 Experimental Equipment and Material

The AlSi10Mg and Ti6Al4V samples were prepared by EOSINT M270 Dual Mode (EOS GmbH) machine. A 200 W Yb (Ytterbium) fiber laser is used to melt powders in an argon atmosphere with a spot of 100 µm and a scan speed up to 5000 mm/s. To reduce thermal residual stresses between the substrate and the part, as well as in the growing part itself, the building platform was kept at 100 °C. A layer thickness of 30 µm was chosen. The gas atomized AlSi10Mg and Ti6Al4V powders have a distribution with particle sizes of 12.87 µm (d_{10}), 27.06 µm (d_{50}), 42.59 µm (d_{90}), and 22.03 µm (d_{10}), 33.35 µm (d_{50}), 47.08 µm (d_{90}) respectively.

3.2 Building of Porous Structures by SLM

Box porous samples (10 mm × 10 mm × 6 mm) were fabricated on a first dense stack of 1.5 mm height, anchored to the building platform by optimized support structures [24] in order not to damage the samples during the removal of these from the platform (Fig. 2a). Then, the thin wall structures were chosen as non-stochastic porous structures [4, 31]. They were built with two different scanning strategies: with line spacing both in x- and y-direction, also named cross-ply, and alternative scanning pattern with line spacing only in the x- or in the y-direction, from a stack of 1.5 mm height to another (Fig. 2b). Foams were chosen as stochastic structures and they were built adopting a rotated scanning strategy, with an angle of 67° with respect to the previous layer (Fig. 1c). The porosity patterns were investigated by taking micrographs of cross sections of the samples by Optical Microscopy (OM - Leica DMI 5000M). The samples were prepared for observation by grinding surface up to 4000 SiC papers. A magnification of 8× and 10× were chosen and 2 images (side and top views) were taken per sample. The thin-walled structures were formed with the choice of the process parameters to obtain a part with the highest density: a laser power of 195 W and a scanning speed of 800 mm/s for AlSi10Mg alloy [24]; while in Ti6Al4V alloy with a laser power of 170 W and a scanning speed of 1250 mm/s. Four different values of hatching distance were chosen for both materials: 0.20 mm, 0.30 mm, 0.40 mm and 0.50 mm.

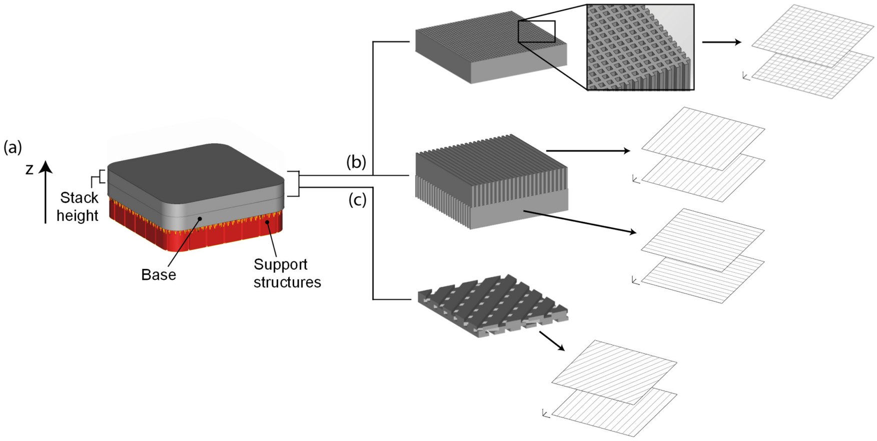

Fig. 2. Schematic representation of the manufacturing porous structures: (a) stl file; (b) non-stochastic porous structures; (c) foams.

4 Results and Discussion

4.1 Non-stochastic Porous Structures

Table 1 shows the results obtained for the as-manufactured thin walls structures. Figure 3 shows the samples built with different scanning strategies to obtain non-stochastic porous structures and foams in aluminum and titanium alloys. In the case of the aluminum samples, a h_d of 0.20 mm does not allow to create defined thin walls but only small scattered porosities. This is mainly due to the size distribution of the starting powders. AlSi10Mg powder, compared to that of Ti6Al4V, has many small particles (<12 μm) that tend to agglomerate on the surface of the bigger ones (d_{90}), creating some clusters of greater than 60 µm. For this reason, it is necessary to consider h_d greater than 0.20 mm. Increasing hatching distance from 0.20 mm to 0.30 mm, the pores grow by creating well-defined walls and therefore well-defined periodic structures. Increasing hatching distance to 0.40 mm leads to the formation of more open channels in which the presence of un-fused particles is reduced (Fig. 4).

Table 1. As-manufactured thin wall structures in AlSi10Mg and Ti6Al4V

Sample	h_d [mm]	Orient.	$\text{Gap}_{\text{width}}$ [mm]	St. dev. [mm]	$\text{Wall}_{\text{width}}$ [mm]	St. dev. [mm]
1_{AlSiMg}	0.20	*x*	0	-	-	-
2_{AlSiMg}	0.20	*y*	0	-	-	-
3_{AlSiMg}	0.30	*x*	0.090	±0.011	0.222	±0.019
4_{AlSiMg}	0.30	*y*	0.095	±0.009	0.219	±0.013
5_{AlSiMg}	0.40	*x*	0.193	±0.014	0.229	±0.018
6_{AlSiMg}	0.40	*y*	0.207	±0.017	0.218	±0.015
7_{AlSiMg}	0.50	*x*	0.360	±0.018	0.150	±0.016
8_{AlSiMg}	0.50	*y*	0.372	±0.022	0.173	±0.025
1_{Ti64}	0.20	*x*	0.086	±0.010	0.130	±0.017
2_{Ti64}	0.20	*y*	0.086	±0.006	0.147	±0.016
3_{Ti64}	0.30	*x*	0.148	±0.017	0.158	±0.014
4_{Ti64}	0.30	*y*	0.150	±0.011	0.150	±0.019
5_{Ti64}	0.40	*x*	0.243	±0.016	0.151	±0.017
6_{Ti64}	0.40	*y*	0.259	±0.027	0.140	±0.015
7_{Ti64}	0.50	*x*	0.355	±0.020	0.139	±0.017
8_{Ti64}	0.50	*y*	0.360	±0.038	0.161	±0.034

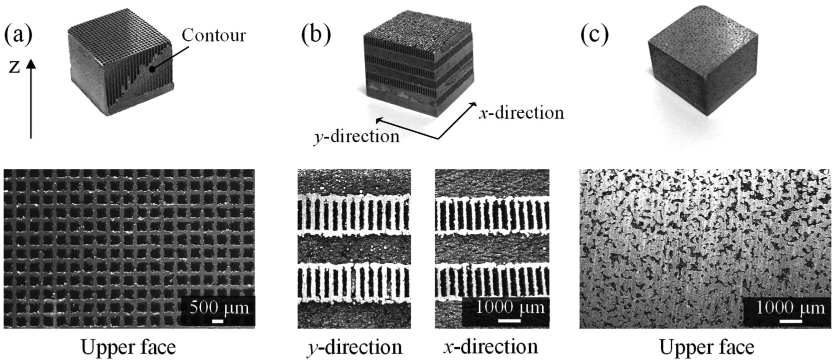

Fig. 3. As built and optical images for AlSi10Mg samples: (a) *x*- and *y*-directions; (b) alternative scanning pattern; (c) rotation of 67°.

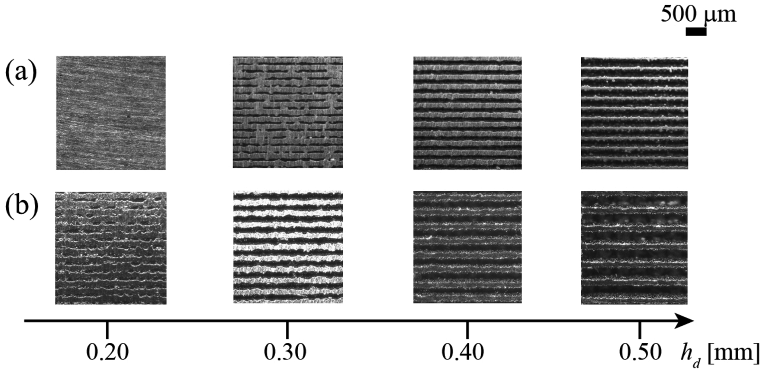

Fig. 4. (a) Optical images of tracks (top view) with various hatching distance: (a) AlSi10Mg and (b) Ti6Al4V samples

If the channel has a size equal to or less than the size of the biggest particles that adhere on the borders, it can be blocked by the powders.

Both materials exhibit dimensional differences of the width of the wall based on the orientation of the walls during the construction. During the formation of the powder layer, some factors contribute to create considerable frictional forces between the blade and the previously melted layer that can cause geometric variations. Among these factors, there is the surface roughness of the previously layer, comparable to the layer thickness, which causes an interference between it and the blade. In addition, the recoating blade pushes a quantity of powder which can cause dynamic pressures against the leading edge of the part being developed. High aspect ratio (tall or wide compared to thickness) wall-like features are particularly vulnerable to these interferences which can also damage the part. For this reason, generally, a part should be oriented so there is not a long line of parallel contact between the part and recoating blade.

The analysis of the structures has confirmed that, irrespective of the material used, the width of the walls depends not only of the laser spot size but also of the process parameters used.

4.2 Foams

Figure 5 shows a foam obtained using the rotated scanning strategy and a hatching distance of 0.50 mm in Al and Ti alloys. By OM image analysis, it was measured a mean porosity value of 43% for AlSi10Mg and 45% for Ti6Al4V foams. The samples have closed pores and two types of open pores, blind and through pores, which have a connection to the surface (Fig. 5c). With lower values of hatching of 0.20 mm and 0.40 mm, foam structures could not be obtained: they were more like dense samples with no interconnected porosity. In all the samples, it was noticed a correct transition from the solid base to the porous structures of the stacks.

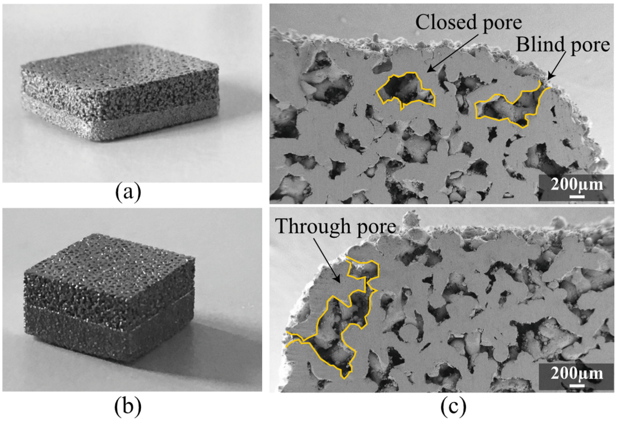

Fig. 5. Foams built by SLM in (a) AlSi10Mg alloy and (b) Ti6Al4V alloy with h_d of 0.50 mm; (c) type of pores.

5 Conclusion

In this study different strategies of manufacturing non-stochastic structures and foams in aluminum and titanium alloys by SLM were analyzed. The results showed that it is possible to obtain porous structure with regular pores that can be tailored by adjusting the hatching distance.

The powder size influences the obstruction of the channels and the size of the walls. From the information that can be obtained by building a well-defined wall using the manufacturing strategy, it's possible to derive a real value of the minimum features, such as thin wall, for certain materials and use it in CAD modeling.

Porous structures have been built on dense bases. This demonstrates the advantage introduced by the AM technologies to minimize the number of components allowing to build structures that possess simultaneously high density zones, necessary to sustain structural loads, and areas with gradual and controlled porosity suitable for other properties, e.g. filters media.

References

1. Hasib, H., Rennie, A., Burns, N., Geekie, L.: Non-stochastic lattice structures for novel filter applications fabricated via additive manufacturing. In: The Filtration Society 50th Anniversary International Conference and Exhibition: Proceedings of the Filtration Society, Filtration Society 50th Anniversary Conference, Chester, United Kingdom, 13–14 November (2014)
2. Tsinoglou, D.N., Eggenschwiler, P.D., Thurnheer, T., Hofer, P.: A simplified model for natural-gas vehicle catalysts with honeycomb and foam substrates. Proc. Inst. Mech. Eng. Part D: J. Automob. Eng. **223**(6), 819–834 (2009)
3. Heikkinen, M.S.A., Harley, N.H.: Experimental investigation of sintered porous metal filters. J. Aerosol Sci. **31**(6), 721–738 (2000)

4. Yadroitsev, I., Shishkovsky, I., Bertrand, P., Smurov, I.: Manufacturing of fine-structured 3D porous filter elements by selective laser melting. Appl. Surf. Sci. **255**, 5523–5527 (2009)
5. Burns, N.R.: Why AM now has the potential to revolutionise filtration solutions. Filtr. + Sep. **51**(2), 42–43 (2014)
6. Vijayakumar, B., Rennie, A., Burns, N., Battersby, P., Burns, M.: Introducing functionality to the filter media. In: Filter Media 6, International Conference and Exhibition. The Filtration Society, Chester, UK (2013)
7. Hasib, H.: Mechanical behavior of non-stochastic Ti-6Al-4V cellular structures produced via electron beam melting (EBM), Master's thesis, North Carolina State University, USA (2011)
8. Abele, E., Stoffregen, H.A., Kniepkamp, M., Lang, S., Hampe, M.: Selective laser melting for manufacturing of thin-walled porous elements. J. Mater. Process. Technol. **215**, 114–122 (2015)
9. Song, C., Yang, Y., Liu, Y., Luo, Z., Yu, J.K.: Study on manufacturing of W-Cu alloy thin wall parts by selective laser melting. Int. J. Adv. Manuf. Technol. **78**, 885–893 (2015)
10. Mumtaz, K.A., Hopkinson, N.: Selective laser melting of thin wall parts using pulse shaping. J. Mater. Process. Technol. **210**, 279–287 (2010)
11. Stamp, R., Fox, P., O'Neill, W., Jones, E., Sutcliffe, C.: The development of a scanning strategy for the manufacture of porous biomaterials by selective laser melting. J. Mater. Sci. Mater. Med. **20**, 1839–1848 (2009)
12. Zhang, S., Wei, Q., Cheng, L., Li, S., Shi, Y.: Effects of scan line spacing on pore characteristics and mechanical properties of porous Ti6Al4V implants fabricated by selective laser melting. Mater. Des. **63**, 185–193 (2014)
13. Song, Y.A., Koenig, W.: Experimental study of the basic process mechanism for direct selective laser sintering of low-melting metallic powder. In: 47th General Assembly of CIRP (1997). Manuf. Technol. **46**(1), 127–130
14. Das, S., Beaman, J.J., Wohlert, M., Bourell, D.L.: Direct laser freeform fabrication of high performance metal components. Rapid Prototyp. J. **4**(3), 112–117 (1998)
15. Simchi, A.: Direct laser sintering of metal powders: mechanism, kinetics and microstructural features. Mater. Sci. Eng. A-Struct. Mater. Prop. Microstruct. Process. **428**(1–2), 148–158 (2006)
16. Agarwala, M., Bourell, D., Beaman, J., Marcus, H., Barlow, J.: Direct selective laser sintering of metals. Rapid Prototyp. J. **1**(1), 26–36 (1995)
17. Wang, X.C., Laoui, T., Bonse, J., Kruth, J.P., Lauwers, B., Froyen, L.: Direct selective laser sintering of hard metal powders: experimental study and simulation. Int. J. Adv. Manuf. Technol. **19**(5), 351–357 (2002)
18. Manfredi, D., Calignano, F., Krishnan, M., Canali, R., Ambrosio, E.P., Atzeni, E.: From powders to dense metal parts: characterization of a commercial AlSiMg alloy processed through direct metal laser sintering. Materials **6**, 856–869 (2013)
19. Ning, Y., Wong, Y.S., Fuh, J.Y.H., Loh, H.T.: An approach to minimize build errors in direct metal laser sintering. IEEE Trans. Autom. Sci. Eng. **3**(1), 73–80 (2006)
20. Ning, Y., Wong, Y.S., Fuh, J.Y.H.: Effect and control of hatch length on material properties in the direct metal laser sintering process. Proc. Inst. Mech. Eng. Part B-J. Eng. Manuf. **219** (1), 15–25 (2005)
21. Yang, L.: Structural design, optimization and application of 3D re-entrant auxetic structures. Ph.D. dissertation. North Carolina State University. Raleigh, NC, USA (2011)
22. Gumruk, R., Mines, R.A.W.: Compressive behaviour of stainless steel micro-lattice structures. Int. J. Mech. Sci. **68**, 125–139 (2013)
23. Yan, C., Hao, L., Hussein, A., Raymont, D.: Evaluations of cellular lattice structures manufactured using selective laser melting. Int. J. Mach. Tools Manuf **62**, 32–38 (2012)

24. Calignano, F.: Design optimization of supports for overhanging structures in aluminum and titanium alloys by selective laser melting. Mater. Des. **64**, 203–213 (2014)
25. Calignano, F., Manfredi, D., Ambrosio, E.P., Iuliano, L., Fino, P.: Influence of process parameters on surface roughness of aluminum parts produced by DMLS. Int. J. Adv. Manuf. Technol. **67**, 2743–2751 (2013)
26. Ventola, L., Robotti, F., Dialameh, M., Calignano, F., Manfredi, D., Chiavazzo, E., Asinari, P.: Rough surfaces with enhanced heat transfer for electronics cooling by direct metal laser sintering. Int. J. Heat Mass Transf. **75**, 58–74 (2014)
27. Spierings, A.B., Levy, G.: Comparison of density of stainless steel 316L parts produced with selective laser melting using different powder grades. In: Proceedings of the Annual International Solid Freeform Fabrication Symposium, Austin, Texas, pp. 342–353 (2009)
28. Spierings, A., Herres, N., Levy, G.: Influence of the particle size distribution on surface quality and mechanical properties in am steel parts. Rapid Prototyp. J. **17**(3), 195–202 (2011)
29. Lee, Y.S., Zhang, W.: Mesoscopic simulation of heat transfer and fluid flow in laser powder bed additive manufacturing. In: Annual International Solid Freeform Fabrication Symposium, Austin, TX, pp. 1154–1165, August 2015
30. Manfredi, D., Calignano, F., Krishnan, M., Canali, R., Ambrosio, E.P., Biamino, S., Ugues, D., Pavese, M., Fino, P.: Additive manufacturing of Al alloys and Aluminium Matrix Composites (AMCs). In: Monteiro, W.A. (ed.) Light Metal Alloys Applications (2014). ISBN 978-953-51-1588-5
31. Klahn, C., Meboldt, M.: Integration of gas-permeable structures in laser additive manufactured products. In: Additive Manufacturing: Innovations, Advances, and Applications. Taylor & Francis Group (2016)

Development and Optimization of an Innovative Double Chamber Nozzle for Highly Efficient DMD

Andrea Marchetti(✉), Federico Mazzucato(✉), and Anna Valente(✉)

SUPSI – University of Applied Science and Arts of Southern Switzerland,
6928 Manno, Switzerland
`{andrea.marchetti,federico.mazzucato,`
`anna.valente}@supsi.ch`

Abstract. Injection nozzles design in Direct Metal Deposition (DMD) critically affects the performances of the process in terms of powder deposition efficiency. In fact, the fluid-dynamic behavior of the powder particles falling into the molten pool strongly depends both on the internal geometry of the deposition nozzle and on the geometry of the nozzle outlet. This efficiency, for commercial nozzles, is usually under 50%, thus implying an unaffordable powder waste. SUPSI implemented an innovative nozzle concept, designed as a coaxial double chamber that enables the concurrent flow of the powder-carrier gas mixture and of the shielding gas. In this configuration, the shielding gas allows to reduce the spread of the blown powder particles, constraining the carrier gas flow and limiting its divergence. Such innovative design also enables the integration of various modules - different in shape - to be nested to the bottom end of the nozzle, in order to adapt its outlet geometry. The main objective of the design is to influence the shape of the powder flux ejected from the nozzle outlet by exploiting the shielding gas while limiting oxidation processes. In order to assess the influence of the feeding parameters on the flow geometry, different concepts and shapes of nozzle outlet have been tested and investigated against the deposition efficiency, both numerically and experimentally. The testing campaign relies upon an image analysis performed on a demonstration setup where the powder flux is tracked using a high-speed camera. Experimental results demonstrate improved deposition efficiency through a significant (up to 18%) spread reduction.

Keywords: Direct Metal Deposition · Nozzle design powder · Deposition efficiency

1 Introduction

Metal Additive Manufacturing (AM) technologies have been deeply studied in the last few years, since the need of sustainable processes has been increasing more and more. In metals AM processing, Direct Metal Deposition (DMD) is widely adopted to manufacture big and complex shaped parts for various sectors, such as aerospace and automotive [1, 3]. This process is obtained by melting the powders ejected from one or

© Springer International Publishing AG 2018
M. Meboldt and C. Klahn (eds.), *Industrializing Additive Manufacturing - Proceedings of Additive Manufacturing in Products and Applications - AMPA2017*,
DOI 10.1007/978-3-319-66866-6_19

more nozzles through a high-energy source, e.g. a laser, which allows generating a high temperature area, i.e. the molten pool, either on the substrate or on a previously deposited layer [2]. Once the molten material cools down by heat dissipation, a continuous metallurgical bond is created, thus forming a new solid layer.

The deposition efficiency, defined as the ratio between the amount of powder directly involved in the component manufacture and the nominal metal powders feed rate, is drastically affected by the solution adopted for the ejecting nozzle.

Commercial nozzles, frequently constituted by axis-symmetric or lateral configurations, exhibit unaffordable deposition efficiency (under 50%) and consequently unreasonable powder waste and high production costs [4, 5]. In such nozzles, the shielding is adopted only for preventing oxidation and not for limiting the powder spread.

In the last years, several authors investigated the fluid-dynamic behaviour of nozzles depending on their geometry. For example, authors like Lin in 1999, Zekovic in 2007, Yang in 2009 and Liu in 2015 [6–9] tried to evaluate the nozzle geometry, proposing different numerical models, with the objective to reduce the powder dispersion during the deposition.

An innovative double chamber nozzle solution, realized by SUPSI [8], is capable of exploiting the shielding gas not only to avoid oxidation, but also as a constrainer for the carrier flow, thus reducing the powder dispersion. For this purpose, the nozzle is conceived with two coaxial chambers (Fig. 1a), where the outer one enables the flow of the shielding gas, which is exploited to control the profile of the particles' flow. The developed nozzle is designed also as a modular solution: different outlets can be nested on the main body. In this way, based on the specific process requirements, the nozzle can rely upon the optimal outlet geometry. In this paper, different outlet geometries, mountable on the aforementioned nozzle, have been tested in order to optimize the powder behaviour. The analysis and assessment of the geometries have been performed firstly at simulation level through CFD analysis; successively, the physical nozzle prototypes have been tested while operating in a desktop demo application.

The rest of the paper is structured as it follows: Sect. 2 describes the investigated geometries, the adopted equipment and the relative experimental methodologies; Sect. 3 outlines the CFD model assumptions; Sect. 4 summarizes the obtained results; Sect. 5 presents conclusions and future work.

2 Experimental Campaign

2.1 Evaluated Geometries and Experimental Apparatus

The optimization of the outlet geometry has been carried out for the nozzle shown in Fig. 1a. The shielding nozzle outlet, depicted in white, can be nested on the rest of the nozzle body, creating a duct through which the gas can flow. In order to understand the dependency of the powder behavior with respect to a certain shape of the nozzle, three different versions, characterized respectively by a slicing angle of 0, 15 and 30°, have been considered (Fig. 1b). For the sake of demonstration, the three different geometries

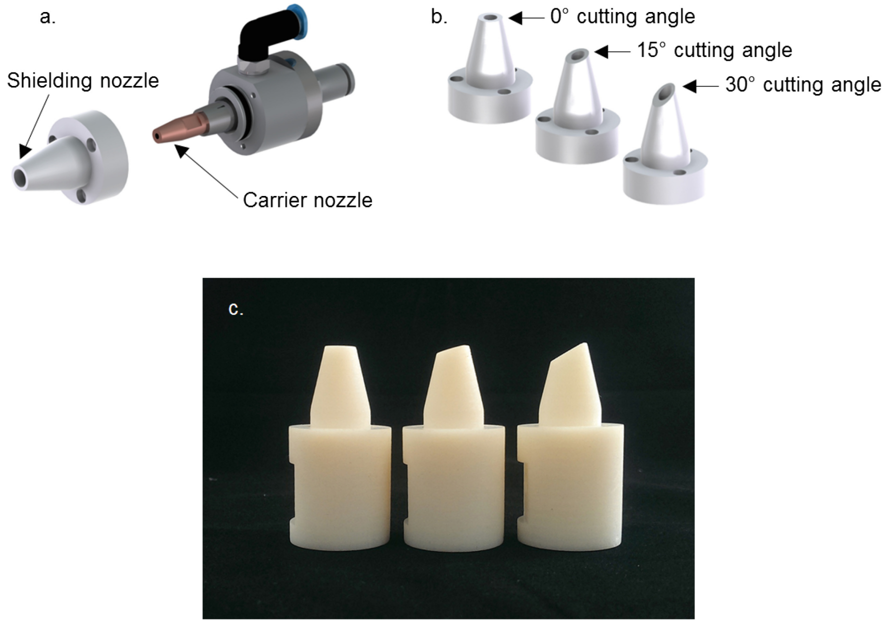

Fig. 1. a. Up-Left: SUPSI modular nozzle b. Up-Right: evaluated geometries. c. Below: printed geometries.

of the complete nozzle (body + modular outlet) have been reproduced in acrylic resin using PolyJet technology, in order to obtain the established cutting angles for both shielding and carrier nozzles (Fig. 1c).

The demonstration setup has been conceived to allow the testing of multiple nozzles. It is constituted by a hermetic box with transparent walls and an internal structure where the nozzles can be positioned and manually adjusted with regard to deposition distance, deposition angle and reciprocal distance. Outside the demonstration setup, a high-speed camera (Emergent HR-4000 CMOS camera) has been positioned with the purpose of monitoring the process flow (Fig. 2). The powders are released through a screw system and transported with Argon gas inside the chamber.

2.2 Experimental Procedure

In order to assess the proposed nozzle efficiency with respect to commercial solutions, some tests at different levels of shielding (0–1.95e−4 kg/s) have been performed on the same initial geometry. The enhancement of the outlet geometry has been studied by relying upon several experiments, performed by maintaining the same fluid-dynamics parameters. Both cases with one and two nozzles were considered for the experimental campaign, aiming at understanding the mutual interaction between fluxes. The demonstration refers to Ti-6Al-4V alloy powder, as demanded by several industrial scenarios that the authors are considering in the aerospace sector [1]. Table 1 resumes the parameters adopted during the experimental campaign.

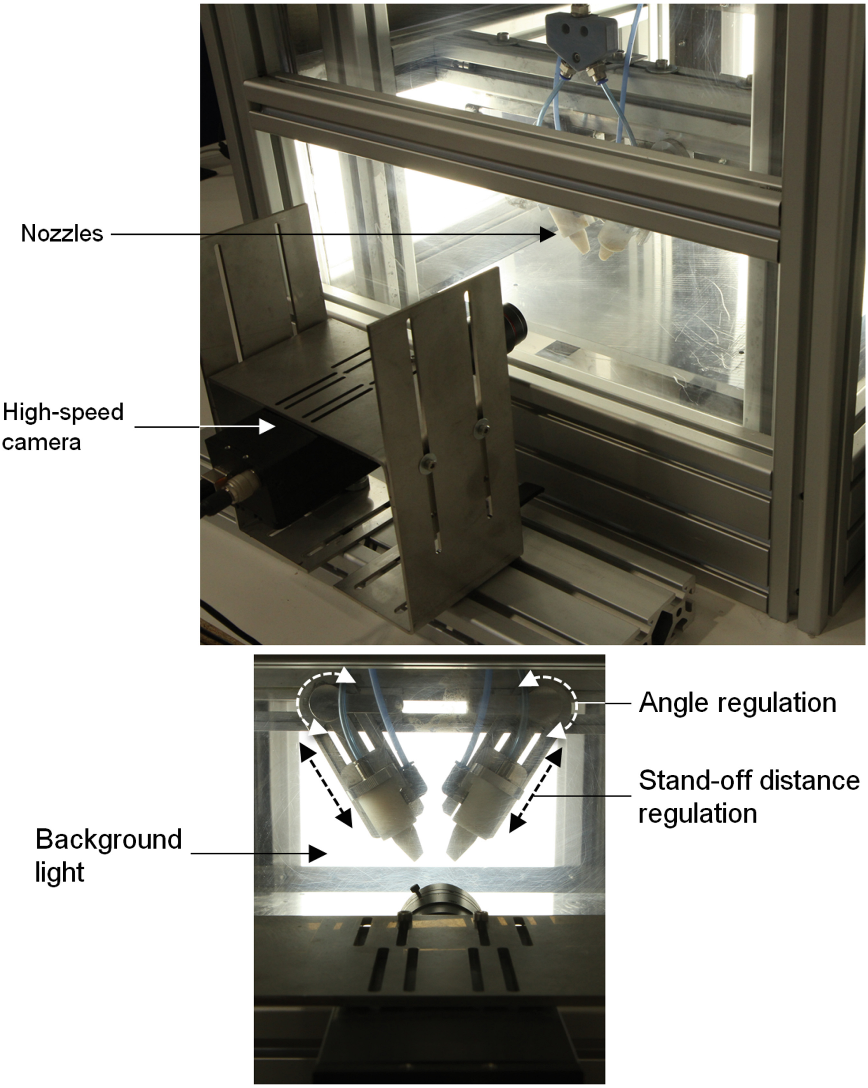
Nozzles
High-speed camera
Angle regulation
Stand-off distance regulation
Background light

Fig. 2. Experimental setup picture.

Table 1. Experimental campaign parameters.

Fluid-dynamics parameters	Outlet angle	Nozzles number
Powder mass flow: 0.1 g/s Carrier gas mass flow: 4.51e−5 kg/s Shielding gas mass flow: 0 kg/s	0°	1/2
Powder mass flow: 0.1 g/s Carrier gas mass flow: 4.51e−5 kg/s Shielding gas mass flow: 1.95e−4 kg/s	0°	1/2
	15°	1/2
	30°	1/2

The nozzles, in order to replicate a usual setup in DMD applications, were mounted at 30° with respect to the vertical direction. In the 2 nozzles analysis, the distance between the intersection point of the two nozzles and the outlet point is fixed at 15 mm, equal to the distance of a hypothetical deposition plane (Fig. 3). The nozzle internal section is not shown, since the geometry is still patent pending [10].

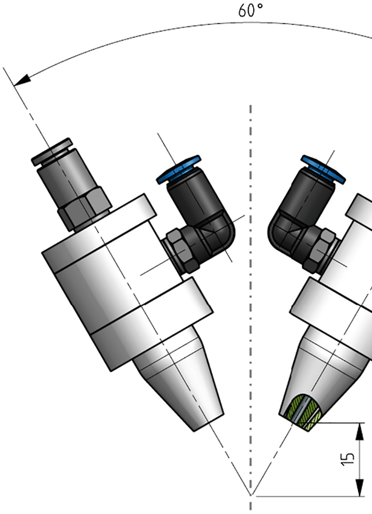

Fig. 3. Disposition of the nozzles for numerical simulations and experimental analysis.

3 Simulations and Numerical Analysis

For the sake of numerical simulation, the nozzle is synthetized by modelling a two-phase flow for the carrier gas and a single continuous phase for the shielding one. The two phases of the carrier flow are composed by the Argon gas, as continuous primary phase, and by the Ti-6Al-4V alloy particles, as the discrete secondary one.

The model has been solved through Ansys Fluent software, considering the Eulerian-Lagrangian approach [7, 11–15]. Carrier and Shielding gas flows were modelled as continuous-phase, applying the standard κ-ε turbulent flow model for Navier-Stokes equations, available in Ansys Fluent. The discrete phase representing the powder particles was computed integrating the differential equation of particle force balance in a Lagrangian coordinate system, considering only drag, inertia and gravity forces. Collisions among particles, which are considered negligible for what concerns their influence on the gas, are not computed during simulations.

Considering two nozzles, a symmetry condition is applied in the vertical plane with respect to the intersection point between nozzles, as represented in Fig. 3. In order to accomplish the geometry variation, a slight modification in the nozzle-domain junction is necessary (Fig. 4). Table 2 synthesizes the boundary conditions adopted for the continuous phase calculation, while Table 3 lists the properties related to the discrete phase.

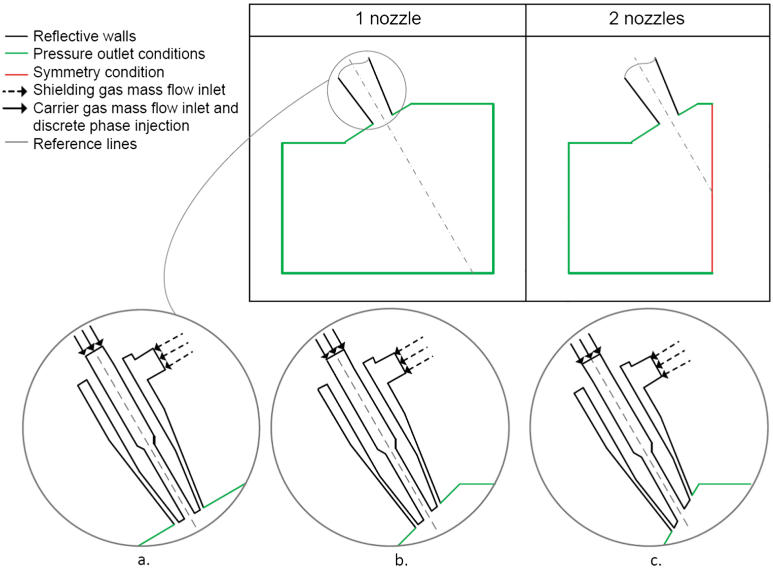
Reflective walls
Pressure outlet conditions
Symmetry condition
Shielding gas mass flow inlet
Carrier gas mass flow inlet and discrete phase injection
Reference lines
1 nozzle
2 nozzles
a.
b.
c.

Fig. 4. Boundary conditions of the CFD model and domain adaption for a. (0°), b. (15°) and c. (30°) geometry.

Table 2. Continuous phase boundary conditions.

Boundary	Value [Unit]	Description
Pressure outlet	0 [Pa]	Ambient pressure in the environment
Carrier gas mass flow inlet	4.51e−05 [kg/s]	Argon gas flowing in the carrier nozzle
Shielding gas mass flow inlet	1.95e−04 [kg/s]	Argon gas flowing in the shielding nozzle

Table 3. Discrete phase properties.

Properties	Value [Unit]	Description
Diameter	70 [µm]	Particle diameter, considering uniform distribution
Velocity magnitude	3.937 [m/s]	Particles injection velocity magnitude
Total flow rate	1e−04 [kg/s]	Particles total mass flow

4 Results and Discussion

4.1 Image Elaboration Methodology

The method employed to characterize the powder flow shape and profile from the experimental data acquired by the high-speed camera is based on process image analysis. The open source software employed for this scope is ImageJ [16]. For each different parameter values combination, 10 images of the powder flow are averaged, and the resulting image is subtracted from the image with no powder flow. In this way, the contours of the powder flow can be better separated from background noise and from the dispersed particles (Fig. 5a). The residual noise remaining in the resulting images can be reduced by applying a band-pass filter for low wavelengths (Fig. 5b). At this stage, an intensity threshold is defined to clearly identify the powder flow from the background. Successively, a binary mask based on this threshold value is applied (Fig. 5c). To characterize the entire profile of the powder flux, 10 lines are drawn along the flow extension with a distance of 1.5 mm from each other. In this way, the last line is located at 15 mm from the nozzle outlet (Fig. 5d). At this distance, similar to the deposition plane location with respect to the nozzle outlet, the width measurement is performed.

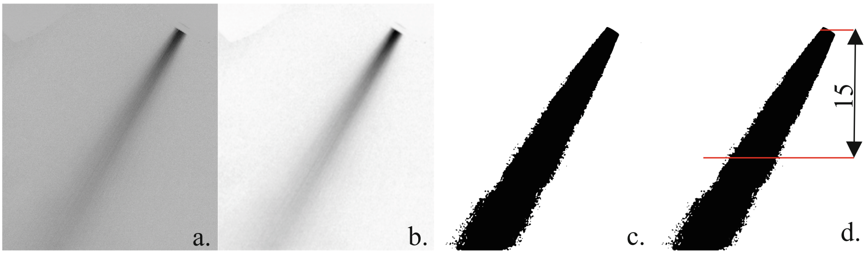

Fig. 5. From left: a. Flux after subtraction b. Flux after band-pass filter c. Flux after binary mask application d. Evaluation line at 15 mm from the outlet.

4.2 Experimental Results

Preliminary experimental results shows how the external shielding gas can reduce the powder spread at the nozzle outlet. For a given value of 1.95e−4 kg/s per nozzle, the powder cross sectional area is reduced from 5.01 mm to 4.37 mm for the one nozzle case and from 5.79 mm to 5.17 mm for the 2 nozzles case, thus targeting an average reduction of 12% (Table 4). Considering the different nozzle geometries, we can see how increasing the slicing angle to 15° provides a significant reduction of the flow width (−5.75% in average) respect to the original geometry with shielding gas, while the results for the 30° geometry are worst with respect to the shielded 0° geometry (+2% deviation in average). For the given shielding velocity, a 30° cut risks to cause turbulence and consequently to increase the dispersion. Values obtained considering only one nozzle are generally lower; nevertheless, considering two nozzles the increment is around 0.8 mm, for all the cases.

Table 4. Preliminary results.

	No shielding		Shielding: 1.95e−4 kg/s					
	0° slice				15° slice		30° slice	
	95% width [mm]	**Variation [%]**	95% width [mm]	Variation [%]	95% width [mm]	Variation [%]	95% width [mm]	Variation [%]
1 nozzle	**5.01**	–	4.37	−13%	4.12	−18%	4.44	−11.5%
2 nozzles	**5.79**	–	5.17	−11%	4.89	−15.5%	5.31	−8.5%

Numerical values computed through Ansys Fluent simulations, with the methods described in Sect. 3, are close but not equal to the experimental ones (average difference 2 mm) with respect to absolute values. For this reason, additional analysis exploiting different methods should be performed in order to obtain a robust numerical model. Since the geometry results are affected by fluid dynamics parameters, further analysis combining the geometry and fluid dynamics parameters can better discriminate the respective influence on the results.

5 Conclusions

In this paper, a new double chamber nozzle solution for DMD is introduced and its performances analysed. Different outlet geometries were exploited in order to further optimize the nozzle behaviour in terms of powder deposition efficiency. The influence of the outlet geometry on the powder flow spread was analysed taking into account the variation of the powder flow at 15 mm from the nozzle outlet. A positive effect in terms of powder distribution, and consequently on powder efficiency, is obtained by the employing an inclined nozzle outlet, which ensures a reduction of the powder spread (up to 18%) while maintaining the same process parameters.

Future works will focus on more efficient experimental validation techniques that do not rely purely upon CFD analysis, in terms of powder spread values. Particularly, an experimental plan with combined fluid-dynamic and geometric parameters will be designed in order to fully understand the parameters mutual influences.

Acknowledgements. The research has been partially funded by European H2020 Borealis Project (Grant agreement no: 636992).

References

1. Borealis project. http://www.borealisproject.eu/project/
2. Thompson, S.M., Bian, L., Shamsaei, N., Yadollahi, A.: An overview of direct laser deposition for additive manufacturing; part I: transport phenomena, modeling and diagnostics. Add. Manuf. **8**, 36–62 (2015). doi:10.1016/j.addma.2015.07.001
3. Shamsaei, N., Yadollahi, A., Bian, L., Thompson, S.M.: An overview of direct laser deposition for additive manufacturing; part II: mechanical behaviour, process parameter optimization and control. Add. Manuf. **8**, 12–35 (2015). doi:10.1016/j.addma.2015.07.002
4. Huang, Y., Khamesee, M.B., Toyserkani, E.: A comprehensive analytical model for laser powder-fed additive manufacturing. Add. Manuf. **12**, 90–99 (2016). doi:10.1016/j.addma.2016.07.001
5. Pinkerton, A.J.: Advances in the modelling of laser direct metal deposition. J. Laser Appl. **27**, S15001 (2005). doi:10.2351/1.4815992
6. Lin, J.: A simple model of powder catchment in coaxial laser cladding. Opt. Laser Technol. **31**, 233–238 (1999)
7. Zekovic, S., Dwivedi, R., Kovacevic, R.: Numerical simulation and experimental investigation of gas-powder flow from radially symmetrical nozzles in laser-based direct metal deposition. J. Mach. Tools Manuf. **47**, 112–123 (2007). doi:10.1016/j.ijmachtools.2006.02.004

8. Yang, N.: Concentration model based on movement model of powder flow in coaxial laser cladding. Opt. Laser Technol. **41**, 94–98 (2009). doi:10.1016/j.optlastec.2008.03.008
9. Liu, S., Zhang, Y., Kovacevic, R.: Numerical simulation and experimental study of powder flow distribution in high power direct diode laser cladding process. Lasers Manuf. Mater. Process. **2**, 199–218 (2015). doi:10.1007/s40516-015-0015-2
10. Brugnetti, I., Colla, M., Marchetti, A., Valente, A.: Nozzle Apparatus for Direct Energy Deposition. Patent Pending. App. Number EP16201499 (2016)
11. Balu, P., Leggett, P., Kovacevic, R.: Parametric study on a coaxial multi-material powder flow in laser-based powder deposition process. J. Mater. Process. Technol. **212**, 1598–1610 (2012). doi:10.1016/j.jmatprotec.2012.02.020
12. Zhu, G., Li, D., Zhang, A., Tang, Y.: Numerical simulation of metallic powder flow in a coaxial nozzle in laser direct metal deposition. J. Opt. Laser Technol. **43**, 106–113 (2011). doi:10.1016/j.optlastec.2010.05.012
13. Zhang, B., Coddet, C.: Numerical study on the effect of pressure and nozzle dimension on particle distribution and velocity in laser cladding under vacuum base on CFD. J. Manuf. Process. **23**, 54–60 (2016). doi:10.1016/j.jmapro.2016.05.019
14. Tabernero, I., Lamikiz, A., Ukar, E., de Lacalle, L.N.L., Angulo, C., Urbikain, G.: Numerical simulation and experimental validation of powder flux distribution in coaxial laser cladding. J. Mater. Process. Technol. **210**, 2125–2134 (2010). doi:10.1016/j.jmatprotec.2010.07.036
15. Wen, S.Y., Shin, Y.C., Murthy, J.Y., Sojka, P.E.: Modelling of coaxial powder flow for the laser direct deposition process. Int. J. Heat Mass Transfer **52**, 5867–5877 (2009). doi:10.1016/j.ijheatmasstransfer.2009.07.018
16. ImageJ, Image Processing and Analysis in Java. https://imagej.nih.gov/ij/

In Situ and Real-Time Monitoring of Powder-Bed AM by Combining Acoustic Emission and Artificial Intelligence

K. Wasmer(✉), C. Kenel, C. Leinenbach, and S.A. Shevchik

Laboratory for Advanced Materials Processing,
Empa – Swiss Federal Laboratories for Materials Science and Technology,
Thun, Switzerland
`kilian.wasmer@empa.ch`

Abstract. At present, the quality control in additive manufacturing is diligently based on temperature of the process zone or high resolution imaging. Hence, various sensors such as pyrometers, photo diodes and matrix CCD detectors are used. The discrepancies in temperature measurements and the real temperature distribution inside the powder medium reduce the reliability of this method. The high resolution imaging monitors the quality *post factum*, after a part is manufactured. So far, no methods are known to monitor the quality of additive manufacturing *in situ* and in real-time. To achieve the goal of accurate real-time quality control, we propose an approach that relies on acoustic emission, which is further analyzed within artificial intelligence framework. We show that the additive manufacturing process has a number of unique acoustic signatures that can be detected, extracted and interpreted in terms of quality.

In this contribution, the processing parameters for the selective laser melting of a 316L steel were modified to create a specimen consisting of sections with three quality levels. During the process, the acoustic emission data were acquired and then processed prior validation. The confidence level achieved in the classification is 79–84% that demonstrates the applicability of this approach for *in situ* and real-time quality monitoring in additive manufacturing. Finally, the proposed method is very flexible in terms of realization and can be integrated in any additive manufacturing machine.

Keywords: Additive manufacturing · Quality control · Acoustic emission · Fiber optical sensors · Artificial intelligence

1 Introduction

In recent years, additive manufacturing (AM) has attracted considerable attention from the industrial world [1, 2]. The main reason is that unlike conventional material removal methods, AM is based on additive material method [3]. This manufacturing strategy has placed AM as one of the most promising future technologies [4] and is recognized, today and by many, as the next industrial revolution [5]. The main reason for this is that AM reduces the geometrical constraints of the parts as compared to conventional manufacturing [5, 6].

© Springer International Publishing AG 2018
M. Meboldt and C. Klahn (eds.), *Industrializing Additive Manufacturing - Proceedings of Additive Manufacturing in Products and Applications - AMPA2017*,
DOI 10.1007/978-3-319-66866-6_20

Several AM technologies exist such as Laser Cusing, Direct Metal Laser Melting, Laser Metal Fusing or Selective Laser Melting (SLM) [7]. In this work, we focused on SLM technology, which is a powder bed AM technology allowing building highly complex 3D geometries layer by layer parts from an alloy powder. This technology has been successfully applied for fast prototyping of unique workpieces and for production of small series of individualized products [7, 8].

Unfortunately, the high expectations are not completely fulfilled as AM is not matured enough. The reason is in the high sensitivity of the AM process to different factors, such as laser parameters, laser optics, mechanical and optical material properties, particles configuration of the powder in the melt zone, etc. [9–11]. Hence, any small changes can have a direct impact on the part quality in terms of pronounced porosity, cracking and accumulation of residual stress inside a part [12]. Under such circumstances, it is obvious that the repeatability of AM processes are limited, preventing the technology from being used in a much wider range. A probable way out of this situation is the development of *in situ* and real-time quality monitoring and control of the part quality [12]. The challenges in such a development are in the complex underlying physics that require interdisciplinary investigations in materials, laser-matter interactions, optical properties of powders and heat propagation [6]. The lack of this knowledge prevents the design of quality monitoring systems [9–12].

At present, the two most common approach for quality monitoring is based on temperature measurements of the process zone and this information is used to keep the melt pool stable [12–14]. The other methodology is based on the image processing of the surface of the manufactured layer [12, 13, 15–18]. Both approaches have drawbacks. The temperature measurements are taken from the surface and no precise estimation of its propagation in depth exists so that the inaccuracies lead to uncontrollable formation of defects. The image processing is a *post mortem* analysis that is carried out after the workpiece is manufactured and no quality improvements are possible [12, 13, 15–18]. Hence, there is a consensus among scientists and industries that there is a lack in reproducibility when producing a workpiece in mass production [1, 3, 12–18].

In recent years, acoustic emission (AE) has been involved for quality monitoring of some industrial processes [19, 20]. Its advantages are in the fast data acquisition and processing since it is represented by 1D sequences, whereas imaging is 2D. Additionally, cutting edge AE sensors, in particular fiber Bragg grating (FBG), are known to be highly sensitive [20, 21]. Thus, some attempts to use either active or passive AE for AM process exist in the literature [22–26] but no link was found between the AE and the quality of the part.

In recent years, significant progresses have been made in terms of artificial intelligence (AI). In a first try of combining FBG sensor and artificial intelligence, we evaluated spectral convolutional neural networks (SCNN) and conventional CNN [27]. The classification accuracy for SCNN was higher than CNN and ranged between 83 to 89% for the three quality levels. In this contribution, a convolutional neural network (CNN) was employed since it is top notch method used in acoustic signals processing, principally for speech recognition [28]. CNN incorporates self-features extraction layers that produce the optimal features for a given task. This makes CNN very interesting for industrial applications as CNN is able to self-optimize the algorithm with a minimum human participation.

2 Experimental Setup, Material and Acoustic Datasets

The experiments were performed on an industrial Concept M2 machine (Concept Laser GmbH, Germany). This machine is based on a selective laser melting (SLM) process. The machine had a fiber laser with wavelength of 1071 nm, a spot diameter of 90 µm, a beam quality $M^2 = 1.02$ and operating in continuous mode. The powder had a particle size distribution ranging from 10 to 45 µm and was made of CL20ES stainless steel (1.4404/316L).

The part produced was a cube with dimensions $10 \times 10 \times 20$ mm^3 shown in Fig. 1a. The process was carried out under N_2 atmosphere so that the O_2 content stayed below 1% during the entire process. Except the laser scanning velocity, the process parameters were kept constant. The laser power P was 125 W, the hatching distance h was 0.105 mm and the layer thickness t was 0.03 mm. Three laser scanning speeds were selected and they were 300, 500 and 800 mm/s. The corresponding energy densities were calculated to be 132, 79, 50 J/mm^3 [29]. The scanning regimes resulted in three pore concentrations inside the part, which was measured on cross-sections via visual inspection of light microscope images. The porosity concentration were 0.07 ± 0.02% (high quality; 500 mm/s; 79 J/mm^3), 0.3 ± 0.18% (medium quality; 300 mm/s; 132 J/mm^3), and 1.42 ± 0.85% (poor quality; 800 mm/s; 50 J/mm^3). The light microscope images of the different qualities are shown in Fig. 1b–d.

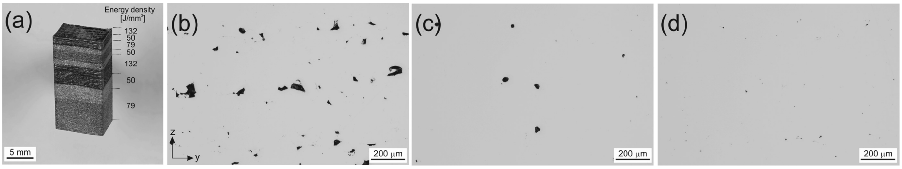

Fig. 1. (a) SLM test part produced with three energy densities where 50 J/mm^3 are bright regions, 79 J/mm^3 are dark regions and 132 J/mm^3 are blueish regions; (b) – (d) Typical light microscope cross-section images of regions produced with (a) 50 J/mm^3, 800 mm/s, poor quality with pores concentration of 1.42 ± 0.85%, (b) 132 J/mm^3, 300 mm/s, medium quality with pores concentration 0.3 ± 0.18% and (c) 79 J/mm^3, 500 mm/s, high quality with pores concentration of 0.07 ± 0.02%.

In this study, the acoustic emission emitted during the process was recorded using a fiber Bragg gratings (FBG) during the whole manufacturing of the part. The FBG was placed inside the machine chamber, at a distance of 20 cm from the process zone. The FBG sensor was pumped with a narrow band laser irradiation at a wavelength of 1547 + 0.01 nm and a light power of 4 mW. The FBG sensor provided a 50% of reflectivity in the optical read out signal and more details about FBGs can be found in [20, 21]. The reflected signal was additional digitized using a high speed photo-diode, connected to data acquisition unit and a data recording software. Both were from Vallen (Vallen Gmbh., Germany). All signals were digitized with a sampling rate of 1 MHz. As an example, the AE signal of a full high quality layer (79 J/mm^3, 500 mm/s) is shown in Fig. 2a.

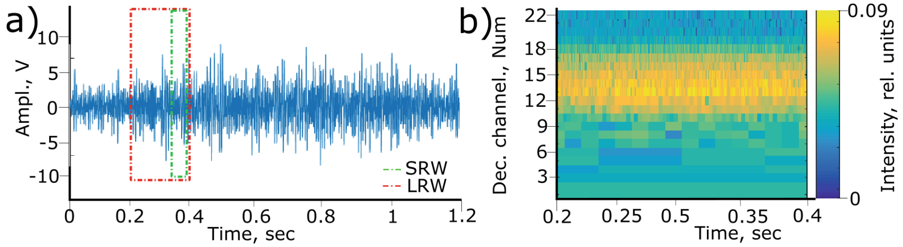

Fig. 2. (a) A typical AE signal from one complete layer of medium quality (132 J/mm^3, 300 mm/s). LRW (red box) and SRW (green box) are the long and short running windows scanning the acquired signal; (b) the complete reconstructed spectrogram from the relative energies of the *M*-band wavelets for the LRW time span bounded by red lines in Fig. 2(a).

3 Data Processing

3.1 Wavelet Spectrograms

In this specific work, the search of distinct features in convolution neural network (CNN) is carried out in the time-frequency domain using wavelet spectrograms. The intensity measurement of the AE components in spectrograms was taken as the relative energies of the narrow frequency bands obtained with *M*-band wavelets.

M-band wavelets are extensions of the traditional wavelet transform [30, 31]. Its advantage is to operate wavelets at various signal subspaces so that they become insensitive to shift-invariance artifacts [31]. The representation of *M*-band wavelets as a multi-channel filtering is defined through finite impulse response filters (FIR) [31]:

$$\varphi_{\mathrm{j}}(n)=\sum_{n}h_0(k)\sqrt{M}\varphi(Mn-k),\ k\subset Z \tag{1}$$

$$\psi_{\mathrm{ji}}(n)=\sum_{n}h_{m-1}(k)\sqrt{M}\psi(Mn-k),\ k\subset Z \tag{2}$$

where M is the channels number, $\varphi(n)$ is a scaling function, j is the current scale, $\psi()$ is the wavelet function, h_0, h_{m-2}, h_{m-1} are the low pass, narrow pass and high pass filters, respectively. The outcomes of Eqs. (1) and (2) are the extraction of the low, narrow and high frequency contents of the signal at a fixed scale j. This is represented by a set of decomposition coefficients $d_{j,s}$ where s denotes the shift within a single frequency band at scale j. In this contribution, the algebraic wavelets from Lin et al. [31] were used.

The use of relative energies allows tracking the energy redistribution between the different frequency bands and those are computed as:

$$\rho_{norm\,j,m}=E_{j,m}/E_j \tag{3}$$

where $E_{j,m}=\int\left|d_{j,m}(t)\right|^2dt=\sum_k\left|d_{j,s}\right|^2$ is the energy of frequency band m at scale j and E_{ij} is a summary of the energy of all frequency bands within the spectrogram. The outcome of Eq. (3) is a spectrogram. An example of an AE signal and a spectrogram are presented in Fig. 2. The spectrogram is reconstructed from a pattern of the signal in Fig. 2a that is bounded by the red lines between 0.2 and 0.4 s.

In this investigation, two AE patterns from the AE signal were analyzed and marked in Fig. 2a by a red and green boxes. These patterns are defined as a LRW (Long Range Window, red box) and SRW (Short Range Window, green box). Both have different span time and have different purposes. The AE signals will be scanned by these two windows. The SRW will provide a higher resolution for more precise spatial localization of single process events in the future. But, its short time span makes it sensitive to noise. This problem is expected to be surmounted thank to the LRW that will be responsible for the whole classification stability. In this work, the LRW is a short term memory of a set of several previous and one current SRW.

3.2 Introduction to Wavelet Spectrograms

In this study, the CNN structure was adjusted to process the flows of the spectrograms from both the LRW and SRW, simultaneously. The scheme of the new CNN structure is presented in Fig. 3. The two spectrograms go through two separate convolution layers from which we get a series of perception maps 1. The information from those is further aggregated in the pooling layers 1. Then, the information from both flows is forwarded into the common convolution layer 2 which is followed by an additional repentance of the pooling operation (see pooling 2 in Fig. 3). The final classification is carried out in fully connected layers as schematically presented in Fig. 3. The classification result is the output of the procedure and this is given in Table 1. More details can be found in Thomas et al. [32] for the pooling operation and Krizhevsky et al. [33] for self-feature extraction and CNN operation principles.

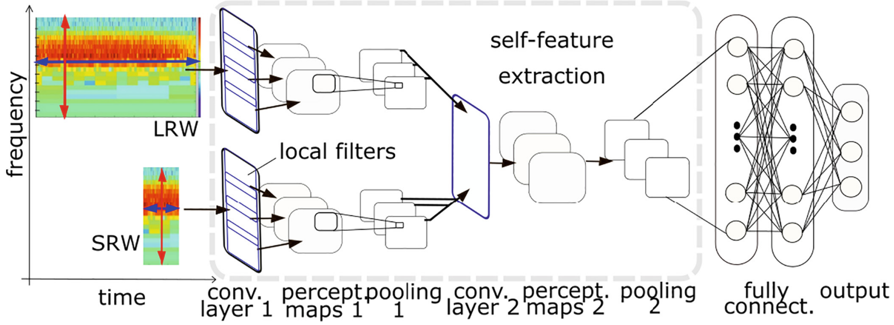

Fig. 3. The structure of the CNN, where LRW and SRW denote the long rang window and short range window, respectively.

Table 1. Test results for different categories (in rows) versus ground truth (in columns). The color intensity encodes the match of the test result to the ground truth. In brackets the classification results only for LRW/SRW are shown

Ground truth / Test categories	Poor	Medium	High
Poor (1.42 ± 0.85 %, 800 mm/s)	84 (84/69)	7 (8/12)	9 (8/19)
Medium (0.3 ± 0.18 %, 300 mm/s)	7 (9/10)	82 (80/63)	11 (11/27)
High (0.07 ± 0.02 %, 500 mm/s)	11 (12/18)	10 (9/21)	79 (79/61)

4 Results and Discussion

4.1 Dynamical Range

As mentioned in Sect. 2, the AM machine employed in this investigation is an industrial Concept M2. Due to their conceptions, such industrial machines have a non-negligible background noise, in particular for acoustic emission (AE). Consequently, it is of utmost importance to be able to decouple the AE of the AM process from the background noise. This was accomplished by recording the machine internal noises without the AM process. Those signals were, then, utilized for the evaluation of the noise background.

It was found from the spectrograms that the background noise of the Concept M2 machine appears in a wide spectral range as for the AM process. However, some discernible dissimilarity was discovered in the range of 9 to 15 KHz (not shown here).

The noise reduction in the industrial mechanic systems are well known and can be effectively suppressed by design of filters. These noises are mainly characterized by low frequencies [34]. But, in this current study, we relied on the ability of CNN to suppress the stationary noises.

4.2 Classification Results

The training dataset included in total 1.200 LRWs and 4.800 SRWs from the three quality categories, which were extracted from the AE signals. In this dataset, each category had the same number of signals. After the training, to test the data, we used a different dataset that was not used in the training procedure. This can be assimilated to newly data recorded for a new part. The test dataset was also constituted by the same number of LRWs and SRWs for each category.

The accuracies of the classification results using the test dataset are given in Table 1. In this table, the numbers without brackets represent the total accuracies (LRW and SRW). The numbers in brackets are the classification results for only either the LRW or the SLRW, respectively. The ground truths, in this table, are given in the columns whereas the classification test categories are in rows. The accuracy is calculated from the number of the true positives divided by the total number of the tests for the individual categories. The total accuracies achieved using the aforementioned time spans for both windows lie between 79 and 84%. The classification errors for each category correspond to the values in the non-diagonal cells of Table 1. For example, the AE test data from poor quality was classified with an accuracy rate of 84% and so it has the lowest error rate. The classification error is the lowest (7%) for the medium quality and the highest (9%) for the highest quality. The situation is completely invers for the medium quality. Finally, the classification error, for the high quality, is almost the same for medium and poor quality.

We would like to point out again here that the poorest quality is made with the highest speed (800 mm/s), followed by the high quality (500 mm/s) and finally the medium quality (300 mm/s). It is also interesting to note that, for the poor quality, the error rates decrease as the differences in the laser scanning speed increases. In contrast, this statement is not valid for the medium quality. In this case, the error rate is highest for the high quality, although the laser scanning speed difference is the smallest as compared to the poor quality, and the error rate is lowest for the poor quality, despite having the largest laser scanning speed difference. As far as the high quality is concerned, although the error rates between the two other quality levels, the lowest value is found to be for the medium quality (10%, 300 mm/s) which has, actually, the closest laser scanning speed with the high quality (500 mm/s) as compared to the poor quality (11%, 800 mm/s). Hence, we can conclude that the laser scanning velocity has no impact on the self-extraction of the distinct features in CNN.

Another source of error may be due to the acoustic echo and noise behavior produced during the additive process. As already mentioned, there are some overlaps in the AE signals coming from the AM process and the noise of the machine. Considering also the stochastic behavior of the AM process and the noise of the machine, it cannot be excluded that some features are not well classified during the training. Such behaviors complicate the extraction of the distinct frequencies and increase the error rates.

The results of the AE signal classification for the LRW and SRW only are presented in brackets in Table 1. It is found that the classification accuracy obtained only considering the LRW is very close or equal to the total classification accuracy, which is obtained from the combined LWR and SRW. In contrast, the classification accuracy of the SRW only is significantly lower than the total and LRW only accuracies. Two reasons may account for this result. First, this may be due to the fact that the SRWs are extremely sensitive to the noises as they operate at much smaller time scales. Second, this could be due to the fluctuations of the acoustic signal from the additive process. The local fluctuations might be caused by very local events which are different from each other due to the non-uniformities of the laser-material interactions. Those are probably caught by the SRWs due to their much smaller time scales. This conveys to higher error rates when splitting all signals only in three categories. Despite its poor classification accuracy, the SRW will bring benefits in the future. Due to the shorter time spans, we will be able to localize more precisely the defects. But, this was out of the scope of this contribution and is the subject for further developments.

5 Conclusions

The main goal of this contribution was to study the feasibility of a very innovative approach which combines acoustic emission (AE) with artificial intelligence (AI) for *in situ* and real-time monitoring of additive manufacturing (AM) processes.

To answer the question, we used an industrial selective laser melting (SLM) machine Concept M2. The material used was a CL20ES stainless steel (1.4404/316L) powder (∅ 10–45 μm). The acoustic sensor selected was a fiber Bragg grating (FBG) due to its high sensitivity. In terms of artificial intelligence, a convolution neural network (CNN) was employed. The CNN employed was modified to be able to analysis input data at two time scales. The CNN was fed with wavelet spectrograms that were are a representation of the AE signals. A part was produced with constant process parameters except for the laser scanning velocity. Three laser scanning speeds were selected to give three levels of quality levels in terms of porosity. The measured porosity concentration were 0.07 ± 0.02% (high quality; 500 mm/s; 79 J/mm^3), 0.3 ± 0.18% (medium quality; 300 mm/s; 132 J/mm^3), and 1.42 ± 0.85% (poor quality; 800 mm/s; 50 J/mm^3). The recorded AE signals were grouped accordingly.

It is known that industrial machines, such as the Concept M2 machine, produce high noise levels resulting in a low signal/noise ratio leading to classification inaccuracies. The approach considered in this work has two tools for effective noise suppression. To start with, we used wavelet spectrograms which allow suppressing noises by excluding the noisy frequency bands. Secondly, the noises can be partly eliminated by the artificial intelligence framework during the training procedure.

The CNN was trained and tested on two different datasets. The classification accuracy was in the range of 79–84%. It was also found that the long range window (LRW) had a very close classification accuracy as compared to the total classification accuracy. The results of the short range window (SRW) are much lower than the LRW and this was explained by the fact that SRW was very sensitive to the local fluctuations of the AE signals.

To conclude, our results show that there are distinct AE features for each manufacturing quality. The extracted features can be differentiated with artificial intelligence technique. Taking into account that it is the first tests carried out, the classification results can be considered as very promising and they showed the feasibility of the quality monitoring of AM process by combining acoustic emission and artificial intelligence.

For improving our actual algorithm to deal with very noisy atmosphere, it requires additional investigation of noises nature and types. Moreover, a further increase of the sensitivity of the AE sensor is possible by utilizing other optical structures. Both ameliorations are our future work.

References

1. Guo, N., Leu, M.: Additive manufacturing: technology, applications and research needs. Front. Mech. Eng. **8**(3), 215–243 (2013). doi:10.1007/s11465-013-0248-8
2. Wohlers Report – 3D Printing and Additive Manufacturing State of the Industry. Annual Worldwide Progress Report. Wohlers Associates, 2013–2016
3. Gu, D.D., Meiners, W., Wissenbach, K., Poprawe, R.: Laser additive manufacturing of metallic components: materials, processes and mechanisms. Int. Mat. Rev. **57**, 133–164 (2012). doi:10.1179/1743280411Y.0000000014

4. Huang, S.H., Liu, P., Mokasdar, A., Hou, L.: Additive manufacturing and its societal impact: a literature review. Int. J. Adv. Manuf. Tech. **7**, 1191–1203 (2013)
5. Zhai, Y.W., Lados, D.A., Lagoy, J.L.: Additive manufacturing: making imagination the major limitation. JOM **66**, 808–816 (2014)
6. Khairallah, S.A., Anderson, A.T., Rubenchik, A., King, W.E., Livermore, L.: Laser powder-bed fusion additive manufacturing: physics of complex melt flow and formation mechanisms of pores, spatter, and denudation zones. Acta Mat. **108**, 36–45 (2016). doi:10.1016/j.actamat.2016.02.014
7. Gibson, I., Rosen, D.W., Stucker, B.: Additive manufacturing technologies, rapid prototyping to direct digital manufacturing. Springer Science + Business Media (2010). 10.1007/978-1-4419-1120-9
8. Frazier, W.E.: Metal additive manufacturing: a review. J. Mater. Eng. Perform. **23**, 1917–1928 (2014). doi:10.1007/s11665-014-0958-z
9. King, W.E., Anderson, A.T., Ferencz, R.M., Hodge, N.E., Kamath, C., Khairallah, S.A., Rubenchik, A.M.: Laser powder bed fusion additive manufacturing of metals; physics, computational, and materials challenges. Appl. Phys. Rev. **2**, 041304 (2016). doi:10.1063/1.4937809
10. Tammas-Williams, S., Zhao, H., Léonard, F., Derguti, F., Todd, I., Prangnell, P.B.: XCT analysis of the influence of melt strategies on defect population in Ti–6Al–4 V components manufactured by selective electron beam melting. Mater. Charact. **102**(4), 47–61 (2015). doi:10.1016/j.matchar.2015.02.008
11. Shifeng, W., Shuai, L., Qingsong, W., Yan, C., Sheng, Z., Yusheng, S.: Effect of molten pool boundaries on the mechanical properties of selective laser melting parts. J. Mater. Process. Tech. **214**(11), 2660–2667 (2014). doi:10.1016/j.jmatprotec.2014.06.002
12. Everton, S.K., Hirsch, M., Stravroulakis, P., Leach, R.K., Clare, A.T.: Review of in-situ process monitoring and in-situ metrology for metal additive manufacturing. Mat. Des. **95**, 431–445 (2016). doi:10.1016/j.matdes.2016.01.099
13. Tapia, G., Elwany, A.: A review on process monitoring and control in metal-based additive manufacturing. J. Manuf. Sci. Eng. **136**, 10 (2014). doi:10.1115/1.4028540
14. Herzog, F., Bechmann, F., Berumen, S., Kruth, J.P., Craeghs, T.: Inventors method for producing a three-dimensional component patent WO1996008749 A3, 2013, 23 August 1995
15. Vaidya, R., Anand, S.: Image processing assisted tools for pre- and post-processing operations in additive manufacturing. Proc. Manuf. **5**, 958–973 (2016). http://dx.doi.org/10.1016/j.promfg.2016.08.084
16. Alhwarin, F., Ferrein, A., Gebhardt, A., Kallweit, S., Scholl, I., Tedjasukmana, O.: Improving additive manufacturing by image processing and robotic milling. In: IEEE Int. Conf. Autom. Sci. Eng. (CASE) 24–28 August, pp. 924–929 (2015). doi:https://dx.doi.org/10.1109/CoASE.2015.7294217
17. Furumoto, T., Alkahari, M.R., Ueda, T., Aziz, M.S.A., Hosokawa, A.: Monitoring of laser consolidation process of metal powder with high speed video camera. Phy. Proc. **39**, 760–766 (2012). doi:10.1016/j.phpro.2012.10.098
18. Furumoto, T., Ueda, T., Alkahari, M.R., Hosokawa, A.: Investigation of laser consolidation process for metal powder by two-color pyrometer and high-speed video camera. CIRP Ann. Manuf. Technol. **62**, 223–226 (2013). doi:10.1016/j.cirp.2013.03.032
19. Wu, H., Yu, Z., Wang, Y.: A new approach for online monitoring of additive manufacturing based on acoustic emission. In: ASME 2016 11th International Manufacturing Science and Engineering, Conference Paper No. MSEC2016–8551, V003T08A013, pp. 1–8 (2016) doi:10.1115/MSEC2016-8551
20. Kashyap, R.: Fiber Bragg Gratting, 2nd edn. Elsevier, Amsterdam (2010). ISBN 978-0-12-372579-0

21. Ramakrishnan, M., Rajan, G., Semenova, Y., Farrell, G.: Overview of fiber optic sensor technologies for strain/temperature sensing applications in composite materials. Sensors **16**(1), 99 (2016). doi:10.3390/s16010099
22. Grosse, C.U., Ohtsu, M.: Acoustic emission testing. Springer-Verlag, Berlin, Heidelberg. doi:10.1007/978-3-540-69972-9
23. Sharratt, B.M.: Non-destructive techniques and technologies for qualification of additive manufactured parts and processes: a literature review, Contract Report DRDC-RDDC-2015-C035 (2015). http://cradpdf.drdc-rddc.gc.ca/PDFS/unc200/p801800_A1b.pdf
24. Cerniglia, D., Scafidi, M., Pantano, A., Łopatka, R.: Laser ultrasonic technique for laser powder deposition inspection. In: 13th International Symposium on Non-dest. Charact. Mat., Le Mans, May 2013.http://www.ndt.net/article/ndcm2013/content/papers/13_Cerniglia.pdf
25. Purtonen, T., Kalliosaari, A., Salminen, A.: Monitoring and adaptive control of laser processes. Phys. Proc. **56**, 1218–1231 (2014). doi:10.1016/j.phpro.2014.08.038
26. Strantza, M., Aggelis, D.G., de Baere, D., Guillaume, P., van Hemelrijck, D.: Evaluation of SHM system produced by additive manufacturing via acoustic emission and other NDT methods. Sensors **15**, 26709–26725 (2015). doi:10.3390/s151026709
27. Shevchik, S.A., Kenel, C., Leinenbach, C., Wasmer, K.: Acoustic emission quality monitoring in additive manufacturing using spectral convolutional neural networks. Submitted in Add. Manf. (s2017)
28. Schmidhuber, J.: Deep learning in neural networks: an overview. J. Neural. Netw. **61**, 85–117 (2015). doi:10.1016/j.neunet.2014.09.003
29. Thijs, L., Verhaeghe, F., Craeghs, T., Humbeeck, J.V., Kruth, J.P.: A study of the microstructural evolution during selective laser melting of Ti–6Al–4 V. Acta Meter. **58**(9), 3303–3312 (2010). doi:10.1016/j.actamat.2010.02.004
30. Daubechies, I.: Ten lectures on wavelets. In: CBMS-NSF Regional Conference Series in Applied Mathematics (1992) 10.1137/1.9781611970104
31. Lin, T., Xu, S., Shi, Q., Hao, P.: An algebraic construction of orthonormal M-band wavelets with perfect reconstruction. Appl. Math. Comput. **172**(2), 717–730 (2006). doi:10.1016/j.amc.2004.11.025
32. Thomas, S., Ganapathy, S., Saon, G., Soltau, H.: Analyzing convolutional neural networks for speech activity detection in mismatched acoustic conditions, Acoustics, Speech and Signal Processing (ICASSP). In: IEEE International Conference on Acoustics Speech and Signal Processing (ICASSP) (2014). 10.1109/ICASSP.2014.6854054
33. Krizhevsky, A., Sutskever, I., Hinton, G.E.: ImageNet classification with deep convolutional neural networks. Adv. Neur. Inf. Proc. Sys. **25** (NIPS 2012) (2012). https://papers.nips.cc/paper/4824-imagenet-classification-with-deep-convolutional-neural-networks
34. Crocker, M.J. (ed.): Handbook of Noise and Vibration Control. Wiley, New Jersey (2007). doi:10.1121/1.2973236. ISBN 978-0-471-39599-7

Quality Related Effects of the Preheating Temperature on Laser Melted High Carbon Content Steels

Livia Zumofen(✉), Christian Beck, Andreas Kirchheim,
and Hans-Jörg Dennig

Centre for Product and Process Development,
Zurich University of Applied Sciences, Winterthur, Switzerland
livia.zumofen@zhaw.ch

Abstract. Additive manufacturing technology selective laser melting (SLM) is an emergent technology allowing generation of complex metal parts layer by layer. During the past years the range of available and processable materials for SLM has been widely extended. However, there is a still a lack of SLM processable high carbon content steels. In the fields of machine elements, especially in advanced cutting tools a large potential of laser melting is identified regarding function integration, topology optimisation and implementation of bionic concepts. In these fields of application high carbon content steels are frequently used. The M2 High Speed Steel (HSS) is a high carbon content steel that belongs to the group of tool steels. As other high carbon content steels, M2 HSS tends to a high susceptibility to cracking. Therefore, the strongly pronounced temperature gradients occurring during the laser melting process lead to part deformation and crack formation. Heating of the SLM baseplate represents a promising approach to reduce temperature gradients and internal stresses. In the present study the quality related effects of reduced temperature gradients on SLM parts were evaluated using a baseplate heating system. Optimized process parameters allowed a stable processing of M2 HSS leading to a relative part density of 99%. Residual stresses decreased with increasing baseplate temperature by trend.

Keywords: High carbon content steel · Selective laser melting · M2 HSS · Tool steel · Internal stresses

1 Introduction

Selective laser melting (SLM) is an emergent additive manufacturing technology, which allows layer-wise generation of complex metal parts based on 3D models [1]. The enormous market expansion of SLM machines in the last years points out the increasing importance of additive manufacturing, particularly in the processing of metals [2]. Due to the new design opportunities offered by SLM, great potential is identified in function integration, topology optimisation and implementation of bionic concepts [1, 3]. In the fields of machine elements, especially in advanced cutting tools high carbon content steels are frequently used.

© Springer International Publishing AG 2018
M. Meboldt and C. Klahn (eds.), *Industrializing Additive Manufacturing - Proceedings of Additive Manufacturing in Products and Applications - AMPA2017*,
DOI 10.1007/978-3-319-66866-6_21

The M2 High Speed Steel (HSS) is a high carbon content steel that belongs to the group of tool steels and is widely used for cutting tools, due to its high hardness, high wear resistance and relatively high toughness [4]. Therefore, processing of M2 HSS is of high interest for advanced tools with high complexity e.g. including internal cooling or lubrication channels. However, high carbon content steels do not yet belong to the standard materials for laser melting, due to their high susceptibility to cracking and deformation when processed with SLM [4–6]. The strongly pronounced temperature gradients occurring during the SLM process are associated with high cooling rates inducing residual stresses [4, 5]. Residual stresses may ultimately lead to warping, part deformation and crack formation. These factors complicate the SLM processing of M2 HSS and currently limit the achievable part quality.

By analogy to laser welding of high carbon content steels, where preheating is a necessity, heating of the SLM baseplate represents a promising approach to reduce occurring temperature gradients. Preliminary studies showed that increased baseplate temperature of up to 200 °C is capable of reducing crack formation in M2 HSS [4, 5]. However, the direct effect of the baseplate temperature on residual stresses remains unknown.

The present work includes a parameter study with focus on scan velocity to allow a stable laser melting process of M2 HSS leading to low porosity. To reduce thermal gradients and internal stresses, a preheating system to heat the baseplate up to 400 °C is applied. Evaluation of porosity and residual stresses in relation to the baseplate temperature represent the main focus.

2 Methods and Experiments

2.1 Powder

Inert gas atomized M2 HSS powder with 0.83% carbon content was supplied from SANDVIK OSPREY LTD. As shown in Fig. 1, the powder has a prevalent spherical shape with small satellites, especially at the larger fraction. The powder has a Gaussian particle size distribution with particle size of 15–48 µm.

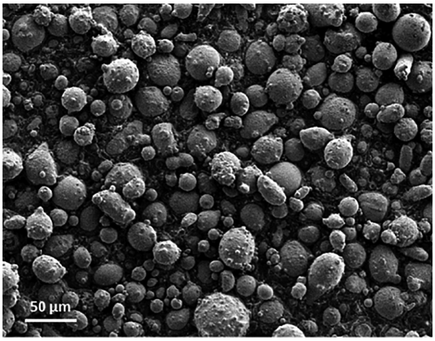

Fig. 1. SEM image of used M2 HSS powder.

2.2 Laser Melting

Selective laser melting is a powder bed based additive manufacturing technology that allows generation of metal parts with low porosity layer by layer. For each layer, a thin powder layer is added, which is selectively melted and connected to the underlying layer, according to 3D data (Fig. 2). Then, the baseplate is lowered and the aforementioned procedure repeated for subsequent layers until the build is completed.

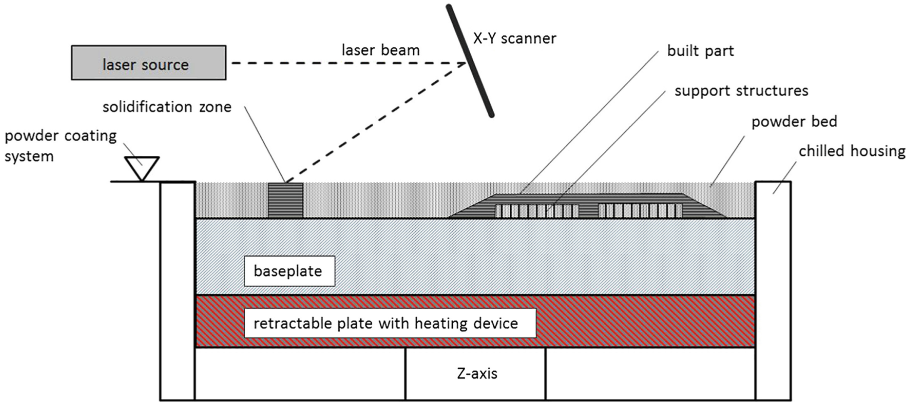

Fig. 2. Schematic representation of the SLM process including the baseplate heating system.

Experiments were carried out on a Renishaw AM 250 laser melting system, which is equipped with a 200 W fiber laser operated in pulsed mode. The beam has a M^2 of < 1.1 and a spot diameter of 70 µm. Argon was used as inert gas with an oxygen threshold of maximum 1000 ppm. An additional baseplate heating device was integrated in the Renishaw AM 250 laser melting system (Fig. 2), which is located below the baseplate.

In order to evaluate effects of scan velocity and baseplate temperature on the part density, cubic specimens were manufactured (2.3). On the basis of specifically designed cantilevers, residual stresses were evaluated with the previously optimized parameter set (2.4). All specimens were manufactured with meander scan strategy, 40 µm layer thickness, 200 W laser power and 80 µm hatch space. Scan velocity varied between 500 mm/s and 1500 mm/s and baseplate temperature between 160 °C and 400 °C for cubic specimens. Cantilevers were manufactured with optimized scan velocity of 750 mm/s and baseplate temperatures of 160 °C–400 °C (2.4).

2.3 Porosity

Low porosity is an essential quality criterion of SLM parts, due to its direct relation to mechanical properties and the demand for comparable strength to bulk material [8]. Porosity is strongly dependent on process parameters and process conditions. Furthermore, an adequate energy input into the powder layer is needed in order to achieve complete melting and generate a homogenous melt track. Therefore, optimum process parameters are required in order to allow a stable SLM process resulting in high part density.

Thereby, the energy density (E_D) represents a common term to describe the energy input of the laser into a defined volume of material [9], whereas the most important parameters are taken into account (Eq. 1). These include the laser power (P_{Laser}), scan velocity (v_{Scan}), hatch space (s_{Hatch}) and layer thickness (t_{Layer}).

$$E_D = \frac{P_{Laser}}{v_{Scan} \cdot s_{Hatch} \cdot t_{Layer}} \tag{1}$$

To evaluate the effects of scan velocity on part density when processing the M2 HSS, specimens with 10 × 10 × 10 mm^3 dimension were manufactured with base parameters as mentioned in (2.2) and varying scan velocity of 500 mm/s–1500 mm/s at 400 °C baseplate temperature. For each set of parameters three specimens were manufactured. As the scan velocity contributes to the energy density, the consequent energy density decreases accordingly with increasing scan velocity (Table 1).

Table 1. Evaluated field of scan velocity and corresponding energy density at 400 °C baseplate temperature.

Sample	Scan velocity [mm/s]	Energy density [Ws/mm^3]
1	1500	42
2	1375	45
3	1250	50
4	1125	56
5	1000	63
6	875	72
7	750	83
8	625	100
9	500	125

The density was evaluated according to the archimedes' principle following the VDI 3405 guideline [10]. Specimens were analyzed using a KERN ABJ 220-4NM measuring device with water as displacement fluid. The relative density was determined based on the ASTM M2 standard density of 8.138 g/cm^3 [11].

2.4 Temperature Gradient Induced Residual Stresses

Previous studies showed the applicability of cantilevers to evaluate residual stresses induced by SLM in various process conditions [12, 13]. Therefore, investigation of residual stresses in the solidified material is carried out using defined cantilever constructions. Subsequent separation of the support structures creates a controlled deformation in the form of deflection. These deflections provide insight into presence of residual stresses. The separation was implemented with a band saw. Subsequent deflections in Z-axis were assessed using a Mitutoyo 192–106 height measuring device.

Cantilevers with two branches are designed and slightly modified to facilitate reproducible support separation (Fig. 3). The cantilever consists of a massive centrally located socket and two symmetrically arranged and supported branches. Supports are 0.5 mm thick arranged with 0.8 mm spacing. The endings of both branches are firmly connected to the base plate, to avoid spontaneous detaching prior to separation. Cantilevers were manufactured at 160 °C, 240 °C, 320 °C and 400 °C with all other parameters remaining identical. At each baseplate temperature, one cantilever per branch thicknesses of 1 mm, 1.5 mm, 2 mm and 4 mm was manufactured. The cantilever dimensions were identical except for the thickness of the branches.

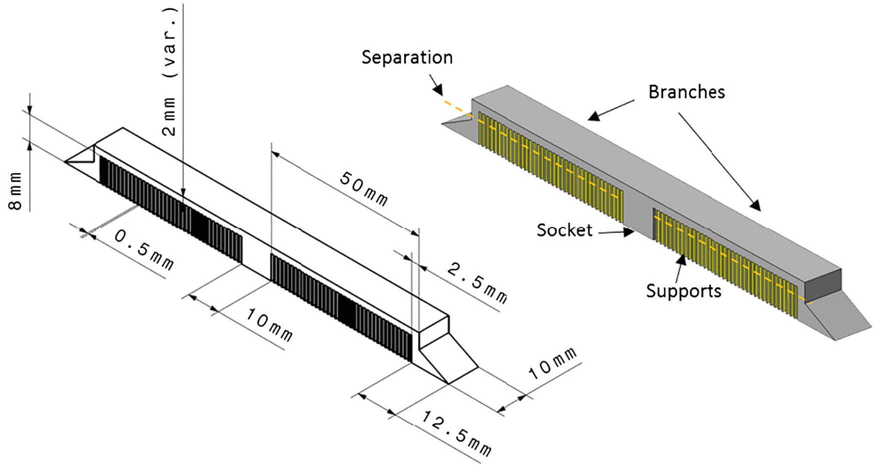

Fig. 3. Dimensions of cantilevers with two branches to evaluate residual stresses.

3 Results and Discussion

3.1 Process Parameters

Investigated specimens possessed a relative density between 98.2% and 99.2%. As displayed in Fig. 4, the density increased with decreasing scan velocity by trend, peaking at around 750–625 mm/s. Considering the melt track homogeneity, scan velocity of 500 mm/s led to strongly pronounced irregularities (Fig. 5).

Scanning electron microscopic evaluation showed homogenous melt tracks at 750 mm/s scan velocity (Fig. 6A). Therefore, scan velocity of 750 mm/s and corresponding energy density of 83 Ws/mm^3 led to both, high part density (Fig. 4) and homogenous melt tracks (Fig. 6A). Besides that, no effect of the baseplate temperature on the specimen density has been recognized (Fig. 6B). Therefore, further experiments were carried out based on the base parameters described in 2.2 and a scan velocity of 750 mm/s.

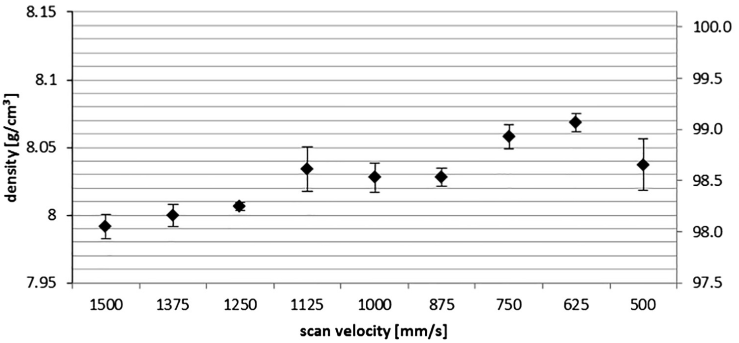

Fig. 4. Absolute and relative density of cubic specimens in relation to scan velocity at 400 °C base plate temperature. Values represent mean ± standard deviation.

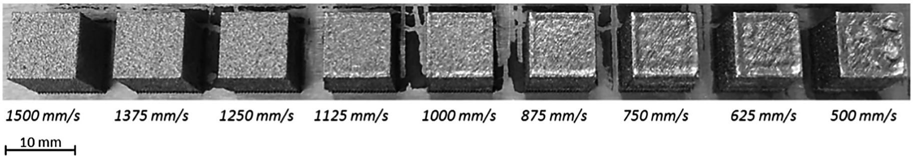

Fig. 5. Top view of cubic specimens with varying scan velocity of 1500 mm/s–500 mm/. Baseplate temperature: 400 °C.

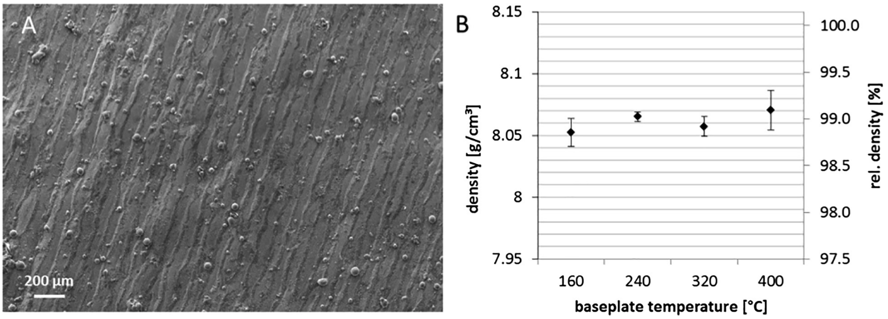

Fig. 6. SEM image of top surface of a cubic specimen manufactured with 750 mm/s scan velocity and 400 °C baseplate temperature (A) and density in relation to baseplate temperature. Values represent mean ± standard deviation (B).

Metallographic cross-sections in horizontal and vertical direction demonstrated a homogenous distribution of spherical shaped pores within specimens manufactured with 750 mm/s scan velocity and 400 °C baseplate temperature (Fig. 7).

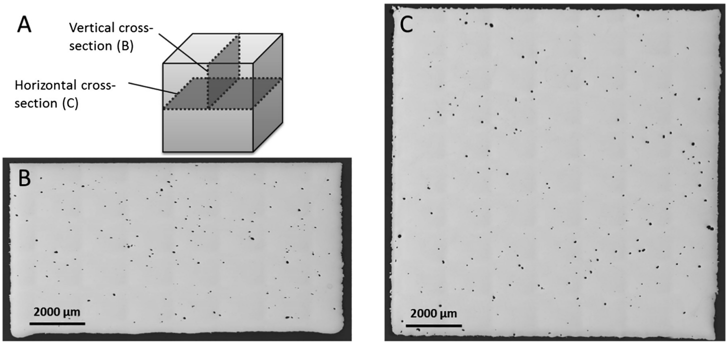

Fig. 7. Cross-sections of cubic specimens (A) in vertical (B) and horizontal (C) direction.

3.2 Effect of Baseplate Temperature on Residual Stresses

As demonstrated in Fig. 8, manufactured cantilevers already contained imperfections, deformations or cracks prior to separation from supports. Early cracking was exclusively observed at baseplate temperatures of 160 °C and below. However, imperfections and deformations were present at baseplate temperatures up to 400 °C. Some of these imperfections have even led to cracking and complete failure during separation, especially at 1 mm branch thickness. Therefore, cantilevers of 1 mm branch thickness were not further pursued.

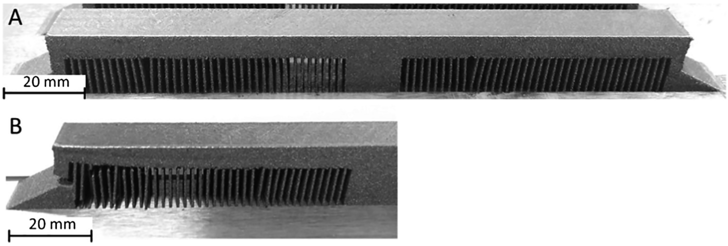

Fig. 8. Cantilevers with 4 mm branches and imperfections at 240 °C baseplate temperature (A); Early deformations and cracks prior to separation at 160 °C baseplate temperature (B).

Deformations of evaluated cantilevers at baseplate temperatures of 160 °C–400 °C are shown in Fig. 9. In consideration of 1.5–4 mm branch thicknesses, the deflection decreased with increasing thickness. The two branches of all cantilevers showed slight deviations between each other. On one hand occurring deviations may be attributed to inconsistent presence of imperfections, but also to temperature differences on the heated baseplate. At 400 °C baseplate temperature negative deflections of cantilever branches with 2 mm and 4 mm thickness were observed. The change of positive to negative deflection from 320 °C to 400 °C indicates a change of tensile stresses to compressive stresses. A similar phenomenon was also observed on H13 tool steel [7].

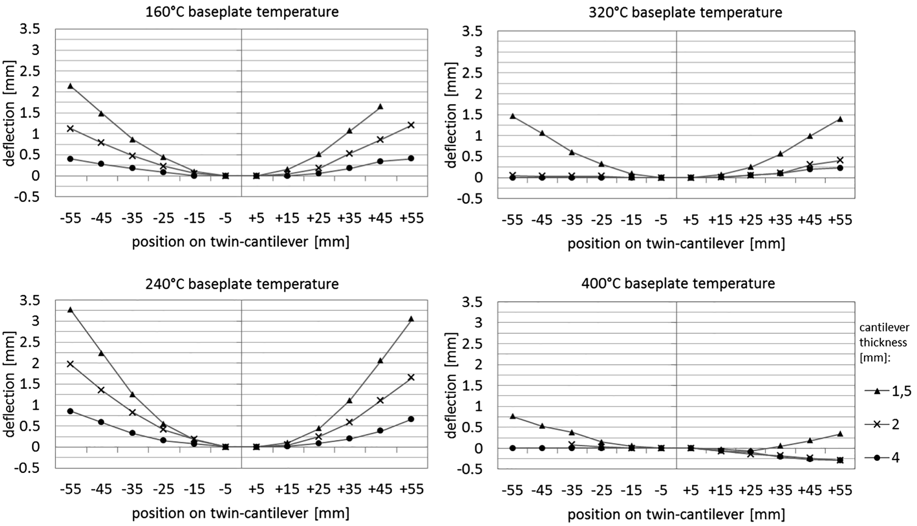

Fig. 9. Deflection of cantilevers with 1.5 mm, 2 mm and 4 mm thickness at different baseplate temperatures of 160–400 °C.

As demonstrated in Fig. 10, the deflection of cantilever branches of 4 mm thickness decreased with increasing baseplate temperature above 240 °C. Therefore, residual stresses are expected to decrease with increasing baseplate temperatures above 240 °C accordingly.

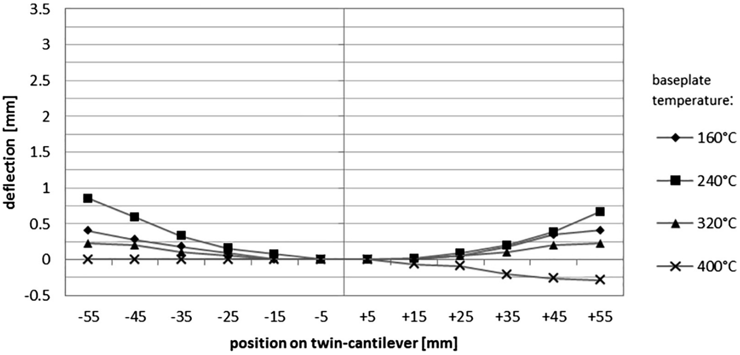

Fig. 10. Influence of temperature on deflection of cantilevers with 4 mm thickness.

Porosity is reported to have an influence on residual stresses [14]. As porosity has been found to be independent of the baseplate temperature within the investigated range (Fig. 6), no such effect is expected to interfere with the aforementioned finding. In contrary, deflection of the cantilever manufactured at 160 °C baseplate temperature was lower than the one at 240 °C (Fig. 10). It is suspected that this result originates from internal stresses above the strength of the material resulting in early relieve of stresses by deformation (Fig. 8B) and micro cracking during manufacturing, lowering the final deflection of the cantilever.

Based on the aforementioned findings, demonstrators of drillers with internal cooling channels were successfully manufactured with 750 mm/s scan velocity and 400 °C baseplate temperature (Fig. 11).

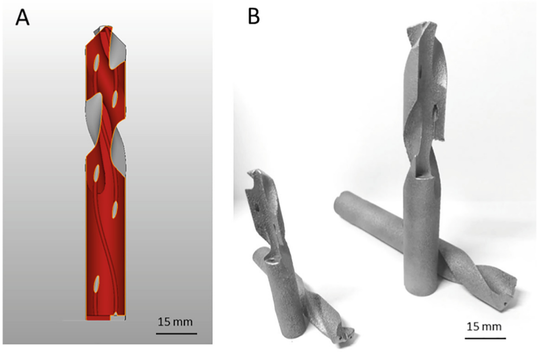

Fig. 11. Sectional view of the 3D model of a driller with internal cooling channels (A) and laser melted M2 HSS drillers (B).

4 Conclusions

Present results showed that M2 HSS may be processed using SLM and a baseplate heating system. Furthermore, the high potential of baseplate heating to reduce internal stresses has been demonstrated. However, residual stresses, imperfections and slight deformations still remained at 400 °C baseplate temperature under investigated conditions. Internal stresses are assumed to be increasingly critical at decreasing feature sizes, especially in parts where a combination of filigree and massive structures is present. By further optimization of process parameters a further reduction of internal stresses, but also porosity are suspected. This includes investigation of the effects of hatch spacing on part porosity and internal stresses. Besides that, investigation of formation of micro cracks and microstructure is of high interest. Further work is also recommended to focus on the characterization of the baseplate heating system and temperature distribution within the build part as a function of build height. It is suggested also to take a combination of the baseplate heating system with additional pre heating systems into account, e.g. infrared radiators to achieve a homogenous preheating temperature throughout the part as well as on the actual powder layer.

Acknowledgements. The authors acknowledge Renishaw plc. for supporting this project.

References

1. Gebhardt, A.: Generative Fertigungsverfahren. Additive manufacturing und 3D-Drucken für Prototying – Tooling – Produktion. 4. neu bearb. und erw. Auflage. Carl Hanser Verlag, München (2013)
2. Wohlers, T., Caffrey, T.: Wohlers Report 2015. 3D-Printing and Additive Manufacturing State of the Industry – Annual Worldwide Progress Report. Wohlers Associates, Fort Collins/US (2015)
3. Gibson, I., Rosen, D., Stucker, B.: Additive manufacturing technologies. 3D Printing, Rapid Prototyping, and Direct Digital Manufacturing. Springer Verlag, Berlin (2010)
4. Kempen, K., Thijs, L., Buls, S., van Humbeeck, J., Kruth, J.-P.: Lowering Thermal gradients in selective laser melting by pre-heating the baseplate. In: Bourell, D.L. (ed) Proceedings of the 2nd Solid Freeform Fabrication Symposium, Austin, TX, pp. 12–24, August 2013. University of Texas at Austin (2013)
5. Taha, M.A., Yousef, A.F., Gany, K.A., Sabout, H.: On Selective Laser Melting of Ultra High Carbon Content Steel: Effect of Scan Speed and Post Heat Treatment. Materialwissenschaften und Werkstofftechnik. Wiley-VCH Verlag GmbH, Weinheim (2012)
6. Liu, Z.H., Chua, C.K., Leong, K.F., Kempen, K., Thijs, L., Yasa, E., van Humbeeck, J., Kruth, J.-P.: A preliminary investigation on selective laser melting of M2 high speed steel. In: 5th International Conference on Advanced Research in Virtual and Rapid Prototyping, Leira, Portugal (2011)
7. Mertens, R., Vrancken, B., Holmstock, N., Kinds, Y., Kruth, J.-P., van Humbeeck, J.: Influence of powder bed preheating on microstructure and mechanical properties of H13 tool steel SLM parts. In: 9th International Conference on Photonic Technologies – Lane 2016, Physics Procedia, vol. 83, pp. 882–890. Elsevier (2016)
8. Yap, C.Y., Chua, C.K., Dong, Z.L., Liu Z.H., Zhang D.Q., Loh L.E., Sing S.L.: Review of selective laser melting: materials and applications, Applied Physics Reviews (2015)
9. Kruth, J.P., Vandenbroucke, B., Van Vaerenbergh, J., Naer, I.: Rapid manufacturing of dental prostheses by means of selective laser sintering/melting. In: Proceedings of the AFPR, S4, (2005)
10. VDI 3405 Part 3, Additive manufacturing processes, rapid manufacturing – Design rules for part production using laser sintering and laser beam melting. Beuth-Verlag, Berlin (2015)
11. OTAI Special Steel Co. Ltd. http://www.astmsteel.com/product/m2-tool-steel-1-3343-hs-6-5-2c-skh51/Accessed 13 Apr 2017
12. Buchbinder, D., Schilling, G., Meiners, W., Pirch, N., Wissenbach, K.: Untersuchung zur Reduzierung des Verzugs durch Vorwärmung bei der Herstellung von Aluminiumbauteilen mittels SLM. RTejournal – Forum für Rapid Technologie (2011)
13. Töppel, T., Müller, B., Hoeren, K. P. J., Witt, G.: Eigenspannungen und Verzug bei der additiven Fertigung durch Laserstrahlschmelzen., pp. 176–186 Schweißen und Schneiden 68, Heft 4 (2016)
14. Mercelis, P., Kruth, J.-P.: Residual stresses in selective laser sintering and selective laser melting. In: Rapid Prototyping Journal, pp. 254–265 (1995)

Business Cases

Additive Manufacturing in Automotive Spare Parts Supply Chains – A Conceptual Scenario Analysis of Possible Effects

Timo Eggenberger, Katrin Oettmeier, and Erik Hofmann(✉)

University of St. Gallen, St. Gallen, Switzerland
`{katrin.oettmeier,erik.hofmann}@unisg.ch`

Abstract. The automotive sector has been very progressive to experiment with additive manufacturing (AM) and early started to adopt it for rapid prototyping. Nonetheless, until the present day the integration of AM in the production of car parts, such as spare parts, proved to be difficult. Spare parts are generally characterized by demand uncertainty. Therefore they require high inventory levels to guarantee short lead times and high service levels for maintenance, repair and overhaul firms. The deployment of AM technologies in spare parts production has the potential to overcome these supply chain-related challenges. This research conceptually investigates the effects of AM in the automotive spare parts business for different supply chain scenarios. As a main contribution of this paper, four scenarios are developed and systematically analyzed regarding their suitability and implications for an AM implementation in the automotive spare parts supply chain.

The results suggest that centralized AM settings generally seem to be beneficial in terms of capacity utilization. Additionally, centralized production appears favorable when short lead-times and minimal downtime costs do not depict major priorities for OEMs. A hybrid scenario offers a high level of flexibility for OEMs to adjust to local demand patterns. In this case, AM is implemented in regional distribution centers. A decentralized production eventually signifies that spare parts are fabricated at repair shops of car dealers. This scenario implies high investment costs paired with considerable uncertainty concerning a sufficient capacity utilization. In contrast to that, a decentralized AM deployment seems to offer the highest potential for a customization of parts and timely deliveries. The outsourcing of AM to an external provider was considered as a fourth scenario. By transferring the production of spare parts to another company, the roles and responsibilities of the OEM shift considerably towards the management of the external production network.

Keywords: Additive manufacturing · Automotive spare parts · Supply chain · Scenario analysis

1 Introduction

Spare parts handling has become a multi-billion dollar business for industry sectors producing durable goods such as cars, planes, machines, household appliances or electronics. (Gallagher et al. 2005). In fact, companies derive a large share of their

© Springer International Publishing AG 2018
M. Meboldt and C. Klahn (eds.), *Industrializing Additive Manufacturing - Proceedings of Additive Manufacturing in Products and Applications - AMPA2017*,
DOI 10.1007/978-3-319-66866-6_22

earnings from the aftermarket business, which also includes services and labour. In certain industries, the aftermarket has become four to five times bigger than the market for first sales and is an important source of profits for original equipment manufacturers (OEM) (Agrawal et al. 2006). About half of the profits of carmakers in the European automotive industry are generated in the aftermarket (Capgemini Consulting & ITEM University of St. Gallen 2010). In Germany, even 75 to 80% of profits originate from the aftermarket (Roland Berger Strategy Consultants 2013). Despite the enormous revenue potential, it remains a great challenge for manufacturers to provide high service levels while at the same time keeping costs for spare parts low (Holmström et al. 2014). Currently, it is often the case that spare parts are produced in high quantities and have to be transported over long distances. They are then stocked in warehouses only to be scrapped at a later point in time if they remain used (Brans and Ponfoort 2012).

Considering the financial importance of the aftermarket business and the challenges that have to be faced, OEMs are continuously trying to find ways to improve their processes. This is the point where additive manufacturing (AM) technologies come into play. However, little is known about the deployment possibilities for AM in automotive spare parts supply chains. Holmström et al. (2014) suggest that the adoption of AM in industries with reduced downtime costs – such as to the automotive sector – is inadequately researched.

The before mentioned aspects suggest that the automotive industry is a relevant research context for studies about the application of AM technologies. It is assumed that AM will not fully substitute conventional manufacturing practices such as injection moulding or subtractive manufacturing, but rather complement established techniques (Johnson and Sasson 2016). The main research question of this paper is as follows:

> *What are the effects of AM in automotive spare parts supply chains when different implementation options (i.e. supply chain scenarios) are considered?*

In order to answer this question, a comprehensive framework is developed, which guides the analyses about the impact of AM technology deployment for different SC scenarios within the automotive spare part sector. Several propositions are elaborated to help practitioners to detect appropriate implementation options for AM.

2 Literature Review

The following literature review assesses the current state of the scientific and professional knowledge with regard to the automotive aftermarket, AM, as well as AM deployments in the automotive spare parts industry.

2.1 Automotive Aftermarket

The spare parts market constitutes around 2 to 4% of all investments in industrial equipment (Brans and Ponfoort 2012). The aftermarket retail value of the European automotive industry was calculated to be around 174 billion Euros in 2008 (Capgemini Consulting & University of St. Gallen 2010). Current spare parts SCs are characterized by high volume production, long transportation distances and capacious warehousing

(Brans and Ponfoort 2012). This leads to high stock levels and eventually obsolete parts, which often need to be scrapped later on (Brans and Ponfoort 2012). The application of AM is perceived as a potential tool to further improve the profitability of the automotive aftermarket by enabling a better customer service and reduced costs.

Different car manufacturers are already experimenting with AM for end-use parts. Audi is testing AM for metal parts construction and has already managed to build a complete 1936 Grand Prix racing car. The accuracy of the parts is claimed to be around half the width of a human hair (Koslow 2015). Although Audi has not applied the AM parts in series production, "using metal 3D printed parts within actual automobile production has suddenly become an arm's reach away from becoming a reality" (Koslow 2015, para. 1). Similarly, BMW is increasingly employing AM for building final parts. "BMW will soon offer their customers the option to include custom 3D printed components made specifically for their car. They have also recently begun using 3D scanning and 3D printing to reproduce hard-to-find parts for classic or collectible cars" (Grunewald 2015, para. 4). The examples from practice demonstrate that spare parts production with AM is a hot topic in the automotive industry, which seems worth investigating.

In the European automotive aftermarket, there is typically an authorized and an independent channel for spare parts. The authorized channel consists of the OEM, its country organizations which operate the warehouses, and the dealer networks with their single- or multi-branded repair shops, e.g. AMAG. The original equipment suppliers (OES) sell their parts to both channels. In the *independent channel*, wholesalers and distributors are buying from independent parts manufacturers and OESs. On the retail level, the parts are then sold to franchise workshops, automotive centres/fast fitters such as Carglass or ATU, and autonomous repair shops (Boston Consulting Group 2012; Roland Berger Strategy Consultants 2013). In the *authorized channel*, spare parts are either delivered from the OEM's production facilities or directly from the OES to the regional distribution centres (RDC). From there, they are transported downstream to the parts distribution centres (PDC) and eventually to the branded service department of the dealership. The OEM typically operates the RDCs and PDCs. Hence, the car dealers' service departments are usually strongly dependent on the distribution network of the OEM (Douglas 2013).

2.2 Additive Manufacturing

AM, sometimes referred to as direct manufacturing (DM), rapid manufacturing (RM) or 3D printing, seems like a fairly new phenomenon. However, the technology has been around for over three decades now (Johnson and Sasson 2016). In recent years, AM has become more advanced in terms of precision, quality and surface finish. Therefore, production of end use products with AM has increasingly become a viable option in several industries (Brooks et al. 2014; Holmström et al. 2014).

In the automotive industry, the AM market is expected to generate revenues of around 1.1 billion USD by 2019 (PR Newswire 2015). Not surprisingly, "Enterprise 3D Printing" has thus arrived in the slope of enlightenment within the Hype Cycle analysis for 2015 (Gartner Inc. 2015). This phase marks the step just before mainstream adoption is achieved. It is not assumed that AM will substitute mass production but rather complements it with specific opportunities like a high productivity of smaller lot sizes, reduced material consumption, optimized designs or faster set-up times (Harrison and Scott 2015; Holmström et al. 2014; Fischer and Rommel 2013; Holmström et al. 2010).

2.3 Current State of Research on AM in the Automotive Spare Parts Industry

Mendis and Reeves (2015) conducted a study concerning AM for spare parts production, specifically in the automotive sector. The authors analysed the general dynamics and drivers for AM adoption in the spare parts market. Most car parts do not seem to be suitable for AM and the ones that are can mostly not be produced at competitive costs (Mendis and Reeves 2015). It is argued that AM for end-use parts will not be a major topic for the automotive industry within the next ten years (Mendis and Reeves 2015). However, the authors do not consider the possibility to improve parts with AM instead of merely replicating them, e.g. through simpler designs, better technical properties or reduced material usage (Berman 2012). If such improvements materialize, parts might be sold at higher prices (Kleer et al. 2015), which could benefit the competitiveness of AM.

At present, an in-depth analysis in the automotive sector about AM deployments in spare parts SCs is still missing. However, the examples of Audi and BMW clearly indicate that the automotive sector is intensively experimenting with the technology to produce not only prototypes but also spare parts or original car parts. This affirms a relevance of research about the requirements and potentials of AM in automotive spare parts SCs.

3 Results

In this chapter, four automotive SC scenarios analysed. The findings are based on a reflection of the relevant literature and conceptual considerations. The idea of considering different SC scenarios draws upon Hou et al. (2014) as well as Holmström et al. (2010, 2014), who conducted a scenario analysis in the aircraft industry. The conceptual analysis of each scenario ultimately yields different testable propositions.

3.1 Centralized AM Implementation

Centralized AM is the first hypothetical scenario that will be illuminated. It is assumed that AM capacities are implemented in the first echelon of the SC at the OEM production facility. Figure 1 provides a schematic and simplified overview of the authorized aftermarket channel with centralized AM. Once the AM parts are finished, they are transported and stocked throughout the SC in RDCs, PDCs and eventually delivered to the dealers. The dealers subsequently mount the AM part in the customer's car. The three different types of arrows illustrate the different process flows between the SC agents, i.e. material, information, and financial flows.

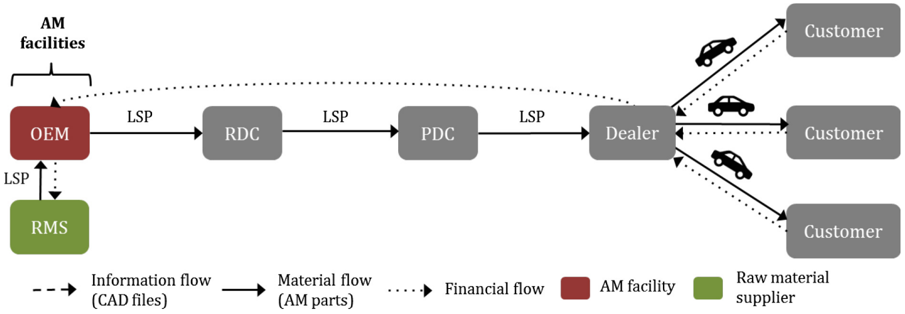

Fig. 1. Centralized SC scenario (Own illustration based on Douglas 2013, para. 12–13)

The main insights from the centralized SC scenario are summarized and translated into propositions, which are the result of the conceptual research approach and have to prove valid in empirical studies within the automotive industry. The first proposition takes up the issue of capacity utilization, which was already tested to some degree in the aerospace industry (Holmström et al. 2010, 2014).

Proposition 1a: A centralized implementation of AM in the automotive spare parts supply chain is associated with bundling advantages in terms of capacity utilization, machine maintenance, and the sourcing of AM materials.

It can be expected that the more central AM is implemented in the supply chain, the higher are the possibilities to monitor and optimize capacity utilization of AM machines. At first, a small number of AM machines can be installed and continually be increased as demand picks up. A centralized scenario may also reduce complexity in the maintenance and operation of the AM facilities. Know-how and manpower for running the AM facilities can be concentrated in fewer locations, which might enable efficiency and cost improvements. Furthermore, raw materials can be sourced centrally and do not have to be supplied to multiple different locations. In contrast to that, all relevant locations need to be equipped with AM machines in a decentralized scenario, which means that there remains less room for improving capacity utilization, but higher flexibility to adapt to demand changes (Holmström et al. 2014). This time aspect informs the next proposition, which reads as follows:

Proposition 2a: A centralized implementation of AM in the automotive spare parts supply chain is favourable when short lead-times and low downtime costs are not key priorities for the OEM.

In order to illustrate this proposition, the aerospace industry serves as an example. Each day an airplane is not operational results in very high costs. For this reason, decentralized production offers advantages, as parts can be produced very quickly on-site. In comparison, the downtime costs in the automotive sector are not as high (Holmström et al. 2014). It is hence reasoned that when short lead-times are not crucial and downtime costs not extremely high, it is advantageous to produce AM spare parts centrally.

Overall, it is concluded that in most cases, centralized AM offers more advantages in the early implementation phase. A pilot project can be started with centralized production and can later be extended gradually to decentralized locations if demand picks up, quality issues are under control and more spare parts become available for AM. Holmström et al. (2004) already introduced this notion for the aircraft industry. Due to the similar circumstances in the automotive industry, it can be assumed that the finding also holds there:

> ***Proposition 3a:*** A centralized implementation of AM in the automotive spare parts supply chain is more suitable at the beginning, when AM is initially deployed and little specific AM know-how exists. At a more advanced stage, spare parts production with AM can gradually be extended to decentralized locations.

3.2 Hybrid AM Implementation

It is important to note that the term "hybrid AM implementation" is not to be confused with hybrid production in the sense of simultaneous use of conventional manufacturing and AM. Throughout this paper, the term "hybrid" refers to a SC setting that is neither centralized nor decentralized. Essentially, it represents a middle course between the centralized and the decentralized scenario.

Hybrid AM in the automotive context means that production is either implemented on RDC level or alternatively on PDC level, depending on the practical circumstances evaluated in a cost-benefit analysis. If the market in a larger region is not particularly big, it can be sensible to install AM facilities in a RDC and then distribute the AM parts through the PDCs to the dealers. This specific situation is illustrated in Fig. 2.

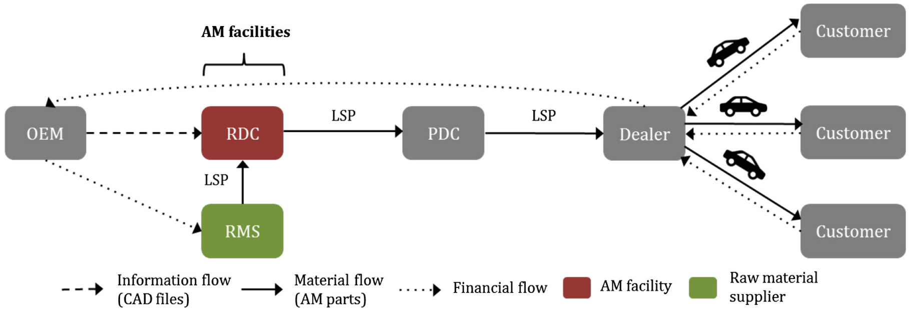

Fig. 2. Hybrid SC scenario on RDC level (Own illustration based on Douglas 2013, para. 12–13)

Alternatively, if demand in a geographical area is high enough to justify AM on PDC level or if markets are very remote to serve, the deployment of AM at PDC level is the preferred solution, as the PDC is located closer to the point-of-use. As Fig. 3 suggests, the horizontal SC is shortened because the RDC, as an additional echelon in the SC, is eliminated.

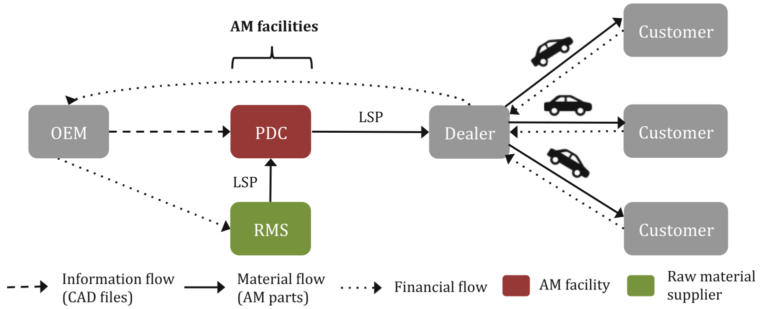

Fig. 3. Hybrid SC scenario on PDC level (Own illustration based on Douglas 2013, para. 12–13)

The two before mentioned scenarios about AM implementations at RDC or PDC level assume that the raw material supplier is responsible for providing the warehouses with AM materials and is refunded by the OEM. Alternatively, it could also be the case that the raw materials are delivered to the OEM, from where the distribution to the warehouses is managed.

The first proposition concerning hybrid deployments of AM in the automotive spare parts SC takes up the fact that this scenario is essentially a compromise between a centralized and a decentralized AM implementation. It corresponds to the results of Hou et al. (2014), who analysed the situation in the aerospace industry:

Proposition 1b: A hybrid implementation of AM in the automotive spare parts supply chain is likely to be an advantageous compromise between a centralized and a decentralized deployment if neither the demand level nor demand fluctuations or manufacturing lead-times are particularly extreme.

When envisaging a hybrid SC scenario as an option for AM technology application, the OEM needs to be aware that the implementation of AM will potentially pose some challenges for the firm's logistics hubs. Most likely, exists little technical know-how to operate the AM machinery. It is assumed that this lack is more evident than in the other settings of AM deployment, particularly the centralized scenario, where profound general manufacturing know-how should readily be available. Hence, the second proposition suggests that considerable investments may be needed in order to build up the required competences at the stage of the RDC or PDC.

Proposition 2b: A hybrid implementation of AM in the automotive spare parts supply chain is associated with a significant need to build up technical know-how since AM is introduced into a logistics environment.

Thirdly, the hybrid scenario has another specific characteristic, which is summarized in the third proposition. It provides the possibility to implement AM on two different echelons in the SC, depending on demand volume and demand variability. In comparison to the centralized approach, flexibility is higher because production happens closer to the customer. In the hybrid, the OEM can carefully evaluate on which level AM should be implemented. Essentially, this means that the hybrid scenario potentially leads to the best mix of quick demand reaction and sufficient capacity utilization. Hence, the following proposition is stated:

Proposition 3b: A hybrid implementation of AM in the automotive spare parts supply chain offers a higher flexibility and greater steering opportunities for the OEM to adjust to local demand patterns compared to a centralized deployment, while at the same time potentially retaining a high capacity utilization.

3.3 Decentralized AM Implementation

The decentralized scenario locates the AM facilities further downstream and hence close to the point of use. In the automotive SC this means to locate AM facilities at the repair shops of the authorized dealer. It represents the highest degree of manufacturing postponement and decentralization analysed within the scope of this paper.

The statement of the American carmaker Ford Motor Company (2016, para. 5) indicates that OEMs consider this production scenario for the future: “As the technology improves, dealer garages might have 3D printers of their own to create replacement parts, making repairs easier than ever”. Figure 4 shows how much the automotive SC for AM spare parts could potentially be streamlined.

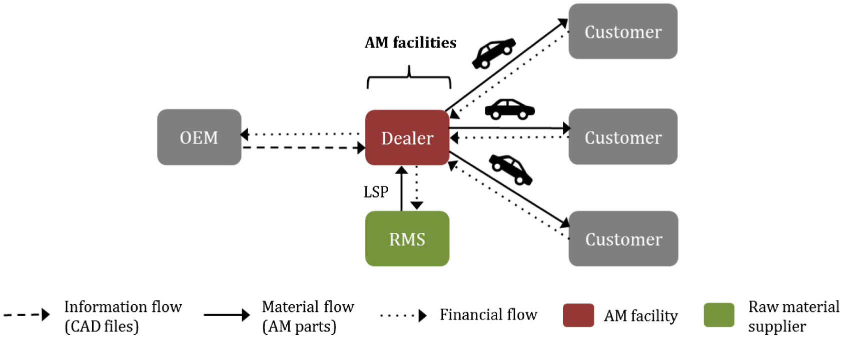

Fig. 4. Decentralized SC scenario (Own illustration based on Douglas 2013, para. 12–13)

The first proposition for the decentralized SC scenario addresses some distinct limitations of a decentralized AM, which refer to capacity utilization and investment costs. The argument is related to existing findings from the aircraft industry (cp. Holmström et al. 2010, 2014).

Proposition 1c: A decentralized implementation of AM in the automotive spare parts supply chain is impeded by the challenge to obtain a high capacity utilization and high investment costs in AM equipment as well as the build-up of specific AM know-how.

Compared to the aircraft industry, the automotive industry has more service points (dealers), which even strengthens the case for this argument. Hence, it seems likely that automotive spare parts SC face even greater challenges in this regard as the aircraft sector. Nonetheless, a decentralized spare parts production can also offer distinct opportunities, which are mainly related to the improved possibility for on-demand and on-location production. No inventory of AM parts needs to be held throughout the SC, which lowers working capital and potential obsolescence risks. Additionally, the transport volume decreases and the SC becomes less prone to disruptions (e.g. bullwhip effect) in case of demand fluctuations (Fischer and Rommel 2013; Holmström et al. 2014). This notion, which relates to logistics, is summarized in the following proposition:

Proposition 2c: A decentralized implementation of AM in the automotive spare parts supply chain is associated with a reduction in transportation and inventory holding costs as well as less distortions in demand information.

In general, any effort undertaken in the field of AM should either lead to reduced overall costs, an improved customer service, or both. The third proposition focuses on the latter. The analysis suggests that decentralized spare parts production with AM offers the highest potential for a better customer service compared to the other three scenarios. On the one hand, on-demand production fosters parts availability and hence speeds up car repair times. On the other hand, a decentralized spare parts production provides the greatest customization opportunities for dealers. Eventually, customers can configure or choose individualized parts, which are then produced upon request. These improved services can lead to a price premium for dealers. In contrast to that, customizing parts in a more centralized setup takes longer and is more complex because production happens farther away from the point-of-use, which results in higher logistics and coordination efforts.

Proposition 3c: A decentralized implementation of AM in the automotive spare parts supply chain is associated with a higher customer service level. On the one hand, a faster response time can be offered and on the other hand, the customization of parts is facilitated, which can potentially lead to a price premium.

3.4 Outsourcing of AM

The last scenario that will be analysed subsequently is not different in terms of the degree of centralization or decentralization, but considers a new actor in the SC. It delineates how the automotive spare parts SC will be affected if logistics service providers (LSPs) or independent AM providers perform AM. This means that the OEM takes a strategic decision to outsource AM to a third party, which then becomes an OES. In the following, particularly the case with LSPs as AM providers will be discussed. Figure 5 illustrates what such a scenario, where spare parts production is outsourced to an LSP could look like. The LSP's warehouses basically replace the RDCs and PDCs of the OEM, apart from that the setup greatly resembles the hybrid scenario.

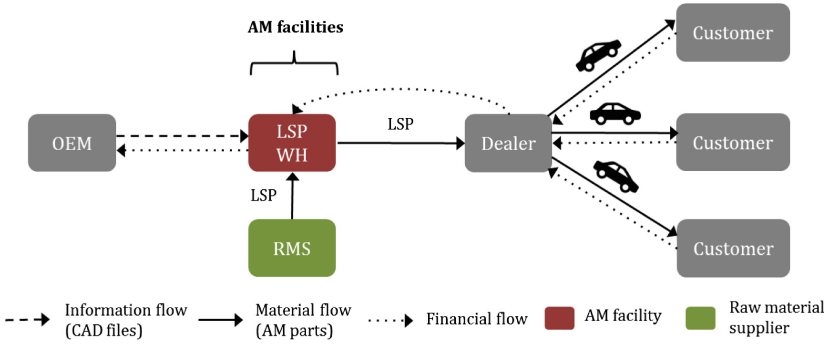

Fig. 5. Outsourcing SC scenario (Own illustration)

By outsourcing the AM activities to an external producer, the tasks for the OEM shift considerably. Even though the OEM is not directly involved in spare parts production with AM anymore, it is important that they still pursue research and development in the field. Only in this way they are able to continuously make more conventional parts available for AM and guarantee premium quality of the blueprints. The blueprints can then be licenced to external producers. By doing so, the OEM needs to make sure that they are designed in a way that the part's originality can be tracked at all times. Additionally, specific processes and management tools need to be in place to monitor the quality of the externally manufactured parts. The following proposition summarizes this change in the responsibilities of the OEM:

Proposition 1d: The outsourcing of automotive spare parts production with AM to an external provider is associated with a rising relevance of product development, quality control, and counterfeit protection tasks for OEMs.

Obviously, the tasks also change substantially for the LSP who was previously only concerned with logistics activities. If LSPs manage to build AM spare parts, they may integrate an additional part of the value chain in their service offering. Moreover, OEMs that outsource AM to LSPs or other providers become more dependent and need to engage in collaborative relationships. This clearly opens up new business opportunities for LSPs:

Proposition 2d: The utilization of AM technologies in the automotive spare parts supply chain by LSPs provides LSPs with additional revenue potential and enables them to internalize an additional step of the automotive value chain.

In automotive spare parts supply chains with AM, the question for the OEM is not just whether to outsource or not, but also to whom. LSPs are not the only players on the market. For example, the development of specialized AM supercentres has to be considered as well. Their business model is to transform manufacturing capacity into a tradeable commodity (Johnson and Sasson 2016). In comparison to LSPs, their core competences are in the field of technology and they operate in big complexes “with no asset specificity and zero changeover costs” (Johnson and Sasson 2016, p. 91). LSPs on the other hand have traditionally been specializing on SC related services and AM represents a rather new business for them. This could have implications that OEMs need to be aware of:

Proposition 3d: Compared to specialized AM providers, the use of an LSP for automotive spare parts production provides the benefit of giving OEMs access to the LSP’s existing distribution network. In order to engage in automotive spare parts production, LSPs may require high investments to build up the necessary AM know-how.

The previous proposition does not suggest that one type of an AM provider or the other is more suitable for the purposes of the OEM. If a LSP is chosen, then it is possible that the OEM needs to enter a strategic partnership in which AM capabilities are developed together with the LSP. In turn, the OEM benefits since it can integrate the AM operations within the distribution network of the LSP. In contrast, if a specialized AM supercentre is selected, the OEM likely does not need to provide assistance in technology development. However, the OEM has to evaluate whether this supplier can be integrated in their logistics processes.

4 Discussion and Conclusion

This paper conceptually investigated the effects of AM in the automotive spare parts business for different supply chain scenarios. As a main contribution of this paper, four scenarios were developed and systematically analyzed regarding their suitability and implications for an AM implementation in the automotive spare parts supply chain. Since the application of AM technologies for the production of spare parts is not well established yet in practice – neither in the automotive industry nor in other sectors, the business cases for the proposed supply chain scenarios cannot easily be studied based on empirical insights. The authors of this paper therefore conceptually derived some first indicatives about specific economic prerequisites, opportunities, and challenges of the scenarios, which are presented in Fig. 6.

Supply chain scenario	**Economic prerequisites / feasibility**	**Opportunities**	**Challenges**
Centralized AM implementation	▪ Sufficiently high global demand volumes for AM spare parts ▪ Low logistics costs	▪ On-demand production of spare parts ▪ Scale economies in manufacturing ▪ Bundling of design and manufacturing competences ▪ High level of control over product quality and distribution for the OEM	▪ Scale economies in manufacturing ▪ Bundling of design and manufacturing competences
Hybrid AM implementation	▪ Sufficiently high regional demand volumes for AM spare parts ▪ Moderate logistics costs ▪ Spare part design blueprints are provided to the PRC or RDC by the OEM	▪ On-demand production of spare parts ▪ Speed advantage / higher proximity to the customer compared to the centralized scenario	▪ Scale economies in manufacturing ▪ Bundling of design and manufacturing competences ▪ Limited level of control over product quality and distribution for the OEM
Decentralized AM implementation	▪ Sufficiently high local demand volumes for AM spare parts ▪ High logistics costs ▪ Spare part design blueprints are provided to the dealers by the OEM	▪ On-demand production of spare parts at the point of consumption ▪ Speed advantage / proximity to the customer	▪ Speed advantage / proximity to the customer ▪ Low level of control over product quality and spare parts distribution for the OEM ▪ Requirement for know-how buildup at the dealers' sites
Outsourcing of AM	▪ Sufficiently high demand volumes for spare parts across clients allows the AM provider to obtain scale economies in manufacturing ▪ Spare part design data blueprints are provided by the OEM	▪ No inventory risk for the OEM ▪ No investments in AM machines, materials and employee trainings needed by the OEM ▪ Specific know-how of the AM provider	▪ OEM has no control over product quality and spare parts distribution ▪ Risk of knowledge spills to competitors (e.g. clients of the AM provider)

Fig. 6. Economic prerequisites, opportunities, and challenges of the supply chain scenarios

Until the present day, AM is not an established fabrication technique for spare parts production in the automotive industry yet. Mendis and Reeves (2015) argue that it will be first necessary for OEMs to start applying AM in their regular manufacturing processes for original car parts. According to them, AM is only an interesting option for spare parts when the respective original car part was already fabricated with AM. Assumingly, they make this point because they do not consider it to be efficient to fabricate a given part with AM and conventional manufacturing at the same time.

Although the technical dimension was not discussed in detail, it is important to understand that technical and economic aspects of AM deployments cannot easily be separated. Especially the reengineering of parts can have significant economic consequences and has to be fostered (Holmström and Partanen 2014). Moreover, redesigning parts can lead to more parts becoming suitable for AM production, which increases AM capacity utilization (Holmström and Partanen 2014). On the other hand, less costly designs in terms of material usage are possible (Petrovic et al. 2011). This in turn allows for a more decentralized production in the long run and can result in cost benefits. In this context, Khan et al. (2012) refer to the importance of "aligning product design with the supply chain". It can be argued that the more parts are "designed for AM" or "AM compatible", the more likely it is that the technology becomes competitive and eventually will be widely adopted. For this reason, R&D and product development are the starting points to leverage AM in the long-term. However, this paper showed that economic impacts of AM need to be researched and considered as well in order to exploit the full potential of AM.

The results of this paper have several implications for research and practice. First and foremost, they support practitioners in their decision-making process for AM implementation. From a strategic perspective, it is emphasized that automotive OEMs have to become even more aware of the disruptive potential of AM for producing spare parts. In fact, the earlier they start to evaluate possible application fields within their operations, the better prepared they are when AM technology is fully ready to fabricate a wide range of car spare parts. In this context, OEMs also have to determine whether it is beneficial to incorporate AM solely in the production of spare parts or whether it can and should be extended to original car parts as well (Mendis and Reeves 2015). From an operational perspective, the conducted scenario analysis highlighted in different scenarios the effects of AM, depending on the degree of centralization. Managers in charge of AM implementations can consult the propositions as guidelines and assess their validity in their specific industrial context.

The research adds to the literature by illuminating the effects of AM implementations in automotive spare parts SCs based on different scenarios. Since AM is not an established technology in automotive spare parts production, the present research lacks a broad data sample of use-cases and tackled this deficiency with a conceptual research approach. Future could provide more detailed insights in this topic and test the developed propositions in empirical studies.

References

Agrawal, N., Agrawal, V., Cohen, M.A.: Winning in the Aftermarket (2006). https://hbr.org/2006/05/winning-in-the-aftermarket. Accessed 5 Apr 2016

Berman, B.: 3-D printing: the new industrial revolution. Bus. Horiz. **55**, 155–162 (2012)

Boston Consulting Group: The European Automotive Aftermarket Landscape (2012). https://www.bcg.com/documents/file111373.pdf. Accessed 2 Apr 2016

Brans, K., Ponfoort, O.: Direct Spare – Final Publishable Report (2012). http://cordis.europa.eu/result/rcn/54707_en.html. Accessed 23 Feb 2016

Brooks, G., Kinsley, K., Owens, T.: 3D printing as a consumer technology business model. Int. J. Manag. Inf. Syst. **18**(4), 271–280 (2014)

Capgemini Consulting & ITEM University of St.Gallen: The Aftermarket in the Automotive Industry (2010). https://www.capgemini.com/resources/the-aftermarket-in-the-automotive-industry. Accessed 4 Mar 2016

Douglas, M.: The Nuts & Bolts of the Automotive Aftermarket Supply Chain (2013). http://www.inboundlogistics.com/cms/article/the-nuts-bolts-of-the-automotive-aftermarket-supply-chain/. Accessed 28 Mar 2016

Fischer, A., Rommel, S.: Additive manufacturing – a growing possibility to lighten the burden of spare parts supply. In: Kochan, D., Kovacs, G.L. (eds.) Digital Product and Process Development Systems, pp. 112–123. Springer, Heidelberg (2013)

Ford Motor Company: Building in the Automotive Sandbox (2016). https://corporate.ford.com/innovation/building-in-the-automotive-sandbox.html. Accessed 25 Apr 2016

Gallagher, T., Mitchke, M.D., Rogers, M.C.: Profiting from spare parts. The McKinsey Quarterly (2005). http://www.werc.org/assets/1/workflow_staging/Publications/666.PDF. Accessed 21 Apr 2016

Gartner Inc.: What's new in Gartner's Hype Cycle for Emerging Technologies, 20 October 2015. http://www.gartner.com/smarterwithgartner/whats-new-in-gartners-hype-cycle-for-emerging-technologies-2015/. Accessed 19 Feb 2016

Grunewald, S.J.: BMW celebrates 25 years of using 3D printing technology to build cars (2015). https://3dprint.com/106539/bmw-25-years-of-3d-tech/. Accessed 26 Apr 2016

Harrison, T.P., Scott, A.: Additive manufacturing in an end-to-end supply chain setting. **2**(2), 65–77 (2015). Mary Ann Liebert Inc.

Holmström, J., Walter, M., Yrjölä, H.: Rapid manufacturing and its impact on supply chain management. In: Logistics Research Network Annual Conference, pp. 1–12 (2004)

Holmström, J., Partanen, J., Tuomi, J., Walter, M.: Rapid manufacturing in the spare parts supply chain. J. Manuf. Technol. Manag. **21**(6), 687–697 (2010)

Holmström, J., Khajavi, S.H., Partanen, J.: Additive manufacturing in the spare parts supply chain. Comput. Ind. **65**, 50–63 (2014)

Holmström, J., Partanen, J.: Digital manufacturing-driven transformations of service supply chains for complex products. Supply Chain Manag.: Int. J. **19**(4), 421–430 (2014)

Hou, L., Huang, S.H., Liu, P., Mokasdar, A., Zhou, H.: The impact of additive manufacturing in the aircraft spare parts supply chain: supply chain operation reference (scor) model based analysis. Prod. Plan. Control **25**, 1169–1181 (2014)

Johnson, J.C., Sasson, A.: The 3D printing order: variability, supercenters and supply chain reconfigurations. Int. J. Phys. Distrib. Logist. Manag. **46**(1), 82–94 (2016)

Khan, O., Christopher, M., Creazza, A.: Aligning product design with the supply chain: a case study. Supply Chain Manag.: Int. J. **17**(3), 323–336 (2012)

Kleer, R., Piller, F.T., Weller, C.: Economic implications of 3D printing: market structure models in light of additive manufacturing revisited. Int. J. Prod. Econ. **164**, 43–56 (2015)

Koslow, T.: Audi Looks to Put 3D Printed Metal End Parts into Their Autos (2015). http://3dprintingindustry.com/2015/11/13/audi-looks-to-put-3d-printed-metal-end-parts-into-their-autos/. Accessed 25 Apr 2016

Mendis, D., Reeves, P.: The current status and impact of 3D printing within the industrial sector: an analysis of six cases studies. The Intellectual Property Office Bournemouth University, pp. 1–80 (2015)

Petrovic, V., Gonzalez, J.V.H., Ferrando, O.J., Gordillo, J.D., Puchades, J.R.B., Grinan, L.P.: Additive layered manufacturing: sectors of industrial application shown through case studies. Int. J. Prod. Res. **49**(4), 1061–1079 (2011)

PR Newswire: Additive Manufacturing in the Automotive Industry: A Ten-Year Forecast (2015). http://www.prnewswire.com/news-releases/additive-manufacturing-opportunities-in-the-automotive-industry-a-ten-year-forecast-300096426.html. Accessed 25 Feb 2016

Roland Berger Strategy Consultants: Customizing Aftersales (2013). https://www.rolandberger.com/media/pdf/Roland_Berger_Customizing_aftersales_20131120.pdf. Accessed 7 Apr 2016

Selection of High-Variety Components for Selective Laser Sintering: An Industrial Case Study

Filippo Fontana(✉), Enrico Marinelli, and Mirko Meboldt

Pd|z Product Development Group Zürich, ETH Zürich, Zürich, Switzerland
`fontanaf@ethz.ch`
`http://www.pdz.ethz.ch`

Abstract. The tool-less manufacturing of lot-size one components by means of Selective Laser Sintering (SLS) can enable companies to enhance their manufacturing flexibility. Especially in the case of high variety manufacturing, companies adopting SLS can potentially reduce order lead times and manufacturing costs. This paper introduces a methodology suitable to assess different manufacturing strategies for high variety component families and leverages a case study from a global manufacturer of packaging machines to show the implications of AM adoption. The case study quantifies the reduction of both manufacturing costs and order lead time in the case of a component with a large amount of possible variants. In the case study, two possible operational strategies for the manufacturing of such with SLS are identified. In a first strategy, SLS adoption can be focused on optimising the specific volume-unit operating cost for producing all component variants, and thus obtain a total manufacturing cost reduction of up to 17% compared to the current conventional set-up. As a second strategy, SLS can be employed for the improvement of service quality. By focusing on the reduction of order lead times over the whole component family, this can be reduced by 48% compared the incumbent set-up. The trade-off among the two strategies is explained with the introduced concept of aggregated lot size.

Keywords: High-variety manufacturing · Selective Laser Sintering · Business case · Cost reduction · Service improvement

1 Introduction

Additive Manufacturing (AM) encompasses a set of production technologies allowing to create physical objects starting from digital models [1]. Selective Laser Sintering is an AM process for the production of polymeric components [2]. Compared to other AM processes, SLS shows the major advantages of not requiring support structures, and of enabling higher throughput [3]. SLS achieves very similar mechanical properties to the ones obtained by injection moulding [4,5]. For these reasons, SLS is often the AM process of choice for the production of polymeric series components [6].

© Springer International Publishing AG 2018
M. Meboldt and C. Klahn (eds.), *Industrializing Additive Manufacturing - Proceedings of Additive Manufacturing in Products and Applications - AMPA2017*,
DOI 10.1007/978-3-319-66866-6_23

AM technologies in general have seen an increased adoption in manufacturing [7]. The work [8] identifies industrial adoption of AM technologies in Aerospace, Automotive and Medical industries. The proliferation of AM technologies in the manufacturing ecosystem [7], has given rise to interest of scholars, with regard to the implications such technologies have on firms operations. The work [9] leverage a case studies approach and interviews, to show that AM can reduce the trade-off between scale and variety, in the domain of highly customised products. They furthermore conclude that, adopters of AM achieve unprecedented flexibility by producing batches of customer tailored products. In [10] the impact of SLS deployment on the aircraft spare parts supply chain is investigated. The authors identify applicability of SLS especially for the manufacturing of spare parts with low average demand. The study shows that AM adoption can reduce inventory along the entire supply chain, however effects on costs are not quantified. The work [11] presents a case study focusing on the manufacturing of an environmental control system for a military aircraft by means of SLS. The contribution identifies that, the deployment of SLS technology can lead to a simplified and less complex supply chain set-up. The same case study is further leveraged by [12] to provide quantitative insights about operating costs for AM in scenarios with a different degree of decentralization.

The manufacturing costs for AM are investigated by [13] among others. The contribution shows that the cost structure of SLS is dominated by machine costs in a first place, followed by material costs. It further defines the inverse relationship between manufacturing costs and build chamber utilization. Findings suggest that unit costs of additively producing components quickly drop and stabilize to a certain value, with increasing filling of the machine chamber. The work [14], investigates the cost structure for the manufacturing of metal parts with Selective Laser Melting (SLM). The contribution argues, that optimisation of the SLM process chain can lead to 50% reduction in manufacturing costs. AM implications in the domain of operations [15], and especially for the efficient production of spare parts have been identified by some scholars, as introduced above. Industrials also attribute vivid interest to the topic, often with strategic commitment of top managers [16]. However applications in the industry are nowadays not widespread, and positive business cases are rare. Companies are still struggling in the mainstream adoption of additive manufacturing for the manufacturing of high variety components. Few scholars address this novel field of research in a quantitative manner. This contribution addresses this gap, and investigates the improvements, that SLS can enable for companies operating in the domain of high-variety manufacturing. The authors therefore formulate the following two research questions to be answered: 1. Which specific variants of a given high-variety component should be produced with SLS? 2. What are the benefits, that SLS can offer in terms of cost and lead time reduction.

2 Methods

The present work uses a case study approach, collecting data from a global manufacturer of machines for food processing with a portfolio of around 800′000 active Stock Keeping Units (SKUs). The project team performed an heuristic component search, combining process expertise about SLS together with several key functions from the company including engineering, service and business development. While conducting the portfolio analysis, the team first set the focus on finding products with an inefficient, intricate and costly order processes, and only in a second phase evaluated technical feasibility with SLS. The component search identified lugs as the subject of the case study.

Lugs are customer specific wear components mounted on a series of roller chains, moving food units along the machine track, for packaging purposes. The lugs portfolio shows an high extent of variability. A customer specific lug variant is shown in Fig. 1. Requirements set on lugs include: resistance to wear, reduced mass, and use of food grade material. Lugs are currently made out of PA6, however tests performed by the company showed that Laser Sintered PA12 also fulfils all application requirements. Customer specific variants of lugs are engineered, depending on food processing format requirements and machine type where the component is mounted on. Data has been collected for 392 lug variants from the company ERP and PDM systems, covering a time-frame of five years from year 2011 to 2015. Collected data is introduced in Table 1.

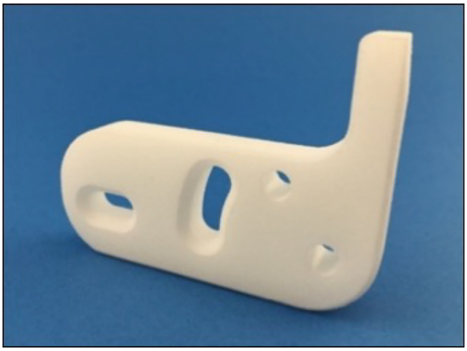

Fig. 1. Customer specific lug variant, manufactured in laser sintered PA12.

The consolidated demand of lugs has been stable over the considered five years time-frame. On average only 31 units of a given variant are produced in a given year. Considering all product variants, the average manufacturing cost per unit produced amounts to about 20 CHF. Two dimensions define the possible manufacturing set-ups for lugs: stock management policy and production site. The stock management policy is decided according to the amount of units historically sold for a given variant. Variants showing stable and relatively high demand are produced in a Make-to-Stock (MTS) configuration. In MTS, inventory is held for the variant, and customer orders are fulfilled from stock. Variants with sporadic and relatively lower sales are produced in a Make-to-Order (MTO) configuration. In MTO, the product is either manufactured from

Table 1. Variant specific data collected from company PDM and ERP information systems.

Data	Description	Unit	Descriptive statistics					
			μ	Median	σ	Min	Max	NAs
m_i	Mass of the a finished lug unit	g	21.57	20.00	14.41	3.00	211.00	5
v_i	Actual material volume of a given lug variant	cm^3	19.88	17.86	13.13	3.19	188.39	0
c_i	Manufacturing cost per unit of manufacturing one specific variant i, includes direct material costs, direct labour costs and work-center rates	CHF	25.21	21.66	13.11	2.97	75.00	0
o_i	Order or manufacturing lot-size for lugs ordered from internal or external suppliers in year 2015	Units	52.70	37.00	58.88	3.00	570.00	47
$N_{i,y}$	Amount of units of variant i produced in year y. Data collected for five years from 2011 to 2015. The descriptive statistic considers the average over five years	Units	30.11	14.00	67.68	0.20	1′034.80	0
T_i	Order-lead time for delivery of lug variant i to the company from supplier	Days	24.83	28.00	4.04	14.00	36.00	271

raw materials or adapted from a semi-finished version kept in stock, upon the issue of a customer order. Lugs manufactured from a semi-finished product are usually processed in house, whereas manufacturing of variants with no parent version is usually outsourced. When lugs share a similar geometry, the company can use common parent versions to reduce the complexity of the process chain and increase its responsiveness. In the current set-up, only 15 variants are manufactured in a MTS configuration, but these few variants account for 23% of the consolidated unit production. All other lug variants show very reduced per variant sales, and are therefore produced in a MTO configuration. Distribution of variants and units produced according to the above discussed dimensions are shown in Table 2. Currently, delivery lead time for lugs, depends on production location, supplier and stock management policy.

Table 2. Characterisation of lug portfolio according to production site and stock management policy.

	In-house	Outsourced
MTO	47 (12%)	330 (84%)
MTS	4 (1%)	11 (3%)

(a) Distribution of product variants.

	In-house	Outsourced
MTO	1’601 (14%)	7’428 (63%)
MTS	122 (1%)	2’651 (22%)

(b) Distribution of average yearly total units manufactured.

This research compares the current situation of producing the product portfolio, with other new scenarios, where SLS is introduced. The reader shall notice that these new scenarios do not necessarily imply the additive production of all lugs variants, but rather a combination of conventional and SLS manufacturing. In order to clearly distinguish variants conventionally produced from the ones manufactured with SLS, a strict notation is defined. Let us consider a lug variant i in the set of all variants considered in this study $\mathcal{L}$. For a given scenario we denote $\mathcal{C}$, where:

$$\mathcal{C} \subseteq \mathcal{L}$$

as the subset of variants produced with current manufacturing technologies, and $\mathcal{S}$ with:

$$\mathcal{S} \subseteq \mathcal{L}$$

as the subset of variants produced by means of SLS. Furthermore, we define, that in a given scenario a product variant i can only be produced either conventionally or with SLS, and therefore following statements apply.

$$\mathcal{C} \cap \mathcal{S} = \emptyset$$
$$\mathcal{C} \cup \mathcal{S} = \mathcal{L}$$

2.1 Operating Costs for Conventional Production

The authors define the total operating costs for conventionally producing variant i, in year y as:

$$\mathrm{TC}^{\mathrm{C}}_{i,y} = \mathrm{MC}^{\mathrm{C}}_{i,y} + \mathrm{OC}^{\mathrm{C}}_{i,y} + \mathrm{IC}^{\mathrm{C}}_{i,y}$$

whereas $\mathrm{MC}_{i,y}$ are total manufacturing costs, $\mathrm{OC}_{i,y}$ are total order costs and $\mathrm{IC}_{i,y}$ are total inventory costs for corresponding lug variant i in year y.

$\mathrm{MC}^{\mathrm{C}}_{i,y}$ is computationally obtained form the manufacturing cost per unit c_i and the amount of units produced $N_{i,y}$, as follows.

$$\mathrm{MC}^{\mathrm{C}}_{i,y} = c_i \cdot N_{i,y}$$

$\mathrm{OC}^{\mathrm{C}}_{i,y}$ are estimated through a per-order fee k^{C}, heuristically defined by the company. An order fee of CHF100 is applied for each order issued for outsourced components, and a fee of CHF50 is applied to each order of in-house produced variants. Hence, total order costs depend on order lot-size, total units produced, and production location.

$$\mathrm{OC}^{\mathrm{C}}_{i,y} = \frac{N_{i,y}}{o_{i,y}} \cdot k^{\mathrm{C}} \quad | \; k^{\mathrm{C}} = \begin{cases} 100\,\mathrm{CHF} \; \forall i \in \mathrm{Outsourced} \\ 50\,\mathrm{CHF} \quad \forall i \in \mathrm{In-house} \end{cases}$$

Total inventory costs are computed and apply only for MTS variants, or in the case of MTO variants with a parent version kept in stock. Computations are performed as follows:

$$\mathrm{IC}^{\mathrm{C}}_{i,y} = \overline{S}_{i,y} \cdot c_i \cdot \zeta \quad | \; \overline{S}_{i,y} = 0.75 \cdot o_{i,y}$$

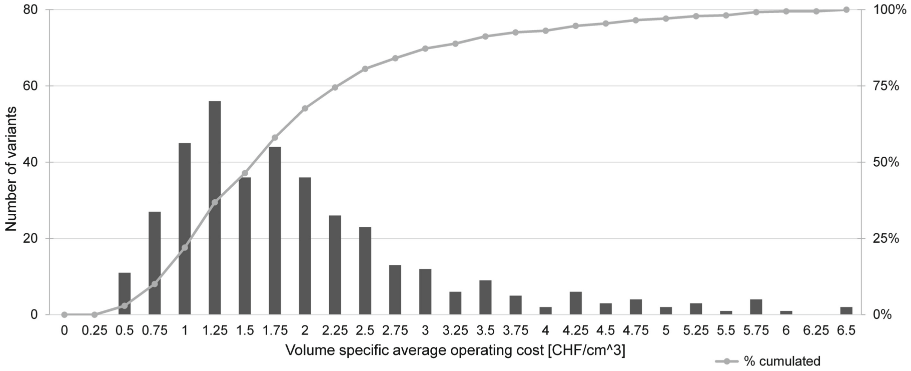

Fig. 2. Volume specific average operating cost distribution of lug variants produced conventionally.

where $\overline{S}_{i,y}$ is the average stock level and ζ is the inventory rate. The average stock level is assumed to be 75% of the order lot-size using a common order point technique [17]. This value includes a 25% safety stock. The average inventory level of a variant is consequently multiplied by the holding costs per variant. We assume an inventory rate ζ of 13% which includes a 9% capital expenses and a 4% warehousing cost. These rates have been suggested by the company, and are applied for internal financial calculations.

The average total operating costs for producing lug variant i over the considered time period can therefore be computed as follows.

$$\overline{\mathrm{TC}}_i^{\mathrm{C}} = \frac{1}{5} \sum_{y=2011}^{2015} \mathrm{TC}_{i,y}^{\mathrm{C}}$$

This value can be further divided by total amount of lugs produced during the observed time period for a given variant, and by the actual material volume of the lug variant.

$$\overline{\mathrm{tc}}_i^{\mathrm{C}} = \frac{\overline{\mathrm{TC}}_i^{\mathrm{C}}}{\overline{N}_i \cdot v_i} \quad | \ \overline{N}_i = \frac{1}{5} \sum_{y=2011}^{2015} N_{i,y}$$

The volume specific average operating costs per variant unit are therefore obtained. This value and its distribution shown in Fig. 2 can be used as a baseline for comparing the current manufacturing set-up, with other possible production scenarios based on the adoption of additive manufacturing.

2.2 Operating Costs for SLS Production

Analogously to the previous section, the authors define the average total operating costs for SLS produced variant i, as follows.

$$\overline{\mathrm{TC}}_i^{\mathrm{SLS}} = \overline{\mathrm{MC}}_{i,y}^{\mathrm{SLS}} + \overline{\mathrm{OC}}_i^{\mathrm{SLS}}$$

Inventory costs do not apply for SLS parts as these are produced in a MTO configuration only. Manufacturing costs per variant unit i in the case of SLS manufacturing $\overline{\mathrm{MC}}_i^{\mathrm{SLS}}$ assume a constant, volume specific manufacturing cost for SLS ν.

$$\overline{\mathrm{MC}}_i^{\mathrm{SLS}} = \nu \cdot v_i \cdot \overline{N}_i$$

The reason behind this assumption is that manufacturing costs with SLS do not depend on part specific geometry, but rather on how the SLS equipment is operated [13]. Order costs in the case of SLS manufacturing are differently as from the current situation. With SLS it is more convenient to consolidate small orders of different lug variants, even of lot size one, into a single manufacturing job and then release a larger order [18]. For this purpose the concept of aggregated lot size is introduced. Aggregated order lot size a is defined as the minimum amount of lugs not necessarily of the same variant, required to release a manufacturing order. The research assumes, that an order is released, as soon as this trigger value is reached. Therefore, average per year order costs for variant i can be expressed as:

$$\overline{\mathrm{OC}}_i^{\mathrm{SLS}} = \frac{\overline{N}_i}{a} \cdot k^{\mathrm{SLS}}$$

where a can be arbitrarily defined by planners. The decision on how to set a, has important implications on the overall order costs, as well as on customer order lead-time. We can define the mean maximal order lead time for SLS $\overline{T}_{\max}^{\mathrm{SLS}}$ as follows.

$$\overline{T}_{\max}^{\mathrm{SLS}} = \frac{a}{\sum_{i \in \mathcal{S}} \overline{N}_i} \cdot 365 + \mathrm{T}^{\mathrm{SLS}}$$

This value estimates the amount of time the company waits, in the worst case, when placing an order for a lug unit. The value is obtained by adding the mean time between SLS orders to the delivery lead time for SLS $\mathrm{T}^{\mathrm{SLS}}$. The formula further highlights the trade-off between cost of orders and lead-time, proportional the parameter a.

Hence, the volume specific average operating costs per variant unit are obtained for SLS produced variants as follows.

$$\overline{\mathrm{tc}}_i^{\mathrm{SLS}} = \frac{\overline{\mathrm{TC}}_i}{\overline{N}_i \cdot v_i}$$

The research considers two possible outsourcing approaches for the production of lugs with SLS: market and partnership. An in house approach has been discarded a priori, as the production of all variants in the considered portfolio with SLS, would imply an average capacity utilisation of a small industrial SLS system of 6% per year.[1] At this capacity utilisation level, operation of SLS equipment is not cost efficient.

In the SLS Market approach, the company relies on a different supplier on the marketplace for each order. Here, a per order fee of 100CHF together with

---

[1] An EOS Formiga P110 was used as a reference system for capacity utilization calculations.

Table 3. Assumptions for considered outsourcing approaches

	SLS market	SLS partnership
Order lead time $\mathrm{T}^{\mathrm{SLS}}$ [days]	5	5
Volume specific manufacturing cost ν [CHF/cm^3]	1.50	1.30
Cost per order k^{SLS} [CHF]	100	60

a volume specific manufacturing cost of 1.50CHF/cm^3 are assumed. In a partnership approach, the company commits to sourcing from a single supplier, and therefore can achieve a reduced per order fee of 60CHF as well as a reduced volume specific manufacturing cost of 1.30CHF/cm^3, thanks to higher negotiation power and consolidation of larger volumes. Assumptions for volume specific manufacturing cost are based on quotes collected from suppliers, and are in line with values proposed by [19]. All approach specific assumptions are reported in Table 3. The reported cost per order k^{SLS} relies on estimations performed together with managers from the company.

2.3 Observed Optimisation Scenarios

The research considers two optimization scenarios targeting distinct parameters. First, a cost minimizing production strategy is addressed. Here, we observe the optimal combination of variants produced conventionally, and variants produced with SLS, such that the total operating costs for offering the entire product portfolio to customers is minimal. Therefore, we define for this scenario the sets $\mathcal{C}$ and $\mathcal{S}$ as follows.

$$\mathcal{C} = \{i \in \mathcal{L} \mid \overline{\mathrm{tc}}_i^{\mathrm{C}} \leq \overline{\mathrm{tc}}_i^{SLS}\}$$
$$\mathcal{S} = \{i \in \mathcal{L} \mid \overline{\mathrm{tc}}_i^{\mathrm{C}} > \overline{\mathrm{tc}}_i^{SLS}\}$$

The research observes the effects, caused by the introduction of SLS, on the average total operating costs for managing the entire portfolio.

$$\overline{\mathrm{TC}} = \sum_{i \in \mathcal{C}} \overline{\mathrm{TC}}_i^{\mathrm{C}} + \sum_{i \in \mathcal{S}} \overline{\mathrm{TC}}_i^{\mathrm{SLS}}$$

Calculations in the cost minimisation scenario furthermore must ensure, that the company can experience at least the same order lead time as the one offered in the current production scenario. To be on the safe side, and ensure the meeting of customer demand the targeted maximal order lead time for SLS has to be lower than 21 days.

In a second scenario, the research observes the costs for improving the service quality over all lugs variants. Target is therefore, to reduce the order lead time from customer perspective, hence applying the most responsive order fulfilment combination. We therefore observe the average total operating costs for managing the entire portfolio, where all MTO variants are produced with SLS. Here,

Table 4. Implications of aggregated lot-size a on machine powder bed filling of a small SLS production system.

Lot-size a	Machine filling
26	One horizontal layer
52	Two horizontal layers
182	Half machine chamber
364	Entire machine chamber

MTS variants are still produced conventionally, as these can be delivered immediately to customer from stock. For this scenario, the sets $\mathcal{C}$ and $\mathcal{S}$ are defined as follows.

$$\mathcal{C} = \{i \in \mathcal{L} \mid sm_i = MTS\}$$
$$\mathcal{S} = \{i \in \mathcal{L} \mid sm_i = MTO\}$$

2.4 Definition of Aggregated Lot-Size

Decision about setting the aggregated lot-size a has crucial implications on the results of the case study. The choice of a not only influences directly the order costs, but must also comply with the assumptions for efficient equipment operation. For the computation of the optimization scenarios, the values presented in Table 4 apply. Predictions are based on test jobs performed on an EOS Formiga P 110.

3 Results and Discussion

Results of the calculations for the cost minimization scenario are reported in Table 5. Results show cost reductions compared to the baseline total operating costs in all computed approaches. Reductions span from a minimum of 9% up to a maximum of 19% depending on selected parameters. However, for both outsourcing approaches SLS Market and SLS Partnership, solutions related to aggregated lot-sizes of $a = 182$ and $a = 364$, show order lead-time values equal or longer than the current situation, and should therefore be discarded. An aggregated lot-size of $a = 52$ provides feasible results in both observed outsourcing scenarios. A detailed comparison of both outsourcing approaches for $a = 52$ is depicted in Fig. 3. As the figure shows, in such cost minimization scenario 46% of product variants are produced with SLS in the market outsourcing approach, and 51% of the variants are produced with SLS in the partnership outsourcing approach. In both outsourcing approaches, no MTS variant has experienced a manufacturing technology switch to SLS. This highlights an already cost effective production of MTS variants. Evidence for this is further supported by a volume specific average operating cost per MTS lug unit of $0.62 \mathrm{CHF/cm^3}$ in the current scenario. Therefore, in this particular case study, SLS is not a cost effective

Table 5. Results of calculations for the cost minimization production strategy in both outsourcing approaches.

SLS market			
Lot-size a	$\lvert\mathcal{S}\rvert$	$\overline{T}^{\text{SLS}}_{\text{max}}$	$\Delta\overline{\text{TC}}$
26	149 (40%)	10	CHF – 24′590 (09%)
52	179 (47%)	11	CHF – 30′139 (12%)
182	194 (51%)	24	CHF – 34′857 (13%)
364	200 (53%)	41	CHF – 35′865 (14%)
SLS Partnership			
Lot-size a	$\lvert\mathcal{S}\rvert$	$\overline{T}^{\text{SLS}}_{\text{max}}$	$\Delta\overline{\text{TC}}$
26	210 (56%)	8	CHF – 39′182 (15%)
52	223 (59%)	10	CHF – 43′792 (17%)
182	231 (61%)	21	CHF – 47′296 (18%)
364	232 (62%)	36	CHF – 48′016 (19%)

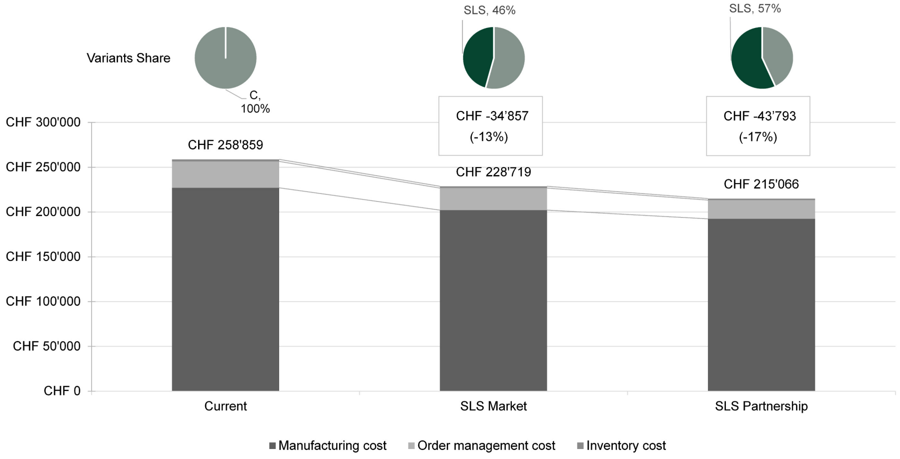

Fig. 3. Comparison of resulting total average operating costs for managing the entire lugs portfolio, in the case of an aggregated lot size $a = 52$.

substitute for MTS variants. Hence, the case study provides evidence for the fact that, components with stable, predictable and relatively high demand are optimally produced conventionally. Furthermore, calculations show, that inventory costs even in the current scenario account up to a very reduced portion of the total costs. The reduction of inventory enabled by SLS is often theorised as one of the possible major advantages of introducing this technology. However, by applying the cost structure defined earlier, the present case study shows that, inventory costs hardly have an impact on total operating costs. This low magnitude of inventory costs can be explained by the consideration of capital expenses only. The inclusion of other hidden costs such as obsolescence might have an impact on the presented figures.

Calculations furthermore show, that SLS has rather a considerable impact on reducing order management costs and manufacturing costs. Lower order costs are achieved through the effects of the aggregated orders, whereas manufacturing costs are reduced by the more variable nature of the SLS cost structure. MTO components conventionally produced show a cost structure largely dominated by fixed-costs originated in frequent equipment set-up and changeover. Such fixed costs are less pronounced in the case of SLS. Further savings from the reduction in complexity in the case of a full switch to SLS might be also of relevance. In the current scenario, lugs undergo different processing routes, and are made of different materials. The manufacturing of all lugs with SLS can reduce this complexity by having one manufacturing process and one material for all variants.

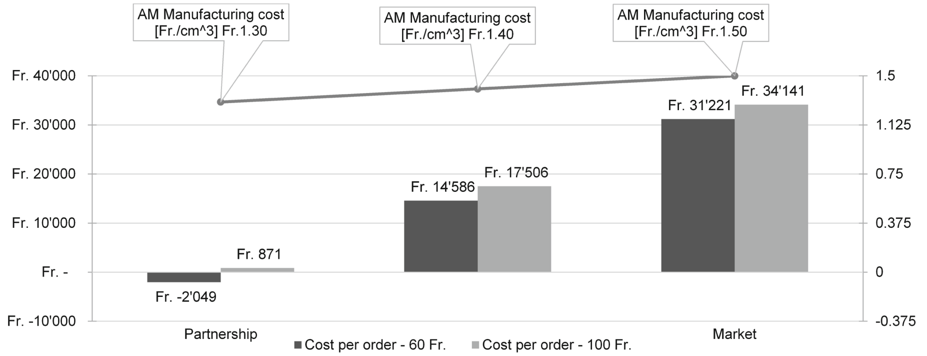

Fig. 4. Difference of total yearly average operating costs for producing the entire lug portgolio between the conventional and the SLS scenarios. Positive values imply lower costs in the conventional set-up.

Results for the service improvement scenario are reported in Fig. 4. The figure shows the difference between the total operating costs in the current scenario and the ones where all MTO lugs are produced with SLS. Varying assumptions of order fees k^{SLS} and volume specific manufacturing costs ν apply. Calculations show that, producing all MTO lugs with SLS is CHF$34'141$ more expensive than the current baseline, when applying market outsourcing assumptions. In this case, the aggregated lot size equals $a = 124$ and the maximal order lead-time is equal to 10 days. However, by considering the SLS partnership outsourcing approach, computed total costs are similar to the ones in the current baseline. Here, the same aggregated lot-size of $a = 124$ and maximal order lead-time of 10 days as above apply. This implies that, a reduction of the maximal order lead-time by 52% can be achieved when producing all MTO lugs additively under SLS partnership outsourcing assumptions, without penalties in total operating costs.

Results show that SLS can be profitably employed in manufacturing, without performing of component redesign, and without the need of owning equipment. However, the re-design of SLS produced variants according to SLS process specific optimization criteria, can further extend the cost savings and further reduce the manufacturing costs [20]. Furthermore, after performing redesign, even more variants might be eligible for manufacturing at a lower cost with SLS than in the current situation. Automation of the order process might also have an impact on reducing the order management costs. For this purpose, a solution including a web configuration portal, where customers can configure and release orders for their specific variants can be of interest. Other possibilities for reducing the order lead time could be to implement shipping of products directly from the SLS provider to the customer, without the need of transiting through the company.

4 Conclusions

The present study provides quantitative results supporting the conclusion that, SLS can enable substantial efficiency improvements for companies operating in the domain of high-variety manufacturing, even without performing component redesign.

With regard to the first proposed research question, the computation and comparison of volume specific average operating costs per variant unit, as defined in this paper, represent a sold basis to algorithmically identify component variants to be produced either with SLS or conventionally. The procedure applied in this work is directly applicable to other high variety component families.

Concerning the second research question addressed in the paper, the proposed model describes the major trade-off encountered in the case of outsourced SLS production, between total operating costs and order lead-time. The critical parameter underpinning this trade-off between time and cost is represented by the definition of the aggregated order lot size. For the specific case of lugs, the paper identifies two counter-posed operating strategies, feasible for either cost reduction or improvement of order-lead time. Calculations performed for the lugs case show that, either an operating cost reductions of 17% or an order-lead time improvement of 52% can be achieved when introducing the SLS manufacturing technology.

Limitations of the study include the fact that, the computations are performed based on the arithmetic mean of the produced units over five years. Therefore, effects of volatility in produced units and in demand are not fully captured by the model. To overcome this limitation, a more sound statistical approach is required. The case study further excludes a make approach a priori, as the conditions for efficient in-house production are not given. However, it can be of interest to capture how in-house production would affect the total costs compared to the presented outsourcing approaches. Furthermore, results are highly dependent upon the definition of the exogenous aggregated lot size a. Hidden costs of inventory are further not considered, in the presented cost structure. Further attempts to include such hidden costs of inventory management of high variety components are much required.

The lug case represent a very specific component, and the possibility to generalise results based on this example is limited. Validity, and range of improvements for other high variety components have to be further investigated. Further effects on the process chain, provided by the introduction of a web based product configuration, allowing the customers to directly order parts with custom dimensions shall be further investigated.

Despite the simplicity of the approach, the case study provides valuable insights about the influence of the most important parameters, and provide decision makers with a set of tools to compare different operating strategies.

References

1. Gibson, I., Rosen, D.W., Stucker, B.: Additive Manufacturing Technologies: Rapid Prototyping to Direct Digital Manufacturing. Springer, Boston (2010)
2. Schmid, M.: Selektives Lasersintern (SLS). In: Additive Fertigung mit Selektivem Lasersintern (SLS), pp. 9–28. Springer (2015)
3. Petrovic, V., Vicente Haro Gonzalez, J., Jordá Ferrando, O., Delgado Gordillo, J., Ramón Blasco Puchades, J., Portolés Portolés Griñan, L.: Additive layered manufacturing: sectors of industrial application shown through case studies. Int. J. Prod. Res. **49**(4), 1061–1079 (2011)
4. Goodridge, R.D., Tuck, C.J., Hague, R.J.M.: Laser sintering of polyamides and other polymers. Prog. Mater. Sci. **57**(2), 229–267 (2012)
5. Wong, K.V., Hernandez, A.: A review of additive manufacturing. ISRN Mech. Eng. **2012**, 1–10 (2012)
6. Meboldt, M., Fontana, F.: Additive Fertigung in der industriellen Serienproduktion: Ein Statusreport. Technical report (2016)
7. Wohlers Associates: Wohlers Report 2013 (2013)
8. Campbell, I., Bourell, D., Gibson, I.: Additive manufacturing: rapid prototyping comes of age. Rapid Prototyp. J. **18**(4), 255–258 (2012)
9. Oettmeier, K., Hofmann, E.: Impact of additive manufacturing technology adoption on supply chain management processes and components. J. Manuf. Technol. Manag. **27**(7) (2016)
10. Liu, P., Huang, S.H., Mokasdar, A., Zhou, H., Hou, L.: The impact of additive manufacturing in the aircraft spare parts supply chain: supply chain operation reference (scor) model based analysis. Prod. Plann. Control **25**(13–14), 1169–1181 (2014)
11. Holmström, J., Partanen, J., Tuomi, J., Walter, M.: Rapid manufacturing in the spare parts supply chain. J. Manuf. Technol. Manag. 21(No.6), 687–697 (2010)
12. Khajavi, S.H., Partanen, J., Holmström, J.: Additive manufacturing in the spare parts supply chain. Comput. Ind. **65**(1), 50–63 (2014)
13. Ruffo, M., Hague, R., Tuck, C.: Cost estimation for rapid manufacturing - laser sintering production for low to medium volumes. Proc. Inst. Mech. Eng. Part B: J. Eng. Manuf. **220**(9), 1417–1427 (2006)
14. Lindemann, C., Jahnke, U., Moi, M., Koch, R.: Analyzing product lifecycle costs for a better understanding of cost drivers in additive manufacturing. Int. Solid Freeform Fab. Symp. **23**, 177–188 (2012)
15. Tuck, C., Hague, R., Burns, N.: Rapid manufacturing: impact on supply chain methodologies and practice. Int. J. Serv. Oper. Manag. **3**(1), 1–22 (2006)

16. Cohen, D.L.: Fostering mainstream adoption of industrial 3D printing: Understanding the benefits and promoting organizational readiness. 3D Printing Addit. Manuf. 1(2), 62–69 (Jan 2014)
17. Schönsleben, P.: Integral logistics management: operations and supply chain management within and across companies. CRC Press (2016)
18. Ruffo, M., Hague, R.: Cost estimation for rapid manufacturing's simultaneous production of mixed components using laser sintering. Proc. Inst. Mech. Eng. Part B: J. Eng. Manuf. **221**(11), 1585–1591 (2007)
19. Baldinger, M., Levy, G., Schönsleben, P., Wandfluh, M.: Additive manufacturing cost estimation for buy scenarios. Rapid Prototyp. J. 22(6) (2016)
20. Atzeni, E., Iuliano, L., Minetola, P., Salmi, A.: Redesign and cost estimation of rapid manufactured plastic parts. Rapid Prototyp. J. **16**(5), 308–317 (2010)

Process Setup for Manufacturing of a Pump Impeller by Selective Laser Melting

Marc Huber[1], Jonas Ess[1], Martin Hartmann[1], Andreas Würms[1,2],
Robin Rettberg[2], Thomas Kränzler[2], and Kaspar Löffel[1](✉)

[1] University of Applied Sciences and Arts Northwestern Switzerland,
5210 Windisch, Switzerland
{marc.huber, jonas.ess, martin.hartmann,
kaspar.loeffel}@fhnw.ch
[2] Sulzer Management Ltd., Pumps Equipment, 8401 Winterthur, Switzerland
{robin.rettberg, thomas.kraenzler}@sulzer.com

Abstract. In the water industry a strong market demand exists for small, high pressure pump systems. However, the casting of impellers for such small pumps in the required quality is difficult or impossible because of their low wall thickness and their unfavorable ratio of impeller diameter to channel height. Selective Laser Melting (SLM), one of the primary metal additive manufacturing technologies, is well-suited to be used for such impellers as the full potential of SLM can be achieved best with such small, complex parts. In this work, we describe the SLM manufacturing of an already existing impeller design at the lower limit of castability. This is motivated by the fact that if this geometry can successfully be SLM-manufactured, there should be no major obstacle for a scale-down to smaller sizes (up to a certain limit), but this SLM-manufactured existing impeller design can be tested on an already existing pump prototype and directly compared to the cast counterpart. The effort described here therefore was to find the optimal orientation of build direction as well as to design suitable support structures. This was done in a heuristic and iterative process with concurrent manufacturing trials. The final SLM-processed prototype impeller fulfilled all geometrical requirements and will be tested in the existing prototype pump in the near future. While the full potential of SLM manufacturing is reached by fundamental part redesigns, the process setup (build orientation optimization and support structure design) for a pre-existing part geometry as performed here is of large practical importance in the service and reconditioning market in the water industry and beyond.

1 Introduction

Starting with the patent by Meiners and co-workers [1] in 1996, there has been a steadily growing interest in the powder-bed additive manufacturing process of Selective Laser Melting (SLM). Over the last decade, industrial applications in different fields have undergone the process from research effort to full-scale serial production [2]. Most prominent among these fields are the biomedical, tool-making, aerospace, and power generation industries (cf., e.g., Yap et al. [3] and references therein).

© Springer International Publishing AG 2018
M. Meboldt and C. Klahn (eds.), *Industrializing Additive Manufacturing - Proceedings of Additive Manufacturing in Products and Applications - AMPA2017*,
DOI 10.1007/978-3-319-66866-6_24

Chief benefit of the SLM technology is that it enables a dramatic size increase of the design space for a given product, meaning that SLM is capable of producing parts that are not manufacturable through any other technology [4]. Furthermore it allows for lead time reduction because no tooling is required. In the pumps industry, pump impellers are complex parts that have long caused manufacturing difficulties [5]. Moreover, there is a size limit below which impellers are not manufacturable anymore at all since the most suited conventional manufacturing method, investment casting, cannot handle the complex 3D geometry at very small scales. There is, however, a large market demand for small, high-pressure pumps - and accordingly, small impellers (below an outer diameter of roughly 100 mm). This makes them a suited target for SLM manufacturing.

For SLM, the situation regarding (impeller) part size is effectively reversed as compared to investment casting. The smaller a part is, the simpler it is to manufacture by SLM (up to a certain limit on the order of SLM manufacturing accuracy of around 0.1 mm). This is because of the main SLM manufacturing constraint, which is the necessity to add support structures to overhang geometries forming an angle of typically less than about 45° with the horizontal [6]. These supports are not needed however if the extent of the overhang is small enough. Thus if scaled down suitably, a given geometry can be SLM-processed without supports even though its scaled-up counterpart cannot.

Because of the above considerations, in this work we describe the manufacturing of a pump impeller by SLM whose size is at the lower limit of castability[1]. We do this with the reasoning that if we can produce this impeller size, there should be no major obstacle to scale it down to smaller sizes. At the same time, the impeller so produced can directly be compared to its cast counterpart in terms of its features and performance. For this endeavor, we choose an already existing impeller geometry, allowing this direct comparison with the cast part also in a full-engine test. The effort therefore lies entirely in finding optimal part orientation, designing the support structure, as well as determining the adequate post-SLM machining steps to obtain the desired geometry. In this work, we describe our heuristic and iterative design process through which we were able to produce the desired impeller with suitable accuracy. While there have been some efforts in the past to manufacture a pump impeller by additive manufacturing via the fused deposition method using polymeric material [9, 10], to our knowledge there exists thus far no documented attempt in the literature toward an SLM processed pump impeller.

We further point out the following: while the potential of SLM manufacturing is greatest if one can come up with an entirely new design that makes use of all design possibilities enabled by SLM, the development of a new design is not possible if a conventionally-produced part shall be produced again by SLM (e.g. as spare part due to shorter lead time). There is thus considerable practical interest in the type of procedure described herein where the SLM support structure for a pre-existing geometry is designed and optimized.

---

[1] The other existing powder bed Additive Manufacturing technique of Electron Beam Melting (EBM) would equally be a possible choice for manufacturing the impeller. SLM and EBM each have their advantages and drawbacks (see, e.g., Niendorf et al. [7] and references therein). In this work we make use of SLM due to its advantage in surface quality as opposed to EBM [8].

2 Impeller Geometry

The part under consideration is a radial impeller with an outside diameter of 92.4 mm and a height of 46 mm; see Figs. 1 and 2. Final machining by milling and turning is possible on all outer surfaces and the shaft bore, however not in the impeller channels. In operation the fluid flows axially into the impeller channels (between hub and cover disk). Due to the rotating blades, the fluid is redirected and finally ejected radially with an increased relative pressure.

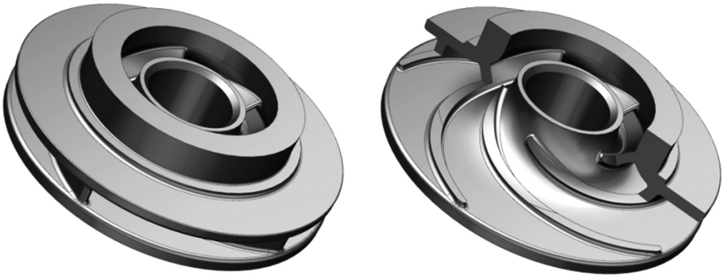

Fig. 1. Investigated impeller geometry.

3 Optimization of Build Direction

In order to determine a suitable orientation of the impeller in the build chamber of the SLM machine, all surfaces of the impeller were first analyzed and divided up into three categories:

A. support removal easily feasible
B. support removal requiring effort but certainly possible
C. support removal difficult or impossible.

These three categories are depicted in Fig. 3. Next, two angles, α and β, were introduced specifying part orientation. α and β stand for rotations about the local (part-specific) x- and z-axis, respectively; see Fig. 4. The range of α and β is 0–72° and 0–180°, respectively, due to cyclic symmetry of the impeller.

Apart from the blades the impeller is completely axisymmetric. The angle α thus has no influence on the orientation of the hub and cover disk regions of the impeller (cf. Fig. 2). It was therefore decided to first examine different angles β and their consequence for necessary support structures of type C on hub and disk, while disregarding necessary support for the blades. The blade support areas could then be optimized via the angle α after finding a suitable β.

Downskin angles (angle between the horizontal plane and a downskin surface, lying between 0° for a horizontal downskin plane and 90° for a vertical plane; cf. the recent VDI norm on Additive Manufacturing [11]) between 0° and 45° were deemed to

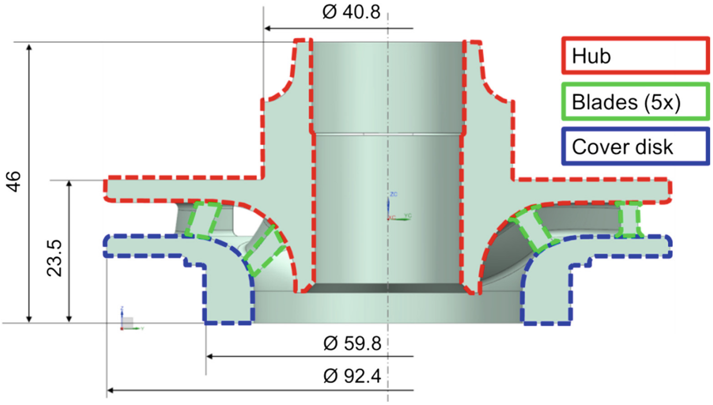
Ø 40.8
Hub
Blades (5x)
Cover disk
46
23.5
Ø 59.8
Ø 92.4

Fig. 2. Impeller nomenclature and main dimensions in mm.

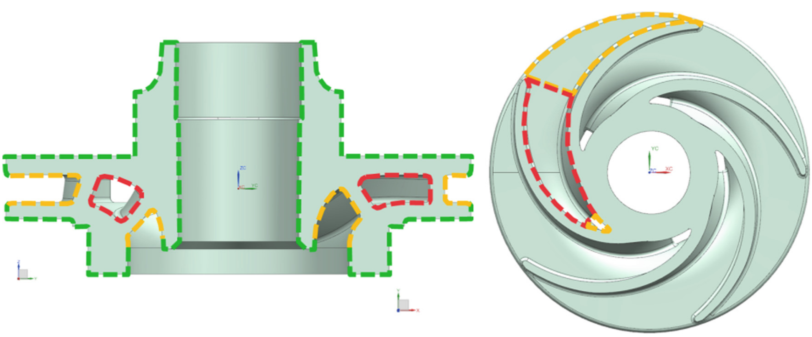

Fig. 3. Surface categorization. Support removal easy: A (green); support removal possible: B (yellow); support removal difficult or impossible: C (red).

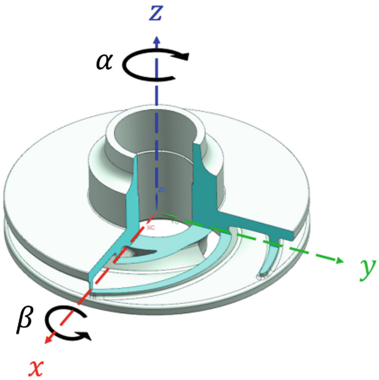

Fig. 4. Definition of orientation parameters α and β.

need supports as mentioned above. In the CAD suite Siemens NX 10.0, downskin angles of surfaces can be suitably visualized.

As evident from Fig. 5, the orientations β = 0° and β = 180° both produce large areas on the hub and cover disk needing supports of type C. Effectively, as β is increased from 0° and beyond 45°, the hub and cover disk areas needing support gradually decrease as shown in Fig. 6. They reach a minimum at β = 90° and then increase again. An angle β of close to 90° thus seems suitable.

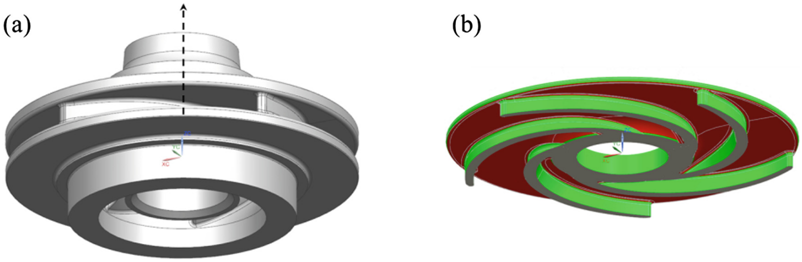

Fig. 5. (a) Impeller for β = 0° and α arbitrary (dashed arrow: build-up direction). (b) Horizontal cut through the blades showing large areas needing support in dark red (green: no support necessary).

Next, for angles β close to 90°, the angle α was examined revealing that the C supports on the blades increase strongly as β approaches 90°. β = 80° was therefore chosen as a first orientation.

Varying α for this β showed that the amount of necessary C supports on the blades is only weakly coupled to α. Minimum C supports are reached for α around 10°, leading to α = 10° as second orientation parameter[2].

We point out that this choice of the two parameters also keeps reasonable the maximum molten cross section in a single layer.

4 Support Design Iteration 1

After the optimal build orientation was determined, a first support structure design was carried out. This was done entirely in the commercial software Materialise Magics 20.0. We generally put supports in all areas with an overhang angle (angle between surface and the horizontal plane) of less than 45°. For all areas accessible with a chisel and lathe, we chose simple block supports as shown in Fig. 7. For the areas not accessible this way, lying mainly between the blades, gusset supports were used as shown in Fig. 8. (Note that both block and gusset supports consist of single laser melt tracks.)

---

[2] We note that instead of our manual approach chosen here, optimization of build orientation can also be performed in commercial programs such as, e.g. Materialise Magics 20.0. However, easy-to-reach surfaces, where support structure removal does not pose a problem, cannot be excluded from the optimization.

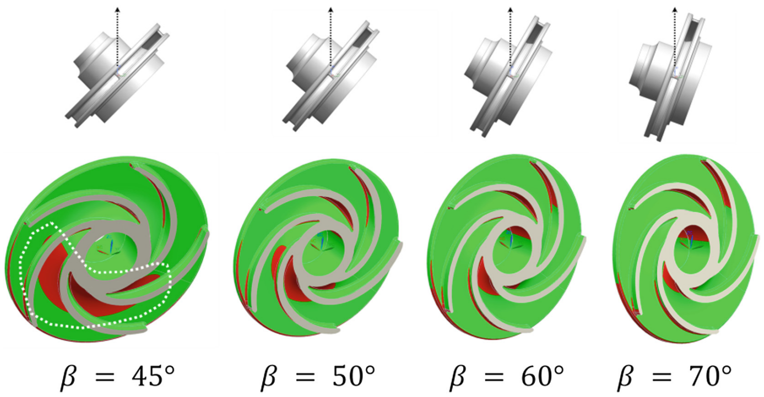

Fig. 6. Analysis of impeller for β between 45° and 70° (red: areas needing support; green: no support necessary). It can be seen that the boomerang-shaped red area (encircled with a dashed line for β = 45°) decreases as β increases.

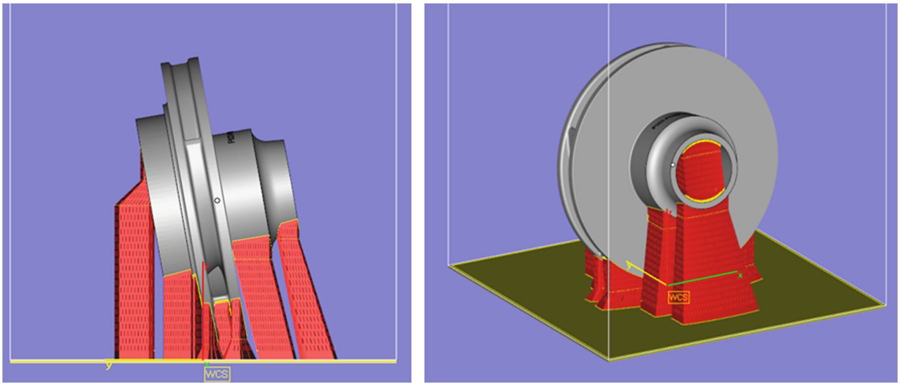

Fig. 7. Block supports in support design iteration 1.

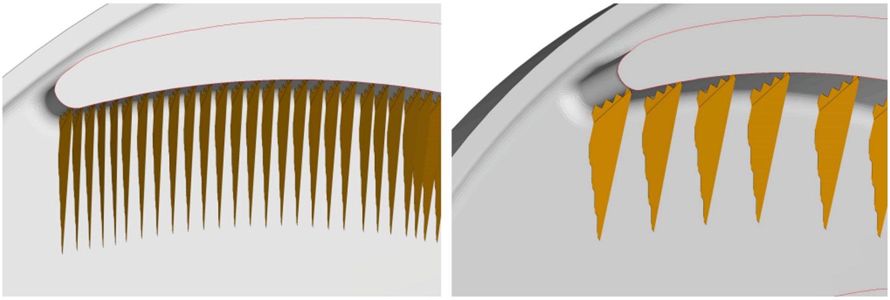

Fig. 8. Gusset supports in support design iteration 1 (on the right, only every fourth gusset is shown for illustration).

A manufacturing trial was performed for the first support design iteration. The target material for the impeller is the nickel-base superalloy IN625; however, the manufacturing trial was performed with a stainless steel of inferior strength than IN625 due to short-term powder unavailability. For this manufacturing trial as well as all manufacturing further discussed in this work, an SLM machine of type Realizer SLM125 was used.

In Fig. 9 the result of the manufacturing trial is depicted. It is clearly visible that the block supports macroscopically cracked in several locations. The reason for the cracks in the supports is the insufficient strength of the supports to "tie down" the massive impeller to the substrate plate, as well as their insufficient ability to conduct heat away from the part being built. This cracking rendered the built part unusable due to excessive part distortion resulting from the supports losing their function. An example of such distortion is the lower hub region of the impeller that is shown in detail on the right in Fig. 9.

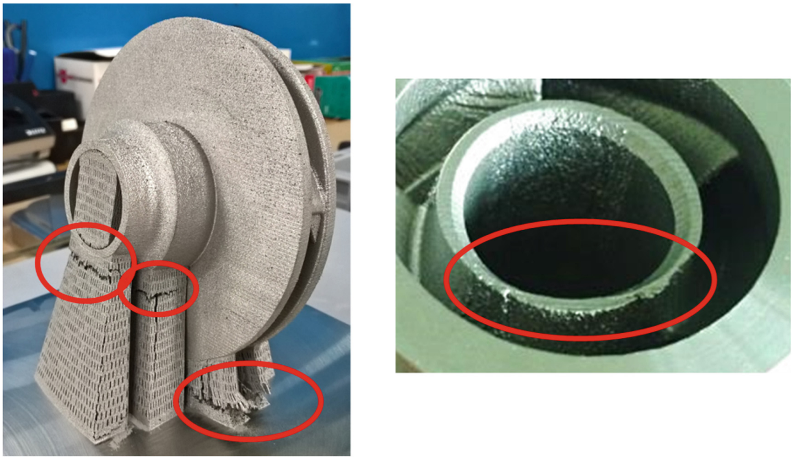

Fig. 9. Manufacturing trial of the first support design iteration. Left: on the substrate plate after SLM, showing large-scale cracking in several areas. Right: after support removal (and post-machining trial), showing severe geometric irregularity in the lower part of the hub.

Removal of the part from the substrate plate was performed with a band saw. The block supports were then broken off with hammer and chisel, while the gussets were successfully removed by shot peening. The part was subsequently used for a trial of the post-machining steps on the lathe.

5 Support Design Iteration 2

Due to the widespread cracking observed in the first manufacturing trial, the support design strategy was subsequently altered. For the second support design iteration, the cracked block supports were replaced by supports created in the native CAD program

Siemens NX 10.0. These new supports are beams as shown in Fig. 10, possessing higher strength and allowing greater heat flux away from the processing zone than in the earlier support design[3]. Their rectangular cross sections have more massive dimensions between 1.5 and 12 mm and are hence termed volume supports. Further, as mentioned before, the angle α only very weakly influences the amount of necessary supports. In order to provide as much local strength as possible in the regions where volume supports are connected to the impeller, the α angle was therefore changed to α = 54°.

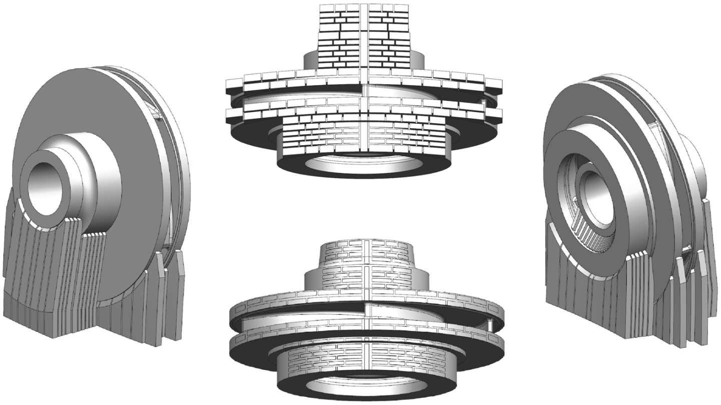

Fig. 10. Volume supports connecting the impeller to the substrate plate in support design iteration 2.

For the lower hub region, volume supports were used too. They are shown in Fig. 11.

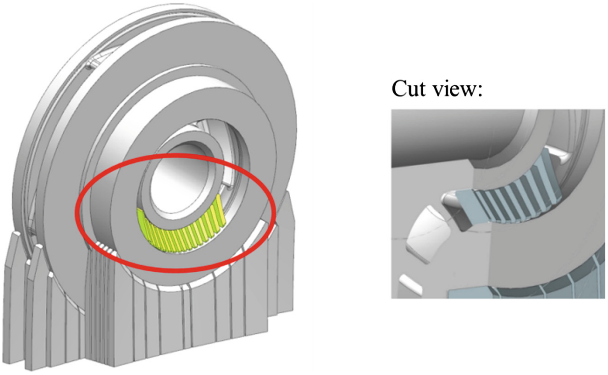

Fig. 11. Volume supports for hub region in support design iteration 2.

---

[3] In SLM, pre-heating of the substrate plate decreases the temperature gradient across the part being built, and hence also decreases thermal stresses. An equally possible strategy for crack mitigation would therefore be to increase substrate pre-heating. In our specific case, however, the pre-heating was already set to its maximum of 200 °C and thus did not allow pursuing this strategy.

A manufacturing trial was then performed in IN625. The result of the trial is shown in Fig. 12. The cracking earlier observed was successfully suppressed. The lower hub region shown in Fig. 13, too, showed clear improvement. The gusset supports, however, were not all successfully removed by shot peening due to the superior strength of IN625 used in this case. For the subsequent prototype manufacturing it was thus decided to attempt the manufacturing with no gussets at all (except single ones at the very ends of two blades), owing to the rather small typical channel widths of around 5 mm.

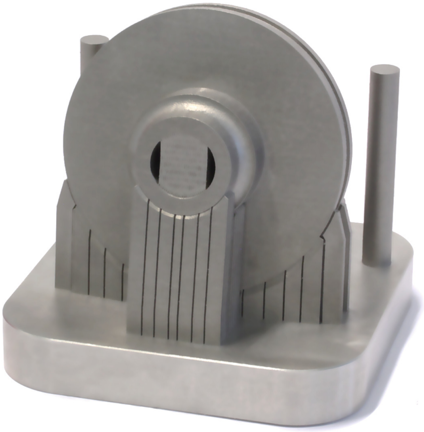

Fig. 12. Manufacturing trial of the second support design iteration on the substrate plate after SLM (tensile specimens also visible).

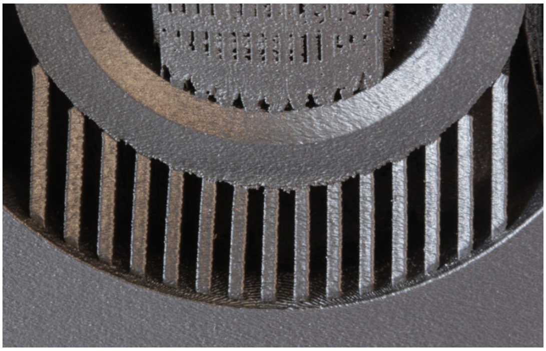

Fig. 13. Manufacturing trial of the second support design iteration: volume supports in the hub region showing clearly improved lower hub geometry.

Regarding the lower hub region, due to the remnants of the volume supports after their removal, this area needed to be post machined on the lathe. Apart from being an additional post-SLM process step, a consequence of this was also the creation of a sharp transition between machined and unmachined surfaces in the waterways that is deemed hydraulically unfavorable. For the prototype a further support modification in this region was therefore decided upon.

6 Prototype Design and Manufacturing

The final prototype design was largely the same as the one of the second support design iteration except for the hub region. There, the volume supports were modified as shown in Fig. 14. Both ends of these volume supports lie on machining stock material; thus any remaining support stub is machined away automatically. Behind these volume supports, only thin line supports are needed (width of one laser melt track) that can be removed without any remainders, thus eliminating the need for post-machining in the waterways.

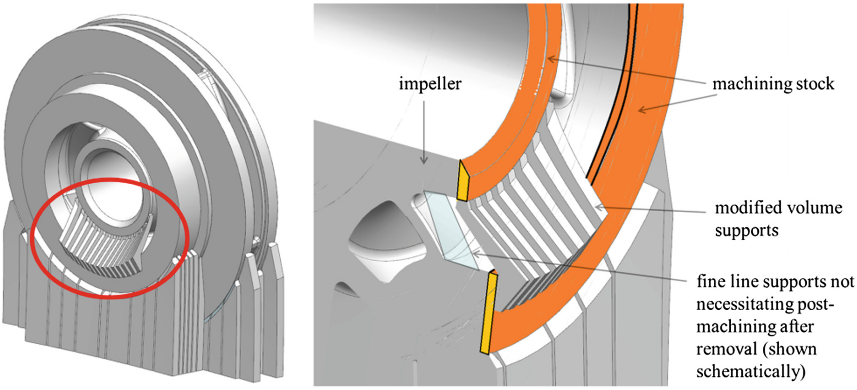
impeller
machining stock
modified volume supports
fine line supports not necessitating post-machining after removal (shown schematically)

Fig. 14. Modified volume supports in the hub region for prototype.

The prototype was manufactured by SLM in IN625. The result is shown in Fig. 15. The manufacturing of the waterways without gusset support proved successful. No cracks were visible, and the modified supports in the hub region also served their purpose as intended.

The prototype was subsequently removed from the substrate, supports were removed, a stress-relief heat treatment was performed, and post-SLM machining followed.

A detailed 3D scan performed with a 3D scanner (type GOM ATOS III Rev. 02) revealed that geometric accuracy of the prototype lies within ±0.2 mm, satisfying the requirements for full-engine testing scheduled in the near future.

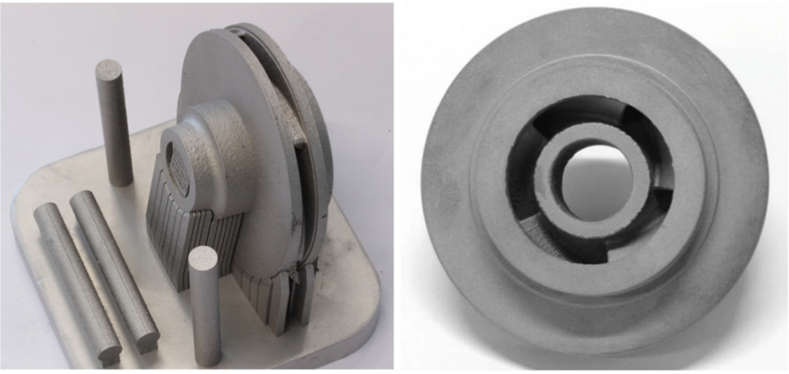

Fig. 15. Left: prototype on the substrate plate after SLM (tensile specimens also visible). Right: prototype after all post-SLM processing steps.

7 Conclusion and Outlook

In this work we demonstrated a process setup to manufacture a pump impeller via SLM. The process setup comprised (a) finding the optimal build direction as well as (b) designing suitable support structures in a heuristic and iterative approach.

First, all impeller surfaces were analyzed and categorized according to the degree of difficulty to remove possible support structures thereon. Possible impeller orientations were considered via two angular parameters and a suitable build direction was chosen. Subsequently, support structures were designed in the commercial software Materialise Magics 20.0. A manufacturing trial, however, showed severe support cracking and part deformation. Therefore a second support design was elaborated with more massive supports designed directly in the native CAD program Siemens NX 10.0. The corresponding manufacturing trial confirmed elimination of the cracking earlier observed. Finally, a prototype was successfully manufactured which fulfilled all geometric requirements. This prototype impeller will be tested in a prototype pump in the near future.

Since a scale-down of size typically increases SLM manufacturability due to small overhang areas being able to support themselves, the successful prototype production implies a large potential for SLM production of impellers of smaller size in the future.

Finally, we point out that the effort documented herein was focused on an existing impeller design in order to be able to test the impeller prototype in an existing pump system prototype. While the full potential is typically reached by fundamental part redesigns unlike done here, the SLM process setup for an existing geometry as described here is of large practical importance in the service and reconditioning market in the water industry and beyond.

Acknowledgment. This work was financially supported by the Commission for Technology and Innovation (CTI).

References

1. Meiners, W., Wissenbach, K., Gasser, A.: Selective laser sintering at melting temperature. US6215093 (B1) (1996)
2. Petrovic, V., Haro Gonzalez, J.V., Jorda Ferrando, O., Delgado Gordillo, J., Blasco Puchades, J.R., Portoles Grinan, L.: Additive layered manufacturing: sectors of industrial application shown through case studies. Int. J. Prod. Res. **49**(4), 1061–1079 (2011)
3. Yap, C.Y., et al.: Review of selective laser melting: Materials and applications. Appl. Phys. Rev. **2**(4), 041101 (2015)
4. Herzog, D., Seyda, V., Wycisk, E., Emmelmann, C.: Additive manufacturing of metals. Acta Mater. **117**, 371–392 (2016)
5. Sulzer Pumps Ltd. (ed.): Sulzer Centrifugal Pump Handbook. Elsevier Science Publishers Ltd., Essex (1989)
6. Introduction to Additive Manufacturing Technology. European Powder Metallurgy Association (2015)
7. Niendorf, T., et al.: Functionally graded alloys obtained by additive manufacturing. Adv. Eng. Mater. **16**(7), 857–861 (2014)
8. Frazier, W.E.: Metal additive manufacturing: a review. J. Mater. Eng. Perform. **23**(6), 1917–1928 (2014)
9. Quail, F.J., Scanlon, T., Strickland, M.: Development of a regenerative pump impeller using rapid manufacturing techniques. Rapid Prototyp. J. **16**(5), 337–344 (2010)
10. Fernandez, S., Jimenez, M., Porras, J., Romero, L., Espinosa, M.M., Dominguez, M.: Additive manufacturing and performance of functional hydraulic pump impellers in fused deposition modeling technology. J. Mech. Des. **138**(2), 024501 (2016)
11. Verein Deutscher Ingenieure (ed.): VDI-Richtlinie 3405: Additive Fertigungsverfahren - Grundlagen, Begriffe, Verfahrensbeschreibungen. Düsseldorf: VDI-Gesellschaft Produktion und Logistik (2014)

Hybrid Integration; Case Study with Sun Sensor for Cube Satellites

Nenad Marjanović[1](✉), Jérémy Disser[1], Frédéric Zanella[1],
Jürg Schleuniger[1], Alessandro Mustaccio[1], Rolando Ferrini[1],
Marc Schnieper[1], and Eyad Assaf[2]

[1] CSEM SA, Tramstrasse 99, 4132 Muttenz, Switzerland
`{nenad.marjanovic,jeremy.disser,frederic.zanella,`
`juerg.schleuniger,alessandro.mustaccio,`
`rolando.ferrini,marc.schnieper}@csem.ch`
[2] HIGHTEC MC AG, Fabrikstrasse 9, 5600 Lenzburg, Switzerland
`eyad.assaf@hightec.ch`

Abstract. An innovative electronic system assembly approach, i.e. hybrid integration combining printed electronic components with/on Flexible Circuit Boards (FCBs) equipped with conventional Surface-Mounted components (SMDs) was implemented in order to realize a sun sensor. Technology-wise, a clear benefit was achieved from the combination of the advantages of both large area printed electronics based on printing processes (e.g. flexibility, light weight, cost effectiveness, etc.) and SMDs with high-end functionalities and robustness. Printed electronics uses additive deposition methods similar to conventional press printing – such as inkjet printing, screen printing, gravure printing, etc. – applying a stack of layers on flexible substrates. By depositing electrically active layers (e.g. conductors, semiconductors and insulators), basic electronic building blocks such as resistors, capacitors, thin film transistors, etc. can be made. On the other hand, FCBs are commonly used where flexibility, space savings, or production constraints limit the use of rigid PCBs. Typically, conventional photolithography and standard SMD integration are combined to realize FCBs. A hybrid sun sensor was demonstrated within the Swiss Space Office funded project hybSat (2014–2016), by HIGHTEC and CSEM. The developed sun sensor comprises inkjet printed organic photodiodes (OPDs), printed resistors, printed capacitors, high-end SMDs and operational amplifiers on a FCB. The fabricated flexible sun sensor is suitable for cube satellites since it is extremely thin, light weight and cost effective. The exampled hybrid technology offers new possibilities to the system designers (towards smart PCBs), material providers (printable functional inks) and extends the current range of products (e.g. wearable, flexible electronics).

Keywords: Printed photo diodes · Hybrid integration · Sun sensor · Cube satellites · Printed electronics

1 Introduction

An innovative electronic system assembly approach, i.e. hybrid integration combines printed electronic components with/on Flexible Circuit Boards (FCBs) equipped with conventional Surface-Mounted components (SMDs). Technology-wise, a clear benefit

© Springer International Publishing AG 2018
M. Meboldt and C. Klahn (eds.), *Industrializing Additive Manufacturing - Proceedings of Additive Manufacturing in Products and Applications - AMPA2017*,
DOI 10.1007/978-3-319-66866-6_25

was derived from the combination of the advantages of both large area printed electronics based on solution processes (e.g. flexibility, light weight, cost effectiveness, etc.) and SMDs with high-end functionalities and robustness. On the one hand, printed electronics uses additive deposition methods similar to conventional press printing – such as inkjet printing, screen printing, gravure printing, etc. – applying a stack of functional ink layers on flexible (lightweight) substrates. By depositing electrically active layers (e.g. conductors, semiconductors and insulators), basic electronic building blocks (such as resistors, capacitors, thin film transistors, invertors, etc.) can be made. At CSEM, the above-mentioned printed building blocks are already demonstrated through their application in smart FCBs by integrating them in a high-pass audio filter [1] or on the recently developed printed pressure sensor embedded in collaboration robots [2]. On the other hand, FCBs are established products, commonly used where flexibility, space savings, or production constraints limit the use of rigid PCBs. Typically, conventional photolithography and standard SMD integration are combined to realize FCBs. Their fabrication may also involve some printing technologies, such as screen printing for very simple device components or functionalities (e.g. connectors). The current trend in the domain is to introduce more added functionalities into FCBs, such as printed large area sensors, energy harvesting elements, etc.

Within the Swiss Space Office funded project hybSat (2014–2016), HIGHTEC and CSEM have developed a hybrid sun sensor comprising inkjet printed organic photodiodes (OPDs), printed resistors, printed capacitors, high-end SMDs and integrated circuits (operational amplifiers) on a FCB. The fabricated flexible sun sensor is suitable for cube satellites since it is extremely thin and light weight.

Generally speaking a wide range of smart flexible FCB-based products as such (smart FCB) are expected out of this hybrid technology such as: health monitoring sensors (heartbeat, temperature sensors, etc.), environment monitoring sensors (pressure, irradiation, etc.), etc.

2 Sun Sensor Fabrication, Characterization and Validation

2.1 Quad Cell Approach

A sun sensor is a device that senses the direction and measures the position of the sun (or another light source) with respect to the sensor position. The working principle of a realized sun sensor is the following: light reaches the sensor through a thin slit on top of a rectangular chamber, whose bottom part is aligned with a group of light-sensitive cells. They convert the incoming photons into electrons and hence a current (analog signal) is generated which is amplified and converted to a digital signal. When two (or four) sensors are placed perpendicular to each other, i.e. quad cell sensing approach, the direction of the sun/light source with respect to the reference of the sensor axis can be determined, see Fig. 1.

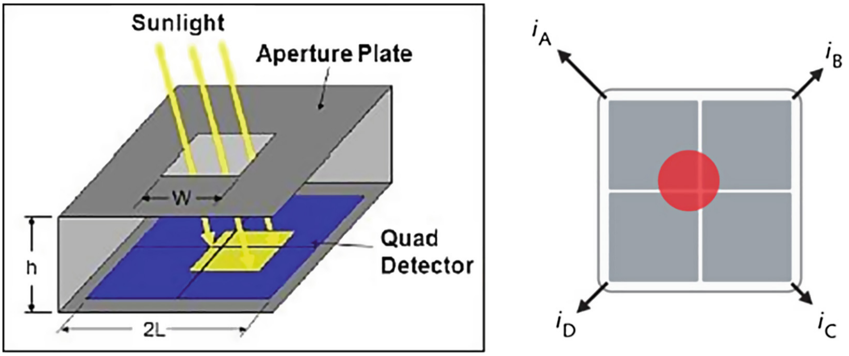

Fig. 1. Quad cell approach (left hand side: image credit: the aerospace corporation) and red spot mimicking light source for visualization reason (right hand side: image credit: A. Cordes and A. Davidson, Detectors: CMOS cameras allow robust active stabilization of laser beams)

Finally the electronics part calculates the position/angle of the sun/light source. The light source position is then calculated using (1):

$$X = \frac{(i_A + i_D) - (i_B + i_C)}{\mathrm{i}_A + i_B + i_c + i_D}\ Y = \frac{(i_A + i_B) - (i_D + i_C)}{\mathrm{i}_A + i_B + i_c + i_D} \tag{1}$$

For example, this approach is followed by Moog Bradford in their Mini Fine Sun Sensor [3]. According to the datasheet of this particular product, the detector active element is made of p-type epitaxial silicon. Common sun sensors e.g. CMOS [4–6], MEMS [7], CCD [8] or photodiodes [9, 10] are indeed produced using processes requiring all silicon industry production facilities such as vacuum, ion implantation (p-type wafer). On the other hand the active material of the proposed hybrid sun sensor is deposited in ambient atmosphere by a digital additive printing process on a flexible substrate. The geometry of the active part can thus be tuned by updating the layout file i.e. omitting masks. The absorbance of the printed active material can be additionally tuned by changing the active material without affecting the process flow. Last but not least the substrate of the hybrid sun sensor can be replaced to fulfil the product requirements.

2.2 Printed Components Fabrication and Characterization

Stand-alone passive and active sun sensor's components such as resistors and OPDs were printed by CSEM on HIGHTEC's pre-patterned polyimide (PI) substrates and characterized. The measured ranges of resistances and photocurrents were used to size the preliminary front-end circuit on standard Printed Circuit Board (PCB). The temperature dependence of the printed resistors was also characterized in order to evaluate the possibility of making a printed thermistor for the demonstrator.

Concerning printed resistors, several different materials based on Poly (3, 4-ethylenedioxythiophene) polystyrene sulfonates (PEDOT:PSS) have been tested on Al pre-patterned PI substrates. Inkjet printed resistors were characterized and assessed with respect to the operating life time, Fig. 3. It shows that with one single conductive ink, several resistance values can be obtained by varying either the geometrical design or the layer thickness/material density (through the variation of the dot spacing). The lowest resistance could withstand 30 mA under 5 V without changes within the measured timeframe (days). The obtained sheet resistances are comprised between 86 Ω/□ and 290 Ω/□.

An aluminium oxide precursor ink was tested as dielectric material candidate for printed capacitors (Fig. 3). The fabrication of the capacitors was performed combining printing techniques (blade and spin coating) to deposit the dielectric film on HIGHTEC pre-patterned PI substrates and photonic sintering to functionalize the dielectric film. CSEM's photonic sintering tool (Novacentrix PF1300) was used to sinter properly the aluminium oxide precursor instead of thermal annealing. Finally working capacitors were obtained, but at low yield and reliability. According to the final demonstrator design the targeted capacitance was fixed to 1 µF. From the obtained results (22.5 nF/cm^2 up to 100 kHz), the capacitor footprint required to achieve the targeted capacitance is 6.7 × 6.7 cm^2 at this dielectric thickness or less by further thinning down the dielectric film. The latter case however increases the short circuit probability of the capacitor.

Finally, a blend of bulk heterojunction Poly-3-hexyl thiophene (P3HT) and Phenyl-C61-butyric acid methyl ester (PCBM) in 1:1 wt./wt. ratio was dissolved in a mixture of ortho-dichlorobenzene and chloroform in a concentration of 80 mg/mL. The printing of OPDs (Fig. 2) was carried out with a single nozzle inkjet printer by Microdrop equipped with a MDK-140 print head. The OPD fabrication details were published elsewhere [11].

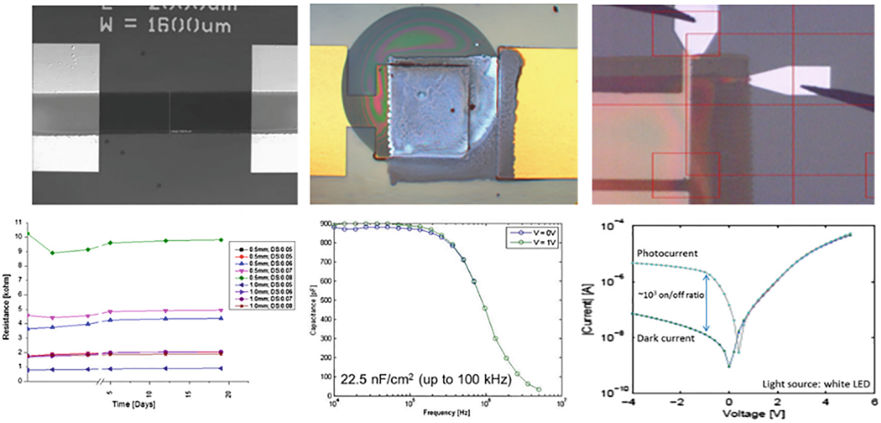

Fig. 2. Top row: inkjet printed resistor (left), capacitor (centre) and OPDs (right) used for realizing the sun sensor bottom row: resistance vs time (left), capacitance vs frequency (centre) and current vs voltage (right) of the printed resistor, capacitor and OPD, respectively.

This thick film was used for minimizing the short-cut risk, decreasing the off current, and increasing the on/off ratio. After printing, annealing on a hotplate was done in a N_2-filled glovebox. The 15-nm Au semi-transparent anode was thermally evaporated through a shadow mask. The fabricated devices were tested using a Keithley 2400 in dark and under illumination in glovebox.

2.3 Sun Sensor Layout and Fabrication

The selected quad cell sensing approach consisting of 4 photodiodes is shown schematically in Fig. 1. Therefore four single Organic Photo Diodes (OPDs) were processed with common bottom contact (a thin aluminum layer), inkjet printed active polymer-based layer, and individual top contacts (a semi-transparent thin gold layer), as described in Sect. 2.2. The sun sensor demonstrator layout is shown in Fig. 3.

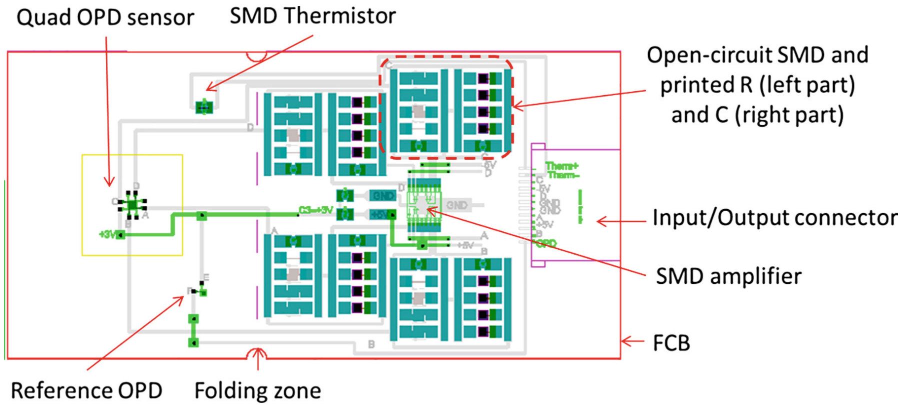

Fig. 3. Sun sensor demonstrator layout

The FCB design relies on the connection-on-demand approach which consists in putting stand-alone printed (see Fig. 2 and Sect. 2.2) and SMD components side-by-side. The connection of the selected printed/SMD component to the whole system is done after characterization of the printed component by inkjet printing a conductive ink. This approach allows enhancing the production yield (on the system level) and minimizing the system integration risks.

After realizing the printed stand-alone components, the sun sensor demonstrator was fabricated according to the layout (Fig. 3). CSEM has printed on the delivered FCBs (HIGHTEC) resistors, capacitors and OPDs, see Fig. 4.

As discussed earlier, attempts were made to print a thinner dielectric film for the capacitors in order to meet the circuit requirements. As discussed earlier, only shorted capacitors were obtained therefore the SMD counterparts were connected to the system.

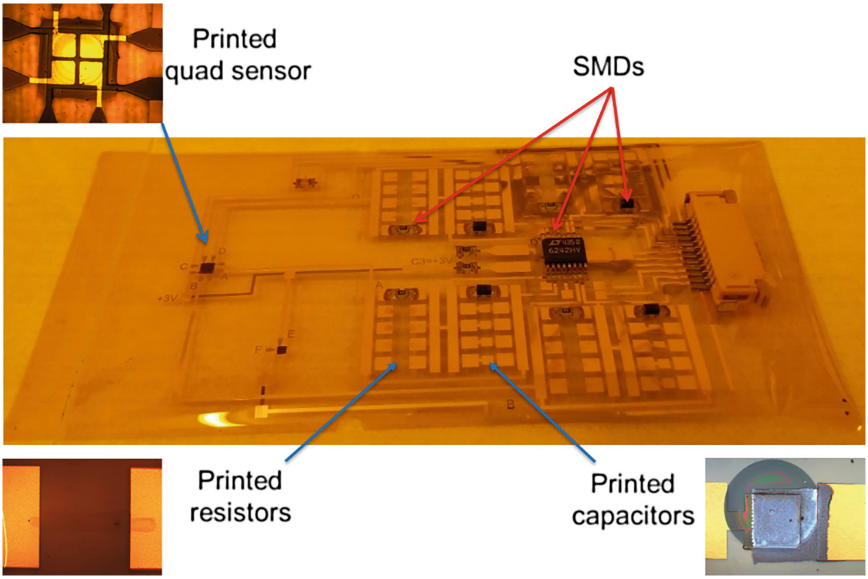
Printed
quad sensor
SMDs
Printed
resistors
Printed
capacitors

Fig. 4. Printed components on the FCBs with embedded SMDs

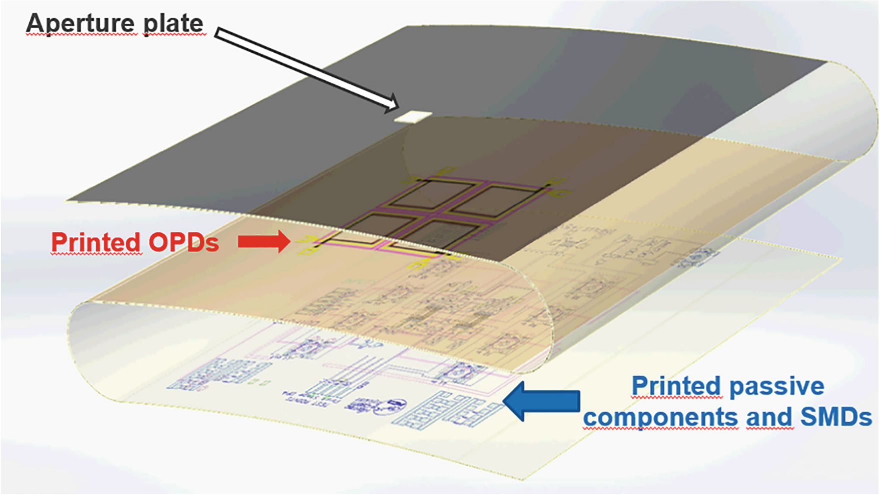
Aperture plate
Printed OPDs
Printed passive
components and SMDs

Fig. 5. Design of the proposed sun sensor applying the quad cell approach given in Fig. 1.

Instead the SMD capacitors were connected according to the layout (Fig. 3). The stiffeners (of a proper thickness) were purchased from the 3M company while the top lids (for the illumination aperture shown in Fig. 1) were opened by laser drilling (Fig. 5). In order to easily fold the PI foil, as shown in Fig. 5, pre-perforation was also performed by laser drilling.

Finally, CSEM and HIGHTEC fabricated and folded the sun sensor demonstrator addressing unique properties of the hybrid technology (Fig. 6) in terms of volume, flexibility, thickness, and weight.

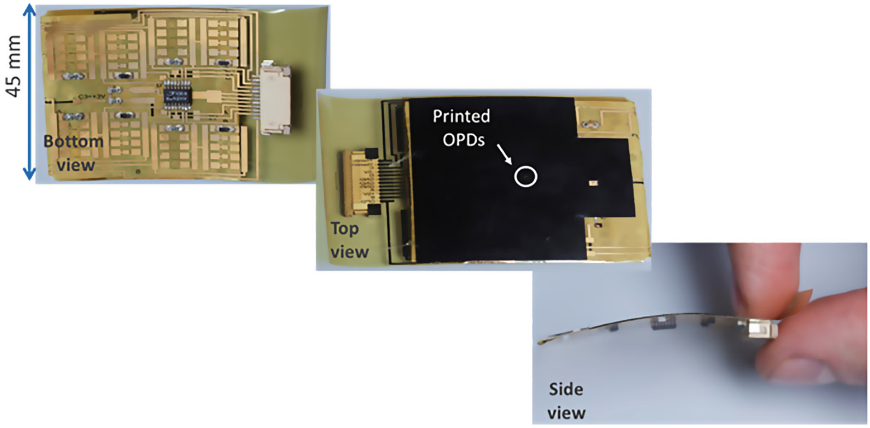

Fig. 6. Assembled and folded flexible sun sensor demonstrator

2.4 Sun Sensor Validation

In order to operate the sun sensor demonstrator CSEM realized a PC interface with a data acquisition card (DAQ) from National Instruments. Figure 7 shows the successful measurement of the OPDs from a quad cell. The light source used is a green laser pointer which was manually aimed at each of the 4 cells (see Figs. 1 and 5).

A green laser pointer was manually aimed at each of the 4 cells and the light spot position was calculated by the software. The quad response is shown in the top graph of each sub-figure of Fig. 7 and the resulting position is illustrated by the red point in the bottom graph. The calculated position follows well the illuminated pattern.

Note: in each sub-figure in Fig. 7, the left 2D graph corresponds to the calculated spot position, sketched with the green dot. The right scale shows the corresponding calculated angle equal to the set one. This validates the demonstration of the working sun sensor between −60° to 60° through the developed PC interface. The accuracy of ~6° was obtained out of this measurements.

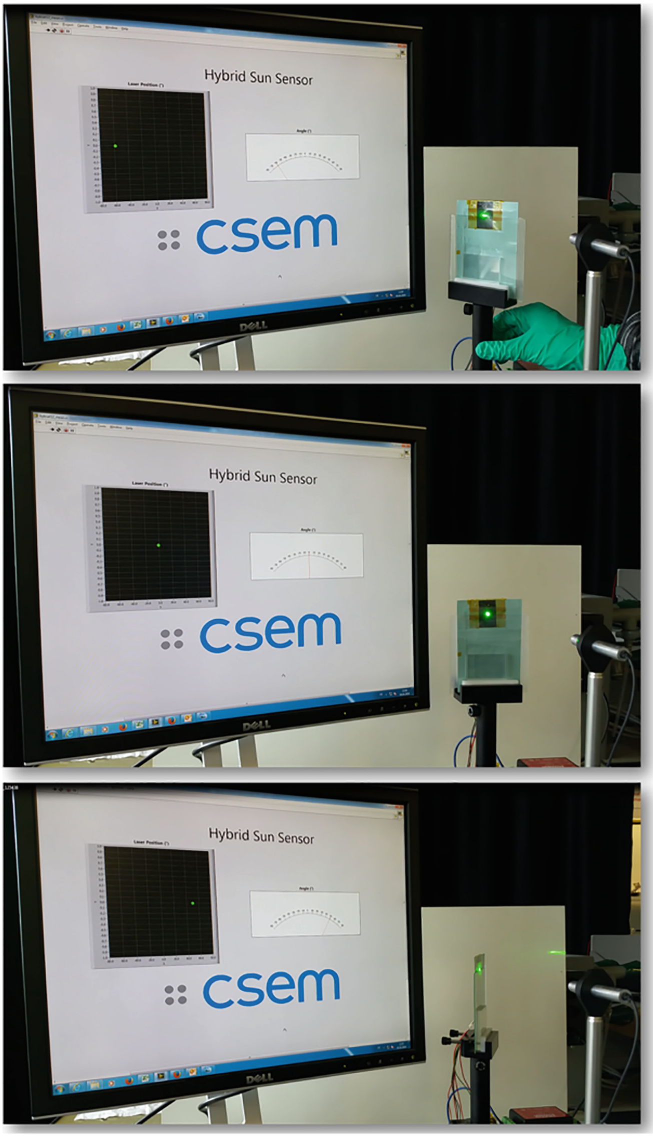
Hybrid Sun Sensor
csem
DELL
Hybrid Sun Sensor
csem
DELL
Hybrid Sun Sensor
csem
DELL

Fig. 7. Hybrid sun sensor validation. Top: −60° incidence angle. Middle: Normal incidence angle. Bottom: +60° incidence angle

3 Conclusions

The presented flexible, hybrid sun sensor is a new kind class of product for e.g. cube-satellites. It demonstrates that the new hybrid sun sensor can be highly compact and tailored out of the selected and designed stand-alone printed components (large area and extremely thin) coupled with high-end SMDs (e.g. amplifier) on flexible FCB.

The gain is in extremely thin sun sensor (thickness of the embedded SMD, i.e. <2 mm), extremely light weight (<2 g), low power (power supply ±5 V), cost-effective (projected cost significantly lower than current solution e.g. Moog Bradford Fine Sun Sensor), etc. whereas the sensor performances are similar.

Furthermore, printing more complex devices, such as Organic Thin Films (OTFTs) and integrated circuits (IC) on FCB can be envisioned in the future which could lead to the next integration level. Thus having more embedded printed components on FCB can further decrease system thickness, weight, costs, etc.

The exampled hybrid technology offers new possibilities to the system designers (towards smart PCBs), material providers (printable functional inks) and extends the current range of products (e.g. wearable, flexible electronics).

Acknowledgments. The development leading to these results has received funding from the Swiss Space Office (SSO)/Swiss Space Center (SSC) in the Framework Programme MdP – Mesures de Positionnement 2014. The authors especially thank to Dr. Tobias Bandi from SSC for the fruitful discussions, support and guidance during this period.

References

1. http://www.youtube.com/watch?v=F035jDS_pU8
2. http://future.arte.tv/fr/innovations-medicales/des-robots-sensibles-au-service-de-lhomme
3. http://bradford-space.com/products/aoce/mfss/
4. Ortega, P., López-Rodríguez, G., Ricart, J., Domínguez, M., Castañer, L.M., Quero, J.M., Tarrida, C.L., García, J., Reina, M., Gras, A., Angulo, M.: A miniaturized two axis sun sensor for attitude control of nano-satellites. IEEE Sens. J. **10**(10), 1623–1632 (2010)
5. Chang, Y.-K., Lee, B.-H.: Development of high-accuracy image centroiding algorithm for CMOS-based digital sun sensors. Sens. Actuators A: Phys. **144**, 29–37 (2008)
6. Wei, M., Xing, F., You, Z.: An implementation method based on ERS imaging mode for sun sensor with 1 kHz update rate and 1 precision level. Opt. Express **21**, 32524–32533 (2013)
7. Abhilash, M., Kumar, S., Sandya, S., Sridevi, T.V., Prabhamani, H.R.: Implementation of the MEMS-based dual-axis sun sensor for nano satellites. In: Metrology for Aerospace (MetroAeroSpace), pp. 190–195. IEEE (2014)
8. Liebe, C.C., Mobasser, S.: MEMS based sun sensor. In: 2001 IEEE Aerospace Conference Proceedings (Cat. No. 01TH8542), Big Sky, MT, vol. 3, pp. 3/1565–3/1572 (2001)
9. Lü, X., Tao, Y., Xie, K., Wang, S., Li, X., Bao, W., Chen, R.: A photodiode based miniature sun sensor. Meas. Sci. Technol. **28**, 055104 (2017). (7pp)
10. Yousefiana, P., Duralib, M., Rashidianc, B., Jalalid, M.A.: Fabrication, characterization, and error mitigation of non-flat sun sensor. Sens. Actuators, A **261**, 243–251 (2017)
11. Maiellaro, G., Ragonese, E., Gwoziecki, R., Jacobs, S., Marjanović, N., Chrapa, M., Schleuniger, J., Palmisano, G.: Ambient light organic sensor in a printed complementary organic TFT technology on flexible plastic foil. IEEE Trans. Circ. Syst.—I: Regul. Pap. **61**(4), 1036–1043 (2014)

Temperature Monitoring of an SLM Part with Embedded Sensor

Philipp Stoll[1](✉), Bastian Leutenecker-Twelsiek[2], Adriaan Spierings[1], Christoph Klahn[2], and Konrad Wegener[3]

[1] Inspire AG icams, St. Gallen, Switzerland
stoll@inspire.ethz.ch
[2] Inspire AG pdz, Zurich, Switzerland
[3] IWF – Institute for Machine Tools and Manufacturing,
ETH Zurich, Zurich, Switzerland

Abstract. Selective Laser Melting (SLM) offers various new possibilities for the production of metallic components with respect to their design and complexity. The manufacturing process in layers enables accessibility and the possibility for manipulation and modification to each section of the part's geometry. Hence the integration of sensors into the component during its manufacturing process is feasible. This approach is of enormous interest for various industrial sectors since sensor integration is a key enabler of industry 4.0. A sensor that has been embedded into a part during SLM production process facilitates not only a monitoring of this metallic part during its use phase in general but a monitoring of a spatially well-defined location within this part. The work presented in this paper specifically targets the integration of a temperature sensor into an SLM part. The sensor is embedded in a section of the part which is not accessible after the production process any more. Different concepts and strategies of sensor positioning and integration are investigated, focussing on an evaluation of the operating ability of these sensors after their embedding with the SLM process. Thus different methods to attach the sensor to the metallic part are presented. Furthermore the paper reports on the analysis of the influence of geometrical design features on the response behaviour and accuracy of the temperature measurement compared to conventionally conducted reference measurements.

Keywords: Selective Laser Melting (SLM) · Industry 4.0 · Part monitoring · Sensor integration · Added value

1 Motivation

Selective Laser Melting (SLM) is an additive manufacturing (AM) technology that currently receives significant attention in the global production industry since it offers entirely new possibilities and strategies for the manufacturing of functional metallic parts. The prime benefits utilised are the option to produce highly complex internal and external geometries and the possibility to design a part based on its core functional purposes, not on the restrictions and limitations of the traditional manufacturing technologies. This results in SLM parts typically exhibiting complex design features,

© Springer International Publishing AG 2018
M. Meboldt and C. Klahn (eds.), *Industrializing Additive Manufacturing - Proceedings of Additive Manufacturing in Products and Applications - AMPA2017*,
DOI 10.1007/978-3-319-66866-6_26

bionic shapes or topology optimized lightweight structures that are of enormous interest for various industrial sectors. Besides design, there is another aspect that is raising industry's interest in SLM technology. Due to the layer by layer manufacturing process, SLM facilitates the integration of functional elements like sensors into the parts produced. Thereby the sensors can be placed in the immediate vicinity of critical locations to be monitored. Thus the users get a more detailed monitoring and consequently a more comprehensive understanding of the conditions within their systems, particularly during operation. The most promising variables to monitor the status of a system or a single work piece are temperature and strain. Knowledge of both parameters is essential to determine structural health and ageing conditions which are of crucial importance for a safe operation mode of various applications. The embedment of sensors into work pieces sets not merely the base line for structural health monitoring applications but also for much wider topics like industry 4.0 or internet of things. These concepts are based on the acquisition of as much data as possible.

The research presented in this paper deals with the embedding of temperature sensors (Pt 100 elements) into stainless steel parts during the SLM manufacturing process. The procedure for the sensor integration is presented focussing on not negatively influencing the sensing capabilities by the embedment process. Additionally a detailed analysis of the measurement accuracy of embedded sensors is conducted.

2 State of the Art

Gausemeier et al. [1] have shown in their roadmap that integration of external components into SLM parts is a field of research that gets more and more attention in industry. They particularly emphasize that the integration of functional elements will be of significant importance in the next years, currently it is just starting. Several research groups have already conducted trials in embedding external elements into SLM parts during the manufacturing process. While Paz et al. [2] investigated the integration of RFID tags into components during the SLM production process, focussing on the analysis of penetration depth with respect to the transmission frequency of the transponder, Sehrt and Witt [3] raised research questions in their paper on RFID tag integration into SLM parts, that are significant for various embedded components in general: beside the analysis of the ability of the embedded component to survive the harsh environmental conditions in an SLM system as well as the SLM process itself, the influence of geometrical features on the sensing or data transmitting capability of integrated elements is a key aspect for further research work in this field. The sensors whose integration into SLM parts during the manufacturing process has recently been investigated in most detail are fibre optical sensors. Li [4] has shown in his dissertation that fibre embedment into metallic parts is feasible in the direct metal deposition (DMD) process. Nevertheless his work can be seen as the fundamental research for integration of external components into metallic parts during additive manufacturing processes in general. His approach is based on a hybrid manufacturing process with alternating additive – laser metal deposition – and subtractive process steps, but nonetheless Li's achievements for the DMD technology have inspired various researchers to think about fibre embedding during different other manufacturing processes as well. Recently this led to a significant increase in the number of research activities and publications dealing with integration of optical fibres in metallic parts during the SLM process. Maier [5] reported the first steps in the direct integration of metallic jacketed fibres into stainless steel coupons on an SLM test setup. In another paper [6] Maier emphasized the aspect of developing optical fibres as sensors that are capable to survive the thermal loads during the direct SLM embedding process. Havermann [7, 8] focussed on the description of an embedment strategy for optical fibres into stainless steel coupons on an SLM test setup. Furthermore he analysed the influences of various process parameters on the embedment procedure and the corresponding bonding qualities. Mathew [9] conducted research on that topic as well, thereby focussing on the embedment of sensors for high temperature measurements up to 1000 °C. Stoll [10] has even been able to transfer the process steps for fibre integration from a lab environment – as it has been used for the aforementioned publications – to a commercial SLM system. Nonetheless despite these great achievements in the cited papers there is a decisive drawback in the integration of optical fibres: the preparation of the fibres, i.e. their coating with one or two protective layers on a specific length, is still a time consuming and manual work. Thus it is not yet possible to purchase these sensors but they are produced for research purposes on demand. Furthermore the papers presented reveal that the way the fibres can be embedded is geometrically limited to straight, horizontal lines. At this point, commercially available, off-the-shelf sensors like Pt 100 elements arouse industry's interest. Although these sensors might require a larger cavity and consequently might negatively influence the mechanical properties of the part, they offer new possibilities for research work since they are cheap, standardized and highly available.

2.1 Focus of the Present Study

The mentioned positive aspects of standardised temperature sensors like Pt 100 elements led to the research presented in this paper. The integration of Pt 100 elements into stainless steel SLM components is investigated with respect to their ability to survive the embedment process. Additionally, different embedment concepts are evaluated based on an analysis of both the measurement accuracy in general and the response behaviour of the sensors in particular.

3 Materials and Methods

3.1 SLM Setup and Material

The experiments have been conducted on a Concept Laser M1 SLM machine with a process chamber of 160 mm × 230 mm and a Nd:YAG laser with maximum power of 100 W. The material used for the embedment trials is stainless steel 316 L.

3.2 Temperature Sensors

The paper presents the integration of temperature sensors – type Pt 100 elements – that are operable at a temperature range from −70 °C to +400 °C and are based on changing resistance in dependence on the temperature.

3.3 Embedding Concepts

Figure 1 schematically shows the single process steps required to embed an external component – e.g. a sensor – into an SLM part during its manufacturing. The subsequent paragraphs will explain in detail the cavity design as well as the strategy to hold the sensor in place and continue the SLM process.

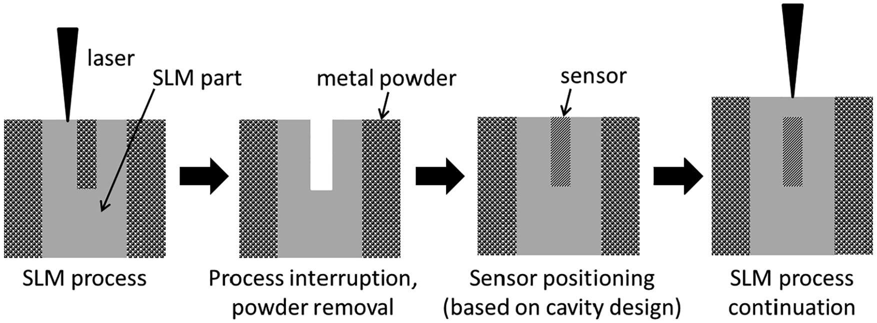
laser
SLM part
metal powder
sensor
SLM process
Process interruption, powder removal
Sensor positioning (based on cavity design)
SLM process continuation

Fig. 1. Process steps to embed external components in SLM parts; modified based on [11]

The different embedding concepts are aiming at the investigation of the parameters predominantly affecting the quality of the temperature measurement:

- Surface roughness, particularly in the cavity
- Positioning of sensor in the cavity with respect to the surface to be measured

3.3.1 Cavity Design

The cavity design is a key aspect in this sensor embedding process since it affects both the manufacturing process and the sensing capability, i.e. the use phase, of the sensor. It determines how the Pt 100 sensor element is located with respect to the surface to be analysed and it sets the orientation of the sensor in relation to the laser beam of the SLM process. In this section the authors focus on the investigation of two different embedding concepts. The geometrical influence on the measuring accuracy is described in the results discussion. While in the first design approach, the sensor is entirely concealed from the laser beam by a cavity that is tilted out of the SLM processing plane (Fig. 2a)), the second cavity design and orientation offers a potential for interaction between the laser and the sensor, since the sensor is merely covered by a 30 µm thick SLM built layer (Fig. 2b)), which is remolten during the scanning of the first layer of

SLM process continuation. The fusion of this sensor covering layer is expected to force the molten metal to surround the sensor and consequently achieve an appropriate embedding of it.

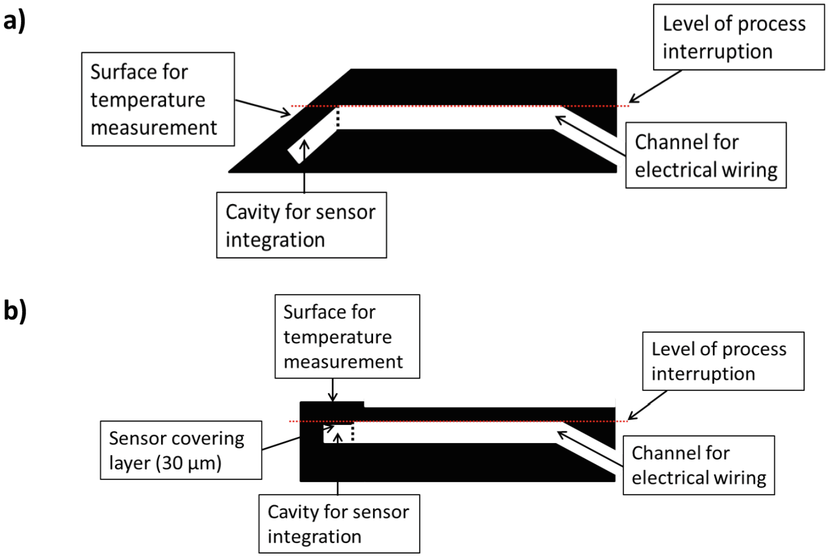
a)
Surface for temperature measurement
Level of process interruption
Channel for electrical wiring
Cavity for sensor integration
b)
Surface for temperature measurement
Level of process interruption
Sensor covering layer (30 µm)
Channel for electrical wiring
Cavity for sensor integration

Fig. 2. (a) Embedding concept a; (b) embedding concept b

3.3.2 Positioning and Fixation of Temperature Sensors

The positioning of the sensors is accomplished by the form of the cavity, which consists of the sensor geometry plus an additional clearance to account for the maximum achievable accuracy of the SLM process. The rough, as-built SLM surface negatively influences the heat conduction properties between the demonstrator geometry and the sensor. To analyse this influence, the design of experiments includes two trials per embedding concept – with and without heat conductive paste surrounding the sensor in the cavity. Furthermore, the embedding concept shown in Fig. 2(a) has been modified for another trial. In this experiment the positioning of the sensor in the cavity is supported by a spring that is inserted during the embedding process step as well (Fig. 3). It presses the sensor to the cavity wall. Thus an optimized heat conduction is expected.

Besides the positioning of the sensor, the extraction of the electrical wires out of the demonstrator geometry is a key aspect of the embedding concept. Since the diameter of these wires exceeds the size of the sensor, their position within the demonstrator geometry is of decisive importance for the structural load capacity of the entire part and needs to be taken into consideration during its design phase. In all cases the channel surrounding the wiring is filled with a fast hardening resin after the sensor and the wiring have been positioned to bond the wires to the cavity preventing the sensors from being pulled out after the integration.

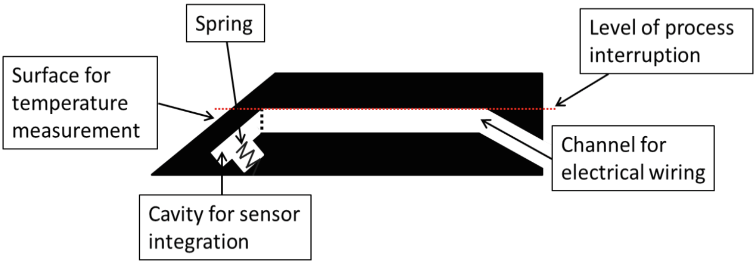
Spring
Level of process interruption
Surface for temperature measurement
Channel for electrical wiring
Cavity for sensor integration

Fig. 3. Embedding concept (a); spring is inserted additionally

3.3.3 Continuation of SLM Process

For both concepts the continuation of the SLM process is feasible without special precaution. In concept b. the part of the geometry covering the embedded sensor is scanned with an SLM process parameter with higher energy density aiming at a fusion of the material surrounding the sensor, consequently resulting in an improved bonding and heat conduction quality.

4 Results and Discussion

4.1 Sensing Capability

4.1.1 Sensor Survival Conditions

To verify if the sensor survived the embedding process, a resistance measurement is conducted. In Fig. 4a comparison of the results before and after the embedding process is displayed. It indicates that the sensors have a good survival probability of the SLM process, independent on the design of the cavity and the embedding concept. Furthermore it can be stated that the measuring accuracy of the sensors that maintained their functionality is not negatively influenced by the embedding process. Nonetheless, Fig. 4 also reveals that all three sensors embedded in geometry a. and pressed to the cavity wall by a spring without using heat conductive paste – sensors number 21, 22, 23 – have lost their functionality during the embedding process, which indicates that a systemic problem is present. It is assumed that a direct contact between the non-isolated part of the electrical wiring and the spring induced a short circuit in the sensing circuit thus destroying the measuring capability of the sensor.

4.1.2 Response Time

The response time of the sensors is dependent on the key influencing parameters surface roughness, particularly in the cavity, and positioning of the sensor in the cavity with respect to the surface to be measured. Additionally the temperature difference between the surface to be measured and the temperature of the demonstrator with embedded sensor is substantially affecting the response time. Thus the measurement setup that is visualised in Fig. 5 is more complex than the setup to evaluate basic functionality of the sensors. The reference temperature value for each analysis is set by the temperature sensor that has been purchased in ready to use configuration, referred

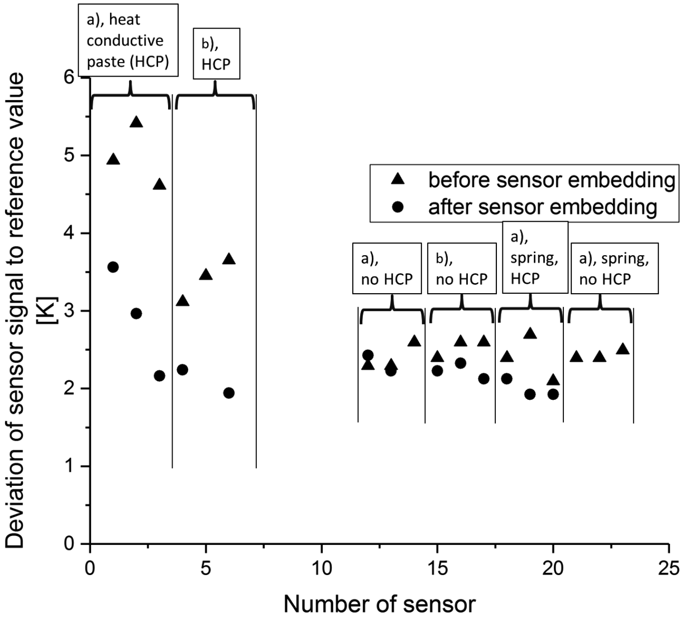

Fig. 4. Assessment of sensor function before and after embedding in SLM part; (HCP = heat conductive paste)

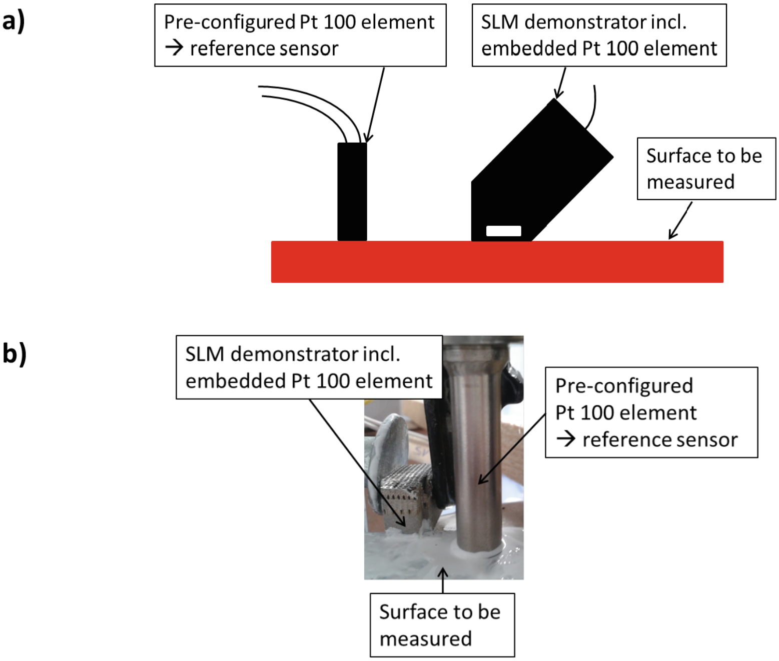
a)
Pre-configured Pt 100 element → reference sensor
SLM demonstrator incl. embedded Pt 100 element
Surface to be measured
b)
SLM demonstrator incl. embedded Pt 100 element
Pre-configured Pt 100 element → reference sensor
Surface to be measured

Fig. 5. Measurement setup for response time assessment of embedded Pt 100 elements. (a) schematically visualized; (b) real measurement setup

to as pre-configured sensor. It is based on a Pt 100 element mounted inside a casing. The embedded sensor is evaluated by bringing the measurement surface of the demonstrator geometry that is indicated in Figs. 2 and 3 for both embedding concepts in contact with the hot surface. To increase heat transfer from this surface to the demonstrator part heat conductive paste is applied. The temperature of the surface to be measured is set to different values in order to get information both on the sensors' response time and measuring accuracy depending on the temperature difference between sensor and analysed surface. The pre-configured sensor continuously monitors the temperature of the measurement surface and sets the reference value while the SLM demonstrator geometry is contacted to and discontacted from this surface repeatedly after having reached saturation for the particular temperature level. The assessment of each sensor's response behaviour and accuracy is based on a relative comparison – i.e. a temperature difference – between the pre-configured sensor and the embedded Pt 100 element. The raw data has been fitted with an exponential decrease function of the form

$$y(t) = y_0 + Ae^{-Bt} \tag{1}$$

However, prior to a quantitative evaluation of the results a qualitative interpretation is conducted first, based on the graphs of the fitted curves for different embedding concepts and temperature levels that are shown in Fig. 6 (for better distinction between the different lines, see online version of the paper). Generally, all curves look rather similar. The differences in the gradients of the curves of the analysis for 50 °C surface temperature originate from the fact that this measurement is the closest to the ambient temperature, i.e. the temperature difference between the set reference temperature and the start temperature of the embedded sensor is the smallest, resulting in the highest impact of the ambient conditions on the measurement. At elevated temperatures, 120 °C and 180 °C, the gradients of the fitted curves are similar.

In order to get a quantitative interpretation of the results anyhow, the time it takes to reach the ±10% range of the surface temperature for each measuring setup has been calculated based on the equations obtained from the data fit according to Eq. (1). The results are displayed in Table 1. In general it can be stated that embedding concept a. leads to shorter response times than concept b based on the ±10% range. Furthermore, the application of heat conductive paste (HCP) surrounding the sensor in the cavity shortens its response time.

While these results reveal merely minor deviations between the two embedding concepts, the accuracy of the measurement in general shows a distinct trend: the sensors embedded according to concept a. have a higher accuracy than the sensors embedded according to concept b. This observation is supported by both the graphs displayed in Fig. 6 and the measuring results listed in Table 2. The sensors embedded according to concept a. have a smaller temperature difference both in measured raw data and in fitted data at the same moment in time. However, it has to be mentioned that a temperature difference of 0 K, meaning the embedded sensor detects the same temperature as the reference sensor does at the surface to be measured, is not possible in a finite time since the embedded sensor is not in direct contact with the analysed surface which leads to an inertia in its measuring capability.

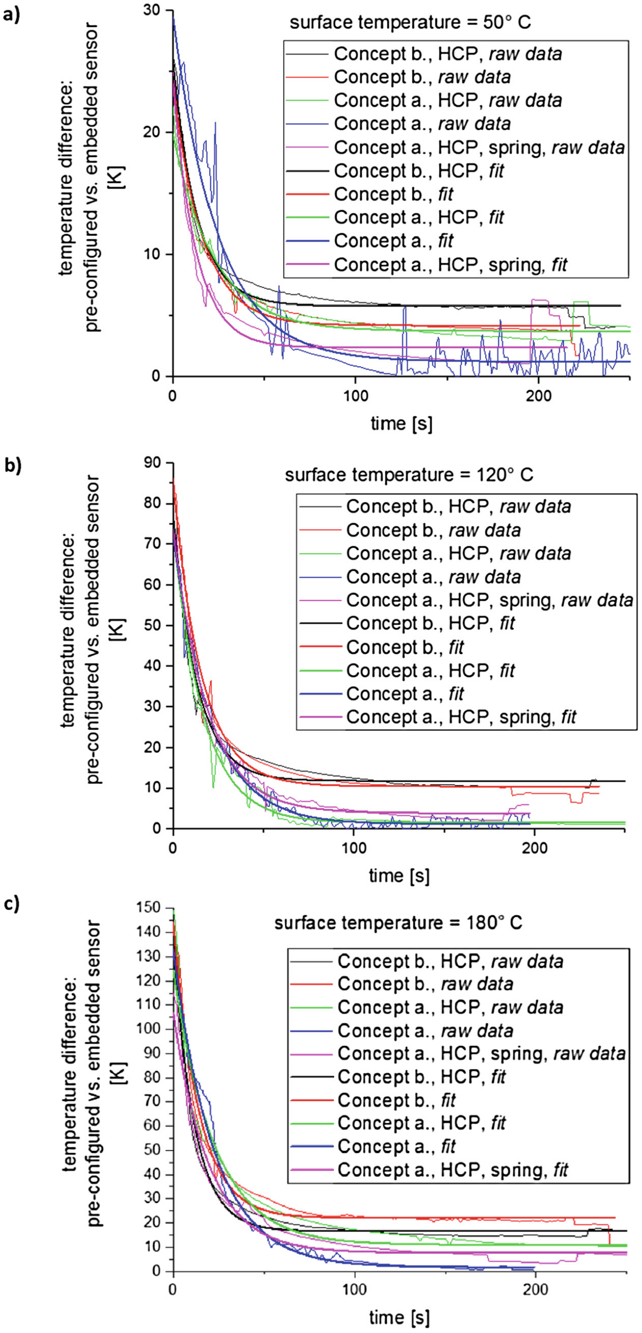

Fig. 6. Assessment of response behaviour of embedded sensors, evaluated at different temperature levels of analysed surface (a) 50 °C (b) 120 °C (c) 180 °C Concepts (a) and (b) according to the schematic representations in Figs. 2 and 3. (HCP = heat conductive paste).

Table 1. Results overview: number of sensors that survived the embedding process; response time [s] till range ±10% of set reference temperature is reached

Set reference temperature		50 °C	120 °C	180 °C
Embedding concept	Functional sensors	Response time [s]		
a.	2/3	50.4	39.2	47.3
a., HCP	3/3	58.2	32.1	61.7
a., HCP, spring	3/3	26.7	40.7	44.3
b.	3/3	52.1	60.9	–
b., HCP	2/3	–	79.8	52.0

In addition to the measurement accuracy that has already been discussed above, Table 2 also lists the damping coefficients B from Eq. (1). In contrast to both the accuracy and the response time to reach the ±10% range of set reference temperature, which are dominated by concept a. sensors, the behaviour of sensors embedded according to concept b. shows larger damping coefficients. Thus concept b. leads to a faster response behaviour when the sensors get in contact with the reference surface.

Table 2. Results overview: difference Δ [K] between reference and embedded sensor in steady state: raw data and fitted data; damping coefficient B from Eq. (1)

Embedding concept	Δ [K]						B [Eq. (1)]		
Set ref. temperature	50 °C		120 °C		180 °C		50 °C	120 °C	180 °C
	Raw	Fit	Raw	Fit	Raw	Fit			
a.	1.6	1.2	2.6	1.3	0.4	1.7	−0.040	−0.048	−0.044
a., HCP	3.3	3.8	2.8	1.7	8.5	10.9	−0.044	−0.060	−0.045
a., HCP, spring	3.8	2.4	6.0	4.0	6.8	7.7	−0.079	−0.053	−0.051
b.	1.9	4.2	8.7	10.5	11.3	22.0	−0.062	−0.064	−0.072
b., HCP	4.2	5.8	12.2	11.9	16.8	16.6	−0.075	−0.076	−0.085

Prior to the conclusion of the results, the authors have to point out two things in particular. First, the numbers and absolute values given in the discussion are merely rough estimates that are highly influenced by the basic measurement setup as well as the sensor embedding process itself. Additionally it has to be noted that no detailed statistical evaluation has been conducted since the results are based on two to three sensors that survived the embedding process per different concept respectively.

5 Conclusions and Outlook

The experiments conducted enable some general conclusions that are of importance for ongoing activities in this field of research:

- It is possible to embed standard Pt 100 sensors in SLM parts without degrading or damaging the sensing capability.
- The application of heat conductive paste in the cavity has a minor positive influence on the response behaviour of the sensor to reach the ±10% range of set reference temperature. Regarding the damping coefficient of the fitted data that is related to the response behaviour in general, i.e. not focussing on the ±10% range of set reference temperature, this effect is not present any more.
- The accuracy of the sensor is not affected by the application of heat conductive paste.
- The accuracy of the sensor is lowered, if the sensor is not entirely shielded from the laser beam as it is in embedding concept b. This might have led to an interaction between laser and sensor.

In order to get a deeper and more comprehensive understanding of these effects, the quality of the sensors' positioning in the cavity has to be analysed based on cross-sectional images in a next step. The results achieved so far act as base line for deeper investigations on integration of Pt 100 elements in SLM parts. In general, the experiments described in this paper are seen as fundamental research work in the field of integration of commercially available, standard sensors in SLM parts. This is an important step to spread out the concept of embedded systems in industry, raise trust in embedding concepts, consequently leading to a strong link between additive manufacturing – SLM in particular – and industry 4.0.

Acknowledgements. The authors like to thank the CTI in Switzerland for financing the project.

References

1. Gausemeier, J., Echterhoff, N., Kokoschka, M., Wall, M.: Thinking ahead the Future of Additive Manufacturing – Future Applications. Heinz Nixdorf Institute (2012)
2. Paz, J.F.I., Wilbig, J., Aumund-Kopp, C., Petzoldt, F.: RFID transponder integration in metal surgical instruments produced by additive manufacturing. Powder Metall. **57**, 365–372 (2014)
3. Sehrt, J.T., Witt, G.: Additive manufacturing of smart parts and medical instruments. In: 17th European Forum on Rapid Prototyping and Manufacturing, Proceedings of AEPR (2012)
4. Li, X.: Embedded sensors in layered manufacturing. Dissertation, Stanford University (2001)
5. Maier, R.R.J., Havermann, D., MacPherson, W.N., Hand, D.P.: Embedding metallic jacketed fused silica fibres into stainless steel using additive layer manufacturing technology. In: Fifth European Workshop on Optical Fibre Sensors, Proceedings of SPIE, vol. 8794, pp. 87942U-1–87942U-4 (2013)
6. Maier, R.R.J., Havermann, D., Schneller, O., Mathew, J., Polyzos, D., MacPherson, W.N., Hand, D.P.: Optical fibre sensing in metals by embedment in 3D printed metallic structures. In: 23rd International Conference on Optical Fibre Sensors, Proceedings of SPIE, vol. 9157, pp. 915707-1–915707-4 (2014)
7. Havermann, D., Mathew, J., MacPherson, W.N., Maier, R.R.J., Hand, D.P.: Temperature and strain measurements with fiber Bragg gratings embedded in stainless steel 316. J. Lightwave Technol. **33**(12), 2474–2479 (2015)

8. Havermann, D., Mathew, J., MacPherson, W.N., Maier, R.R.J., Hand, D.P.: In-situ measurements with fibre bragg gratings embedded in stainless steel. In: 23rd International Conference on Optical Fibre Sensors, Proceedings of SPIE, vol. 9157, pp. 9157A1-1–9157A1-4 (2014)
9. Mathew, J., Schneller, O., Polyzos, D., Havermann, D., Carter, R.M., MacPherson, W.N., Hand, D.P., Maier, R.R.J.: In-fiber fabry-perot cavity sensor for high-temperature applications. J. Lightwave Technol. **33**(12), 2419–2425 (2015)
10. Stoll, P., Mathew, J., Spierings, A., Bauer, T., Maier, R.R.J., Wegener, K.: Embedding fibre optical sensors into SLM parts. In: Proceedings of the 27th Annual International Solid Freeform Fabrication Symposium (2016)
11. Lausch, H., Töppel, T., Petters, R., Gronde, B., Herrmann, M., Funke, K.: Multi-material approach to integrate ceramic boxed temperature-sensitive components in laser beam melted structures for bio and other applications. In: Proceedings of 3rd Fraunhofer Direct Digital Manufacturing Conference (2016). ISBN (E-Book): 978-3-8396-1001-5

Unique Customer Benefits

Integration of Fiber-Reinforced Polymers in a Life Cycle Assessment of Injection Molding Process Chains with Additive Manufacturing

Thomas Hofstätter[1](✉), Niki Bey[2], Michael Mischkot[1], Philippe M. Stotz[2],
David B. Pedersen[1], Guido Tosello[1], and Hans N. Hansen[1]

[1] DTU Mechanical Engineering, Technical University of Denmark,
2800 Kongens Lyngby, Denmark
`thohofs@mek.dtu.dk`
[2] DTU Management Engineering, Technical University of Denmark,
2800 Kongens Lyngby, Denmark

Abstract. Additive manufacturing technologies applied to injection molding process chain have acquired an increasingly important role in the context of tool inserts production, especially by vat polymerization. Despite the decreased lifetime during their use in the injection molding process, the inserts come with improvements in terms of production time, costs, flexibility, as well as potentially improved environmental performance as compared to conventional materials in a life cycle perspective.

This contribution supports the development of additively manufactured injection molding inserts with the use of fiber-reinforced vat polymerization technology. The life cycle assessment of the prototyping process chain for rapid prototyping with high flexibility provides a base for industrial applications in injection molding.

Keywords: Fiber-reinforced polymers · Life cycle assessment · Additive manufacturing · Injection molding · Process chains

1 Introduction

The conventional injection molding (IM) pilot production cycle is modified in a form where the cavity of the steel mold is generalized in geometry making room for inserts shaping the final geometry of the produced part. The generalized cavity is equipped with a smaller insert which is cheaper and more flexible in production and handling. Those standard inserts can be manufactured conventionally by milling of metals.

Newly developed technologies such as additive manufacturing (AM) show their major advantages in terms of flexibility and speed of production. [1–5] Moreover, finer details such as corners are limited to the voxel size of the AM machine (in the lower μm range), not the diameter of the milling machine.

© Springer International Publishing AG 2018
M. Meboldt and C. Klahn (eds.), *Industrializing Additive Manufacturing - Proceedings of Additive Manufacturing in Products and Applications - AMPA2017*,
DOI 10.1007/978-3-319-66866-6_27

Prior investigations by [6,7] have shown a significant difference in potential environmental contributions such as Climate Change (Global Warming Potential, GWP) [8] and Human Toxicity (HT) [9] of IM inserts made from photopolymer exposed in a vat polymerization (VP) process [1,10] compared to conventional inserts made from brass and steel. Despite the described advantages, the lifetime (i.e. number of shots) of AM inserts is significantly lower than the lifetime of conventionally machined metal tools. A general review on environmental impact of AM compared to conventional manufacturing was performed by [11].

This investigation targets the life cycle of an advancement of IM inserts by fiber-reinforced polymers (FRPs) [12,13]. Introduced by [1], FRPs in IM inserts reduced the crack propagation velocity in the insert and increased the lifetime by a factor of 2.6 at 5$\%_{\mathrm{wt}}$ short carbon fibers (CFs) and 5.2 at 10$\%_{\mathrm{wt}}$ compared to plain inserts without fiber-reinforcement as well as inserts made conventionally from aluminum, brass and steel [1,14,15].

This paper elaborates on previous research by comparing plain inserts without fibers to FRP inserts in the perspective of a life cycle assessment (LCA) according to ISO 14040/44 [16] on screening level. It therefore contributes to the understanding of the effects if IM with AM inserts on environmental factors.

2 Methods

The LCA was performed on inserts produced with the proprietary photopolymer HTM-140 by the company Envisiontec. The inserts were shaped in the dimensions of 3 mm x 19 mm x 19 mm equipped with micro features such as sharp corners, cylindrical cavities and edges as shown in Fig. 1.

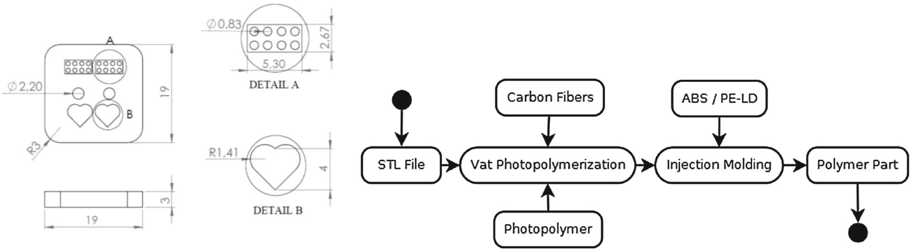

Fig. 1. Geometry of the investigated insert with sharp corners, cylindrical cavities and edges (left, source: [10], used with permission) and diagram of the IM process (right).

The FRP inserts were produced from a mixture of 5$\%_{\mathrm{wt}}$ and 10$\%_{\mathrm{wt}}$ of short virgin carbon fibers with dimensions 7.2 mm diameter and 100 mm average length [17]. They were modeled in SimaPro according to [18,19] and will be referred to as VP 0%, VP 5%, and VP 10%

The manufactured inserts were grouped to a number of 4 inserts since the tool used 4 inserts per shot as shown in Fig. 2 whereas each insert of the compared materials had different specific weights shown in Table 1. The material is injected from the back of the machine from a granular primary material. The IM process parameters were not changed from conventional IM manufacturing. Therefore, the process was also not included in the LCA as the focus is on the comparison of different insert materials as well as the impact of waste generation on the IM process.

The lifetime was experimentall determined for PE-LD as part material in [1,7,14,15] and is listed in Table 2. It can be expected that the lifetime of ABS as part material is lower due to the higher process temperature.

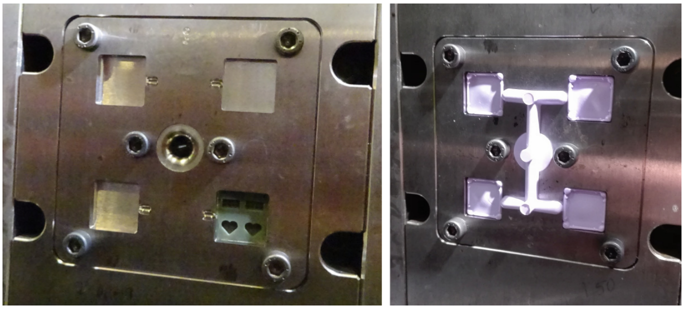

Fig. 2. Single insert in the IM machine (left). The process has a capacity of 4 inserts producing one part each. All inserts are connected by hot runners (right) resulting in waste material (source: [1], used with permission).

Table 1. Weight of 1 insert of the different kinds.

VP 0%	VP 5%	VP 10%	Aluminum	Brass	Steel
1.3 g	1.325 g	1.35 g	3.2 g	10.2 g	9.4 g

Table 2. Lifetime of 1 insert of the different kinds for injection of PE-LD as determined from [1,7,14,15].

VP 0%	VP 5%	VP 10%	Aluminum	Brass	Steel
500 shot	1300 shot	2600 shot	10000 shot	10000 shot	10000 shot

In order to investigate the inserts' share of environmental impact of the entire IM process, the waste of injected polymer was additionally calculated and compared to the used inserts. Acrylonitrile butadiene styrene (ABS) and Low-density polyethylene (PE-LD) were chosen as injected materials. The weight characteristic of 1 shot is shown in Table 3. Polymer waste is responsible for approximately 60% of the injected polymer weight in the process.

Table 3. Weight of 4 produced parts and residual material of the IM process that was not used in the final parts for 1 shot.

	ABS	PE-LD
Weight of 4 parts	2.00 g	1.60 g
Weight of waste	2.72 g	2.28 g
Total weight	4.72 g	3.88 g

It was chosen to use GWP in CO_2 equivalent as well as HT in kg 1,4-DB equivalent, as indicators for the life cycle impact of the investigated inserts and parts.

3 Results

It was shown that the GWP increased at increasing CF content whereas the contributions to HT decreased. An increase in GWP of approximately 5% and a reduction of HT by less than 1% is reached when adding 1% CF to the AM insert compared to an insert without CF.

Brass leads to a significantly higher impact on HT as shown in Table 4 where influencing factors of 1 kg of the materials are listed. ABS has a higher impact on the LCA as compared to PE-LD with an accelerated impact due to its chemical composition and its production chain (Table 5).

Table 4. LCA data for 1 kg of the inserts' materials.

	VP 0%	VP 5%	VP 10%	Aluminum	Brass	Steel	Carbon fibers
GWP in kg CO_2eq	3.118	3.769	4.419	18.971	5.045	1.744	16.127
HT in kg 1,4-DB eq	621.790	596.313	570.835	269.738	4772.948	85.757	112.236

Table 5. LCA data for 1 kg of the parts' materials.

	ABS	PE-LD
GWP in kg CO_2 eq	3.995	1.896
HT in kg 1,4-DB eq	7.057	2.486

Waste is responsible for 60% of the necessary injected polymer and makes up for up to 33% of the contributions for 1 shot as shown in Table 6 for 1 shot. The factors were calculated as ratio of impact of waste to overall impact of necessary parts and waste. ABS can be considered more influential in both factors with a high impact on the LCA.

Table 6. Ratios of waste material as compared to the total of GWP and HT impacts for 1 shot.

	VP 0%	VP 5%	VP 10%	Aluminum	Brass	Steel
GWP ratio of ABS	0.3301	0.2857	0.2508	0.0159	0.0194	0.0569
HT ratio of ABS	0.0043	0.0044	0.0046	0.0020	0.0000	0.0022
GWP ratio of PE-LD	0.1576	0.1318	0.1128	0.0061	0.0075	0.0224
HT ratio of PE-LD	0.0012	0.0013	0.0013	0.0006	0.0000	0.0006

When neglecting the contributions of the polymer waste, CFs have a strong impact on the LCA of the IM process. Even at higher shot numbers, the GWP contributions to the 4 inserts VP 10% in the IM machine remains significantly below the GWP of the metal materials and VP 5% competes with steel at higher shot numbers as can be seen in Fig. 3.

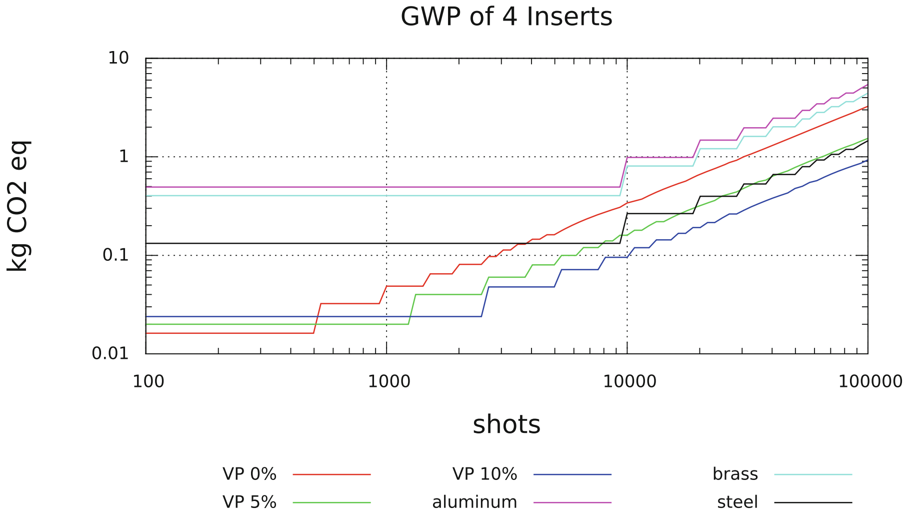

Fig. 3. Cumulative GWP impact neglecting the polymer waste.

Due to the high effects of the photopolymer on HT, the AM inserts remain between aluminum and steel below and brass exceeding the impact. Still, smaller production numbers below 5000 shots favor the AM inserts as suitable alternatives for prototyping applications as shown in Fig. 4.

It is moreover noticeable that the GWP of both ABS as well as LD-PE waste remains high compared to the inserts' materials. The contributions of the waste component of the IM process overrules the contributions of the insert material on the GWP as shown in Figs. 5 and 6. At higher shot numbers, the ratio converges to 1 meaning that the inserts' materials have negligible contribution to the global impact.

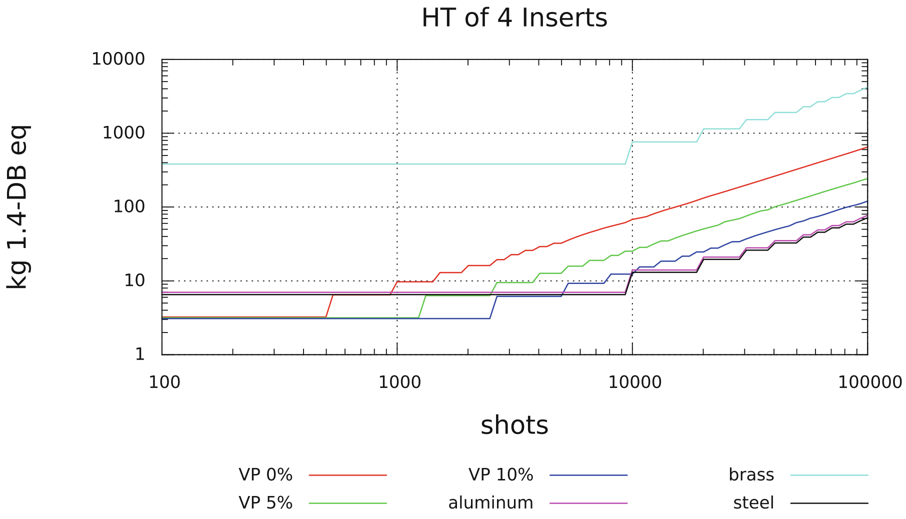

Fig. 4. Cumulative HT impact neglecting the polymer waste.

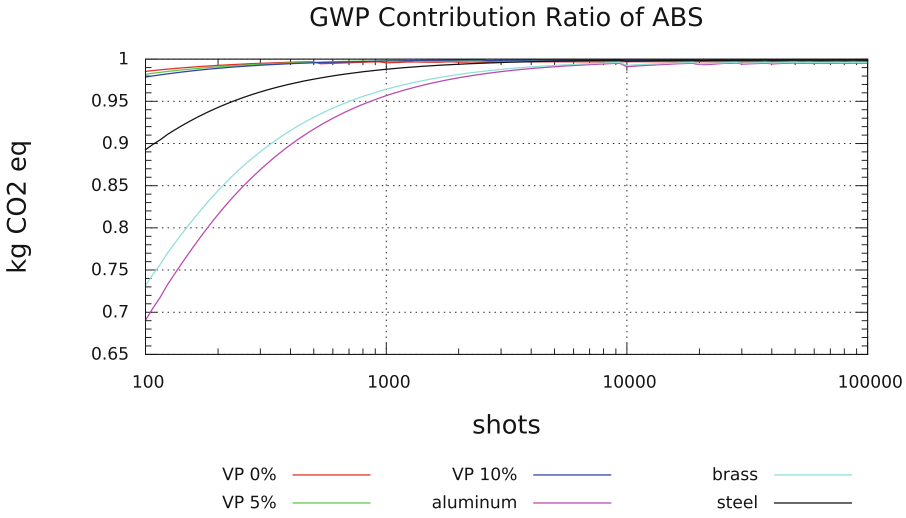

Fig. 5. Ratio of GWP impact of ABS waste material as compared to the total impact on the LCA.

Due to the poor performance of brass in terms of HT, the contributions of waste ABS and PE-LD remains at 20% for brass in terms of ABS waste (Fig. 7) and 10% for brass in terms of PE-LD waste (Fig. 8). Production of VP 0% inserts

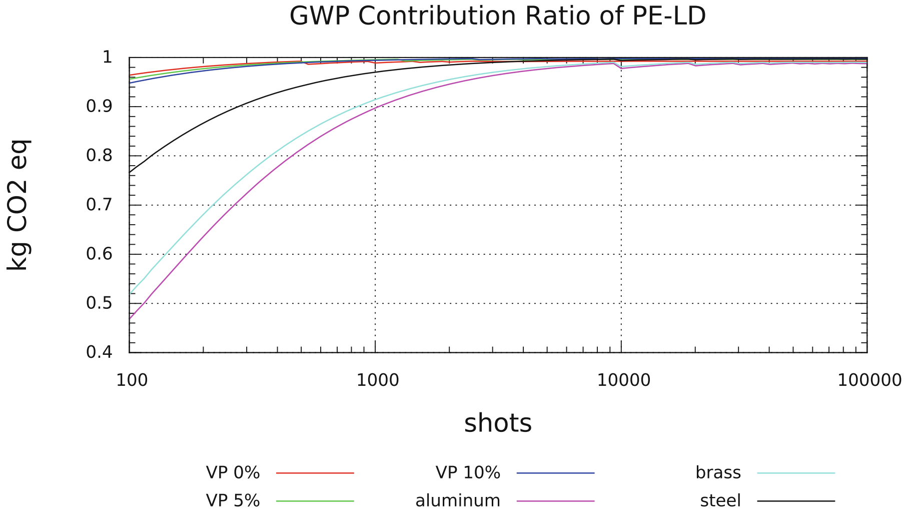

Fig. 6. Ratio of GWP impact of PE-LD waste material as compared to the total impact on the LCA.

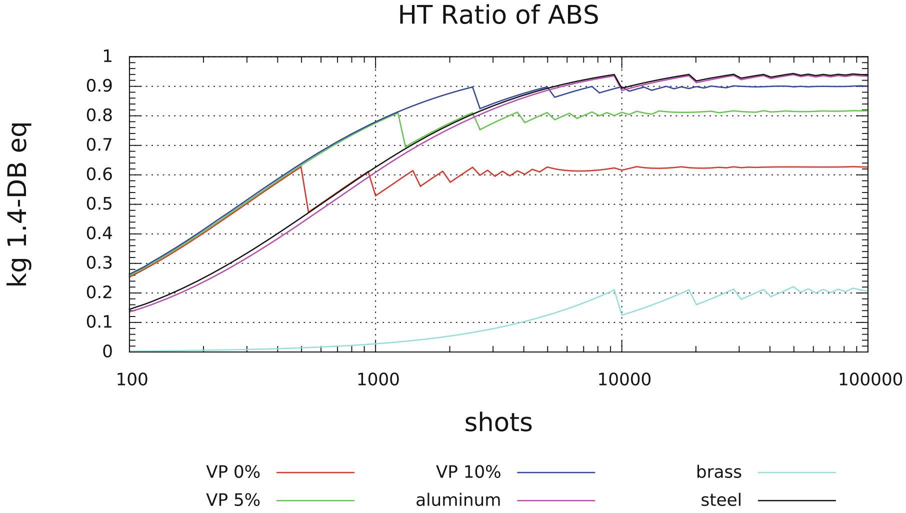

Fig. 7. Ratio of HT impact of ABS waste material as compared to the total impact on the LCA.

is influenced up to 63% in terms of ABS waste and up to 40% in terms of PE-LD waste. Better performance of FRPs in the AM inserts in terms of lifetime results in a higher contribution of the waste material.

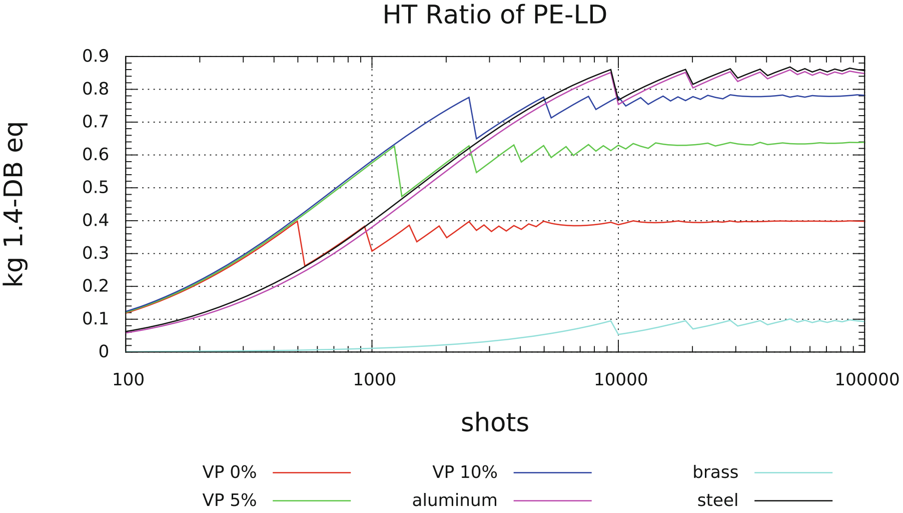

Fig. 8. Ratio of HT impact of PE-LD waste material as compared to the total impact on the LCA.

4 Conclusion

As a conclusion, the IM manufacturing process needs revision in terms of produced polymer waste that does not contribute to the part or the mold. Production of ABS and PE-LD parts was not dominated by the difference in the insert material, but by the environmental impact of ABS and PE-LD parts and waste production.

CFs have a significant influence on the performance of AM inserts in the LCA. Concerning GWP contributions, AM inserts with a ratio of $10\%_{\mathrm{wt}}$ have a preferable performance than metal inserts.

AM inserts are most suitable for smaller production volumes in terms of their environmental impact, manufacturing costs and time as well as feature accuracy.

Due to the lower lifetime of AM inserts in the IM process, metal inserts are preferred for series production of high part volumes whereas AM inserts are preferred in all key aspects for prototyping of low to medium volume production.

References

1. Hofstätter, T., Mischkot, M., Pedersen, D.B., Tosello, G., Hansen, H.N.: Evolution of surface texture and cracks during injection molding of fiber-reinforced, additively-manufactured, injection molding inserts. In: Proceedings of Aspe Summer Topical Meeting 2016. ASPE–The American Society for Precision Engineering (2016)
2. Kovacs, J.G.: Construction of pre-deformed shapes for rapid tooling in injection molding. In: Macromolecular symposia, vol. 239, pp. 259–265. Wiley-Blackwell, 111 River Street Hoboken NJ 07030-5774 USA (2006)

3. Kovacs, J.G., Kortelyesi, G., Kovacs, N.K., Suplicz, A.: Evaluation of measured and calculated thermal parameters of a photopolymer. Int. Commun. Heat Mass Trans. **38**(7), 863–867 (2011)
4. Tábi, T., Kovács, N.K., Sajó, I.E., Czigány, T., Hajba, S., Kovács, J.G.: Comparison of thermal, mechanical and thermomechanical properties of poly (lactic acid) injection-molded into epoxy-based rapid prototyped (polyjet) and conventional steel mold. J. Therm. Anal. Calorim. **123**(1), 349–361 (2016)
5. Rahmati, S., Dickens, P.: Rapid tooling analysis of stereolithography injection mould tooling. Int. J. Mach. Tools Manuf. **47**(5), 740–747 (2007)
6. Mischkot, M., Hofstätter, T., Bey, N., Pedersen, D.B., Hansen, H.N., Hauschild, M.Z.: Life cycle assessment injection mold inserts: additively manufactured, in brass, and in steel. In: Proceedings of the DTU Sustain Conference 2015. DTU–Technocal University of Denmark (2015)
7. Hofstätter, T., Bey, N., Mischkot, M., Lunzer, A., Pedersen, D.B., Hansen, H.N.: Comparison of conventional injection mould inserts to additively manufactured inserts using life cycle assessments. In: Proceedings of Euspen's 16th International Conference & Exhibition. EUSPEN–European Society for Precision Engineering and Nanotechnology (2016)
8. Parry, M., Canziani, O.F., Palutikof, J.P., van der Linden, P.J., Hanson, C.E., et al.: Climate Change 2007: Impacts, Adaptation and Vulnerability, vol. 4. Cambridge University Press, Cambridge (2007)
9. Rosenbaum, R.K., Bachmann, T.M., Gold, L.S., Huijbregts, M.A.J., Jolliet, O., Juraske, R., Köhler, A.L., Larsen, H.F., MacLeod, M., Margni, M., McKone, T.E., Payet, J., Schuhmacher, M., van de Meent, D., Hauschild, M.Z.: Usetox - the unep-setac toxicity model: recommended characterisation factors for human toxicity and freshwater ecotoxicity in life cycle impact assessment. Int. J. Life Cycle Assess. **13**(7), 532–546 (2008)
10. Mischkot, M., Hansen, H.N., Pedersen, D.B.: Additive manufacturing for the production of inserts for micro injection moulding. In: Proceedings of Euspen's 15th International Conference & Exhibition (2015)
11. Kreiger, M., Pearce, J.M.: Environmental life cycle analysis of distributed three-dimensional printing and conventional manufacturing of polymer products. ACS Sustain. Chem. Eng. **1**(12), 1511–1519 (2013)
12. Song, Y.S., Youn, J.R., Gutowski, T.G.: Life cycle energy analysis of fiber-reinforced composites. Compos. A Appl. Sci. Manuf. **40**(8), 1257–1265 (2009)
13. La Mantia, F.P., Morreale, M.: Green composites: a brief review. Compos. A Appl. Sci. Manuf. **42**(6), 579–588 (2011)
14. Hofstätter, T., Pedersen, D.B., Tosello, G., Hansen, H.N.: Applications of fiber-reinforced polymers in additive manufacturing. In: Proceedings of the 1st Cirp Conference on Composite Materials Parts Manufacturing, CIRP (2017)
15. Hofstätter, T., Pedersen, D.B., Tosello, G., Hansen, H.N.: State-of-the-art of fiber-reinforced polymers in additive manufacturing technologies. J. Reinf. Plast. Compos. **36**(15), 1061–1073 (2017). doi:10.1177/0731684417695648
16. International Organization for Standardization: Iso 14040/44:2006 environmental management – life cycle assessment – principles and framework (2006)
17. Zoltek. Zoltek px35 milled carbon fibers technical data sheet (2015)
18. Schmidt, J.H., Watson, J.: Eco island ferry: comparative LCA of island ferry with carbon fibre composite based and steel based structures. Technical report, 2.-0 LCA consultants (2014)
19. Toray Industries Inc.: Carbon fiber and global environment (2017)

Advantages in Additive Manufacturing for a Medium Format Metrology Camera

Ralph Rosenbauer[1(✉)], Filippo Fontana[2], Heidi Hastedt[3],
Thomas Luhmann[3], David Ochsner[1], Dirk Rieke-Zapp[4],
and Robin Rofallski[3]

[1] ALPA Capaul & Weber AG, Zürich, Switzerland
`{ralph,david}@alpa.ch`
[2] ETH Zürich, Zürich, Switzerland
`fontanaf@ethz.ch`
[3] Jade Hochschule, Oldenburg, Germany
`{Heidi.hastedt,luhmann,robin.rofallski}@jade-hs.de`
[4] AICON 3D Systems GmbH, Meersburg, Germany
`dirk.rieke-zapp@hexagon.com`

Abstract. The following paper describes the possibilities of additive manufacturing technology for small-series production of specialised measurement solutions for research and industry by means of the upgrade of a conventional medium format system camera for the photogrammetric solution ALPA 12 add|metric. Particular attention is paid to the description of the design process as well as to the comparison with the experience from conventionally produced predecessors. The resulting camera yields much better photogrammetric accuracy than previous models.

Keywords: Additive design · Laser sintering · Photogrammetry · Metrology

1 Introduction

The increasing establishment of additive manufacturing processes over the past approximately twenty years has given rise to new opportunities for small and medium-sized companies [1, 2]. They especially benefit from the option of realising small to extremely small series [3–5] as well as individual production without high costs for mould construction [6] (in the case of injection moulding) or for toolmaking and programming costs [7, 8] (with CNC methods).

In addition, the additive manufacturing process allows for short innovation cycles because very early in the different stages of the design process (see Fig. 1), both the general shaping and the detail solutions can be tested directly with the exact same manufacturing technology that is also used for the final product [9].

This rapid availability of functional patterns, but above all functional prototypes, allows the early involvement of users and customers into the product development process [10]. This approach, where functional prototypes are directly validated under real market conditions is called bridge manufacturing. Bridge manufacturing avoids

© Springer International Publishing AG 2018
M. Meboldt and C. Klahn (eds.), *Industrializing Additive Manufacturing - Proceedings of Additive Manufacturing in Products and Applications - AMPA2017*,
DOI 10.1007/978-3-319-66866-6_28

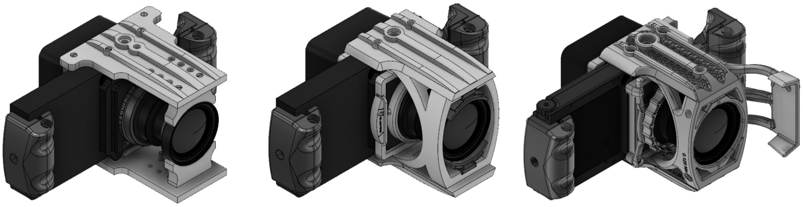

Fig. 1. The ALPA 12 FPS add|metric in different development stages during the process of construction and testing.

time-consuming and costly aberrations, since specific requirements of the users, which can only manifest themselves over the course of the use, can be considered, and implemented on a timely basis.

Several engineering applications require metrology techniques that allow for high-precision 3D measurements e.g. for deformation measurement, manufacturing or quality management. Applications can be found in many different business parts, such as aerospace, shipbuilding, car industry, general production industry or material testing. Object sizes vary from large-volume metrology (20 m × 20 m × 1−10 m) to standard volumes (2–3 m for each dimension). The resulting accuracy of a single object point is expected to be within 100–300 µm for large-volume applications and less than 10 µm for standard volumes.

In order to guarantee the high accuracy requirements, a lasertracking or photogrammetric system can be used. A lasertracker is a polar laser distance measurement technique that allows for the 3D coordinate measurement of an object point that is referenced by a specific reflector. This is a contact-based method. A photogrammetric system works with the contactless acquisition of a specific group of images taken over the object volume and a ray-based triangulation estimation. High-quality cameras and lenses are required and need to be connected perfectly and stable with respect to each other during the whole image acquisition process. Rieke-Zapp et al. [11] gained an accuracy level for an off-the-shelf camera of 52 µm for a maximum length of 2 m when the ring flash was not being fixed to the lens. Comparative analyses with the Alpa 12 WA lead to an accuracy of 124 µm for standard processing with a ring flash fixed to the lens, indicating the influence of one source of instability. Applying algorithmic developments that compensate for instabilities of the camera-to-lens stability or lack of sensor quality improve the accuracy to 29 µm [12]. The subsequent remodification to the Alpa 12 metric gained higher accuracies without algorithmic modelling [13] that were also validated by Reznicek et al. [14], achieving an accuracy level of 40 µm for the length measurement error.

Algorithmic modelling allows for compensation of many hardware imperfections that are constant for each image, e.g. correction of lens distortion. An important prerequisite for standard algorithmic modelling is the minimization of hardware imperfection that will vary for each image. Therefore, the mechanical stabilisation of the camera-lens-sensor system in non-metric cameras is often identified as the key component for accurate results.

Nowadays standard SLR-bodies of the best quality (tested out of a batch) are combined with adapted metric lenses to be used as photogrammetric systems. The typically guaranteed precision is specified to 5 µm ± 5 ppm (1σ) [15]. A theoretical length measurement error is then given for a length of 2 m by 50 µm (2σ). The INCA4 from GSI systems is, besides the preceding ALPA 12 WA metric and INCA cameras, one of a very few metric or metrology cameras. A drawback of this system is the limited usage due to the manufacturers' software. Martin et al. [16] published results of a comparative test of the INCA3 and an off-the-shelf camera system of lower cost to measurements of a lasertracker in a volume of 13.5 m x 8 m x 3 m. While the resulting 3D points of the INCA measurement fit within an accuracy of ± 86 µm (2σ) to the single-station lasertracker points, the usage of the off-the-shelf camera leads to deviations of up to ± 373 µm (2σ). Reznicek et al. [17] achieved a length measurement error in large volumes of less than 250 µm using the Alpa 12 WA metric.

The need of a metric camera for high-precision metrology has been an issue for years. Algorithmic developments enable different improvements in the photogrammetric results, but their application is limited in acceptance and verification of the imaging geometry. Metric stability allows for pre-calibration which is necessary for many applications. A reissue of a metric camera by ALPA was desirable and lead to a cooperation in order to build a new metric camera considering metrology and manufacturing aspects.

2 Requirements for Metric Cameras and Development of the ALPA 12 Metric

A metric camera is defined as a "camera with stable optical-mechanical design" [18], leading to a constant relationship between the perspective centre, the principal distance and the location of the principal point, referred to as "interior orientation" [18]. This constant relationship is assumed in photogrammetric camera models, despite not being necessarily present in current systems (i.e. non-metric cameras). Stable housings and lens mountings are not guaranteed by manufacturers, resulting in minimal movements of the lens that cause deviations from the assumed model. For highest accuracies in photogrammetric applications, a metric camera is thus highly desirable.

Any displacement within the camera system and variations in focus and focal length introduced during image acquisition are to be avoided in order to keep a constant interior orientation. The sensor should offer a high resolution on a plane pixel architecture and a large pixel pitch, enabling a high signal to noise ratio. A lens with a static mounting on the camera body and low distortions is another aspect, improving the accuracy of metrology tasks. According to the achievable precision of measured image coordinates, the stability of a metric camera should be better than 1 µm in all dimensions.

Using retroreflective targets for object signalisation, a ring flash has to be mounted to the camera lens in order to illuminate the targets and reflect them to the optical axis. Table 1 illustrates the aforementioned parameters and categorizes them whether or not they are widely available in current photogrammetric systems.

Table 1. Requirements of a metric camera for photogrammetric purposes

	Property	Use
Camera-lens-architecture	Fixed focus	Constant interior orientation
	Fixed focal length	
	Stable housing	
	Low lens distortions	Improves image quality
Image sensor	Sensor flatness	Unmodeled parameter
	Large pixel pitch	Improves image quality
	High resolution	
Flash	Ring flash	Illumination along optical axis

Practical experience results from a preceding non-additive manufactured metric camera, which fulfils all of the requirements mentioned above. The ALPA 12 camera platform combines medium format camera backs with high-quality lenses to provide optimal image quality for photographic applications. Since particular attention is paid to the precise alignment of all parts the ALPA 12 is well suited as a candidate for photogrammetric applications. Nevertheless, contemporary metric requirements for economic and practical work are no longer fulfilled using the standard ALPA 12 WA. In addition, the manufacturing of small units of a metric camera needs to be considered when designing a new metric camera.

First tests with a non-modified ALPA 12 were carried out in 2005 [19, 20]. At that time the ALPA 12 system was chosen to take advantage of the very large pixel count available from digital medium format backs and the possibility to get lenses with fixed displacement of the principal point. The first being an advantage for applications using image correlation, the latter allowing for better overlap of stereo models. Berger et al. [13] report on a laboratory study using an ALPA 12 TC camera in combination with a lens with a displaced principle point to calculate digital elevation models from soil surfaces. The first accuracy evaluation according to VDI/VDE 2634 [21] of the ALPA 12 [11] revealed a good potential accuracy of the camera system but also showed that the interior geometry of the camera was not completely stable. The results of that study convinced ALPA to build the first ALPA 12 metric camera (see Fig. 2). The digital back was fixed to the camera body using screws, just as the lens board was fixed to the camera by screws rather than using the regular clamping mechanism. This design required a modified camera body while no modifications to camera back or lenses were required. The ALPA 12 metric accomplished a maximum length measurement error of 45 µm in a 2 m x 2 m x 1.5 m measurement volume according to VDI/VDE 2634 [13]. This result was accomplished with a 35 mm lens with fixed focus distance. Other lenses where the regular focusing ring was only taped in place, revealed larger length measurement errors of 50 µm and more. In general, shorter and lighter lenses yielded better length measurement errors than longer lenses with more complex designs. Several camera backs were tested as well. Sensor size or pixel count had no significant influence on length measurement error. Monochrome camera backs yielded a significant improvement in point measurement precision in the images and reduced the data volume to one third compared to RGB sensors with the same pixel count. An improved length measurement error was not observed. The ALPA 12 metric is still mostly used for terrestrial surveys [22].

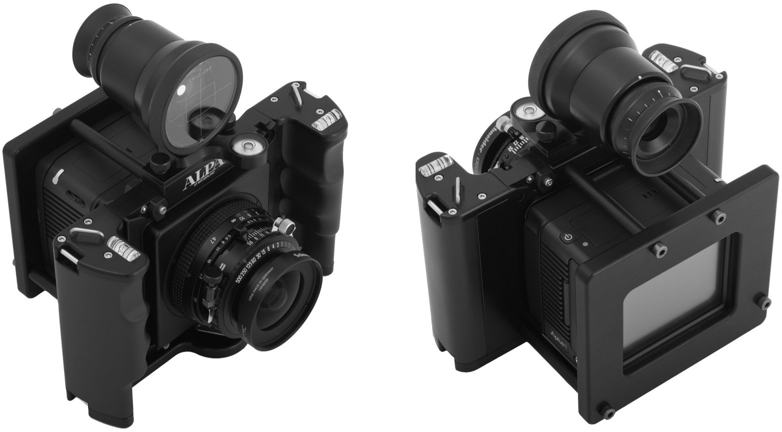

Fig. 2. The first ALPA 12 metric from 2005, still produced with "traditional" substractive methods. Notice the back and lens are fixed to the camera body directly using screws.

3 The ALPA 12 FPS Add|Metric: Technical Basis and Metrical Enhancement

The experience gained from the tests and practical applications of the ALPA 12 metric impressively demonstrated the potential of a photogrammetry solution developed by the conversion of a modular medium format camera. However, the weakness of the concept also very clearly came to light: profitable production of such a specialised solution was difficult to achieve. This was particularly due to the fact that the innovation cycles for digital backs as well as lenses are so short that specialised press plates and reinforcements can only be produced in small series, which results in very high unit costs. Even more serious, however, was the need for mechanical modifications of the base camera (bores for bolting to the backside as seen in Fig. 2), which made the respective cameras useless for other utilisation, as well as not permitting easy upgradability to newer components.

Based on these observations, it was decided to implement the second version of a photogrammetric camera only with additively manufactured parts to be attached to a completely unmodified standard camera. Due to the current requirements of the cooperation partners, the designers chose the ALPA 12 FPS model [23] instead of the ALPA 12 WA model used in the first edition. The new camera offers a focal plane shutter as well as electronically controlled leaf shutter integrated into the lens, thus making manual cocking of the shutter unnecessary. In addition, the ALPA 12 FPS model has very solid screw points on two sides, enabling problem-free installation of the parts for the conversion to the measuring camera. To fit the modular design of the ALPA medium format camera system, the design should be easily adaptable to different lenses as well as digital back parts.

For the initial tests, the choice was based on a Rodenstock HR Digaron-W 40 mm [24] with a diagonal image angle of approximately 70° to 80° (depending on the type of back used), which also enabled working in tight spaces found in production halls and museum facilities etc. thanks to its wide-angle design. Its optical construction is largely free of astigmatism, coma, and chromatic aberrations, resulting in a resolution that matches the resolution recommended for current high-resolution digital rearrangements. In order to realize short flash synchronisation times (<1/250 s), the lens was mounted on an electronic central circuit. This allows both the electronic adjustment of the shutter and a very vibration-free exposure. A PhaseOne IQ350 [25], which is based on a 33 × 44 mm large CMOS sensor with 50 megapixels, was used as a digital back for testing. Due to the sensor technology and the comparatively large pixel pitch (approx. 5 µm), it facilitates very noise-free recording.

4 Design Process

At the beginning of the project, various approaches and manufacturing techniques were considered. Among other things, manufacturing by means of laser-melting metal, hybrid combinations of metal and polymers, or purely polymeric designs were investigated. The decision in favour of a pure polymeric construction was made mainly on the basis of the extensive experience in laser sintering collected by ALPA through several applications in prototyping as well as through serial part construction. With PA3200 GF [26], a comparatively strong material is now available for this technique, which allows very precise and fine-grained parts on EOS Formiga P-110 system [27] with 100 µm layer thickness [28]. The method of additive laser sintering offers the advantage of not requiring support structures, which allows for more freedom in printable shapes compared to other techniques [29]. The chamber size of the EOS Formiga makes it possible to seamlessly produce the parts required for the project. In addition, proven methods for surface treatment (such as dyeing and compacting) are now available, which allow a series-ready finish without manual rework.

The chosen approach for the design is based on the use of the solid threads of the ALPA 12 FPS, mentioned above, as a starting point for external support structures. While a constant distance between the lens and the sensor plane is necessary for the application in photography, the fixation perpendicular to the objective axis is of crucial importance in photogrammetry. To ensure this, the additively made extensions serve as a frame, which fixes the position of the lens and the digital back to the ALPA 12 FPS in all spatial directions and thus also keeps them constant with one another. The design of the brackets has been chosen during the design process in such a way as to ensure a decoupling of the operating forces from the lens-back unit: the handgrips are only connected to the camera housing and not to the additional external frame structures. This is essential for the consistency of the alignment lens-back and thus for the measuring accuracy.

To combine this increased precision with easy modifiability, the construction of the ALPA 12 add|metric is based on two longitudinal brackets which are fastened at the top and bottom of the camera body via two M5 and one 3/8" UNC screws (see Fig. 3). In order to achieve maximum strength with minimum weight, they have three ribs, which in turn are filled with a honeycomb structure to increase the torsional stiffness. These brackets fit two frames for the lens and the digital back, both of which are fixed with special pins (see Fig. 4): When tightening the longitudinal beams, their profile ensures optimal contact pressure for both brackets. The fixings for the digital back and the lens are each implemented with inserted rubber profiles, minimising play in the image plane (see Fig. 3). This is significant because conventional cameras for photographic use are optimised only for exact positioning along the optical axis of the lens while a lateral displacement of the planes is not critical. However, for use in measurement technology, it is essential to precisely exclude this variability of the principal point position.

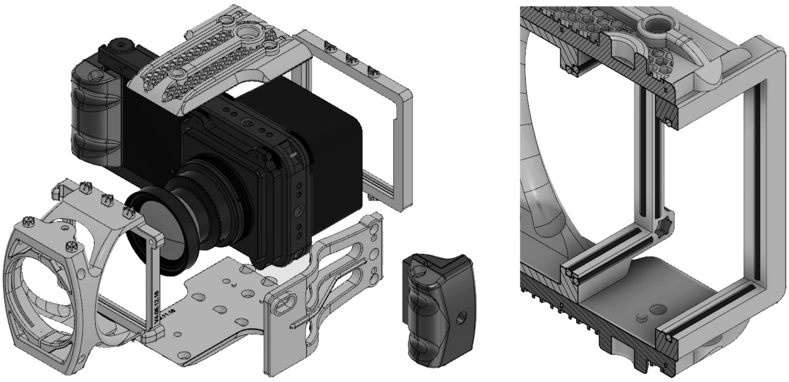

Fig. 3. Exploded view of the current state of the ALPA 12 FPS add|metric. The detail on the right-hand side shows the position of the additional rubber profiles eliminating mechanical play.

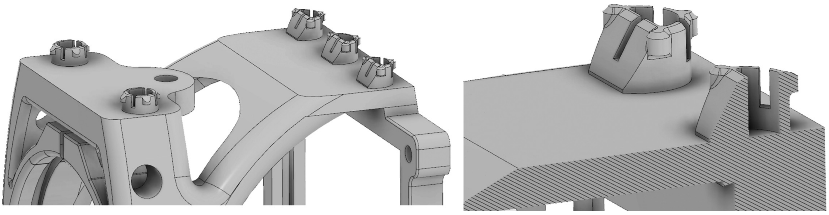

Fig. 4. Two detail drawings showing the connection between the longitudinal brackets and the frames for the lens and digital back. The special profile provides additional retention force in both longitudinal and latitudinal direction.

Like the elimination of the mechanical play, fixing the focusing of the lens is of crucial importance. This is achieved in the ALPA 12 add|metric in two ways: first, clamping the focusing ring takes place by means of a lockable lever, which engages in a toothed ring on the helical of the lens. Secondly, the front ring of the lens is also covered and fastened with two clamping screws. This solution also allows the lens to be supported, thus eliminating the effect of gravity.

In order not to influence the unit formed by the two longitudinal beams and the lens and the jaw holder, which is responsible for the stability of the principal point position and thus the metrological usability of the ALPA 12 add|metric, all further attachments were decoupled from this unit. This applies to the flash holder whose weight thus has no influence on the lens, since it is not attached to the filter thread of the lens, as is generally the case, but by means of an additional holder (see Fig. 3). This is directly screwed to the additional left handgrip, which allows a comfortable grip.

The experience gained in the design and manufacturing process proves that the additive manufacturing from PA3200 GF is generally suitable for the production of special parts for the modification of serial products. In the authors' view, the following factors are decisive for the feasibility:

The process of laser sintering is very vulnerable to geometry changes due to thermal influences: increased heat input induced by high-mass constructions can easily lead to unwanted material growth and strongly asymmetrically scaled components entail the risk of distortion [28]. These factors, as well as the powder removal after sintering, should already be considered in the early stages of the design as much as possible.

Equally important is the earliest possible definition of the material used, the manufacturing process (layer thickness), and in particular the orientation of the part during the sintering process. Depending on the arrangement of the components in the system, different tolerances occur that must be taken into account. Key is at this point especially the close cooperation with the manufacturers of the parts as early as possible in the design process. Subsequent changes in the manufacturing technique almost invariably lead to modifications of the fits and tolerances.

The strengths of additive designs are obvious especially when retro-engineering is required during the course of the design. In our case study, the three-dimensional CAD models were available for ALPA 12 FPS and the lens, but not for the digital back, which also has oblique surfaces that are difficult to measure. Due to the choice of the additive technique, the fit could be optimised at an early stage in the design process by means of function patterns (see Fig. 1 for different stages of the design process).

Since the design of the ALPA 12 add|metric was a new development, the authors involved in the design relied on the "pair construction" approach, which used regular convergence and divergence phases. Between the project meetings, which were held on a weekly basis, the designers independently prepared solutions for the new tasks or current problems. These were then each compared and evaluated. If the discussion of the variants did not provide a clear priority for one of the solution approaches, the choice of the additive manufacturing method permitted the problem-free, time-saving, and cost-effective comparison of both variants. Due to the short innovation cycles, it was possible in most cases to have the new test parts, samples, and prototypes available on a weekly basis for the work meetings.

5 Cost Aspect

Taking into account the expenses for the intermediate samples, the realisation in selective laser sintering proves to be an extremely economic solution. In contrast to the previous model, a photogrammetry solution can also be produced and delivered with the additively modified camera for customer orders within weeks. Even more important is the easy modifiability of the design, which allows quick adaptation to customer-specific needs. This aspect is especially important for SMEs who are dependent on responding as flexibly as possible to customer requirements [1, 30].

6 Evaluation of the ALPA 12 FPS Add|Metric

The internationally recognised German Guideline VDI/VDE 2634 [21] describes practical acceptance and reverification methods to evaluate the accuracy of a point-based optical 3D measuring system such as a single camera. Based on the guideline a volumetric testing field (see Fig. 5) including 58 calibrated lengths, each defined between two signalised points, and three scales is used for the camera calibration. The photogrammetrically estimated lengths are compared as a target-performance evaluation. The maximum deviation, known as maximum length measurement error (LME_{max}), is taken as the system's accuracy.

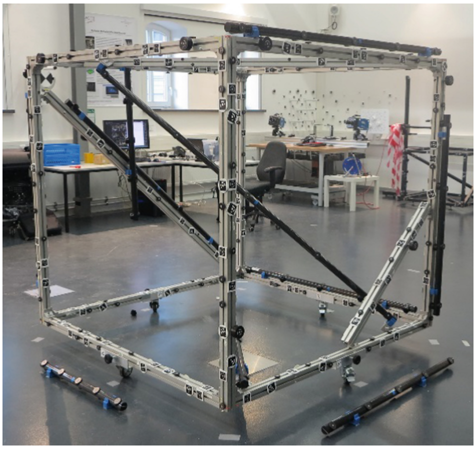

Fig. 5. VDI/VDE 2634 testfield with additional scales

For the evaluation, a standard processing, as well as an image-variant parameter processing was used with AICON 3D Studio, a standard photogrammetric analysis software. The aim is, on the one hand, the assessment of the achievable accuracy of the metric camera within a standard processing workflow while aiming at an LME_{max} of less than 30 µm. On the other hand, the camera-to-lens stability has to be checked in particular with respect to its impact on the results and the evaluation of the Alpa 12 FPS add|metric.

For the standard processing, a set of images is taken in a calibration scheme. The calibration scheme includes images taken while rolling the camera through the optical axis in four main orientations (standard 0°, −90°, +90° and 180°). Table 2 shows a representative selection of the results. The inner precision of the adjustment reaches values in object space of less than 5 µm for each coordinate direction and a 1/30th pixel in image space respectively. The maximum length measurement error remains below 26 µm.

Table 2. Selection of evaluation results with standard processing

Set	Images	Precision object space X-Y-Z [µm]	Precision image space [pixel]	LME_{max} [µm]
1	144	5.1 – 4.9 – 4.0	1/30	19.74
2	172	4.5 – 4.4 – 3.6	1/30	25.74

Additionally, an image-variant processing was added to set 1 (see Table 2). The algorithm describes the calibrated focal length and the point where the optical axis passes through the image plane separately for each image (while in standard processing this is averaged). These values allow for the analysis of the camera-to-lens stability during the acquisition process. Figure 6 exemplarily shows the values of the calibrated focal length for set 1. The table is divided into four parts of the same camera orientation and one part of different camera orientation. The varying values do not show any systematic deviations as they would appear with instabilities e.g. due to gravity influences. The improvement on the length measurement error of 1.7 µm is marginal and demonstrates the stability and metric quality of the camera.

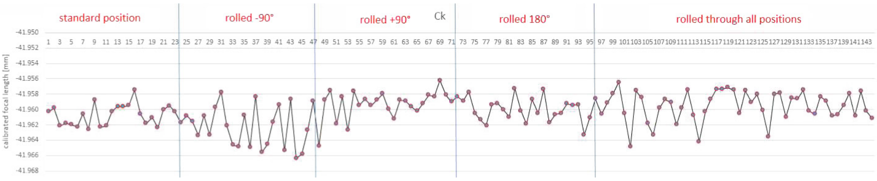

Fig. 6. Values of calibrated focal length for set 1

Comparing the results to the latest tests done with the preceding Alpa 12 WA camera [17] a significant improvement of more than 10 µm (30%) can be determined for the standard processing, using the same test environment. The achievement of high accuracies is decoupled from algorithmic processing. The new Alpa 12 FPS add|metric with additive manufactured fixations allows for its usage in standard processing with concurrent high accuracy.

7 Summary

Photogrammetric techniques allow for a fast, contact-less and accurate acquisition of complex geometries. Currently, the available cameras lack the mechanical stability in combination with high-resolution sensors, thus not exploiting the full potential of photogrammetric systems. Using additive techniques, a digital medium format camera was optimised for these applications. The development process benefits not only from the producible shapes but also from short innovation cycles and cost advantages with respect to the production of small charges. First metrological tests prove the modification's success, as preceding studies are outperformed by a significant amount. Furthermore, the postulated stable mechanical composition is observable in the analysis with variant interior orientation.

References

1. Ahuja, B., Karg, M., Schmidt, M.: Additive manufacturing in production: challenges and opportunities. In: Helvajian, H., et al., (eds.) Laser 3D Manufacturing II. p. 935304 (2015)
2. Mellor, S., Hao, L., Zhang, D.: Additive manufacturing: a framework for implementation. Int. J. Prod. Econ. **149**, 194–201 (2014)
3. Ruffo, M., Hague, R., Tuck, C.: Cost estimation for rapid manufacturing laser sintering production for low to medium volumes. Proc. Inst. Mech. Eng. Part B: J. Eng. Manuf. **220** (9), 1417–1427 (2006). http://sdj.sagepub.com/lookup/10.1243/09544054JEM517
4. Berman, B.: 3D printing: the new industrial revolution. Bus. Horiz. **55**(2), 155–162 (2012). http://dx.doi.org/10.1016/j.bushor.2011.11.003
5. Gibson, I., Rosen, D.W., Stucker, B.: Additive Manufacturing Technologies: Rapid Prototyping to Direct Digital Manufacturing. Springer US, Boston (2010). http://link.springer.com/10.1007/978-1-4419-1120-9
6. Tuck, C.J., et al.: Rapid manufacturing facilitated customization. Int. J. Comput. Integr. Manuf. **21**(3), 245–258 (2008). http://www.tandfonline.com/doi/abs/10.1080/09511920701216238
7. Ahn, D.G.: Applications of laser assisted metal rapid tooling process to manufacture of molding & forming tools - state of the art. Int. J. Precis. Eng. Manuf. **12**(5), 925–938 (2011)
8. Rosochowski, A., Matuszak, A.: Rapid tooling: the state of the art. J. Mater. Process. Technol. **106**(1–3), 191–198 (2000)
9. Lopez, S.M., Wright, P.K.: The role of rapid prototyping in the product development process: a case study on the ergonomic factors of handheld video games. Rapid Prototyp. J. **8** (2), 116–125 (2002). http://dx.doi.org/10.1108/13552540210420989, Accessed 28 October 2016
10. Enkel, E., Perez-Freije, J., Gassmann, O.: Minimizing market risks through customer integration in new product development: learning from bad practice. Creat. Innov. Manag. **14**(4), 425–437 (2005). http://dx.doi.org/10.1111/j.1467-8691.2005.00362.x
11. Rieke-Zapp, D., Tecklenburg, W., Peipe, J., Hastedt, H., Haig, C.: Evaluation of the geometric stability and the accuracy potential of digital cameras—comparing mechanical stabilisation versus parameterisation. ISPRS J. Photogramm. Remote Sens. **64**(3), 248–258 (2009)
12. Ebert, A., Rieke-Zapp, D., Herwegh, M., Ramseyer, K., Gnos, E., Decrouez, D.: Microstructures of coarse grained marbles, analyzed using a new technique based on the bireflectance of calcite. Tectonophysics **463**(1), 175–184 (2009)

13. Berger, C., Schulze, M., Rieke-Zapp, D., Schlunegger, F.: in press. Rill development and soil erosion: a laboratory study of slope and rainfall intensity. Earth Surface Processes and Landforms. doi:10.1002/esp.1989, Accessed 3 June 2010
14. Reznicek, J., Luhmann, T., Jepping, Ch.: Influence of raw image preprocessing and other selected processes on accuracy of close-range photogrammetric systems according to VDI 2634. Int. Arch. Photogram. Remote Sens. Spat. Inf. Sci. **XLI-B5**, 107–113 (2016). doi:10.5194/isprsarchives-XLI-B5-107-2016
15. GSI, 15 March 2017. http://www.geodetic.com/products/systems/v-stars-n.aspx
16. Martin, O.C., Muelaner, J.E., Dhokia, V., Robson, S., Kayani, A., Maropoulus, P.G.: Comparative performance between two photogrammetric systems and a reference laser tracker network for large-volume industrial measurement. Photogram. Record **21**(155), 348–360 (2016). doi:10.1111/phor.12154
17. Reznicek, J., Hastedt, H., Ekkel, T., Luhmann, T., Jepping, Ch.: Analysen zur Datumsfestlegung in photogrammetrischen Projekten großer Volumina. Publikationen der DGPF **25**, 259–270 (2016)
18. Luhmann, T., Robson, S., Kyle, S., Harley, I.: Close-range Photogrammetry. Principles, Methods and Applications. Whittles, Dunbeath (2014)
19. Rieke-Zapp, D., Oldani, A., Peipe, J.: Eine neue, hochauflösende Mittelformatkamera für die digitale Nahbereichsphotogrammetrie. Publikationen der Deutschen Gesselschaft für Photogrammetrie und Fernerkundung **14**, 263–270 (2005)
20. Rieke-Zapp, D., Peipe, J.: Performance evaluation of a 33 megapixel Alpa 12 medium format camera for digital close range photogrammetry. Int. Arch. Photogram. Remote Sens. Spat. Inf. Sci. **36**(5), 4 (2006). (on CD-ROM)
21. VDI: German Guideline on Optical 3D measuring systems – Imaging systems with point-by-point probing VDI/VDE 2634 Part 1 (2002)
22. Caduff, R., Rieke-Zapp, D.: Registration and visualisation of deformation maps from terrestrial radar interferometry using photogrammetry and structure from motion. Photogram Rec **29**, 167–186 (2014). doi:10.1111/phor.12058
23. http://www.alpa.ch/en/article/alpa-12-fps, 22 March 2017
24. http://www.alpa.ch/_files/Rodenstock%20digital%20foto%20lenses%20EN.pdf, 22 March 2017
25. https://www.phaseone.com/~/media/NEW_WEB/Tech-Spec/Backs/IQ%20Digital%20Back%20Range.ashx, 22 March 2017
26. http://eos.materialdatacenter.com/eo/material/pdf/30971/PA3200GF?sLg=de&rnd=1490192876573, 22 March 2017
27. https://www.eos.info/systems_solutions/plastic/systems_equipment/formiga_p_110, 22 March 2017
28. Schmid, M.: Selektives Lasersintern (SLS). In: Additive Fertigung mit Selektivem Lasersintern (SLS). Springer, pp. 9–28 (2015)
29. Horn, T.J., Harrysson, O.L.A.: Overview of current additive manufacturing technologies and selected applications. Sci. Progress **95**(3), 255–282 (2012)
30. Eyers, D., Dotchev, K.: Technology review for mass customisation using rapid manufacturing. Assem. Autom. **30**(1), 39–46 (2010)

Patient Specific Implants from a 3D Printer – An Innovative Manufacturing Process for Custom PEEK Implants in Cranio-Maxillofacial Surgery

Florian M. Thieringer[1,2](✉), Neha Sharma[2], Azagen Mootien[2],
Ralf Schumacher[3], and Philipp Honigmann[2,4]

[1] Department of Oral and Cranio-Maxillofacial Surgery,
University Hospital Basel, Spitalstrasse 21, 4031 Basel, Switzerland
`Florian.Thieringer@swiss-mam.ch`
[2] MAM Research Group, Department of Biomedical Engineering,
Hightech Research Center, University of Basel, Allschwil, Switzerland
[3] MAM Lab, School of Life Sciences, Institute for Medical and Analytical
Technologies, University of Applied Sciences, Basel, Switzerland
[4] Hand Surgery Kantonsspital Baselland, Liestal, Switzerland

Abstract. Additive Manufacturing (AM) is rapidly gaining acceptance in healthcare. Computer-assisted planning of surgical procedures, fabrication of anatomical 3D models, and patient specific implants are well-established processes at the author's department. Surgical planning and medical 3D printing are firmly integrated technologies in the clinical course of treatment at the University Hospital Basel.

Polyether-ether-ketone (PEEK) has been observed, mainly in Cranio-maxillofacial surgery, Spine-, Neuro- and Hand surgery, as a reliable alternative to materials such as titanium for the production of patient-specific implants. The manufacture of medical PEEK implants has been limited mainly to subtractive manufacturing processes such as Computerized Numerical Control (CNC) milling. This production method leads to significant limitations as opposed to AM. 3D printing of PEEK allows construction of almost any complex geometry such as hollow implant bodies or implants in lightweight bio-mimicking design which cannot be manufactured using other technologies.

Recently, it has become possible to process PEEK in the Fused Filament Fabrication (FFF) method, which opens up a number of innovative options for medical-surgical use. With the latest PEEK 3D printers which are now available, inexpensive and compact production intervals for custom implants are conceivable.

Although the medical certification of this workflow is a challenge, the fabrication of patient-specific implants in the operating room in the near future could be possible. In this article, the possibilities and limitations of the production of patient-specific implants from PEEK by 3D printing methods are described, as well as the recent experiences in the field of 3D printing of PEEK implants.

This research project is based on a collaboration of the above-mentioned research institutes and the Apium Additive Technologies GmbH, Karlsruhe, Germany; Brando Okolo, Uwe Popp et al.

© Springer International Publishing AG 2018
M. Meboldt and C. Klahn (eds.), *Industrializing Additive Manufacturing - Proceedings of Additive Manufacturing in Products and Applications - AMPA2017*,
DOI 10.1007/978-3-319-66866-6_29

Keywords: Polyether-ether-ketone · PEEK · FFF/FDM · AM · 3D printing · PSI

1 Introduction

Additive manufacturing (AM) is developing and gaining significance at a very fast rate in the medical field for the reproduction of surgical planning as it is superior to the fabrication processes like subtractive manufacturing processes [e.g. computer numerical control (CNC milling)] as this gives the advantages of being superior in "one-off" production, since there is no need for tooling, no apparent waste and, objects being manufactured with similar precision. AM techniques like Fused filament fabrication (FFF) can be used to create virtually any geometry such as hollow implant bodies and 3D patient specific implants, and are also lightweight in design [1, 2].

There are several different technologies for AM such as stereolithography (SLA), photopolymer jetting, selective laser sintering (SLS), electron beam melting (EBM), direct metal laser sintering (DMLS), fused deposition modeling (FDM), also known as fused filament fabrication (FFF) [3, 4]. Among the current AM technologies, FFF provides a major advantage of low start-up time prior to production; which means that after a short commissioning time, the machine is ready to produce parts. It should also be noted that the purchasing cost of an FFF 3D printer is far below than those of the comparable production techniques. These printers are also of low maintenance, quick to repair and easy to clean [5].

The most important selection criteria for FFF materials are heat transfer characteristics and rheology [6]. Various thermoplastic materials like polycaprolactone (PCL), polyglycolic acid (PGA) etc. have been used in the reconstruction of CMF defects using FFF. However, among the various thermoplastic materials under evaluation, recently polyether-ether-ketone (PEEK) has come out to be a very promising material [7]. PEEK is resistant to many chemicals and features excellent combination of strength, stiffness, durability, environmental resistance and has been used in medical implants, aerospace, automotive, and electrical industries for more than 20 years [8].

It is suitable for load bearing implants because of its favorable bio-mechanical properties, radiolucency, magnetic resonance imaging (MRI) compatibility and chemical inertness [9].

Until now, the bulk of PEEK medical implants could only be manufactured by subtractive manufacturing methods, such as CNC milling. The PEEK implants produced by CNC milling are time consuming and more expensive than AM. Relvas et al. [13] estimated the value of the initial investment of the implemented system about 36.000 Euro, and the cost of surgery, about 400 Euro. The authors obtained the values based on a scenario of five years of use for the equipment and 200 days of work per year. However, no rates of return for the initial investment costs were taken into consideration.

Although manufacturing of 3D PEEK materials has been widely investigated for use in different industries, its use in medical field is still limited as the fabrication of PEEK using FFF 3D printers is quite challenging and difficult due to its very high melting temperature [11]. A large number of publications are still based on preliminary technical results on extrusion based AM of PEEK [12].

In Cranio-maxillofacial (CMF) surgery, reconstructive procedures in the region of the face and the skull often present a challenge to the surgeon. Especially due to the complex anatomy and the need of an optimal rehabilitation of the appearance of the patients, congenital and acquired defects are difficult to treat [10]. The loss of complex or extended bone structures due to trauma or oncologic resection involves a considerable physical and emotional stress for the patients while leaving the surgeon with the consideration of how the defect can be covered in the best possible way. Patient-specific implants (PSI) can be an effective solution in this situation, helping to overcome these difficulties and the resulting uncertainties [14]. The PSI are designed to fit precisely in the anatomical defects or malformations. After having finalized the Computer-aided design (CAD), the implant shape is controlled visually and, if needed, modified in the course of an iterative process, using an AM model of the implant in combination with the patient's anatomy as to control and optimize the shape and fit of the implant on the bone [15].

In this view point article, we present the preliminary observations and potential of specialized FFF 3D printer to generate PEEK PSI. This manufacturing process produces complex three- dimensional parts using layered printing process directly from a computer model without a need of further tooling.

2 Materials and Printing Process

2.1 3D Printer

The 3D printer used in our study is HPP155 based on the FFF technology manufactured by Apium Additive Technologies GmbH, Karlsruhe, Germany (formerly known as Indmatec HPP155/Gen. 2). The printer uses Apium Controlling Software (CS) utilizing STL format files.

2.2 PEEK Filament

For the printing process, Apium PEEK 450 Natural 1.75 mm filament was used which is a semi-crystalline polymer with density of 1.30 g/cm3 and tensile strength of 97 MPa with the ASTM D638 test method was used (https://apiumtec.com/en/filaments/).

2.3 Printing Process

For the printing process, first, the radiological raw data of the patient is obtained in a Digital Imaging and Communications in Medicine (DICOM) and is then imported into a medical modeling program to generate a virtual 3D patient specific model. This step is also called segmentation. After this, the 3D model is manipulated on the computer to design the "spare-part" that will eventually become the custom implant to be modeled. The final data sets are then converted and separa-ted as a Standard Tessellation Language (STL) and send to the 3D printer, which then generates the implant.

The current FFF technique involved deposition of molten thermoplastic materials through one nozzle in a specific laydown pattern. In this process, the object including support structures is printed layer by layer. The filament is supplied to the machine through a nozzle. The nozzle follows a raster pattern in the X, Y plane and forms a layer. After, a layer is finished, the working bed in the Z direction is lowered and the new layer is extruded. Support structures were incorporated in the geometry of the implants. Thus, the part is built in a layer by layer fashion fusing the layers together [4].

3 Preliminary Results

The first tests were made with FFF 3D PEEK printer. These tests confirm the possibility of processing PEEK in the desired way (extrusion through a small nozzle). Figure 1 shows 3D printed osteosynthesis plates. Figure 2 shows one of the latest parts in the shape of a skull implant used in cranioplasty for repair of cranial vault defects. Figure 3 shows a 3D-printed PEEK implant with support structures for immediate replacement of the zygomatic bone after tumor surgery of the midface.

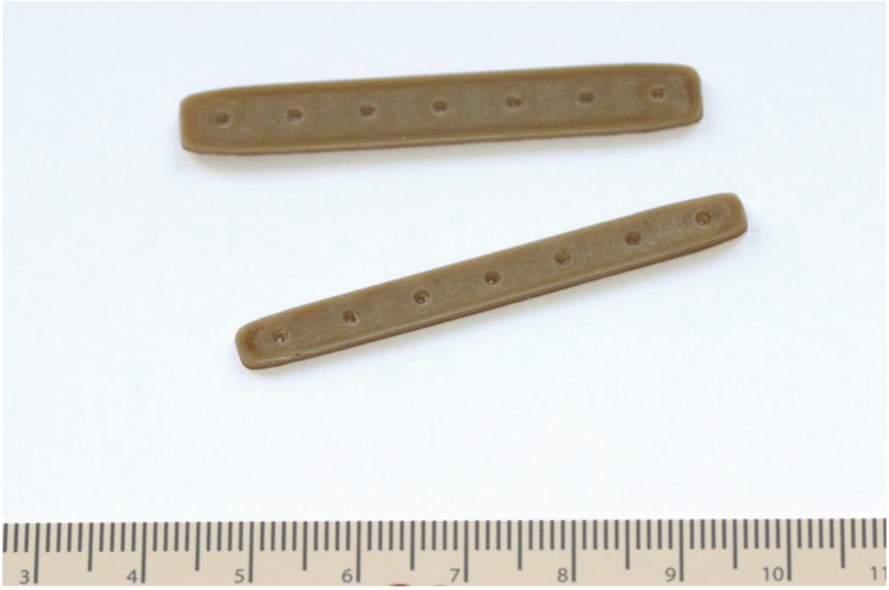

Fig. 1. 3D-printed PEEK osteosynthesis plates (length of 50 mm)

The 3D printed PEEK implants fabricated by this process were without any discoloration (improper crystallization) and deformation. The bed temperature (about 100 °C) and the print temperature (about 400 °C) of the printer were high enough to provide a good thermal control over the entire build chamber leading to a good layer bonding and thereby, preventing black specks in the PEEK prints. As the print chamber is entirely enclosed, another aspect to consider when preparing an object for 3D printing at such high temperatures is the method to hold the print to the surface. Therefore, a special fixative (DimaFix, DIMA 3D, Valladolid, Spain) spray applied to a "cold" printbed for adhesion was used in this technique.

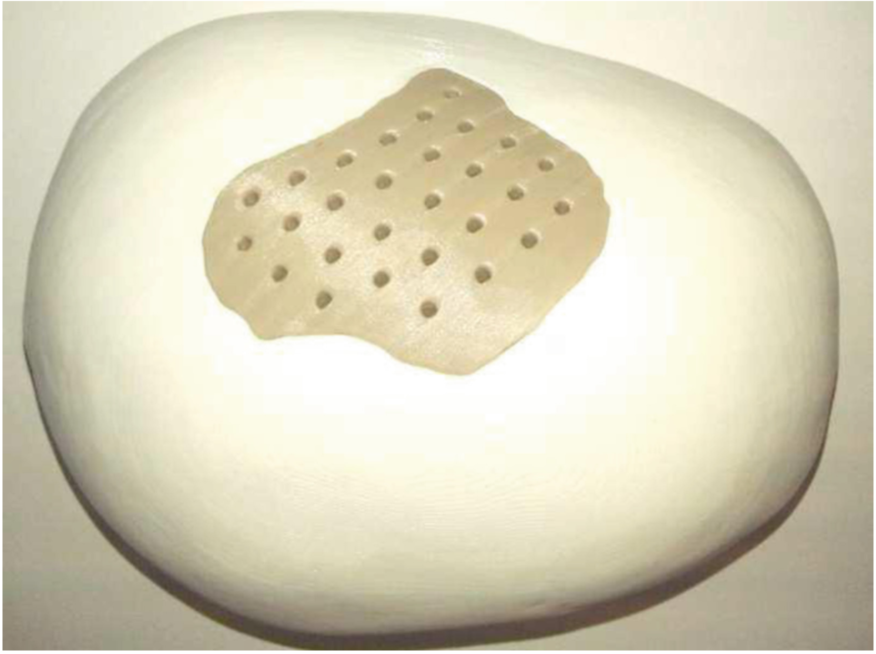

Fig. 2. 3D-printed cranioplasty PSI for repair of defects in the cranial vault

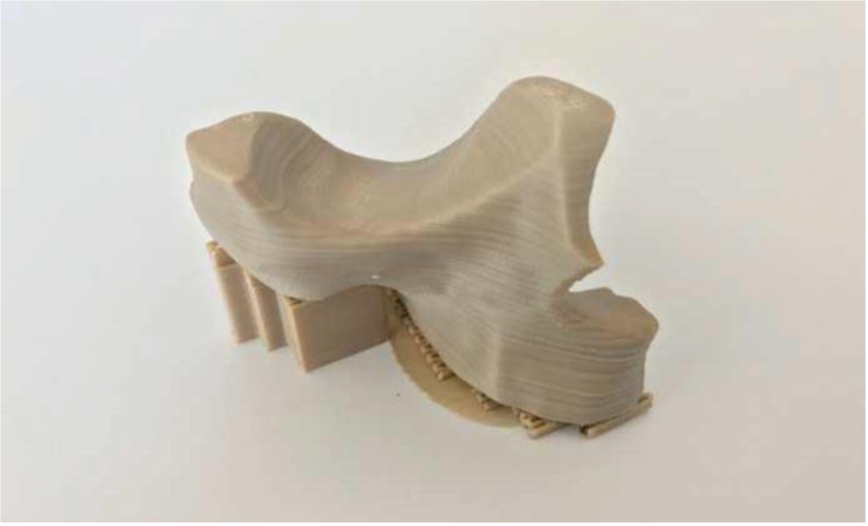

Fig. 3. Exactly fitting 3D-printed lightweight PEEK implant for immediate replacement of the zygomatic bone after tumor surgery

The result findings suggest that the goal of the 3D printer to produce even complex anatomical/geometrical shapes is possible.

4 Discussion

With the introduction of computer aided design and manufacturing techniques in surgery, it has become possible to fabricate implants using various modern biocompatible materials. Many of these materials can only be processed with great difficulties using traditional production methods. One of these newer materials is the thermoplastic high-performance polymer known as PEEK. PEEK has been conventionally fabricated by using subtractive techniques like CNC milling and additive techniques like SLS. However, all these processes are expensive and material-consuming. More recently, with the introduction of FFF printers, 3D printing of PEEK PSI is conceivable. In contrast to CNC milling, the AM of PEEK PSI by FFF has substantial benefits in the medical field.

This process not only provides cost advantages, but also reduces the manufacturing time in comparison with the conventional production methods. While being highly cost-effective with little material waste, the 3D printing of PEEK allows an almost unlimited geometry of the implant body to be selected with outstanding biomechanical properties in the case of reduced stress-shielding effects (in the bone-healing process) and weight savings, which would hardly be possible with traditional milling methods [16].

However, the process of manufacturing PEEK by FFF 3D printing is complex due to coupled interactions of many parameters. The critical factors for 3D printing of PEEK by FFF are high-temperature extrusion head design, and efficient heat management throughout the process, so as to achieve continuous printing. Nevertheless, with the introduction of an all metal hot-end extruder capable of attaining temperatures up to 520 °C, working on PEEK in FFF 3D printing has become possible. The preliminary findings from the PEEK prints suggest that anatomically complex PSI can be printed using an FFF 3D printer. The authors believe that such a process, can provide various advantages like less wastage of material, cost-effectiveness, low investment on machine (cost of the printer about 20.000 Euro) and operator training, faster in-house implant production and a better personalized patient care approach. All these factors have a potential in reducing the overall healthcare management cost.

Nevertheless, the FFF 3D printing process also carries certain disadvantages like requirement of support structures for complex anatomy of implants with overhangs, temperature fluctuations during production that may lead to delamination, and restricted accuracy due to the diameter of the building filament. Another key drawback that needs attention is the anisotropic behavior of the FFF 3D printed PEEK implants. As FFF 3D printers melt polymers layers on top of layers, leading to a mechanical adhesion, the emerging FFF-printed objects may have different mechanical properties based on the direction of mechanical stress applied on them.

This anisotropic behavior needs to be addressed and tested in future experiments. Within the framework of the cooperation of the institutions listed above, a PEEK FFF printer, which has been introduced to the industrial market for some time, is undergoing the certification process for medical applications. The test specimens required for the certification were prepared, evaluated and passed through other test methods (e.g. cleaning, sterilization and surface modification). In a further step, the integration of 3D printing is additionally examined from the medico-legal point of view in the clinical environment.

5 Conclusion

Though this article presents only a limited amount of the research done in the project to process PEEK by means of FFF, it indeed opens up a huge scope for innovation in the medical-surgical applications.

To produce 3D manufactured PEEK parts with maximum precision, it is crucial to observe critical factors such as accurate printing temperature, printing speed, nozzle size and viscosity of the PEEK and requirement of special devices to control the thermo-mechanical processes that lead to the solidification of the extruded thermoplastic material. Additionally, medico-legal aspects and Medical Device Regulation (MDR) also needs to be addressed to successfully integrate the 3D printing process of PSI on-the-spot.

With the advent of inexpensive compact 3D printers, a one-stop-shop solution is conceivable in which the surgeons of the future will manufacture medically certified 3D PSI in their own clinics. This would have a major advantage for cutting, planning, and production intervals for PSI and save a substantial amount of time compared with off-site implant production by third-party providers thereby leading to a more cost-effective healthcare management.

References

1. Ventola, C.L.: Medical applications for 3D printing: current and projected uses. PT **39**(10), 704–711 (2014)
2. Hoang, D., Perrault, D., Stevanovic, M., Ghiassi, A.: Surgical applications of three-dimensional printing: a review of the current literature & how to get started. Ann. Transl. Med. **4**(23), 456 (2016). doi:10.21037/atm.2016.12.18
3. Dickens, P.M., Stangroom, R., Greul, M., Holmer, B., Hon, K.K.B., Hovtun, R., Neumann, R., Noeken, S., Wimpenny, D., et al.: Conversion of RP models to investment castings. Rapid Prototyp. J. **1**(4), 4–11 (1995). doi:10.1108/13552549510104401
4. Zein, I., Hutmacher, D.W., Tan, K.C., Teoh, S.H.: Fused deposition modeling of novel scaffold architectures for tissue engineering applications. Biomaterials **23**(4), 1169–1185 (2002). doi:10.1016/S0142-9612(01)00232-0
5. Novakova-Marcincinova, L., Kuric, I.: Basic and advanced materials for fused deposition modeling rapid prototyping technology. Manuf. Ind. Eng. **11**(1), 1338–6549 (2012)
6. Chia, H.N., Wu, B.M.: Recent advances in 3D printing of biomaterials. J. Biol. Eng. **9**, 4 (2015). doi:10.1186/s13036-015-0001-4
7. Kim, M.M., Boahene, K.D.O., Byrne, P.J.: Use of customized polyetheretherketone (PEEK) implants in the reconstruction of complex maxillofacial defects. Arch. Facial Plast. Surg. **11**(1), 53–57 (2009). doi:10.1001/archfaci.11.1.53

8. Rigby, R.B.: Polyetheretherketone. In: Margolis, J.M. (ed.) Engineering Thermoplastics: Properties and Applications, pp. 299–314. Marcel Dekker Inc., New York (1985). doi:10.1002/pol.1986.140240616
9. Najeeb, S., Khurshid, Z., Matinlinna, J.P., Siddiqui, F., Nassani, M.Z., Baroudi, K.: Nanomodified peek dental implants: bioactive composites and surface modification - a review. Int. J. Dent. **2015**, 381759 (2015). doi:10.1155/2015/381759
10. Dérand, P., Rännar, L.E., Hirsch, J.M.: Imaging, virtual planning, design, and production of patient-specific implants and clinical validation in craniomaxillofacial surgery. Craniomaxillofac Trauma Reconstr. **5**(3), 137–144 (2012). doi:10.1055/s-0032-1313357
11. Petzold, R., Zeilhofer, H.F., Kalender, W.A.: Rapid prototyping technology in medicine-basics and applications. Comput. Med. Imaging Graph. **23**(5), 277–284 (1999). doi:10.1016/S0895-6111(99)00025-7
12. Guevara-Rojas, G., Figl, M., Schicho, K., Seemann, R., Traxler, H., Vacariu, A., et al.: Patient- specific polyetheretherketone facial implants in a computer-aided planning. J. Oral Maxillofac. Surg. **72**(9), 1801–1812 (2014). doi:10.1016/j.joms.2014.02.013
13. Relvas, C., Reis, J., Potes, J.A., Fonseca, F.M., Simões, J.A.: Rapid manufacturing system of orthopedic implants. Rev. Bras. Ortop. **44**(3), 260–265 (2015). doi:10.1016/S2255-4971(15)30077-X
14. Chen, H.L., Porter, R.S.: Melting behavior of poly (ether ether ketone) in its blends with poly (etherimide). J. Polym. Res. **31**(12), 1845–1850 (1993). doi:10.1002/polb.1993.090311217
15. Vaezi, M., Yang, S.: Extrusion-based additive manufacturing of PEEK for biomedical applications. Virtual Phys. Prototyp. **10**(3), 123–135 (2015). doi:10.1080/17452759.2015.1097053
16. Thieringer, F., Popp, U., Okolo, B., Schumacher, R., Honigmann, P.: Custom Implants for Humans from a 3-D Printer – An Innovative Manufacturing Process for Custom PEEK Implants. Kunststoffe international, April 2016

Teaching and Training

Work-Process Orientated and Competence Based Professional Training for Skilled Workers in Laser Additive Manufacturing

Christian Daniel(✉), Bianca Schmitt, and Maren Petersen

Institute Technology and Education ITB, University of Bremen,
28359 Bremen, Germany
christian.daniel@uni-bremen.de

Abstract. In production technology innovative machining methods such as additive manufacturing are changing the work-fields and work-processes of skilled workers and thus their professional training needs to be altered. Laser additive manufacturing currently experiences introduction in serial applications in aircraft or medical industry. In this context parts of very high quality are mandatory and to achieve this it is necessary to set up processing strategies and parameters. Nevertheless a high complexity in the relationship between parameter setting and process outcome is characteristic for additive technology. Due to this fact comprehensive experience and know-how, which is yet few to be found, is demanded from machine operators. Surveys conducted in the industry show that consequently changed qualification requirements upon skilled workers can already be defined in detail for additive manufacturing. Therefore a corresponding professional training was developed which is work-process orientated and focuses on the specialized competencies for professional decision-making and responsibilities. In this context the training approach explicitly does not concentrate only on simple machine or process instruction for additive manufacturing. Rather the methodical didactic concept bases on a blended learning approach which includes the combination of multiple learning locations as well as project based learning in a professional context. Here technical contents are connected to a sequence of tasks in form of modules each with a reference to the professional practice. In this way also the shift towards close to engineering tasks and methods for continuous self-learning are addressed. Finally learning systems regarding the infrastructure and capacities that are required for a learning environment are assessed. In conclusion additive manufacturing and its digital process chain represents a typical example for changing work settings for trained professionals in the context of increasingly interconnected industrial processes. Therefore the developed professional training can perspectively also be transferred to further processes in Industry 4.0.

1 Introduction

Additive manufacturing (AM) currently experiences introduction in serial applications for example in aircraft or medical industry. Especially the aircraft and aerospace industry represents important fields of application for AM as a high degree of

© Springer International Publishing AG 2018
M. Meboldt and C. Klahn (eds.), *Industrializing Additive Manufacturing - Proceedings of Additive Manufacturing in Products and Applications - AMPA2017*,
DOI 10.1007/978-3-319-66866-6_30

geometrical freedom for lightweight design and series with a small lot size can be achieved [1, 2]. In this context direct manufacturing of final products by selective laser melting (SLM) represents the field of application with the biggest developing potential which is expected to significantly expand further throughout the following years [1]. Already within a timespan of about 10 years a growth from 3.9% in the year 2003 to 19.2% in the year 2012 in directly manufactured final products based on the overall manufactured parts, prototypes and models by additive manufacturing shows this increase which is expected to continue further [3]. Nevertheless the enormous potential provided by AM can only be exploited when there are appropriately skilled workers available in the industry throughout all steps of the process chain [4]. Consequently, based on the continuous development and the increasing wide spread use of AM technology, a built-up of well-trained skilled workers should be aspired. Therefore the present paper makes an approach for an innovative training method contributing to the situation of training and education in the field of AM.

2 State of the Art in Professional Training for Additive Manufacturing

As Germany represents a significant corporative actor in AM technology its situation of education and vocational training is exemplarily analyzed. In the German vocational training and education system the introduction of AM methods has already taken place for six professions such as production technologists (Produktionstechnologe/-in), technical product designers (Techn. Produktdesigner/-in), technical model makers (Techn. Modellbauer/-in), engravers (Graveur/-in) and casting mechanics (Gießereimechaniker/-in) [5].

A performed analysis of curricula for these professions in the metal industrial sector shows that training contents of AM are already placed within the standard formal guidelines between the 2nd and 4th year of vocational training [5]. For these professions the following exemplary competencies regarding AM methods are to be studied [5]:

- Preparation of AM production processes
- Planning and manufacturing of prototypes and samples
- Choosing suitable methods for transferring data in exchange formats like STL etc.
- Computer assisted manufacturing of models, forms and samples
- Developing parts from plastic regarding methods from forming and primary shaping in the context of assemblies

Nevertheless, regarding that there is a total number of more than 30 professions in which a professional career can be aspired in the metal processing industry, this situation shows that AM it still few to be found in professional curricula when compared to conventional manufacturing methods such as milling or turning and if it is found the detailed AM technologies are not explicitly named [6]. In contrast to this the introduction of more contents regarding AM would be desirable especially for substantial professions like aircraft device mechanics (Fluggeräte-mechaniker/-in), precision mechanics (Feinwerkmechaniker/-in), industrial mechanics (Industriemechaniker/-in), mold makers (Werkzeugmechaniker/-in) or product developers [7].

Furthermore, besides the initial vocational training, trainings for skilled workers with advanced professional experience are already provided e.g. by research institutes, universities, companies or professional associations such as ‘Hochschule Schmalkalden’, ‘Fraunhofer IFAM’, ‘LZH Laser Akademie GmbH’ or ‘LZN Laser Zentrum Nord GmbH’ in terms of workshops or longterm courses of studies [8–11]. LZH offers a training for “Specialists for additive manufacturing methods/rapid technologies” in accordance to guideline DVS®3602-1 which represents a certified professional training [10].

The amount of training possibilities underlines that there is a significant offer and demand of professional AM training present in the market. From the perspective of the AM users this provides the opportunity to choose between different forms of training and to decide the best suitable training method for each specific need. The work-process in AM represents the focus for learning in the present paper and learning methods in terms of an educational scientific point of view are subordinated given that approved methods are combined in an innovative setting focusing on a vocational scientific point of view [12–15].

3 Identification of Competencies for Additive Manufacturing

In AM professional reality it is necessary to be able to apply knowledge in consistently new and challenging situations and potentially also to be able to transfer knowledge to variable AM technologies. Therefore the acquirement of competencies is necessary. In this context the term of competencies includes the subjective perspective of employees and is therefore more comprehensive than a qualification [12, 13]. For the purpose of the identification of required competencies for AM in a first step a sector analysis was performed followed by a questionnaire based survey regarding topics such as utilized laser based manufacturing methods, field of activities, state of knowledge and type of experienced training. The questionnaire provided access to a feedback of 40 professional respondents from companies in the laser based manufacturing branch. Though the sample of the survey does not allow a statistical analysis or verification yet results were consistent so that it was possible in this manner to specifically design the framework for the following interviews [16]. The interviews were conducted with selected experts from the industry. They were executed with regards to a determination of up-to date qualitative data directly from the industrial application of AM. To be able to compare the results from the surveys these were structured using an interview guideline organized by the topics ‘future development of AM methods’, ‘skilled labor in this context’ and ‘demands for qualification’. The structured but open interviews were executed with 5 stakeholders from different branches of the metal processing industry such as dental technology, suppliers for aerospace industry, small and medium-sized businesses from mold making, research centers and service suppliers. The interviewees were holding functions in divisions of technical management, development, design and manufacturing and represented both personnel in leading positions as well as employees in technical executing positions.

To be able to acquire target-oriented information from the interviews specific AM methods need to be chosen. This is also necessary for the development of an exemplary learning situation thus the training needs to address specific AM methods. Based on the analysis in Sect. 2, the initial inquiry towards interview partners and the following interview preparation on the one hand powder-bed based SLM was selected due to a high significance for industrial applications in metal and plastic. On the other hand fused deposition modeling (FDM) based on extrusion of filament was selected. This considers the suitability of FDM for training regarding costs for machines and raw plastic material. Furthermore also end products and functional prototypes are usually manufactured in an industrial context by FDM [17].

For the evaluation of the interviews audial recordings were transcribed and analyzed based on determined categories in accordance to the steps of the process chain in AM. This approach was chosen due to the fact that the competencies for skilled workers in AM were expected to be well correlated to the steps of the process chain in AM. The process chain is complex due to its manifold steps and thus demands an expertise in different disciplines from skilled workers. The process chain contains steps in Pre-, In- as well as Post-processing such as a discussion with a customer, 3D-CAD design, revision of digital data, slicing, manufacturing, finishing and collaborative discussion [18, 19] (Fig. 1). In this context the didactical concept of learn and work assignments (LWA) is introduced which consist of ‘Assignment of order’, ‘Planning’, ‘Execution’ and ‘Closure’ [14]. In conjunction to the steps of the AM process chain analogies to the phases of learn and work assignments can be seen (Fig. 1). Therefore this connection is exploited in the development of a didactic concept in the following section.

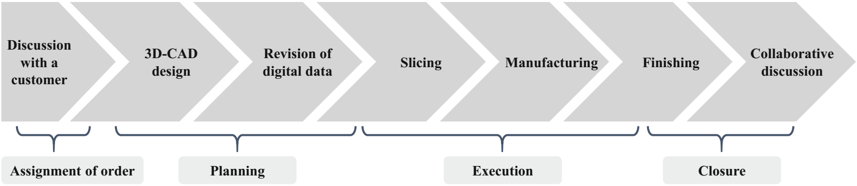

Fig. 1. Process chain in additive manufacturing regarding the work-processes

The results of the interviews emphasize demands of competencies within the fields shown in Fig. 2. Furthermore the aggregation of identified competencies from the interviews is shown (Fig. 2). For the development of creative solutions in a discussion with a customer, competencies such as problem solving, planning as well as social and technological competencies are required. Throughout the following steps of the process chain competencies are demanded that comprise the adept handling of computers and software. Competencies in information technology (IT) have to be applied to knowledge in design for AM as well as to technological competencies covering e.g. AM specific process knowledge. Therefore interdisciplinary thinking and acting is necessary.

In the context of the design and data preparation process it depends on the size, the organizational structures and thus the degree of division of labor within each business unit how intensively the skilled worker is involved in this step. Nevertheless within

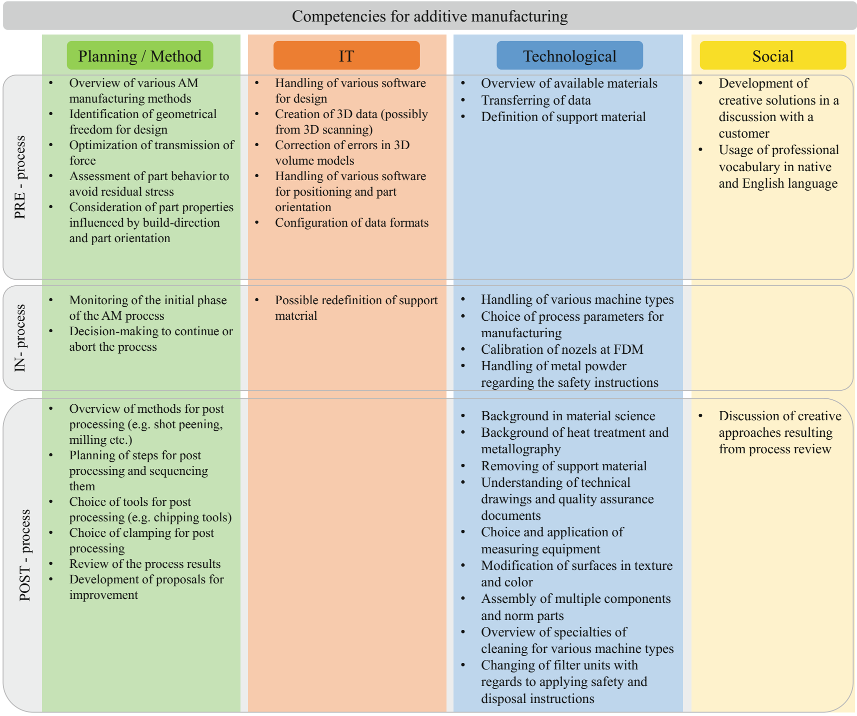

Competencies for additive manufacturing

	Planning / Method	IT	Technological	Social
PRE - process	• Overview of various AM manufacturing methods • Identification of geometrical freedom for design • Optimization of transmission of force • Assessment of part behavior to avoid residual stress • Consideration of part properties influenced by build-direction and part orientation	• Handling of various software for design • Creation of 3D data (possibly from 3D scanning) • Correction of errors in 3D volume models • Handling of various software for positioning and part orientation • Configuration of data formats	• Overview of available materials • Transferring of data • Definition of support material	• Development of creative solutions in a discussion with a customer • Usage of professional vocabulary in native and English language
IN- process	• Monitoring of the initial phase of the AM process • Decision-making to continue or abort the process	• Possible redefinition of support material	• Handling of various machine types • Choice of process parameters for manufacturing • Calibration of nozels at FDM • Handling of metal powder regarding the safety instructions	
POST - process	• Overview of methods for post processing (e.g. shot peening, milling etc.) • Planning of steps for post processing and sequencing them • Choice of tools for post processing (e.g. chipping tools) • Choice of clamping for post processing • Review of the process results • Development of proposals for improvement		• Background in material science • Background of heat treatment and metallography • Removing of support material • Understanding of technical drawings and quality assurance documents • Choice and application of measuring equipment • Modification of surfaces in texture and color • Assembly of multiple components and norm parts • Overview of specialties of cleaning for various machine types • Changing of filter units with regards to applying safety and disposal instructions	• Discussion of creative approaches resulting from process review

Fig. 2. Competencies for additive manufacturing structured in matrix form

training for AM all steps of the process chain should at least be addressed in a basic manner to enable e.g. problem solving competencies when manufacturing problems arise from other parts of the process chain than the ones in which certain trained staff is specialized in.

In summary the surveys conducted in the industry show that competency requirements upon skilled workers can already be defined in detail for additive manufacturing and that a high demand throughout all levels of degrees including also technicians, master craftsmen and engineers is persistent. Therefore in the next step a corresponding professional training is developed which explicitly does not concentrate only on simple machine or process instruction for additive manufacturing but is work-process orientated and focuses on the specialized competencies for professional decision-making and responsibilities.

4 Development of Work Process Orientated Professional Training

Since the qualification and competency requirements upon skilled workers are identified a corresponding professional training is developed in the following section. It is work process orientated and focuses on the specialized competencies for professional decision-making and responsibilities. Furthermore it addresses homogenous as well as heterogeneous target groups from various professions and experience levels. Therefore the derived exemplary learning situation for AM can be integrated in initial basic vocational training as well as in the advanced training of skilled workers.

As described in the prior section the acquirement of competencies for skilled workers in AM is necessary. Nevertheless competencies are greatly difficult to be taught in ex-cathedra teaching situation in which solely theoretical knowledge is transferred. The ability to self-organized and creative acting under the uncertainty of open system environments is rather imparted in process orientated learning with self-reflection of technical content. This can be achieved by applying the approved didactic concept of learn and work assignments (LWA) [14]. These represent situations in project form which are process- and task-orientated, containing problem situations with regards to real vocational context [14]. The configuration of the learning situation should be orientated towards the principle of wholly acting and should address the steps ‘Informing’, ‘Planning’, ‘Executing’ and ‘Checking’ to achieve the superordinate aim of acting orientation [15]. Therefore a LWA consists of the four phases ‘Assignment of order’, ‘Planning’, ‘Execution’ and ‘Closure’ in which a product or a service is realized in context to a reality based customer and manufacturing order. Based on specific operational challenges trainees realize and deliberate practical solutions within a team while the implementation of the above named competencies is achieved by embedding them into the each LWA’s project step (Fig. 3).

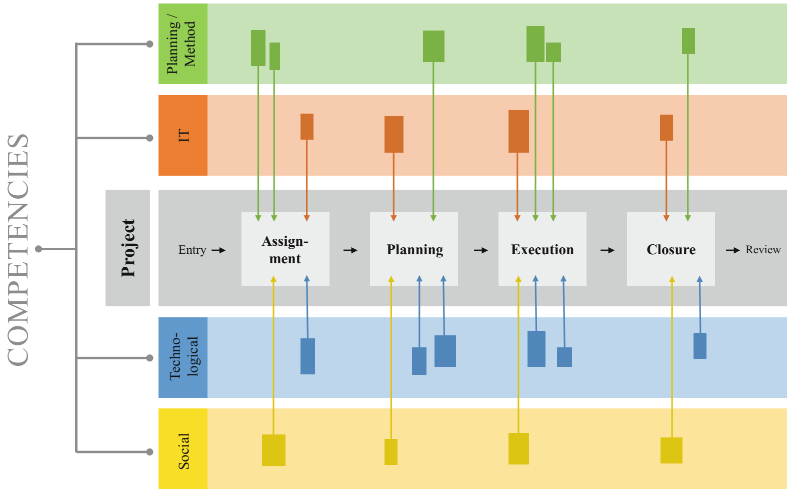

Fig. 3. Structure of learn and work assignments (LWA)

Furthermore as an innovative approach in this contribution the conception of a LWA for AM training is simultaneously merged with the methodical didactic concept of a blended learning approach which includes the combination of multiple learning locations (Fig. 4). These are specifically used to address each particular content in an each suitable learning environment and thus enhance the learning process overall. By this combination of two didactic methods conventional teaching structures can be overcome and a project based learning approach is realized which imparts the necessary professional competencies for AM.

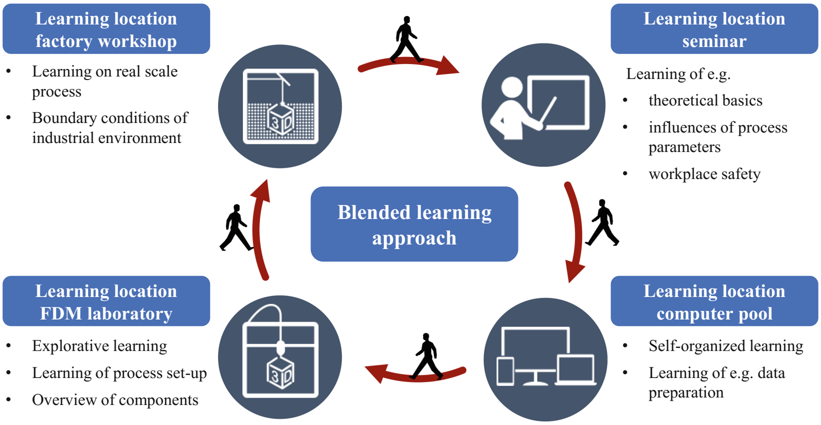
Learning location factory workshop
- Learning on real scale process
- Boundary conditions of industrial environment
Learning location seminar
Learning of e.g.
- theoretical basics
- influences of process parameters
- workplace safety
Blended learning approach
Learning location FDM laboratory
- Explorative learning
- Learning of process set-up
- Overview of components
Learning location computer pool
- Self-organized learning
- Learning of e.g. data preparation
3D
3D

Fig. 4. Blended learning approach with different learning locations

For the developed training four learning locations can be identified. These consist of a seminar room, a PC-pool, an AM laboratory e.g. equipped with a FDM machine and an industrial sized workshop with access to SLM machines.

The learning location of a seminar room as well as a PC-pool is suitable for the first phase of the LWA. A customer order is introduced by the trainer where the manufacturing of a prototype part is queried first from plastic material and in a later serial production from metal material. The queried part contains AM relevant elements that demand an AM specific design. Aspects such as lightweight potential, integrated functions, individualized components or a minor lot size can be addressed. Also necessary theoretical basics about AM are introduced. The trainees form project groups and process assigned tasks within the prepared project framework under supervision of the trainer. The first application of the developed LWA showed that groups of up to 5 people are feasible. Depending on the training situation also the introduction of a group design challenge with the aim to achieve the best technical solution for the projected part can be taken into consideration. The teams gather information about relevant AM methods autonomously and after inquiry the stakeholders exchange their achieved results. In this way besides the technical competencies also methodical and social competencies are trained simultaneously. The trainer chairs the learning process, complements neglected content, corrects in case of mistakes and directs towards the next phase of the LWA. Also the learning location of an AM laboratory can be used to provide the trainees first hand insight of the components of AM machines.

In the planning phase of the LWA the trainer introduces the steps of the AM process chain and demonstrates the handling and possibilities of data preparation software such as the placement of support structures and part orientation in the building chamber. Therefore a learning location equipped with digital media is necessary. Further the trainees themselves apply the creation and configuration of CAD-data as well as the correction of digital models and final data preparation for the AM process with corresponding software on computer workplaces under the guidance of the trainer.

In the execution phase of the LWA the trainees transfer the prepared production data of their group to the FDM machine followed by the definition of process parameters and set-up of the process. In this context learning locations such as an AM laboratory and also a seminar room or PC-pool can be used e.g. to learn about influences of process parameters in the AM process. Finally the trainees observe the start-up phase of the building process and after finishing of the building process the groups execute the prior planned steps of post-processing.

In the closure phase of the LWA the reflection of achieved results is carried out. After finishing of the manufacturing process the quality of the manufactured part of each group is assured. The trainees therefore are coached in handling of corresponding measurement equipment and they document the results in quality protocols. This proceeding aims towards a self-responsible reflection of the process results by the trainees. Successfully passed process steps as well as occurred problems are documented and propositions for improvement are made. These are subsequently discussed with the trainer and modifications are defined for the derivation of a manufacturing procedure for the metallic serial part.

Since the application of FDM cannot reproduce the whole complexity in each step of the process chain for industrially relevant, metal processing SLM the trainees commence a second manufacturing cycle. Else e.g. the handling of metal powder and filter components would be neglected and also the post-processing for both manufacturing method differs. The project groups are therefore passing through the steps of the process chain for the metallic part where the trainer focusses on imparting SLM specific differing competencies while the group works more self-reliant on the process steps analogous to FDM.

Nevertheless also limitations of the LWA can be observed from an initial application of the training. In this way the evenly integration of all group members turned out to be challenging. Also setting up of small groups means a splitting of the learning group and thus demands a high commitment of the trainer. In term of the project timeline the LWA needs to be divided in multiple sessions due to the time consuming manufacturing process which could mean a limitation e.g. in a scholar context. Finally also limited view and space in front of AM machines may conflict with the fact that manufacturing may be started at once from multiple groups which therefore are all meant to observe the proper start-up of the process at the same time.

5 Summary and Outlook

In the presented contribution a professional training was developed combining two didactic concepts. In this way the training provides future perspectives for employees in initial basic vocational training as well as in the advanced training of skilled workers. The learning situation enhances a straight forward access to innovative technologies of

AM and prospectively important competencies can be acquired by a variety of target groups. The AM training furthermore reacts to a typical example for changing work settings for trained professionals in the context of increasingly interconnected industrial processes. Therefore the developed training can perspectively also be transferred to further processes in the context of Industry 4.0. Following steps can be seen in the detailed evaluation during an implementation of the developed professional training. With future development also approaches of learning in a virtual additive manufacturing environment is thinkable and learning content can be provided by this media.

Acknowledgments. The authors would like to thank Mr. Springer, P. whose graduation thesis resulted from the course of this work.

References

1. Wohlers, T.: Wohlers Report 2014–3D Printing and Additive Manufacturing State of the Industry. Wohlers Associates, Fort Collins (2014)
2. Campbell, I., Bourell, D., Gibson, I.: Additive manufacturing: rapid prototyping comes of age. Rapid Prototyping J. **18**(4), 255–258 (2012)
3. Breuninger, J., et al.: Generative Fertigung mit Kunststoffen – Konzeption und Konstruktion für Selektives Lasersintern. Springer, Heidelberg (2013)
4. VDI - Verein Deutscher Ingenieure e.V.: Statusreport Additive Fertigungsverfahren September 2014 (2014)
5. Rahmenlehrplan für den Ausbildungsberuf Produktionstechnologe/Produktionstechnologin, Technischer Modellbauer_in, Technischer Produktdesigner_in, Gießereimechaniker_in, Graveur_in Graveurin, Metallbildner_in (Beschluss der Kultusministerkonferenz vom 15.02.2008, 23.04.2009, 27.05.2011, 26.03.2015, 17.03.2016)
6. IHK Berlin, Handwerkskammer Berlin (Hrsg.): Bildung in Zahlen - Ausgabe 2016, Berlin (2016)
7. EFI - Expertenkommission für Forschung und Innovation: EFI Gutachten 2015-Additive Fertigung “3D-Druck” (2015)
8. Form+Werkzeug: Startschuss für Studium zum Anwendungstechniker/in für additive Verfahren/Rapid-Technologien Hochschule Schmalkalden (2016)
9. Fraunhofer-Institut für Fertigungstechnik und Angewandte Materialforschung IFAM: Pulvertechnologie Schulungen und Weiterbildung (2017)
10. LZH Laser Akademie GmbH: Fachkraft für additive Fertigungsverfahren nach Richtlinie DVS® 3602-1 (2016)
11. LZN Laser Zentrum Nord GmbH: Die Light Academy - Aus- und Weiterbildung im Bereich der (laser-)additiven Fertigung bzw. des industriellen 3D Drucks (2017)
12. Becker, M., Spöttl, G. (eds.): Berufswissenschaftliche Forschung – Ein Arbeitsbuch für Studium und Praxis. Peter Lang Internationaler Verlag der Wissenschaften, Frankfurt am Main (2008)
13. Rauner, F.: Qualifikation, Kompetenz und berufliches Wissen – ein aufklärungsbedürftiger Zusammenhang, In: Schlögl, P., Dér, K. (Hrsg.) Berufsbildungsforschung alte und neue Fragen eines Forschungsfeldes. Transcript Verlag, Bielefeld (2010)
14. Howe, F., Knutzen, S.: Kompetenzwerkstatt - Band 4: Entwickeln von Lern- und Arbeitsaufgaben, Christiani (Hrsg.) (2011)

15. Dehnbostel, P.: Berufliche Kompetenzentwicklung im Kontext informellen und reflexiven Lernens – Stärkung der Persönlichkeit - und Bildungsentwicklung?, In: K. Barre/Hahn, C. (Hrsg.) (2012)
16. Hackel, M., Blötz, U., Reymers, M.: Berichte zur beruflichen Bildung: Diffusion neuer Technologien - Veränderungen von Arbeitsaufgaben und Qualifikationsanforderungen im produzierenden Gewerbe. W. Bertelsmann Verlag, Bielefeld (2015)
17. Berger, U., Hartmann, A., Schmid, D.: Additive Fertigungsverfahren. Verlag Europa Lehrmittel, Haan-Gruiten (2013)
18. Gebhardt, A.: Generative Fertigungsverfahren – Additive Manufacturing und 3D Drucken für Prototyping-Tooling-Produktion, 4th edn. CarlHanser Verlag, München (2013)
19. Möhrle, M., Emmelmann, C.: Fabrikstrukturen für die additive Fertigung, ZWF, Jahrgang 111. Carl Hanser Verlag, München (2016)

Why Education and Training in the Field of Additive Manufacturing is a Necessity

The Right Way to Teach Students and Professionals

Andreas Kirchheim(✉), Hans-Jörg Dennig, and Livia Zumofen

Centre for Product and Process Development (ZPP),
Zurich University of Applied Science (ZHAW), Winterthur, Switzerland
andreas.kirchheim@zhaw.ch

Abstract. Complexity for free? This is one of the big advantages of additive manufacturing. But what does that mean in reality? In the case of additive manufacturing freedom in general is also a new restriction. For this reason, it needs appropriate education and further training to recognize the new possibilities and also the limits of the additive manufacturing.

At the Centre for Product and Process Development (ZPP) of the Zurich University of Applied Sciences ZHAW, the additive production has been part of the training program for several years both in the teaching of mechanical engineering for students and in the continuing education of professionals.

In this paper, the experiences with the new education and training modules “Additive Manufacturing” will be presented. The program includes theory and practice on the machines (AM Laboratory) including the economic and ecological aspects. In particular, a special semester-accompanying project work is carried out, in which the students learn the constructive and technological peculiarities of the product development up to the additive manufacturing process, after-treatment and quality control of the components. The education in bachelor degree relies on the problem-based learning concept, where the student learns about additive manufacturing through the experience of solving an open-ended problem.

Keywords: Additive manufacturing · Education · Training · Continuing education · Design rules · Additive manufacturing laboratory

1 Introduction

The additive manufacturing processes have been developed from the 1980s, from rapid prototyping to additive manufacturing, or also called direct manufacturing [1]. Today, the 3D printers in the area of rapid prototyping are omnipresent. In addition, the various additive manufacturing processes for plastics and metals have already found their way from development to the industrial production environment [2–4].

With the layer-by-layer manufacturing directly from the CAD model, product or design advantages can be used against the conventional subtractive manufacturing. Complex structures, particularly in lightweight construction for aerospace, customer-specific

© Springer International Publishing AG 2018
M. Meboldt and C. Klahn (eds.), *Industrializing Additive Manufacturing - Proceedings of Additive Manufacturing in Products and Applications - AMPA2017*,
DOI 10.1007/978-3-319-66866-6_31

products in medical and dental technology, but also in the jewellery industry, etc. are producible [5]. Functional integration is another advantage that results in an additional value, an “added value” in the application, e.g. conformal cooling in injection molding or in assemblies by component reduction [6].

“Complexity for free” is one of the promising arguments for additive manufacturing (Fig. 1). Only when you have mastered the innovative technology you will be able to apply it properly, and it will be successful in the market. Therefore, it’s a need to establish a deep theoretical and practical education in AM for students or professionals [2, 7–9]. Only if a new technology has penetrated the market, it leads to consequences in the education system. Today there is the problem that a new technology as additive manufacturing will not be educated in a wide range [7]. Step by step the education and training becomes reality in the education of students as well as in continuous education [9–12].

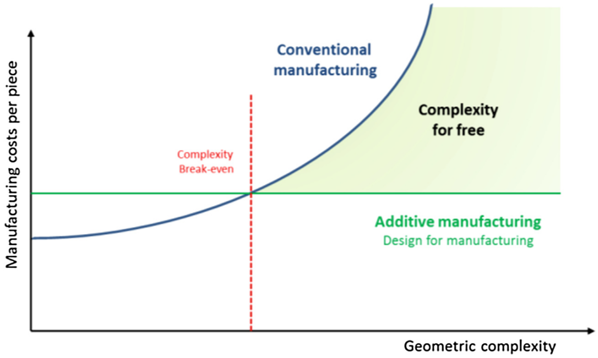

Fig. 1. Complexity for free using additive manufacturing

Education in additive manufacturing should include at least aspects as followed:

- Identification of meaningful components for additive production with regard to economic and technical aspects
- Understanding the additive production techniques, in particular laser beam melting in powder bed
- Application of the “additive” design rules
- Preparation of the build job (e.g. orientation of the components in the work area, arrangement of support structures, etc.)
- Development and application of the correct post-treatment and post-processing methods
- Development and application of methods for quality assurance.

An advanced education and training is necessary for the mechanical engineering students and also for the professional who works in related fields. However, who should or can be educated? What are the prerequisites for a successful training?

At the ZHAW a special module in “Additive Manufacturing” in the 3rd year of the Bachelor’s degree in Mechanical Engineering has been carried out last year successfully. A uniform training base is the main advantage; students have corresponding and uniform training in material technology, CAD and especially in the general design theory and practice for an innovative and integrated product development. In the continuing education, such uniform knowledge base is often not given - The challenge is to teach a heterogenic group with the same educational objective. Beginners want to get an overview and production engineers, design engineers and machine operators focus more detailed on the manufacturing method.

2 Bachelor Degree

The study of mechanical engineering at the ZHAW focuses on the innovative and integrated product development process. In addition to classical design principles and machine elements, creativity and an inventive spirit are promoted from the outset. Tools such as CAx, 3D-Experience and new manufacturing technologies as 3D-printing are trained. Within the framework of a team based semester project with four credits, rapid prototyping is put in place so that the students are quickly given an understandable, real and tangible feedback for their developments. A discrete prototype can be used to answer questions about size, design and ergonomics, and mistakes are difficult to obscure. Problem solving competences, creativity, motivation and communicative abilities of the students are encouraged. The students experience a real "start-up-feeling".

With this education, the students have, very good prerequisites for a deepening in the "additive manufacturing" of the main study. In this module, the students learn the prerequisite for successful additive manufacturing and how this is to be carried out. After the students get a broad overview of the additive manufacturing-technologies in general and in the selective laser beam melting (SLM) for metallic components in particular, very important is the identification of meaningful components and parts for additive manufacturing with regard to economic and technical aspects. Additive manufacturing, especially in metal, makes sense only if a certain added value is achieved in the product itself, through the production or later in the application (Fig. 2). To realize an added value, is a must. If a component is selected, it must be constructed "additive-ready", therefore state of the art design recommendations for additive manufacturing [13, 14] are communicated and applied.

Now the correct parameters for the SLM process have to be defined. The basic parameters of selective laser melting are taught so that the students are able to define them. The necessary supports have to be positioned sensibly and massively and the component must be aligned in the working area of the SLM machine (Fig. 3).

It is also important to experience how the components are removed from the build plate, how the supports are removed from the component and which post-processes are needed. Based on the lesson content learned during the semester (14 × 4 h), the student is able to successfully carry out the semester accompanying project work, especially for the selective laser melting of metallic components.

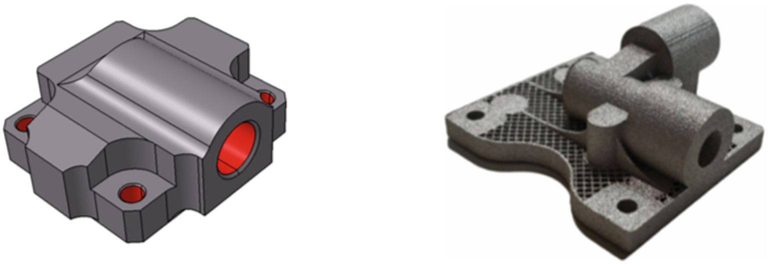

Fig. 2. Weight-optimization of a housing of a hydraulic safety valve for aerospace application, original, conventional manufactured, 100% weight (left), optimized, additive manufactured, 20% weight (right)

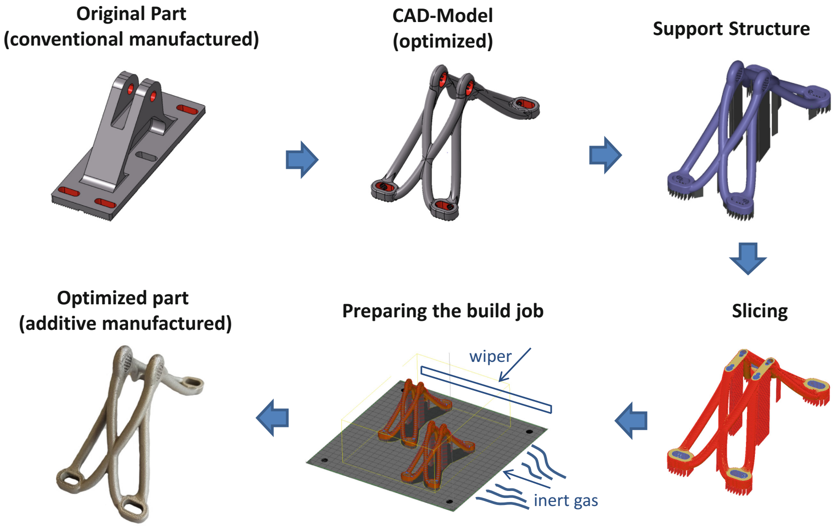
Original Part
(conventional manufactured)
CAD-Model
(optimized)
Support Structure
Slicing
Preparing the build job
wiper
inert gas
Optimized part
(additive manufactured)

Fig. 3. Work flow of the pre-processing of the additive manufacturing process on the example of a galley attachment of an air craft

2.1 Educational Model - Semester Accompanying Project Work

The project includes the research of a component (own ideas, industry, literature, Internet), which has the potential to be additively manufactured. It is important to highlight the profitability and customer benefit of such an implementation. The boundary condition of the component size is max. $150 \times 150 \times 200$ mm^3. Separate solutions have to be developed. As soon as the component is fixed and also the material is evaluated, it has to be designed or adapted according to the design guidelines for additive manufacturing, in order to guarantee a safe construction and to emphasize its advantages constructively. In addition, the preparation, the post-processing and the quality assurance processes are taken into account and described.

A brief report summarizes the “additive” product development and additive manufacturing process, which is finally presented in a poster presentation and demonstrated on the basis of a printed component. With this semester accompanying project the mediated knowledge of the students may be reviewed by lecturer in a very comprehensive way.

The pedagogic concept of the semester accompanying project is predicated on the problem based learning [15]. It needs a high complexity level which is feasible to implement during the semester. With the own research and evaluation of a potential component, the students define their own problems. Of course, this has to be led by the senior lecturers. Problem-based Learning (PBL) is a focused, experimental learning around the exploration, explanation and solving important problems. In the additive manufacturing course, the students work in teams of two people – guided by lecturers or tutors respectively. Besides the lesson contents, the module is based on self-directed learning, which leads the students directly to their defined component. The learning process is based on the methodical “7-Step” or “7-jumps” [17]:

1. Clarifying Concepts
2. Defining the Problem
3. Analysing the problem/Brainstorming
4. Categorizing
5. Formulating Learning Issues
6. Self-Study
7. Discussion of newly acquired knowledge.

Several 7-Step processes are included in the semester project. In the design phase, the students need to develop their product concept to an additive manufactured model. In this phase, they need to clarify the problems and to isolate the main questions (Step 1–2). Afterwards, they have to activate the existing knowledge (Step 3–4) and need to know, for what reasons, the need the knowledge. The Formulation of the learning issues is a important step in the process. The self-study phase (Step 6) is one of the biggest part, for i.e. design guidelines for AM. At the End, they need to summarize there gained knowledge.

There are milestones within the semester like the intermediate presentation or the final documentation at the end of the last lecture. There is also an intermediate exam where only the theoretical knowledge is checked. The final examination is divided into a dialogue session with a poster and a presentation of the additive manufactured part in metal or plastic (Fig. 4). Through the assessment and the presentation of a real product with a high potential, the benefits can be harvested effectively.

The whole course is supported in the learning platform “Moodle”. The students can not only download and see documents, but also upload the data for the presentation and the final documentation. A diversified design of the learning process, e.g. a variation of the teaching-learning method (PBL, e-Learning, frontal teaching) improves the learning motivation of the students. Through the use of various teaching-learning methods (with different social forms), the individual characteristics of the students with regard to preferred learning styles can be considered [16].

An evaluation of the module by the students, pointed out the very good balance between theoretical input and practical work at the software as well at the 3D printer. Also, the semester accompanying project work with final presentation as a test has been appreciated. They could practice the learned theory directly in the project work.

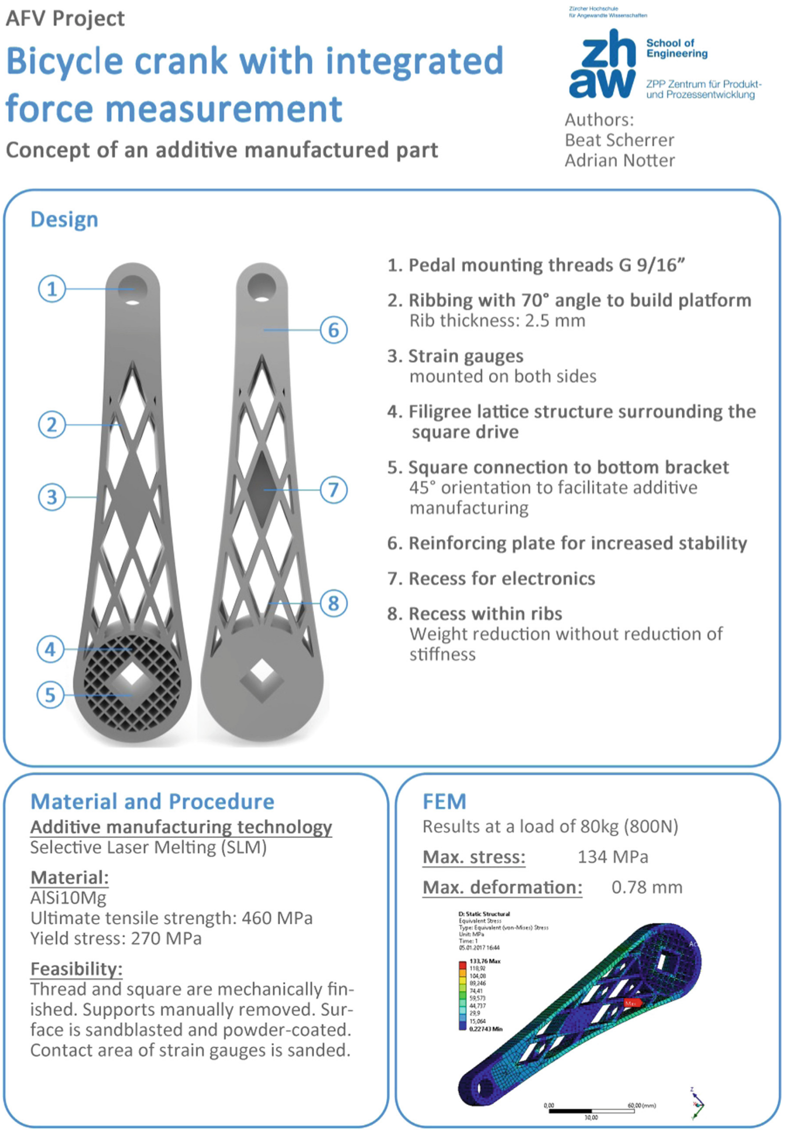

AFV Project

Bicycle crank with integrated force measurement

Concept of an additive manufactured part

Zürcher Hochschule für Angewandte Wissenschaften

zh aw School of Engineering

ZPP Zentrum für Produkt- und Prozessentwicklung

Authors:
Beat Scherrer
Adrian Notter

Design

1. Pedal mounting threads G 9/16"
2. Ribbing with 70° angle to build platform
   Rib thickness: 2.5 mm
3. Strain gauges
   mounted on both sides
4. Filigree lattice structure surrounding the square drive
5. Square connection to bottom bracket
   45° orientation to facilitate additive manufacturing
6. Reinforcing plate for increased stability
7. Recess for electronics
8. Recess within ribs
   Weight reduction without reduction of stiffness

Material and Procedure

Additive manufacturing technology
Selective Laser Melting (SLM)

Material:
AlSi10Mg
Ultimate tensile strength: 460 MPa
Yield stress: 270 MPa

Feasibility:
Thread and square are mechanically finished. Supports manually removed. Surface is sandblasted and powder-coated. Contact area of strain gauges is sanded.

FEM

Results at a load of 80kg (800N)

Max. stress: 134 MPa

Max. deformation: 0.78 mm

①
②
③
④
⑤
⑥
⑦
⑧
D: Static Structural
Equivalent Stress
Type: Equivalent (von-Mises) Stress
Unit: MPa
Time: 1
05.01.2017 16:44
133,76 Max
118,92
104,08
89,246
74,41
59,573
44,737
29,9
15,064
0,22743 Min
Max
0,00
30,00
60,00 (mm)
Z
X
Y

Fig. 4. Example of a student poster presentation of a bicycle crank

3 Training in Continuing Education for Professionals

The ZHAW is currently offering a continuing education course "Additive Manufacturing" (9 × 4 half-days) for professionals, in which the different additive manufacturing technologies and the corresponding processes for pre-processing and post-processing are taught for various applications and deepened in practical exercises. The course is designed for beginners and people with a technical background, such as engineers or technicians and similar professionals.

The learning objectives of the students include the understanding of the additive manufacturing chain (from the CAD to the additively manufactured components) as well as the different industrially used additive manufacturing processes (3D printing processes). The professionals learn about the possibilities and limitations of additive manufacturing as well how the materials are used. They understand and exercise the digital data preparation for additive manufacturing, use the design recommendations for additive manufacturing and initiate the additive production from the CAD. In the end, they are able to evaluate the additively manufactured components with regard to qualitative characteristics and are familiar with the usual post-processing methods. A further aim is to separate the additive manufacturing processes in industrial technical applications from conventional production processes (economic, ecological) and to access the perspectives of additive manufacturing.

In the future, it is certainly necessary to expand this entry-level course into a Certificate of Advanced Studies (CAS) with at least 12 credits. Furthermore, an alignment is required for professionals such as engineers, design engineers or machine operators.

4 Summary and Outlook

These courses lead to more graduates and skilled professionals that understand the potential and are able to successfully apply additive manufacturing technologies. This is supposed to support broad application and industrialization of additive manufacturing processes and enable enhanced, innovative product development to exploit the full potential of additive manufacturing. The offered education of the ZHAW in the field of additive manufacturing (design rules, material knowledge, after-treatment, quality management) provide a balance between theory and practice and lead to improved skills for new design thinking and production methods.

The challenge is continuing education with a heterogeneous training base. In this case, it is certainly necessary to offer adapted courses for the right target groups in the future.

References

1. Wohlers, T.: Wohlers Report 2012 - Additive Manufacturing and 3D Printing State of the Industry. Wohlers Associates, Colorado (2012)
2. acatech – Deutsche Akademie der Technikwissenschaften, Nationale Akademie der Wissenschaften Leopoldina, Union der deutschen Akademien der Wissenschaften (Hrsg.): Additive Fertigung. München (2016)
3. VDI- Verein Deutscher Ingenieure e.V. (2016): Statusreport Additive Fertigung, Düsseldorf, April 2016
4. VDMA-Arbeitsgemeinschaft Additive Manufacturing (Hrsg.): Technology Scout 2017, Technologien, Anwendungen und Hersteller, Frankfurt am Main, 2017

5. Yap, C.Y., Chua, C.K., Dong, Z.L., Liu, Z.H., Zhang, D.Q., Loh, L.E., Sing, S.L.: Review of selective laser melting: Materials and applications. Appl. Phys. Rev. (2015)
6. Gibson, I., Rosen, D.W., Stucker, B.: Additive Manufacturing Technologies. Springer US, Boston (2010)
7. Marschall, H.: Personal für die additive Fertigung, Kompetenzen, Berufe, Aus- und Weiterbildung, Sringer Fachmedien Wiesbaden (2016)
8. Huang, Y., Leu, M.: Frontiers of Additive Manufacturing, Research and Education, Report of NSF Additive Manufacturing Workshop, 11–12 July 2013, Published by University of Florida, Gainesville (2014)
9. EFI Expertenkommission Forschung und Innovation (Hrsg.): Gutachten zu Forschung, Innovation und technologischer Leistungsfähigkeit Deutschlands Additive Fertigung (3D-Druck) (2015)
10. Additive manufacturing and design master’s degrees to be offered in fall 2017. PENN STATE NEWS, Penn State University, April 14 2017
11. Anwendungstechniker/-in (FH) für additive Verfahren/Rapidtechnologien, Wissenschaftliche Weiterbildung, University of Applied Science Schmalkalden (2017)
12. Fachingenieur Additive Fertigung VDI, Zertifikatslehrgang, Veranstalter: VDI Wissensforum GmbH, Düsseldorf (2017)
13. VDI 3405 Part 3, Additive manufacturing processes, rapid manufacturing – Design rules for part production using laser sintering and laser beam melting. Beuth-Verlag, Berlin, December 2015
14. Adam, G.: Systematische Erarbeitung von Konstruktionsregeln für die additiven Fertigungsverfahren Lasersintern, Laserschmelzen und Fused Deposition Modeling. Shaker Verlag (2015)
15. Müller, C.: Gestaltung von problembasierten Lernumgebungen (Problem-based Learning). Eine Analyse aus motivations- und kognitionspsychologischer Sicht, Netzwerk, Januar 2008
16. Kolb, D.A.: Experiential Learning: Experience as the Source of Learning and Development. Prentice-Hall, Englewood Cliffs (1984)
17. Schmidt, H.G.: Problem-based learning: rationale and description. Med. Educ. **17**(1), 11–16 (1983)

The Experience Transfer Model for New Technologies - Application on Design for Additive Manufacturing

Bastian Leutenecker-Twelsiek[1], Julian Ferchow[1](✉),
Christoph Klahn[1], and Mirko Meboldt[2]

[1] Inspire AG, Leonhardstrasse 21, 8092 Zurich, Switzerland
ferchow@inspire.ethz.ch
[2] ETH Zürich, Leonhardstrasse 21, 8092 Zurich, Switzerland

Abstract. To apply new technologies in industry, it requires knowledge about the specific technology. Since a new technology, such as Additive Manufacturing (AM), enters the industry slow, the knowledge transfer must be supported. AM is capable to produce end user parts by serial production. To implement this new technology into industry an Experience Transfer Model (ETM) supports the transfer of knowledge from the academic environment to professional engineers in industry. This paper presents the concept of the ETM, which transfer experience knowledge about identification expertise and design expertise in three steps: Input of theory, implementation of the theoretical knowledge and reflection of the approach. The validation of the ETM with Swiss SME showed a successful implementation of experience knowledge.

Keywords: New technology · Experience Transfer Model · Design for additive manufacturing · Identification expertise · Design expertise

1 Introduction

To implement new technologies, such as AM, companies with new product development, need the expertise to identify suitable parts. Additionally, a new technology process create new possibilities but also new restrictions to the design (Leutenecker-Twelsiek et al. 2016). To unlock the full potential of a new technology, such as AM it needs additionally to existing academic design guide lines a training to transfer design expertise (Wohlers 2015). The challenge to transfer a new technology expertise from the academic environment to industry is not limited to AM. Rather, the way to transfer expertise for a new technology can be used for new technologies in general.

Additive Manufacturing (AM), or 3D printing - as it is referred to in the media, is a group of manufacturing technologies which produce three-dimensional objects by adding material, usually in a layer by layer process (VDI 3405 2015). In the beginning of the manufacturing technologies in the 1980th, the first applications were the production of prototypes. During the following decades the manufacturing technology and materials evolved and nowadays, new fields of application are possible.

© Springer International Publishing AG 2018
M. Meboldt and C. Klahn (eds.), *Industrializing Additive Manufacturing - Proceedings of Additive Manufacturing in Products and Applications - AMPA2017*,
DOI 10.1007/978-3-319-66866-6_32

Additive Manufacturing processes are technologically mature for industrial production and due to a sufficient process stability and a rising competition between service providers (Baldinger and Duchi 2013). Additive Manufacturing becomes economically feasible for a growing number of industrial and end-user applications (Gebhardt 2012; Gibson et al. 2015; Wohlers 2015). Today there are many different Additive Manufacturing processes available, some of which provide sufficient stability and robustness for serial direct part production. Processes like Selective Laser Melting (SLM), Selective Laser Sintering (SLS) and, with some limitations, Fused Deposition Modeling (FDM) are used to produce end-user parts.

To transfer knowledge about a new technology it needs a didactical appropriate approach. The knowledge of a human is divided into two different types: Explicit and implicit knowledge. Explicit knowledge is a factual knowledge and clearly teachable by formulas or models. However, it doesn't correlate to skills or experience (Notté 2013). Explicit knowledge for design for AM can be transferred by design guide lines. In contrast to explicit knowledge, implicit knowledge is not clearly illustratable, verbalizable or definable. Implicit knowledge can be learned for instance by gathering experience and is hard to transfer (Notté 2013). Implicit knowledge represents the most important knowledge for company's and the engineers (North 2005). For Engineers, usually, implicit knowledge is already existing for design knowledge for conventional manufacturing technologies such as milling, casting or turning, since design engineers have experience in designing products for this technologies since decades. However, for additive manufacturing the implicit knowledge for engineers is not jet existing. Due to the fact that AM is a young technology, and offers different design restriction compared to conventional manufacturing technologies.

In this paper, a general experience transfer model is developed, to transfer experience knowledge for new technologies in general, from academic environment to industry.

2 Need for Experience Transfer in Design for AM

Additive Manufacturing (AM) offers a large variety of design potentials for new products. To utilize the full potential of additive manufacturing the specific AM design should be adopted (Gebhardt 2012). Therefore, design guidelines shall support the engineer in developing the optimal AM design. At present, a large number of academic design guide lines exist (Becker et al. 2005) (Hietikko 2014) (Kumke et al. 2016) (Kranz et al. 2014) (Adam 2015; Wegner and Witt 2012). However, this academic design guidelines entering industrial practice very slow. A main reason is the scientific focus of the academic design guidelines, which makes it difficult for engineers in industry to understand and to apply it (Wohlers and Caffrey 2015). Scientific studies showed a need in transferring the knowledge of the academic design guidelines to the professional engineers in industry (Kohlhuber et al. 2016).

In this paper, the expression professional engineer mean general technical engineers with work experience. For professional engineers in industry, design for AM is not just a simple extension of domain knowledge of conventional manufacturing technologies. The key to unlock the design potential of AM is to overcome the fixed mind-sets of conventional manufacturing technologies (Hopkinson 2006). The modality of the knowledge transfer is not done by modifying the AM design guidelines from an academic AM design guideline to the application oriented AM design guideline. AM knowledge is divided in process knowledge about the manufacturing and in application knowledge of AM. To transfer the AM knowledge to the industry, the fixed mind-sets must be overcome by supplementing the AM design guidelines by application oriented design workshops for professional engineers in industry.

To implement the AM technology into series production, not only the knowledge about the AM design must be transferred, but also the knowledge about the suitable AM manufacturing technology.

Both, explicit and implicit knowledge is not jet transferred into industry. To implement AM into industrial series production, a practice oriented knowledge transfer is needed in form of a workshop. The transfer workshop communicate both, theoretical explicit knowledge but in particular implicit knowledge. A workshop is important that the participator become proactive and generate implicit knowledge.

3 Theory and Concept of the General Experience Transfer Model for New Technology

The experience transfer model (ETM) transfers in a systematical way experience knowledge. It based on the experience and Education theory of Dewey that human education is based on experiences (Dewey 1938). The Karlsruhe education model for product development (KaLeP) introduced Deweys theory in the academic education for engineers. KaLeP showed a significant improvement in supporting the learning process in the human brain, compared to the conventional way of academic education (Albers et al. 2004; Albers et al. 2006). Based on the theory of Dewey and KaLeP, the ETM continues the idea of experience based learning and introduce the experience based learning of Dewey into the knowledge transfer from the academic environment to industry (Schön 1983; Kolb 1981; Lemos 2007; Valkenburg and Dorst 1998).

The Experience Transfer Model (ETM) describes a systematical approach to gain experience knowledge about new technologies by three steps: Input of theory, implementation of the theoretical knowledge and reflection of the theoretical knowledge, plotted in Fig. 1. The aim of the ETM is to generate experience knowledge in identification and design expertise to implement new technologies in industry.

Identification: Here the participator generate the experience knowledge about how they can identify elements that have a potential to produce them by another technology. At the end, the old technology should be replaced by a new technology and should create an additional technological and economical value.

Design: The participator gain an experience knowledge about how to create a design of a new technology, either of an identified existing element or of a new element.

To transfer the identification expertise and the design expertise the ETM is applied. The knowledge is transferred by technology experts. The technology experts are professionals with explicit and implicit knowledge. Following the three successive steps of the ETM are explained:

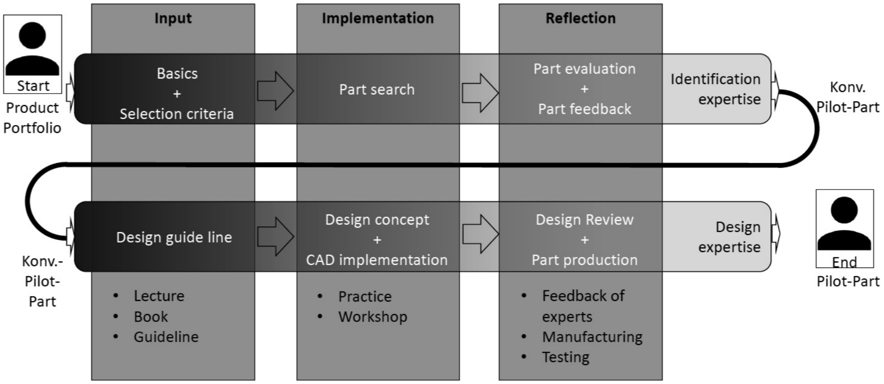
Input
Implementation
Reflection
Start
Product Portfolio
Basics + Selection criteria
Part search
Part evaluation + Part feedback
Identification expertise
Konv. Pilot-Part
Konv.-Pilot-Part
Design guide line
Design concept + CAD implementation
Design Review + Part production
Design expertise
End
Pilot-Part
Lecture
Book
Guideline
Practice
Workshop
Feedback of experts
Manufacturing
Testing

Fig. 1. The general Experience Transfer Model (ETM) concept including the expected schedule.

Before participants gain experience, they need an input of the theoretical knowledge. The first step is an effective teaching of the explicit knowledge about the technology in form of an initial kick-off workshop.

Second, after the introduction of explicit knowledge, the implementation of the explicit knowledge in the industrial environment follows. The aim is to build up experience knowledge. During the implementation step of the identification expertise, the participator applies either the explicit knowledge to identify elements with a potential to redesign it for a new technology. In the implementation step of the design expertise he applies his explicit knowledge to design a element which fits to a new technology. Through this step the participants generate implicit knowledge based on his own experience cf. (Albers et al. 2006).

In the third step, the technology expert analyses the work of the participator and offer them a feedback. That gives the participating engineer the opportunity reflecting their own approaches of the implementation step. This step consolidate the implicit knowledge in a sustainable way. In addition, this step avoids mistakes during the first two steps. The reflection is carried out in an oral or written way.

The application of the ETM is described in the following chapter for additive manufacturing.

4 Experience Transfer Model for the Application of Design of Additive Manufacturing

The process of the Experience Transfer Model (ETM) is applied to build up two different expertise. First the Identification expertise to detect an AM part with a potential for an AM design. Secondly the design expertise to design an AM part. The Workshop is managed by AM – technology experts (AM experts). The participator of the workshop are professionals from industry.

Identification Expertise for AM

The aim is to transfer the experience knowledge to the participator, that they generate the expertise to identify parts where additive manufacturing creates the highest value to the customer (Klahn et al. 2015).

Input: Before a participant searches an AM part in a product portfolio, he needs an explicit knowledge about Additive Manufacturing (AM) basics. As a kick-off workshop the participator receives a basic input of the theoretical knowledge by the AM-Experts. Further, engineers learning which materials are suitable and which part sizes can realized by AM. For instance, it is not reasonable to produce every part by AM, because the costs directly linked to the part volume. However, design complexity is for free. From this, it follows that additional costs must be compensated by function integration and a volume efficient design. Four selection criterions are introduced (Klahn et al. 2014) to identify AM parts. Based on a demonstration part, the application of the selection criterions is illustrated during the kick-off workshop (Fontana et al. 2016).

Implementation: Based on the initial kick-off workshop, participating engineers performing the search for a part with potential to be redesigned for the AM technology. A template supports the engineers to document the parameters of their identified parts including drawings and pictures. Figure 2 shows an example template.

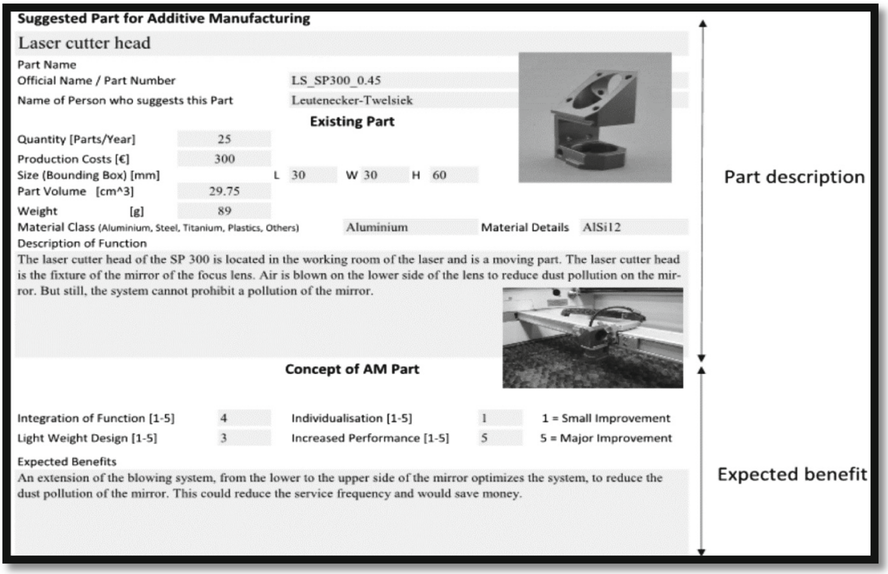

Suggested Part for Additive Manufacturing

Laser cutter head

Part Name

Official Name / Part Number LS_SP300_0.45

Name of Person who suggests this Part Leutenecker-Twelsiek

Existing Part

Quantity [Parts/Year] 25

Production Costs [€] 300

Size (Bounding Box) [mm] L 30 W 30 H 60

Part Volume [cm^3] 29.75

Weight [g] 89

Material Class (Aluminium, Steel, Titanium, Plastics, Others) Aluminium Material Details AlSi12

Description of Function

The laser cutter head of the SP 300 is located in the working room of the laser and is a moving part. The laser cutter head is the fixture of the mirror of the focus lens. Air is blown on the lower side of the lens to reduce dust pollution on the mirror. But still, the system cannot prohibit a pollution of the mirror.

Concept of AM Part

Integration of Function [1-5] 4

Individualisation [1-5] 1

Light Weight Design [1-5] 3

Increased Performance [1-5] 5

1 = Small Improvement

5 = Major Improvement

Expected Benefits

An extension of the blowing system, from the lower to the upper side of the mirror optimizes the system, to reduce the dust pollution of the mirror. This could reduce the service frequency and would save money.

Fig. 2. Template for a suggested part for an AM redesign – Laser cutter head

Reflection: The AM-Experts evaluate the suggestions of the suggestions of the participating engineers. The evaluation is relating to the feasibility of production, necessary post processing, estimations of AM costs and possible benefits for the OEM and the customer. The feedback is depicted in Fig. 3, including the evaluation criteria and the corresponding quantification.

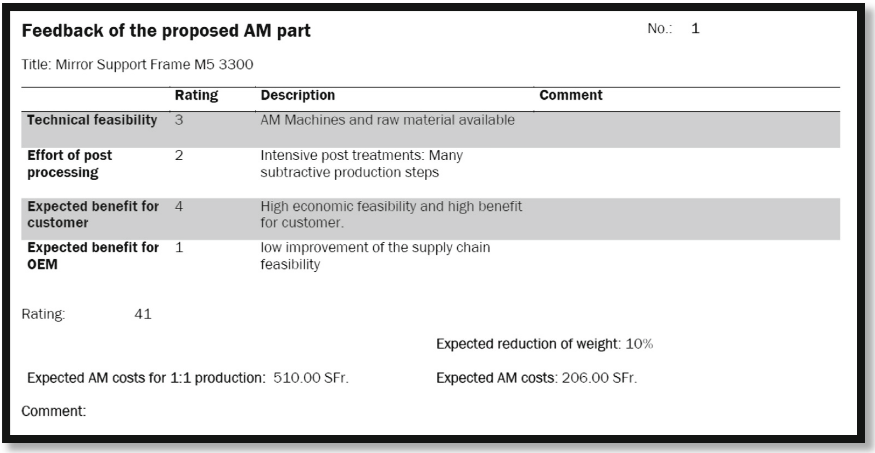

Feedback of the proposed AM part

No.: 1

Title: Mirror Support Frame M5 3300

	Rating	Description	Comment
Technical feasibility	3	AM Machines and raw material available	
Effort of post processing	2	Intensive post treatments: Many subtractive production steps	
Expected benefit for customer	4	High economic feasibility and high benefit for customer.	
Expected benefit for OEM	1	low improvement of the supply chain feasibility	

Rating: 41

Expected reduction of weight: 10%

Expected AM costs for 1:1 production: 510.00 SFr.

Expected AM costs: 206.00 SFr.

Comment:

Fig. 3. AM expert feedback to participating engineer. Here the proposed AM part is a Mirror Support Frame M5 3300

If the feedback shows, that there is a significant potential to change from the conventional manufacturing technology to AM, the part will be redesigned. The result of the redesign will be a pilot part. During this step, the participator had the effect of learning and generating implicit knowledge.

Design Expertise

For an engineer, experience knowledge in AM design is essential to reduce manufacturing costs and to unlock the full potential of the AM technology. Either the participating engineers uses the AM technology as a manufacturing technology with cost benefits at complex parts and small lot sizes, or he also uses the advantage of the little restrictions of the additive manufacturing (Klahn et al. 2015). According to ETM the first step is the theoretical input workshop.

Input: During the input workshop, the design guidelines are explained in detail. The design guide lines containing process features and design principles (Leutenecker-Twelsiek et al. 2016; Klahn et al. 2015). For a better understanding sample parts out of the industry are used during this step.

Implementation: The implementation step of the ETM includes first the concept development and secondly the detailed design of the AM part. The concept development takes place in an ideation workshop under the moderation of an AM – expert. The location of the workshop takes place in a new environment for the participating engineer, which is outside of his company. A new environment stimulates creative mindsets in product development (Rittiner et al. 2016; Deigendesch 2009), which helps that the full potential for AM design is used. Here the participating engineers are proactive and experience the AM design directly under a subtle guidance of the AM experts. At the end of the ideation workshop, the participators design one to three pilot parts in the form of sketches or in low fidelity prototypes cf. Fig. 4(a). In Fig. 4(b) shows a concept of a laser cutter head. The next step for the participating engineer is to implement the ideas and concepts of the workshop into a detailed designed CAD model in his company by his own. The participators execute it in their company, because there they have the have their own system and on digital tools. Figure 4(c) shows a CAD model of a laser cutter head. The implementation part is central for the experienced based learning of the participator. The theory behind it is explained in Sect. 3.

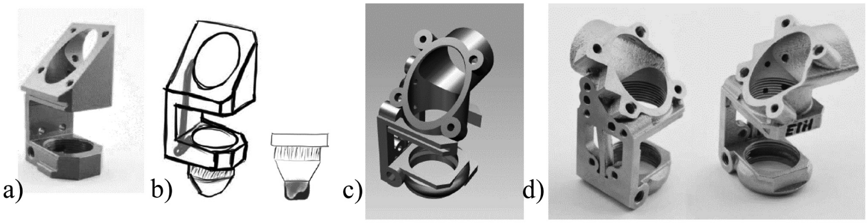

Pilot part Concept drawing CAD part AM prototype

Fig. 4. Implementation and reflection process including: (a) pilot part, (b) concept drawing, (c) CAD part, (d) AM prototype – Laser cutter head

Reflection: The final step of the design expertise is the reflection. Therefor the AM – expert analyses the CAD part of the engineer. Then, the participator receives a feedback due to his designed AM-Part. If necessary, the AM –Part will be re-designed by the participating engineer. The last step of reflection is the validation of the designed AM pilot part by building cf. Fig. 4(d) and testing. Under supporting of the AM expert, the iteration process helps to reflect his own design like learning by doing and generating implicit knowledge. The iterative process takes usually place in the company of the participator respectively if they have no 3D printer at the suppliers place.

5 Validation of the ETM with a Swiss SME

Following, the application of the ETM, according to Fig. 1, is illustrated by an industry case. Several small and medium sized companies of the textile machinery sector where participating in this case.

Identification Expertise: After the theoretical input workshop of a half day, the attendees had explicit knowledge about how to identify potential AM parts in general cf. Sect. 4. To implement the explicit knowledge from the input workshop the participants had 4 weeks to selected between five and twenty parts with AM potential, depending on the company size and the number of participating engineers per company. The AM experts then evaluated the submitted parts and recommended a pilot part. As a reflection of the selected part, the AM experts returned the evaluation to the attendees and where discussed. The part evaluation and the implementation of the redesigned part where carried out specific to the single company and their needs in a half day session. The discussion of the evaluation generated an implicit knowledge of the participators and consequently an identification expertise.

Design Expertise: As a pilot part, a Swiss textile machinery company selected a thread separator. Up to the input workshop, the thread separator was manufactured by conventional manufacturing technologies and it consisted several components (Fig. 5a). In the half-day input Workshop, the participator learned how to redesign the part into an AM design. To implement the explicit knowledge of the input, in a one-day ideation workshop, the participating engineers developed a design concept. The AM Experts supported the participator and gave some advices for the concept. After the workshop, the participator implemented the concept into CAD (Fig. 5b) in his company. To check the design features, some single part geometries where produced (Fig. 5c). By an iterative process, the participators reflected their design and generated implicit knowledge by manufacturing, testing and optimizing the AM part. Finally, the participant get the design expertise. The reflection of the AM design was executed in a half-day workshop.

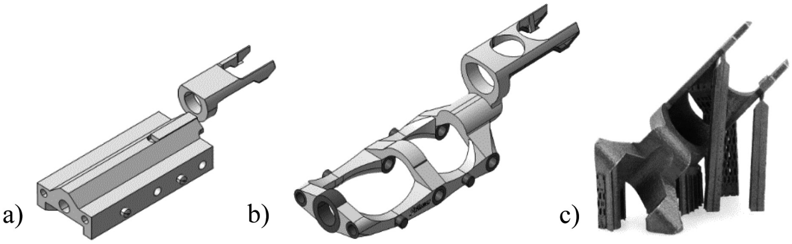

Fig. 5. Successive procedure of a AM design of a thread disposer. (a) Conventional manufactured part; (b) AM redesign; (c) test geometry.

Validation: During the design expertise workshop, the attending engineer proposed new AM parts, which they have not proposed during the implementation workshop. One identified part with AM potential is a rotating lock, plotted in Fig. 6(a). Here the parts are conventional manufactured, the gear assembly has two axis and many single parts. This indicates that the engineer improved his identification expertise during the design workshop. After the engineer identified new potential AM parts, they redesigned the parts in a proactive way by them self. Figure 6(b), shows such a redesigned part. Here, the gear mechanism combined in one axis and one part.

The fact, that participator of the ETM workshop identified and redesigned several parts in there company by them own, it indicates that the ETM successfully implements expertise in identification and design into industry. The ETM workshop provides the local Swiss SME an experience knowledge in design for AM, to establish on the international highly competitive markets.

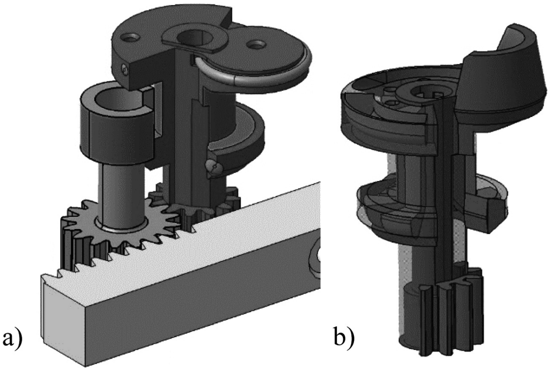

Fig. 6. (a) Conventional manufactured part; (b) AM redesigned part

6 Conclusion

The experience transfer model (ETM) for new technology transfers explicit and especially implicit knowledge from the academic environment to the industry. In this paper, the general ETM is developed, in the form of workshops executed for the technology of additive manufacturing (AM) and empirical validated by the feedback of the workshop participators of AM. The feedback showed that the participator where satisfied with the expertise they took out of the ETM workshops for AM. Additionally the participating engineers identified new AM parts by them self. Then they independently and proactive the participator redesigned new AM parts.

However, there are some limitations: For a statistical validation, more data must be collected in a systematical investigation. Further, to validate the ETM for an application in new technologies in general, it must executed and validated for another technology. According to the feedback of the participator, the present ETM workshop for AM showed successfully the transfer of explicit and especially implicit knowledge in design for AM.

Acknowledgments. The authors would like to thank the Swiss industry association SWISSMEM for supporting its members in participating in our AM technology transfer program.

References

Adam, G.A.O.: Systematische Erarbeitung von Konstruktionsregeln für die additiven Fertigungsverfahren Lasersintern, Laserschmelzen und Fused Deposition Modeling, 1. Aufl. Forschungsberichte des Direct Manufacturing Research Centers, vol. 1. Shaker, Herzogenrath (2015)

Albers, A., Burkardt, N., Ohmer, M.: The constructivist aspect of design education in the Karlsruhe education model for industrial product development KaLeP (2004)

Albers, A., Burkardt, N., Meboldt, M.: The karlsruhe education model for product development “KALEP”, in higher education (2006)

Baldinger, M., Duchi, A.: Price benchmark of laser sintering service providers. In: High Value Manufacturing: Advanced Research in Virtual and Rapid Prototyping. CRC Press, pp. 37–42 (2013)

Becker, R., Grzesiak, A., Henning, A.: Rethink assembly design. Assem. Autom. **25**(4), 262–266 (2005). doi:10.1108/01445150510626370

Dewey, J.: Experience and Education. The Kappa Delta Pi Lecture Series, 1st edn. Simon & Schuster, New York (1938)

Fontana, P., Klahn, C., Mebold, M.: AM Network- Additive Fertigung in der industriellen Serienproduktion - Ein Statusreport (2016)

Gebhardt, A.: Understanding additive manufacturing: rapid prototyping-rapid tooling-rapid manufacturing. Carl Hanser Verlag GmbH Co. KG (2012)

Gibson, I., Rosen, D., Stucker, B. (eds.): Additive Manufacturing Technologies: 3D Printing, Rapid Prototyping and Direct Digital Manufacturing, 2nd edn. Springer, New York, Heidelberg, Dodrecht, London (2015)

Hietikko, E.: Design for additive manufacturing – DFAM. Int. J. Eng. Sci. (IJES) **3**(12), 14–19 (2014). ISSN (e) 2319 –1813, ISSN (p) 2319 –1805

Hopkinson, N.: Rapid Manufacturing an Industrial Revolution for the Digital Age. Wiley, Chisester (2006). ISBN 978-0-470-01613-8

Klahn, C., Leutenecker, B., Meboldt, M.: Design for additive manufacturing – supporting the substitution of components in series products. Procedia CIRP **21**, 138–143 (2014). doi:10.1016/j.procir.2014.03.145

Klahn, C., Leutenecker, B., Meboldt, M.: Design strategies for the process of additive manufacturing. Procedia CIRP **36**, 230–235 (2015). doi:10.1016/j.procir.2015.01.082

Kohlhuber, M., Kage, M., Karg, M. (eds.): Stellungnahme Additive Fertigung, München (2016). https://www.leopoldina.org/uploads/tx_leopublication/2016_Stellungnahme_AdditiveFertigung.pdf. ISBN 978-3-8047-3676-4

Kolb, D.A.: Experiential learning theory and the learning style inventory: a reply to Freedman and Stumpf. Acad. Manag. Rev. **6**(2), 289–296 (1981)

Kranz, J., Herzog, D., Emmelmann, C.: Methodik für die fertigungsgerechte Konstruktion von laseradditiv gefertigten bionischen Leichtbaustrukturen aus TiAl6V4. In: Rapid. Tech 2014 (2014)

Kumke, M., Watschke, H., Vietor, T.: A new methodological framework for design for additive manufacturing. Virtual Phys. Prototyp. **11**(1), 3–19 (2016). doi:10.1080/17452759.2016.1139377

Lemos, N.: An Introduction to the Theory of Knowledge. Cambridge University Press, Cambridge (2007)

Leutenecker-Twelsiek, B., Klahn, C., Meboldt, M.: Considering part orientation in design for additive manufacturing. Procedia CIRP **50**, 408–413 (2016). doi:10.1016/j.procir.2016.05.016

North, K.: Wissensorientierte Unternehmensführung. Wertschöpfung durch Wissen, 4th edn. Gabler, Wiesbaden (2005).ISBN 978-3-322-95334-6

Notté, K.: Wissensmanagement im Vertrieb. Springer Gabler (Springer Gabler Results), Wiesbaden (2013). ISBN 978-3-658-02700-1

Rittiner, F., Heck, J., Meboldt, M., Steinert, M.: Space Utilization Patterns and Workshop Furniture–Affordances for New Product Development and Design (2016)

Schön, D.A.: The Reflective Practitioner: How Professionals Think in Action. Basic Books, New York (1983)

Deigendesch, T.: Kreativität in der Produktentwicklung und Muster als methodisches Hilfsmittel: Creativity in Product Development and Patterns as a Methodological Means of Support. Karlsruher Institut für Technologie (2009)

Valkenburg, R., Dorst, K.: The reflective practice of design teams. Des. Stud. **19**(3), 249–271 (1998). doi:10.1016/S0142-694X(98)00011-8

VDI 3405: Additive manufacturing processes, rapid manufacturing; design rules for part production using laser sintering and laser beam melting. Verein Deutscher Ingenieure, Berlin (2015)

Wegner, A., Witt, G.: Design rules for laser sintering. J. Plast. Technol. **8**(3), 253–277 (2012)

Wohlers, T.: Wohlers Report 2015: 3D printing and additive manufacturing state of the industry; annual worldwide progress report. Wohlers Associates, Fort Collins (2015)

Wohlers, T.T., Caffrey, T.: Wohlers report 2015: 3D printing and additive manufacturing state of the industry annual worldwide progress report. Wohlers Associates, Fort Collins (2015)

Decision-Making in Additive Manufacturing – Survey on AM Experience and Expertise of Designers

Johanna Spallek(✉) and Dieter Krause

Institute of Product Development and Mechanical Engineering Design,
Hamburg University of Technology, Hamburg, Germany
j.spallek@tuhh.de

Abstract. Technological advancements in additive manufacturing (AM) has enabled the usage of AM for end-use parts more than ever before. Deciding whether or not to apply AM for final parts and knowing how to design for AM is fundamental in the design phase, which is why Design for AM (DfAM) methods are currently being elaborated.

This paper analyzes the current experiences and knowing of designers concerning additive manufacturing technologies and, hence, provides a foundation for the development of DfAM methods. This study presents a survey with designers asking them about their experience with and knowledge on additive manufacturing technologies. The study reveals the disparate experience with AM, reaching from highly skilled AM experts to designers who have never held an AM part in the own hands before. While a good basic knowledge concerning AM seems present, detailed knowledge is lacking, especially with regard to general restrictions and the differentiation of the AM technologies. Interest and intentions in using AM for final part production is high, combined with a slight skepticism. For further implementations of AM in final part production, DfAM methods are meaningful and desired by designers, e.g. for decision-making processes for direct AM. These DfAM approaches should be focused on AM specific requirements and characteristics while covering the proven discrepancies in the experiences and the skills of designers concerning AM.

Keywords: Additive manufacturing · Design for AM · Decision-making in AM · Industry survey

1 Introduction

The term ‘additive manufacturing’ (AM) subsumes production technologies which build parts by adding material layer-by-layer, line-by-line, piece-by-piece, or surface-by-surface. Technological progress in the last three decades has improved part quality, materials, and prices for a variety of AM technologies [1]. Main benefit and innovation of AM is that it eliminates tooling which, in turn, allows for high geometrical freedom as well as production flexibility, especially for low quantities [2]. Tool-less fabrication direct from digital information offers various application possibilities, taking into account that various AM technologies offer different advantages and

© Springer International Publishing AG 2018
M. Meboldt and C. Klahn (eds.), *Industrializing Additive Manufacturing - Proceedings of Additive Manufacturing in Products and Applications - AMPA2017*,
DOI 10.1007/978-3-319-66866-6_33

restrictions [3, 4]. AM applications in product life cycle can be divided into three main groups: (1) Fabricating prototypes, e.g. for concept models, functional or technical prototypes used in the design phase, or as display models in marketing and sales, was the earliest application of AM technologies [1]. In the two remaining groups, AM is used either directly (2) or indirectly (3) for producing end-use parts. In direct additive manufacturing – also known as rapid manufacturing or direct digital manufacturing [4] – a final part of a product is manufactured additively. AM technologies combine geometrical freedom with flexible production of small lot sizes, which can be used for mass personalization [4, 5]. In the third group, AM technologies are used to fabricate production tools, whereby short-run tooling, e.g. for prototype tooling, and long-run tooling, e.g. for mass production purposes, differ from each other [4].

The industrial use of AM has been frequently discussed in the literature, as in [6]. These reports indicate that one challenge for final part production using AM comes with traditional attitudes in companies, as AM is relatively young compared to the conventional production technologies [6]. To bring a better understanding of AM into industry, Design for AM (DfAM) approaches are relevant for clarifying when and how to design for AM. These approaches often focus on design rules for direct AM considering the geometrical constraints to ensure manufacturability [7, 8]. DfAM approaches on the design process and practice take the unique characteristics of AM technologies, the specific fabrication capabilities and restrictions into consideration [1], e.g. for AM-enabled mass personalization [5].

While DfAM approaches are highly relevant to overcome the barriers of traditional attitudes in the industry and to eliminate “cognitive barriers associated with designing for AM” [9], studies on current attitudes towards AM technologies are very rare or still unpublished, as [10]. In order to develop expedient DfAM approaches, e.g. for improving decision-making processes in AM-enabled mass personalization, it is essential to know which current expertise and opinions designers actually have with AM technologies. Therefore, this paper aims at supporting DfAM methods by providing a foundation to the development of approaches in this area by answering the question: Which experiences and skills do designers have with AM? It presents the results of an industry survey on designers’ knowing, experience and opinions of AM, focusing on decision-making for direct AM.

2 Methods

The study was organized as an online survey with the title ‘Survey on 3D-Printing: Experience and Expertise of Engineers in Development and Design’. Due to its popularity, the term ‘3D-printing’ was consistently applied to all AM technologies, as was explained to the participants during the survey. Invitations to German-speaking participants were distributed through contacts in the industry, academic networks, and 3D-printing and industrial newsletters. Two versions of the voluntary questionnaire, which differed in length and range, were accessible online from February 2017 until April 2017. The short version (SV, on average 8 min) focused on AM experiences as well as designers’ expertise and opinions concerning the fields of AM application. The long version (LV, on average 15 min) contained additionally questions, e.g. on basics of design rules for AM and the various AM technologies. Designers' experience and knowing concerning AM usually include both the production of prototypes and final part production. Both versions contained general questions on AM and questions focused on final part production, as the latter is highly relevant for decision-making for direct AM. The questionnaires were made up of 25 (SV) or 50 (LV) single or multiple choice questions, additional free text questions for analyzing the basic knowledge concerning AM application fields, and rankings for personal reasons for being pro/con AM final production.

3 Results

After the description about participants of the survey, the results are presented in four sections: basic and detailed knowledge of designers concerning AM, experiences with AM, and attitudes of designers towards final AM production. Results of both versions are consolidated, unless otherwise indicated as LV (long version).

3.1 Participants of the Survey

172 (91 LV, 81 SV) out of 254 (127 LV, 127 SV) survey respondents answered all questions (see Table 1). Target participants were defined as those respondents which are concerned with making decisions relevant to AM for final part production: product planning, component design, comparing or deciding about materials and production technologies, and production planning. 101 completely processed participants fulfilled the target prerequisite (61 LV, 40 SV), whose **working areas** are displayed in Fig. 1. Results of the study are based on completed answers by those target participants, hereafter defined as 'participants'.

Table 1. Distribution of survey respondents.

	LV + SV	LV	SV
Number of total respondents	254	127	127
Number of all-question respondents	172	91	81
Target participants	101	61	40

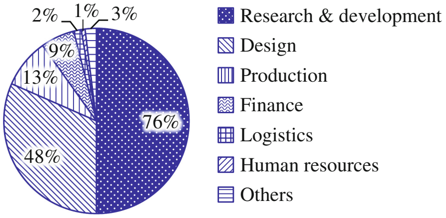

Fig. 1. Working areas of target participants (multiple answers were possible)

Figure 2 shows the distribution of the **age** and **company branches** of participants. Multiple choices of predefined answers were possible when choosing a company branch. Since 'shipbuilding' was named multiple times in the category 'other' it was added to the results. In terms of **business size**, 31% of the target participants were working in small and medium-sized enterprises (less than 249 employees), 9% in companies with 250–499 employees, 24% in companies with 500–9,999 employees, and 32% in companies with 10,000 or more employees.

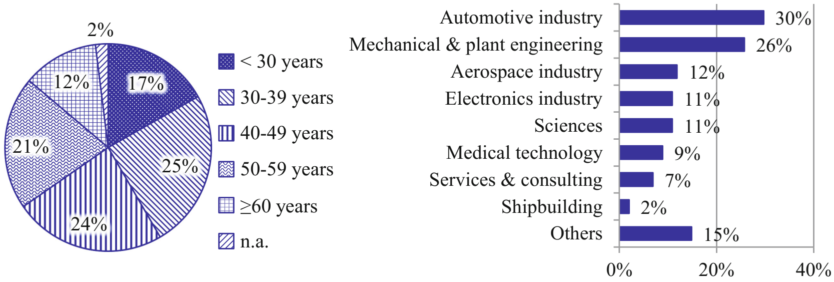

Fig. 2. Distribution of target participants: age (left) and company branches (right)

3.2 Basic AM Knowledge of Designers

At the beginning, participants were asked to intuitively describe their **understanding of '3D-printing' or 'additive manufacturing'** (maximum 2–3 sentences; the general meaning of 3D-printing and AM was then explained in more detail). These free text answers show that the majority of designers have the basic understanding that 3D-printing means to fabricate a part in layers from a digital file (97%), whereby 37% explained AM even in further detail. In 42% of the free texts, the variety of multiple materials and technologies was mentioned additionally. In over one third of the answers, participants gave detailed explanations of AM technologies. Some answers were only specialized on laser-based AM technologies (9%) or on rapid prototyping (4%). 2% mentioned that they knew 3D-printing, but not 'Additive Fertigung', the German word for AM.

The majority of the participants had a very good understanding as to **why AM can be used for final part production**. Participants were asked to name intuitively up to five reasons for direct AM application in their own words and these answers were then clustered and evaluated. Frequent answers were: geometrical freedom of AM for complex structures, cavities, and freeform surfaces (mentioned by 60%), as well as the fabrication of low quantities for small batches or lot size one (45%), which enables product customization/personalization (mentioned by 17%). The rapidness of AM allows for short production and lead times, and fast time to market, which was mentioned by 36% of participants. Advantages for lightweight design, material and weight saving were mentioned by 23%. Tool-less fabrication with savings of tool construction time and costs (14%), functional integration (11%), as well as part consolidation and improved assemblies (11%) were also mentioned as reasons for using AM for final parts. 13% of the participants mentioned prototype fabrication, although the question was to state reasons for the use of AM for *final* part production. 6% of the participants did not know or did not mention any application cases of AM for final part production.

Knowledge levels concerning **general advantages** (see Fig. 3) and **disadvantages** (see Fig. 4) of one or more AM technologies were asked in multiple choice questions, which included true [2, 4] and false answer possibilities. The long version contained more answer possibilities (marked 'LV'); percentage is referred to total respondents of each answer possibility. 1% of the participants mentioned that they do not know any dis-/advantages of AM. It is important to note that not selected answers cannot distinguish between non-chosen and non-processed answers. The results on the advantages exhibit a clear differentiation between chosen, correct answers and the selection of false answer possibilities (Fig. 3). Such a clear distinction is not recognizable for the selected disadvantages of AM, which meant that also wrong answers were chosen (Fig. 4).

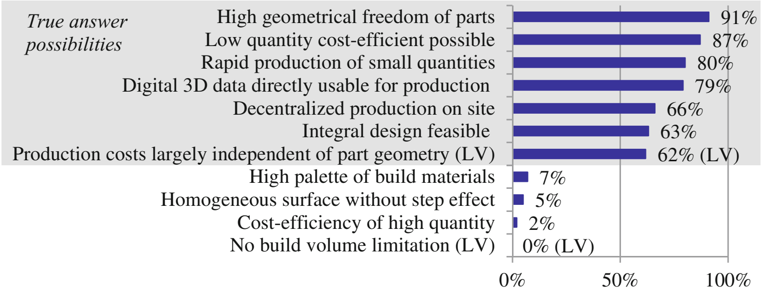

Fig. 3. Percentage of participants selecting general advantages of AM technologies

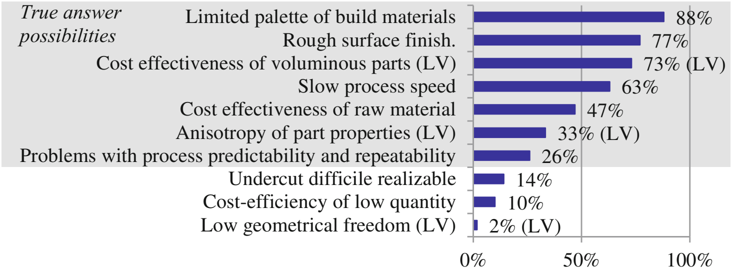

Fig. 4. Percentage of participants selecting general disadvantages of AM technologies

3.3 Detailed Knowledge of AM Technologies and Design Rules

Skills in differentiating various AM technologies were analyzed by asking participants to match pictures of AM machines and AM parts to the names of the AM technologies (only LV participants). Approximately half of the LV participants chose the correct answer in every case, see Fig. 5. 64% of the LV participants matched 2 or more technologies correctly. Those participants were then asked to compare two AM technologies with respect to material strength, material, and smoothness of the surface; more than 80% of these answers were correct.

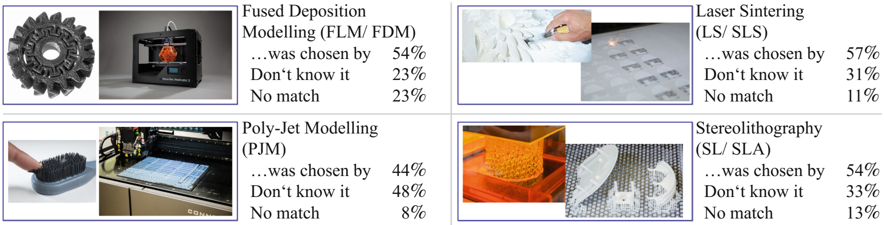
Fused Deposition Modelling (FLM/ FDM)
…was chosen by 54%
Don‘t know it 23%
No match 23%
Laser Sintering (LS/ SLS)
…was chosen by 57%
Don‘t know it 31%
No match 11%
Poly-Jet Modelling (PJM)
…was chosen by 44%
Don‘t know it 48%
No match 8%
Stereolithography (SL/ SLA)
…was chosen by 54%
Don‘t know it 33%
No match 13%

Picture sources: www.resins-online.com; www.3dprod.com; www.fkm-lasersintering.de; www.mack-technik.com; www.rapidobject.com; www.heise.de; www.1zu1prototypen.com

Fig. 5. Matching pictures of AM machines and parts to the name of the technology

The LV participants were asked to mark those predefined **aspects, which have to be considered for design and production planning** of AM parts in some or all AM technologies; results of this multiple-choice question are displayed in Fig. 6. The predefined aspects are based on [1, 8, 11] and contain four supplementary wrong answers of production-ready design for other manufacturing technologies.

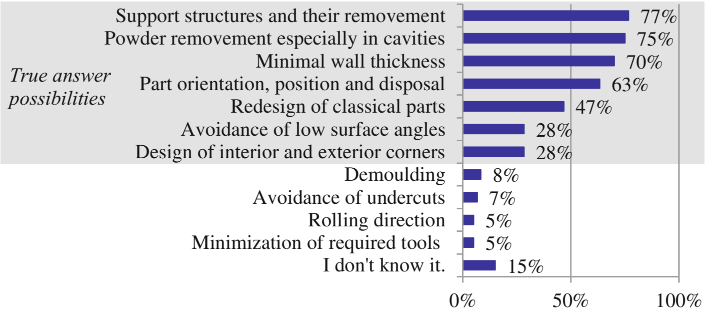

Fig. 6. Percentage of LV participants choosing relevant aspects to design and production planning for AM

3.4 AM Experience of Designers

Nearly all of the participants had **held AM parts in their hands** before (98%). 18% of the LV participants stated that they did not know the technologies of the parts that they had held in their hands. Most **hand-held parts were made by** Laser Sintering, as 77% of those who had correctly matched the SLS picture mentioned, which are 44% of all LV participants (compare Fig. 5; multiple choices were possible). The second most frequent technology of the hand-held parts were Fused Deposition Modeling (73% of all who match the FDM-picture correctly, which means 39% of all LV participants) followed by Stereolithography (67% of correctly matched pictures, resp. 36% of all LV participants). Parts made by Poly-Jet Modeling (MJM/PJM) were not often held in hands (30% of correct PJM matchings, which are 13% of all LV participants).

16% of the participants had never **ordered or fabricated a part with AM** before. 29% of the participants had fabricated or ordered 1 to 9 3D-printed parts, 25% 10 to 49 parts and 31% 50 parts or more. Percent specifications in this section relate to all those participants who had ordered or fabricated 3D-printed parts (in sum 84% of all participants, 85% of all LV participants). These participants **used 3D-printed parts** mostly for display models and prototypes, as 86% of them stated (multiple answers were possible). Less than one third of these participants stated that they used the fabricated components for final parts (27%), and only 12% use AM for serial part production. The AM-fabricated parts were also used for private occasions or gifts (24%), or spare parts (18%). 9% spontaneously stated in 'other usages' that they used AM parts for testing and for exploring material and machine characteristics. **Additive manufacturing was chosen** mostly because of rapid production (chosen by 75% of the LV participants who fabricated or ordered 3D-printed parts, multiple answers were possible). 58% of these LV participants chose AM because of cost-efficient production of low quantities. 37% of these LV participants exploited the geometrical freedom through AM, 31% fabricated parts because of their interest in AM or in testing AM machines.

Half of all participants stated that they had already **designed** a part especially for AM and had considered construction guidelines for AM (50%).

Participants who had fabricated parts with AM were asked how often they had already **handled a 3D-printer**. This question was posed to 52 LV participants and to 8 SV participants. Due to a technical error other 25 SV responses were missing. The following results and analyses concerning the experience level leave these missing participants out of consideration and are marked as *. 38% of the participants* who fabricated AM parts had already handled a 3D-printer before (12% 1 to 9 times, 8% 10 to 49 times and 18% 50 times or more), whereby most of them **operated** a Fused Deposition Modeling machine.

Three categories are defined for the experience level of participants* with AM: inexperienced, slightly experienced, and experienced. These categories are based on the four equally loaded statements concerning the hand-held AM fabricated parts, the number of fabricated AM parts, the frequency of operating AM machines, and the construction for AM. The yes/no choices concerning AM parts held in hands and concerning the design for AM are valued as 1/0.25. The frequency of fabricated or ordered AM parts, and operations of AM machines are valued as 0.25 for none, 0.5 for 0 to 9 times, 0.75 for 10 to 49 times, and 1 for 50 times or more. The sum of this value range from 1 to 2 for inexperienced, over 2 to 3 for slightly experienced, and over 3 to 4 for experienced. Using this gradation, 34% of the participants* belong to the category 'inexperienced' (LV 33%), 29% to 'slightly experienced' (LV 33%) and 37%, LV 34% respectively, belong to the 'experienced' category.

The majority of the participants* worked in **companies that own AM machine(s)**. The distribution of the participants working in companies owning or not owning AM machines is displayed in Fig. 7 – both for all participants and separated for participants* by categories for experience level with AM.

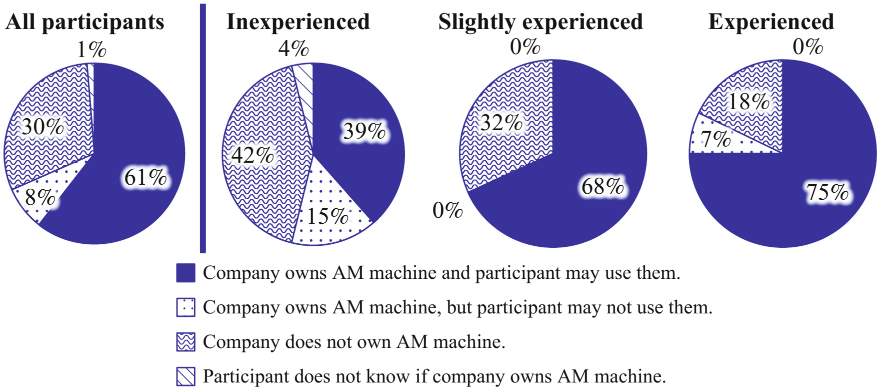

Fig. 7. Distribution of participants in companies with/without AM machine(s) and their accessibilities. Left: all participants; right: participants* separated by experience level with AM

3.5 Attitude of Designers Towards AM Technologies for Final Parts

Next to knowing about AM, personal attitudes towards AM are highly relevant when designers are considering whether or not to use AM for final parts production. Thus, participants were asked for which **personal reason they would/would not fabricate final parts with AM**. They were prompted to choose reasons to be for/ against direct AM by selecting (1) which reasons were essential to them, and (2) to order them according to their personal relevance. Seven predefined reasons were presented in random order in questions for and against direct AM (Fig. 8).

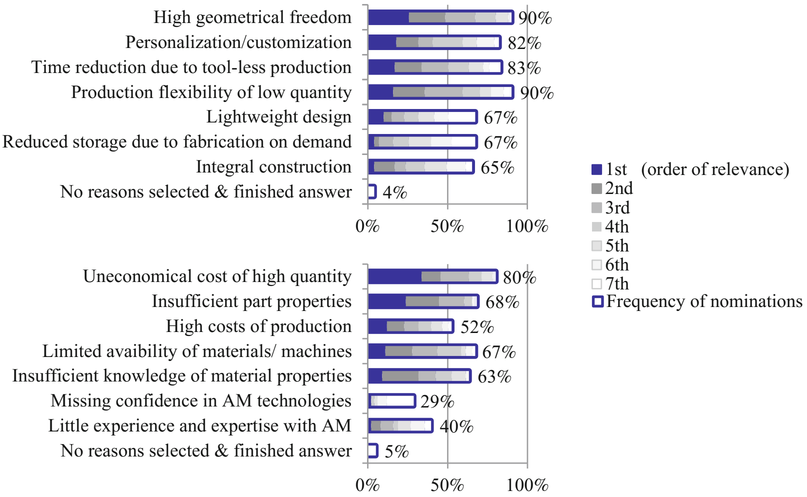

Fig. 8. Ranking of personal reasons for being in favor of (above) or against (below) AM for final part production, sorted by 1st order of relevance.

2% of the participants did not answer the two questions on personal ranking. 4% of the participants selected no reason to be *for* direct AM while they stated that they had finished the answer; 5% selected no reason to be *against* direct AM.

Geometrical freedom was rated as the number one reason *for* using AM-fabricated final parts (see Fig. 8, above). Production flexibility in low quantity was mentioned equally often but with lower relevance, especially with regard to the first order of relevance (16% of nomination vs. 26% for geometrical freedom). Personalization/customization and time reduction due to tool-less production were similarly relevant reasons, followed by lightweight design, integral construction and cost reduction of storage due to on-demand fabrication.

Reasons *against* AM-fabricated final parts are distributed more unevenly in number of nominations (see Fig. 8, below). Main reason for being against direct AM was the uneconomical cost of high quantities, followed by insufficient part properties, which exhibited a similar relevance but was less frequented mentioned. Reasons which were rated with less relevance were: insufficient expertise and experience with AM and missing confidence in AM technologies. In sum, reasons *against* direct AM are less frequented than reasons *for* direct AM.

The more experienced the participants, the more they **felt certain** that they could evaluate whether AM or conventional technologies were more suitable for the production of *final* parts, see Fig. 9. LV participants were asked if they would like to have a **decision support** when considering AM for final part production. The majority of the participants stated that such a support would be helpful (LV 64%). 25% of the LV participants – the majority of them are well experienced and skilled – said that they didn't need any decision-support as they were well versed with additive manufacturing. 11% of the LV participants (most of them are members of the 'inexperienced' category) did not need or want to make this decision.

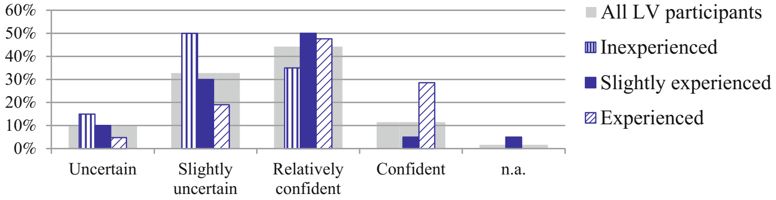

Fig. 9. Certainty of LV participants that they could judge whether AM or conventional technologies were reasonably for the production of final parts. Percentages refer to entirety of category.

Statements concerning the **intention of using final part production with AM in the next 5 years** showed that the majority stated that they 'plan on' or 'absolutely plan on' using AM for final parts, i.e. 60% of all participants and even 75% of the experienced participants*, see Fig. 10. 16% of all participants were unsure because of too little information or uncertain progress in 3D-printing technologies.

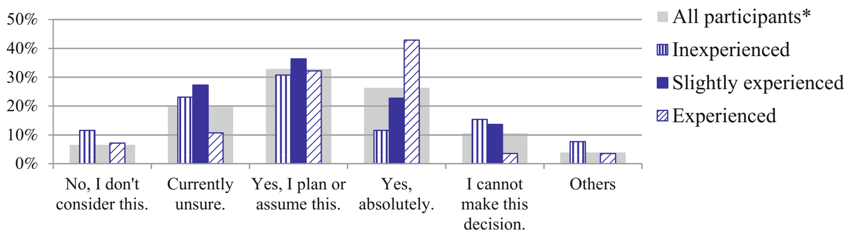

Fig. 10. Participants'* intention of fabricating final parts with AM in the next 5 years. Percentages refer to entirety of category.

4 Discussion

4.1 AM Knowing of Designers

Understanding how AM technologies work is important in making design decision for AM and consequently in exploiting AM specific potentials and implementing AM for final part production. Designers have a firm basic understand of AM, as proven by free text answers on AM and its application cases for final part production. Especially the astonishing high quality of answers about application cases of AM for final parts reveals that the general understanding on the AM-specific possibilities is given for designers. Only the occasionally reference to prototype fabrication in the question about AM for final parts indicates a poor distinction between the application groups in prototyping and final part production.

Advantages and disadvantages of the AM technologies are known by designers but not to in same degree. Existing differences between AM technologies may possibly influence the selection of answer: For example, SLS has lower restrictions with regard to anisotropy than FDM parts, so that SLS experts maybe not chose this point. However, the separation between true and wrong answers should be clearly visible in Figs. 3 and 4. Advantages can be clearly separated into a majority of true answers and a minority of incorrect answers. The results of the disadvantages, however, do not offer such a clear distinction between disadvantages and non-disadvantages. Disadvantages of AM seem to be known by fewer designers and this lack of knowledge, especially concerning non-disadvantages of AM technologies, has to be overcome as it influences the decision-making in AM and late complications could be reduced in advance.

As various AM technologies contain different possibilities and restrictions, e.g. the feasible material, mechanical strength or accuracy, it is relevant that decision makers know the different AM technologies. Assigning pictures of AM parts to AM technologies was challenging for the participants (Fig. 5). Too often, the differences between the AM technologies remained unknown. As the clear majority of experienced designers answered these questions correctly, the assumption is reasonable that there is a high discrepancy in the knowledge concerning the various AM technologies.

The designers were aware of design rules for AM – a separation between correctly chosen true aspects how to design for AM and wrong answers was recognizable (Fig. 6). Some designers stated that they do not know AM design rules; they may benefit from design guidelines about how to design for AM. This topic could be analyzed in more in detail than this study focusing on decision-making in AM allows for.

The presented analysis of AM expertise of designers exposes that the general understanding about AM is good while there is a deficit in knowing about general restrictions of AM. Many designers show difficulties in differentiating various AM technologies so that the advantages and especially restrictions of the different AM technologies need to be further clarified in DfAM approaches. The definitions and wording of AM and of AM technologies need to be unified. Finally, categorizing the application groups in product life phases (prototyping, direct AM, and indirect AM) in DfAM approaches can be helpful, especially for working on an improved understanding for decision-making about AM for *final* part production.

4.2 AM Experience of Designers

Not only expertise but also experience levels vary greatly with regard to various AM technologies. This study shows that, unfortunately, nearly one fifth of the participants did not know which technology was used to make the parts that they were holding in hands. Holding AM parts in own hands does not substitute in-depth experiences through self-designed and self-fabricated AM parts, but it supports the understanding of part properties, advantages and restrictions of that particular technology. Current purchase prices and operation efforts of AM machines compared to desktop 3D-printer explain the fact that FDM machines are being used the most. Thus it comes somewhat of a surprise that most participants had held parts fabricated with Laser Sintering. The (still distant) goal is that designers can say that they have held parts in their hands fabricated by different AM technologies – and that they also know name and properties of those technologies.

AM fabricated parts are used in different product life phases for prototypes, final components and spare parts. Survey results with companies in [6] show that companies use AM to produce functional parts more than for fabricating prototypes. The presented survey with engineers show that individual engineers act differently than companies, as 86% of the participants used 3D-printed parts for display models and prototypes and only 28% for final parts/ final parts in series.

The analysis of designers' experience with AM proves that experience levels of designers with AM vary strongly. DfAM methods should consider these discrepancies in experiences and offer tailored approaches for different target groups.

4.3 Attitude of Designers Towards AM Technologies for Final Parts

Expertise and experience concerning AM influence the attitude of designers towards the decision about direct AM. It is astonishing that around 60% of all participants want to build final products in the next 5 years – even the inexperienced ones. The more experienced the participants were, the more confident they felt about making decisions on final part productions with AM, and the more definite they stated their intention of fabricating final parts with AM in the next years. Experiences with AM are related proportionally to the access to an AM machine in a company (Fig. 7). Achieving right estimations about final part production with AM and the expedient application of additive manufacturing technologies can, thus, be supported through easy accessibility of AM machines in companies.

Most important personal reasons for direct AM were: geometrical freedom, production flexibility in low quantity, time reduction, and personalization possibilities. Since these reasons are also main advantages of AM, it is a good sign that between 82% and 90% of the designers did choose them as relevant. The most frequented personal reason against direct AM (i.e. uneconomical cost of high quantity) was chosen less often (80%) than these four reasons for direct AM, which approves the high interest in direct AM.

Only two-fifths of the designers stated that a lack of knowledge and experience with AM was a relevant reason against direct AM. Anyway, over three-fifths of designers would appreciate a decision support to decide whether or not to design for direct AM. Furthermore, almost of half of participants felt (slightly) uncertain about deciding when to use AM or conventional production technologies for final part production. These three statements show that designers are not against using AM for final parts but that further support for the decision concerning the design for AM is necessary. The reflection on when to design for direct AM and the consideration of AM specific impacts should be supported by DfAM methods.

One third of the designers stated that they were experienced with AM for final part production, only around half of them in serial part production. Detailed experiences and any existing complications in the design process for direct AM should be further analyzed in order to improve the understanding of the current situation.

The presented analysis of the designers' attitude towards direct AM exposes that there is a high interest and intention in using AM for final parts production, yet this is combined with a slight skepticism. A decision support of when to design for direct AM is needed now, especially by the less experienced and skilled designers concerning AM. It is meaningful to support the highest rated reasons for direct AM, because these main advantages of AM are also well accepted by designers. Those different characteristics for using direct AM need different kinds of design support. For example: high geometrical freedom can be supported through design rules or topological optimizations in the detail design phase, while mass personalization of products need special processes in product structure design in order to fulfill the individual needs with reduced variety-induced complexity. Thus, it is essential in DfAM to reflect upon the reasons for AM usages separately without neglecting their mutual influences and the overall characteristics of AM.

5 Conclusion and Outlook

Additive manufacturing can be used for different purposes in product life cycle because it allows for high geometrical freedom and fabrication flexibility, e.g. enabling an economical production of small lot sizes. With focus on decision-making of designers for direct AM, this paper presents an industrial survey about the current attitudes of designers on AM. Answers of the target group (i.e. working in product planning and design, decision-making of materials and production, or production planning) were analyzed with respect to their experience, expertise and attitude towards AM fabricated (final) parts. The data shows that the experience with AM is very different, reaching from never having held an AM part in their own hands to high skilled AM experts. While the basic knowledge about AM and its application cases is present, in-depth knowledge concerning the restrictions and the different AM technologies is lacking. The presented analyses reveal that there is a high interest and intention in using AM for final parts production, combined with a slight skepticism. Further DfAM methods should address those aspects about missing detailed knowledge and skepticism. In order to use AM specific possibilities, DfAM approaches are meaningful in supporting the decision-making process in direct AM for different application cases.

Against the backdrop of recent technological improvements of AM, this study reveals that it is also important to implement DfAM approaches. At this point, the high discrepancies found in AM experience and knowledge levels should be covered while continuously supporting the usage of AM for final part production. DfAM approaches about when to and how to design for AM are needed and should reflect overall AM characteristics while focusing on specific reasons for AM applications, e.g. geometrical freedom or fabrication of low quantities.

References

1. Thompson, M.K., Moroni, G., Vaneker, T., Fadel, G., Campbell, R.I., Gibson, I., Bernard, A., Schulz, J., Graf, P., Ahuja, B., Martina, F.: Design for additive manufacturing. Trends, opportunities, considerations, and constraints. CIRP Ann. – Manuf. Technol. (2016). doi:10.1016/j.cirp.2016.05.004
2. Baumers, M., Dickens, P., Tuck, C., Hague, R.: The cost of additive manufacturing. Machine productivity, economies of scale and technology-push. Technol. Forecast. Soc. Change **102**, 193–201 (2016). doi:10.1016/j.techfore.2015.02.015
3. Spallek, J., Frölich, A., Buhk, J., Fiehler, J., Krause, D.: Comparing technologies of additive manufacturing for the development of vascular models. In: 2016 Conference on Fraunhofer Direct Digital Manufacturing (2016). doi:10.13140/RG.2.1.2847.0169
4. Gibson, I., Rosen, D., Stucker, B.: Additive Manufacturing Technologies: 3D printing, rapid prototyping, and direct digital manufacturing, 2nd edn. Springer, New York (2015). doi:10.1007/978-1-4939-2113-3
5. Spallek, J., Sankowski, O., Krause, D.: Influences of additive manufacturing on design processes for customised products. In: 14th International Design Conference - DESIGN 2016 (2016). doi:10.13140/RG.2.1.1112.4080
6. Wohlers Associates: Wohlers Report 2016. 3D printing and additive manufacturing state of the industry: annual worldwide progress report. Wohlers Associates, Fort Collins (2016)
7. Adam, G.A.O., Zimmer, D.: On design for additive manufacturing. Evaluating geometrical limitations. Rapid Prototyp. J. **21**(6), 662–670 (2015). doi:10.1108/RPJ-06-2013-0060
8. Kranz, J., Herzog, D., Emmelmann, C.: Design guidelines for laser additive manufacturing of lightweight structures in TiAl6V4. J. Laser Appl. **27**(S1), S14001 (2014). doi:10.2351/1.4885235
9. Seepersad, C.C.: Challenges and opportunities in design for additive manufacturing. 3D Print. Addit. Manuf. **1**(1), 10–13 (2014). doi:10.1089/3dp.2013.0006

10. Pradel, P.: Survey for Design for Additive Manufacturing (2016). http://www.d4am.eng.cam.ac.uk/research/d4am-project/survey, https://lboro.onlinesurveys.ac.uk/dfam-survey. Accessed 29 May 2017
11. Adam, G.: Konstruktionsregeln für Additive Fertigungsverfahren. Eine Grundlage für die Ausbildung und Lehre. OptoNet-Workshop, 06 November 2013. http://www.spectronet.de/story_docs/vortraege_2013/131106_optonet_workshop/131106_03_adam_dmrc.pdf

Author Index

A
Abdulstaar, Mustafa, 104
Assaf, Eyad, 264

B
Bach, Miriam, 93
Beck, Christian, 210
Bellet, Michel, 49, 82
Bey, Niki, 287
Bianchi, Giovanni, 117
Bibb, Richard, 24
Bonnard, Renan, 127
Briand, Danick, 137

C
Calignano, Flaviana, 181
Cattano, Giulio, 181
Chandran, Olivier, 137
Chavarri, Carlos Herrán, 162
Chen, Qiang, 49
Clemens, Frank, 93

D
Daniel, Christian, 319
Delrot, Paul, 145
Dennig, Hans-Jörg, 210, 329
Disser, Jérémy, 264
Dunan, Barthelemy, 137

E
Efthymiou, Evangelos, 34
Eggenberger, Timo, 223
Eisenbarth, Daniel, 152
Ess, Jonas, 252

F
Ferchow, Julian, 337
Ferrini, Rolando, 264
Fontana, Filippo, 238, 296

G
Gandin, Charles-André, 49, 82
Grekavicius, Lukas, 34
Guillemot, Gildas, 49, 82

H
Hamilton, Kelvin, 70
Hansen, Hans Nørgaard, 162, 287
Hartmann, Martin, 252
Hastedt, Heidi, 296
Hoffmann, Patrik, 104
Hofmann, Erik, 223
Hofstätter, Thomas, 162, 287
Honigmann, Philipp, 308
Huber, Marc, 252
Hughes, Jack Antony, 34

I
Iuliano, Luca, 181

K
Kenel, C., 200
Kirchheim, Andreas, 210, 329
Klahn, Christoph, 3, 273, 337
Kränzler, Thomas, 252
Krause, Dieter, 347

L
Lachmayer, Roland, 14
Lani, Sebastien, 137
Le Dantec, Marie, 104
Leinenbach, C., 200
Leistner, Matthias, 104
Leparoux, Marc, 104
Leutenecker-Twelsiek, Bastian, 273, 337
Lippert, Rene Bastian, 14
Löffel, Kaspar, 252
Loterie, Damien, 145

© Springer International Publishing AG 2018

M. Meboldt and C. Klahn (eds.), *Industrializing Additive Manufacturing - Proceedings of Additive Manufacturing in Products and Applications - AMPA2017*,
DOI 10.1007/978-3-319-66866-6

Luhmann, Thomas, 296
Lunzer, Andreas, 162
Lusiola, Tony, 93

M
Manfredi, Diego, 181
Marchetti, Andrea, 59, 191
Marinelli, Enrico, 238
Marjanović, Nenad, 264
Mazzucato, Federico, 59, 191
Meboldt, Mirko, 3, 238, 337
Melnykowycz, Mark, 93
Michailidou, Ifigeneia, 162
Mischkot, Michael, 162, 287
Mootien, Azagen, 308
Moser, Christophe, 145
Moultrie, James, 24
Mustaccio, Alessandro, 264

O
Ochsner, David, 296
Oettmeier, Katrin, 223
Omidvarkarjan, Daniel, 3
Ortona, Alberto, 117

P
Pedersen, David Bue, 162, 287
Petersen, Maren, 319
Pradel, Patrick, 24
Psaltis, Demetri, 145

R
Rettberg, Robin, 252
Rieke-Zapp, Dirk, 296
Rofallski, Robin, 296
Roland, Lachmayer, 169
Rosenbauer, Ralph, 296

S
Santoliquido, Oscar, 117
Scharf, D., 93
Schleuniger, Jürg, 264
Schmitt, Bianca, 319
Schnieper, Marc, 264
Schumacher, Ralf, 308
Sebastian, Tutu, 93
Sharma, Neha, 308
Shevchik, S.A., 200
Spallek, Johanna, 347
Spieldiener, Kevin, 152
Spierings, Adriaan, 273
Stoll, Philipp, 273
Stotz, Philippe M., 287

T
Thieringer, Florian M., 308
Tosello, Guido, 162, 287
Tsavdaridis, Konstantinos Daniel, 34

V
Valente, Anna, 59, 191
Voirin, Guy, 137

W
Wasmer, K., 200
Wegener, Konrad, 152, 273
Wirth, Florian, 152
Würms, Andreas, 252

Y
Ya, Wei, 70
Yousif, Zghair, 169

Z
Zanella, Frédéric, 264
Zhang, Yancheng, 82
Zhu, Zicheng, 24
Zumofen, Livia, 210, 329